Rooney, Rebecca Audrey (2024) *Extracellular vesicle mediated delivery of angiotensin (1-9) after ischaemic stroke.* PhD thesis.

https://theses.gla.ac.uk/84466/

Enlighten: Theses
https://theses.gla.ac.uk/
research-enlighten@glasgow.ac.uk

Extracellular Vesicle mediated delivery of Angiotensin (1-9) after Ischaemic Stroke

Rebecca Audrey Rooney

MSc, MRes, BSc (hons)

Submitted in fulfilment of the requirements of the degree of Doctor of Philosophy in the College of Medical, Veterinary and Life Science, University of Glasgow

School of Cardiovascular and Metabolic Health, College of Medical, Veterinary and Life Sciences, University of Glasgow

April 2024

© R A Rooney 2024

<u>Author's Declaration</u>

I declare that this thesis has been entirely written by myself and is a record of work performed by myself with the exception of:

- Article screening for in chapter 3 was conducted by myself and Dr Lorraine Work.
- Plasma samples from SHRSPs were collected by Dr Lorraine work and Dr Josie Fullerton, until such time that I was trained and assessed as competent to extract blood samples from SHRSPs that could be used to generate plasma.
- SHRSP brain tissues (n=3) were provided by Dr Josie Fullerton following completion of her successful tMCAO surgeries until such time that I was trained and assessed as competent to conduct tMCAO surgeries (Figure 7.1-7.5).
- Organs from SHRSPs subjected to intranasal delivery of EVs were collected by Dr Lorraine Work and Dr Josie Fullerton (Figure 6.8-6.17).
- On occasion tail cuff plethysmography and perfusion fixation of SHRSPs used in this experiment were conducted by Mrs Wendy Beattie (Figure 7.11).
- On occasion neuroscoring was conducted by Dr Lorraine Work, Dr Josie Fullerton and Mrs Wendy Beattie (Figure 7.13).
- Blood samples from AT_2R deficient mice were collected by Dr Lisa McArthur until such time that I was trained and assessed as competent to perform cardiac puncture.
- Genotyping of AT_2R deficient mice was conducted by myself, Dr Lisa McArthur, Mrs Elaine Friel.
- Neo-natal SHRSP brains were isolated by Dr Josie Fullerton and Mrs Nicola Britton until such time that I was trained and assessed as competent to do so.
- Transmission electron microscopy and imaging of extracellular vesicles was conducted by Mrs Margaret Mullin (Figure 5.19).
- Mr Jamie Cooper of Oxford Brookes University conducted nano flow cytometry set-up and gating for extracellular vesicles (Figure 4.5-4.12).

Rebecca Rooney

April 2024

__Acknowledgements__

To my wee family. Mum and Dad, as you say, you made smart kids, which is why I must first talk about my big brother. Matt, you were my childhood best friend, a constant, and someone who I have always looked up to and will continue to do so for as long as we are together. Mum and Dad, thank you for listening to me talk about EVs for the past half a decade. I'm so glad I have such supportive parents like you who will stop what they are doing at any minute to be there for me. To my sister-in-law, Bee, and my soon-to-be sister-in-law, Patty, thank you for being the sisters I never had. I would like to thank Anita and Jörg for their kind words of support and encouragement. Our family has grown over the years; from Scotland to England to Switzerland. I love you all no matter where you are.

Lastly, I would like to thank Dr Philipp Boder, my best friend and fiancé. When I first met you on this PhD programme, I knew you were special, both academically and personally, but little did I know I would end up marrying you. Thank you for being the greatest partner anyone could ask for. Your kindness, loyalty, passion, and love are unwavering. You, Philipp, above all else, are the greatest gift this life has given me.

<u>List of publications, awards and presentations</u>

Publications and Awards

Fullerton, JL., Cosgrove, CC., **Rooney, RA**., & Work, LM. (2022) Extracellular vesicles and their microRNA cargo in ischaemic stroke. Journal of Physiology. DOI:10.1113/jp282050

The Guarantors of Brain Travel Grant- £1,000

Graham Wilson Travel Grant- £800

MVLS Travel Grant- £750

Conference presentations

Poster presentation at the Gordon Research Conference on Extracellular Vesicles 2022 in Maine, USA for the project entitled: *"Characterisation of circulating EV populations from wildtype or Angiotensin II Type 2 Receptor knockout mice".*

Poster presentation at BRAIN & BRAIN PET 2022 in Glasgow, UK for the project entitled: *"Characterisation of circulating EV populations from wildtype or Angiotensin II Type 2 Receptor knockout mice".*

Poster presentation at UK society for Extracellular Vesicles 2022 in Edinburgh, UK for the project entitled: "*Assessing the effects of RVG-targeted extracellular vesicles in novel stroke therapies".*

Oral presentation at Alzheimer's Research UK ERC day Scotland 2019 in Dundee, UK for the project entitled:*" Therapeutic extracellular vesicle-mediated delivery of angiotensin-(1-9) peptide after ischaemic stroke".*

Poster presentation at BHF student conference 2021 (virtual) for the project entitled: *"Therapeutic extracellular vesicle-mediated delivery of angiotensin-(1-9) peptide after ischaemic stroke."*

<u>Summary</u>

Stroke remains a leading cause of global disability and mortality. For those who experience a stroke, interventions such as mechanical thrombectomy, or more commonly, rtPA are used to enable total or partial reperfusion that can save lives and reduce the degree of disability. With advancements in medicine, 80% of stroke incidences are preventable, and hopefully one day, with further advancements in pioneering medical science, the degree of disability and morbidity from stroke will be minimal. Recently, extracellular vesicles (EVs) have been studied for their role in disease, including stroke, due to their cell signalling potential and internalised cargo. In doing so, EVs are now understood to be excellent delivery vectors, whereby beneficial microRNAs, compounds or peptides may be encased within EVs that can be used to treat various diseases. Activation of the receptors within the counter-regulatory axis of the Renin Angiotensin Aldosterone system (RAAS), such as the Angiotensin II Type II receptor, AT_2R, can lead to vasodilation, inhibition of inflammation, prevention of cell death and stimulation of cell growth, all of which are crucial pathways in the brain following stroke. Several preclinical and clinical stroke studies have highlighted the potential benefit of targeting RAAS to improve post-stroke outcomes. By eliciting the activation of AT_2R by its novel functional ligand Angiotensin-(1-9) [Ang-(1-9)], these protective downstream pathways can be activated. It was therefore hypothesised that loading EVs with Ang-(1-9) would activate neuroprotective mechanisms in a comorbid model of experimental stroke. Consequently, this research would establish the therapeutic potential of Ang-(1-9) in ischaemic stroke, along with assessing the ability of EVs to successfully deliver potentially therapeutic, internalised cargo.

In chapter 3, published peer-reviewed data was systematically reviewed to summarise whether RAAS targeting interventions improved post-stroke functional outcomes, including neurological outcomes, infarct volumes and the expression of peptides or cognate receptors, in experimental stroke models. From the available literature there were 414 hits from which a total of 27 publications met the inclusion criteria and were included in further data analysis. Of the studies that assessed the effects of RAAS targeting interventions on neurological outcomes, 31 out of 42 studies demonstrated that RAAS targeting interventions improved post-stroke neurological outcomes. These positive findings were also reflected in infarct volume, whereby, of the studies that assessed the effects of RAAS targeting interventions on infarct volume, 12 out of 16 studies found that RAAS targeting interventions reduced infarct size following stroke. RAAS targeting interventions also led to differential expression of genes coding for cognate receptors and

key enzymes in the RAAS. These findings put into perspective the beneficial effects of activating the counter regulatory axis of the RAAS and inhibiting the classical axis of the RAAS, on post-stroke outcomes.

In chapter 4, it was hypothesised that AT_2R deficiency in C57BL/6 mice would influence the characteristics of circulating EVs. EVs were isolated from plasma samples of male and female wildtype C57BL/6 mice or AT_2R deficient mice and were characterised using conventional nanoparticle tracking analysis (NTA), protein quantification and nano flow cytometry. AT_2R deficiency in female mice led to a significantly increased concentration of EVs compared to wildtype female mice, indicative that AT_2R deficiency can directly impact EV characteristics. A sex-based difference was identified in AT_2R deficient mice, whereby EV particle size was significantly greater in AT_2R deficient females compared to AT_2R deficient males. EV protein content was similar between groups. To understand if knocking down AT_2R affected EV surface markers, and potentially the cellular origin of EVs, plasma derived EVs were analysed for the presence of platelet marker CD41 and endothelial cell marker CD31 using nano flow cytometry. Again, sex-based differences were identified in the AT_2R deficient mice, whereby it was found that EVs from AT_2R deficient female mice possessed significantly greater levels of CD41 and CD31 compared to EVs derived from AT_2R deficient male mice. From current literature, miRNAs were identified that were linked with the RAAS. Two miRNAs, miRNA-132 and -146a, were expressed within EVs isolated from plasma of wildtype mice or AT_2R deficient C57BL/6 mice, however the expression of these miRNAs was similar between groups. Overall, it was determined that AT_2R deficiency led to differences in EV concentration compared to wildtype mice and that AT_2R deficiency led to sex-based difference in EV size and surface marker expression.

In chapter 5, EV isolation methods were compared to determine whether isolation method influenced EV concentration, size and protein content. Size exclusion chromatography (SEC) was the method that provided the greatest EV concentration from SHRSP plasma samples and was used for further downstream experiments. EVs were loaded with peptides or miRNAs by electroporation which led to a significant reduction in EV concentration. SEC isolation of EVs following electroporation led to the greatest EV concentration compared to other isolation techniques. Over and above NTA characterisation and in line with standardised characterisation guidelines, SEC isolated EVs were found to possess common EV biomarkers, as determined by western blot, and structure, as determined by transmission electron microscopy. EVs and their loaded cargo were then assessed in preclinical cell culture models of stroke. Ang-(1-9) peptide and Ang-(1-9) electroporated

EVs did not affect the viability of immortalised B50 rat neuronal cells or SHRSP rat primary neuronal cells, suggesting their safety for use in animal models. EVs were electroporated with fluorescently-labelled Ang-(1-9) peptides or lipophilic dyes, as it may have provided information into the location of EVs and potentially the delivery site of internalised cargo in further *in vivo* studies. Treatment of immortalised B50 rat neuronal cells and GPNT rat cerebral endothelial cells with 5-FAM-Ang-(1-9) or electroporated EVs did not produce fluorescence, however primary neuronal cells treated with 5-FAM-Ang-(1-9) peptide demonstrated abundant fluorescence. Lipophilic labelling of EVs led to unreproducible red fluorescence in GPNT cerebral endothelial cells and primary neuronal cells. Ultimately loading of EVs with 5-FAM-Ang-(1-9) or labelling with lipophilic dye was unreproducible and could not be carried forward to *in vivo* studies.

In chapter 6 intranasal administration of EVs and EV brain targeting ability was assessed. EVs were loaded with exogenous *Cel-miR-39* and administered intranasally to SHRSP rats. The expression of *Cel-miR-39* EV cargo was identified throughout the brain, demonstrating the effectiveness of intranasal EV administration and the subsequent delivery of internal EV cargo. To target EVs to the brain, EVs were linked to Rabies virus glycoprotein (RVG) peptide using a CP05 linker previously reported to conjugate to CD63 tetraspanin on the surface of EVs. Primary neuronal cells expressed the receptor for RVG, CHRNB2, at greater levels than immortalised B50 rat neuronal cells, and as such primary neuronal cells were used in further targeting investigations. SEC isolated EVs were also shown to possess CD63 tetraspanin required for RVG-CP05 targeting conjugation. Non-targeted, *Cel-miR-39* loaded EVs, and RVG-targeted, *Cel-miR-39* loaded EVs at various concentrations were compared for their ability to deliver miRNA cargo throughout SHRSP rat brain following intranasal administration. Overall RVG targeting did not improve EV miRNA cargo delivery to the brain using the intranasal EV administration method, and as such RVG targeting of EVs was not used in further *in vivo* studies.

In the final results chapter, chapter 7, the effects of occlusion and reperfusion duration on post-stroke gene expression within brain tissue was determined. Genes related to the RAAS, such as ACE, ACE2 and Mas1, and growth, such as VEGFA and VEGFB, were assessed whereby occlusion duration led to differential expression of RAAS-related genes. The subsequent *in vivo* study aimed to assess the effects of intranasally administered Ang-(1-9) electroporated EVs on functional outcomes following tMCAO. In this stage the difficulty of *in vivo* research was highlighted and some functional outcomes that were originally planned could not be conducted due to animals exceeding humane endpoints as a result of tMCAO surgery. Nevertheless, the effects of Ang-(1-9) EVs on gene expression

within brain tissue of SHRSPs in the acute phase following tMCAO was determined, whereby Ang-(1-9) EVs led to differential expression of genes related to RAAS, growth and inflammation.

The findings of this thesis highlight the possible benefit of RAAS targeting interventions, including Ang-(1-9), and how EVs may be used as a delivery vector to facilitate the use of RAAS targeting interventions in ischaemic stroke. Some aspects of this preclinical study were challenging; however, the data demonstrates the potential application of EVs in disease treatment. Further study must be carried out to conclusively determine the likely benefits of Ang-(1-9) in ischaemic stroke.

<u>Table of Contents</u>

List of Tables

List of Figures

List of Abbreviations

ACE .... angiotensin converting enzyme

ACE2 .... angiotensin converting enzyme 2

ACEi .... ACE inhibitors

AD... Alzheimer disease

AF .... atrial fibrillation

AFC .... automated fraction collector

Akt .... protein kinase B

Ang I .... angiotensin I

Ang II .... angiotensin II

Ang-(1-7) .... angiotensin-(1-7)

Ang-(1-9) .... angiotensin-(1-9)

ARBs .... angiotensin II receptor blockers

AT_1R .... angiotensin II type I receptor

AT_2R .... angiotensin II type II receptor

AT_4R .... angiotensin II type IV receptor

ATP .... adenosine triphosphate

BAMs .... border-associated macrophages

BBB .... blood brain barrier

BCA .... bicinchoninic acid

Bcl-2 .... B-cell lymphoma 2

BDNF ....brain derived neurotrophic factor

BMI .... body mass index

BMSCs .... bone marrow derived stem cells

BoC .... brains-on-chips

bp .... base pairs

C21 .... Compound 21

CaCM .... calcium calmodulin

CBF .... cerebral blood flow

CBP .... cerebral blood pressure

CCA .... common carotid artery

CCB .... calcium channel blockers

CD31 .... cluster of differentiation 31

CD41 .... cluster of differentiation 41

CD61... cluster of differentiation 61

CD63.. cluster of differentiation 63

CD81.. cluster of differentiation 81

CD9 .... cluster of differentiation 9

Cel-miR-39.. *Caenorhabditis elegans* mimic microRNA 39

IHC .... immunohistochemistry

IL .... interleukin

ILF .... intraluminal filament

ILV .... intraluminal vesicles

iNOS.. inducible nitric oxide synthase

IP_3 .... inositol triphosphate

IP_3R .... IP_3 receptors

IRAP ....insulin-regulated membrane aminopeptidase

JAK/STAT .... Janus kinase/signal transducers and activators of transcription

JNKs .... c-jun N-terminal kinases

KOF ....AT_2R knockout females

KOM ....AT_2R knockout males

LCMS .... liquid chromatography mass spectrometry

LDH .... lactate dehydrogenase

MACE.. major adverse cardiovascular events

MAK-1 .... MAP kinase phosphatase-1

MasR .... Mas receptor

MCA ....middle cerebral artery5

MCAO ....middle cerebral artery occlusion

MCP-1 .... monocyte chemoattractant protein-1

MI .... myocardial infarction

miRNAs ....microRNAs

MLCK ....myosin light-chain kinases

MRI ....magnetic resonance imaging

mRS .... modified Rankin scale

MSCs ....mesenchymal stem cells

MTT .... 3-(4,5-dimethylthiazol-2-yl)-2,5-diphenyltetrazolium bromide

MVB .... multivesicular bodies

N_2 ....nitrogen

nanoFC .... nano flow cytometry

NDMAR ....N-methyl-D-aspartate receptor

NDS .... neurological deficit score

NEP ....neprilysin

NFκB .... nuclear factor kappa light chain enhancer of activated B cells

NGF .... nerve growth factor

NIHSS ....National Institute for Health Stroke Scale

nNOS ....neuronal nitric oxide synthase

NO ....nitric oxide

NOR .... object recognition

NOS ....nitric oxide synthase

NOX .... NADPH oxidase activity

nSMase .... neutral Sphingomylinase

NTA .... nanoparticle tracking analysis

NVU .... neurovascular unit

O_2 .... oxygen

OGD .... oxygen glucose deprivation

p38s .... p38 mitogen-activation protein kinases

PA .... pterygopalatine artery

PBS .... phosphate buffer solution

PCR .... polymerase chain reaction

PEG .... polyethylene glycol

PET... positron emission tomography

PFA .... paraformaldehyde

PIP_2 .... phosphatidylinositol-4,5-bisphosphate

PKG .... protein kinase G

PLCβ .... phospholipase C beta

pMCAO .... permanent middle cerebral artery occlusion

PP2A .... protein phosphatase 2A

PPI .... protease and phosphatase inhibitor

qPCR .... quantitative polymerase chain reaction

RAAS .... Renin Angiotensin Aldosterone System

RI .... recognition index

RIPA .... Radioimmunoprecipitation assay buffer

RNA.. ribonucleic acid

RNS .... reactive nitrogen species

ROS.. reactive oxygen species

RQ .... relative quantity

rtPA .... recombinant tissue plasminogen activator

RUNX .... Runt-related transcription factor

RVG .... rabies virus glycoprotein

SEC .... size exclusion chromatography

SEM .... standard error of the mean

SHP-1 .... tyrosine phosphatase Src homology region domain containing phosphatase-1

SHR .... spontaneously hypertensive

SHRSP .... spontaneously hypertensive stroke prone

SVZ .... subventricular zone

TBI .... traumatic brain injury

TCR .... T cell receptor

TEM .... transmission electron microscopy

TGF-β... transforming growth factor beta

TIA ....transient ischaemic attack

TLRs .... toll-like receptors

tMCAO .... transient middle cerebral artery occlusion

TNF-α .... tumour necrosis factor alpha

TRAF2 .... TNF receptor associated factor 2

TTC .... triphenyltetrazolium chloride

UC.. ultracentrifugation

VEGF .... vascular endothelial growth factor

VLDL ....very-low density lipoproteins

VSMCs .... vascular smooth muscle cells

WKY ....Kyoto Wistar rats

WTF .... wildtype females

WTM .... wildtype males

Chapter 1 Introduction

1.1 Stroke

"Stroke is a clinical syndrome of presumed vascular origin characterized by rapidly developing signs of focal or global disturbance of cerebral functions which lasts longer than 24 hours or leads to death" (National Institute for Health and Care Excellence, 2023c).

Stroke is a debilitating disease that affects nearly 12 million people worldwide annually (World Stroke Organisation, 2022). During stroke blood supply to the brain is prevented or reduced due to occlusion of a cerebral vessel as a result of thrombus or embolism, known as ischaemic stroke, or due to a brain bleed, known as haemorrhagic stroke (Stroke Association, 2024).

The most common form of stroke, ischaemic stroke, is defined as:

"an episode of neurological dysfunction caused by focal cerebral, spinal, or retinal cell death due to infarction following vascular occlusion or stenosis"(National Institute for Health and Care Excellence, 2023c).

The less common form of stroke, haemorrhagic stroke, is defined as:

"rapidly developing neurological dysfunction due to a focal collection of blood from within the brain parenchyma or ventricular system (intracerebral haemorrhage), or bleeding into the arachnoid space (subarachnoid haemorrhage) that is not caused by trauma"(National Institute for Health and Care Excellence, 2023c).

An alternative form of ischaemia affecting the brain, transient ischaemic attack (TIA), occurs when blood supply to the brain is transiently reduced and is self-resolving, often defined as:

"a transient (less than 24 hours) neurological dysfunction caused by focal brain, spinal cord, or retinal ischemia, without evidence of acute infarction" (National Institute for Health and Care Excellence, 2023c).

Stroke may be fatal or devastating for individuals. With acquired disability observed in approximately 60% of stroke patients and mortality rate of 30%, stroke remains a leading cause of global disability and mortality. Today it is now understood that nearly 80% of all

strokes are preventable (American Stroke Association, 2023a). Advancements in modern medicine have improved these survival rates and the degree of disability post-stroke.

1.1.1 Stroke subtype

There are two main forms of stroke, haemorrhagic and ischaemic. The least common form of stroke, haemorrhagic stroke, occurs when a blood vessel within the brain ruptures. Haemorrhagic stroke can be subcategorised into subarachnoid and intracerebral strokes depending on the location of the haemorrhage. A subarachnoid haemorrhagic stroke is located between the inner and outer layer that surround the brain, while an intracerebral stroke occurs within the cerebrum of the brain. Vessel rupture may be a result of aneurysm or arteriovenous malformation (American Stroke Association, 2023b). The most prevalent form of stroke, ischaemic stroke, can occur as a result of a thrombus or an embolus. In the case of thrombosis, blood vessels within the brain can be narrowed due to atherosclerotic build up. With embolic stroke, a blood clot may form within the body that can travel to the brain and block cerebral blood flow. The severity of stroke is dependent on both the location of the vessel blockage or rupture and the duration of blockage or bleed (American Stroke Association, 2023c).

1.1.2 Stroke presentation and assessment.

A stroke patients may present with a variety of symptoms including unilateral muscle weakness, numbness in regions of the body, loss of vision, difficulty with moving/poorly coordinated movement and issues with speech (Stroke Association, 2023). The acronym FAST (Face, Arms, Speech, Time) is often used as a tool to help individuals recognise the signs of stroke. Expanding upon this acronym, individuals may identify facial drooping, inability to raise both arms and slurred speech. If the aforementioned criteria are met, then individuals will be urged to contact emergency medical care (Stroke Association, 2023). The onset of these symptoms can be sudden and must be treated quickly. Upon clinical examination, certain symptoms may also provide insight into the location of the stroke within the brain. Non-contrast computed tomography (CT) scans are commonly carried out to identify whether the patient has experienced a stroke. Further, positron emission tomography (PET), single photon emission computed tomography (SPCT) or magnetic resonance imaging (MRI) may also be used to visualised the brain following stroke

(Markus, 2004). Imaging assessments are used in tandem with stroke scale scoring to deliver an accurate assessment of patients presenting with symptoms of stroke.

The National Institute for Health Stroke Scale (NIHSS) is used to assess the neurological function in stroke patients at the onset of symptoms and during recovery. Previous stroke severity scoring systems such as the Cincinnati prehospital stroke scale created by Brott and colleagues in 1989, allowed for the creation of the modern NIHSS (Brott et al., 1989). Today the NIHSS is a 42-point score, whereby a high score is correlated with more severe stroke and greater disability. The NIHSS includes assessment of levels of consciousness, vision, muscle weakness, mobility, speech and cognition (The National Institutes of Health, 2024). Other forms of acute stroke assessment such as the Glasgow Coma Scale (GCS) can be used to assess neurological impairment following stroke (Teasdale and Jennett, 1974). During the recovery period following stroke intervention, various scoring systems can be used to monitor changes in a patients impairment or disability, for example by use of the modified Rankin scale (mRS) (Rankin, 1957, van Swieten et al., 1988). By scoring patients during the acute period, clinicians can obtain an overview of prognosis and have better insight into which intervention is appropriate for a patient presenting with stroke symptoms. Further use of these scales may allow for more streamlined preventative treatments and rehabilitation in stroke patients.

1.1.3 Epidemiology and risk factors of Stroke

In 2019, there were approximately 12.2 million strokes worldwide, of which 7.6 million (62.4%) were categorised as ischaemic stroke. Haemorrhagic and subarachnoid strokes accounted for 27.9% and 9.7% of all strokes in 2019. The mortality rate of ischaemic stroke is approximately 40%, whereby in 2019 there were 3.3 million deaths caused by ischaemic stroke (World Stroke Organisation, 2022). From 1990 to 2019 the incidence of ischaemic stroke increased by 88%, while disability-adjusted life years (DALYs) and mortality rate increased by 57% and 61% respectively (GBD 2019 Stroke Collaborators, 2021). DALYs are the number of life years that a person has lost due to a given disease and is often a measure of disease burden (Arnesen and Nord, 1999). In 2019 approximately 63.5 million life years were lost due to ischaemic stroke which includes life years lost due to mortality and disability (World Stroke Organisation, 2022). In the INTERSTROKE case control study of almost 27,000 participants from 32 different countries there were at total of 10 modifiable risk factors for stroke occurrence including: hypertension, smoker status, waist-to-hip ratio, diet, regular physical activity, alcohol

intake, apolipoprotein B/A1 score, history of diabetes mellitus or HbA$_{1c}$ >6.5%, psychophysical factors, cardiac causes, and atrial fibrillation (O'Donnell et al., 2016). According to the global burden of disease (GBD) published in 2019, there were 19 risk factors influencing all stroke DALY, including but not limited to: pollution, diet, alcohol consumption, physical activity, smoker status, BMI, blood glucose and blood pressure (GBD 2019 Stroke Collaborators, 2021). Risk factors for stroke include both modifiable and non-modifiable risks, whereby modifiable risks are those that may be changed or modified to prevent the occurrence of disease (National Institute for Health and Care Excellence, 2023d). Of the 21 global regions assessed within the GBD 2019, high systolic blood pressure was the leading modifiable risk factor for ischaemic and haemorrhagic stroke related DALYs (GBD 2019 Stroke Collaborators, 2021).

Hypertension is defined as an average systolic blood pressure over 140 mmHg and diastolic blood pressure of over 90 mmHg (National Institute for Health and Care Excellence, 2022). Changes within the vascular system of the brain due to high blood pressure may be a contributing factor for stroke occurrence (Siedlinski et al., 2023). Hypertension is a largely treatable disease and reduction in blood pressure has been shown to reduce cerebrovascular risk (PROGRESS Collaborative Group, 2001). A study by the University of Oxford found that a reduction in systolic blood pressure by 5 mmHg reduced the risk of cardiovascular events by approximately 10%, demonstrating the importance of blood pressure management in reducing disease risk (Blood Pressure Lowering Treatment Trialists' Collaboration, 2021). Stroke patients commonly present with a clinical history of hypertension (Pathak et al., 2018). High blood pressure can lead to changes in brain vasculature and may exacerbate vascular damage within the brain following stroke (Siedlinski et al., 2023). In a survey study of over 500,000 patients evaluated following stroke, 63% had increased systolic blood pressure over 140 mmHg, while 38% of patients had a diastolic blood pressure of over 90 mmHg (Qureshi et al., 2007). In a study evaluating data from over 11,000 ischaemic stroke patients, a total of 72.7% of patients had a history of hypertension, nearly 20% of whom would go on to experience recurrent stroke within a one-year period (Wang et al., 2013b). Several clinical trials have assessed the effects of antihypertensive treatment on stroke risk and post-stroke outcomes. In the PROGRESS trial individuals who had TIA or ischaemic stroke were treated with antihypertensives and functional outcomes were assessed. In the proceeding 4 years following combination antihypertensive treatment, stroke risk decreased compared to single antihypertensive treatment (PROGRESS Collaborative Group, 2001). The RIGHT-2 trial investigated whether transdermal glyceryl trinitrate (GTN), a nitric oxide donor, could

improve functional outcomes in elderly stroke patients whereby GTN showed no benefit to post-stroke functional outcomes (RIGHT-2 Investigators, 2019). The CATIS trial investigated the effects of antihypertensive treatment in patients following ischaemic stroke, whereby they found that administration with antihypertensives to achieve a blood pressure of 140 mmHg/90 mmHg within the first 7 days following stroke did not affect disability or mortality rate (Zhang et al., 2019). In a separate study, 72-hours of intensive antihypertensive treatment combined with alteplase did not improve functional outcomes in ischaemic stroke patients compared to conventional guideline blood pressure management plus recombinant tissue plasminogen activator alteplase (Anderson et al., 2019). However, it is suggested that ischaemic stroke patients presenting with blood pressure greater than 180mmHg/105mmHg must be treated with antihypertensives prior to intervention with alteplase (Powers et al., 2019). Overall, the effects of antihypertensives on post-stroke outcomes vary between summarised clinical trials, however these studies identify that reducing blood pressure may improve functional outcome post-stroke. Additionally, maintenance of other factors such as blood glucose level, temperature and other factors that may exacerbate stroke pathology, may also better patient outcome following stroke.

As of 2019 approximately 59.70 million people were affected by Atrial fibrillation (AF), a heart condition that leads to irregular heart rhythm. Due to irregular heart rhythm, blood may pool in the heart and may form a clot, which, when dislodged, can lead to ischaemic stroke. It is estimated that 1 in 4 strokes in patients over the age of 40 are caused by AF (Heart and Stroke Foundation of Canada, 2023). Another common risk factor for stroke is high blood glucose level. As of 2019 there were 460 million people living with diabetes. Diabetes can lead to changes in the vasculature, leading to endothelial dysfunction, artery stiffening and inflammation, and as such is a risk factor for stroke (Chen et al., 2016c).

A healthy lifestyle is a main way of reducing the risk of stroke which includes frequent activity, healthy eating/drinking/smoking habits and maintaining a healthy weight (Centers for Disease Control and Prevention, 2022b). It has been found that implementing healthy lifestyle factors significantly reduces stroke risk (Larsson et al., 2015). While some may be genetically predisposed to stroke, one study found that genetic and lifestyle factors were independent risk factors for stroke occurrence, emphasising the importance of maintaining a healthy lifestyle irrespective of genetic risk (Rutten-Jacobs et al., 2018). By preventing stroke, other diseases and complications that are linked to stroke, such as dementia or depression, may also be prevented (Hachinski et al., 2019, White et al., 2011). The list of risk factors associated with stroke is extensive, however a large number of these risk

factors are modifiable. A number of stroke prevention initiatives exist to help educate the population on stroke risk, however obstacles such as access to information, health care, and healthy food remain.

1.1.4 Current treatments for ischaemic stroke

Reperfusion post-stroke is critical in preserving normal brain function whilst restoring normal physiological function (Powers et al., 2015). Recombinant tissue type plasminogen activator (rtPA) is effective in treating ischaemic stroke, myocardial infarction, pulmonary embolism and deep vein thrombosis (Hacke et al., 2008, Neuhaus et al., 1989, Klok et al., 2023, Goldhaber et al., 1990). In such diseases or medical conditions, rtPA binds to fibrin molecules on the surface of blood clots and activates fibrin bound plasminogen. The rtPA protease cleaves plasminogen from the fibrin molecules to form the fibrinolytic enzyme plasmin. Plasmin then breaks the crosslinks between fibrin molecules, destroying the blood clot structure (Schneider and Nesheim, 2004). rtPA medications, such as Alteplase, can be used in the acute stage, approximately 4 hours, following ischaemic stroke at a standard dose of 0.9 mg/kg over a one hour infusion period (Cheng et al., 2021). rtPA medications can significantly improve reperfusion post-stroke, however adverse side effects for example intracranial haemorrhage (ICH) has been observed in such notable clinical trials as NOR-TEST (Logallo et al., 2017). The ENCHANTED trial was carried out to assess whether lowering the dose of rtPA would reduce adverse side effects. The ENCHANTED trial concluded that, within a predominantly Asian cohort, there was no difference in the rates of death or disability between low-dose (0.6 mg/kg) and standard dose (0.9 mg/kg), however, the low dose resulted in fewer symptomatic ICH compared to standard dose (Anderson et al., 2016). Similarly, the Japan Alteplase Clinical Trial II (J-ACT II) found that recanalisation could be achieved when patients were treated with low dose, 0.6 mg/kg, of Alteplase while no cases of ICH were reported (Mori et al., 2010). Overall, rtPA at various doses can successfully increase reperfusion post-stroke.

Intra-arterial thrombectomy (IAT) also known as mechanical thrombectomy is an alternative method of achieving reperfusion following ischaemic stroke. With this method, cranial blood clots can be removed using a catheter inserted into the transfemoral or radial artery. Clots may be aspirated or a stent may be inserted into the affected artery, both techniques were compared in the COMPASS trial for their impacts on functional outcome following ischaemic stroke, whereby there was no significant difference in 90-day functional outcomes observed between treatment groups (Turk et al., 2019). One of the

benefits of IAT over rtPA is that IAT may enable recanalisation at a later timepoint following the onset of stroke symptoms compared to rtPA. The MR CLEAN trial assessed the effects of IAT up to 6 hours following the onset of stroke presentation compared to non-IAT control patients. Approximately 90% of participants in the MR CLEAN trial also received rtPA. This trial found that ischaemic stroke patients that had undergone IAT showed improved functional outcomes by 90-days post-intervention compared to non-IAT controls, while IAT did not increase mortality rates compared to non-IAT controls (Berkhemer et al., 2015). Similar findings were also observed in the SWIFT PRIME trial, whereby IAT intervention within 6 hours of stroke presentation combined with rtPA led to improved functional outcomes by 90-days post-intervention compared to rtPA only patients (Saver et al., 2015). In some incidences, an occlusion may remain in the brain of ischaemic stroke patients longer than 4-6 hours, for example, rtPA may not have fully removed the occlusion, or the patient may have poor access to immediate hospital care. The ESCAPE trial hoped to assess recanalisation using IAT up to 12 hours post-stroke. Unfortunately, only 15.5% of trial participants underwent treatment >6 hours after symptom onset, with most patients undergoing reperfusion treatment within 4 hours after symptom onset. Nevertheless, patients that underwent IAT + rtPA showed improved mRS and other functional outcomes compared to rtPA only patients, while mortality rate was reduced in patients that had undergone IAT + rtPA treatment compared to their rtPA counterparts (Goyal et al., 2015). The DEFUSE-3 trial demonstrated that reperfusion could be achieved using arterial thrombectomy 16 hours after the development of stroke symptoms. In this trial, patients that received IAT + rtPA showed significantly improved functional outcomes compared to their rtPA counterparts (Albers et al., 2018). Further elongating the time to recanalisation assessment, the DAWN trial investigated the effects of IAT recanalisation in patients up to 24 hours after the onset of stroke symptoms. They found that achieving recanalisation with IAT and rtPA even after 24 hours following stroke symptom onset led to improvements in functional outcomes by 90-days post-intervention (Nogueira et al., 2017)

Despite the evident success of IAT in achieving reperfusion post-stroke, few patients receive this form of intervention. Clinical trials have proven on numerous occasions that IAT in combination with rtPA triumphs over conventional rtPA treatment. One study found that administration of rtPA prior to IAT reduced clot area and was hypothesised to aid in the removal of cerebral blood clots (Rossi et al., 2021). Access to IAT treatment varies dramatically between healthcare regions. It is estimated that 10% of all stroke patients in the United Kingdom (UK) are eligible for IAT treatment (McMeekin et al.,

2017). The clinical need of patients remains unmet due to lack of training. There are only 24 specialised neuroscience centres that are able to provide IAT within the UK, however they are not easily accessible to all patients requiring thrombectomy (Zhang et al., 2021).

1.1.5 Pathology of ischaemic stroke

Under normal conditions, approximately 15% of total cardiac output is required by the brain (Claassen et al., 2021). The preservation of this blood supply is maintained by cerebral blood pressure (CBP). CBP is tightly regulated by cerebral perfusion pressure (CPP) and cerebrovascular resistance (CVR) and is tightly intertwined with cerebral blood flow (CBF) (Markus, 2004). Normal CBF is approximately 50 mL/100 g/min, which, for the average brain weight, equates to almost 1 L of blood every minute (Lassen, 1985). When blood flow to the brain is reduced or is halted altogether during stroke, oxygen supply to the brain tissue is reduced, which leads to altered ion exchange, increased reactive oxygen species and nitric oxide synthase production and activity, increased inflammation and immune cell recruitment/deployment, excitotoxicity and irreparable damage to brain tissue culminating in cell death (Figure 1.1).

Within the stroke brain exists two hemispheres, the ipsilateral (ischaemic) and contralateral (non-ischaemic) hemispheres. In the ischaemic ipsilateral hemisphere exists three broad zones: the ischaemic core, the ischaemic penumbra, and the unaffected oxygenated tissue (Figure 1.1). The effects of ischaemia will be discussed in detail later in this chapter; however, it is important to briefly discuss the effects of stroke on the contralateral side of the brain. Cerebral blood flow within the contralateral hemisphere following ischaemic stroke has been identified as a possible prognostic marker for post-stroke neurological recovery (Thamm et al., 2019). The mechanisms of which may be linked to gene expression whereby genes related to neurogenesis and inflammation, such as the frizzled class receptor 8 (Fzd8) and suppressor of cytokine signalling 3 (Socs3) genes, may be differentially expressed within the contralateral hemisphere in rodent models of transient middle cerebral artery occlusion (tMCAO) (Buga et al., 2008, Filippenkov et al., 2023). In ischaemic stroke patients the integrity of contralateral hemisphere structure has been correlated with the degree of cognitive impairment (Dacosta-Aguayo et al., 2014). With that being said, much focus is given to the ipsilateral side of the brain following stroke as reperfusion is the key to improved functional outcomes in stroke patients.
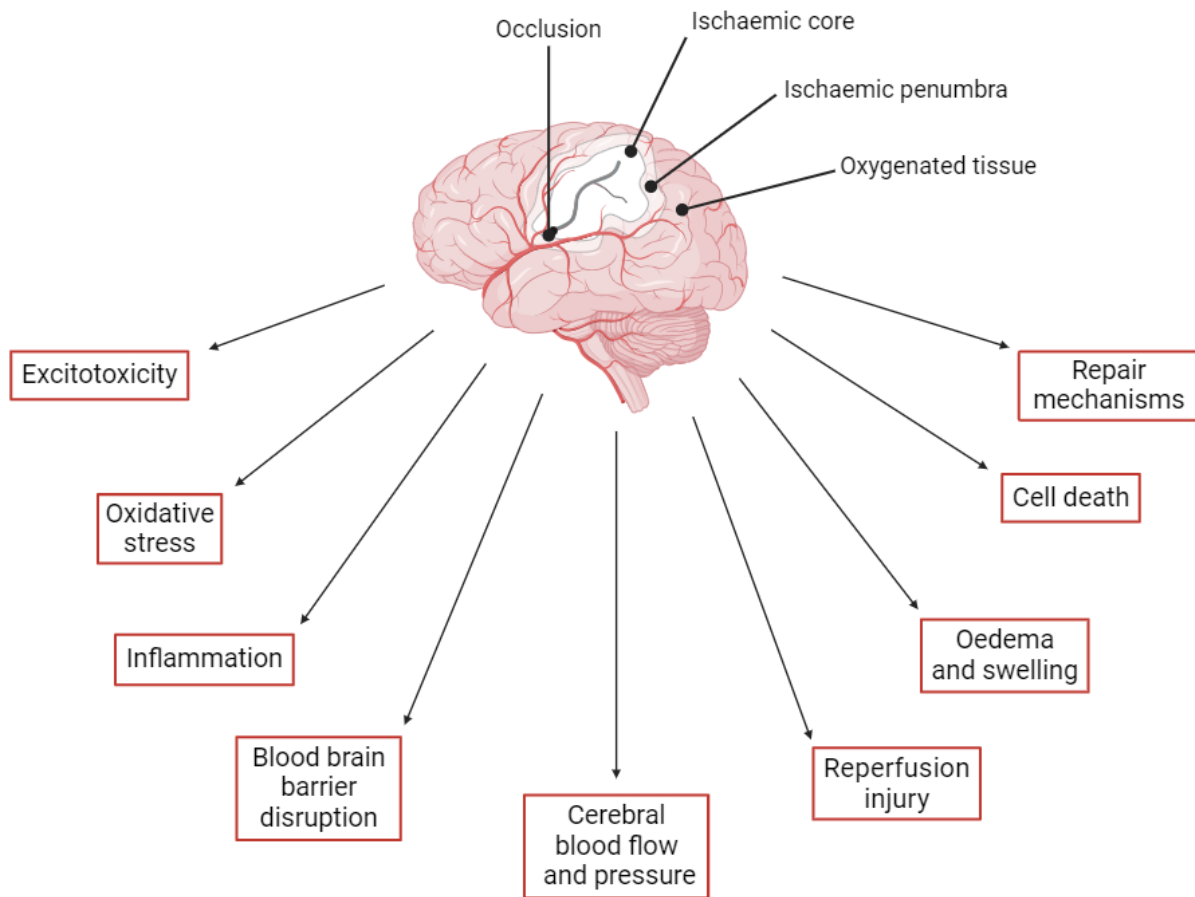
Figure 1.1 Pathological mechanisms in stroke.
Pathological mechanisms may include cerebral blood flow and pressure, inflammation, oedema, swelling, blood brain barrier disruption, reperfusion injury, cell death, repair mechanisms, excitotoxicity and oxidative stress. Figure created in BioRender.

1.1.5.1 Excitotoxicity and blood brain barrier dysfunction

N-methyl-D-aspartate receptor (NDMAR) is bound by the neurotransmitter glutamate and is required for normal neuronal functions such as synaptic plasticity and memory (Jewett and Thapa, 2022). After ischaemic stroke, oxygen levels within the brain become reduced leading to a reduction in negatively charged adenosine triphosphate (ATP) (Hurtado et al., 2003). As a result, the net charge of neurons switches from negatively charged to positively charged. These changes within cellular charge cause voltage gated calcium channels to open, releasing calcium into the presynaptic space and glutamate into the synapse. Increased intracellular calcium can result in mitochondrial and endoplasmic reticulum dysfunction, as well as increased production of damage associated molecular patterns (DAMPs) and reactive oxygen species (ROS) (Starkov et al., 2004). There are several forms of glutamate receptor, however, due to high calcium concentrations post-stroke, glutamate preferentially binds to NDMAR, leading to influx of further calcium and sodium into neurons (Crupi et al., 2019). This influx of calcium and sodium initiates cell swelling and cell death pathways and contributes to ischaemic disease pathology. Further, excitotoxicity can lead to changes within the blood brain barrier (BBB). The BBB is formed of tightly packed endothelial cells, between which exist tight junctions containing proteins such as claudin, occludin and tight junction adhesion molecules which mediate BBB integrity (González-Mariscal et al., 2003). The BBB tightly regulates the movement of circulating blood constituents from the periphery into the central nervous system (CNS) and protects the CNS from inflammation, diseases and other harmful properties than may be found within the wider circulation (Daneman and Prat, 2015). Following stroke, the influx of peripheral blood constituents into the CNS can lead to increased intercranial pressure that may cause further damage within the ischaemic brain.

1.1.5.2 Oxidative stress and reperfusion injury

The brain consists of a high level of polyunsaturated fats. Fatty acids within polyunsaturated fats are highly susceptible to oxidative stress due to the highly unstable electrons in proximity to the carbon-carbon bonds within the lipid chain (Milatovic et al., 2011). Following ischaemic insult, ROS may be produced within the brain tissue by resident and infiltrating immune cells. NADPH oxidase activity (NOX) can lead to ROS production which may activate apoptotic pathways, such as the caspase pathway, and may lead to BBB dysfunction and immune cell activation (Hernandes et al., 2022). In low

oxygen environments, such as the ischaemic brain, the oxygen radical dihydrogen dioxide can be produced and metabolised to form toxic hydroxide radicals (Halliwell, 1992). Oxidative stress within the ischaemic brain is not limited to ROS, but also include reactive nitrogen species (RNS). Nitric oxide synthases (NOSs), such as neuronal (nNOS), inducible (iNOS) and endothelial (eNOS) can produce nitric oxide (NO), which in turn can affect blood pressure and the immune response. In inflammatory states such as stroke, immune cells can produce O_2- and NO to form the extremely toxic peroxynitrite that can cause lipid, mitochondrial and deoxyribonucleic acid (DNA) damage and presence of which within the brain may be used to identify lesion area (Ballinger et al., 2000, Burney et al., 1999, Yang et al., 2021b). iNOS can reduce mitochondrial respiration and can cause increased glutamate concentration which perpetuates damaging excitotoxicity (Zorov et al., 2000). The rich ROS/iNOS environment can lead to the death of BBB endothelial cells, breakdown of tight junction proteins and eventual BBB permeability (Pun et al., 2009). In order to combat oxidative stress, the body can produce superoxide dismutases and other enzymes (Spranger et al., 1997). Reduction of ROS production by use of NOX inhibitors such as Apocynin has been shown to significantly reduce infarct volume in experimental stroke (Tang et al., 2007). Oxidative stress remains a major component of damage within the ischaemic brain and inhibition of these damaging pathways may improve post-stroke outcomes.

Despite effective intervention following stroke, some patients are left with life-changing disabilities post-stroke and it is theorised that reperfusion injury may be the cause. Reperfusion injury relates to the damage caused to the microvasculature of the brain following reperfusion. One of the first to note the occurrence of reperfusion injury was Jennings and colleagues in 1960, where they hypothesised that reperfusion may increase levels of necrosis within the ischaemic canine heart (Jennings et al., 1957). Within *in vivo* models, reperfusion injury may occur after blood flow to the brain is restored following ischaemia. However, in these models, the degree to which reperfusion may cause damage to the stroke brain is often overlooked as the experimental objective is, generally, to assess the overall effects of ischaemia on the brain, not the effects of reperfusion. A prospectively collected database study attempted to understand the impact of reperfusion injury in ischaemic stroke patients following IAT. They found that of the 27 eligible patients who underwent IAT intervention following ischaemic stroke, reperfusion injury frequency was approximately 48%. Further when analysing a cohort of 226 patients they found that reperfusion injury was associated with poorer functional outcomes following stroke (Zhou et al., 2023b). Interestingly one study found that reperfusion was the strongest predictor of

BBB disruption following ischaemic stroke as determined by MRI (Warach and Latour, 2004). Further investigation into the mechanisms of reperfusion injury following ischaemic stroke must be carried out to better understand how current interventions may be optimised to prevent further damage to the stroke brain.

1.1.5.3 Inflammation and apoptosis

Macrophages are the most common immune cell within the CNS and are subcategorised into microglia and border-associated macrophages (BAMs) depending on their location (Pedragosa et al., 2018). Microglia are the most common resident immune cell within the brain so much so that they make up approximately 10% of all cells in the brain (Salter and Stevens, 2017). In the past, microglia have been rigidly characterised as M1 (proinflammatory) or M2 (anti-inflammatory) (Colonna and Butovsky, 2017). With more in-depth understanding of microglial complexity, terminology used to describe microglia is more reflective of spectrum of microglial function. Within the ischaemic brain, microglia can potentiate damage and promote repair. Activated microglia secrete cytokines such as interleukin (IL) IL-1β, IL-6 and TNF-α, while regenerative microglia secrete IL-4 and IL-10 cytokines, along with transforming growth factor β (TGF-β) (Smith et al., 2012, Xiong et al., 2016). Following ischaemic stroke, ROS and DAMPs can lead to the activation of microglia and activation of matrix metalloprotease (MMP)-9 which can enhance vascular injury and BBB disruption (Fujimura et al., 1999). Activated microglia secrete cytokines and MMPs that alter the expression of adhesion molecules, such as intercellular adhesion molecule-1, on the surface of endothelial cells within the brain, enabling neutrophil recruitment to the site of ischaemia. Phagocytic neutrophils are recruited to the ischaemic lesion within minutes and remain in the brain for up to three days in experimental stroke (Gelderblom et al., 2009). In the acute phase following ischaemic stroke, toll-like receptors (TLRs) 2 and 4 become activated on the surface of neutrophils and microglia which stimulates the production of nuclear factor kappa light chain enhancer of activated B cells (NFκB) and simultaneously drives ROS production (Morgan and Liu, 2011). Neutrophil deployment is reliant upon inflammatory stimuli provided by microglia and other cellular necrosis. Post-stroke, neutrophils can also be activated by mast cells that, under normal conditions, reside in the brain and meninges (Arac et al., 2019). Mast cells are known to contribute to BBB dysfunction post-stroke (McKittrick et al., 2015). Transcription factor NFκB activation leads to the production of proinflammatory cytokines such as IL-1β and IL-18. Along with BAMs, other immune cells such as T, B and natural killer cells are

located within the border zones of the CNS. Approximately 24 hours following stroke, T cells infiltrate into the brain tissue. αβ and γδ T cells are activated by proinflammatory cytokines and chemokines and further exacerbate neuroinflammation, while in later stages post-stroke, microglia and BAMs can produce TGF-β that stimulates recruitment of neuroprotective T regulatory cells (Magnus et al., 2012, Santamaría-Cadavid et al., 2020). Ultimately the activation of immune cells and the immune cascade directly following and in the days after stroke act to restore normal cellular homeostasis within the brain but may end up potentiating brain damage and cell death.

There are two forms of cell death, apoptosis and necrosis, which may occur when cells become damaged or harmful. Apoptosis is an active regulated, non-inflammatory form of cell death, while necrosis is a passive form of cell death due to aberrant environmental conditions, leading to inflammation (Fink and Cookson, 2005). Regulated cell death is an essential part of normal homeostasis (Cui et al., 2021). The ischaemic core of the stroke brain consists of the most severely injured cells that will undergo necrosis following occlusion (Sodaei and Shahmaei, 2020, Arroja et al., 2019). The ischaemic penumbra is the tissue surrounding the lesion that may be rescued by clinical intervention following a stroke. However, some cells within the penumbra may be too damaged to undergo repair and will undergo apoptosis. Apoptosis within the penumbra can last for days following ischaemic stroke and may contribute to the expansion of the infarct zone (Naito et al., 2020).

1.1.5.4 Repair mechanisms.

Following ischaemic stroke, cells within the ischaemic core and penumbra may die. However, cells can proliferate in the brain following ischaemic insult. CNS progenitor cells within the subventricular zone (SVZ) may differentiate into neuroblasts and migrate to the lesion site (Lindvall and Kokaia, 2015). Neurogenesis has been linked with the potent angiogenic vascular endothelial growth factor (VEGF), whereby mice overexpressing VEGF displayed increased neurogenesis within the SVZ (Wang et al., 2007). In one study, rodents subjected to permanent middle cerebral artery and treated with VEGF immediately following ischemic insult demonstrated increased vascular permeability, however when administration was delayed to 48 hours, cerebrovascular perfusion increased while neurological outcomes were improved (Zhang et al., 2000). It is thought that VEGF may bind to intact vascular basement membrane to enable the

proliferation of endothelial cells within the brain (Rosenstein et al., 1998, Ingber et al., 1986). Astrocytes have also been shown to play a role in repair following ischaemic stroke, whereby they may produce proliferation factors such as brain derived neurotrophic factor (BDNF), a key modulator of neurogenesis and neuronal survival (Quesseveur et al., 2013). Other neurotrophic factors and growth factors may be produced by cells within the brain that stimulate regeneration following ischaemic stroke.

1.1.6 Models of the brain

A common model of the neurovascular unit (NVU) is *in vitro* cell culture. Here, immortalised cell lines, such as neurons, can be investigated in culture to mimic the brain outside a living system. Brain organoids have also been developed over the years to create a model of the brain that contains multiple complementary brain regions and cell types (Lancaster et al., 2013). Advancements in technology have allowed for the development of 'brains-on-chips' (BoC) which enable for more accurate *in vitro* modelling of the brain compared to conventional cell lines. Three-dimensional models of the brain, such as organoids or BoC, better represent the interplay between brain regions and cells, and are therefore important in modelling NVU dysfunction (Amirifar et al., 2022).

Animal models have been used in the quest to advance medical science for centuries. The place of animal use in science allows for better understanding of disease pathology and development of novel medicines within a living system. In whole, live system models of disease, animals such as rodents are commonly used when studying the brain preclinically, including their use in experimental models of stroke (Johnson et al., 2015).

1.1.6.1 *In vitro* models of stroke

Cell culture models provide an important insight into disease models, and how these models may react to possible therapies. *In vitro* stroke models rely upon the depletion of oxygen and/or glucose from culture conditions to mimic the occlusion of blood flow in the brain that provides both oxygen and glucose to brain tissue (Goldberg and Choi, 1993). When using combined oxygen glucose deprivation (OGD) culture media containing glucose is replaced with low or no glucose culture media. The plate or dish of cells is transferred to a hypoxic chamber, whereby a set flow and percentage of oxygen is pumped into the chamber and the chamber is sealed. Alternatively, hypoxic incubators may be used

to mimic low oxygen environments. The cells are maintained under OGD where they have access to a limited supply of oxygen and low/no glucose. Stroke models can also be achieved chemically or enzymatically. In such cases chemicals such as antimycin-A, rotenone and sodium azide can be used to disrupt the electron transport chain, mimicking hypoxic conditions associated with stroke (Wevers et al., 2021, Kurian and Pemaih, 2014). *In vitro* stroke models can also rely on inducing excitotoxicity, whereby NMDAR subtype 2A can be antagonised to induce neuronal cell death (von Engelhardt et al., 2007). Additionally substances such as cobalt chloride have also been used to induce hypoxia in cell culture models (Kim et al., 2013).

1.1.6.2 *In vivo* models of stroke

Rodent *in vivo* models of cerebral ischaemia can be achieved using various methods such as intraluminal filament (ILF), electrocoagulation, endothelin-1 (ET-1) injection or introduction of emboli (Figure 1.2). The most common form of *in vivo* stroke model relies upon the ILF method. With this an ILF may be surgically inserted into great arteries of the brain to occlude blood flow. One common example is the middle cerebral artery (MCA) occlusion (MCAO) method, whereby an ILF equal to the size of the vessel is inserted into the common carotid artery and advanced to block the opening of the MCA (Longa et al., 1989). MCAO may be transient (tMCAO), wherein following ILF insertion, the ILF may be removed, mimicking both occlusion and reperfusion. Alternatively, ILFs may be left in place leading to a permanent model of MCAO (pMCAO).

Permanent occlusion of rodent vessels or arteries in the brain, such as the MCA, can also be achieved through electrocoagulation (Bederson et al., 1986, Llovera et al., 2014). Upon isolation of the vessel or artery, electrocoagulation forceps may be closed over the artery and a voltage applied through the forceps. This voltage generates heat that is capable of burning through tissue, in this case a vessel or artery (Cordero, 2015). Electrocoagulation is known to reduce blood loss in tissue incisions compared to conventional scalpels, and as such may be a preferential stroke model (Prakash et al., 2015). In terms of *in vivo* stroke models, this method allows for precise cessation of blood flow through the vessel or artery with the added benefit of reducing blood loss associated with common filament occlusion methods.

In ET-1 models of ischaemic stroke, ET-1 binds to endothelin-A or endothelin-B receptors on the vessel surface, leading to severe vasoconstriction that results in cerebral ischaemia,

which over time, gradually reduces to allow for reperfusion (Chan et al., 2017). Other models of ischaemic stroke include photothrombotic models which rely upon the systemic injection of photosensitive dyes. A laser of specified wavelength is applied to the exposed brain resulting in cerebral ischaemia (Labat-gest and Tomasi, 2013). Embolic stroke model relies upon the delivery of clotted blood or chemicals that induce a clot using a cannula inserted into the internal carotid artery (Macrae, 2011). This model is often used to assess the effectiveness of thrombolytic medication, with or without additional intervention, in experimental stroke. *In vivo*, post-stroke outcomes, such as infarct volume and neurological and/or cognitive outcomes, can provide important insight into the severity of stroke and benefit of potential new therapies. Post-stroke outcomes may be measured in several different ways. An extensive list of post-stroke outcomes will be discussed at length in chapter three of this thesis.
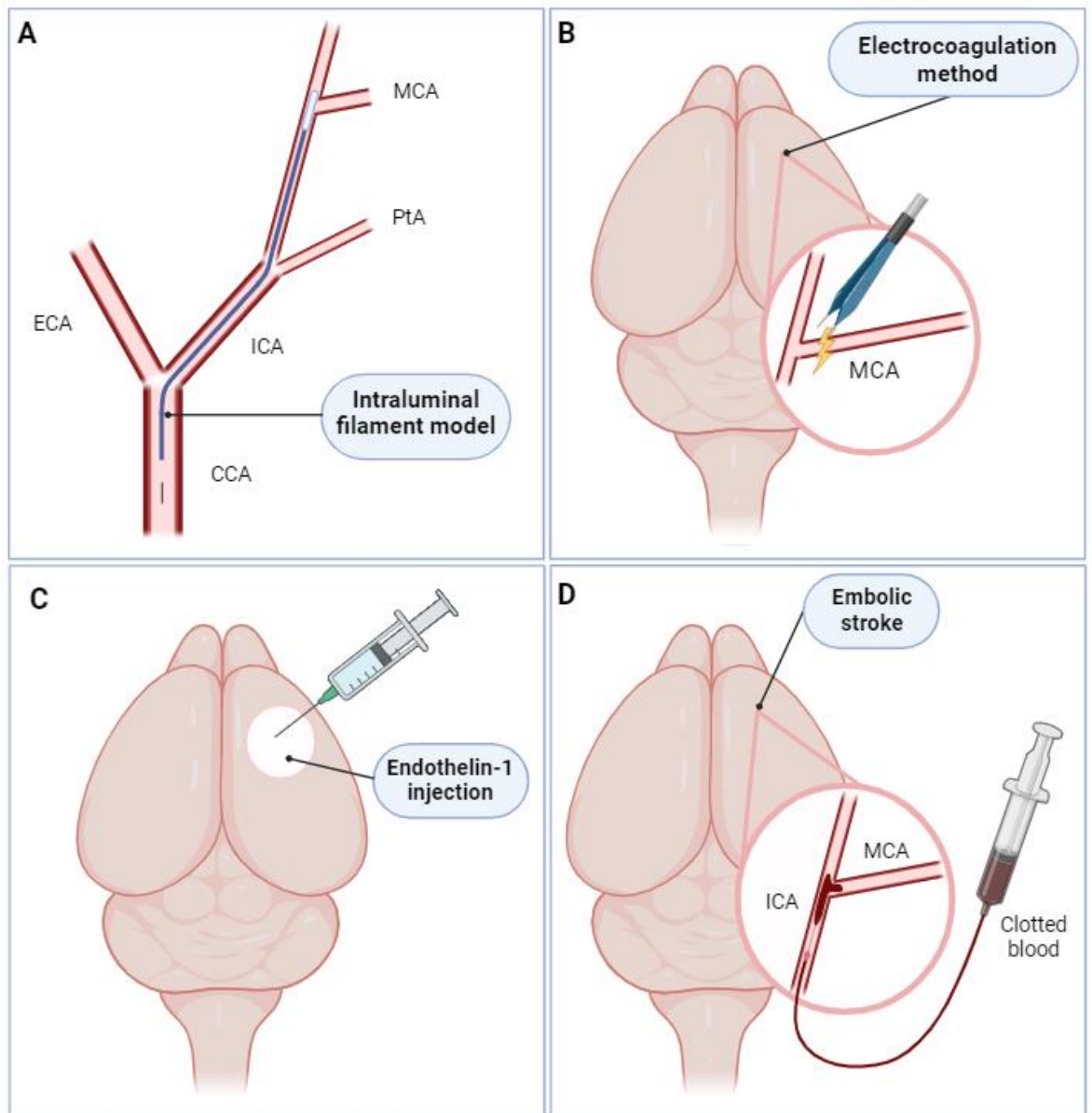
Figure 1.2 *In vivo* experimental stroke models.
Depiction of common *in vivo* models of ischaemic stroke. A) ILF model of MCAO, B) electrocoagulation method of MCAO, C) ET-1 injection model of MCAO and D) Embolic model of MCAO. Figure created in BioRender.

1.2 The Renin Angiotensin Aldosterone System

There are two main axes of the Renin Angiotensin Aldosterone System (RAAS): the classical axis and the counter-regulatory axis, each of which work to maintain long-term blood pressure and extracellular volume (Figure 1.3) (Navar, 2014). RAAS dysfunction is closely associated with cardio- and cerebro-vascular diseases such as hypertension and stroke.
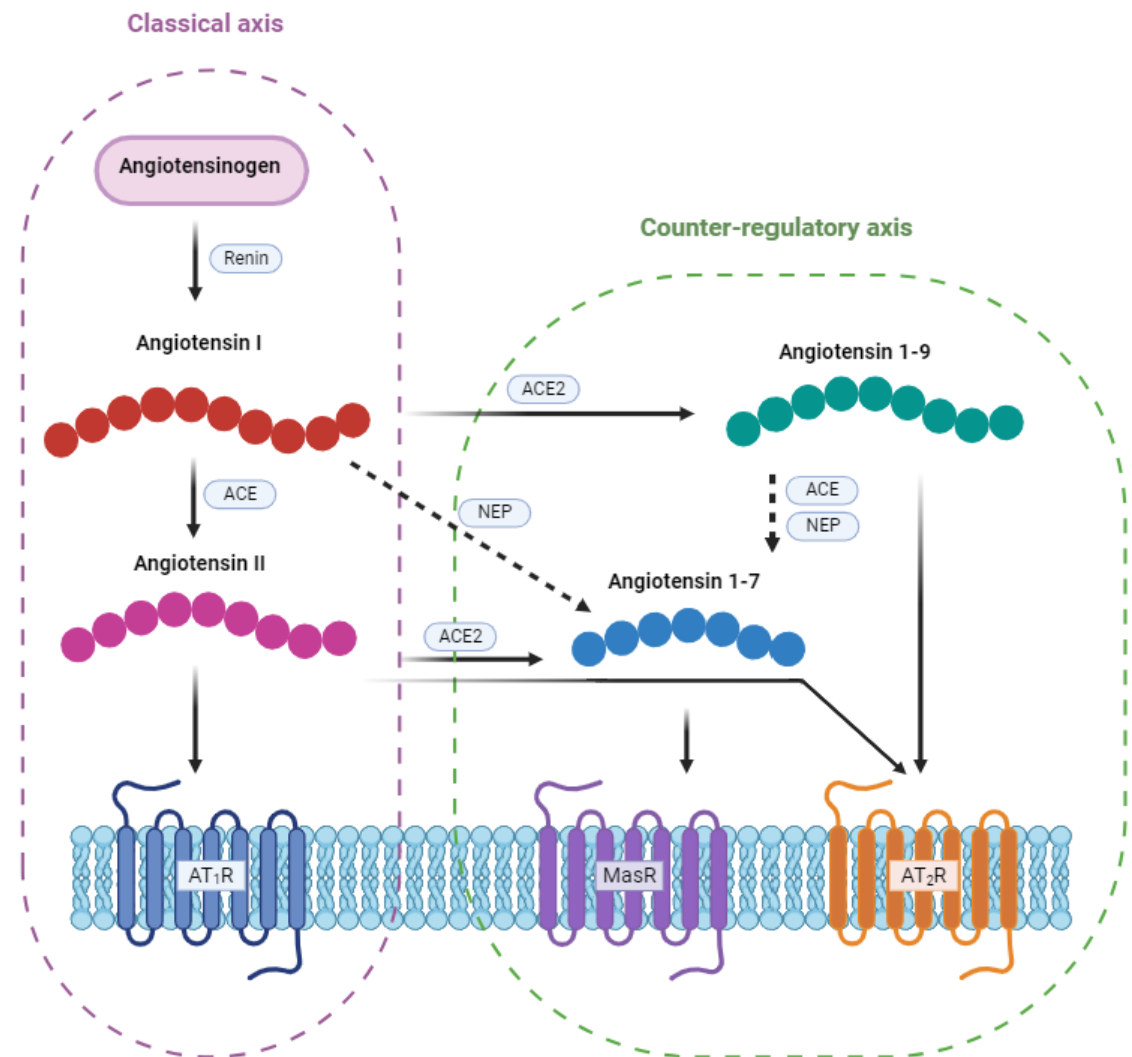
Figure 1.3 The classical and counterregulatory axis of RAAS.
Pathway includes the breakdown of angiotensinogen by renin to form Ang I. Ang I can be broken down into Ang II by ACE. In the classical axis of RAAS Ang II may stimulate the AT_1R. In the counterregulatory axis Ang II may be broken down by ACE2 into Ang-(1-7). Ang I may also be broken down directly into Ang-(1-7) by NEP. Ang I can be broken down by ACE2 to form Ang-(1-9) that can be further broken down by ACE and NEP to form Ang-(1-7). Ang-(1-7) may stimulate the MasR. Ang I can be broken down into Ang-(1-9) by ACE2. Both Ang II and Ang-(1-9) may stimulate the AT_2R. Figure created in BioRender.

1.2.1 The classical axis

Within the kidney, the release of the aspartyl protease, renin, from activated granular cells of the juxta-glomerular apparatus is tightly regulated by renal baroreceptors, Angiotensin II and sodium chloride levels in the macular densa (Bock et al., 1992, Bührle et al., 1987, Schlatter et al., 1989). The substrate of renin, angiotensinogen is produced by the liver and found within the circulating plasma. Renin binds to the Agt substrate of angiotensinogen and cleaves it to form Angiotensin I (Ang I). Angiotensin converting enzyme (ACE), commonly found in endothelial cells of the lung, binds to Ang I, which is then converted to bioactive Angiotensin II (Ang II). The angiotensin II type I receptor (AT_1R), expressed on vascular endothelial cells and smooth muscle cells, is bound by Ang II leading to vasoconstriction and eventual increase in blood pressure (Santos et al., 2018) (Figure 1.3). The classical axis of the RAAS is important in maintaining blood pressure under normal conditions and during incidents of severe changes in blood pressure, such as trauma, for example, cessation of blood flow within the kidneys (Anderson et al., 1979). However, overactivation of the classical pathway of the RAAS increases levels of fibrosis, oxidative stress and proinflammatory responses, therefore it must be tightly regulated (Wright and Harding, 2013).

1.2.1.1 Angiotensin II type I receptor

The functional ligand of the G-protein coupled receptor AT_1R, Ang II, initiates a signalling cascade that ultimately leads to an increase in blood pressure (Figure 1.4). The AT_1R is expressed on vascular smooth muscle cells (VSMCs), endothelial cells, cardiac fibroblasts and renal mesangial cells, all of which are closely associated with vascular health and function (Kawai et al., 2017). Following activation by Ang II, the AT_1R is then coupled with four G-proteins, $G_{\alpha q/11}$, $G_{\alpha i}$, G_{12} and G_{13} leading to activation of downstream phospholipase C β (PLCβ) which breaks down phosphatidylinositol-4,5-bisphosphate (PIP_2) to inositol triphosphate (IP_3) and diacylglycerol (DAG). IP_3 then binds to IP_3 receptors (IP_3R) on sarcoplasmic reticulum leading to increased intracellular calcium concentration (Woll and Van Petegem, 2021). Intracellular calcium levels are known to be increased in hypertension and contribute to hypercontractility and vascular remodelling (Touyz et al., 2018). Intracellular calcium complexes with calmodulin to form calcium calmodulin (CaCM) which, in combination with proto-oncogene tyrosine-protein kinase Src (c-SRC), activates and phosphorylates myosin light-chain kinases (MLCK). Phosphorylated MLCK enables binding of myosin to actin cytoskeleton within VSMC,

leading to contraction of VSMC (Wynne et al., 2009). The contraction of VSMC within the cardiovascular system increases vascular resistance and consequently blood pressure. Additionally, activation of AT_1R leads to downregulation of peroxisome proliferator-activated receptor gamma coactivator 1-alpha (PGC-1α) which ultimately causes the downregulation of eNOS and NO, reducing vasodilation (Li et al., 2016).

AT_1R activation is linked with immune response, whereby Ang II stimulation of cardiomyocytes has been shown to increase inflammatory cytokine concentrations such as TNF-α due to upregulation of the JAK/STAT pathway (Wang et al., 2012). TNF can then interact with TNF receptor associated factor 2 (TRAF2) to activate mitogen-activated protein kinases (MAPKs) and the transcription factor NFκB (Malinin et al., 1997). TNFα binding to TNF receptors (TNFR) can lead to the activation of TNFR associated death domain (TRADD) and subsequent activation of apoptotic caspase cascade (Bender et al., 2005). In rodent models of myocardial infarction (MI), antagonism of the AT_1R has been shown to reduce the expression of proinflammatory IL-1β, IL-6, monocyte chemoattractant protein-1 (MCP-1) and MMPs in myocardial tissue (Song et al., 2014). Mechanistically, when Ang II binds to AT_1R, NOX may be produced that promote the production of ROS which can also activate MAPK. MAPK signalling is important in normal physiological homeostasis and is responsible for regulating cell proliferation, stress response, apoptosis and immune responses. MAPK signalling is activated by extracellular signal-related kinases (ERK), c-jun N-terminal kinases (JNKs) and p38 mitogen-activation protein kinases (p38s) that can drive detrimental inflammatory responses (Huang et al., 2009). MAPK can activate cyclic AMP response element binding protein (CREB) which is important in neuronal proliferation, differentiation and survival (Koga et al., 2019, Landeira et al., 2018).

Figure 1.4 Signalling mechanism of the AT₁R.

Illustration of the downstream cascades following AT$_1$R activation by Ang II. Arrows demonstrate the connection between cascade components of the pathway. Components highlighted in pink relate to the vasoconstrictive properties of AT$_1$R activation. Components highlighted in blue relate to the growth and remodelling properties of AT$_1$R activation. Components highlighted in green relate to inflammation, immune cell activation/recruitment, oxidative stress and apoptosis that occurs following AT$_1$R activation. Component abbreviations: PLCβ, phospholipase C β; PIP2, phosphatidylinositol-4,5-bisphosphate; IP3, inositol triphosphate; DAG, diacylglycerol; Ca, calcium; CaCM, calcium calmodulin; cSRC, proto-oncogene tyrosine-protein kinase Src; MLCK, myosin light-chain kinases; NOX, NADPH oxidase; ROS, reactive oxygen species; MAPK, mitogen-activated protein kinases; ERK, extracellular signal-related kinases; JNK, c-jun N-terminal kinases; p38s, p38 mitogen-activation protein kinases; CREB, cAMP-response element binding protein; eNOS, endothelial nitric oxide synthase; NO, nitric oxide; AP-1, activator protein-1; NFκB, nuclear factor kappa-light-chain-enhancer of activated B cells; MCP-1, monocyte chemoattractant protein-1; JAK, Janus kinase; STAT, signal transducers and activators of transcription; TNFα, tumour necrosis factor alpha; TRAF2 TNF receptor associated factor 2; TRADD, tumour necrosis factor receptor associated death domain; IL-1β, Interleukin-1 beta. Figure created in BioRender.

1.2.1.2 Angiotensin II

The octapeptide, Ang II, binds to G-protein coupled receptors AT_1R and AT_2R. Activation of each receptor elicits distinct counteractive biological responses, for example, when binding to the AT_1R on VSMC, Ang II can stimulate vasoconstriction, however, Ang II binding to the AT_2R on smooth muscle cells leads to vasodilation (Katada and Majima, 2002). Alternatively, within the zona glomerulosa of the adrenal cortex, Ang II may stimulate the release of the mineralocorticoid hormone aldosterone, increasing water and sodium retention leading to an increased blood volume, and, resultantly, increased blood pressure (Toda et al., 2013).

The role of Ang II in cerebrovascular disease will be discussed later in this introduction and in further chapters. Aside from the contribution of Ang II in stroke, Ang II is associated with several diseases, most commonly, cardiovascular disease (CVD). Due to its role within the vasculature, Ang II has been linked to numerous pathologies. In humans, Ang II binding to the AT_1R activates classical RAAS signalling leading to increased blood pressure, which if sustained may lead to cardiac hypertrophy, fibrosis and organ damage (Zhang et al., 2008). Circulating and cardiac Ang II concentrations have been shown to be increased in rodent models following MI due to changes in left ventricular end diastolic pressure (Ruzicka et al., 1995). Ang II can stimulate cardiac fibrosis in rodent models of MI (Ruzicka et al., 1995, Sun et al., 1998). RAAS inhibition following MI has shown to reduce remodelling/cardiac fibrosis, whilst reducing the progression of heart failure (Davies et al., 2000). Mechanistically, Ang II mediated remodelling may be linked to NFκB which has been shown to promote Ang II mediated inflammation (Wolf et al., 2002). In other diseases such as cancer, Ang II may also facilitate tumour angiogenesis and growth via AT_1R stimulation in rodent models of malignant melanoma (Egami et al., 2003).

Angiotensin converting enzyme (ACE) inhibitors (ACEi) have been developed to prevent the breakdown of angiotensin I into Ang II. ACEi, such as Captopril, are frequently used to treat hypertension and prevent major adverse cardiovascular events (MACE) in various diseases, including hind limb ischaemia (National Institute for Health and Care Excellence, 2023b, Armstrong et al., 2015). Similarly, to prevent the actions of Ang II, angiotensin II receptor blockers (ARBs) antagonise the AT_1R to prevent Ang II binding. Like ACEi, ARBs, such as Candesartan, are also prescribed to treat hypertension and MACE, including heart failure and stroke prevention (National Institute for Health and Care Excellence, 2023a).

1.2.2 The counter-regulatory axis of the RAAS

The counter-regulatory axis of the RAAS, also known as the non-classical axis of the RAAS can counteract the effects of Ang II binding the AT_1R. Angiotensinogen is broken down by renin to form Ang I which is cleaved by ACE2 into Ang-(1-9), a functional ligand of the AT_2R (Flores-Muñoz et al., 2012). Cleavage of Ang I leads to reduced Ang II concentrations as initially Ang I is converted into Ang-(1-9). Ang-(1-9) can be broken down by ACE into Angiotensin-(1-7) [Ang-(1-7)], the functional ligand of the Mas receptor (MasR) (Santos et al., 2003). Ang-(1-7) may also be created by the catalysis of Ang II by neprilysin (NEP). ACE and NEP have varying activities, for example, Ang-(1-9) is preferentially cleaved by NEP into Ang-(1-7) more so than ACE, whereby the catalytic activity of NEP is greater than ACE, however the binding affinity of ACE to Ang-(1-9) is greater than NEP (Rice et al., 2004). Activation of AT_2R and MasR results in vasorelaxation, directly combating the vasoconstrictive properties of the classical axis of the RAAS (Katada and Majima, 2002, Durand et al., 2016). The role of the counter regulatory axis of the RAAS in cerebrovascular disease will be discussed later in this introduction and in further chapters of this thesis. In rodent models of MI, treatment with the AT_1R antagonist Telmisartan and Olmesartan led to increased cardiac function and increased plasma levels of Ang-(1-7) (Wang et al., 2017a). In cancer, MasR activation through use of AVE0991 agonist reduced cancer cell growth in mouse models of adenocarcinoma (Murphy et al., 2019). From CVD to cancer, the counter-regulatory axis of RAAS has demonstrated its importance in disease pathology.

1.2.2.1 The ACE2/Ang-(1-7)/MasR axis

Within the counter-regulatory axis of the RAAS, Ang-(1-7) is produced by the breakdown of: Ang I by NEP or Ang II by ACE2 or Ang-(1-9) by ACE. Ang-(1-7) mediated activation of the MasR counteracts the effects of Ang II binding the AT_2R (Figure 1.5). The potential role of Ang-(1-7) and Ang-(1-9) in cerebrovascular disease will be extensively discussed later in this introduction and in further chapters of this thesis. In CVD, ACE2/Ang-(1-7)/MasR axis stimulation demonstrated that, following experimental MI, rats treated with AT_1R antagonists Telmisartan and Olmesartan showed improved cardiac function, and increased plasma levels of Ang-(1-7) (Wang et al., 2017a). While in a similar study, Telmisartan significantly increased the expression of MasR and ACE2 within heart tissue of experimental autoimmune myocarditis (EMA), along with an increase in serum Ang (1-

7) concentration (Sukumaran et al., 2012). Ang-(1-7) has also been shown to reduce the expression of pro-fibrotic chemokine TGF-β1 in rodent cultured cardiomyocytes (Iwata et al., 2005), while antagonism of MasR by A-779 has been shown to increase levels of fibrotic TGF-β1 within the liver of hepatic fibrosis rats (Pereira et al., 2007). Further detail on the benefit of ACE2/MasR/Ang-(1-7) axis in ischaemic stroke will be discussed in chapter three of this thesis.

Mechanistically, ACE2/Ang-(1-7)/MasR axis activation has been demonstrated decreased expression of NOX components such as p47 and nitrotyrosine, which may lead to decreased ROS activation (Sukumaran et al., 2012). Agonism of the MasR by Ang-(1-7) can activate protein kinase B (Akt)-dependent phosphorylation of eNOS and NO production (Sampaio et al., 2007). Cyclic guanosine monophosphate (cGMP) and cGMP-dependent protein kinase type I (cGKI) combine with NO to cause smooth muscle relaxation and thusly vasodilation associated with the counter-regulatory axis of RAAS (Koeppen et al., 2004). Activation of MasR leads to the production of PI3K and subsequent production of PIP_2 and downstream PIP_3 leading to the recruitment of effectors such as Akt that can further influence vasodilation (Burke, 2018).

Moreover, stimulation of ACE2/Ang-(1-7)/MasR axis has shown to reduce phospho-JNK, phospho-ERK, phospho-p38 and phospho-MAPKAPK-2 signalling pathways through phosphorylation of upstream Src homology region domain containing phosphatase-2 (SHP-2) (Sukumaran et al., 2011, Sampaio et al., 2007). Downregulation of phosphor-p38 can reduce pro-inflammatory responses associated with hypertension, by inhibiting pro-inflammatory cytokine production (Rajashekhar et al., 2011, Olzinski et al., 2005, Bachstetter and Van Eldik, 2010). Indeed, ACE2/MasR/Ang-(1-7) axis is known to reduce pro-inflammatory factors such as iNOS, IL-1β, NFκB and monocyte chemoattractant protein-1 (MCP-1) in rodent models of dilated cardiomyopathy (Sukumaran et al., 2012).
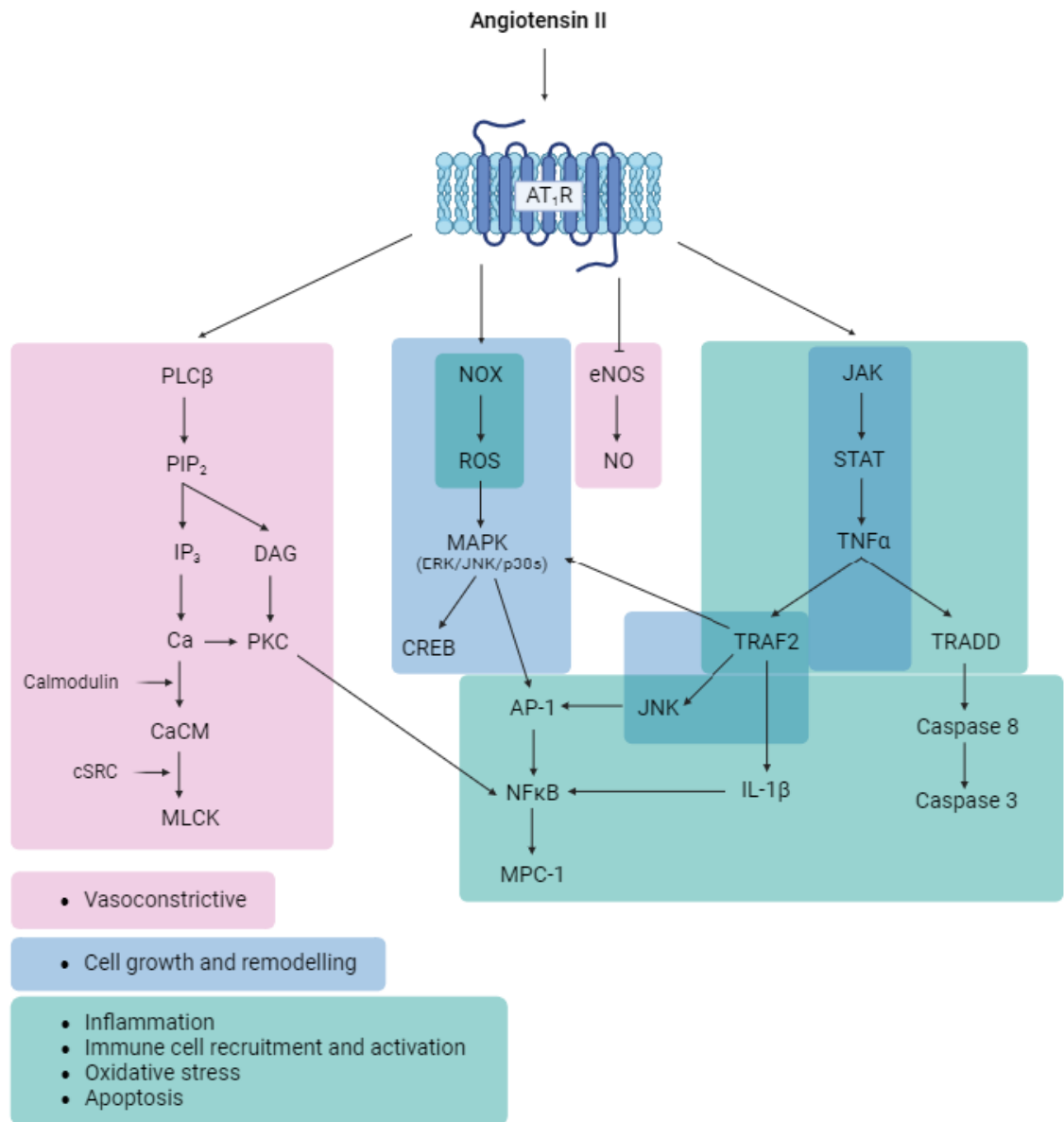
Figure 1.5 Signalling mechanism of the MasR.
Illustration of the downstream cascades following MasR activation by Ang-(1-7). Arrows demonstrate the connection between cascade components of the pathway. Components highlighted in pink relate to the vasodilative properties of MasR activation. Components highlighted in blue relate to the growth and remodelling properties of MasR activation. Components highlighted in green relate to inhibition of oxidative stress and vasoconstriction that occurs following MasR activation. Component abbreviations: SHP-2, Src homology region domain containing phosphatase-2; MAPK, mitogen-activated protein kinases; ERK, extracellular signal-related kinases; JNK, c-jun N-terminal kinases; p38s, p38 mitogen-activation protein kinases; PI3K, phosphoinositide 3-kinases; PIP2, phosphatidylinositol-4,5-bisphosphate; PIP3, phosphatidylinositol-4,5-triphosphate; Akt, protein kinase B; eNOS, endothelial nitric oxide synthase; NO, nitric oxide; cGMP, cyclic guanosine monophosphate; PKG, cGMP-dependent protein kinase or protein kinase G; cGK, cGMP-dependent protein kinase; RhoA, Ras homolog family member A; RhoK; Rho kinase; NOX, NADPH oxidase; ROS, reactive oxygen species. Figure created in BioRender.

1.2.2.2 The Angiotensin II type II receptor

The G-protein coupled receptor, AT_2R, shares 34% homology with the AT_1R (Mukoyama et al., 1993). Ang-(1-9) and Ang II are functional ligands of the AT_2R and activate the counter-regulatory axis of the RAAS (Figure 1.6). Stimulation of the AT_2R by Ang II leads to activation of multiple phosphatases including: tyrosine phosphatase Src homology region domain containing phosphatase-1 (SHP-1), MAP kinase phosphatase-1 (MAK-1) and protein phosphatase 2A (PP2A), which in turn reduces cell proliferation enabled by the MAPK signalling pathway (Zhang and Liu, 2002). Reduction in MAPK activation also leads to a reduction in MAPK-dependent B-cell lymphoma 2 (Bcl-2) mediated apoptosis (Torcia et al., 2001). Additionally, stimulation of the AT_2R may leads to JNK activation and increased FasL expression that stimulates caspase mediated cell death (Zhu et al., 2019). SHP-1 activates MMS2 and subsequently PPARγ which is important in promoting neuronal cell differentiation and prevention of neural inflammation (Hofsaess and Kapfhammer, 2003, Gurley et al., 2008). SHP-1 negatively regulates PI3K-dependent Rac1 activation, leading to reduced NOX activation (Krötz et al., 2005). Reduced NOX activation leads to reduced ROS concentrations and dampened inflammatory immune response. Stimulation of the AT_2R by Ang II also leads to increased bradykinin production and in turn NO-cGMP-dependent signalling to increase vasodilation (Siragy and Carey, 1999, Abadir et al., 2003). cGMP can stimulate protein kinase G (PKG) and cGKI which increases vasodilation and reduces RhoA/RhoK MLC mediated vasoconstriction, respectively (Francis et al., 2010, Savoia et al., 2005). With regards to immune response, SHP-1 has been shown to reduce T cell receptor (TCR) mediated T cell activation (Kosugi et al., 2001). Agonism of the AT_2R, such as through the use of the small molecule, Compound 21, C21, has proven beneficial in models of hypertension, sepsis and ischaemic stroke (Rehman et al., 2012, Jabber et al., 2023, Ahmed et al., 2019). Activation of the AT_2R can reduce JAK/STAT activation and subsequent production of proinflammatory factors such as NFκB, that may be detrimental in stroke (Harari and Liao, 2010). The potential benefits of AT_2R agonism in ischaemic stroke will be further discussed in depth in chapter three of this thesis.

1.2.2.3 Angiotensin-(1-9)

The nonapeptide Ang-(1-9) is produced by the hydrolysis of Ang I by ACE2. Preclinically, the novel peptide Ang-(1-9), from the counter-regulatory RAAS axis, is capable of counteracting the effects of Ang II by acting as a functional ligand of the AT_2R (Figure 1.6). In recent years, Ang-(1-9) has been investigated in various pathologies, though most research focuses on its role in CVD. Studies investigating the role of Ang-(1-9) in CVD have utilised various delivery methods, concentrations and models, however most studies have identified the beneficial effects of Ang-(1-9) in models of CVD (Fattah et al., 2016, Norambuena-Soto et al., 2020, Flores-Muñoz et al., 2012). Be it positive, neutral, or negative, these studies provide better understanding of the potential benefit of Ang-(1-9) and, importantly, its possible mechanisms of actions.

Numerous groups have studied the effects of Ang-(1-9) on functional cardiac outcomes, including ejection fraction, left ventricular function, infarct size and blood pressure. For example, in one such study, Ang-(1-9) reduced the number of apoptotic cells within the left ventricle, increased left ventricular ejection fraction and systolic function, and decreased infarct size in rodent models of MI (Mendoza-Torres et al., 2018). Another study utilised an Adeno-associated virus to deliver Ang-(1-9) to mice following MI which led to preserved left ventricular systolic function (Fattah et al., 2016). High doses of Ang-(1-9) (1200 ng/kg/min) delivered to spontaneously hypertensive SHR rats reduced systolic and diastolic blood pressure and vascular remodelling by decreasing VSMC proliferation (Norambuena-Soto et al., 2020). In another study, Ang-(1-9) has been shown to reduce cardiac and kidney fibrosis and decreased numbers of infiltrating monocytes in both renal and cardiac tissues in renin-independent, salt-loaded hypertensive deoxycorticosterone acetate (DOCA) rats. Additionally, Ang-(1-9) was able to improve cardiac function and restore blood pressure in salt-loaded DOCA rats (Gonzalez et al., 2018). Ang-(1-9) delivered by osmotic minipump to Spontaneously hypertensive stroke prone rats (SHRSPs) reduced cardiac fibrosis (Flores-Muñoz et al., 2012).

Cell models of the cardiovascular system have also been crucial in understanding the protective mechanisms behind Ang-(1-9). For instance, when Ang-(1-9) was delivered to norepinephrine stimulated cardiomyocytes *in vitro* using polymeric nanoparticles, cardiomyocyte area was reduced, suggesting the use of Ang-(1-9) in preventing cardiac hypertrophy (Sepúlveda-Rivas et al., 2021). Several studies have identified the role of Ang-(1-9) in intracellular calcium sensitisation, whereby isolated cardiomyocytes treated with Ang-(1-9) led to an increase sarcoplasmic reticulum calcium content, which was

thought to be a result of Ang-(1-9) mediated Protein Kinase A activation (Fattah et al., 2016). In another study, Ang-(1-9) was found to alter calcium uptake through AT_2R/miR-129-3p/PKA signalling pathway (Sotomayor-Flores et al., 2020). However, the protective mechanisms of Ang-(1-9) has also been linked to Ang-(1-9) mediated increase in NOX4 bioavailability, FoxO1 transcription factor activation, which is important in gluco-neogenesis and -lysis, Akt activation, a component of the Akt/PKB signalling pathway that promotes cell survival and growth, and stimulation of atrial natriuretic peptide secretion, a cardiac specific hormone that can stimulate the release of water from the blood and lead to vasodilation (Norambuena-Soto et al., 2020, Mendoza-Torres et al., 2018, Cha et al., 2013, Song et al., 2015). With that being said, groups have also shown that Ang-(1-9) can influence mitochondrial morphology through Drp1 phosphorylation, an enzyme important in mitochondrial fission/fusion, and ultimately cell growth and apoptosis (Sotomayor-Flores et al., 2020, Guo et al., 2023).

Diverging somewhat from studies investigating the effects of Ang-(1-9) in classically developed CVD to drug-induced forms of CVD, one study looked at the effects of Ang-(1-9) in chemotherapy induced cardiomyopathy. When Ang-(1-9) was administered to Adriamycin-induced cardiomyopathy rats it led to improved left ventricular function and reduced pro-inflammatory immune response (Ma et al., 2023). While in models of prostate cancer Ang-(1-9) appears to drive cancer pathology by stimulating the expression of pro-inflammatory NFκB and VEGF expression (Domińska et al., 2019). Such studies provide helpful insights into the potential mechanisms of action of Ang-(1-9). As evidenced by the above, Ang-(1-9) may reduce fibrosis, blood pressure and pro-inflammatory responses in models of CVD. It may therefore be suggested that Ang-(1-9) may be beneficial in treating post-stroke pathology.
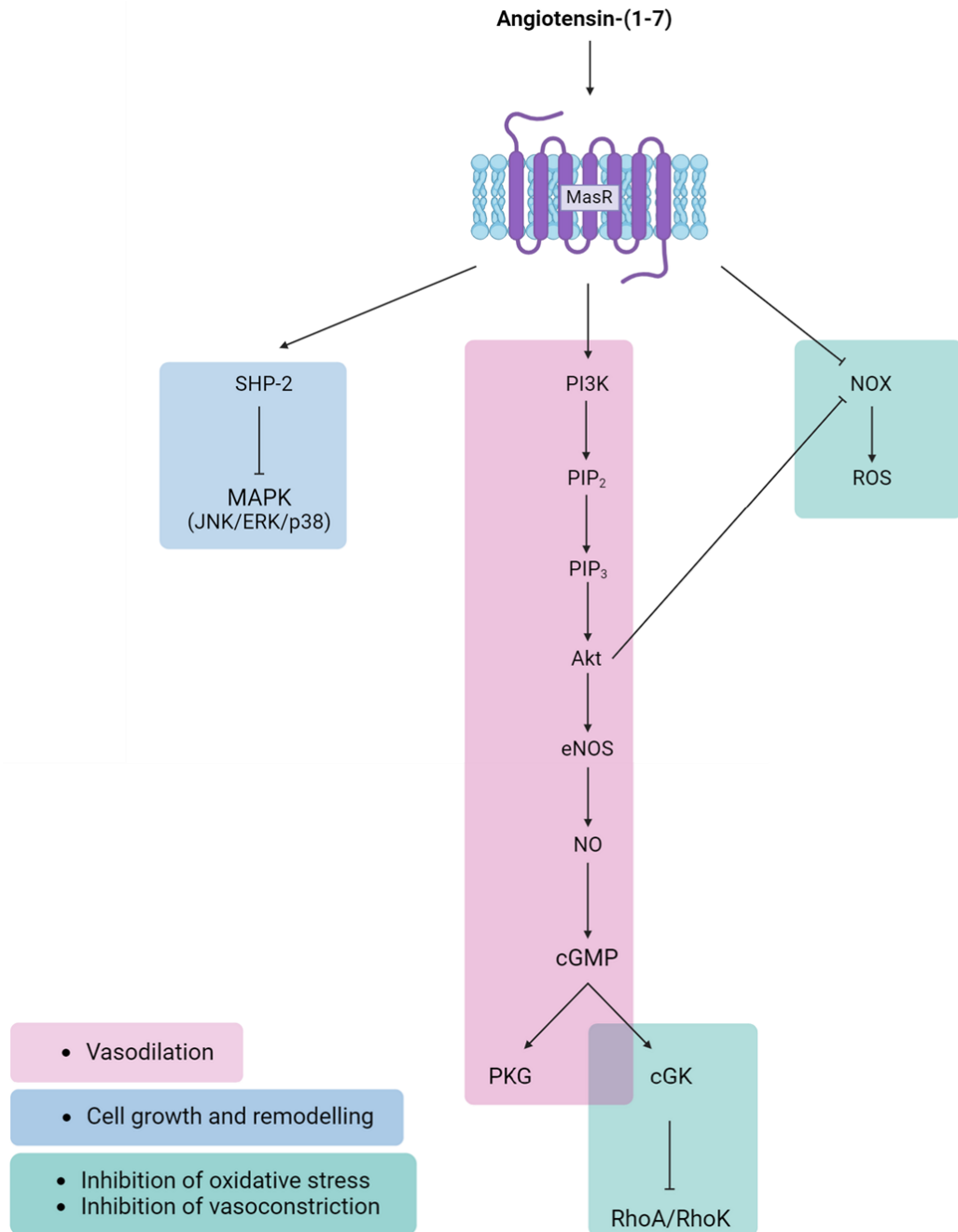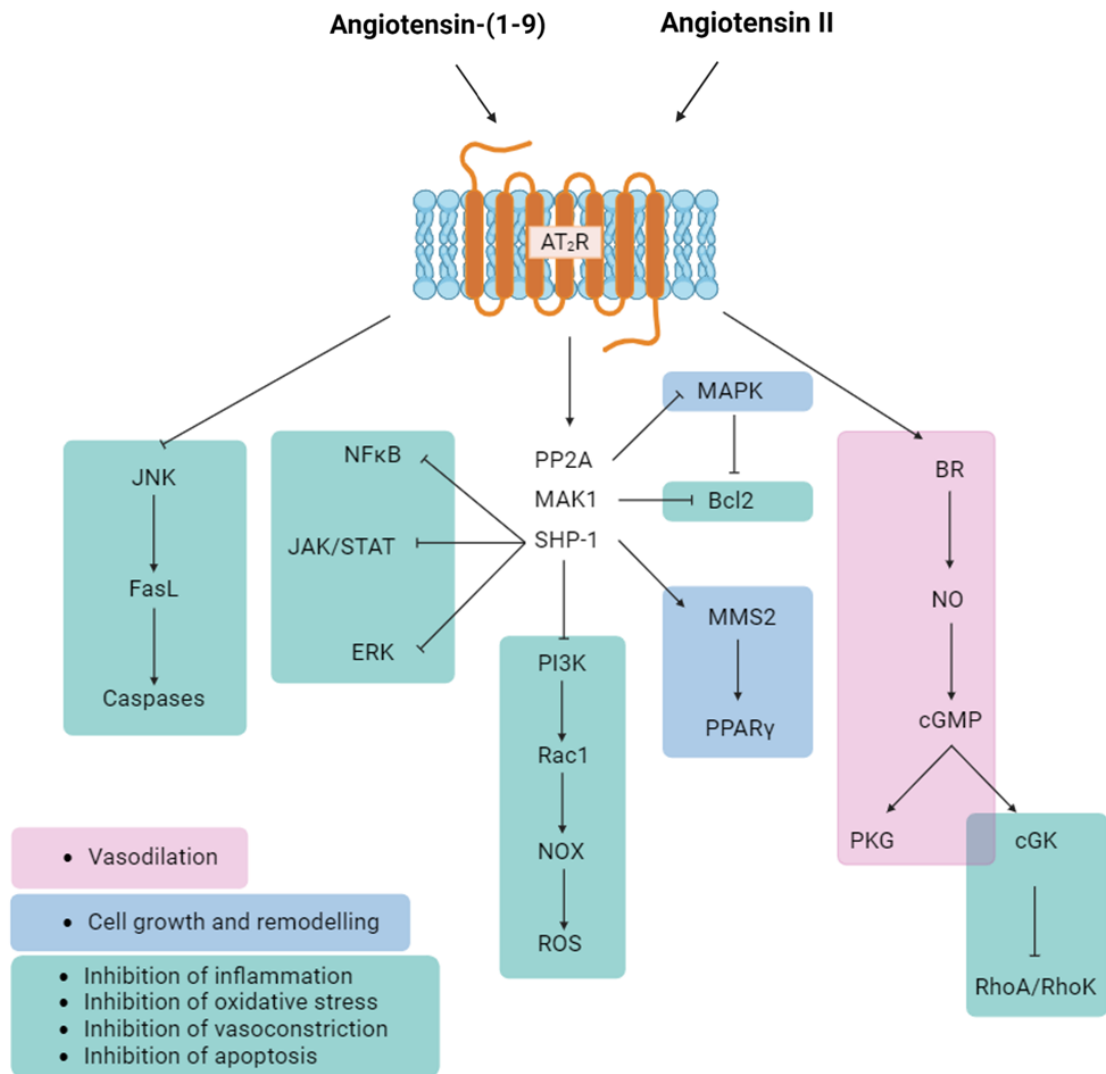
Figure 1.6 Signalling mechanism of the AT₂R.
Illustration of the downstream cascades following AT$_2$R activation by Ang II and Ang-(1-9). Arrows demonstrate the connection between cascade components of the pathway. Components highlighted in pink relate to the vasodilative properties of AT$_2$R activation. Components highlighted in blue relate to the growth and remodelling properties of AT$_2$R activation. Components highlighted in green relate to inhibition of inflammation, oxidative stress, apoptosis and vasoconstriction that occurs following AT$_2$R activation. Component abbreviations: JNK, c-jun N-terminal kinases; FasL, Fas ligand; NFκB, nuclear factor kappa-light-chain-enhancer of activated B cells; JAK, Janus kinase; STAT, signal transducers and activators of transcription; ERK, extracellular signal-related kinases; PP2A, protein phosphatase 2A; MAK1, male germ cell-associated kinase-1; SHP-1, Src homology region domain containing phosphatase-1; PI3K, phosphoinositide 3-kinases; Rac1, Ras-related C3 botulinum toxin substrate-1; NOX, NADPH oxidase; ROS, reactive oxygen species; MAPK, mitogen-activated protein kinases; MMS2, E2 ubiquitin-conjugating protein MMS2; PPARγ, peroxisome proliferator-activated receptor gamma; BR, bradykinin; NO, nitric oxide; cGMP, cyclic guanosine monophosphate; PKG, cGMP-dependent protein kinase or protein kinase G; cGK, cGMP-dependent protein kinase; RhoA, Ras homolog family member A; RhoK; Rho kinase. Figure created in BioRender.

1.2.3 RAAS in the brain

The brain RAAS and central RAAS exist as connected but separate arms. Initial evidence identified that Ang II was able to activate neuronal cells within the subfornical organ (SFO) of cat brains, the region of the brain responsible for fluid balance (Phillips and Felix, 1976). The expression of AT_1R has been identified within brain tissues, whereby AT_1R has been shown to be expressed in regions such as the lateral septum, SFO, paraventricular nucleus of the hypothalamus, arcuate nucleus, nucleus tractus solitarii (NTS) and area postrema (Sumners et al., 2020). AT_2R is widely expressed throughout the brain, but appears to be densely clustered within the NTS, medial prefrontal cortex, medial amygdala (Sumners et al., 2020). Of note, the NTS is the region of the brain responsible for baroreflex function and sympathetic outflow, thus the expression of both AT_1R and AT_2R in this region are indicative of the key role the brain RAAS exerts on the cardiovascular system (Waki, 2012).

With regard to key enzymes of RAAS, both renin and ACE2 have been identified within different regions and cell types of the brain. For example renin is found at low concentrations in the brain, however it is present within neurons and glial cells (Bodiga and Bodiga, 2013). ACE2 has been shown to be expressed in the cell body of neurons in the piriform cortex, caudate putamen, hypoglossal nucleus and primary motor cortex of mouse brains (Doobay et al., 2007). Following the COVID-19 pandemic, ACE2, the receptor for COVID-19, has been widely assessed. Interestingly, data investigating the expression of ACE2 has shown that ACE2 is predominantly expressed within pericytes of the brain, while MasR ligand, Ang-(1-7), has been shown to be expressed within the hypothalamus (Muhl et al., 2022, Block et al., 1988). Novel studies into the role of components of RAAS within health and disease continue to expand our knowledge on the importance of RAAS within the brain. Combined, these studies clearly demonstrate the presence of critical components of RAAS within the brain.

1.2.4 RAAS in ischaemic stroke

The presence of RAAS in the brain and the role of RAAS post-stroke may have implications in stroke pathogenesis and recovery. With that said, modification of RAAS by common anti-hypertensive medications such as ACEi or ARBs have demonstrated varied neuroprotection clinically (Schrader et al., 2005, Gilliot et al., 2018). Over and above reducing hypertension, altering expression of both classical and counter-regulatory axes of

RAAS may increase vasodilation, reduce inflammation, and prevent cell death (Francis et al., 2010, Sukumaran et al., 2012). Overactivation of the classical axis of the RAAS is known to increase inflammatory mediators, fibrosis and oxidative stress (Wright and Harding, 2013). Rats treated prophylactically with ARBs demonstrated increased cerebral reperfusion and decreased infarct volumes following MCAO (Engelhorn et al., 2004). Current research focusing on Ang-(1-7) has also found the MasR to be upregulated as early as 6 hours following ischaemic stroke, as well as increased levels of cerebral and circulating Ang-(1-7) (Lu et al., 2013). Central infusion of Ang-(1-7) prior to ET-1-MCAO led to decreased infarct volumes (Mecca et al., 2011). Similar results were also demonstrated when investigating the effects of C21, an AT_2R agonist, after ET-1-MCAO, whereby infarct volumes and neurological deficits were decreased (Joseph et al., 2014). Further studies into CGP42112 AT_2R agonist have also demonstrated improved motor function and decreased lesion size after tMCAO (McCarthy et al., 2009). Primary cortical neuronal cell viability after OGD was increased following treatment with CGP42112 (Lee et al., 2012). Both *in vitro* and *in vivo* evidence has demonstrated the importance of RAAS modification on ischaemic stroke and how, by altering RAAS peptide levels and/or inhibiting or stimulating RAAS receptors, novel therapies may be developed to treat ischaemic stroke. Positive investigations such as these into Ang-(1-7) pave the way for further studies into the possible beneficial effects of Ang-(1-9) following ischaemic stroke. The effects of RAAS modulation in ischaemic stroke will be discussed in depth in chapter three of this thesis.

1.3 Introduction to Extracellular Vesicles

Extracellular vesicles (EVs) are small lipid bilayer molecules that are capable of trafficking internalised cargo systemically throughout the body and are a key component in cell signalling (Salomon et al., 2022). Due to their small nature and structural stability, largely protected from the environment in which they reside, EVs have demonstrated negligible immunogenicity, making them a promising drug delivery vector.
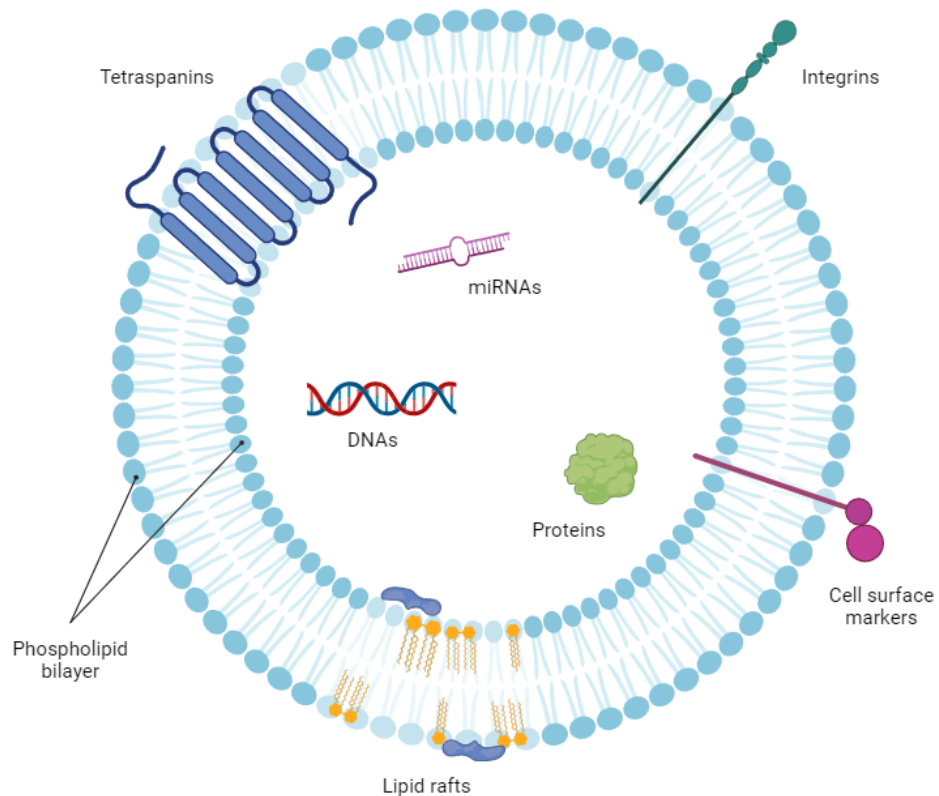
Figure 1.7 Extracellular vesicle structure and membrane components.
Image depicting the overall structure of an extracellular vesicle including the phospholipid bilayer, tetraspanins, lipid rafts, cell surface markers and integrins. Image also depicts internal extracellular vesicle cargo such as miRNA, DNA and proteins. Figure adapted from (Newman et al., 2022). Figure created in BioRender.

1.3.1 EV formation

EVs are comprised of a phospholipid bilayer outer membrane and an internal, luminal compartment that contains vital cargo (Zaborowski et al., 2015). This cargo may include DNA and ribonucleic acid (RNA) molecules, such as microRNAs (miRNAs), as well as proteins. The phospholipid bilayer of EVs may contain tetraspanins, integrin molecules, cell-specific markers, and lipid rafts (Figure 1.7). There are three main forms of EVs;

exosomes, microvesicles and apoptotic bodies, all of which are defined by their morphology (Yáñez-Mó et al., 2015). The formation of exosomes relies upon invagination of the plasma membrane of a cell which ultimately breaks off to form an early-stage endosome. Within the cytoplasm of the cell, early-stage endosomes may bind to key cytosolic organelles or other endosomes to form late-stage endosomes. Late-stage endosomes undergo further invagination to form internal intraluminal vesicles (ILV) and are transformed into multivesicular bodies (MVB) (Hanson and Cashikar, 2012). Regulators ARF6 and PLD2 are responsible for membrane budding to form ILVs within MVB (Ghossoub et al., 2014). MVBs can be processed differently within the cell, whereby MVBs may be degraded within the cytosol or may fuse with the plasma membrane to release internal exosomes (Figure 1.8).

There are four endosome sorting complexes required for transport (ESCRT) proteins, each playing their individual role in exosome formation and secretion from parental cells. ESCRT-0 complexes with ubiquitinated proteins on the surface of endosomes. ESCRT-0 itself is formed of HRS, Eps15 and clathrin. HRS of ESCRT-0 binds to TSG101 on ESCRT-I. ESCRT-I recruits ESCRT-III to the complex through means of either ESCRT-II or ALIX. ESCRT-I and -II are thought to mediate membrane budding during ILV formation, while ESCRT-III cleaves membrane buds to create cargo containing ILVs within MVBs (McCullough et al., 2018). ILVs formation may also be dependent of sphingolipids, whereby one study identified that inhibition of sphingomyelinases reduced EV secretion by hindering of ceremide-dependent ILV budding into MVB (Menck et al., 2017). ESCRTs and accessory proteins are required for budding and have been shown to play an essential role in EV secretion; knockdown of these proteins can alter EV secretion (Colombo et al., 2013). Similarly, inhibition of sphingomyelinase-2 required for sphingolipid breakdown, has been shown to reduce EV secretion (Guo et al., 2015, Choezom and Gross, 2022). MVB-mediated EV secretion has also been achieved in the absence of ESCRT proteins, demonstrating the complex nature of EV biogenesis and secretion (Stuffers et al., 2009). Independent of ESCRT, tetraspanins, such as CD63, have been examined for their role in secretion. Knockout of CD63 in HEK293 cells by CRISPR technology demonstrated fewer secreted EVs quantified by nanoparticle tracking analysis (Hurwitz et al., 2016a). Additionally, siRNA knockdown of ARF6 has shown to reduce exosome release and reduce breast cancer cell migration *in vitro* (Li et al., 2017a).
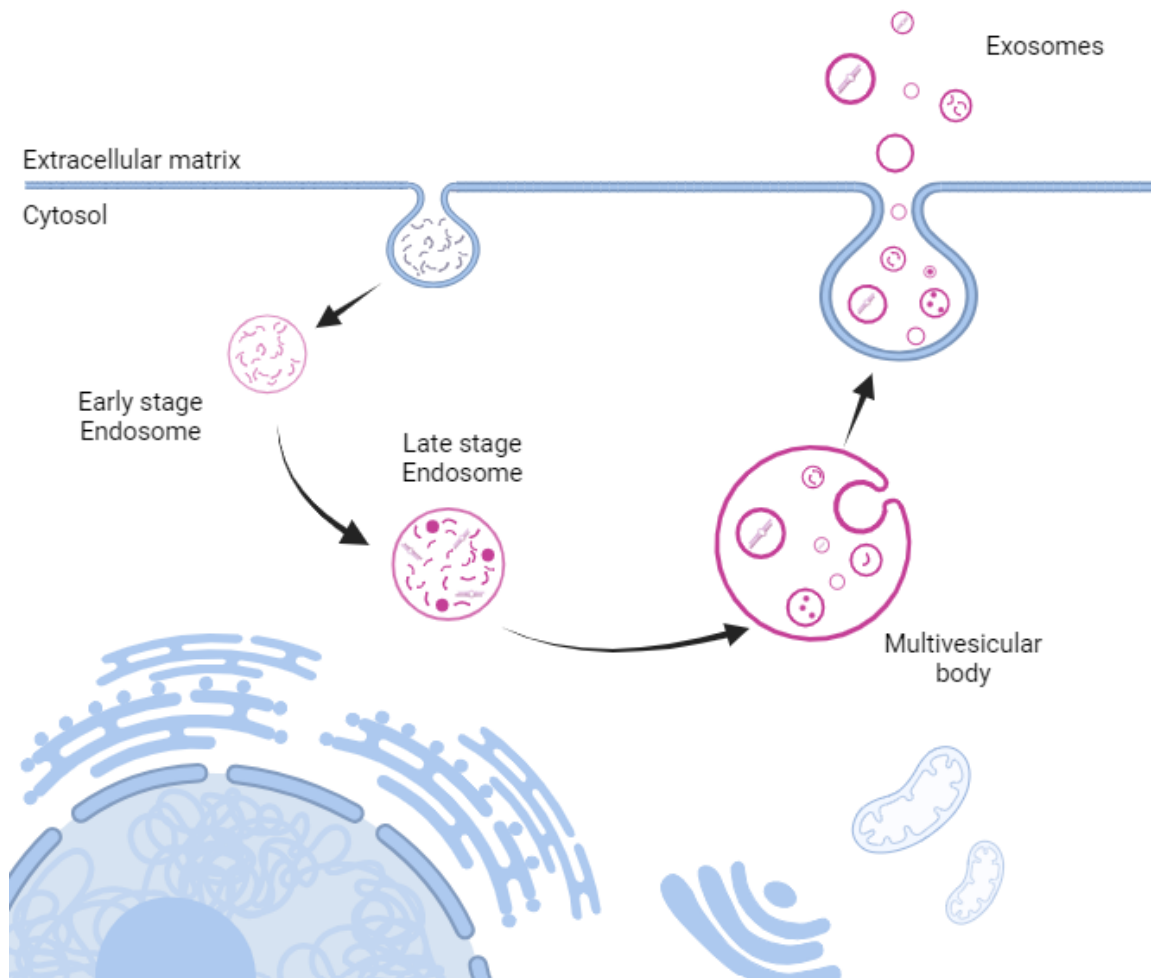
Figure 1.8 Formation of extracellular vesicles from parental cells.
Image depicts the formation of early-stage endosomes by invagination of the plasma membrane. Early-stage endosomes may interact with organelles or other endosomes to form late-stage endosomes. Late-stage endosomes undergo further invagination to form intraluminal vesicles (ILVs), where late-stage endosomes are transformed into multivesicular bodies (MVBs). MVBs may bind to the plasma membrane where ILVs are released into the extracellular matrix as exosomes. Figure created in BioRender.

1.3.2 EV cargo

A single cell can produce heterogenous EV populations with different bilayer components and cargo. During EV formation, specifically the invagination steps and interactions with ILVs, precursor EVs are exposed to extracellular matrix and parental cell components that may be incorporated into the final EV structure. Incorporation of parental components within EVs may enable therapeutic targeting (Rädler et al., 2023, Gao et al., 2018) which will be discussed in a later chapter of this thesis. During the ILV formation stage, parental cytoplasmic components including proteins and miRNA can be encapsulated in ILVs that are later released as EVs. Similarly, MVBs may influence the composition of EVs, whereby the tetraspanin CD63 commonly found on MVBs, are subsequently identified on the surface of EVs and are thusly used as EV biomarkers (Pols and Klumperman, 2009). One study showed that EVs secreted from the apical and basolateral side of a polarised cell carry individually distinct cargo (Chen et al., 2016b).

MiRNAs remain at the forefront of therapeutic EV studies due to their ability to alter gene expression at a transcriptional level (Catalanotto et al., 2016). MiRNAs can be trafficked systemically around the body, protected from extracellular microenvironments by EVs. KRAS, the gene responsible for the activation of the Ras-MAPK pathway may play a role in miRNA cargo loading into and eventual secretion of EVs. EVs isolated from KRAS mutant colorectal cancer cells showed reduced RISC-complex protein Ago2 localisation to MVB and subsequent reduction in Ago2 within EVs (McKenzie et al., 2016). RISC ribonucleoprotein incorporates miRNAs to target genes while Ago2 is required for mRNA degradation and aids in miRNA-mediated inhibition of translational gene expression (Martinez and Gregory, 2013). miRNA profiles are altered within mutant KRAS colorectal cancer derived EVs, thus consolidating the importance of gene expression in miRNA cargo-loading of EVs. Sequence motifs have been identified in miRNAs which are bound by sumoylated ribonuclear proteins, such as hnRNPA2B1, to control miRNA localisation within EVs (Villarroya-Beltri et al., 2013). Numerous EV derived miRNAs have demonstrated potential biomarker properties and therapeutic value.

1.3.3 EVs in cell signalling

EVs are able to deliver internal cargo such as phospholipids, proteins and RNA molecules from parental cells to other cells throughout the body (Anand et al., 2019). EVs may directly bind to cell surface receptors on the surface of target cells to directly deliver internal cargo to the target cell, such as miRNAs (Mittelbrunn et al., 2011). This cargo may lead to alteration of cell pathways or may even effect gene expression. EV binding to target cells can result in transfer of genetic information to recipient cells (Camussi et al., 2010). As such, EVs have significant potential in treating numerous diseases, especially systemic disease, due to their stability within the body, allowing for intact cargo delivery to desired sites (Salomon et al., 2022). There are three main methods of EV integration into target cells; direct endocytosis, paracrine or endocrine signalling (Wang et al., 2017b). Microvesicles including EVs are more susceptible to changes within the microenvironment compared to exosomes. This can be eloquently demonstrated within the tumour microenvironment whereby EV cargo transfer and receptor expression can confer drug-resistance to cancer cell types, promoting tumorigenesis. With that being said EVs can be modified within the tumour microenvironment to express oncogenic proteins which in turn aid in tumour cell growth (Rak and Guha, 2012). Related to this, the pattern recognition receptor P2X7R, commonly found in microglia, is bound by pathogen/damage associated molecular patterns, which leads to membrane blebbing and microvesicle release. P2X7R activation by ATP can lead to increased microvesicle blebbing and is associated with ATP-mediated apoptotic cell death (Kanellopoulos and Delarasse, 2019). To summarise, EVs may bind to and interact with cells to alter signalling pathways throughout the body in both health and disease.

1.3.4 EV research guidelines

Over the past 15 years the number of published EV articles has grown exponentially. These publications include EVs isolated from various samples and their use in a wide variety of diseases. As such guidelines have been developed in order to assist researchers in their EV research, namely EVTrack and MISEV guidelines (Lötvall et al., 2014, Van Deun et al., 2017, Thery et al., 2018, Welsh et al., 2024). EVTrack consortium first shed light on the need to standardise EV research, after noting that in EV papers published from 2010 to 2015, there were 190 different EV isolation methods listed, demonstrating the heterogeneity in EV research (Van Deun et al., 2017). Initial guidelines emphasise the need to identify EV-specific protein markers through use of flow cytometry, western blotting or

mass spectrometry (Lötvall et al., 2014). MISEV guidelines were expanded in later years to include further guidance on methods for sample preparation, EV isolation, EV characterisation and storage (Thery et al., 2018). As the quality of EV research improves in line with these standard guidelines, additional information uncovered in this research has led to the development of the most up-to-date MISEV 2023 guideline in the field of EV research which was published in early 2024 (Welsh et al., 2024). Methods of EV isolation and characterisation will be discussed in depth in chapters two, four and five.

1.3.5 Application of EVs in diseases

EV treatment may be beneficial in diseases including CVD, renal disease, wound healing, and ischaemic stroke. In models of CVD, cardiosphere derived EVs have previously been shown to reduce Ang II-induced cardiac hypertrophy and organ damage in mice (Cambier et al., 2018). Within the infarcted myocardium of mice, EVs enriched with miRNA-21 reduced the number of apoptotic cardiomyocytes (Song et al., 2019). EVs have also improved wound healing in preclinical models of diabetes (Guo et al., 2017b, Li et al., 2018). In models of renal ischaemia reperfusion injury, administration of ACE2 overexpressing mesenchymal stem cells (MSCs) derived EVs improved renal function (Zhang et al., 2023). EVs have also proven beneficial in slowing senescence in preclinical models of aging (Gong et al., 2020). In experimental models of cortical injury, MSC-derived EV treatment enhanced dendritic plasticity and behavioural recovery (Medalla et al., 2020).

There are various studies that have identified the benefits of EVs in ischaemic stroke models. EVs derived from MSCs, bone marrow derived stem cells (BMSCs) and other cell types have been shown to improve post-stroke outcomes in a large number of studies. In terms of functional outcomes, studies have shown that MSC-EVs or cerebral endothelial cell derived EVs delivered with or without tPA to experimental models of stroke improved neurological scores, increased BBB integrity markers and reduced infarct volume (Qiu et al., 2022, Li et al., 2021a, Otero-Ortega et al., 2020, Doeppner et al., 2015). Neural progenitor cell derived EVs, adipose-derived MSC derived EVs and anti-inflammatory microglial cells derived EVs delivered to experimental stroke models have demonstrated improved neurological recovery (Zheng et al., 2021, Chen et al., 2016a, Hu et al., 2022, Li et al., 2021b). The benefits of MSC-derived EVs (MSC-EVs), inducible pluripotent stem cell derived EVs and anti-inflammatory microglial cells derived EVs in experimental stroke are attributed to: increased number of neuroblast and neuronal cell proliferation,

decreased neuronal cell death, increased endothelial cell markers, reduced glial scar formation, reduced astrocyte activation, reduced BBB dysfunction and reduced expression of pro-inflammatory cytokines (Xin et al., 2013, Otero-Ortega et al., 2020, Li et al., 2023b, Li et al., 2021b).

The use of EVs in ischaemic stroke treatment may be enhanced by altering EV cargo to contain potentially therapeutic miRNAs, proteins and other compounds. In the context of stroke research, the most assessed therapeutic EV cargo is miRNA. EV miRNAs have long been thought of as prognostic markers for disease, indeed miRNAs are differentially expressed following ischaemic stroke (Mens et al., 2021). As such by loading EVs with miRNAs, or any other beneficial peptide or compound, post-stroke functional outcomes may be improved. The benefits of EVs miRNAs in ischaemic stroke has previously been reviewed in detail (Fullerton et al., 2023). EVs loaded with proteins such as brain derived neurotrophic factor improved post-stroke neurological outcomes and reduced infarct volume post-stroke (Zhou et al., 2023a). Expanding upon the idea that EVs may be altered or designed to contain therapeutic cargo, EVs may be conjugated with targeting molecules or may be designed to be integrated with targeting molecules that enhance the delivery of EV cargo to desired organs (Murphy et al., 2019). For example, in experimental models of ischaemic stroke Rabies virus glycoprotein targeted EVs has successfully increased EV delivery to the brain (Yang et al., 2020b, Haroon et al., 2024, Gao et al., 2018). The prospect of targeting EVs to the brain will be discussed in length in chapter six of this thesis.

The benefit of RAAS interventions and EVs have independently been established in ischaemic stroke. This thesis research aims to combine the benefits of EVs and the novel peptide Ang-(1-9) from the counter-regulatory axis of RAAS to assess their effects on post-stroke outcome, research that, until this point, has not previously been published.

1.4 Overall hypothesis

- Circulating extracellular vesicles from spontaneously hypertensive stroke prone (SHRSP) rats loaded with Angiotensin-(1-9) from the counter-regulatory axis of the RAAS, will influence outcome measures in SHRSPs following experimental stroke.

- Application of targeting Rabies virus glycoprotein to extracellular vesicles will improve cargo delivery in animal models.

- Modulation of RAAS by means of Angiotensin II type II receptor deficiency in C57BL/6 mice will influence the characteristics of circulating extracellular vesicles.

- Systematic comparison of peer-reviewed publications will demonstrate improvement in outcome measures in experimental stroke models following treatment with RAAS targeting interventions.

1.5 Overall aims

- Characterise EVs isolated from total plasma of SHRSPs.

- Optimise *in vitro* models to assess Ang-(1-9) peptides and loaded EVs on cells associated with the neurovascular unit.

- Determine whether Rabies virus glycoprotein conjugation of EVs will increase targeting towards the brain.

- Deliver Ang-(1-9) loaded EVs to SHRSP rats following tMCAO and assess levels of gene expression.

- Characterise circulating extracellular vesicles from wildtype and AT_2R deficient C57BL/6 mice.

- Systematically compare peer-reviewed publications to ascertain whether treatment with RAAS targeting interventions influences outcome measures in preclinical models of ischaemic stroke.

Chapter 2: Methods

2.1 *In vivo* methods

2.1.1 Animal methods

Male and female Spontaneously Hypertensive Stroke Prone Rats (SHRSPs), male and female C57BL/6 mice and male and female C57BL/6 AT_2R knockout mice were bred within the Biological Services facility at the University of Glasgow. Animals were housed in cages singly or with same sex littermates prior to the start of the study. Animals were allowed free access to rodent feed (RM1 expanded or pelleted diet, SDS, England) and water. All studies were carried out in accordance with the Animals Scientific Procedures Act 1986 under project licences PP5760534 and PP05FE1F82 and were approved by the University of Glasgow's Ethics Review Committee

2.1.2 SHRSP procedures

2.1.2.1 Tail cuff plethysmography

Systolic blood pressure was measured using the rat platform BP-2000 Blood pressure Analysis system™ (Visitech Systems, Bioseb, UK). SHRSPs were restrained within the apparatus and were given habituation sessions prior to experimental measurements. Prior to starting measurements, rats were allowed to warm to base plate temperature of 37°C. Five practice readings were taken to further habituate the animals to the sensation of the blood pressure cuff. The number of experimental readings was set to a maximum of 15 and the blood pressure reading was set to a maximum of 240 mmHg. The time within restraint would not exceed 30 minutes. From the readings generated outliers greater than 2X standard deviation were automatically removed by the software. For the therapeutic Ang-(1-9) electroporated EV study, tail cuff plethysmography measures were determined at least twice before the commencement of antihypertensive treatment and prior to stroke surgery to ensure blood pressure had been reduced.

2.1.2.2 Antihypertensive treatment

Animals were given 16 mg/kg/day of hydralazine (Merck, UK) and hydrochlorothiazide (Merck, UK) orally within a soft egg custard food mix (Heinz, UK). Treatment

commenced 2-weeks prior to stroke surgery and continued daily until the completion of the experiment. Blood pressure was assessed before and after antihypertensive treatment.

2.1.2.3 Burrhole and tMCAO surgery

Male SHRSPs of 270-306 grams underwent burrhole and tMCAO surgery at 17-19 weeks of age. Animals were initially anaesthetised in a box using 2 L/min 100% oxygen plus 5% isoflurane. Animals were then endotracheally intubated and artificially ventilated with 0.35 L/min 100% oxygen at a rate of 68 breaths per minute with 3.5-4% isoflurane throughout the duration of the procedure. A rectal thermometer was used to monitor body temperature and was maintained between 35-37°C using a heated mat and/or heat lamp. Both burrhole and tMCAO surgery was conducted under a microscope at various magnifications. For burrhole surgery, animals were placed in a stereotactic frame. Animals were given 10 mg/mL analgesic Naropin subcutaneously at the sight of incision (GSK, UK) and 2.5 mL saline subcutaneously before and after surgery. An incision was made in the scalp of the animal and connective tissue was removed to expose the skull. Two 1 mm transcranial burrholes were drilled on either side of the sagittal suture on the parietal bone with a microdrill. The dura was then pierced (Microtorque II, Harvard Apparatus) and the scalp sutured and the animal was removed from the stereotactic frame and placed in a supine position on an operating pad. An incision was made in the neck of the animals to the left of the trachea. Using blunt dissection tools, the common carotid artery (CCA) was isolated and ligated proximal to the bifurcation of the external carotid artery (ECA) and the internal carotid artery (ICA). The ECA was then ligated, and a loop tie was placed on the ICA. Carotid branches transversing from the ECA towards the pterygopalatine artery (PA) were electrocauterised and the PA was then ligated. An incision was made in the common carotid artery and a silicone coated intraluminal filament (Catalogue number: 503356PK10, Doccol Corporation, USA) was inserted into the CCA and was advanced 22mm through the ICA to the origin of the left MCA (Figure 2.1). The filament was kept in place for 10 minutes while heartbeat and body temperature were monitored. After removal of the intraluminal filament, the loop tie on the ICA was tightened to prevent back flow of blood from the brain. An additional ligation was made distal to the incision on the CCA. The incision in the CCA was then sealed by electrocautery and ligations on the ICA, ECA and PA were removed. The incision on the neck was sutured and the animal was slowly removed from artificial respiration until able to breathe independently. The animal was then transferred to a recovery cage and placed in a dark, quiet recovery room and was

monitored daily to assess their level of overall health and distress or discomfort. An example of the surgical monitoring sheet used throughout the duration of the experiment is found in Table 2.1. Animals were maintained for 24 hours or 10 days, for assessment of gene expression following stroke or functional outcomes respectively.
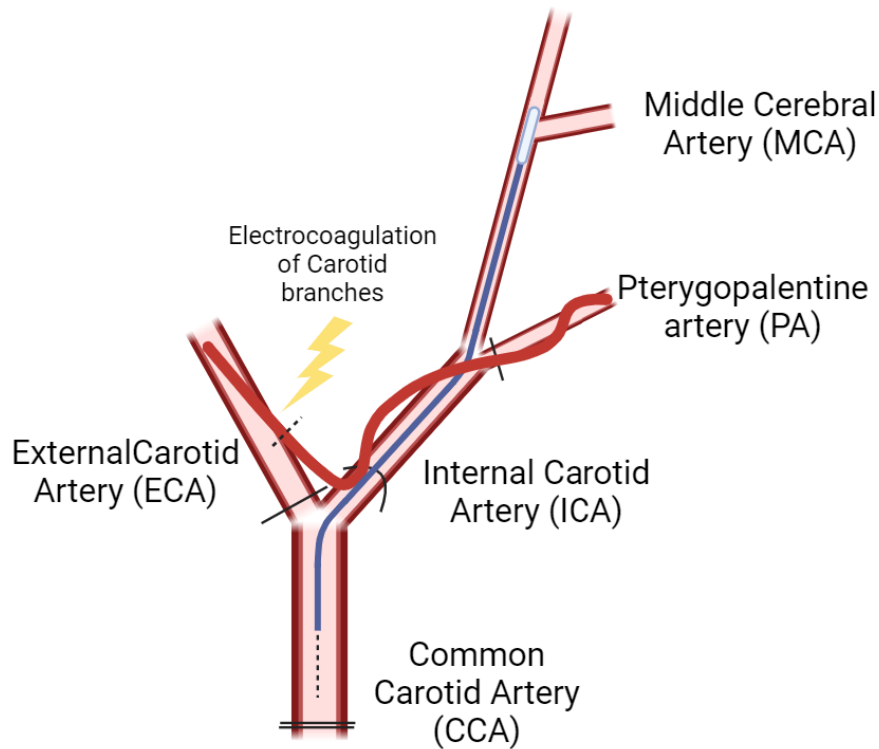
Figure 2.1 Illustration of intraluminal filament MCAO model.
CCA was isolated proximal to the bifurcation of the ECA and ICA. CCA was ligated approximately 10 mm from the bifurcation point. ECA was ligated at the base of the bifurcation. A loop was placed round the ICA and carotid branches were electrocauterised. The PA was ligated, and a small incision was created in the CCA. A silicone coated intraluminal filament was inserted into the CCA incision and was advanced to the origin of the MCA (typically 18-22mm). The intraluminal filament was ligated in place for the duration of occlusion. The ligation was then eased to remove the intraluminal filament. A further ligation was placed above the incision site on the CCA and the incision site on the CCA was electrocauterised. Ligations on the ECA and PA were then removed and initial incision was sutured before the animal was recovered.

Table 2.1 Example of post-operative monitoring sheet.

Example post-operative monitoring sheet

PPL: LMW Procedure number: 9	Pre-operative weight: 300g					Surgery date: 15/11/2022 Suture removal date: N/A
Animal ID: 1A Animal strain: SHRSP	10% weight loss* *NB. Call NVS if body weight falls below 10% of pre-operative weight or recovery is not as expected by day 3.					Days to recover to pre-operative weight:
Surgery/expected adverse effects: tMCAO+burrhole						
Date and time:	Weight	Appetite	Faeces	Urine	Wound	Comments
15/11/2022; 11am	N/A	No	Yes	Yes	Minor Bleeding	Unconscious after surgery, minor wound bleeding
15/11/2022; 2 pm	N/A	No	Yes	Yes	No bleeding	Responsive to touch, wound has stopped bleeding, groggy after anaesthetic
15/11/2022; 4.30 pm	N/A	No	Yes	Yes	No bleeding	Responsive to touch, wound has stopped bleeding, more awake and
16/11/2022; 9 am	290 g	No	Yes	Yes	No bleeding	Never ate baby food given overnight, responsive, weight loss okay
16/11/2022; 11 am	N/A	Yes	Yes	Yes	No bleeding	Mildly alert, responsive, has eaten baby food
16/11/2022; 2 pm	N/A	Yes	Yes	Yes	No bleeding	Mildly alert, responsive, has eaten baby food
16/11/2022; 4:30 pm	N/A	Yes	Yes	Yes	No bleeding	Mildly alert, responsive, has eaten baby food
17/11/2022; 9 am	282g	Yes	Yes	Yes	Good	Eating baby food, responsive and alert, lost more weigh but that is to be expected
17/11/2022; 12 pm	N/A	Yes	Yes	Yes	Good	Eating baby food, responsive and alert
Drugs given:			Dose:			Frequency:
Monitoring continued until desired timepoint						

2.1.2.4 RVG (+/-) *Cel-miR-39* mimic miRNA electroporated EV treatment

Male SHRSPs of 246-313 grams in weight were anaesthetised with 2 L/min oxygen and 4% isoflurane. Rats were transferred to a mask and were reflex assessed before proceeding. In line with the ARRIVE guidelines, EV preparations were delivered to SHRSPs in a randomised, blinded manner (Percie du Sert et al., 2020, Kilkenny et al., 2010). Randomisation and blinding were conducted by Dr Lorraine Work ahead of any *in vivo* delivery of EVs. EV preparations of 12 µL were administered to each nare twice, allowing for a total of 48 µL per delivery. EVs were delivered on day one and two with a six-hour pause between deliveries. Control EVs ($2.1x10^9$ particles/µL per single 48 µL dose) or RVG$^-$ *Cel-miR-39* mimic miRNA electroporated EVs ($2.1x10^9$, $5.2x10^9$, or $1.04x0^{10}$ particles/µL per single 48 µL dose) or RVG$^+$ *Cel-miR-39* mimic miRNA electroporated EVs ($5.2x10^9$ particles/µL per single 48 µL dose) were administered to each animal intranasally per 48 µL dose. The total number of EVs delivered per group were as followed: Control EVs, $1x10^{11}$ particles total, RVG$^-$ *Cel-miR-39* mimic miRNA electroporated EVs, $1x10^{11}$, $2.5x10^{11}$ or $5x10^{11}$ particles total and RVG$^+$ *Cel-miR-39* mimic miRNA electroporated EVs $2.5x10^{11}$ particles total. On the fourth day, animals were culled under terminal general anaesthesia.

2.1.2.5 Ang-(1-9) electroporated EV treatment

In line with the ARRIVE guidelines, EV preparations were delivered to SHRSPs in a randomised, blinded manner. Randomisation and blinding were conducted by Dr Lorraine Work ahead of any *in vivo* delivery of EVs. EVs loaded with Ang-(1-9) peptide (Phoenix Pharmaceuticals Ltd., US) were administered to rats subjected to tMCAO at a 4-hour timepoint post-stroke. The animals were lightly anaesthetised in a box using 2 L/min Oxygen and 4% isoflurane before being transferred to a mask where 2 L/min oxygen and 4% isoflurane was maintained. As with previous intranasal delivery methods, rats were given a maximum delivery volume of 48 µ L per dose. The total number of Ang-(1-9) electroporated EVs delivered per animal was $2.5x10^{10}$.

2.1.2.6 Neurological deficit score

A 30-point neurological deficit score (NDS) was conducted prior to and at days 3, 7 and 10 post-stroke. The NDS was used to assess post-stroke outcomes such as mobility, reflex, limb function and general health. A list of all NDS assessment criteria and scores are included in Table 2.2.

Paw placement: The animal was placed on a flat surface. One at a time each paw was moved from beneath them. If an animal immediately compensated and attempted to place the paw back in the original position, the animal was given a maximum score. If an animal was unable to compensate for paw placement, the animal scored zero for that paw.

Horizontal bar: the animal was held by its tail until it was within grasp of the horizontal bar. If the animal was able to grasp the horizontal bar and raise all four limbs to the bar, the animal was given the maximum score. If the animal fell from the bar, it was given the lowest score possible.

Rotation: The animal was placed on a flat surface and held by the base of the tail. The animal was then moved by the tail in both a clockwise and anticlockwise direction. If the animal was able to counteract the movement in both directions, the animal was given the maximum score. If the animal was able to counteract the rotation on one side, it was given a score of one.

Visual forepaw reaching: The animal was held by the base of the tail above a flat surface. If the animal was able to reach for the surface with both forepaws, the animal was given the maximum score of two. If the animal was only able to reach with one paw, it was given a score of one.

Grip strength: The animal was held by the base of the tail above a cage top and lowered so that it was able to grasp the cage wires. The animal was gently pulled backwards over the wires. If the animal was able to grip wire with normal strength across both paws, the

animal was given the maximum score. If the animal was not able to grip the wire, it was given the lowest score.

Response to vibrissae touch: the animal was placed on a flat surface. Out of eyesight and from behind, the whiskers of the animal were brushed with a pen. If the animal responded normally with the whisker touch on both sides, it was given the maximum score. If the animal did not respond to whisker touch on either side, it was given the lowest score.

Circling: The animal was placed on a flat surface and was allowed to freely roam. If the animal exhibited no circling behaviour, then the animal was given the maximum score. If the animal was spinning in tight circles or was immobile, it was given the lowest score.

Mobility: The animal was placed on a flat surface and was allowed to freely roam. If the animal exhibited normal movement, it was given the maximum score. If the animal was reluctant to move or immobile, it was given the lowest score.

General condition: The animals overall state, including weight and overall behaviour/appearance was assessed. If the animal appeared normal with no weight loss, then the animal was given the maximum score. If the animal was in fair condition and had lost weight and showed some form of bodily secretion, it was given the lowest possible score.

Table 2.2 Assessment type and points score of the Neuroscore.

Test type	Point scoring	Max score (30)
Paw Placement	1 point for each successful paw placement	4
Horizontal Bar	3 if both hindlimbs raised onto the bar 2 if one hindlimb raised onto the bar 1 if the animal hangs from the bar 0 if the animal falls	3
Rotation	1 for each side	2
Visual Forepaw Reaching	1 for each successful paw placement	2
Grip Strength	3 for normal strength 2 for good but weakened strength 1 for weak strength 0 for no grip	3
Response to Vibrissae Touch	3 equal responses on both sides 2 weakened response on affected side 1 no response on affected side 0 no response on either side	3
Circling	5 if the animal does not circle 4 if the animal tends to one side 3 for large circles (> 50 cm radius) 2 for medium circles (15-50 cm radius) 1 for small circles (> 15 cm radius) 0 for spinning or refusing to move	5
Mobility	4 for normal mobility 3 for very active 2 for lively 1 for unsteady 0 if reluctant to move	4
General Condition	4 if normal 3 if very good, but less weight gain 2 if very good but showing secretions 1 if good 0 if fair	4

2.1.2.7 Tissue collection

Following completion of the *in vivo* study, animals were humanely culled. Animals were anaesthetised in a box using 2 L/min oxygen and 5% isoflurane before being transferred to a mask where 2 L/min oxygen and 5% isoflurane was maintained. After reflexes were tested an incision was made below the sternum which continued up both sides of the ribcage. The diaphragm was cut to expose the heart and lungs. The pericardium around the heart was removed to allow the heart to drop within the chest. The left ventricle was pierced using a 16-gauge needle and approximately 3-5 mL of blood was withdrawn and collected in BD Vacutainer Plastic Lithium Heparin Tubes (Medisave, UK). The heart and lungs were removed to arrest blood flow. Upon completion of cardiac puncture, rats were decapitated, and brains were removed from the skull. As appropriate for the experiment brains were sectioned either rostocaudally in both hemispheres (Figure 2A) or in accordance with ischaemia zones across both hemispheres (Figure 2B). Afterwards the heart, lungs, liver, kidneys, and spleen were all removed. All tissue samples were either frozen in liquid nitrogen or placed in 4% paraformaldehyde (PFA). Collected blood was centrifuged at 2,000 g for 10 minutes, after which time the top plasma layer was collected and stored at -80°C until use.

2.1.2.8 Historical samples

Historical SHRSP plasma samples were provided for initial experimentation from animals culled by Dr Lorraine Work and Dr Josie Fullerton. Historical brain tissue samples were provided by Dr Josie Fullerton that were later used in combination with samples prepared by myself for experiments assessing the effects of reperfusion time and stroke occlusion time on gene expression.
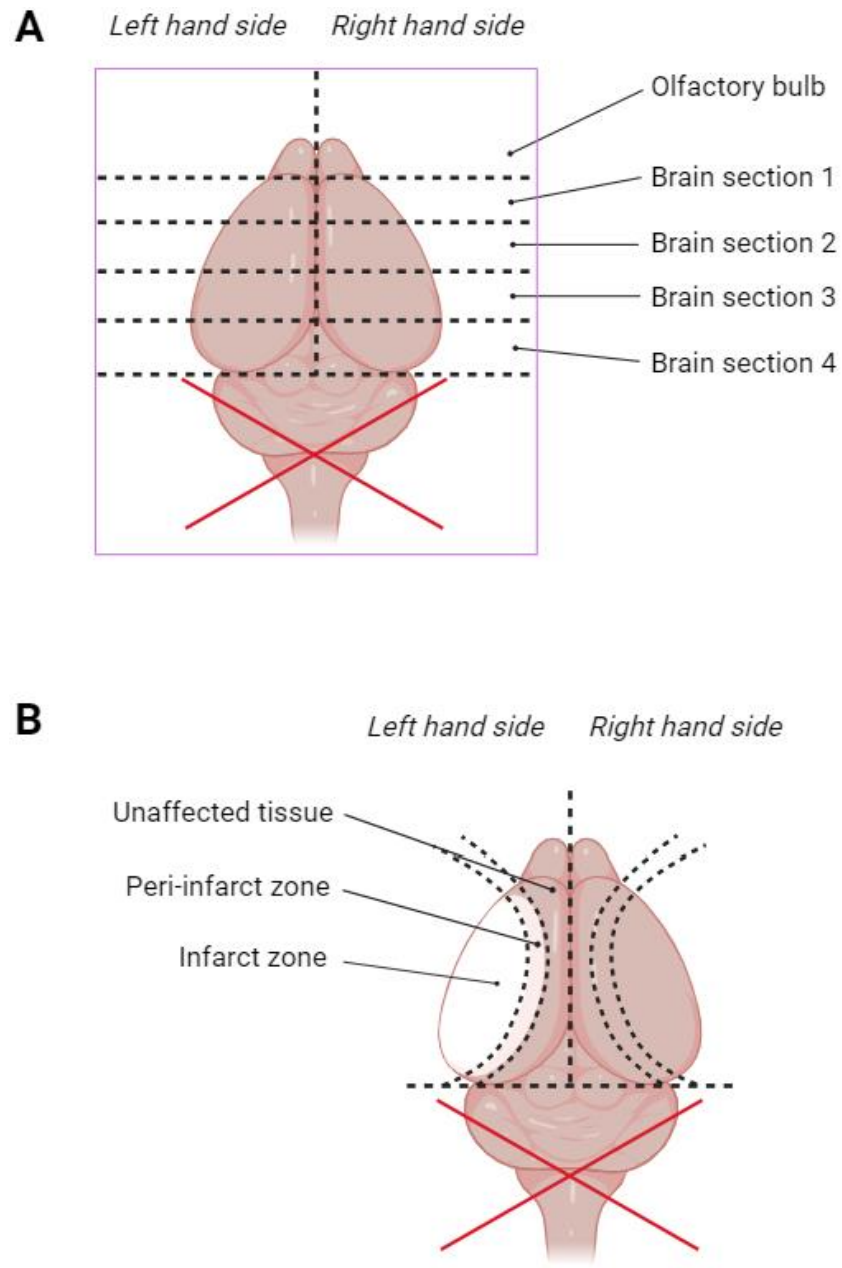
Figure 2.2 Brain sectioning methods.
Image depicts rostrocaudal sectioning of the left and right side of the brain to include A) Olfactory bulb, brain section 1, brain section 2, brain section, 3 and brain section 4, while cerebellum was discarded. B) Image depicts brain infarct sectioning. On the ipsilateral side, unaffected tissue, peri-infarct tissue and infarct tissue were collected. Reflective brain regions were also collected on the contralateral side of the brain. Cerebellum was discarded.

2.1.3 C57BL/6 mice

2.1.3.1 AT$_2$R mouse cardiac puncture

C57BL/6 mice were weighed at the start of each procedure. Mice were anaesthetised in a box using 1 L/min oxygen and 4% isoflurane. Mice were transferred to a mask where 1 L/min oxygen and 4% isoflurane was continued. After reflex testing, an incision was made below the sternum which continued up both sides of the ribcage. The diaphragm was cut to expose the heart and lungs. Connective tissue attached to the heart was severed to allow the heart to drop within the chest. A 22-gauge needle was inserted into the apex of the heart, piercing into the left ventricle. Blood was drawn of approximately 100-500 µL in volume and collected in BD Vacutainer Plastic Lithium Heparin Tubes (Medisave, UK). Upon completion of cardiac puncture, the heart and lungs were removed to arrest blood flow. The mouse was decapitated and the scull was exposed. The scull was slowly removed, and the brain was exposed. The optic nerve was severed, and the brain was removed from the cranium. Left and right hemispheres were either fixed in 4% PFA or frozen in liquid nitrogen. Collected blood was centrifuged at 2,000 g for 10 minutes, after which time the top plasma layer was collected and stored at -80°C until use.

2.1.3.2 AT$_2$R mouse genotyping

Ear tags were collected by biological services. Ear tag samples were lysed in alkaline lysis reagent and incubated at 95°C for 30 minutes. Samples were then neutralised with neutralising reagent. A volume of 1 µL sample was added directly into a cDNA plate. cDNA mastermix was comprised of 1X Go Taq Buffer (Promega, UK), 40 µM dNTPs (ThermoFisher Scientific, UK), 20 µM MgCl$_2$ (ThermoFisher Scientific, UK), 0.2µM AT$_2$R KO primer 1 (5'-CCACCAGCAGAAACATTACC-3')(Eurofins Genomics, Germany), 0.2µM AT2R KO primer 2 (5'-GAACTACATAAGATGCTTGCCAGG-3') (Eurofins Genomics, Germany), 0.2µM Neo 1 primer (5'-GGCAGCGCGGCTATCGTGG-3') (Eurofins Genomics, Germany), 1.5 U/µL Go Taq polymerase (Promega, UK) and nuclease-free water (Qiagen, UK) to create a maximum reaction volume of 25 µL. The DNA was amplified using the following thermal cycling conditions; one cycle of 95°C for 5 minutes, 30 cycles of 95°C for 30 seconds then 60°C for 30 seconds then 72°C for 45 seconds, followed by one cycle of 72°C for 7 minutes and a hold temperature of 12°C. A 1% agarose gel (ThermoFisher Scientific, UK) was made. cDNA product was combined with 5 µl Blue/Orange Loading Dye, 6X (Promega, UK).

cDNA product was then loaded onto the agarose gel, along with Thermo Scientific™ GeneRuler 100 bp DNA Ladder (ThermoFisher Scientific, UK). The agarose gel was then run for 1.5 hours at 100 volts. The gel was then imaged using the ChemiDox XRS+ system (Bio-Rad, UK). For AT_2R wildtype animals, a single band should be observed at approximately 470 bp. For AT_2R heterozygous animals, two bands should be observed at approximately 470 bp and 800 bp. For AT_2R knockout animals, a single band should be observed at approximately 800 bp.

2.2 *In vitro* methods

2.2.1 Extracellular vesicle methods

2.2.1.1 Precipitation isolation

EVs were isolated from plasma samples from naïve male SHRSPs using Total Exosome Isolation Kit from plasma (ThermoFisher Scientific, UK) as per manufacturer's instructions. Plasma samples were initially centrifuged to pellet residual erythrocytes. The supernatant was then transferred into a new Eppendorf tube. On most occasions EVs were isolated from 200 µL of plasma, to which 100 µL of PBS (ThermoFisher Scientific, UK) was added before 10 µL of Proteinase K was added. The solution was vortexed and incubated at 37°C for 10 minutes. To the solution 60 µL of exosome precipitation reagent (from plasma) was added. The solution was mixed by vortex and was incubated on ice for 30 minutes. The solution was then centrifuged at 10,000 g for 5 minutes for rat plasma or 30 minutes for mice plasma to pellet EVs. EV pellets were resuspended in 200 µL sterile PBS.

2.2.1.2 Ultracentrifugation isolation

Samples requiring EV isolation using ultracentrifugation (UC) were transferred into 13.2 mL, Open-Top Thin wall Ultra-Clear Tubes (Beckman Coulter, UK). UC tubes were then filled to the brim with sterile PBS. UC tubes were inserted into UC spin cylinders of the Optima L-80 XP Ultracentrifuge (Beckman Coulter, UK) and the cylinder was placed in the UC rotor. Samples were then centrifuged at 120,000 g for 1.5 hours at 4°C. After this time, supernatant was discarded, and EV pellets were washed in sterile PBS. UC tubes were then filled to the brim with sterile PBS. UC tubes were inserted into UC spin cylinders and placed within the rotor. Samples were then centrifuged at 120,000 g for 1.5 hours at 4°C. After this time, supernatant was discarded, and EV pellets were resuspended in 200 µL of sterile PBS.

2.2.1.3 Size exclusion chromatography

For initial plasma EV isolation, plasma was centrifuged at 1,500 g for 10 minutes and the supernatant was transferred to a new Eppendorf. Plasma was further centrifuged at 9,000g to remove large particulates. Supernatant was transferred to a new Eppendorf in preparation for SEC isolation. Using qEVsingle/35 nm columns (IZON) EVs were isolated

from 100 µL of cleared plasma with the assistance of Automated Fraction Collector (AFC) (IZON). A total of 4 x 0.2 mL fractions, along with the void volume, were collected and pooled. Using qEVoriginal columns (IZON), EVs were isolated from a maximum of 500 µL of cleared plasma with the assistance of AFC. A total of 3 x 0.5 mL fractions were collected and pooled. For both column types, all pooled fractions were concentrated to approximately 200 µL.

2.2.1.4 Pierce BCA protein assay

Pierce™ BCA Protein Assay Kits (ThermoFisher Scientific, UK) was used to determine protein content as per manufacturer's instructions. A dilution range of 25-2000 µg/mL was used for BCA standards. BCA standards and EVs samples were diluted in sterile PBS. EVs were diluted 1:1 in sterile PBS and a total volume of 10 µL of sample was added to the 96 well plate while a total of 20 µL of standard was added to the plate. BCA working reagent was diluted 50 parts reagent A to 1 part reagent B, after which 200 µL of working reagent was added to each well of the 96 well plate. The plate was incubated at 37°C for 30 minutes protected from light. After this time, the VICTOR X3 multilabel plate reader (Perkins Elmer) was used to measure sample absorbance at a wavelength of 560 nm. BCA standard concentration and absorbance reading were used to create a standard curve from which protein concentration could be derived.

2.2.1.5 Nanoparticle tracking analysis

EVs were characterised by nanoparticle tracking analysis (NTA) using the Malvern NanoSight LM10 (Malvern, UK). Samples were diluted to the appropriate volume to give a range of 30-60 particles per frame with a concentration range of 1×10^{7} to 1×10^{9} particles per mL as per manufacturer's instructions in a 1 mL volume. The sample was then injected into the sample chamber and individual EVs could be visualised under a conventional upright microscope at 20X magnification. A camera attached to the NanoSight was able to capture videos of EVs. A total of 5 videos each 60 seconds in length were taken at various fields of views. Videos were analysed using the NanoSight NTA 3.2 software to provide information on particle concentration and size.

2.2.1.6 EV electroporation loading

EVs were loaded with miRNAs and Ang-(1-9) peptides using electroporation. The desired concentration of EVs were incubated with miRNAs (1 nmol miRNA: 14 µg/µL) or peptides (1mM Ang-(1-9): 1.18 µg/µL; 1mM 5-FAM-Ang-(1-9): 1.58 µg/µL) and 50 mM Trehalose (Merck, UK) for 45 minutes on ice. A volume of 125 µL of EV samples mix was added to 1 mm electroporation cuvettes (Geneflow, UK) and pulsed with 0.4V using a MicroPulse Electroporator (Bio-Rad, UK). Immediately after pulsing 875 µL 1% BSA (Merck, UK) was added to electroporated EVs and thoroughly mixed. Electroporated EV mixes were either immediately re-isolated or kept at 4°C for 24 hours before re-isolation. For UC re-isolation techniques, electroporated samples were transferred to UC tubes and were filled with sterile PBS. Electroporated samples were centrifuged at 120,000g for 1.5 hours at 4°C. After which, supernatant was removed and electroporated EVs were resuspended in PBS. Samples were centrifuged one final time before the electroporated EV pellet was resuspended in 200 µL of sterile PBS and stored at -80°C. For SEC re-isolation techniques, electroporated EV mix was concentrated to approximately 100 µL before isolating using qEVsingle/35 nm columns (IZON) according to previously mentioned methods.

2.2.1.7 PKH26 labelling

EVs were labelled with PKH26 using the PKH26 Red Fluorescent Cell Linker Kit for General Cell Membrane Labelling (Merck, UK). A total of 300 µg of EVs diluted in PBS was ultracentrifuged at 120,000g for 1.5 hours at 4°C. Supernatant was discarded and EVs were resuspended in 1 mL of diluent C and 4 µL of PKH26 label was added and incubated at room temperature for 5 minutes. An equal volume of 5% (w/v) Bovine Serum Albumin (BSA) (Merck, UK) was then added and incubated at room temperature for 1 minute. UC tubes were filled to the top with sterile PBS and were centrifuged at 120,000g for 1.5 hours at 4°C. Supernatant was removed and labelled EVs/control were resuspended in 2 mL of sterile PBS. UC tubes were filled to the top with sterile PBS and were centrifuged at 120,000g for 1.5 hours at 4°C. Supernatant was removed and labelled EVs were resuspended in 200 µL of PBS.

2.2.1.8 RVG-CP05 EV targeting

Cel-miR-39 mimic miRNA was loaded into plasma derived EVs using electroporation. The equivalent of 30 µg of EVs was incubated with 30 µg of Rabies Virus Glycoprotein (RVG) peptide with CP05 linker peptide (CP05-RVG sequence: CRHSQMTVTSRL-YTIWMPENPRPGTPCDIFTNSRGKRASNG; LifeTein, LLC., USA) overnight at 4°C. Conjugated EVs were then washed five times using Millipore 100kDa diafiltration columns (Merck, UK) in PBS-Tween 0.1%. Washed EVs were then concentrated to a volume of approximately 100 µL.

2.2.1.9 Transmission electron microscopy of EVs

Electroporated and non-electroporated EVs were prepared and resuspended in 50 µL of 2 % PFA (Merck, UK). EVs were prepared and imaged using transmission electron microscopy (TEM) by Mrs Margaret Mullin at the University of Glasgow histology facility. TEM imaged were analysed using FIJI software.

2.2.2 Cell culture methods

2.2.2.1 Immortalised cell line maintenance

Under the laminar flow hood, immortalised cells were defrosted from storage in liquid nitrogen, and media was drop added to minimise osmotic shock. Cells were centrifuged at 1,000g for 5 minutes. Supernatant was discarded and cells were resuspended in 10 mL media. Cells were then transferred into T150cm^2 flask and additional media was added to the flask. Cell flasks were incubated at 37°C until confluent. When confluent, media was removed from flasks and cells were washed twice with sterile PBS. Cells were then treated with 3 mL trypsin-EDTA (ThermoFisher Scientific, UK) and incubated at 37°C for 5 minutes. After this time, 10 mL media was added to neutralise the trypsinisation process. Cells were then transferred to a Falcon tube and were centrifuged at 1,000g for 5 minutes. Supernatant was removed and cells were resuspended in media to be further split. Alternatively, cells were cryopreserved in 10% DMSO (Merck, UK) and 90% media and aliquoted into 1 mL cryotubes. A list of immortalised cells, their descriptions and media components can be found in Table 2.3.

2.2.2.2 Primary neuronal cell isolation and cultures

Cell culture plates were coated with 6 µg/mL laminin (ThermoFisher Scientific, UK) and 4 µg/mL poly-D-lysine (ThermoFisher Scientific, UK) in sterile distilled water. Plates were washed with sterile PBS prior to cell plating. Primary neuronal cells were isolated from brains of gestational day 18 SHRSP neonates. Brain tissue was finely chopped and was washed twice in Hanks' Balanced Salt Solution (HBSS) (Merck, UK). Brain tissue in HBSS was transferred to 50 mL Falcon tube and 4 mL of trypsin-EDTA (ThermoFisher Scientific, UK) was added. Brain tissue was incubated at 37°C for 10 minutes and 4 mL of DMEM 10% FBS was added. Sample was titrated with a fine glass pipette. Cells were counted and resuspended in neurobasal media (ThermoFisher Scientific, UK) containing B27 supplement (ThermoFisher Scientific, UK) to form a solution of 1.2x10^6 cells/mL. Cells were plated on coated wells and additional media was added. Information on primary neuronal cell description and media components can be found in Table 2.3.

Table 2.3 Cell lines, descriptions and media components

Cell line	Cell type	Media	Media supplements
B50	Rat neuroblastoma cells	DMEM	• 10% (50 mL Foetal Bovine Serum [FBS] in 500 mL media) FBS (ThermoFisher Scientific, UK) • 100 units/mL (5 mL) Penicillin/Streptomycin mix (ThermoFisher Scientific, UK) • 2 mM (5 mL) L-Glutamine (ThermoFisher Scientific, UK)
GPNT Isolated	Rat cerebral endothelial cells	Ham's F10	• 10% (50 mL FBS in 500 mL media) FBS (ThermoFisher Scientific, UK) • 100 units/mL (5 mL) Penicillin/Streptomycin mix (ThermoFisher Scientific, UK) • 2 mM (5 mL) L-Glutamine (ThermoFisher Scientific, UK)
Primary neuronal cells	SHRSP rat neonatal neuronal cells	NBM	• 10% (50 mL FBS in 500 mL media) FBS (ThermoFisher Scientific, UK) • 2% (10 mL in 500 mL) B27 Supplement (ThermoFisher Scientific, UK) • 100 units/mL (5 mL) Penicillin/Streptomycin mix (ThermoFisher Scientific, UK) • 1.25 mM (5 mL) L-glutamine (ThermoFisher Scientific, UK)

2.2.2.3 Cell-derived EVs

For experiments requiring the production of cell-derived EVs, cell media was created using exosome-depleted FBS (ThermoFisher Scientific, UK) at the same v/v percentage as standard media. Media was collected from cells cultured in EV-depleted media and filtered using a 0.22 µm syringe (Sartorius, UK). EVs were then isolated from filtered culture media using the UC methods above.

2.2.2.4 Oxygen glucose deprivation

Primary neuronal cells were plated at a seeding density of 6×10^4 cells per well in a 96 well plate, while B50s and GPNTs were plated at a seeding density of 1×10^4 cells per well in a

96 well plate. Cells were grown in 96 well plates until approximately 80% confluent. Media was removed and washed twice with sterile PBS. Glucose free DMEM was added before oxygen glucose deprivation (OGD). Lid-less plates were added to the hypoxic chamber (Bilrups-Rothenburg Inc.) and the chamber was clamped shut. Gas mixture was as follows: 1% Oxygen (O_2), 5% Carbon dioxide (CO_2) and 200 bar Nitrogen (N_2) (BOC, Guildford, UK). Both chamber valves were open to allow for flow at a rate of 20 L/min for 4 minutes. The exit valve was then closed, and the oxygen flow was reduced to 10 L/min until the exhaust flow was heard. The entry valve was closed, and the chamber was placed in the incubator for either 3 or 6 hours at 37°C. After this time, the chamber was returned to the hood, media removed and replaced with complete media. Plates were incubated at 37°C for 18 hours reperfusion time. Cells maintained under normal conditions were provided with complete media and were kept in 37°C 5% CO_2 incubator.

2.2.2.5 EV and peptide treatment

All cells were grown and maintained at 37°C with 5% CO_2. EVs were electroporated with either *Cel-miR-39* mimic miRNA (ThermoFisher Scientific, UK), Ang-(1-9) peptide (Phoenix Pharmaceuticals Ltd., US) or 5-FAM-Ang-(1-9) peptide (GenScript, Netherlands). For cells treated with electroporated EVs prior to MTT assay, cells were grown in 96 well plates until approximately 80% confluent. Prior to EV treatment, normal culture media was removed and replaced with EV depleted media. Three EV concentrations 5×10^8, 5×10^9 and 5×10^{10} particles/mL were added to each well under normal culture conditions for 24 hours or during an 18-hour reperfusion phase following a 6-hour OGD phase. For cells treated with Ang-(1-9) peptides, cells were grown in 96 well plates and were treated with 1, 5, 10 and 20 µM of Ang-(1-9) or fluorescent 5-FAM-Ang-(1-9) during normal conditions for 24 hours or during an 18-hour reperfusion phase following a 6 hours OGD phase. For cells treated with PKH26 labelled EVs, 2.5×10^9 particles/mL were added to 6 well plates and were incubated for 3, 6 or 18 hours before cell fixation. For cells treated with *Cel-miR-39* mimic miRNA electroporated EVs with or without conjugated RVG targeting peptide, cells were incubated with EVs for either 4 or 18 hours prior to cell lysis. All EVs were diluted in EV depleted media before applying to cells.

2.2.2.6 MTT assay

Cells were plated and treated with EV or peptides under normal conditions or following OGD. MTT was used from the CyQUANT™ MTT Cell Viability Assay (ThermoFisher Scientific, UK) to determine cell viability. Briefly, 10 µL of MTT solution (0.5 mg/mL) was added to each well of the plate. Plates were shielded from light and incubated at 37°C for 3 hours. Media was then removed and 100 µL of DMSO (Merck, UK) was added to each well to resuspend MTT crystals. Plates were then covered and placed on the rocking shaker for 15 minutes. VICTOR X3 multilabel plate reader (Perkins Elmer) was used to measure sample absorbance at a wavelength of 560 nm. Percentage cell viability was calculated as follows:

$$\% \ viability = \frac{Treated \ cell \ absorbance - Background \ media \ absorbance}{Untreated \ cell \ absrbance - Bckground \ media \ absorbance} \ x \ 100$$

2.2.2.7 Cell fixation and imaging

Cells were incubated with PKH26 labelled EVs or 5-FAM-Ang-(1-9) electroporated EVs or were treated with 5-FAM-Ang-(1-9) peptide to assess potential uptake. Cells were washed 3 times with sterile PBS and were then fixed with 4% PFA (Merck, UK) for 10 minutes at room temperature. PFA was removed and cells were washed 3 times with PBS at 5-minute intervals. Coverslips were removed and washed in distilled water before being mounted face-down on slides with Prolong Gold with DAPI. Slides were left to dry overnight at room temperature and were then refrigerated until imaging. Slides were imaged using the Olympus IX71 inverted microscope (Olympus) with pE0300 series microscope illuminator (CoolLED, UK) at 40x magnification and imaged using QCapture Pro software (Teledyne Photometrics). Images were merged using FIJI software.

2.2.2.8 Immunocytochemistry

Cells were grown until approximately 80% confluent. Cells were washed 3 times with sterile PBS and were then fixed with 4% (w/v) PFA for 10 minutes at room temperature. PFA was removed and cells were washed 3 times with PBS at 5-minute intervals. Cells were permeabilised with PBST (PBS with 0.1% (v/v) Triton X) for 10 mins at room temperature. Cells were washed 3 times with PBS at 5-minute intervals. Cells were

blocked with 10% (v/v) goat serum in PBS for 30 minutes at room temperature. Cells were washed once with PBS at 5-minute intervals. Cells were incubated with the Anti-Nicotinic Acetylcholine Receptor beta 2/CHRNB2 primary antibody (ab41174, Abcam, UK) (1:100, 1:200 and 1:300 dilution factor; dilute in 1% (v/v) goat serum) and 1or IgG control (1:100 dilution factor) for 1 hour at room temperature. Cells were washed 3 times with PBS at 5-minute intervals. Cells were incubated with Goat anti-Rabbit IgG (H+L) Cross-Adsorbed ReadyProbes™ Secondary Antibody, Alexa Fluor™ 488 (ThermoFisher Scientific, UK) diluted to 1:500 diluted in PBS for 1 hour at room temperature. Cells were washed 3 times with PBS at 5-minute intervals. Coverslips were removed and washed in distilled water before being mounted face-down on slides with ProLong™ Gold Antifade mount with DNA Stain DAPI (ThermoFisher Scientific, UK). Slides were left to dry overnight at room temperature and then refrigerated. Slides were imaged using the Olympus IX71 inverted microscope (Olympus) with pE0300 series microscope illuminator (CoolLED, UK) at 40x magnification and imaged using QCapture Pro software (Teledyne Photometrics). Images were merged using FIJI software.

2.2.3 Gene and miRNA expression analysis

2.2.3.1 RNA extraction

RNA was isolated from approximately 50 mg of tissue or cells grown in 6 well plates. RNA was isolated from lysed samples using the miRNeasy extraction kit (Qiagen, UK) according to manufacturer's instructions. Briefly, a total of 700 µL of QIAzol Lysis Reagent (Qiagen, UK) and one 5 mm stainless steel bead (Qiagen, UK) were added to tissue samples and samples were homogenised using the Tissue Lyser Universal Laboratory Mixer-Mill Disruptor (Qiagen, UK) at two repetitions of 30 Hz for 20 seconds. To the homogenised sample 140 µL of chloroform was added before the tube was vigorously shaken and incubated at room temperature for 3 minutes. Samples were then homogenised for 15 minutes at 4°C after which the clear, top aqueous layer was transferred into a new Eppendorf, to which 525 µL of 100% ethanol was added and mixed. A maximum volume of 700 µL of the solution was transferred to a 2 mL RNeasy spin column and was centrifuged at 8,000 g for 15 seconds at room temperature and the flow through was discarded. This step was repeated if the sample volume following the addition of ethanol was greater than 700 µL. A total of 700 µL of RWT buffer was added to the column and was centrifuged at 8,000 g for 15 seconds at room temperature and the flow through was discarded. Then 500 µL of RPE buffer was added to the column and was

centrifuged at 8,000 g for 2 minutes at room temperature and the flow through was discarded. The column was then dried by centrifugation at 8,000g for 2 minutes at room temperature. The column was then transferred to a new Eppendorf and 50 µL of RNase free water was added to the column and incubated at room temperature for 1 minute. The column and was centrifuged at 8,000 g for 1 minute at room temperature and the RNA was collected. The RNA was eluted back into the column and centrifuged one final time at 8,000 g for 1 minute at room temperature and the RNA was collected for quantification. For EV-derived miRNA extraction, EV preparations were spiked with 20 pg of an exogenous *Cel-miR-39* miRNA to use as a spike in housekeeper before (mi)RNA extraction.

2.2.3.2 Nanodrop quantification

The NanoDrop 1000 spectrophotometer (ThermoFisher Scientific, UK) was used to quantify the concentration of RNA samples. All samples were stored on ice during measurement.

2.2.3.3 miRNA reverse transcription

Reverse transcription (RT) product was created from 5 ng RNA samples using TaqMan™ MicroRNA Reverse Transcription Kit (ThermoFisher Scientific, UK) containing 0.75mM dNTPs, 3.33 U/µL MultiScribe reverse transcriptase, 1X RT buffer, 2.5 U/µL RNase inhibitor, RNase free water and 1 µL of 5X sample probe to create a final volume of 7.5 µL. Samples underwent amplification using the following thermal cycling profile: 16°C for 30 minutes, 42°C for 30 minutes, 85°C for 5 minutes and 12°C until removal from block. Plates were stored at -20°C prior to qPCR. For EV-derived miRNA cDNA plates, a second housekeeping *A. thaliana* spike (50 pg) was introduced to the mastermix. A list of housekeeping miRNA probes can be found in Table 2.4, while a list of miRNAs of interest can be found in Table 2.5.

Table 2.4 List of housekeeping miRNA probes

Gene	ThermoFisher Assay ID	Dye	Species
U87	001712	FAM	Rat

Table 2.5 List of miRNA probes of interest

Gene	ThermoFisher Assay ID	Dye	Species
Mir29a	002247	FAM	Mouse
Mir33a	465396_mat	FAM	Human
Mir132	000457	FAM	Mouse
Mir146a	000468	FAM	Rat
Mir155	002571	FAM	Mouse
Mir188	002320	FAM	Mouse
Mir212	461768_mat	FAM	Mouse
Mir483	002560	FAM	Mouse
Cel-miR-39	000200	FAM	Rat
Ath-miR159a	000338	FAM	Rat

2.2.3.4 cDNA synthesis

cDNA was created from 1 µg RNA samples using TaqMan™ Reverse Transcription Reagents (ThermoFisher Scientific, UK) containing 0.5 mM dNTPs, 2.5 U/µL MultiScribe reverse transcriptase, 1X RT buffer, 1 U/µL RNase inhibitor, 2.5 µM random hexamers,

5.5 mM MgCl$_2$ and RNase free water to a total volume of 20 µL. The thermocycle profile was as follows: 25°C for 10 minutes, 48°C for 30 minutes, 95°C for 5 minutes and 12°C until removal from block. Plates were stored at -20°C prior to qPCR.

2.2.3.5 Quantitative real-time polymerase chain reaction

Appropriate Taqman™ probes (ThermoFisher Scientific, UK) was combined with TaqMan™ Universal Master Mix II (ThermoFisher Scientific, UK). cDNA product was taken directly from the cDNA plate and combined with Taqman mastermix to form a maximum volume of 10 µL. The thermocycle profile was carried out at 95°C for 15 seconds and 60°C for 60 seconds for a total of 40 cycles using QuantStudio 12K Flex Real-Time PCR System (ThermoFisher Scientific, UK). A list of housekeeping gene probes can be found in Table 2.6, while a list of genes of interest can be found in Table 2.7.

Table 2.6 List of housekeeping gene probes

Gene	ThermoFisher Assay ID	Dye	Species
ACTB	Rn00667869_m1	FAM	Rat
B2M	Rn00560865_m1	FAM	Rat
GAPDH	Rn01775763_g1	VIC	Rat
HPRT1	Rn01527840_m1	FAM	Rat
UBC	Rn01499642_m1	FAM	Rat

Table 2.7 List of genes of interest probes

Gene	ThermoFisher Assay ID	Dye	Species
ACE	Rn00561094_m1	FAM	Rat
ACE2	Rn01416293_m1	FAM	Rat
AGTR1A	Rn02758772_s1	FAM	Rat
AGTR2	Rn00560677_s1	FAM	Rat
BDNF	Rn01484928_m1	FAM	Rat
CHRNB2	Rn00570733_m1	FAM	Rat
CLAUDIN 5	Rn01753146_s1	FAM	Rat
IL10	Rn99999012_m1	FAM	Rat
IL1	Rn00580432_m1	FAM	Rat
111B	Rn00580432_m1	FAM	Rat
IL6	Rn01410330_m1	FAM	Rat
MAS1	Rn00562673_s1	FAM	Rat
NFKB	Rn01399572_m1	FAM	Rat
RUNX1	Rn01645281_m1	FAM	Rat
TGFA	Rn00446234_m1	FAM	Rat
TGFB1	Rn00572010_m1	FAM	Rat
TNF	Rn99999017_m1	FAM	Rat
VEGFA	Rn01511602_m1	FAM	Rat
VEFGB	Rn01454585_g1	FAM	Rat

2.2.4 Western Blotting

EVs were isolated and protein content was determined using BCA. EVs (30 µg) were lysed in RIPA buffer (Merck, UK) containing protease and phosphatase inhibitor (PPI) (RIPA:EVs; 5:1) and needle sonicated at 20 Hz for 5 seconds on three occasions. EVs of the appropriate concentration for each antibody were mixed with NuPAGE™ LDS sample buffer 4X (ThermoFisher Scientific, UK) and incubated at 95°C for 5 minutes. Pre-set NuPAGE™ 10%, Bis-Tris Midi protein gel (ThermoFisher Scientific, UK) was placed in the electrophoresis tank (BioRad, UK) and were submerged in MES SDS running buffer (ThermoFisher Scientific, UK). The gel comb was removed, and EV samples and Chameleon® Duo Pre-stained Protein Ladder (LI-COR Biosciences Ltd., UK) were added to gel wells. The gel was run at 120 volts until the sample dye had almost run off the gel. Proteins were then transferred from the gel to Power Blotter Pre-cut Membrane (ThermoFisher Scientific, UK) using Power Blotter–Semi-dry Transfer System (ThermoFisher Scientific, UK). Membranes were then blocked for 1 hour using SEA BLOCK (ThermoFisher Scientific, UK), and were washed in TBST (TBS with 0.05% Tween-20). Membranes were incubated with primary antibodies overnight at 4°C. A list of primary antibodies and dilutions can be found in Table 2.8 List of Primary and Secondary Antibodies used for Western Blotting.Table 2.8. Membranes were then further washed in TBST and incubated with secondary antibodies for 1 hour at room temperature. A list of secondary antibodies and dilutions can be found in Table 2.8. Membranes were washed before imaging using Licor Odyssey CLx at the appropriate wavelength.

Table 2.8 List of Primary and Secondary Antibodies used for Western Blotting.

Antibody	Company	Catalogue number	Dilution Factor
Annexin A2	Abcam	ab189473	1:5000
CD81	Santa Cruz Biotechnology	sc-166029	1:500
TSG101	Abcam	ab125011	1:5000
Annexin XI	Santa Cruz Biotechnology	sc-46686	1:200
CD9	Abcam	ab92726	1:2000
CD63	Abcam	ab59479	1:2000
Goat anti-Mouse	ThermoFisher Scientific	A11357	1:15000
Goat anti-Rabbit	ThermoFisher Scientific	A11367	1:15000

2.2.5 Ang-(1-9) ELISA

The concentration of Ang-(1-9) in various samples were analysed using Angiotensin 1-9 ELISA Kit (Generon, UK) as per manufacturer's instructions. Briefly, Ang-(1-9) electroporated EVs were lysed in 1X RIPA containing PPI while Ang-(1-9) peptide was diluted in PBS. Ang-(1-9) standards were created ranging from 12.35 to 1,000 pg/mL. Detection reagent A and B were diluted 1 in 100 in assay diluent as per the manufacturer's instructions. A total of 50 µL of PBS, peptide or EVs were added to a 96 well plate, before adding 50 µL of detection reagent A. The plate was sealed and incubated for 1 hour at 37°C. Each well was washed with 350 µL of wash buffer four times. A total of 100 µL of detection reagent B was added to each well and the plate was sealed and incubated for 1 hour at 37°C. Each well was washed with 350 µL of wash buffer five times. A volume of 90 µL of substrate solution was added to each well and the plate was sealed and incubated for 10-20 minutes at 37°C protected from light. To stop the reaction, 50 µL of stop solution was added to each well and the absorbance was immediately measured using the VICTOR X3 multilabel plate reader at a wavelength of 450 nm. Ang-(1-9) standard concentration and absorbance reading were used to create a standard curve from which Ang-(1-9) EV or peptide concentration could be derived.

2.2.6 NanoFC

NanoFC studies were conducted in the lab of Dr Ryan pink at Oxford Brookes University under the guidance of Mr Jamie Cooper. EV surface markers were analysed using nano flow cytometry (nanoFC). To prepare antibodies of interest, Dynabeads Protein G (Invitrogen, UK) were used to concentrate antibodies as per manufacturer's instructions. EVs were diluted to a concentration of $1x10^9$ events/mL and were incubated with Carboxyfluorescein succinimidyl ester (CFSE) (Abcam, UK) for 30 minutes at 37°C. CFSE-EVs were then incubated with 0.75 µg/mL of CD81 antibody (BioLegend, UK) and 3 µg/mL CD63 antibody (BioLegend, UK) EV markers for 1 hour at 37°C. To this mixture 3 µg/mL CD41 antibody (BioLegend, UK) and 2 µg/mL CD31 antibody (BioLegend, UK) were added and incubated for 1 hour at 37°C. IgG controls were used at the same concentration as the antibodies of interest. Samples were loaded in duplicate into 96 well plate and inserted into the Amnis CellStream flow cytometer (Luminex, UK). CellStream parameters and flow cytometry gating strategy was performed by Mr Jamie Cooper from Oxford Brookes University, United Kingdom. The number of events related to each marker were normalised to background CFSE staining.

2.2.7 Statistical analysis

Data generated in this thesis was initially curated in Excel. Measurements such as averages, standard error of the mean (SEM) or equations related to CT values were also analysed using Excel. For higher power statistical analysis GraphPad Prism version 10 was used whereby significance was deemed to be $p<0.05$. Details of statistical calculations can be found in figure legends below results figures. In instances where there were two unpaired groups with differing standard deviations, a Welches t-test was carried out. In instances where there were two paired groups, Gaussian distribution was assumed and a paired t-test was carried out. In unmatched/unpaired or matched/repeated groups larger than two, a One-way ANOVA was carried out assuming Gaussian distribution. Multiple comparisons were carried out comparing the mean of each column with every other column. For matched/repeated data equal variables of difference were assumed and a post-hoc Tukey's was carried out on the multiple comparisons. If the standard deviation was not assumed to be equal for the unmatched/unpaired data, then Brown-Forsythe and Welch ANOVA was conducted with post-hoc Dunnett's T3 multiple comparison. In incidences where there were matched or repeated measures then the data was analysed using a Repeated measures of mixed-effect with post-hoc Tukey's multiple comparison test.

D'Agostino-Pearsons omnibus normality test, Anderson-Darling test, Shapiro-Wilk normality test or Kolmogorov-Smirnov normality test, was carried out on all data assuming Gaussian distribution. One-way ANVOA Outliers were identified using ROUT test at an aggressive value of $Q=1\%$ unless otherwise stated. If outliers were identified in matched/paired samples, then all matched/paired numerical values for the sample were removed from all comparisons. To understand correlation, Gaussian distribution was assumed, and Pearsons' correlation coefficient was used. Power calculations for group sizes required in this investigation were carried out by Dr Lorraine Work in consultation with statistician Dr John McClure. A sample size of 12 per group was calculated as sufficient enough to detect a difference in infarct size and neurological assessments at a power of 80% and a significance level of 5% using ANOVA with post-hoc analyses.

Chapter 3: Do renin angiotensin aldosterone system targeting interventions effect post-stroke functional outcomes?

3.1 Introduction

The function of RAAS is important for normal homeostasis and has been mechanistically described in the introduction chapter of this thesis. Briefly, RAAS can be characterised into two main axes, the classical and counter-regulatory axes. In the classical axis, Angiotensinogen is cleaved by renin to form angiotensin I (Ang I). Ang I is broken down by angiotensin converting enzyme (ACE) to form Angiotensin II (Ang II), the functional ligand of the angiotensin II type I receptor (AT_1R). Activation of the AT_1R is known to cause vasoconstriction, inflammation, oxidative stress, fibrosis, and apoptosis (Wynne et al., 2009, Wang et al., 2012, Griendling et al., 2000). Within the counter-regulatory axis, Ang I can be converted to Angiotensin-(1-9) [Ang-(1-9)] under the action of angiotensin converting enzyme 2 (ACE2). Ang-(1-9) is a functional ligand of the angiotensin II type II receptor (AT_2R). Activation of AT_2R can lead to vasodilation, cell growth, remodelling and apoptosis (Abadir et al., 2003, Savoia et al., 2005, Siragy and Carey, 1999). Ang I can be converted to Angiotensin-(1-7) [Ang-(1-7)] by Neprilysin (NEP), or alternatively, Ang II can be converted to Ang-(1-7) by ACE2. Additionally, Ang-(1-9) may be broken down by ACE to form Ang-(1-7). Ang-(1-7) is the functional ligand of the Mas receptor (MasR), which when activated, can lead to vasodilation, reduced inflammation, and reduced remodelling (Sukumaran et al., 2012, Souza Á et al., 2013). Other extensions of RAAS exist outside of the conventional classical and counter-regulatory axes, such as the insulin-regulated membrane aminopeptidase (IRAP), Angiotensin II type IV receptor (AT_4R) which is activated by Angiotensin IV (Ang IV). Stimulation of AT_4R has been shown to increase calcium uptake within the brain and is associated with increased synaptic transmission and potentiation of hippocampal neurons (Davis et al., 2006).

To treat certain diseases, components of RAAS may be modulated by RAAS-specific interventions. Clinically, targeting components of RAAS may be achieved by direct renin inhibitors (DRI), Angiotensin converting enzyme inhibitors (ACEi) and Angiotensin receptor blockers (ARBs) (Ma et al., 2010). Aside from inhibitors, also referred to as antagonists, agonists, or activators, may also be used to modulate RAAS. From the

publications analysed in this systematic review, several RAAS targeting agonists and antagonists (herein referred to as RAAS targeting interventions) were assessed to determine their benefits in preclinical stroke models. These RAAS targeting interventions are known to interact with the AT_1R, AT_2R, MasR and AT_4R components of RAAS. Specifically, studies used ARBs, Valsartan and Candesartan to antagonise the AT_1R of the classical axis of RAAS. Within the counter-regulatory axis of RAAS, the AT_2R was activated by the agonists CGP42112 or Compound 21 (C21) and activation was antagonised by PD123319. Further, Ang-(1-7) was used to activate the MasR while A779 was used to antagonise MasR. AT_4R neutralising antibodies were used to antagonise AT_4R (Figure 3.1). Although other forms of RAAS targeting interventions exist, the aforementioned interventions were investigated by publications that met the inclusion criteria of this systematic review protocol and their impacts in preclinical stroke models will be discussed in depth in this chapter.

Activation or inhibition of RAAS is widely used to treat cardiovascular disease (CVD), mainly hypertension. Administration of direct inhibition of renin can be used to reduced hypertension, while hypertensive patients treated with ACEi have a reduced rate of major adverse cardiac events and even death (Yusuf et al., 2000, Jamerson et al., 2008, Stanton et al., 2003). Aside from treating hypertension, ARBs are also used to treat diabetic nephropathy in type 2 diabetes, chronic heart failure and migraines (National Institute for Health and Care Excellence, 2023a, National Institute for Health and Care Excellence, 2024b, National Institute for Health and Care Excellence, 2024a). As the leading modifiable risk factor for stroke is hypertension, RAAS targeting interventions are used to decrease blood pressure in hypertensive patients, reducing the risk of stroke (GBD 2019 Stroke Collaborators, 2021). This has been demonstrated in clinical trials, such as the notable PROGRESS trial, whereby stroke risk was reduced following dual treatment with ACEi thiazide diuretics in both hypertensive and non-hypertensive patients with prior history of stroke or transient ischaemic attack (PROGRESS Collaborative Group, 2001). Post-hoc analysis of the BP TARGET clinical trial identified that acute ischaemic stroke patients receiving RAAS inhibitors displayed better post-stroke neurological outcomes compared to patients not receiving RAAS inhibitors (Maïer et al., 2022). Combining these findings, RAAS targeting interventions have been shown to reduce stroke risk and better functional outcomes post-stroke.

Following acute stroke, patients are neurologically assessed to determine the impacts of stroke on functional outcomes. Neurological assessments include, but are not limited to, the NIH Stroke Scale (NIHSS), Glasgow Coma Scale and Rankin Scale, all of which

assess cognitive and motor function post-stroke (Brott et al., 1989, Teasdale and Jennett, 1974, Rankin, 1957). Additionally, imaging techniques can be used to assess the size of ischaemic lesions in stroke patients that provide key insights into patient treatment plans. In preclinical models, neurological and infarct assessments can be conducted following experimental stroke to provide information about the neurological impacts of stroke and are similar to neurological assessments conducted in humans (Bederson et al., 1986). There are a wide range of preclinical neurological assessments, several of which will be discussed in length in this systematic review. One benefit of using preclinical models in stroke research is that biological samples are more readily available, such as whole brain homogenates. With this, in-depth, tissue specific analyses can be carried out to better understand how disease may affect a given organ, or, alternatively, how one tissue-specific disease may affect the whole system. Using experimental models of stroke, novel therapies may be produced, or new drug targets may be identified that are beneficial post-stroke, some of which may already be widely understood in the context of other diseases.

By targeting the counter-regulatory axis of the RAAS and activating protective downstream mechanisms, such as anti-inflammatory or growth mechanisms, post-stroke outcomes may be improved. Studies investigating the effects of RAAS targeting interventions in preclinical models are compelling and will be discussed in detail in this systematic review. Interventions targeting the RAAS have been assessed in experimental stroke models, however animal species/strain, stroke model, type of intervention, intervention concentration, administration timing and route of administration vary between studies. It is for this reason a systematic review of published, peer-review studies was conducted in order to compare studies assessing the effects of RAAS interventions in preclinical stroke models. With this, similarities and differences were identified and discussed in length, providing insight into the potential therapeutic effects of RAAS targeting interventions post-stroke.

Figure 3.1 Illustration of how notable interventions target aspects of the RAAS.
Within the classical axis of the RAAS, angiotensin IV (Ang IV) is the functional ligand of
the angiotensin II type IV receptor (AT_4R). The AT_4R can be antagonised by AT_4R
neutralising antibodies. Angiotensin II is the functional agonist of the angiotensin II type I
receptor (AT_1R), while Valsartan and Candesartan are antagonist of the AT_1R. The Mas
receptor (MasR) can be activated by the functional ligand Angiotensin-(1-7) [Ang-(1-7)],
while MasR can be antagonised by A779. CGP42112 and Compound 21 (C21) can agonise
the AT_2R, while PD123319 can agonise AT_2R. Agonists are highlighted in dark blue while
antagonists are highlighted in light blue. Figure created in BioRender.

3.1.1 Hypotheses and Aims

3.1.1.1 Hypothesis

RAAS targeting interventions will improve post-stroke functional outcomes in preclinical models of stroke.

3.1.1.2 Aim

To systematically review data from peer reviewed journals to assess post-stroke neurological outcomes, infarct volume and expression profiles following treatment with RAAS targeting interventions in preclinical stroke models.

3.2 Methods

3.2.1 Study design

A search strategy entitled "Do components of the counter-regulatory axis of the renin angiotensin aldosterone system effect post-stroke functional outcomes?" was designed and published on SyRF systematic Review Facility published on 28th September 2020 and can be found at https://syrf.org.uk/protocols. Two searches were conducted on 29th September of 2020 and 11th November of 2021 using MEDLINE and EMBASE databases, after which results were identified and screened relative to inclusion exclusion criteria to provide a bank of appropriate studies.

3.2.2 Screening

Titles and abstracts obtained from the search strategy were screened by two independent researchers (Rebecca Rooney [RR] and Lorraine Work [LMW]) using the SyRF screening application to assess their eligibility. Studies were then selected for inclusion after full-text analysis by two independent researchers (RR, LMW). A consensus was met between reviewers to resolve any inclusion/exclusion differences.

3.2.3 Specified outcome measures

Specified post-stroke outcome measurements included the following:

- Neurological outcomes
- Infarct volume
- Expression levels of relevant peptides or cognate receptors.

3.2.4 Inclusion and exclusion criteria

Inclusion criteria:

- Interventions that target the counter-regulatory axis of RAAS (limited to: Ang-(1-9), Ang- (1-7), C21, AT_2R agonist/antagonists) in preclinical and clinical models of stroke (patients/animals).

- Clinical case series and observational cohorts. For interventional trials, the potential effect of the intervention on the counter-regulatory axis of the RAAS will be considered and a study level decisions will be made on inclusion of complete data or only inclusion of control arm data (if available).

- Animal models and studies in humans of all ages and both sexes.

- Any dose of RAAS targeting interventions delivered at any point in preclinical stroke models or controlled trial setting, given time before humane killing or discharge from study.

- English language papers only.

- Publications published during or after 1990.

- Papers published in peer reviewed scientific journals.

Exclusion criteria:

- Non-stroke studies (e.g. we will not include traumatic brain injury and subarachnoid haemorrhage).

- Human patients < 18 years of age.

- No outcome measure described.

- Non-English language papers.

- Publications published before 1990.

- Publications not published in peer reviewed scientific journals – such as published abstracts theses, posters.

3.2.5 Cohort analysis

Paper title, author, year of publication, stroke model, assessments and intervention were itemised. Titles of neurological and infarct volume assessments, along with gene, protein or mRNA expression analysis were directly taken from papers. However, in the instance where a research group described a scored functional assessment as "modified point-scale"

a new category was created for point scales. If the descriptions of these point scales matched those in other papers, they were grouped together.

3.2.6 Data extraction

Data were extrapolated from published figures using WebPlotDigitizer (https://apps.automeris.io/wpd/) for all studies to standardise data extraction method between studies and entered into standardised spreadsheets.

3.2.7 Comparisons and statistical analysis

Assessments were categorised and scored against frequency within paper text. For assessments receiving a score of ≥3, whereby 3 or more studies used a specific assessment method, in-depth comparisons were made. For assessments receiving a score of ≤2 whereby less than 2 studies used a specific assessment method, brief comparisons were made. Fold change was used as a measure of improvement or decline after intervention. Fold change was determined as:

$$Fold\ change = \frac{B - A}{A}$$

Using this equation, A was the initial value, for example the value of the control, while B was the final value, for example the value following intervention. For comparisons that were statistically significant, statistics were taken directly from the paper text, whereby $p < 0.05$ was considered significant. For ease of comparing the effects of RAAS targeting intervention in preclinical models of stroke, all individual outcomes were arranged in terms of animal species and strains.

3.3 Results

3.3.1 Inclusion of reviewed literature

Searching both the MEDLINE and EMBASE databases for the terms included in the search strategy led to the identification of 414 records. A total of 354 records were excluded as they did not meet the inclusion criteria. Sixty records were taken forward for abstract screening and a further 13 studies were excluded. Full text screening was conducted on 47 records, from which a further 20 were excluded and 27 publications were taken forward for final data analysis.
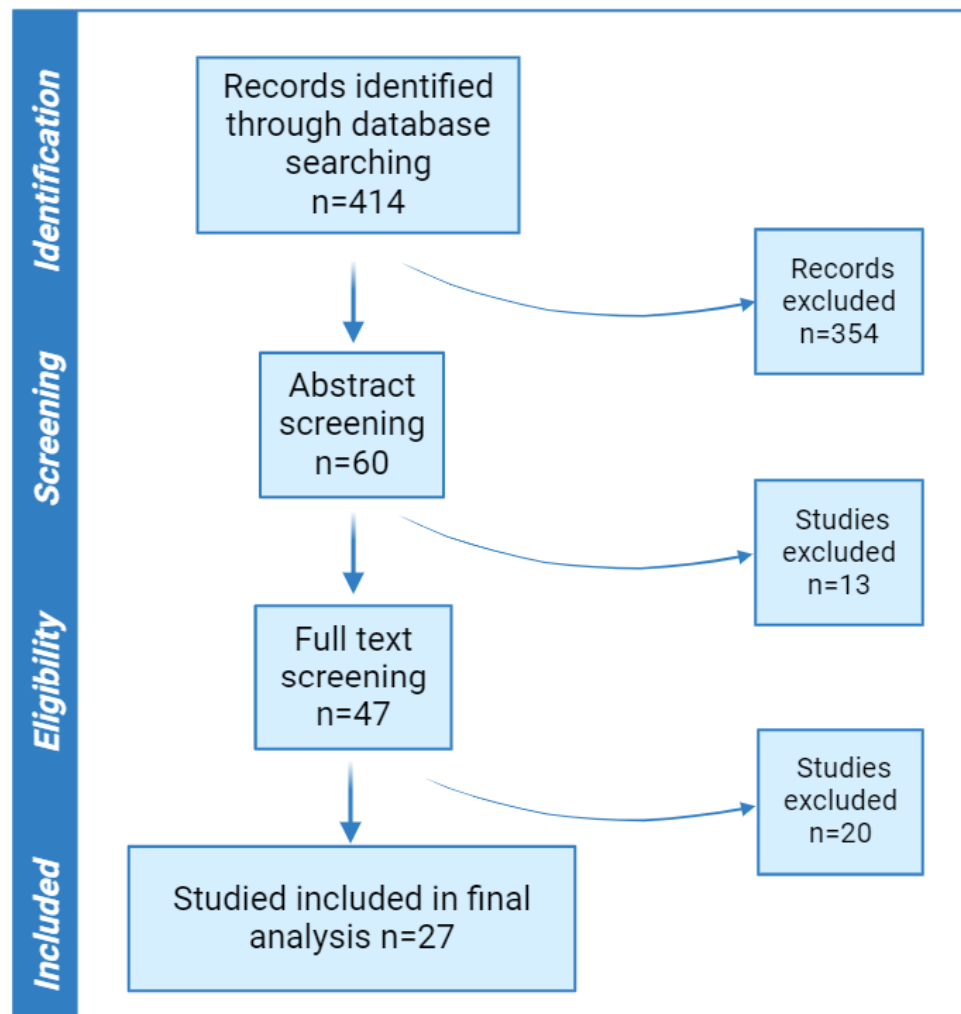
Figure 3.2 PRISMA flow diagram of reviewed literature.
Articles were excluded using a set of inclusion/exclusion criteria. Studies that included diseases other than ischaemic stroke and those that did not provide a relative intervention were excluded. From the 414 records identified a total of 27 studies were included in the final review.

3.3.2 Effects of RAAS targeting interventions on neurological outcomes post-stroke

Neurological outcomes are commonly used as a functional outcome post-stroke. Compared to baseline measurements, stroke significantly reduces functional outcomes in the acute phase post-stroke, while in the recovery/rehabilitation functional outcomes gradually improve before ultimately plateauing (Kwakkel et al., 2003). There are various forms of neurological assessments used in the field of preclinical stroke research, as outlined in this systematic review and other publications (Hietamies et al., 2018). A total of 25 publications included in this systematic review assessed neurological outcomes post-stroke, with a total of 27 different types of neurological assessments identified. Of the 27 neurological assessments identified, a total of 10 assessment types were used by 3 or more publications, as outlined in Table 3.1.

The beam test was the most common form of neurological assessment, whereby a total of 8 publications used beam test to assess the effects of RAAS targeting interventions on post-stroke neurological outcomes (Ahmed et al., 2018, Alhusban et al., 2015, Eldahshan et al., 2019, Fouda et al., 2017, Ishrat et al., 2019, McCarthy et al., 2014, McCarthy et al., 2009, McCarthy et al., 2012). The second most common method of neurological assessment was Bederson (0-3) test which was used in a total of 7 publications included in this systematic review (Ahmed et al., 2019, Ahmed et al., 2018, Bennion et al., 2018a, Bennion et al., 2017, Fouda et al., 2017, Joseph et al., 2014, Bennion et al., 2018b). The third most common assessment method, Garcia score (0-18), was used by a total of 4 publications to assess the effects of RAAS interventions on post-stroke neurological outcomes (Bennion et al., 2018a, Bennion et al., 2017, Joseph et al., 2014, Schwengel et al., 2016). Of the remaining assessment types, 4 publications used NOR (Ahmed et al., 2019, Ishrat et al., 2019, Jackson-Cowan et al., 2021), 4 publications used Bederson 5-point score (Alhusban et al., 2015, Eldahshan et al., 2019, Min et al., 2014, Jiang et al., 2014), 3 publications used a 5-point scale (Shan et al., 2018, Iwai et al., 2004, Lee et al., 2012) 3 publications used passive avoidance test (Ahmed et al., 2018, Ahmed et al., 2019, Eldahshan et al., 2021), 3 publications assessed paw grasp (Alhusban et al., 2015, Eldahshan et al., 2019, Ishrat et al., 2019), 3 publications used rotarod test (Alhusban et al., 2015, Bennion et al., 2017, Ishrat et al., 2019), and 3 publications used paw adhesive to assess the effect of RAAS targeting interventions post-stroke (Bennion et al., 2017, Bennion et al., 2018b, Jackson et al., 2020).

Table 3.1 Classification of post-stroke neurological assessments

Main Intervention	Author	Neuroscore										Memory & Cognition									Sensory & Motor							
		Bederson (0-3)	Garcia Score (0-18)	Bederson (5-point)	5-point scale	Bedersons (0-8)	7-point scale	Bedersons (6-point)	Bedersons (4-point)	Modified neurological severity score	18-point score	Novel object recognition	Passive avoidance test	Morris water maze	2-trail Y maze	Step test	Object placement	Elevated plus maze	Open field test	Spontaneous alternation performance	Beam test	Paw adhesive test	Paw grasp	Rotarod test	Grip strength	Hang test	Forelimb placement	Body swing
C21	Ahmed et al., 2018	1										1	1							1								
	Ahmed et al., 2019	1										1	1	1														
	Alhusban et a.,. 2015			1					1												1		1	1	1			
	Bennion et al., 2018	1	1																			1						
	Bennion et al., 2017	1	1																					1				
	Eldahshan et al., 2019				1	1															1		1					
	Eldahshan et al., 2021				1								1				1	1	1		1							
	Fouda et al., 2017	1																			1							
	Ishrat et al., 2019							1				1									1		1	1	1			
	Jackson et al., 2020														1							1						
	Jackson-Cowan et al., 2021											1			1													
	Joseph et al., 2014	1	1																									
	Mateos et al., 2016					1																						
	McCarthy et al., 2014																				1							
	Min et al., 2014			1																								
	Schwengel et al., 2016		1																									
	Shan et al., 2018						1																					
Ang-(1-7)	Arroja et al., 2019										1																	
	Bennion et al., 2018	1																				1						
	Jiang et al., 2014			1																								
	Kuipers et al., 2020									1						1											1	1
Other	Iwai et al., 2004			1																								
	Lee et al., 2012				1																					1		
	McCarthy et al., 2009																				1							
	McCarthy et al., 2012																				1							
Total number of studies		7	4	4	3	2	1	1	1	1	1	4	3	1	2	1	1	1	1	1	8	3	3	3	2	1	1	1

3.3.2.1 Bederson (0-3) score

A total of 7 studies used Bederson (0-3) score to determine the effects of the RAAS interventions on neurological outcomes post-stroke (Ahmed et al., 2018, Ahmed et al., 2019, Bennion et al., 2018a, Bennion et al., 2017, Fouda et al., 2017, Joseph et al., 2014, Bennion et al., 2018b). Four of these studies investigated the effects of RAAS targeting interventions on Sprague-Dawley (SD) rats following MCAO, while 2 of these studies assessed the effects of RAAS targeting interventions on Wistar rats following either transient MCAO (tMCAO) or permanent MCAO (pMCAO). Only one study looked at the effects of RAAS targeting interventions on spontaneously hypertensive (SHR) rats following tMCAO. RAAS targeting interventions used in the following studies included C21, Ang-(1-7), Candesartan and PD123319, with or without IL-10 antibodies.

A low Bederson score is indicative of a better functional outcome, as such improvements in Bederson score, as shown by fold-change, may be presented as a negative value. Neurological outcomes were largely improved across various studies and interventions at multiple assessment timepoints. For example, SD rats treated with C21 (0.03 mg/kg; intraperitoneal injection [i.p.]) following endothelin-1 (ET-1) middle cerebral artery occlusion (MCAO) [ET-1-MCAO] demonstrated improved Bederson score (0-3) by day 3 (-0.31-fold change) until day 21 (-0.53-fold change) post-stroke compared to saline control at each time point ($p<0.05$) (Bennion et al., 2017). In a related study, SD rats subjected to pMCAO and treated with C21 (1.5 µg/kg intranasal [i.n.]) post-stroke showed improvement in Bederson (0-3) score at 24 hours (-0.70-fold change; $p<0.01$) and 72 hours (-0.46-fold change; $p<0.05$) post-stroke compared to saline control (Bennion et al., 2018a). Further, C21 (0.03 mg/kg; i.p.) delivered to SD rats following pMCAO led to an improvement in Bederson score (0-3) (-0.77-fold change) compared to saline controls 24 hours post-stroke ($p<0.05$) and by day 3 post-stroke (-0.75-fold change) depending on administration time ($p<0.05$). Pre- and post-stroke treatment with C21 significantly improved Bederson score (0-3) at a concentration of 0.03 mg/kg (-0.89-fold-change) or 0.1 mg/kg (-0.88-fold change) compared to saline control by day 3 post-stroke ($p<0.05$). Pre-treatment of C21 (0.0075 µg/µL/h) intracerebroventricularly for 7 days before stroke led to an improvement in Bederson score (0.3) compared to vehicle control on day 3 post stroke ($p<0.05$). However, administration of PD123319 (0.3 µg/µL/h; intracerebroventricular administration [i.c.v.]) annulled these protective effects (Joseph et al., 2014). When SD rats were subjected to tMCAO and treated with Ang-(1-7) (125 µg/kg; oral) Bederson score (0-3) was improved by day 3 (-0.25-fold change) compared to day 0 ($p<0.05$) (Bennion et al.,
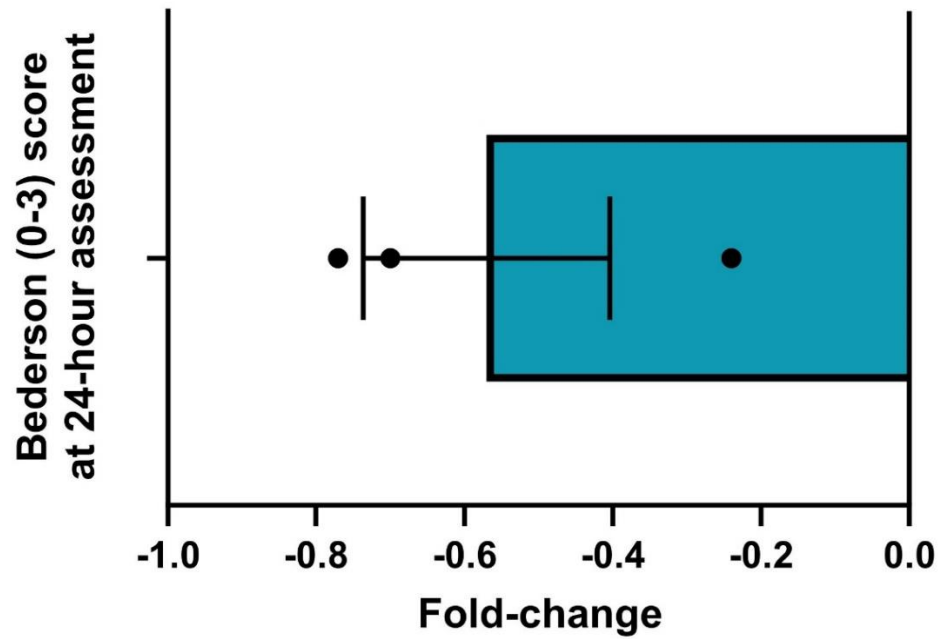
2018b). All studies using SD rats to assess the effects of C21 on Bederson (0-3) score found significant improvement in neurological score following C21 treatment.

Moving onto Wistar rats, C21 treatment had varying effects on neurological outcomes. Twenty-four hours following tMCAO Wistar rats treated with C21 (0.03 mg/kg/day; i.p.) combined with IgG antibodies led to improved Bederson (0-3) score (-0.24-fold change) compared to saline control ($p<0.05$) (Fouda et al., 2017). Conversely, Wistar rats treated with C21 (0.12 mg/kg/day; oral) for 30-days post-pMCAO showed no improvement in Bederson score (0-3) compared to saline control at 24 hours or 28 days post-stroke (Ahmed et al., 2019).

In a separate species, male spontaneously hypertensive (SHR) rats treated with C21 (0.03 mg/kg/day; i.p.) for 7 days post-tMCAO led to improvement in Bederson score (0-3) (-0.80-fold-change) by 28-days post-stroke compared to 24 hours post-stroke. When C21 was combined with Candesartan (-0.80-fold change) or Candesartan was given without C21 (-0.80-fold-change) Bederson (0-3) score was also improved ($p<0.0001$) (Ahmed et al., 2018).

When comparing all 7 studies that used Bederson (0-3) score to assess the neuroprotective effects of C21, 6 studies concluded C21 treatment led to improved neurological outcomes post-stroke, while one study found no difference in C21 treatment compared to saline control. Overall, 24 hours and 3 days post-stroke were the most common timepoints for assessing Bederson (0-3) score, whereby three of more studies used either timepoint in their investigations (Bennion et al., 2017, Bennion et al., 2018b, Fouda et al., 2017, Bennion et al., 2018a, Jiang et al., 2014). For the studies who investigated the effects of RAAS targeting interventions on Bederson (0-3) score at 24 hours post-stroke, the mean fold change in Bederson (0-3) score was -0.57 ± 0.17 (mean $\pm$ standard error of the mean [SEM]) (Figure 3.3 A). For the studies who investigated the effects of RAAS targeting interventions on Bederson (0-3) score at 3 days post-stroke, the mean fold change in Bederson (0-3) score was -0.44 ± 0.11 (mean $\pm$ SEM) (Figure 3.3 B).
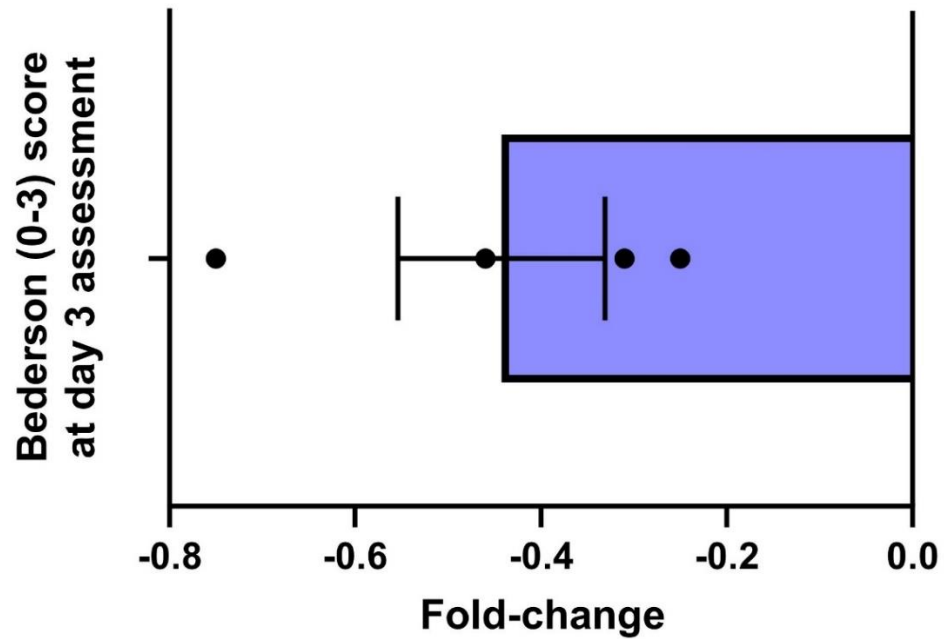
Figure 3.3 Effects of RAAS targeting interventions on Bederson score (0-3) post-stroke.
Fold-change Bederson (0-3) score was calculated from raw data extracted from tables and figures. Bederson (0-3) assessments conducted on preclinical stroke models following treatment with RAAS targeting intervention at 24 hours (A) or 3 days (B) post-stroke. Data may include publications that conducted multiple experiments at a given timepoint. Data presented at mean fold-change ± SEM (n=3-4) (Bennion et al., 2017, Bennion et al., 2018a, Bennion et al., 2018b, Fouda et al., 2017, Jiang et al., 2014).

3.3.2.2 Bederson 5-point score

A total of 4 studies were identified that used Bederson 5-point score to assess the effects of RAAS targeting interventions on neurological outcome post-stroke (Alhusban et al., 2015, Eldahshan et al., 2019, Min et al., 2014, Jiang et al., 2014). Two of these studies investigated the effects of RAAS targeting interventions on Wistar rats following tMCAO, two studies investigated the effects of RAAS targeting interventions on SD rats, while one study assessed the effects of RAAS targeting interventions on C57BL/6 mice following pMCAO. RAAS interventions included C21 and Ang-(1-7) with or without A779 or PD123319.

Male Wistar rats subjected to tMCAO that were treated with C21 (0.03 mg/kg; i.p.) demonstrated improved Bederson 5-point score (-0.35-fold change) compared to saline control ($p<0.05$). However, when stroke rats were treated with C21 plus PD123319 or PD123319 alone, there was no improvement in Bederson 5-point score (Alhusban et al., 2015). Additionally, improvements in Bederson 5-point score were also observed in female Wistar rats subjected to tMCAO, where it was found that C21 treatment significantly improved Bederson 5-point score (-0.27-fold change) compared to saline control ($p<0.05$) (Eldahshan et al., 2019).

Similar improvements were also observed in SD rats and C57BL/6 mice. SD rats subjected to pMCAO and treated with Ang 1-7 (1.11 nmol/L; i.c.v.) with or without A779 (1.14 nmol/L; i.c.v.) showed improved Bederson 5-point score following Ang-(1-7) treatment (-0.28-fold change) compared to vehicle control ($p<0.05$), while combined treatment of Ang-(1-7) and A779 significantly worsened Bederson 5-point score (0.34-fold change) compared to Ang-(1-7) treatment alone ($p<0.05$) (Jiang et al., 2014). C57BL/6 mice treated with C21 (10 µg/kg/day; i.p.) for 14 days prior to pMCAO showed improvement in Bederson 5-point score on days 3 (-0.32-fold change), 5 (-0.40-fold change) and 7 (-0.43-fold-change) post-stroke compared to time-matched vehicle control ($p<0.05$) (Min et al., 2014).

Of the 4 studies using Bederson 5-point score to assess neurological outcome following RAAS intervention post-stroke, all showed significant improvement in neurological outcomes. Overall, 24 hours post-stroke was the most common timepoint for assessing Bederson 5-point score, whereby 3 or more studies used the 24-hour timepoint in their investigations (Alhusban et al., 2015, Eldahshan et al., 2019, Jiang et al., 2014). For the studies who investigated the effects of RAAS targeting interventions on Bederson 5-point

score at 24-hours post-stroke, the mean fold change in Bederson 5-point score was -0.30 ± 0.03 (mean ± SEM) (Figure 3.4).
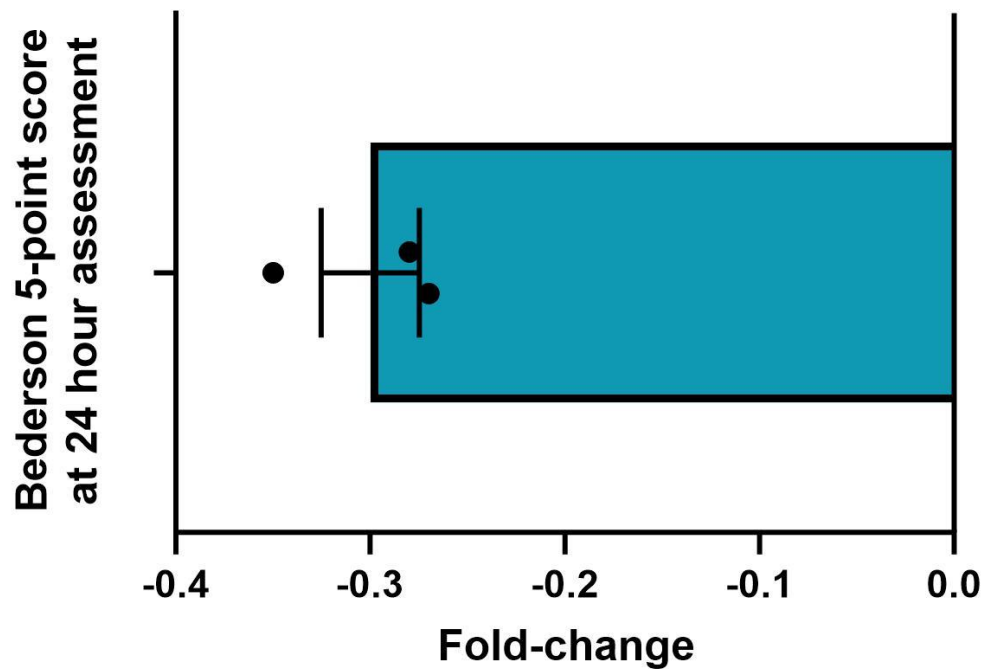
Figure 3.4 Effects of RAAS targeting interventions on Bederson 5-point post-stroke. Fold-change Bederson 5-point score was calculated from raw data extracted from tables and figures. Bederson 5-point assessments conducted on preclinical stroke models following treatment with RAAS targeting intervention at 24 hours post-stroke. Data may include publications that conducted separate experiments at a given timepoint. Data presented at mean fold-change ± SEM (n=3) (Alhusban et al., 2015, Eldahshan et al., 2019, Jiang et al., 2014).

3.3.2.3 Garcia score (0-18)

A total of 4 studies identified used the Garcia Score to assess the neurological benefits of C21 post-stroke (Bennion et al., 2018a, Bennion et al., 2017, Joseph et al., 2014, Schwengel et al., 2016). Of these studies, 3 studies investigated the effects of C21 on SD rats following MCAO, while one study assessed the effects of C21 on C57BL/6 mice post-stroke. RAAS targeting interventions included C21 with or without PD123319.

Delivery of C21 at various timepoints and administration routes has proven beneficial post-stroke. For example, SD rats pre-treated with C21 (0.0075 µg/µL/hr; i.c.v.) 7 days before ET-1 MCAO led to an improvement in Garcia score by day 3 post-stroke (0.19-fold change) compared to vehicle control (p<0.05). C21 (0.01 mg/kg or 0.03 mg/kg; i.p.) delivered 2 hours before, and up to 48 hours post-stroke did not improve Garcia score by 3 days post-stroke. C21 (0.03 mg/kg; i.p.) delivered post-stroke, up to 12 hours (0.40-fold change) or 48 hours (0.12-fold change) post-stroke, led to improved Garcia score compared to saline control on day 3 (p<0.05). Co-administration of C21 with PD123319 (0.3 µg/µL/hr; i.c.v) prevented improvement in Garcia score (Joseph et al., 2014). Similarly, SD rats subjected to pMCAO and treated with C21 (0.03 mg/kg; i.p.) up to 48 hours post-stroke showed improved Garcia score at 24 hours (0.24-fold change), day 3 (0.23-fold change) and day 7 (0.26-fold-change) post-stroke, while there was no improvement in Garcia score after 7 days (Bennion et al., 2017). Additionally, SD rats treated with C21 (1.5 µg/µL; intranasal administration [i.n.]) up to 48 hours post-stroke significantly improved Garcia score at 24 (0.14-fold change) and 72 hours (0.13-fold change) post-stroke (p<0.05) (Bennion et al., 2018a). All studies using SD rats to assess the effects of C21 treatment on Garcia score (0-18) at various timepoints and route of administration found that C21 treatment improved neurological outcomes.

Moving from studies investigating rats to one that assessed the effects of RAAS targeting interventions on mice, wildtype (WT) and AT_2R knockout (AT2RKO) C57BL/6 mice subjected to tMCAO were treated with C21 (0.03 mg/kg; i.p.) up to 4 days post-stroke. Within the WT group, C21 treatment improved Garcia score at 24 hours (0.23-fold change), day 2 (0.26-fold change) and day 4 (0.20-fold change) post-stroke compared to time-matched vehicle control (p<0.05), while there was no difference in Garcia score in AT2RKO mice at any timepoint (Schwengel et al., 2016).

All 4 studies using the Garcia (0-18) score showed significant improvement in neurological outcomes following treatment with RAAS targeting interventions. Overall, 24 hours post-stroke was the most common timepoint for assessing Garcia (0-18) score, whereby 3 or

more studies used the 24-hour timepoint in their investigations (Bennion et al., 2017, Bennion et al., 2018a, Schwengel et al., 2016). For the studies who investigated the effects of RAAS targeting interventions on Garcia (0-18) score at 24-hours post-stroke, the mean fold change in Garcia (0-18) score was 0.20 ± 0.03 (mean $\pm$ SEM) (Figure 3.5).

Figure 3.5 Effects of RAAS targeting interventions on Garcia (0-18) score post-stroke.
Fold-change Garcia (0-18) score was calculated from raw data extracted from tables and figures. Garcia (0-18) assessments conducted on preclinical stroke models following treatment with RAAS targeting intervention at 24 hours post-stroke. Data may include publications that conducted separate experiments at a given timepoint. Data presented at mean fold-change $\pm$ SEM (n=3) (Bennion et al., 2017, Bennion et al., 2018a, Schwengel et al., 2016).

3.3.2.4 5-point neuroscore

Of the studies included in this search, 3 studies used a 5-point neurological score to assess the effects of C21 and other RAAS interventions on post-stroke neurological outcomes (Shan et al., 2018, Iwai et al., 2004, Lee et al., 2012). All 3 studies investigated the effects of RAAS targeting interventions of in C57BL/6 mice. RAAS targeting interventions C21, CGP42112 or Valsartan with or without GW9662 (a peroxisome proliferator activated receptor γ inhibitor).

C57BL/6 mice were treated with C21(10 µg/kg/day; oral) with or without GW9662 (0.35 mg/kg/day; oral) for 2 weeks prior to pMCAO. Twenty-four hours post-stroke, neurological outcome was assessed using a 5-point score system. C21 treatment significantly improved neuroscore (-0.15-fold change; $p<0.05$) compared to control, however, when C21 was combined with GW9662, neuroscore was significantly worse (0.17-fold-change) compared to C21 only treatment ($p<0.05$) (Shan et al., 2018). Atgr2$^+$ and Agtr2$^-$ mice, derived from the C57BL/6 species, were treated with the AT$_1$R antagonist valsartan (3 mg/kg/day; minipump) for 10 days prior to pMCAO. Atgr2$^+$ animals treated with Valsartan had improved neuroscore (-0.29-fold change) compared to non-valsartan treated Agtr2$^+$ mice 24 hours post stroke ($p<0.05$). Valsartan treatment did not alter neuroscore in Agtr2$^-$ mice compared to non-valsartan treated Agtr2$^-$ mice 24-hours post-stroke (Iwai et al., 2004). Male C57BL/6 mice subjected to tMCAO were treated with CGP42112 (1 mg/kg; i.p.) post-stroke. Twenty-four hours following stroke, C21 treatment significantly improved (-0.75-fold change) neuroscore compared to vehicle control ($p<0.05$) (Lee et al., 2012).

Overall, 3 studies found that RAAS interventions improved neurological outcomes post-stroke as measured by 5-point neuroscore. The most common timepoint for assessing 5-point score was 24 hours (Shan et al., 2018, Iwai et al., 2004, Lee et al., 2012). For the studies who investigated the effects of RAAS targeting interventions on 5-point score at 24-hours post-stroke, the mean fold change in 5-point score was -0.40 ± 0.18 (mean $\pm$ SEM) (Figure 3.6).
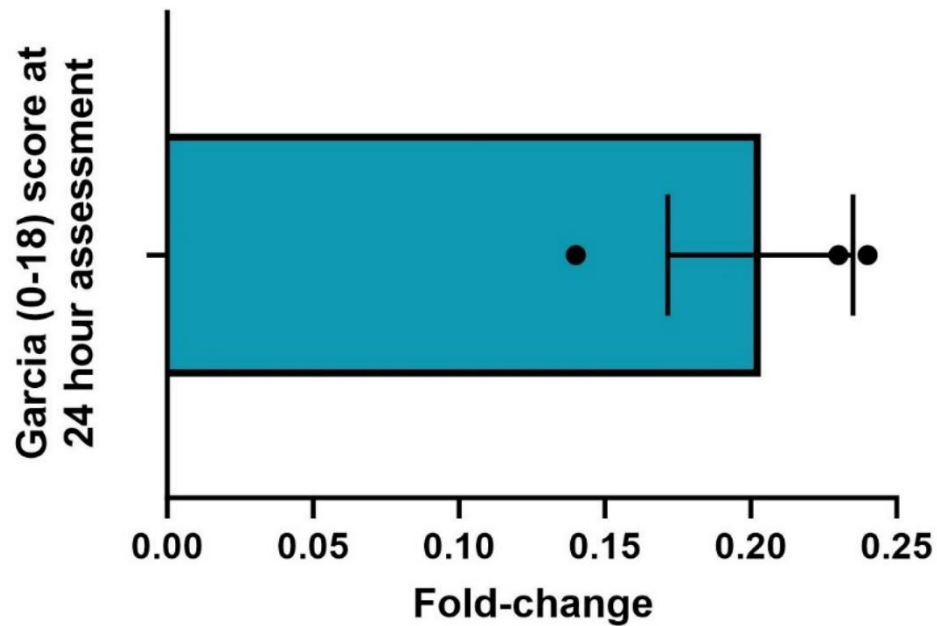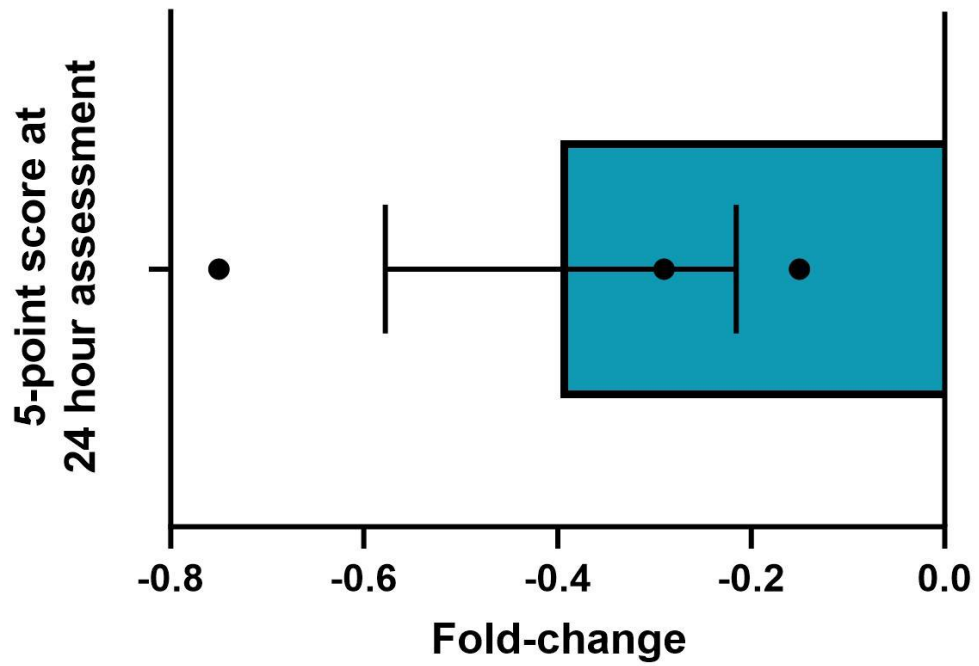
Figure 3.6 Effects of RAAS targeting interventions on 5-point score post-stroke.
Fold-change 5-point score was calculated from raw data extracted from tables and figures.
5-point assessments conducted on preclinical stroke models following treatment with
RAAS targeting intervention at 24 hours post-stroke. Data may include publications that
conducted separate experiments at a given timepoint. Data presented at mean fold-change
± SEM (n=3) (Shan et al., 2018, Iwai et al., 2004, Lee et al., 2012).

3.3.2.5 Beam Test

A total of 8 studies identified used beam walk test to assess neuroprotective qualities of RAAS targeting interventions post-stroke (Ahmed et al., 2018, Alhusban et al., 2015, Eldahshan et al., 2019, Fouda et al., 2017, Ishrat et al., 2019, McCarthy et al., 2014, McCarthy et al., 2012, McCarthy et al., 2009). The beam test assesses an animal's ability to traverse a ledged beam that gradually narrows. Here, the number of foot falls is directly related to sensory deficits post-stroke. Of these studies, 4 studies investigated the effects of RAAS targeting interventions on Wistar rats following MCAO, while 3 studies assessed the effects of RAAS targeting interventions and the remaining study investigated the effects of RAAS targeting interventions on SHR rats post-stroke. RAAS targeting interventions included C21, GGP42112 with or without PD123319.

Male Wistar rats were subjected to embolic MCAO (eMCAO) followed by C21 treatment at various concentrations. Animals that received 0.01mg/kg of C21 intravenously at 3 hours post-stroke had improved (1-fold change) beam walk score compared to 0.03 mg/kg of C21 by day 5 post-stroke (p<0.05). However, animals that received 0.03 mg/kg of C21 at 3 hours post-stroke showed a worsened beam score (-0.34-fold change) compared to saline control on day 7 post-stroke (p<0.05). There was no change in beam walk score at 24 hours post stroke compared to saline control. When C21 treatment (0.01 mg/kg) was delayed to 3-, 6- and 24-hours post-stroke, there was no improvement in beam walk score from 24 hours to 7 days post stroke. Additionally, when C21 (0.01 mg/kg) was combined with tPA there was no observed improvement in beam walk score on day 7-28 post-stroke (Ishrat et al., 2019). Conversely, Wistar rats subjected to tMCAO and treated with C21 (0.03 mg/kg/day; i.p.) combined with IgG at the point of reperfusion had improved beam walk score (-0.34-fold change) compared to saline control 24 hours post-stroke (p<0.05). When C21 was combined with IL-10 neutralising antibodies this improvement in beam walk score was reduced (Fouda et al., 2017). Wistar rats subjected to tMCAO and treated with C21 (0.03 mg/kg/day; i.p.) at the point of reperfusion resulted in an improved beam walk score (-0.54-fold change) compared to saline control 24 hours post-stroke (p<0.05). This improvement in beam walk was reversed when C21 was combined with PD123319 treatment (3 mg/kg; i.p.) (Alhusban et al., 2015). Female Wistar rats were subjected to tMCAO before treatment with C21 (0.03 mg/kg; i.p.) at the point of reperfusion. There was no significant difference in beam score with C21 treatments (-0.27-fold change) compared to saline control 24-hours post-stroke (Eldahshan et al., 2019). Of the studies investigating the effects of C21 on Wistar rats varying benefits of RAAS targeting interventions on neurological outcomes were observed.

Administration of C21 (0.03 mg/kg/day; i.p.) to male SHR rats 2 hours following tMCAO and continued for 7 days led to an improvement in beam walk score. C21 (-0.75-fold change), saline plus Candesartan (-0.77-fold change) and C21 plus Candesartan (-0.83-fold change) resulted in improved beam walk score by 28 days post-stroke compared to 24 hours post-stroke ($p < 0.0001$) (Ahmed et al., 2018). Further, SHRs pre-treated with C21 (50 ng/kg/min) over 8 days followed by ET-1 MCAO showed improvement in beam walk score (-0.83-fold change) compared to saline control at 24-hours post-stroke ($p < 0.01$), however, no improvement in beam walk score was observed at 3 days post-stroke. Additionally, when C21 (50 ng/kg/min) was delivered post-stroke no improvement in beam walk score was observed compared to saline control at 24-hours (-0.04-fold change) and 3 days (-0.49-fold change) post-stroke. When PD123319 (36 ng/kg/min) was administered either alone or with C21 prior to or following stroke beam walk score was unaltered (McCarthy et al., 2014). SHR rats were treated with CGP42112 (0.1, 1 or 10 ng/kg/min; i.c.v.) five days before ET-MCAO and continued for 3 days post-stroke. Percentage error in beam walk was increased at both 1- and 3-days post-stroke in vehicle treated animals. CGP42112 at a concentration of 0.1 ng/kg/min led to reduced percentage error at day three post-stroke compared to vehicle treated animals (-0.75fold change; $p < 0.05$). Treatment with 1 ng/kg/min of CGP42112 led to reduced percentage error at both day 1 (-0.82-fold change; $p < 0.05$) and day 3 (-0.93-fold-change; $p < 0.01$) post-stroke compared to vehicle treated animals. Treatment with 10 ng/kg/min CGP42112 led to reduced percentage error at both day 1 (-0.81-fold change; $p < 0.05$) and day 3 (-0.89-fold-change; $p < 0.01$) post-stroke compared to vehicle treated animals. CGP42112 combined with PD123319 and PD123319 treatment showed similar percentage error compared to vehicle control post-stroke (McCarthy et al., 2009). Similar positive effect of RAAS targeting interventions on post-stroke beam walk assessment were observed when the same group investigated the effects of CGP42112 (3 µg/kg/dose; i.c.v.) in SHR rats five days before ET-MCAO and continued for 3 days post-stroke, whereby compared to time-matched vehicle control, percentage error at both day 1 (-0.81-fold change; $p < 0.05$) and day 3 (-0.91-fold-change; $p < 0.01$) post-stroke were reduced following CGP42112 treatment (McCarthy et al., 2012).

When comparing these 8 studies, 6 studies found that RAAS targeting interventions improved beam walk score post-stroke, one study found no change in beam walk score with RAAS targeting interventions and one study found that RAAS targeting interventions may result in worse beam walk score. Overall, 24 hours post-stroke was the most common timepoint for assessing beam walk, whereby three of more studies used the 24-hour

timepoint in their investigations (Fouda et al., 2017, Alhusban et al., 2015, Eldahshan et al., 2019, McCarthy et al., 2012, McCarthy et al., 2014, McCarthy et al., 2009). For the studies who investigated the effects of RAAS targeting interventions on beam walk at 24-hours post-stroke, the mean fold change in beam walk score was -0.56 ± 0.11 (mean ± SEM) (Figure 3.7).
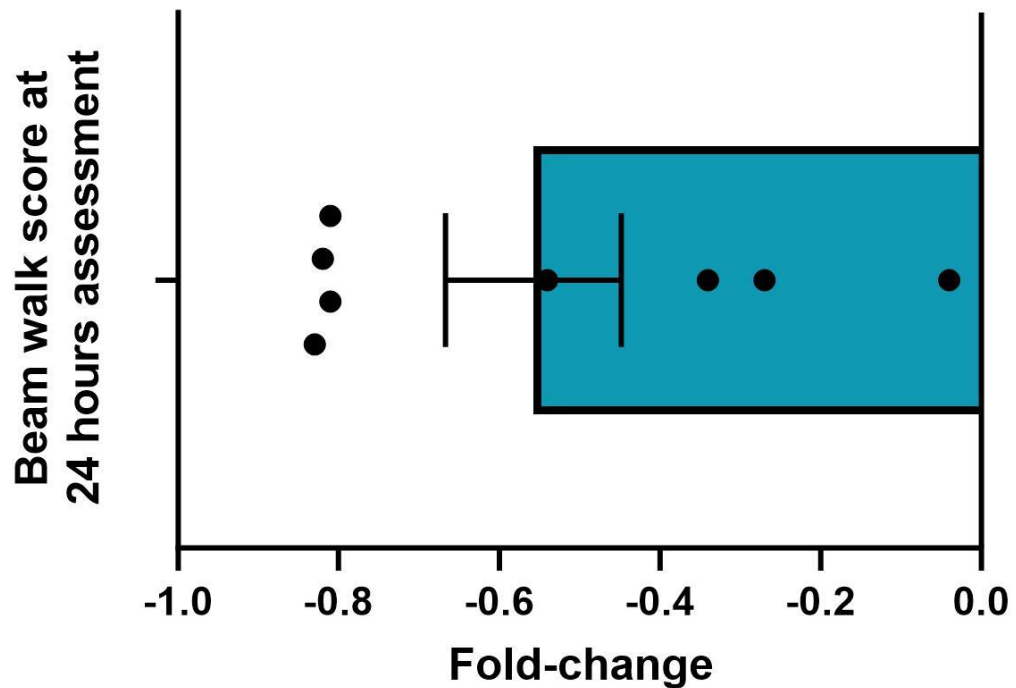
Figure 3.7 Effects of RAAS targeting interventions on beam walk score post-stroke. Fold-change in beam walk score was calculated from raw data extracted from tables and figures and the mean fold-change was determined. Studies that investigated the effects of intervention at 24- hours post-stroke were grouped; this may include one group carrying out multiple experiments using C21 with 24-hour assessment timepoint. Data presented at mean fold-change ± SEM (n=8) (Fouda et al., 2017, Alhusban et al., 2015, Eldahshan et al., 2019, McCarthy et al., 2012, McCarthy et al., 2014, McCarthy et al., 2009).

3.3.2.6 Rotarod test

Three studies used rotarod testing to determine the effects of RAAS targeting interventions on post-stroke neurological outcomes (Alhusban et al., 2015, Ishrat et al., 2019, Bennion et al., 2017). Rotarod test measures motor learning, whereby animals are placed on a rotating cylindrical rod and are expected to keep up with the movement of the rod. Animals that have been subjected to stroke are more likely to fall off the rod more frequently and within a smaller timeframe compared to healthy controls (Deacon, 2013). In this systematic review, 2 studies investigated the effects of C21 in Wistar rats, while one group assessed the effects of C21 on SD rats following stroke using rotarod test.

C21 (0.03 mg/kg; i.p.) delivered to male Wistar rats at 90 mins following tMCAO showed improved percentage running time following C21 treatment (0.03 mg/kg; i.p.) compared to saline control animals on day 4 (0.59-fold change) and day 7 (0.26-fold change) post-stroke ($p<0.05$) (Alhusban et al., 2015). However, in a similar study, Wistar rats subjected to eMCAO and treated with C21 (0.01 mg/kg; intravenous injection [i.v.]), tPA (10 mg/kg; i.v.) or C21 combined with tPA 2-hours post-stroke found no improvement in rotarod time and speed in all studies by day 28 (Ishrat et al., 2019). Of the two studies investigating the effects of C21 on rotarod outcome in Wistar rats, one showed post-stroke improvement following C21 treatment, while the other showed no improvement with C21 treatment.

Moving onto a different rodent model, SD rats subjected to pMCAO had significantly improved (1.03-fold change) percentage rotarod time by day 7 post-stroke following C21 (0.03 mg/kg i.p.) treatment compared to saline control. From day 7 to day 28 post-stroke, there was no significant difference in percentage rotarod time compared to baseline control between saline and C21 treated animals. Overall area under the curve for rotarod time was improved with C21 treatment (0.88-fold change) compared to saline control ($p<0.05$) (Bennion et al., 2017).

In summary, 2 of the 3 studies assessing the effects of C21 treatment on rotarod test outcome identified improvement in rotarod outcome following C21 post-stroke, while one group did not demonstrate improvement in rotarod outcome following C21 treatment post-stroke.

3.3.2.7 Paw Grasp

A total of 3 studies used paw grasp score to assess the effects of C21 on motor function post-stroke (Alhusban et al., 2015, Eldahshan et al., 2019, Ishrat et al., 2019). During paw grasp assessment, animals are suspended by the tail and allowed to grasp a pole or wire and their ability to grasp the pole by both, one or no paws directly relates to motor function. All three of these studies identified in this systematic review investigated the effects of C21 on paw grasp in the same Wistar rodent strain post-stroke.

C21 (0.03 mg/kg i.p.) administered to Wistar rats at 90 mins following tMCAO led to improved paw grasp score on day 4 (-0.45-fold change) and 7 (-0.34-fold change) compared to time-matched saline controls ($p<0.05$) (Alhusban et al., 2015). Conversely, Wistar rats subjected to eMCAO and treated with C21 (0.01, 0.03 or 0.06 mg/kg; i.v.) 3 hours post-stroke had no significant improvement in paw grasp score from 24-hours to 7 days post-stroke. Nor did they find any significant difference in paw grasp score when C21 was given at either 3-, 6- or 24 hours post-stroke by day 7 post-stroke. Furthermore, they found no difference in paw grasp score when C21 (0.01 mg/kg; i.v.) was combined with tPA (10 mg/kg; i.v.) by 28 days post-stroke (Ishrat et al., 2019). Likewise, female Wistar rats subjected to tMCAO were treated with C21 (0.03 mg/kg; i.p.), whereby there was no significant improvement in paw grasp score 24 hours post-stroke following C21 treatment (Eldahshan et al., 2019). Overall, from the three studies, two studies did not find a significant improvement in paw grasp with C21 treatment whereas one group found that C21 improved paw grasp post-stroke.

3.3.2.8 Novel object recognition

A total of 4 studies used NOR to assess neuroprotective qualities of RAAS targeting interventions post-stroke (Ahmed et al., 2018, Ahmed et al., 2019, Ishrat et al., 2019, Jackson-Cowan et al., 2021). Novel object recognition assesses recognition memory. The time taken in interacting with the novel object is directly related to recognition memory (Leger et al., 2013). Animals that have undergone stroke will have reduced recognition memory and as such will spend less time interacting with the novel object. The discrimination index (DI) is the time taken for the animal to differentiate between novel objects and recognisable objects, while the recognition index (RI) is the time taken to investigate the novel object. DI is represented as a value between -1 and +1, while RI is represented as a value between 0 and +1. If the value of DI is positive the animal spent a greater amount of time investigating the novel object (Bekci et al., 2024). If the value of RI

is positive the animal possesses greater object recognition memory (Joung et al., 2020). Three of the 4 studies identified in this systematic review investigated the effects of RAAS targeting interventions on Wistar rats, while one group assessed the effects of C21 on SHR rats post-stroke. RAAS targeting interventions included C21 and Candesartan.

Twenty-four hours following pMCAO, male Wistar rats were treated with C21 (0.12 mg/kg/day; oral) and treatment continued for 30 days post-stroke. Saline control animals showed a significant reduction in DI (-0.32-fold change) and RI (-0.14-fold change) compared to baseline controls (p<0.0001). C21 and Candesartan treatment led to DI or RI similar to baseline measurements (prior to ischaemic insult) by 21 days post-stroke. Further, saline control animals also showed a significant reduction in DI and RI compared to both sham and C21 groups by 21 days post-stroke (p<0.0001) (Ahmed et al., 2019). Wistar rats subjected to eMCAO followed by C21 treatment (0.01, 0.03 or 0.06 mg/kg; i.v.) at 3 hours post-stroke showed no significant difference in DI by day 7 post-stroke. C21 treatment improved 5-minute DI (9-fold change) compared to C21 plus tPA treatment by 28 days after stroke (p<0.05) (Ishrat et al., 2019). Similarly, diabetic female Wistar rats subjected to tMCAO and treated with C21 (0.03 mg/kg; i.v.) demonstrated no difference in DI and RI compared to vehicle treated or sham rats by 4 weeks following tMCAO (Jackson-Cowan et al., 2021). All 3 studies using Wistars to assess the effects of C21 on NOR did identify any significant improvements in DI/RI following C21 treatment post-stroke.

Male SHR rats were subjected to tMCAO and were treated with C21 (0.03mg/kg/day; i.p.) or Candesartan (0.3 mg/kg/day; i.p.) at 2 hours post-stroke and continued for 7 days. Saline control animals showed a decline in DI (-0.72-fold change) and RI (-0.30-fold change) compared to baseline control (prior to ischaemic insult) at 21 days post-stroke (p<0.0001). Importantly, C21 and Candesartan treatment led to no significant decline in NOR in terms of discrimination and recognition index after 21 days compared to saline controls. (Ahmed et al., 2018). Overwhelmingly, studies studying the effects of C21 using NOR demonstrated no significant change in DI/RI following C21 treatment post-stroke.

3.3.2.9 Passive avoidance test

A total of 3 studies were identified that used passive avoidance test to measure the effect of RAAS targeting interventions on memory post-stroke (Ahmed et al., 2018, Ahmed et al., 2019, Eldahshan et al., 2021). Passive avoidance assesses learning and memory whereby

animals are allowed to learn an adverse environmental stimulus, such as a short electric shock within a portion of a holding chamber (Eagle et al., 2016). Animals with greater memory retention will have longer step-through latency compared to impaired stroke animals. In this systematic review, 2 studies assessed the effects of RAAS targeting interventions on SHR rats, while one study assessed the effects of RAAS targeting interventions on Wistar rats post-stroke. RAAS targeting interventions included C21 and Candesartan.

Longer step-through latency is indicative of better memory retention. SHR rats subjected to tMCAO experienced increased step-through latency following C21 treatment (0.12 mg/kg/day; oral) (12.82-fold change), saline plus Candesartan (10.96-fold change) and C21 plus Candesartan (8.10-fold change) by 28 days post-stroke compared to baseline controls ($p<0.0001$). Saline control animals showed reduced step through latency compared to other treatment groups ($p<0.0001$) (Ahmed et al., 2018). In ovariectomised female SHRs subjected to tMCAO and treated with C21 (0.03 mg/kg/; i.p. then 0.12 mg/kg; oral) step-through latency significantly increased step through latency (1.24-fold change) compared to saline control ($p<0.05$). Following stroke, saline control animals had significantly poorer step through latency (-0.61-fold change) compared to pre-stroke saline control post-stroke ($p<0.05$) (Eldahshan et al., 2021).

Wistar rats subjected to pMCAO treated with C21 (0.12 mg/kg/day; oral) or sham animals retained their retention of step through latency compared to baseline controls by 28 days post-stroke. C21 treatment did not affect step through latency post-stroke compared to sham control and pre-stroke measurement. Vehicle control animals showed a significant decrease in their step through latency (-0.59-fold change) compared to baseline measurements ($p<0.00001$). Additionally, vehicle control animals also showed a significant reduction in step through latency compared to sham (-0.62-fold change) and C21 treated (-0.58-fold change) ($p<0.00001$) (Ahmed et al., 2019).

From the 3 studies investigating the effects of C21 on passive avoidance tests, 2 studies found that C21 increased step-through latency post-stroke, while one group found that C21 prevented a reduction in step through latency post-stroke.

3.3.2.10 Paw adhesive test

A total of 3 studies used paw adhesion test to investigate the effects of RAAS interventions on cognitive and motor outcomes post-stroke (Bennion et al., 2017, Bennion et al., 2018b,

Jackson et al., 2020). Paw adhesive test is used to measure somatosensory deficit, whereby animals subjected to stroke will take longer to touch and remove adhesive labels compared to non-stroke animals. Two studies investigated the effects of RAAS interventions in SD rats post-stroke, while one group investigated the effects of RAAS interventions in Wistar rats post-stroke. RAAS targeting interventions included C21 and Ang-(1-7).

SD rats subjected to tMCAO were treated with C21 (0.03 mg/kg; i.p.) post-stroke and paw adhesive tests were carried out at 4 hours, 1-, 3-, 7-, 14-, 21- and 28-days following stroke. Paw adhesive time to touch was significantly reduced following C21 treatment at day 14 (-0.65-fold change) and 21 (0.51-fold change) post-stroke compared to saline control (p<0.05). Paw adhesive time to remove sticker was significantly reduced following C21 treatment (-0.48-fold change) at day 14 compared to saline control (p<0.05). There was no difference in paw adhesive time to touch or removal at any other timepoint (Bennion et al., 2017). In a related study by the same group, SD rats were subjected to ET-1-MCAO and were treated with Ang-(1-7) (125 µg/kg; oral) at 4 hours, day 1 and day 2 post-stroke. Paw adhesive time to touch was similar between Ang-(1-7) and water control from day 1 to day 3 post-stroke. Paw adhesion time to removal was significantly decreased following Ang-(1-7) treatment compared to water control at day 3 post-stroke (p<0.05), however paw adhesion time to removal was similar between groups at day 1 post-stroke (Bennion et al., 2018b)

Moving onto another rat strain, C21 (0.12 mg/kg) was administered to Wistar rats 3 days following tMCAO, which significantly decreased paw adhesive removal time in both control and diabetic animals compared to vehicle control or diabetic animals from week 1 to week 8 post-stroke (p<0.05-0.001) (Jackson et al., 2020). Overall, all studies found that RAAS interventions significantly reduced time taken to touch or remove the adhesive stickers on the paws of both SD and Wistar rats.

3.3.2.11 Overall effects of RAAS targeting interventions on neurological outcomes

The effects of RAAS targeting modulations on neurological outcome post-stroke, determined by various neurological assessments, varied between research studies as illustrated in Table 3.2. The effects of RAAS targeting interventions on neurological outcomes were characterised as: significant improvement, no significant change, both improvement and decline or significant decline. Of the 42 assessments conducted, 31 assessments showed significant improvement in neurological outcome following RAAS targeting interventions, irrespective of assessment method, and 10 assessments showed no change in neurological outcomes following RAAS targeting interventions. One assessment found both improvement and decline in neurological outcome following RAAS targeting interventions Table 3.3.

Table 3.2 Neurological benefits of RAAS targeting interventions post-stroke.

Main Intervention	Author	Neurological assessment									
		Beam test	Bederson (0-3)	Garcia Score (0-18)	Novel object recognition	Bederson (5-point)	5-point scale	Passive avoidance test	Paw grasp	Rotarod test	Paw adhesive test
C21	Ahmed et al., 2018	1	1		1			1			
	Ahmed et al., 2019		1		1			1			
	Alhusban et al., 2015	1				1			1	1	
	Bennion et al., 2018		1	1							
	Bennion et al., 2017		1	1						1	1
	Eldahshan et al., 2019	1				1		1			
	Eldahshan et al., 2021							1			
	Fouda et al., 2017	1	1								
	Ishrat et al., 2019	1			1				1	1	
	Jackson et al., 2020										1
	Jackson-Cowan et al., 2021				1						
	Joseph et al., 2014		1	1							
	McCarthy et al., 2014	1									
	Min et al., 2014					1					
	Schwengel et al., 2016			1							
	Shan et al., 2018						1				
	Bennion et al., 2018		1								1
	Jiang et al., 2014					1					
Other	Iwai et al., 2004						1				
	Lee et al., 2012						1				
	McCarthy et al., 2009	1									
	McCarthy et al., 2012	1									
Total number of studies		8	7	4	4	4	3	3	3	3	3

Significant improvement	(green)
No significant change	(yellow)
Both improvement and decline	(purple)
Significant decline	(orange)

Table 3.3 Overview of the improve and decline in neurological outcomes following RAAS targeting interventions post-stroke.

Effect of RAAS intervention	Beam test	Bederson (0-3)	Garcia Score (0-18)	Novel object recognition	Bederson (5-point)	5-point scale	Passive avoidance test	Paw grasp	Rotarod test	Paw adhesive test	Total number of assessments
Notable improvement	6	6	4	0	4	3	2	1	2	3	**31**
No significant change	1	1	0	4	0	0	1	2	1	0	**10**
Both improvement and decline	1	0	0	0	0	0	0	0	0	0	**1**
Significant decline	0	0	0	0	0	0	0	0	0	0	**0**

3.3.3 Effects of RAAS interventions on Infarct volume post-stroke

Infarct volume is commonly used as an outcome measure in experimental stroke models. Infarct volume is an independent predictor of post-stroke functional outcome (Zaidi et al., 2012). Preclinically, a common method of determining infarct volume is 2,3,5-Triphenyltetrazolium chloride (TTC) staining, as illustrated by this systematic review. Within live cells, TTC is reduced by mitochondria to produce a vibrant red colour, while dead cells within the infarct region remained stained. Image analysis of TTC stained brain sections can be used to quantify the infarcted region of the brain in experimental stroke models (Benedek et al., 2006). The practice of magnetic resonance imaging (MRI), frequently used by studies in this systematic review, can be used to measure infarct volume. Clinically, MRI can be used to quantify the size of ischemic lesion in stroke patients and provides information relating to expected clinical outcomes (Lövblad et al., 1997). *In vivo*, MRI can be used to determine the impacts of interventions on infarct volume post-stroke (Bennion et al., 2017, Min et al., 2014).

Of the studies included in this systematic review, a total of 22 studies assessed the effects of RAAS interventions on infarct volume post-stroke, as shown in Table 3.4 (Alhusban et al., 2015, Bennion et al., 2017, Bennion et al., 2018a, Eldahshan et al., 2019, Eldahshan et al., 2021, Fouda et al., 2017, Ishrat et al., 2019, Joseph et al., 2014, Mateos et al., 2016, McCarthy et al., 2014, Min et al., 2014, Schwengel et al., 2016, Shan et al., 2018, Arroja et al., 2019, Bennion et al., 2018b, Jiang et al., 2014, Regenhardt et al., 2013, Ma and Yin, 2016, Iwai et al., 2004, Lee et al., 2012, McCarthy et al., 2009, McCarthy et al., 2012). The most common form of assessing infarct volume post-stroke following RAAS intervention was TTC staining, with 12 studies using TTC staining (Alhusban et al., 2015, Bennion et al., 2018a, Eldahshan et al., 2019, Fouda et al., 2017, Ishrat et al., 2019, Joseph et al., 2014, Shan et al., 2018, Bennion et al., 2018b, Jiang et al., 2014, Regenhardt et al., 2013, Ma and Yin, 2016, Iwai et al., 2004). The second most common form of assessing infarct volume following RAAS intervention post-stroke was MRI, with 4 studies using MRI (Bennion et al., 2017, Eldahshan et al., 2021, Min et al., 2014, Schwengel et al., 2016). Other studies identified in this systematic review used a variety of methods to assess infarct volume including ballistic light method with thionin staining, unstained histology, nissl staining, crystal violet staining and diffusion weighted imaging.

Table 3.4 Classification of infarct assessment methods

Main Intervention	Author	Infarct assessment						
		TTC	MRI	Balistic light method & thionin staining	Unstained histology	Nissl staining	Crystal Violet staining	Diffusion weighted imaging
C21	Alhusban et al., 2015	1						
	Bennion et al., 2018	1						
	Bennion et al., 2017		1					
	Eldahshan et al., 2019	1					1	
	Eldahshan et al., 2021		1					
	Fouda et al., 2017	1						
	Ishrat et al., 2019	1						
	Joseph et al., 2014	1						
	Mateos et al., 2016					1		
	McCarthy et al., 2014				1			
	Min et al., 2014		1					
	Schwengel et al., 2016		1					
	Shan et al., 2018	1						
Ang-(1-7)	Arroja et al., 2019				1			1
	Bennion et al., 2018	1						
	Jiang et al., 2014	1						
	Regenhardt et al., 2013	1						
Other	C. Y. Ma & L. Yin., 2016	1						
	Iwai et al., 2004	1						
	Lee et al., 2012			1				
	McCarthy et al., 2008							
	McCarthy et al., 2012			1				
Total number of studies		**12**	**4**	**2**	**2**	**1**	**1**	**1**

3.3.3.1 TTC staining

A total of 12 studies used TTC staining to assess the effects of RAAS interventions on infarct volume post-stroke (Alhusban et al., 2015, Bennion et al., 2018a, Bennion et al., 2018b, Fouda et al., 2017, Eldahshan et al., 2019, Ishrat et al., 2019, Joseph et al., 2014, Shan et al., 2018, Jiang et al., 2014, Regenhardt et al., 2013, Ma and Yin, 2016, Iwai et al., 2004). A total of 6 studies investigated the effects of RAAS interventions on SD rats (Bennion et al., 2018a, Joseph et al., 2014, Bennion et al., 2018b, Jiang et al., 2014, Regenhardt et al., 2013, Ma and Yin, 2016). Four studies that investigated the effects of RAAS interventions on Wistar rats (Alhusban et al., 2015, Fouda et al., 2017, Eldahshan et al., 2019, Ishrat et al., 2019). Two studies investigated the effects of RAAS interventions on C57BL/6 mice (Shan et al., 2018, Iwai et al., 2004). RAAS targeting interventions included in these studies include C21, Ang-(1-7), CGP42112 and Valsartan, used either alone or in some studies combined with A779, PD123319 or anti-IL-10 antibodies.

C21 (15 µg/kg; i.n.) administered to SD rats following pMCAO led to reduced infarct volume (-0.42-fold change) compared to saline control after 72-hours post-stroke ($p<0.05$) (Bennion et al., 2018a). SD rats treated with C21 (0.0075 µg/µL/hr; i.c.v.) prior to pMCAO showed significant reduction in infarct volume (-0.48-fold change) compared to aCSF control by 3-days post-stroke ($p<0.05$). Additionally, delivery of C21 (0.03 mg/kg; i.p.) 2 hours before and 4-, 24- and 48-hours after stroke significantly reduced infarct size (-0.60-fold change, $p<0.05$) compared to aCSF at day 3 post-stroke, while treatment of 0.1 mg/kg (i.p.) of C21 before and after stroke also reduced infarct volume compared to aCSF (-0.49-fold change, $p<0.05$). Further, delivery of C21 (0.03 mg/kg; i.p.) after stroke at 4-, 24- and 48-hours post-stroke significantly reduced infarct size compared to aCSF at day 3 post-stroke (-0.44-fold change, $p<0.05$). When C21 (0.03 mg/kg; i.p.) was delivered at 4 and 12 hours post stroke, infarct volume was reduced compared to aCSF control when assessed at 24-hours post-stroke (-0.58-fold change, $p<0.05$) (Joseph et al., 2014). Using another AT$_2$R agonist, CGP42112, SD rats subjected to tMCAO and treated with CGP42112 (1 mg/kg/day; i.p.) showed reduced infarct volume (-0.15-fold change) compared to saline control by day 7 post-stroke ($p<0.05$), while treatment with PD123319 (1 mg/kg/day i.p.) increased infarct volume (0.41-fold change) compared to saline control ($p<0.01$) (Ma and Yin, 2016).

SD rats were subjected to ET-1 MCAO and were treated with Ang-(1-7) (125 µg/kg; oral) at 4-, 24- and 48 hours post-stroke. After 3 days the percentage infarct volume was reduced following Ang-(1-9) treatment (-0.23-fold change) compared to water control ($p<0.05$)

(Bennion et al., 2018b). SD rats were treated with Ang-(1-7) (1.1 nmol/L; i.c.v.) with or without Mas antagonist A779 (1.4 nmol/L; 0.25 µL/h) for 4 weeks prior to pMCAO. Twenty-four hours post-stroke, infarct volume was reduced following Ang-(1-7) treatment (-0.28-fold change, $p<0.05$), however, infarct volume was increased when Ang-(1-7) was combined with A779 (0.35-fold change, $p<0.05$) (Jiang et al., 2014). In another study investigating Ang-(1-7), SD rats subjected to ET-1 MCAO and treated with Ang-(1-7) (1.1 nmol; i.c.v.) showed reduced percentage infarcted grey matter (-0.61-fold change) compared to vehicle control 24-hours post-stroke ($p<0.05$) (Regenhardt et al., 2013).

C21 (0.03 mg/kg; i.p.) delivered to Wistar rats 90 mins after tMCAO led to a significant reduction in infarct volume (-0.35-fold change) compared to saline control 24-hours post-stroke ($p<0.05$). A combination of C21 and PD123319 (3 mg/kg; i.p.) or treatment with PD123319 alone did not reduce infarct volume post-stroke (Alhusban et al., 2015). Wistar rats subjected to tMCAO that were treated with C21 (0.03 mg/kg/day; i.p.) led to a reduction in infarct volume (-0.34-fold change) compared to saline control 24 hours post-stroke ($p<0.05$). C21 treatment combined anti-IL-10 neutralising antibodies or saline combined with anti-IL-10 neutralising antibodies did not improve infarct volume (Fouda et al., 2017). Male Wistar rats subjected to eMCAO and treated with C21 via i.p. at a concentration of 0.01 mg/kg, 0.03 mg/kg, or 0.06 mg/kg also did not show any significant difference in infarct volume compared to control (Ishrat et al., 2019). In female Wistar rats, C21 (0.03 mg/kg; i.p.) treatment following tMCAO did not reduce infarct volume compared to controls by 24-hours post-stroke (Eldahshan et al., 2019).

C21 (10 µg/kg/day; i.p.) delivered to male C57BL/6 mice post-tMCAO led to a reduction in infarct volume (-0.38-fold change) compared to saline controls 24-hours post-stroke ($p<0.01$) (Shan et al., 2018). Agtr2^{+} and Agtr2^{-} C57BL/6 mice were treated with AT_1R antagonist valsartan (3 mg/kg/day; mini.) for 10 days prior to pMCAO. Valsartan treated Agtr2^{+} mice showed reduced ischaemic area in coronal sections 2 through 5 (-0.27 ± 0.01; average fold change through coronal sections $\pm$ SEM) compared to untreated Agtr2^{+} controls ($p<0.05$). Valsartan treated Agtr2^{-} mice showed no difference in ischaemic area compared to untreated Agtr2^{+} control (Iwai et al., 2004).

A total of 12 studies investigated the effects of RAAS interventions on infarct volume, as assessed by TTC staining. Of these 12 studies, 10 studies identified reduction in infarct volume after RAAS intervention, whereas 2 studies did not find any difference in infarct volume after RAAS intervention. Overall, 24 hours and 3 days post-stroke were the most common timepoints for assessing infarct volume by TTC staining, whereby three of more

studies used either timepoint in their investigations (Joseph et al., 2014, Jiang et al., 2014, Regenhardt et al., 2013, Alhusban et al., 2015, Fouda et al., 2017, Shan et al., 2018, Iwai et al., 2004). For the studies who investigated the effects of RAAS targeting interventions on infarct volume at 24 hours post-stroke, the mean fold change in infarct volume was $-0.40 \p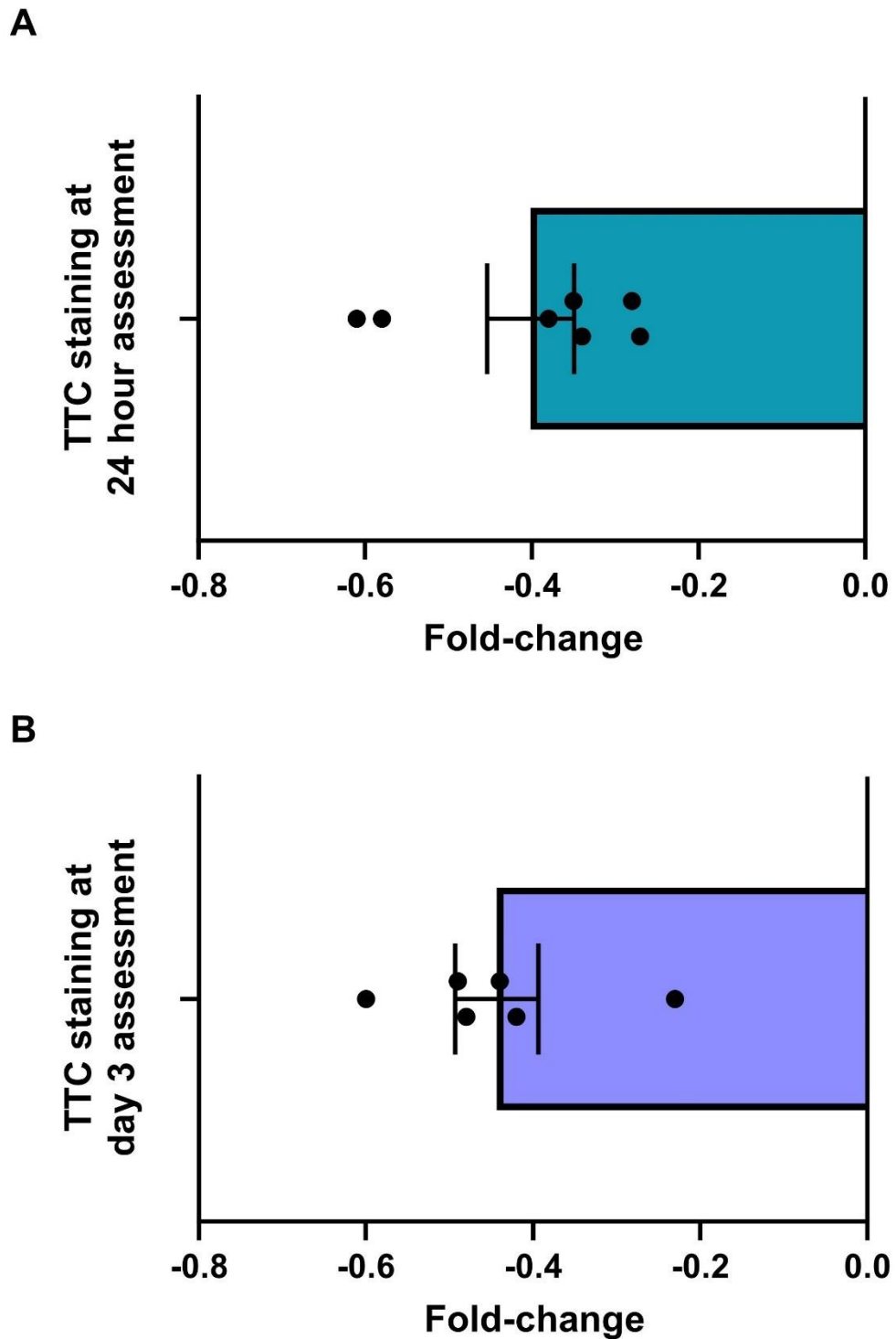m 0.05$ (mean $\pm$ SEM) (Figure 3.8 A). For the studies who investigated the effects of RAAS targeting interventions on infarct volume at 3 days post-stroke, the mean fold change in infarct volume was -0.44 ± 0.05 (mean $\pm$ SEM) (Figure 3.8 B).

Figure 3.8 Effects of RAAS targeting interventions on TTC-determined infarct volume post-stroke.
Fold-change infarct volume as determine by TTC staining was extracted from raw data given within tables and figures. TTC staining was conducted on preclinical stroke models following treatment with RAAS targeting intervention at 24 hours (A) or 3 days (B) post-stroke. Data may include publications that conducted separate experiments at a given timepoint. Data presented at mean fold-change ± SEM (n=6-7) (Joseph et al., 2014, Jiang et al., 2014, Regenhardt et al., 2013, Alhusban et al., 2015, Fouda et al., 2017, Shan et al., 2018, Iwai et al., 2004).

3.3.3.2 MRI assessment

A total of 4 studies investigated the effects of C21 on infarct volume using MRI (Bennion et al., 2017, Eldahshan et al., 2021, Min et al., 2014, Schwengel et al., 2016). Two studies investigated the effects of RAAS interventions on C57BL/6 mice (Min et al., 2014, Schwengel et al., 2016). One group investigated the effects of RAAS interventions on SD rats (Bennion et al., 2017), while another investigated the effects of RAAS interventions on SHR rats (Eldahshan et al., 2021).

Wildtype (WT) or AT_2R KO C57BL/6 mice were treated with C21 (10 µg/kg/day; i.p.) 14 days prior to pMCAO. C21 treated WT mice showed reduced ischaemic area compared to untreated WT mice from 24-hours to day 5 post-stroke ($P<0.05$), while C21 treated AT_2R KO mice showed no improvement in infarct volume compared to AT_2R KO saline control animals. When C21 (10 µg/kg/day; i.p.) was delivered to WT mice at the point of reperfusion, ischaemic volume was decreased on day 3 (-0.25-fold change) and 5 (-0.45-fold change) during a 7-day assessment period compared to saline control ($p<0.05$) (Min et al., 2014). Conversely, in a similar study, WT and AT_2R KO mice subjected to tMCAO and treated with C21 (0.03 mg/kg/day; i.p.) showed no improvement in infarct volume compared to vehicle control by day 4 post-stroke ($p<0.05$) (Schwengel et al., 2016).

Male SD rats subjected to pMCAO were treated with C21 (0.03 mg/kg; i.p.) 1.5 hours, 1 day and 2 days post-stroke. Using MRI, infarct volume was reduced with C21 treatment (-0.35-fold change) compared to saline control by three-weeks post-stroke ($p<0.05$) (Bennion et al., 2017). Ovariectomised female SHRs were treated with C21 (0.03 mg/kg/day; i.p.) at 24-hours post-tMCAO and continued at a higher dose then (0.12 mg/kg/day; o.) for 5 days post-stroke. No difference in infarct size/cavitation as a percentage of the contralateral side was identified following C21 treatment compared to saline control (Eldahshan et al., 2021). Overall, 2 studies found that C21 reduced infarct volume as determined by MRI (Bennion et al., 2017, Min et al., 2014), while 2 studies did not find any difference in infarct volume following C21 treatment as determined by MRI (Eldahshan et al., 2021, Schwengel et al., 2016).

3.3.3.3 Overall effects of RAAS targeting interventions on infarct volume

The effects of RAAS targeting interventions on infarct volume post-stroke, determined my TTC staining and MRI imaging, varied between research studies as illustrated in Table 3.5Table 3.5. The effects of RAAS targeting interventions on infarct volume were characterised as: significant reduction, no significant change, both reduction and expansion (i.e. low concentration of RAAS targeting intervention led to increased infarct volume while high concentration led to reduced infarct volume) or significant expansion. Of the 12 assessments using TTC staining to measure infarct volume, a total of 10 assessments identified a significant reduction in infarct volume, while 2 studies showed no change in infarct volume. Of the 4 assessments using MRI to measure infarct volume, a total of 2 assessments identified a significant reduction in infarct volume, and 2 studies showed no change in infarct volume following RAAS targeting intervention as shown in Table 3.6. Overall, 12 assessments showed significant improvement in infarct volume following RAAS targeting interventions, irrespective of assessment method, while 4 assessments showed no change in infarct volume following RAAS targeting interventions as outlined in Table 3.6.

Table 3.5 Benefits of RAAS targeting interventions on post-stroke infarct volume.

| Main Intervention | Author | Infarct assesment | |
		TTC	MRI
C21	Alhusban et al., 2015	1	
	Bennion et al., 2018	1	
	Bennion et al., 2017		1
	Eldahshan et al., 2019	1	
	Eldahshan et al., 2021		1
	Fouda et al., 2017	1	
	Ishrat et al., 2019	1	
	Joseph et al., 2014	1	
	Min et al., 2014		1
	Schwengel et al., 2016		1
	Shan et al., 2018	1	
Ang-(1-7)	Bennion et al., 2018	1	
	Jiang et al., 2014	1	
	Regenhardt et al., 2013	1	
Other	C. Y. Ma & L. Yin., 2016	1	
	Iwai et al., 2004	1	
Total number of studies		**12**	**4**

Significant reduction	(green)
No significant change	(yellow)
Both reduction and expansion	(magenta)
Significant expansion	(orange)

Table 3.6 Overview of the reduction or expansion of infarct volume following RAAS targeting interventions post-stroke.

Effect of RAAS intervention	TTC	MRI	Total number
Notable reduction	10	2	**12**
No significant change	2	2	**4**
Both reduction and expansion	0	0	**0**
Significant expansion	0	0	**0**

3.3.4 Effects of C21, Ang-(1-7) or other RAAS modulators on relevant peptides and receptor expression post-stroke

Molecular techniques such as western blotting, Enzyme Linked-Immunosorbent Assay (ELISA) and quantitative polymerase chain reaction (qPCR) can be used to assess levels of gene and protein expression. These techniques have been widely used by studies included in this systematic review to investigate the effects of RAAS targeting interventions on post-stroke expression profiles. A total of 7 publications investigated the effects of RAAS targeting intervention on relevant RAAS proteins and cognate receptors expression of said RAAS targeting interventions (Alhusban et al., 2015, Bennion et al., 2018a, Shan et al., 2018, Arroja et al., 2019, Chang et al., 2014, Ma and Yin, 2016, McCarthy et al., 2009). A total of 5 types of expression assessments were used in these 7 publications including: immunohistochemistry (IHC), qPCR, ELISA, western blot and liquid chromatography mass spectrometry (LCMS) as shown in Table 3.7.

Table 3.7 Classification of expression assessment methods

Main Intervention	Author	Expression assessment				
		IHC	qRT-PCR	ELISA	WB	LCMS
C21	Alhusban et al., 2015				1	
	Bennion et al., 2018					1
	Shan et al., 2018		1			
Ang-(1-7)	Arroja et al., 2019		1			
	Chang et al., 2014			1		
Other	C. Y. Ma & L. Yin., 2016	1				
	McCarthy et al., 2009	1				
Total number of studies		**2**	**2**	**1**	**1**	**1**

A total of 7 studies used various methods to better understand the effects of RAAS interventions on expression profiles following ischaemic stroke (Alhusban et al., 2015, Bennion et al., 2018a, Shan et al., 2018, Arroja et al., 2019, Chang et al., 2014, Ma and Yin, 2016, Iwai et al., 2004, McCarthy et al., 2009). Three studies assessed the effects of RAAS intervention on relevant expression profiles in SD rats post-stroke (Chang et al., 2014, Ma and Yin, 2016, Bennion et al., 2018a). Two studies investigated the effect of RAAS intervention on relevant expression profiles in Wistar rats post-stroke (Alhusban et al., 2015, Arroja et al., 2019). One group investigated the effect of RAAS intervention on relevant expression profiles in SHR rats post-stroke (McCarthy et al., 2009), while another group investigated the effect of RAAS intervention on expression profiles in C57BL/6 mice (Shan et al., 2018). RAAS interventions included Candesartan, CGP42112, C21 and Ang-(1-7) administered with or without other interventions such as PD123319, A779, AT_4R antiserum or GW9662.

SD rats were pretreated with either Candesartan (5 nmol), PD123319 (5 nmol), A779 (5 nmol), AT_4R antiserum (unknown starting concentration diluted 1:20) or vehicle prior to tMCAO. Within the RVLM of stroke rats 60 minutes post-stroke, Ang II levels were significantly increased in all treatment groups relative to sham control animals as determined by ELISA. Ang-(1-7) and Ang IV were decreased in all treatment groups relative to sham control animals, while angiotensinogen concentration remained similar between treatment groups and sham control animals (Chang et al., 2014). SD rats subjected to tMCAO were treated with CGP42112 (1 mg/kg/day; i.p.) or PD123319. On day 7 animals were humanely culled and expression of AT_2R within brain tissue was assessed using IHC. AT_2R expression was increased in CGP42112 treated stroke animals (0.46-fold change; $p<0.05$) compared to saline control, while stroke animals that received PD123319 showed reduced levels of AT_2R expression (-0.43-fold change; $p<0.05$) (Ma and Yin, 2016). SD rats were subjected to MCAO and were treated with C21 (1.5 µg/kg) either intranasally or intraperitoneally. C21 concentration was similar in the right olfactory bulb, cortex and striatum in stroke and non-stroke animals following i.n. C21 treatment as determined by LCMS. However, following i.p. C21 treatment, C21 concentration was significantly increased in the right cortex (5.31-fold change) and right striatum (6.25-fold change) of stroke animals compared to non-stroke C21 treated animals ($p<0.05$) (Bennion et al., 2018a).

Wistar rats subjected to tMCAO were treated with C21 (0.03 mg/kg; i.p.). Twenty-four hours post-stroke, within ipsilateral brain homogenates, AT_1R (AGTR1A 60 kDa isoform) expression was reduced following C21 treatment (-0.26-fold change) compared to saline

treated stroke animals as determined by western blot ($p<0.05$). Additionally, AT_1R (AGTR1B 45 kDa isoform) expression was decreased following C21 treatment (-0.35-fold change) compared to stroke saline treated animals ($p<0.01$). Interestingly, AT_2R expression was increased in contralateral brain homogenates following C21 treatment (1.88-fold change) compared to sham controls ($p<0.01$), and saline treated stroke animals (0.70-fold change; $p<0.05$), while AT_2R expression was similar in the ipsilateral hemisphere of C21 and saline treated stroke rats (Alhusban et al., 2015). Wistar rats subjected to tMCAO were treated with Ang-(1-7) (1.1 nmol; 1 mL/hr; i.c.v.) and the expression of various genes within the peri-infarct zone were assessed using qPCR at 24 hours and 7 days post-stroke. Mas1 was downregulated in both vehicle control (-0.62-fold change) and Ang-(1-7) treated animals (-0.54-fold change) compared to sham control by day 7 post-stroke ($p<0.05$). Interestingly, Agtr2, the gene encoding the AT_2R, was downregulated in vehicle treated animals (0.43-fold change), but not in Ang-(1-7) treated animals, compared to sham control by day 7 post-stroke ($p<0.01$). Mas 1 and Agtr2 expression was similar between treatment groups 24 hours post-stroke, while Agtr1, ACE and ACE2 expression was similar between treatment groups at both 24 hours and 7 days post-stroke (Arroja et al., 2019).

SHRs were treated with CGP42112 (1 ng/kg/min; i.c.v.) for 5 days before and continued 3 days after tMCAO. By day 3 post-stroke animals were humanely culled, and brain sections were frozen in preparation for IHC to determine AT_2R expression. Within the ipsilateral infarct zone after CGP42112 treatment, AT_2R expression was increased (1.79-fold change) relative to the vehicle control ($p<0.05$). AT_2R expression was similar in the non-infarcted ipsilateral or representative non-infarcted and infarcted areas of the contralateral hemisphere after CGP42112 treatment (McCarthy et al., 2009).

C57BL/6 mice were treated with C21 (10 µg/kg/day; i.p.) for a period of 8 weeks prior to tMCAO. Animals were humanely killed 24-hours post-stroke and expression of AT_1R and AT_2R were assessed in the ischaemic cortex using qPCR. AT_1R and AT_2R levels were unchanged after C21, C21 combined with GW9662 or GW9662 treatment (Shan et al., 2018). Relevant RAAS peptides and cognate receptors expression identified various different patterns of change and have been summarised in Table 3.8. Most prominently, three studies found that AT_2R expression was upregulated post-stroke following C21 and CGP42112 treatment (Alhusban et al., 2015, Ma and Yin, 2016, McCarthy et al., 2009).

Table 3.8 Overview of expression patterns following RAAS targeting interventions post-stroke.

Author	Date	Model	Intervention	Assessment method	Pattern of change
Alhusban et al.,	2015	Wistar rats	C21	Western blot	↓AT1R; ↑AT2R
Bennion et al.,	2018	Sprague-Dawley rats	C21	LCMS	↑C21
Shan et al.,	2018	C57BL6/J mice	C21 and GW9662	qPCR	▬ AT1R; ▬ AT2R
Arroja et al.,	2019	Wistar rats	Ang-(1-7)	qPCR	↓Mas1; ▬Agtr1; ▬ Agtr2; ▬ Ace; ▬ ACE2
Chang et al.,	2014	Sprague-Dawley rats	Candesartan, PD123319, A779 and AT4R antiserum	ELISA	↑ Ang II; ↓ Ang-(1-7); ↓ Ang IV
McCarthy et al.,	2009	Spontaneously hypertensive rats	CGP42112	IHC	↑ ▬ AT2R
Ma & Yin.	2016	Sprague-Dawley rats	CGP42112 and PD123320	IHC	↑↓ AT2R

↑ Increased   ↓ Decreased   ▬ Unchanged

3.4 Discussion

In this systematic review a total of 414 hits were identified from an online screening of EMBASE and MEDLINE databases, in line with the published protocol entitled "Do components of the counter-regulatory axis of the renin angiotensin aldosterone system effect post-stroke functional outcomes?" (https://syrf.org.uk/protocols). Of these 414 hits a total of 27 publications met the inclusion criteria and were included in further data analysis. Specific outcome measures were categorised into neurological outcomes, infarct volume and expression profiles. Various forms of neurological and infarct volume assessment were conducted, by 3 or more studies, to determine the effects of RAAS targeting interventions post-stroke. Additionally, the effects of RAAS targeting interventions on expression profile were also assessed. A total of 42 neurological assessments were conducted, 31 assessments found that RAAS targeting interventions improved neurological outcomes in preclinical stroke models. Of the 16 infarct volume assessments carried out, 12 assessments found that RAAS targeting interventions reduced infarct volume in preclinical stroke models. RAAS targeting interventions led to differential expression of components of RAAS, such as ACE, ACE2 and cognate receptors for individual interventions. Overall, RAAS targeting interventions improved functional outcomes following experimental stroke.

Broad neuroscoring was conducted in several studies, whereby those using Garcia score (0-18), Bederson (5-point) score and 5-point scale unanimously demonstrated improvement in neuroscore. Although those using Bederson (0-3) score ultimately showed overwhelming improvement in neuroscore following RAAS targeting intervention, not all studies noted improvement. Of the 7 studies that used Bederson (0-3) to assess neurological outcomes (Ahmed et al., 2018, Ahmed et al., 2019, Bennion et al., 2018a, Bennion et al., 2017, Fouda et al., 2017, Joseph et al., 2014, Bennion et al., 2018b) only one study found no change in neurological outcomes following RAAS intervention in preclinical models of stroke (Ahmed et al., 2019). When comparing Bederson (0-3) score there were several variables between studies for example experimental stroke models, animal strain/species and type of RAAS targeting intervention. Interestingly, the one study that found no change in Bederson (0-3) score following RAAS targeting intervention was the only study in this assessment group to use tandem distal pMCAO and was the only study to administer RAAS targeting interventions orally. Therefore, one may speculate that type of experimental stroke or route of administration could be the reason for no improvement in Bederson (0-3) score compared to the other 6 studies (Ahmed et al., 2019).

For those using Bederson (0-3) score, some authors did not provide information on size of infarct volume following MCAO in their studies included in this comparison of Bederson (0-3) score (Ahmed et al., 2018, Ahmed et al., 2019). However, other studies provided a value for the infarct volume of control stroke animals not receiving RAAS targeting interventions, whereby infarct volume caused by stroke in control animals in the absence of intervention ranged from 33-55%. The infarct volume in these animals demonstrates the expected infarct volume cause by the type of stroke surgery. Infarct volume is known to differ between experimental stroke models (Zhang and Faber, 2019). The ischaemia induced by distal MCAO is known to result in smaller infarct volumes, and one may speculate that this may be correlated to better neurological outcomes (Carmichael, 2005). It is well established that poorer neurological outcomes are correlated with larger infarct volumes (Haranhalli et al., 2020). Consequently, one may suggest this lack of change in neurological outcome following RAAS targeting intervention may be related to smaller initial infarct volume, thus reducing the ability of RAAS targeting interventions to cause notable improvements in neurological outcomes.

To assess the effects of RAAS targeting interventions on post-stroke cognition, studies used NOR and passive avoidance tests. All studies using NOR to determine the effects of RAAS targeting intervention post-stroke found no significant improvement in DI/RI. Importantly, this does not mean that C21 did not improve DI/RI compared to baseline control. In actuality, saline control stroke animals showed declined DI/RI, while C21 returned DI/RI to levels reflective of baseline reading in 3 of the 4 studies, demonstrating the benefits of C21 post-stroke (Ahmed et al., 2018, Ahmed et al., 2019, Jackson-Cowan et al., 2021). Clinically, stroke patients experience vascular cognitive impairment immediately after stroke onset which can remain for 3 to 40 months post-stroke, depending on stroke type, before gradually improving or resolving (Jokinen et al., 2015, Garcia et al., 2013). Therefore, the timing at which cognition is assessed in experimental stroke models is an important factor. In the studies that investigated the effects of RAAS targeting interventions on cognition using NOR, 2 groups assessed NOR at 21 days post-stroke, one assessed NOR at 2- and 4-week post-stroke, while the final study assessed NOR at 7 days post-stroke. Perhaps if these studies included later NOR assessment timepoints, for example 3 months, then the benefits of RAAS targeting interventions on cognition may have been more easily separated from expected basal improvements in cognition post-stroke.

Studies utilising passive avoidance test to determine the effects of RAAS intervention on post-stroke cognition demonstrated varying improvements in outcomes (Ahmed et al.,

2018, Ahmed et al., 2019, Eldahshan et al., 2021). The studies that found significant improvement in passive avoidance test subjected SHRs to tMCAO, while the study that showed no change in passive avoidance test subjected Wistar rats to distal pMCAO. Perhaps the difference in experimental stroke surgery or even rat strain may explain why no changes were observed in passive avoidance test score in one of the 3 studies (Ahmed et al., 2019). Previously it has been shown that Wistar rats have significantly smaller infarct volumes following 60- and 75- minutes of occlusion compared to SHR counterparts (Encarnacion et al., 2011). Similarly, compared to SHR rats that are stroke prone, Wistar rats demonstrate reduced basal blood pressures (Hannawi et al., 2021a). Unfortunately, infarct volume values were not described in two of the three studies using passive avoidance test to fully determine base infarct volume for SHRs (Ahmed et al., 2018, Ahmed et al., 2019). Despite this, it is plausible that differences in rat strains may influence infarct volume and subsequently neurological outcomes.

The effects of RAAS targeting interventions on sensory and motor function post-stroke were determined by paw adhesive test, rotarod test and paw grasp. All studies that used paw adhesive test unanimously demonstrated improvement in sensory motor function following RAAS targeting intervention (Bennion et al., 2017, Jackson et al., 2020, Bennion et al., 2018b). Rotarod and paw grasp, however, showed varying improvement in post-stroke motor function following RAAS intervention (Alhusban et al., 2015, Ishrat et al., 2019, Eldahshan et al., 2019, Bennion et al., 2017). The 2 studies that found improvement in rotarod test post-stroke following C21 treatment used the same concentration of C21 (0.03 mg/kg) delivered through IP injection. However, the study that found no difference in rotarod test following C21 treatment used a smaller dose of C21 (0.001 mg/kg) delivered intravenously (Ishrat et al., 2019). Intravenous injection can result in receptor saturation and rapid elimination of compounds from the circulation therefore IP injection may be more beneficial in delivering drugs to the brain following stroke, thus allowing prolonged exposure to C21 (Al Shoyaib et al., 2019). These differences in concentration and route of administration may explain why this study did not show similar improvements of C21 on post-stroke rotarod test compared to other studies using this assessment method. Paw grasp was used to assess the effects of RAAS targeting interventions on motor function post-stroke which yielded mostly neutral results. This may be due to the small number of studies using this method and the variables of the comparison. For example, concentration of C21, route of administration, assessment timeframe and type of experiment stroke varied between study, all of which may impact the observed benefit of

C21 post-stroke. Perhaps if there were more studies to compare the effects of C21 on paw grasp, the larger dataset would consolidate the effects of C21 on paw grasp post-stroke.

When investigating the effects of RAAS targeting interventions in preclinical models of ischaemic stroke, the most common method of assessing infarct volume was TTC staining. This method provided the greatest ratio of studies showing reduction in infarct volume to those showing no change in infarct volume whereby a total of 10 studies showed improvement in infarct volume following RAAS targeting intervention post-stroke (Alhusban et al., 2015, Bennion et al., 2018a, Bennion et al., 2018b, Fouda et al., 2017, Eldahshan et al., 2019, Ishrat et al., 2019, Joseph et al., 2014, Shan et al., 2018, Jiang et al., 2014, Regenhardt et al., 2013, Ma and Yin, 2016, Iwai et al., 2004). Irrespective of final infarct volume, all Wistar rats were treated with C21 as the RAAS targeting intervention and all received similar doses of C21. One study that found no change in infarct volume following RAAS targeting intervention used eMCAO method compared to all other Wistar studies using tMCAO and as such perhaps this lack of reduction in infarct volume may be related to the stroke model used (Ishrat et al., 2019). Indeed, compared to the other two studies using tMCAO in Wistar rats, whereby infarct volume ranged from approximately 37-42% in saline treated animals 24 hours post-stroke, Wistar rats subjected to eMCAO showed an infarct volume of approximately 23% in saline treated stroke animals 24 hours following eMCAO (Alhusban et al., 2015, Fouda et al., 2017, Ishrat et al., 2019). Possibly this lack of improvement in infarct volume, as determined by TTC staining, may be due to small initial infarct volumes. Another notable difference between studies was the co-administration of tPA with RAAS targeting interventions (Ishrat et al., 2019). Application of tPA with novel stroke interventions has previously been shown to reduce the benefit of novel stroke interventions, for example in the ESCAPE-NA1 trail (Hill et al., 2020). One may therefore postulate that lack of reduction in infarct volume in certain studies may be due to their use of tPA in combination with C21, however baseline C21 treatment independent of tPA did not yield any significant difference in infarct volume (Ishrat et al., 2019). Methodologically, TTC staining poses several issues such as variance in incubation time, tissue infiltration of mitochondrial enzyme-containing macrophage and difficulty delineating brain architecture within unstained infarcted regions, all of which may contribute to discrepancies between studies (Liszczak et al., 1984, Wexler et al., 2002). Another important factor to consider is that TTC staining is usually conducted at relatively acute timepoints post-stroke, most commonly 24 hours following stroke induction (Türeyen et al., 2004). In the days following stroke, lesion volumes can continue to expand due to inflammation (Schwamm et al., 1998). Therefore, assessing infarct volume at 24

hours post-stroke using TTC staining may not accurately determine the full extent of the infarct volume post-stroke.

Using MRI to assess the effects of RAAS targeting interventions on preclinical stroke models, a total of four assessments were conducted with varying results. Comparing all studies that used MRI to assess infarct volume, there were 3 animal strains/species, various intervention administration routes and 2 forms of experimental stroke. Importantly, all studies used the same RAAS targeting intervention, C21, at similar concentrations. Grouping these models into pMCAO and tMCAO, all studies using tMCAO model showed no change in infarct volume following RAAS intervention, while both studies using pMCAO showed reduction in infarct volume following RAAS targeting intervention. The time at which the MRI was conducted post-stroke varied significantly between studies, from 24 hours to 6 weeks post-stroke and as such the degree of lesion expansion and reduction may vary between studies and may give way to the variances observed between studies. For example, in humans, infarct lesion volume continues to expand from onset to day 3 post-stroke, and reduces in size after day-3 as recovery mechanisms take affect (Lansberg et al., 2001). Similarly, the infarct volumes also varied between studies and stroke model. pMCAO is known to cause larger infarct volumes than tMCAO (Zhang and Faber, 2019). Infarct volume ranged from approximately 15-50%, so too did the method of quantifying infarct size by MRI vary between studies, for example infarct volume as determined by the percentage total of the whole brain or infarct volume as a percentage of the contralateral side (Min et al., 2014, Bennion et al., 2017, Eldahshan et al., 2021, Schwengel et al., 2016). Additionally, one may also assume that, due to differences in the extent of lesion size and the degree of neuroinflammation between models, the downstream pathways activated by AT_2R stimulation may also be altered between studies, thus affecting the observed impact of RAAS targeting interventions post-stroke. Combined, these identified variables may in part contribute to the variation observed in MRI assessments to determine the effects of RAAS targeting interventions in preclinical models of stroke.

The time point of RAAS targeting intervention administration is also a key aspect to consider in terms of translatability. A total of 19 of the 27 studies administered RAAS targeting interventions post-stroke (Ahmed et al., 2018, Ahmed et al., 2019, Alhusban et al., 2015, Arroja et al., 2019, Bennion et al., 2017, Bennion et al., 2018a, Ma and Yin, 2016, Eldahshan et al., 2019, Eldahshan et al., 2021, Fouda et al., 2017, Jackson et al., 2020, Jackson-Cowan et al., 2021, Jiang et al., 2014, Kuipers et al., 2020, Lee et al., 2012, Mateos et al., 2016, Min et al., 2014, Schwengel et al., 2016, Shan et al., 2018), while 5

administered RAAS targeting interventions prior to- and post-stroke (Bennion et al., 2018b, Joseph et al., 2014, McCarthy et al., 2009, McCarthy et al., 2012, Regenhardt et al., 2013) and 3 studies administered RAAS targeting interventions prior to stroke (Chang et al., 2014, Iwai et al., 2004, McCarthy et al., 2014). A therapeutic that can prevent stroke does not exist, rather, therapies may be prescribed to a patient to prophylactically reduce the risk of stroke or the reoccurrence of stroke. One may question the protective effects that these RAAS targeting interventions may have post-stroke when solely administered under basal conditions prior to the onset of stroke and not following stroke when these interventions may beneficially effect stroke pathology. Therefore, studies that elected to administer RAAS targeting interventions both before and after stroke, may be more reflective of relativity of treating stroke pathology and the drug regimens of stroke patients. It may also be argued that administration of RAAS targeting interventions post-stroke may also be reflective of clinical care, whereby only after the occurrence of stroke do patients receive interventions, such as tPA or antihypertensives, that may positively affect stroke pathology.

3.4.1 Mechanisms of RAAS-mediated neuroprotection

Although not the aim of this systematic review, the data included in these publications also provided insight into the mechanisms behind how these RAAS targeting interventions may be beneficial post-stroke. Oxidative stress occurs when cells possess high levels of reactive oxygen species (ROS) (Allen and Bayraktutan, 2009). ROS, due to unpaired electrons, are capable of causing cellular damage, and within the ischaemic brain, can potentiate stroke pathology as discusses in the introduction chapter (Hernandes et al., 2022). Post-stroke ROS can lead to lipid peroxidation and changes within endothelial cell permeability, which is a key component that drives tissue damage in tMCAO and pMCAO stroke models (Peters et al., 1998). Several studies in this systematic review identified a link between reduced ROS and improved post-stroke outcomes following treatment with RAAS targeting interventions (Arroja et al., 2019, Jiang et al., 2014, Regenhardt et al., 2013, Shan et al., 2018).

In ischaemic stroke, immune cells called monocytes are recruited to the lesion site from 24-hours post-stroke and plateau at approximately 4 days post-stroke (Gliem et al., 2012). Within the brain, monocytes differentiate into macrophage, phagocytic cells that clear damaged tissue and release proinflammatory cytokines within the area to stimulate the recruitment of further immune cells (Miro-Mur et al., 2016). Immune cell recruitment and

release of proinflammatory cytokines often leads to collateral damage to the brain. This systematic review demonstrated that RAAS targeting interventions reduced monocyte attraction and proinflammatory cytokine profiles providing a degree of neuroprotection (Arroja et al., 2019, Min et al., 2014, Lu et al., 2008, Joseph et al., 2014, Regenhardt et al., 2013). Neutrophils, phagocytic immune cells are also recruited to the brain post-stroke. Over and above their clearance roles, neutrophils release ROS within the brain leading to increased blood brain barrier (BBB) permeability (Matsuo et al., 1994). Treatment with RAAS targeting C21 correlated with increased BBB integrity post-stroke (Shan et al., 2018). Additionally, neuronal formation and neuronal growth were also shown to be upregulated after RAAS modulation (Alhusban et al., 2015, Schwengel et al., 2016, Shan et al., 2018). Combined, it appears that the beneficial effects of RAAS targeting interventions in preclinical models of stroke are related to reduction in ROS, modulation of immune response, improvement in BBB integrity and stimulation of neuronal cell growth.

3.4.2 Data reporting and limitations

Heterogeneity in outcome measures in preclinical stroke has been highlighted in literature (Hietamies et al., 2018). Due to the heterogeneity seen in assessment methods only assessment methods used by $3\geq$ or more studies were analysed in-depth. With that being said there were 10 different neurological assessments used in downstream data analysis. The number of studies that used each neurological assessment varied. Assessment methods used by a greater number of publications provided greater power for comparison. Other neurological assessments used by fewer than 3 studies may have also supported or contradicted the hypothesis that RAAS targeting interventions are neuroprotective post-stroke, however as these studies were not subjected to data extraction and analysis, one cannot be certain. Perhaps if the subject of this systematic review was solely in relation to the effects of RAAS targeting interventions on post-stroke neurological outcomes, then these studies could have been included. TTC staining and MRI were the most common methods of assessing infarct volume post-stroke, however 5 additional methods were also used to determine infarct volume at a frequency of less than 3 publications. Again, if the subject of this systematic review was solely in relation to the effects of RAAS targeting interventions on post-stroke infarct volume, then these studies could have been included. In providing a more comprehensive overview of the impact of RAAS targeting interventions post-stroke, some assessment methods were excluded.

One reason why TTC staining is a common method of assessing infarct volume, and certainly TTC staining was the most common method identified in this systematic review, is because it is a simple and inexpensive technique, but it does come with its drawbacks as previously discussed. More advanced methods of measuring infarct volume such as MRI are highly expensive and specialised training is required to carry out *in vivo* imaging. A benefit of using MRI over TTC staining is that imaging can be conducted on live animals and changes in infarct volume can be assessed at various time points. With that being said, the interpretation of MRI images may be subjective, and images may be distorted due to small brain sizes and acquisition parameters (Chow et al., 2016, Xu et al., 2022).

Western blot, ELISA and qPCR were used to determine changes in gene and protein expression. Each study investigated different genes and proteins, with a small number overlapping between interventions. Here, qPCR provides information about gene expression but also provides insight into relative protein expression. Empirically, protein concentration can be determined by western blot and ELISA; however, ELISA is a far more sensitive quantification method than western blot. All methods of determining expression profiles are relatively inexpensive and are commonly used in research laboratories. High powered LCMS can be used in place of ELISA, qPCR and western blot to determine expression profiles, however at a greater cost.

As data was collected from English language, peer-reviewed journals, studies that may contain valuable information related to this subject may have been omitted from this systematic review as they were not written in English. In future, translation tools may be used to convert non-English journals into English, allowing for the incorporation of relevant data. The timeframe of publication search was from 1990 to present day (at time of screening). RAAS related research has vastly expanded from 1986 and research continues to this day. Consequently, due to continuous publication in the field, data published outside the data extraction timepoint may also prove beneficial in this comparison. It should be noted that, with any publication, there may be bias in reporting, for example where studies only publish data that supports the overall hypothesis. With that being said, more recent publications are subject to more stringent review processes. The stroke therapy academic industry roundtable (STAIR) meeting led to the development of proposed criteria to strengthen preclinical and clinical stroke research (Saver et al., 2009, Stroke Therapy Academic Industry Roundtable (STAIR), 1999, Fisher et al., 2009). Coupled with the animal research; reporting of *in vivo* experiments (ARRIVE) guidelines that provide a checklist for transparent reporting of animal research, publications are more reputable now than they have ever been (Percie du Sert et al., 2020, Kilkenny et al., 2010).

In fact, the quality of preclinical stroke research has increased over the past 10 years, enhancing confidence in preclinical stroke publications (Ramirez et al., 2017). In future studies it may be beneficial to widen the scope of assessment from solely ischaemic stroke to both ICH and TIA to better understand the potential role of RAAS modulations within other forms of cerebrovascular disease.

As discussed within the methodology, neurological assessment methods were modified in numerous studies. Cross-referencing was used to create an accurate understanding of assessment methods to allow for appropriate grouping. However, slight differences in assessment methods between studies may have introduced variance and ultimately led to the creation of new assessment method groups. For example, a publication may have stated a 5-point score was used to determine neurological outcome, however upon closer review this 5-point score ranged from 0-5 points, effectively making the assessment method a 6-point score.

3.4.3 Conclusions

Systematically reviewing the use of RAAS targeting interventions may identify new ways in which they can be used. This systematic review evaluated the potential neuroprotective qualities of RAAS targeting interventions following experimental stroke. An overwhelming number of studies demonstrated that RAAS targeting interventions were neuroprotective post-stroke and led to improvements in neurological outcomes and reduction in infarct volume. Mechanistically, some RAAS targeting interventions were able to modulate key aspects of RAAS in preclinical models of stroke. The result of this systematic review strengthens the conclusion that RAAS targeting interventions, some of which are already clinically approved for treatment of hypertension, may be neuroprotective post-stroke.

Chapter 4: Characterisation of circulating extracellular vesicles derived from wildtype or AT$_2$R deficient C57BL/6 mice

4.1 Introduction

4.1.1 RAAS and the AT$_2$R in stroke

As hypertension is the leading modifiable risk factor in stroke occurrence and outcome, the RAAS may be modulated to reduce blood pressure and in turn alter stroke pathology (GBD 2019 Stroke Collaborators, 2021). Overactivation of the classical axis of the RAAS is known to increase inflammatory mediators, fibrosis and oxidative stress, all of which are detrimental in stroke (Wright and Harding, 2013). Modulation of the central RAAS includes the use of angiotensin receptor blockers (ARBs), angiotensin converting enzyme inhibitors (ACEi), βeta adrenergic inhibitors, calcium channel blockers (CCB), and renin inhibitors, all of which have different mechanisms of action, but ultimately lead to a reduction in blood pressure. With this, common anti-hypertensive medications such as ACEi or ARBs have demonstrated varied neuroprotection in transient ischaemic attack, ischaemic stroke, and cerebral haemorrhage patients (Schrader et al., 2005, Gilliot et al., 2018).

It has widely been accepted that there is a separate RAAS axis within the brain, commonly known as b-RAS (brain-renin angiotensin system) (Ganten et al., 1971, Cosarderelioglu et al., 2020). Despite conflicting evidence, it is generally concluded that b-RAS can produce the same components as the peripheral RAAS, such as the brain specific isoform of renin (Shinohara et al., 2017). Numerous groups have identified key RAAS components in the brains of humans and other models. Of particular interest is the presence of RAAS-related receptors and their associated ligands and their potential beneficial effects in stroke.

Within the counter-regulatory axis of the RAAS, Ang-(1-7) binds to the G-protein-coupled receptor Mas receptor (MasR) (Santos et al., 2003). The ACE2-Ang-(1-7)-MasR axis may play a protective role in stroke. Mas1 and ACE2 expression was increased in the ischaemic brain cortex of Sprague-Dawley rats from 6-48 hours following permanent middle cerebral artery occlusion (pMCAO), while Ang (1-7) levels were increased in serum and brain homogenates post-pMCAO (Lu et al., 2013). Intracerebroventricular infusion of Ang-(1-7)

prior to endothelin-1-induced middle cerebral artery occlusion (ET-1-MCAO) led to a decrease in infarct volumes (Mecca et al., 2011).

Preclinically, AT_1R antagonists improve cerebral perfusion post-stroke, whilst AT_2R stimulation has been shown to reduce infarct volume and improve neurological outcome in spontaneously hypertensive rats following reversible middle cerebral artery occlusion and ET-1-MCAO (Nishimura et al., 2000, McCarthy et al., 2014). C21, an AT_2R agonist, delivered intracerebroventricularly after ET-1-MCAO led to decreased infarct volume and improved neurological outcomes in Sprague-Dawley rats following stroke (Joseph et al., 2014). Another AT_2R agonist, CGP42112, has demonstrated improved motor function and decreased infarct volume post-tMCAO *in vivo* (McCarthy et al., 2009), while *in vitro* CGP42112 treatment increased primary cortical neuronal cell viability (Lee et al., 2012). Additionally, EVs isolated from AT_2R overexpressing bone marrow-derived stem cells delivered intravenously to rodent models of carotid artery injury reduced levels of restenosis (Zou et al., 2023). To date no studies have assessed the effects of EVs in AT_2R deficient stroke models. Regulation of b-RAS via central RAAS regulation, for instance by stimulation of AT_2R, may lead to the development of treatments for cerebrovascular diseases. By harnessing the potential of EVs to deliver modulators of RAAS, stroke outcomes may be improved.

4.1.2 Extracellular vesicle signalling, cargo, and source

EVs directly bind to cell surface receptors to influence downstream signalling pathways or EVs can integrate into cells to release internalised cargo, such as proteins, RNA molecules and lipids to alter cellular processes, that may directly influence gene transcription (Anand et al., 2019, Gurung et al., 2021). After sorting, loading and budding, EVs deliver internalised cargo through autocrine, paracrine, and endocrine signalling (Wang et al., 2017b). There are two main methods of EV cargo sorting: the ESCRT complex dependent and ESCRT complex independent pathways (Sherman et al., 2021). With the former, ESCRT proteins allow for the formation of multivesicular bodies and budding and can also be responsible for cargo sorting from parental cell to EVs (Katzmann et al., 2001). The ESCRT complex-independent manner includes lipid rafts, tetraspanin-enriched microdomains and the neutral Sphingomyelinase (nSMase) pathway (Perez-Hernandez et al., 2013, Trajkovic et al., 2008). Recent research has demonstrated that nSMase regulates miRNA sorting into EVs independently of ESCRT proteins (Kosaka et al., 2010).

miRNA cargo contained within EVs can alter gene expression at a transcriptional level by binding target RNA and altering resultant protein production (Catalanotto et al., 2016). Sequence analysis has found that miRNAs are the most abundant RNA molecule within EVs, accounting for approximately 42% of raw read and 76% of mappable reads (Huang et al., 2013). The expression of miRNAs is altered in disease states and between sexes, illustrating the diversity of their signalling capacity (Guo et al., 2017a). As miRNAs have a range of effects throughout the body, what may be beneficial in stroke may be detrimental in other diseases and what may be upregulated in plasma EVs may be downregulated in tissues. For example, preclinically, EV-derived miRNA-126 has been shown to increase vascular endothelial growth factor receptor 2 (VEGFR2), expression and is thought to promote neurogenesis and neuronal cell migration post-stroke in diabetic mice subjected to pMCAO (Wang et al., 2020). Similarly, adipose-derived stem cell EVs overexpressing miRNA-126 delivered intravenously to Sprague Dawley rats two hours following tMCAO improved neurological outcomes (Geng et al., 2019). Conversely, after acute myocardial infarction EV-derived miRNA-126 has been found to stimulate immune cascades that exacerbate myocardial infarct size (Akbar et al., 2022). Preclinically, the most abundant plasma EV-derived miRNA, miRNA-99a, is downregulated in prostate cancer cells and suppresses tumorigenesis *in vitro* (Sun et al., 2011). However, C57BL/6 mice subjected to middle cerebral artery occlusion treated with miRNA-99a agomir by intracerebroventricular injection demonstrated reduced infarct volume compared to untreated stroke mice (Tao et al., 2015).

Various studies have demonstrated the beneficial and possible pathogenic effects of EV miRNAs in preclinical models of ischaemic stroke. For instance, miRNA-98 loaded EVs were found to decrease infarct volume and improved neurological score in Sprague Dawley rats and C57BL/6 mice following tMCAO (Yang et al., 2021a). Whereas, miRNA-9 and miRNA-124 were upregulated in serum derived EVs of acute ischaemic stroke patients and were positively correlated with infarct volume (Ji et al., 2016).

Based on current literature, miRNA-29a, miRNA-33a-5p, miRNA-132, miRNA-146a, miRNA-155, miRNA-188-5p, miRNA-212-5p and miRNA-483 were identified for their relation to RAAS, for example by targeting the AT_1R, AT_2R, MasR or ACE2 directly or differential expression of miRNAs after receptor-substrate interaction (Jeppesen et al., 2011, Zheng et al., 2010, Adamcova et al., 2021, Pacurari and Tchounwou, 2015, Sun et al., 2020, Wang et al., 2013a, Obama and Eguchi, 2014). Of significance, miRNA-132, found on the miRNA-132/-212 gene cluster, is important in neuronal development and function, synaptogenesis, synaptic transmission and neural angiogenesis (Qian et al.,

2017). Within the miRNA-146 family of miRNAs exists two separate genes that code for miRNA-146a and miR-146b (Paterson and Kriegel, 2017). miRNA-146a has been shown to negatively regulate upstream components of the proinflammatory NFκB pathway (Saba et al., 2014). As a result, the expression of these EV miRNAs may be beneficial post-stroke.

In humans and animals, EVs can be isolated from many different biological fluids such as blood serum and plasma, urine, breast milk, saliva, cerebrospinal fluid and lymph (Zhang et al., 2022, Pisitkun et al., 2004, Admyre et al., 2007, Chiabotto et al., 2019, Akers et al., 2016, Milasan et al., 2016). As heterogeneous blood EVs are derivatives of parental cells, they can provide insight into diseases throughout the body and are considered non-invasive liquid biopsies (Irmer et al., 2023). EV composition is dependent on cell source which resultantly may influence EV function (Hurwitz et al., 2016b). The presence of CD31 and CD41 cell markers on EVs from AT$_2$R deficient and wildtype mice was assessed. Individually, CD31 is a marker of endothelial cells and is expressed on the surface of immune cells, while CD41 is a transmembrane protein often expressed on platelets (Marelli-Berg et al., 2013). As endothelial cells, immune cells and platelets play crucial roles in stroke pathology, the presence of CD31 and CD41 on EVs of AT$_2$R deficient mice may also influence stroke outcome. With the wide variety of cell types within the body, it is difficult to define the exact type of parental cells from which EVs are derived. This process would require a large collection of data from numerous cell types to identify commonalities in EV surface markers between cell types. However, as guidelines have been developed in order to standardise EV research the idea of determining the source of EVs is not out-of-reach. By building on these experimental guidelines, for example through use of nano flow cytometry, EV surface markers can be detected and could provide insight into the role of cell origin on possible EV function.

4.2 Hypotheses and aims

4.2.1 Hypotheses

- AT_2R deficiency may alter EV characteristics compared to wildtype mice.
- AT_2R deficiency may alter EV surface markers and in turn may affect cell source compared to wildtype mice.
- miRNA content may be altered in EVs derived from AT_2R deficient mice compared to wildtype mice.

4.2.2 Aims

- Characterise EVs derived from wildtype and AT_2R deficient C57BL/6 mice.
- Identify CD31 and CD41 surface markers of EVs derived from wildtype and AT_2R deficient C57BL/6 mice to understand cell source.
- Characterise miRNA cargo within EVs derived from wildtype and AT_2R deficient C57BL/6 mice.

4.3 Methods

Methods used in Chapter 4 can be found in Chapter 2 of this thesis and are outlined below:

- 2.1.3.1 AT_2R mouse cardiac puncture
- 2.1.3.2 AT_2R mouse genotyping
- 2.2.1.1 Precipitation isolation
- 2.2.1.4 Pierce BCA protein assay
- 2.2.1.5 Nanoparticle tracking analysis
- 2.2.3.1 RNA extraction
- 2.2.3.2 Nanodrop quantification
- 2.2.3.3 miRNA reverse transcription
- 2.2.3.5 Quantitative real-time polymerase chain reaction
- 2.2.6 NanoFC
- 2.2.7 Statistical analysis

4.4 Results

4.4.1 AT$_2$R mice genotyping

AT$_2$R expression was determined by genotyping ear notch tissue samples from each mouse used in this investigation. Following tissue lysis, cDNA was amplified and run through a DNA gel to expose DNA banding. Wildtype, AT$_2$R expressing mice, were identified by one band at approximately 470 base pairs (bp), while heterogeneous AT$_2$R mice were identified by two bands at approximately 470 bp and 800 bp. AT$_2$R deficient mice were identified by one band at approximately 800 bp (Figure 4.1).
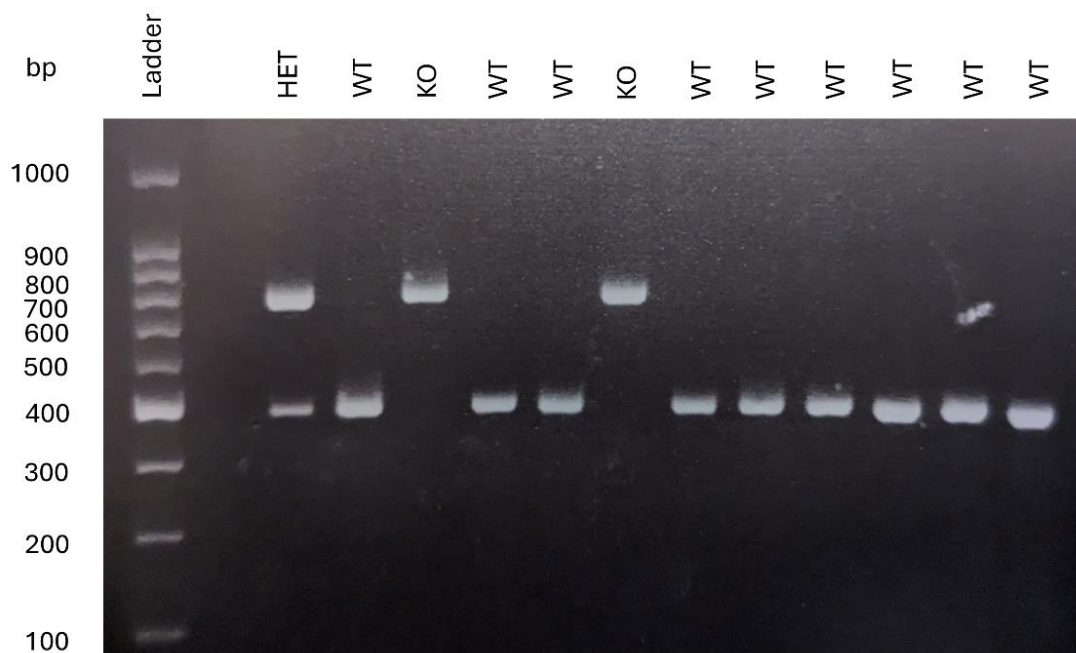
Figure 4.1 Representative image of DNA gel to determine genotype of wildtype and AT₂R deficient mice.
Mouse ear notch tissue samples were lysed, and DNA was amplified using RT-PCR. DNA samples were run through a 1% Agarose gel to allow for separation of DNA bands within the gel along with a 100bp ladder for size reference. The DNA gel was the imaged and DNA banding, representative of the size of DNA fragments, were used to determine whether mice were wildtype (WT), heterogenous for AT₂R (HET) or AT₂R deficient (KO).

4.4.2 AT$_2$R body weight

To assess whether knocking out the AT$_2$R affected overall body weight, wildtype and AT$_2$R knockout mice of approximately 8-10 weeks in age were weighed prior to cardiac puncture and isolation of plasma EVs. There was no significant difference in body weight between the wildtype males (WTM) (24.10 ± 0.72 g; mean ± SEM) and AT$_2$R knockout males (KOM) (23.67 ± 0.59 g). There was no significant difference in body weight between the wildtype females (WTF) (18.44 ± 0.29 g) and AT$_2$R knockout females (KOF) (18.56 ± 0.58 g). WTF weighed significantly less than WTM ($p<0.0001$), while KOF weighed significantly less that KOM ($p<0.0001$) (Figure 4.2).
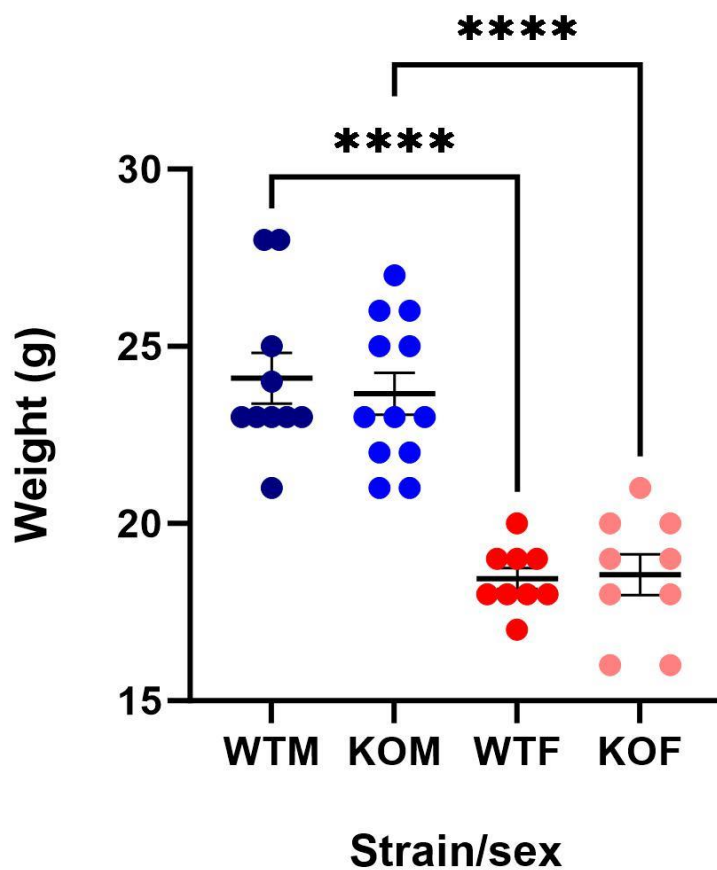
Figure 4.2 Body weight of wildtype and AT₂R knockout mice prior to cardiac puncture.
Mice of approximately 8-10 weeks old were weighed prior to cardiac puncture of plasma EV isolation and characterisation. Weight in grams (g) (WTM-EVs; n=10, KOM-EVs; n=12, WTF-EVs; n=9, KOF-EVs; n=9, $p<0.0001$, Brown-Forsythe and Welch ANOVA with post-hoc Dunnett's T3 multiple comparison).

4.4.3 Effects of sex and AT$_2$R expression on EV particle concentration, size and protein content

To assess whether sex or knocking out the AT$_2$R influenced EV characteristics, EVs were assessed using NTA (Figure 4.3) and bicinchoninic acid (BCA) assay (Figure 4.4). NTA data demonstrated an increase in particle concentration in KOF plasma-derived EVs (KOF-EVs) (2.98×10^{12} p/mL $\pm 0.31 \times 10^{12}$ p/mL; mean $\pm$ SEM) compared to WTF plasma-derived EVs (WTF-EVs) (1.73×10^{12} p/mL $\pm 0.23 \times 10^{12}$ p/mL; p=0.0063) (Figure 4.3 A). There was no difference in particle concentration between WTM plasma-derived EVs (WTM-EVs) (3.26×10^{12} p/mL $\pm 0.72 \times 10^{12}$ p/mL) and KOM plasma-derived EVs (KOM-EVs) (3.52×10^{12} p/mL $\pm 0.52 \times 10^{12}$ p/mL) (Figure 4.3 A).

NTA data also showed there was no difference in EV particle size between WT and AT$_2$R deficient mice in either sex. However, there was an increase in EV size in KOF-EVs (84.0 ± 3.5 nm; mean $\pm$ SEM) compared to KOM-EVs (71.01 ± 2.04 nm; p<0.05). EV size was comparable between WTF-EVs (80.64 ± 2.38 nm) and WTM-EVs (73.97 ± 3.38 nm) (Figure 4.3 B).

EV protein content, determined by BCA assay, was similar between WTM (515.82 ± 57.73 µg/mL; mean $\pm$ SEM) KOM (510.43 ± 50.24 µg/mL), WTF (746.87 ± 84.79 µg/mL and KOF (563.97 ± 51.85 µg/mL) (Figure 4.4).

A
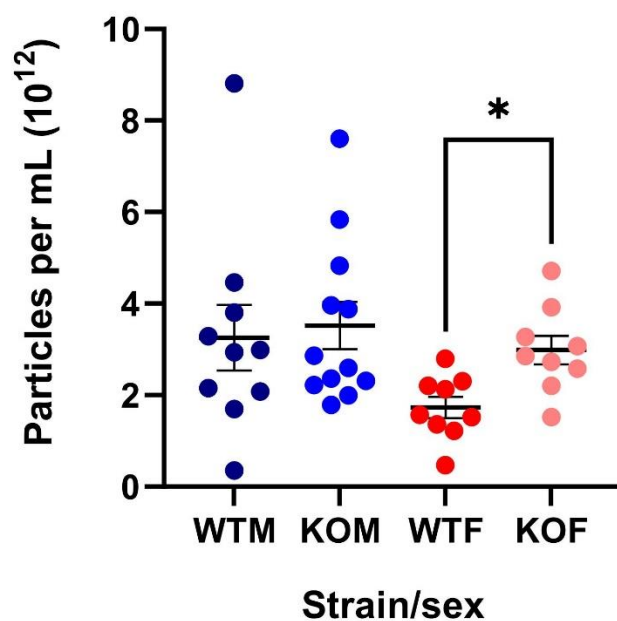
B
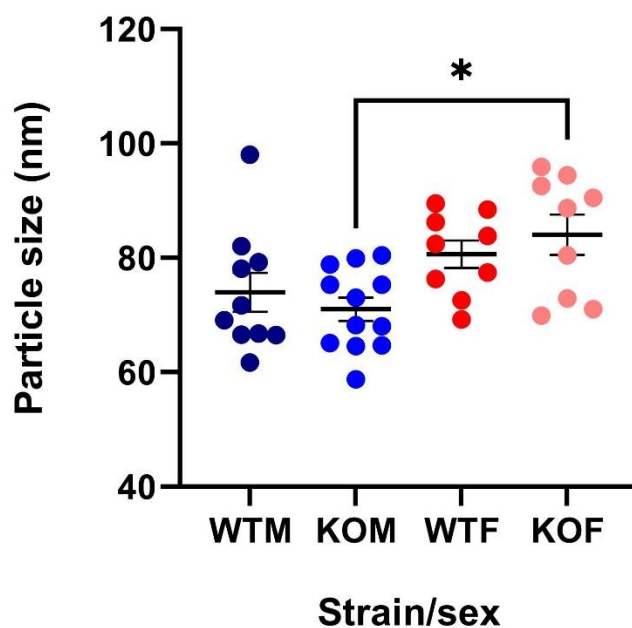
Figure 4.3 Characteristics of circulating EV from wildtype and AT$_2$R deficient mice. Comparison of EV particle concentration (A) and particle size (B) between wildtype or AT$_2$R deficient mice determined by NTA (WTM-EVs; n=10, KOM-EVs; n=12, WTF-EVs; n=9, KOF-EVs; n=9, p<0.05, Brown-Forsythe and Welch ANOVA with post-hoc Dunnett's T3 multiple comparison).
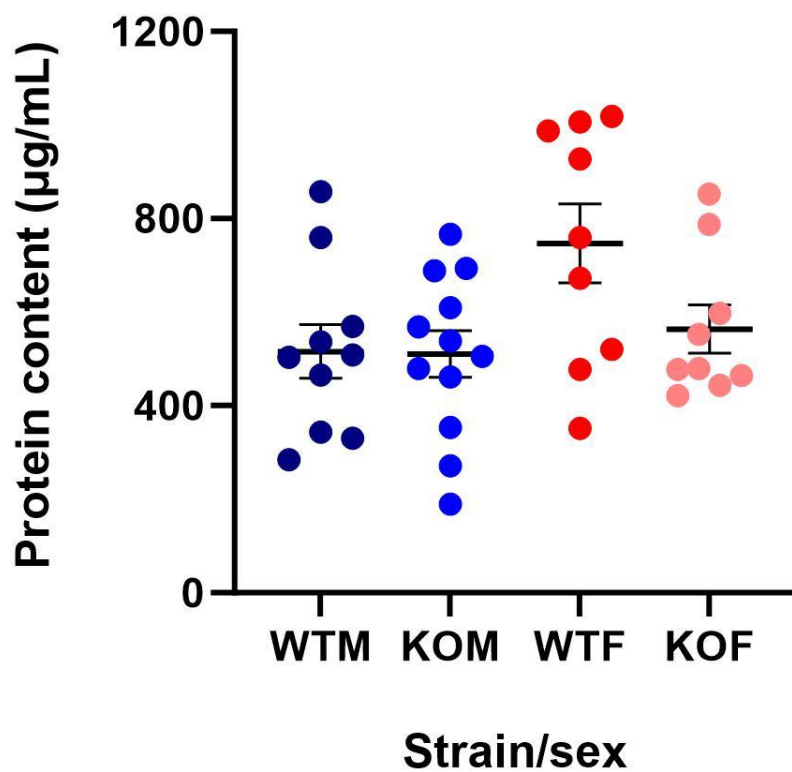
Figure 4.4 Protein content of circulating EV from wildtype and AT$_2$R deficient mice. Comparison of EV total protein content between wildtype or AT$_2$R deficient mice determined by BCA (WTM-EVs; n=10, KOM-EVs; n=12, WTF-EVs; n=9, KOF-EVs; n=9, p>0.05, Brown-Forsythe and Welch ANOVA with post-hoc Dunnett's T3 multiple comparison).

4.4.4 Effects of sex and AT$_2$R expression on EV cell sources

To understand if knocking out the AT$_2$R affected EV surface markers, plasma-derived EVs were analysed for the presence of platelet marker CD41 and endothelial cell marker CD31 using nano flow cytometry (nanoFC). NanoFC studies were conducted in the lab of Dr Ryan pink at Oxford Brookes University using the Luminex Amnis CellStream benchtop flow cytometer under the guidance of Mr Jamie Cooper. NanoFC gating strategy was conducted by Mr Jamie Cooper.

The number of CD41$^+$ events per mL between wildtype and AT$_2$R deficient groups in each sex were comparable (Figure 4.5 & Figure 4.6). There was no difference between WTM group (2.89 x 10^3 ± 0.89 x 10^3 events/mL; mean ± SEM) and WTF group (5.25 x 10^3 ± 1.63x10^3 events/mL) (Figure 4.7). There was a significant increase in the number of CD41$^+$ events per mL in KOF group (7.75 x 10^3 ± 1.01 x 10^3 events/mL) and KOM group 3.36 x 10^3 ± 0.57 x 10^3 events/mL, $p<0.01$) (Figure 4.8).

The number of CD31$^+$ events per mL between wildtype and AT$_2$R deficient mice in each sex were similar (Figure 4.9 & Figure 4.10). Within the wildtype groups, there was no difference in the number of CD31$^+$ events between WTM group (0.64x10^3 ± 0.14x10^3 events/mL; mean ± SEM) and WTF group (6.58x10^4 ± 3.47x10^4 events/mL) (Figure 4.11). The number of CD31$^+$ events per mL were significantly increased in KOF group (2.11x10^4 ± 0.39x10^4 events/mL) compared to KOM group (0.98x10^3 ± 0.23x10^3 events/mL, $p<0.05$) (Figure 4.12).
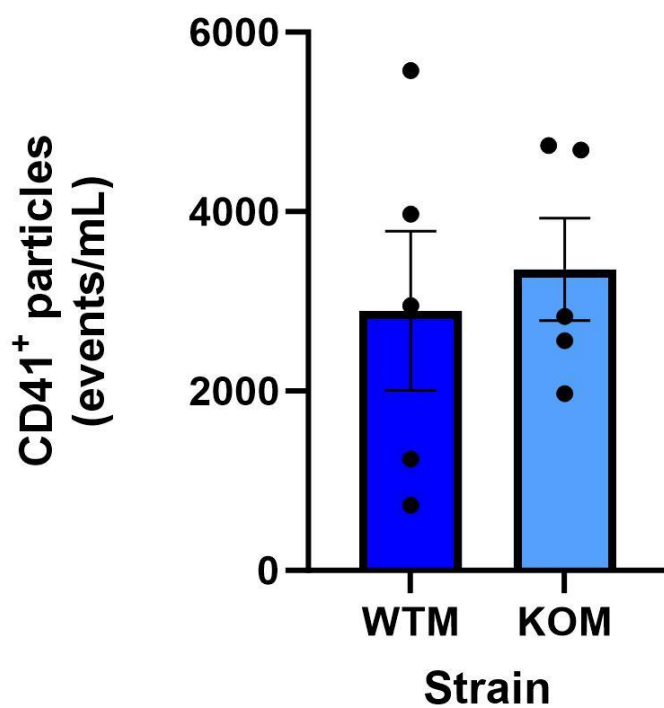
Figure 4.5 CD41$^+$ events in circulating EV samples from wildtype and AT$_2$R deficient male mice.
Number of CD41$^+$ event in WTM and KOM EV samples as determined by nanoFC.
(WTM; n=5, KOM; n=5, p>0.05, Welch's t-test).
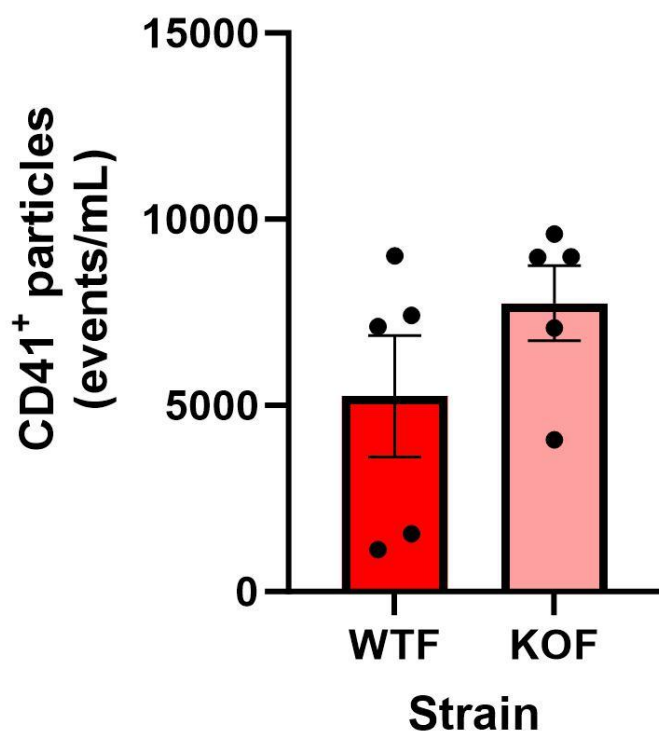
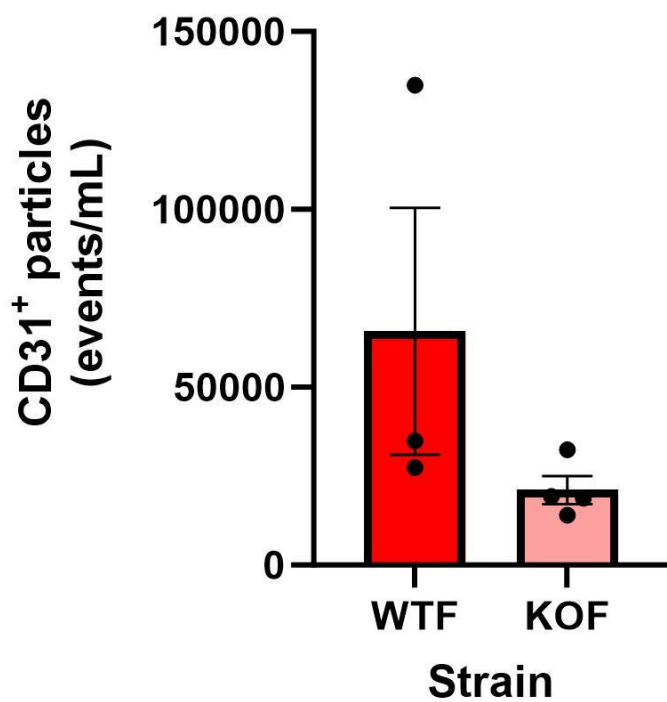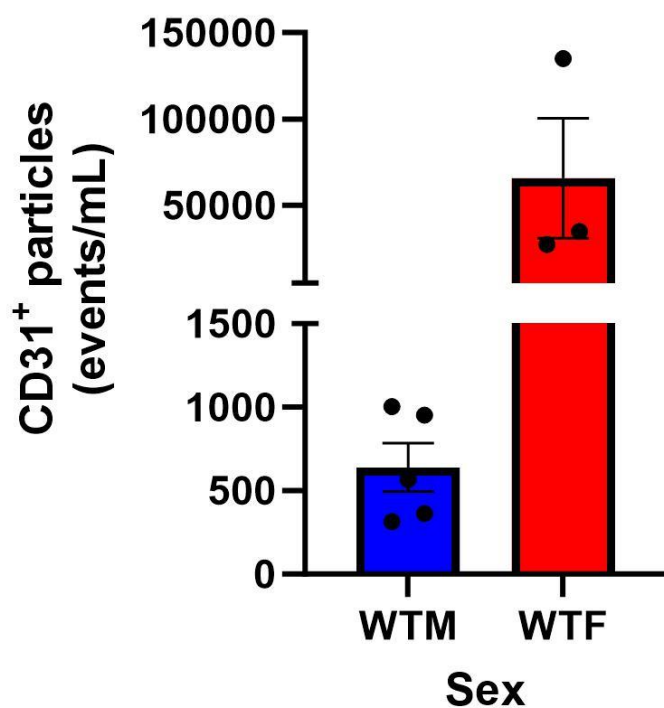**Figure 4.6 CD41$^+$ events in circulating EV samples from WT and AT$_2$R deficient female mice.**
Number of CD41$^+$ event in WTF and KOF EV samples as determined by nanoFC. (WTM; n=5, KOM; n=5, p>0.05, Welch's t-test).
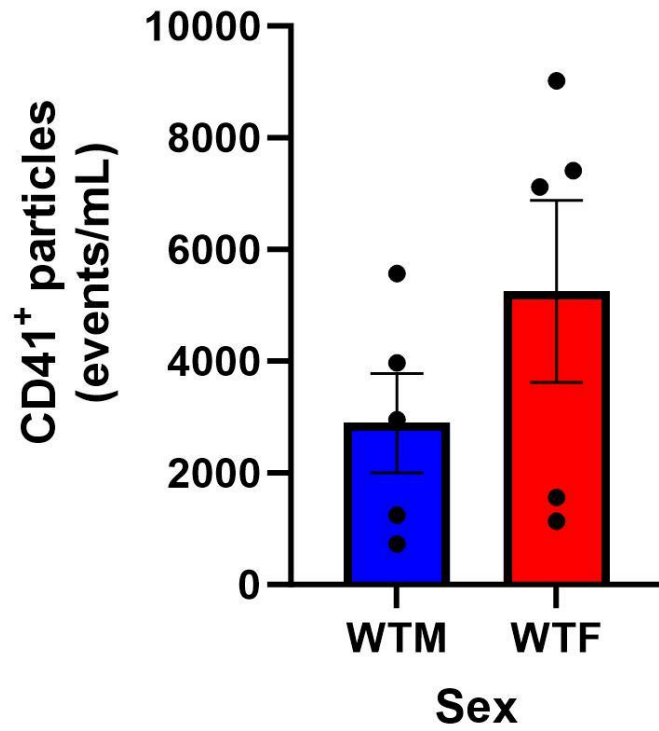
Figure 4.7 CD41$^+$ events in circulating EV samples from WT mice.
Number of CD41$^+$ event in WTM and WTF EV samples as determined by nanoFC.
(WTM; n=5, KOM; n=5, p>0.05, Welch's t-test).
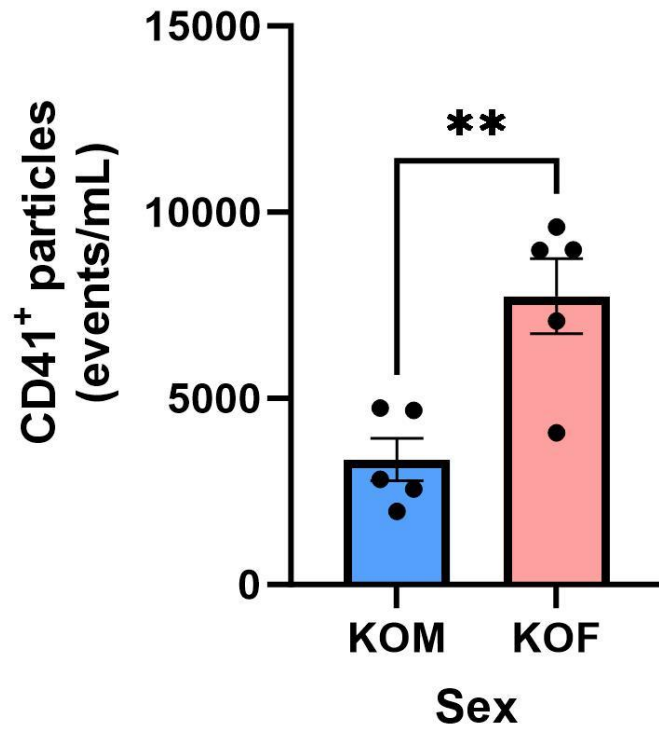
Figure 4.8 CD41$^+$ events in circulating EV samples from AT$_2$R deficient mice.
Number of CD41$^+$ event in KOM and KOF EV samples as determined by nanoFC. (WTM; n=5, KOM; n=5, **p<0.01, Welch's t-test).
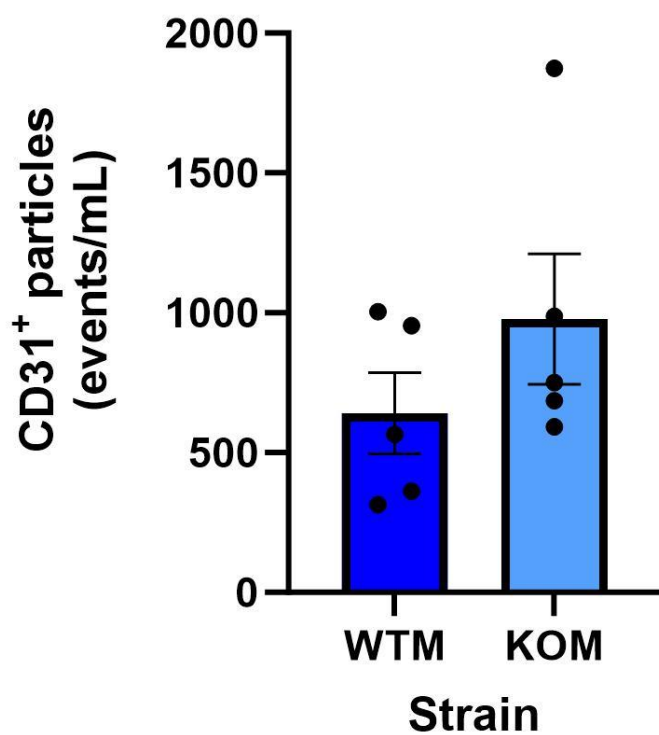
Figure 4.9 CD31+ events in circulating EV samples from WT and AT₂R deficient male mice.
Number of CD31+ event in WTM and KOM EV samples as determined by nanoFC.
(WTM; n=5, KOM; n=5, p>0.05, Welch's t-test).

Figure 4.10 CD31$^+$ events in circulating EV samples from WT and AT$_2$R deficient female mice.
Number of CD31$^+$ event in WTF and KOF EV samples as determined by nanoFC. (WTM; n=3, KOM; n=4, p>0.05, Welch's t-test).

Figure 4.11 CD31$^+$ events in circulating EV samples from WT mice.
Number of CD31$^+$ event in WTM and WTF EV samples as determined by nanoFC.
(WTM; n=5, WTF; n=3, p>0.05, Welch's t-test).
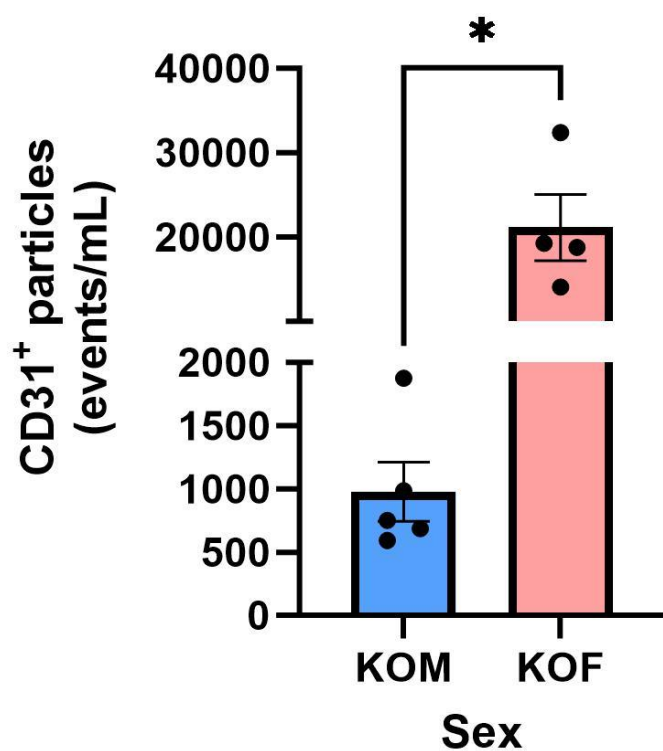
Figure 4.12 CD31$^+$ events in circulating EV samples from AT$_2$R deficient mice.
Number of CD31$^+$ event in KOM and KOF EV samples as determined by nanoFC. (KOM; n=5, KOF; n=4, *p<0.05, Welch's t-test).

4.4.5 Effects of sex and AT$_2$R expression on miRNA cargo

From a literature search, a bank of 8 miRNAs, miRNA-29a, miRNA-33a, miRNA-132, miRNA-146a, miRNA-155, miRNA-188, miRNA-212 and miR483, were linked to RAAS. From this list, only miRNA-132 and miRNA-146a were detected in plasma-derived EVs from wildtype and AT$_2$R deficient mice. These miRNAs are known to target the AT$_1$R, AT$_2$R, MasR or ACE2 or expression of these miRNAs may be altered following after finctional ligands bind the AT$_1$R, AT$_2$R and MasR (Jeppesen et al., 2011, Zheng et al., 2010, Adamcova et al., 2021, Pacurari and Tchounwou, 2015, Sun et al., 2020, Wang et al., 2013a, Obama and Eguchi, 2014). Individually, there was similar EV-derived miRNA-132 expression between wildtype or AT$_2$R deficient mice within each sex, and in either wildtype or AT$_2$R deficient mice between sexes, when compared to WTM. Values as follows: WTM-EVs (dCT $\pm$ SEM, 8.48 $\pm$ 0.23; RQ $\pm$ RQ$_{max}$, 1.00 $\pm$ 0.18), KOM-EVs (dCT $\pm$ SEM, 8.23 $\pm$ 0.29; RQ $\pm$ RQ$_{max}$, 1.19 $\pm$ 0.26), WTF-EVs (dCT $\pm$ SEM, 8.47 $\pm$ 0.15; RQ $\pm$ RQ$_{max}$, 1.01 $\pm$ 0.11) and KOF-EVs (dCT $\pm$ SEM, 8.73 $\pm$ 0.29; RQ $\pm$ RQ$_{max}$, 0.84 $\pm$ 0.19) (Figure 4.13 A & B).

Individually, there was similar levels of EV-derived miRNA-146a expression between wildtype or AT$_2$R deficient mice within each sex, and in either wildtype or AT$_2$R deficient mice between sexes, when compared to WTM. Values as follows: WTM-EVs (dCT $\pm$ SEM, 7.07 $\pm$ 0.51; RQ $\pm$ RQ$_{max}$, 1.00 $\pm$ 0.42), KOM-EVs (dCT $\pm$ SEM, 7.72 $\pm$ 0.66; RQ $\pm$ RQ$_{max}$, 0.64 $\pm$ 0.37), WTF-EVs (dCT $\pm$ SEM, 9.02 $\pm$ 0.34; RQ $\pm$ RQ$_{max}$, 0.26 $\pm$ 0.07) and KOF-EVs (dCT $\pm$ SEM, 9.28 $\pm$ 0.24; RQ $\pm$ RQ$_{max}$, 0.22 $\pm$ 0.04) (Figure 4.14 A & B).
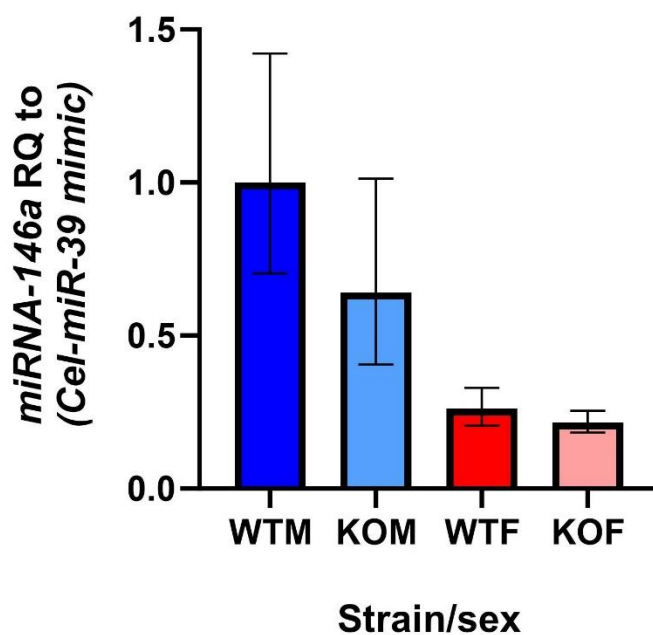
A

B
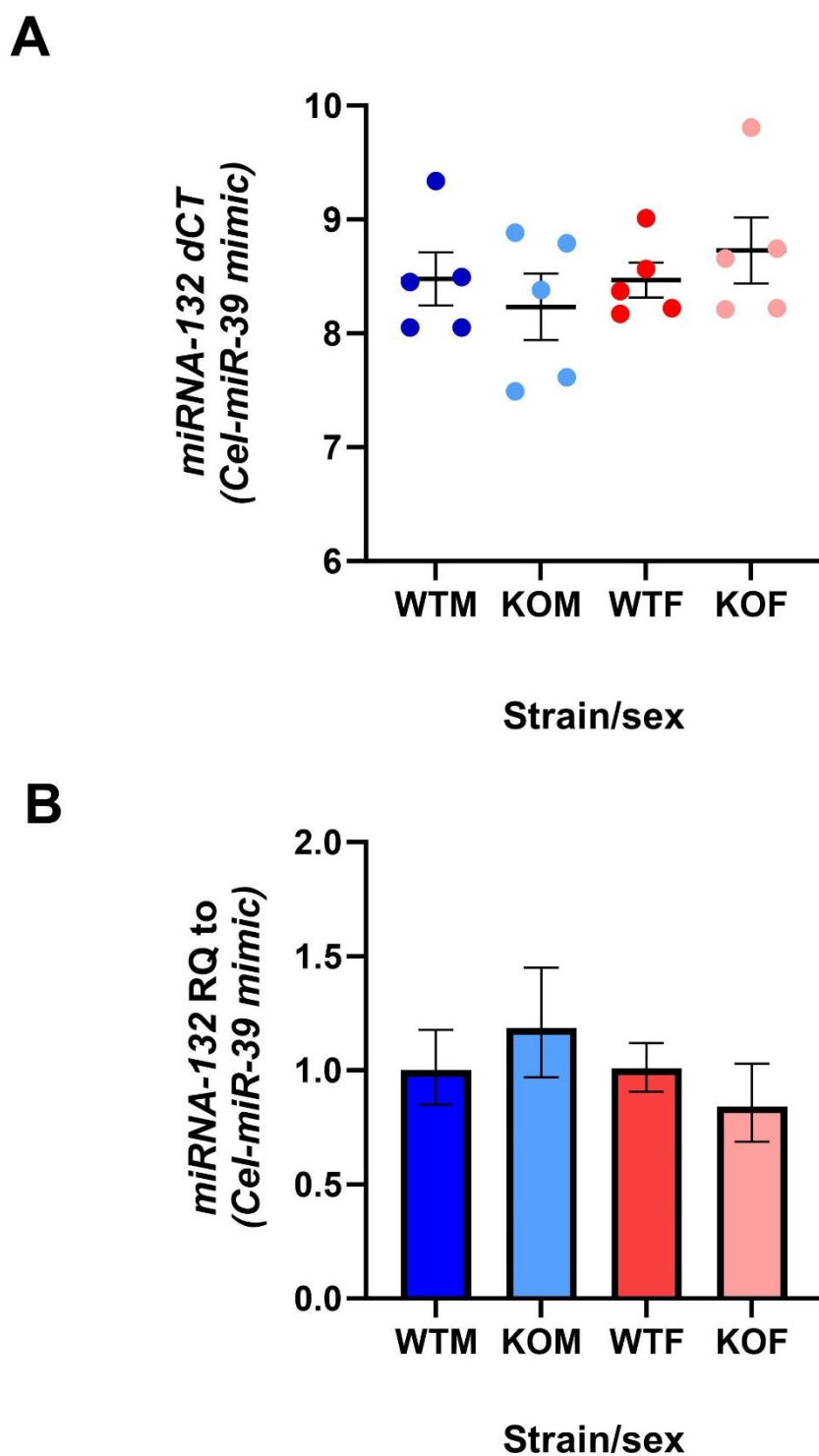
Figure 4.13 miRNA-132 expression within EV-derived miRNA from WT or AT$_2$R deficient mice plasma EVs.
qPCR of miRNA-132 expression was performed from miRNA isolated from EVs derived from plasma samples from 8–10-week-old WT or AT$_2$R deficient C57BL/6 mice. EV miRNA expression was normalised to *C. elegans miRNA-39* spike-in housekeeper. A) Delta cycle threshold (dCT) demonstrated the abundance of miRNAs and error bars represent standard error of the mean (SEM). B) Relative Quantity (RQ) is accompanied by error bars denoting RQ min/max (n=5, p>0.05, One-way AVOVA with post-hoc Dunnett's multiple comparison correction).

A
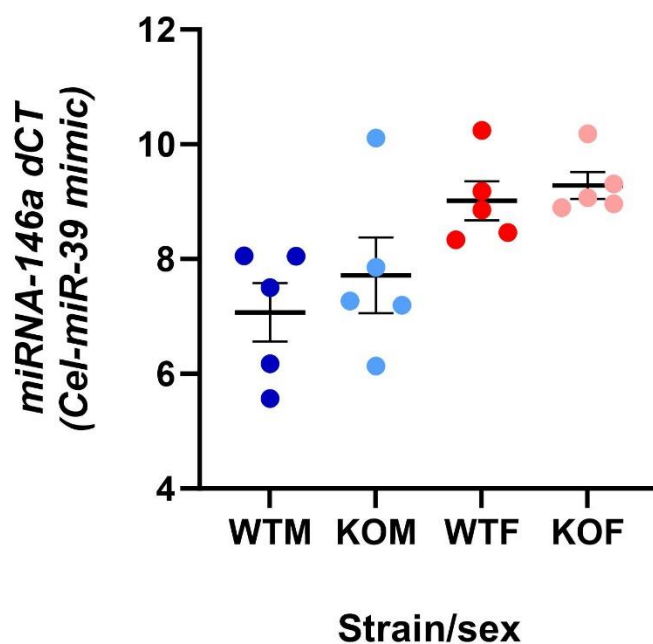
B

Figure 4.14 miRNA-146a expression within EV-derived miRNA from WT or AT$_2$R deficient mice plasma EVs.
qPCR of miRNA-146a expression was performed from miRNA isolated from EVs derived from plasma samples from 8–10-week-old WT or AT$_2$R deficient C57BL/6 mice. EV miRNA expression was normalised to *C. elegans miRNA-39* spike-in housekeeper. A) Delta cycle threshold (dCT) demonstrated the abundance of miRNAs and error bars represent standard error of the mean (SEM). B) Relative Quantity (RQ) is accompanied by error bars denoting RQ min/max (n=5, p>0.05, One-way AVOVA with post-hoc Dunnett's multiple comparison correction).

4.5 Discussion

In this investigation, sex-based differences were observed in AT_2R deficient animals, including EV particle size and surface markers. EV particle size was larger in AT_2R deficient females compared to AT_2R deficient males. Within the AT_2R deficient group, the number of $CD31^+$ or $CD41^+$ events were increased in females compared to males. EV protein content was similar between wildtype and AT_2R deficient groups, while miRNA-132 and miRNA-146a expression was also similar between wildtype and AT_2R deficient groups. Interestingly, EV particle concentration was the only aspect of this study to identify a difference between wildtype and AT_2R deficient animals within the same sex, whereby particle concentration was increased in AT_2R deficient females compared to wildtype females.

In line with the MISEV2018 guidelines, EVs that were isolated from AT_2R deficient and wildtype C57BL/6 mice were characterised by NTA and BCA (Thery et al., 2018). There was an increase in EV particle concentration within AT_2R deficient females compared to wildtype females. Research has shown that in certain disease states EV particle concentrations can vary. For example, microparticle concentration has been correlated with CAD in male diabetic patients, whereby it was demonstrated that patients with higher microparticle concentrations were more likely to suffer cardiovascular-related deaths (Sinning et al., 2011). Additionally, EV particle concentrations have been shown to be increased in patients following stroke and myocardial infarction (Couch et al., 2017, Ji et al., 2016, Akbar et al., 2022). It could be hypothesised that the increase in EV concentration in AT_2R deficient females may lead to poorer outcomes following experimental stroke compared to their wildtype counterpart. Poorer clinical outcome may be related to blood pressure in AT_2R deficient mice; indeed hypertension is the leading modifiable risk factor for stroke (GBD 2019 Stroke Collaborators, 2021). In other preclinical models, AT_2R deficient mice were shown to have blood pressure 15 mmHg higher and have greater renal vascular resistance than their wildtype counterparts (Gross et al., 2000). It should be noted that the AT_2R deficient colony at the University of Glasgow have never previously shown an outward hypertensive phenotype. However, animals were not subjected to tail cuff plethysmography in this study, and one cannot rule out possible drift in blood pressure since last the blood pressure of the colony was assessed. Any increase in blood pressure may increase cardio- and cerebro-vascular disease risks in the AT_2R deficient model and the effects of AT_2R deficiency on EV characteristics following experimental stroke should be further investigated.

EV protein content was similar between groups. It may have been expected, since EV particle number was greatest in the AT_2R deficient male group, that this group would have a greater protein content. However, as will be discussed in chapter 5 of this thesis, no significant correlation between EV concentration and protein content could be established. Additionally, in this study the AT_2R deficient females presented with larger EV size compared to AT_2R deficient males, however there was no difference in EV size between wildtype males and females, suggesting a link between sex and AT_2R deficiency. There has been limited study into sex-based difference in EV particle size. One group identified difference in EV particle size between males and females that were influenced by exercise and calorie intake (Conkright et al., 2022). However, a lack of data perhaps reflects the paucity of research studying mixed sex groups or sex differences in the EV field. As disease often affects males and females differently, more studies should include both sexes in preclinical research to better understand sex as an independent variable.

In terms of EV biogenesis, it is well known that cells produce EVs of various sizes and that EV size may be influenced by disease state, for example, cerebral spinal fluid derived EVs have been shown to be smaller in size in Lewy body dementia patients compared to healthy control patients (Longobardi et al., 2022). It could be theorised that the increase in EV size identified in AT_2R deficient female may be due to difference in EV biogenesis and composition which may influence EV cargo content. One study identified a significant increase in insulin signalling proteins pATK and pIGF-1R, proliferative proteins, p-p53 and ERK 1/2, and apoptosis protein, caspase-3 within plasma EVs of females compared to plasma EVs of males (Hooten et al., 2019). Common EV tetraspanins also provide an insight into EV biogenesis and composition, and so it would have been interesting to characterise EV tetraspanins through such methods as western blotting.

EV cargo and surface markers are predicted by parental cells (Hurwitz et al., 2016b). This study demonstrated the presence of CD31 and CD41 on nanoparticles derived from AT_2R deficient and wildtype mice. Platelet endothelial cell adhesion molecule-1, also known as CD31, expressed on endothelial cells and platelets, plays an important role in immune cell activation, while CD41 is often expressed on platelets (Marelli-Berg et al., 2013). In line with our understanding of how EV surface markers are influence by parental cells, circulating blood may contain EVs produced from endothelial cells and platelets, as blood passes over endothelial cells that line the interior surface of blood vessels and platelets make up a small proportion of blood, it is understandable why both CD41 and CD31 may be found on the surface of these EV samples (Grozovsky et al., 2015).

The number of CD31+ events was significantly higher in EV samples from AT_2R deficient females compared to AT_2R deficient males. Of note, AT_2R deficiency results in increased infarct volume, poorer neurological outcomes and increased reactive oxygen species in mice models of stroke compared to AT_2R wildtype control mice (Iwai et al., 2004, Mogi et al., 2006). CD31 may contribute to stroke pathology and recovery due to its role in cell-cell adhesion and angiogenesis (Albelda et al., 1990). Clinically, the number of CD31+ cells has been correlated with improved patient outcomes following stroke (Boeckh-Behrens et al., 2017). Male AT_2R knockout C57BL/6 mice were shown to have reduced neurological outcomes post-stroke following AT_2R stimulation my C21, while male wildtype mice demonstrated significant improvement in neurological outcomes following AT_2R stimulation (Schwengel et al., 2016). This group did not assess C21 mediated AT_2R stimulation in female AT_2R knockout mice. With that in mind, it would have been interesting to carry out *in vivo* tMCAO surgery on both AT_2R deficient males and females to determine if AT_2R females demonstrated reduced infarct volumes and improved neurological outcomes compared to their male counterparts.

Mechanistically, a link between AT_2R expression and the benefit of CD31 in normal endothelial function has also been identified, whereby treatment with Ang II, which primarily binds the AT_1R, was shown to decrease CD31 and eNOS expression within the endothelium of the aortic vascular wall in APOE deficient mice. However, when treated with the AT_2R agonist NP-6A4, CD31 and eNOS expression returned to control levels (Sharma et al., 2020). Post-stroke, endothelial dysfunction can occur due to immune cell infiltration and further potentiates damage to the brain (Hu et al., 2017). Activation/increase expression of AT_2R may restore or improve endothelial function by reducing oxidative stress as a result of increasing CD31 and eNOS. Further study must be carried out to better understand the effects of CD31^{+} EVs in the context of ischaemic stroke and whether the number of CD31^{+} events may be correlated with blood brain barrier (BBB) integrity.

The increase in the number of CD31^{+} events could be attributed to increased endothelial cell activation in AT_2R deficient female mice compared to AT_2R deficient males. It has been reported that endothelial cells derived from males and females are genetically and functionally distinct from one another. One study demonstrated that female human umbilical vein endothelial cells (HUVECs) were enriched in immune-related genes compared to male HUVECs (Lorenz et al., 2015). Aside from its expression on endothelial cells, CD31 is also expressed on immune cells such as macrophage, dendritic and T and B cells (Marelli-Berg et al., 2013). This increase in CD31^{+} events may be in part due to

increased numbers of immune cell derived EVs within AT_2R deficient mice. Pregnant AT_2R deficient mice have been shown to have increased renal proinflammatory T cells compared to wildtype pregnant mice (Mirabito et al., 2014). Inhibition of CD31 has been shown to reduce infarct volume in FVB/n LysM-eGFP mice following tMCAO, however blocking CD31 did not alter the number of infiltrating leukocytes (Nadkarni et al., 2022). One may speculate that CD31 inhibition may alter immune cell activation state to prevent proinflammatory damage to the brain, however further research should be carried out to evaluate this theory.

The number of CD41^{+} events were increased in AT_2R deficient females compared to their male counterparts to concentrations like that of CD31^{+} events. One may have expected that the number of CD31^{+} events would be greater than the number of CD41+ events in EV samples from wildtype and AT_2R deficient mice, solely due to the fact that endothelial cells represent a much larger source of EVs rather than the small number of platelets within circulation, however this was not the case. One hypothesis is that endothelial cell derived EVs, or CD31^{+} EVs, may be taken up by target cells at a greater rate than CD41^{+} platelet derived EVs. Another hypothesis may be that the production rate of EVs may differ between platelets and endothelial cells, therefore one cell type may appear to produce more EVs than the other. A study found that the ratio of EVs to cells within plasma samples varied greatly between plasma cell type, for example, red blood cell or neutrophil derived EVs represented low ratio of EVs to cell, while cells such as monocytes and lymphocyte represented high ratio of EVs to cell (Auber and Svenningsen, 2022). EV labelling combined with imaging may be used in future to investigate differences in EV uptake between WT and AT_2R deficient mice.

CD41 complexes with CD61 which goes on to bind the coagulation factor fibrinogen and as such is implicated in platelet aggregation (Phillips et al., 1988). The presence of CD41 on the surface of EVs from AT_2R deficient mice may be of significance in stroke outcome. One group identified the relationship between re-canalisation and CD41^{+} microparticle concentrations in patients following ischaemic stroke, whereby the number of CD41^{+} microparticles was increased in re-canulated patients compared to patients without canulisation (Bivard et al., 2017). It was suggested that this increase in the number of CD41^{+} microparticles may be due to increased reperfusion within re-canalised patients resulting in an increase in the number of microparticle shedding from circulating platelets (Bivard et al., 2017). In AT_2R deficient mice (AT2RKO) subjected to transient bilateral carotid artery occlusion the number of rolling and adhesion platelets within pial veins and arteries was significantly increased compared to AT2RKO sham controls at both 3- and 6-

hour time points. Although not significant, there was an increase in the number of rolling and adhesion platelets in AT2RKO mice compared to C57BL/6J wildtype control mice at both 3- and 6-hours post-occlusion (Fukuoka et al., 2015). One may hypothesise that AT_2R deficiency may lead to increased platelet cell number which in turn may lead to greater numbers of platelet cell derived EVs within circulation. Overall, limited research into sex-based difference in EV characterisation represents a gap in the literature which this study may hope to expand upon. Further research should be carried out on additional surface markers for EVs derived from wildtype and AT_2R deficient males and females, in order to better understand the key roles both sex and AT_2R expression may play in EV function.

Initially, qPCR was carried out to assess the expression of miRNAs within the cargo of EVs isolated from wildtype and AT_2R deficient mice. From the list of miRNAs mentioned in the introduction, miRNA-29a, miRNA-33a-5p, miRNA-155, miRNA-188-5p, miRNA-212-5p and miRNA-438 were undetectable in miRNA derived from EVs of wildtype or AT_2R deficient mice, while miRNA-132 and miRNA-146a were detected. There was no difference in EV-derived miRNA-132 and miRNA-146a expression between wildtype and knockout animals, nor was there any difference in the expression of these miRNAs between sexes. Differences in miRNA expression between males and females have widely been investigated in neurological diseases, while some yielded clear sex-based difference in miRNA expression, others did not. For example, plasma miRNA-132 expression was significantly greater in male patients with Parkinson's disease than female counterparts, while in patients with mild cognitive impairment, there was no difference in plasma miR-132 expression between males and females (Yang et al., 2019, Sheinerman et al., 2013).

miRNA-132 plays a key role in synaptogenesis, synaptic transmission, and neural development/function, as well as angiogenesis (Qian et al., 2017). As miRNA-132 and miRNA-212 share the same gene locus and can be simultaneously induced and repressed, it could be expected that both miRNAs would be detected using qPCR (Wanet et al., 2012). However, each miRNA can be induced to differing degrees by various factors. For example, miRNA-132 was induced more so than miRNA-212 during herpes simplex virus 1 or cytomegalovirus infection, leading to suppression of antiviral responses, enabling viral replication (Lagos et al., 2010). Differences in miRNA induction may account for why miRNA-212 was not detected within EVs. *In vitro*, miRNA-132 has been shown to target genes associated with nervous system development, neuronal migration, and endocytosis (Antoniou et al., 2023). One study demonstrated that NMRI mouse cultured primary cortical neurons treated with brain derived neurotrophic factor led to the production of EVs containing increased levels of miRNAs compared to controls, including miRNA-132

(Antoniou et al., 2023). The mice investigated as part of this thesis were not subjected to any form of stimulation that may in turn alter the expression of EV derived miRNAs.

In this study EVs were isolated from plasma of AT_2R deficient and wildtype mice and were not isolated from specific organs such as the brain. Within the stroke brain, miRNA-132 has been shown to play a crucial role in maintaining the BBB and preventing neuronal cell death (Yan et al., 2021). In preclinical models, C57BL/6 mice pre-treated with agomir-132 prior to tMCAO led to improved neurological outcomes and reduced infarct volume. It was found that the expression of proteins associated with vascular endothelial cell tight junctions, VE-cadherin and β-catenin, were increased with agomir-132 treatment compared to agomir control. These findings were mirrored when agomir-132 treatment was replaced with an MMP-9 inhibitor. Later, targeted prediction identified that MMP-9 was a target for miRNA-132 which was further confirmed via *in vitro* analysis (Zuo et al., 2019). It could be suggested that if EVs were derived from brain tissue of both AT_2R deficient and wildtype mice, then the miRNA profiles may have been different and miRNA-132 may have been detected within brain-derived EVs. Indeed, the finding that miRNA-132 is associated with vascular endothelial cell tight junctions, an integral component of the BBB, suggests that miRNA-132 loaded EVs may protect against BBB deterioration following ischaemic stroke. This study could be expanded to include various different tissues within the body, importantly the brain, to determine whether AT_2R deficiency may lead to differences in EV derived miRNA.

Although not significant, there was a trend towards a decrease in miRNA-146a expression between wildtype males and females. MiRNA-146a appears to play a role in stroke pathology and risk, and as such highlights the importance of EV derived miRNA-146a as a possible biomarker in stroke. Decreased expression of miRNA-146a has been identified in stroke patients and has been corelated with poorer clinical outcomes (Kotb et al., 2019, Zhu et al., 2015, Li et al., 2015, Li et al., 2017b). In preclinical models of Alzheimer's disease miRNA-146a targets upstream of the TNFα pathway and reduces the expression of proinflammatory mRNAs such as complement factor-H and interleukin-1 receptor associated kinase-1 (Li et al., 2011). Perhaps the benefit of miRNA-146a in neurological diseases may rely upon reducing the expression of proinflammatory mediators, which are responsible for post-stroke cell death (Sekerdag et al., 2018). With this in mind, the reduction in EV derived miRNA-146a observed in wildtype female mice compared to their male counterparts may suggest that female mice may experience worse strokes than males. However, one may also postulate that miRNA-146a may be released from EVs at a faster rate in females than males and may provide females with greater protection from the

negative impact of stroke compared to males. Indeed one study found that C57BL/6 female mice subjected to permanent distal middle cerebral artery occlusion had significantly smaller infarct volumes than their male counterparts (Zhao et al., 2017). Inhibition of miRNA-146b in Sprague-Dawley rats following transient middle cerebral artery occlusion (tMCAO) reduced neuronal cell differentiation within the peri-ischaemic striatum and subventricular zone compared to tMCAO control animals (Zhang et al., 2020). Together, it can be suggested that the miRNA-146 family of miRNAs may play a protective roll following stroke and if EVs were to be loaded with miRNA-146a, it may improve post-stroke outcomes.

As AT_2R deficient and wildtype mice were not subjected to experimental stroke prior to EV isolation and miRNA quantification, it would be interesting to determine whether AT_2R deficiency, and sex may also influence EV derived miRNA expression following tMCAO, and in turn post-stroke outcomes including infarct volume, levels of neurogenesis and inflammation. Additionally, expanding upon the EV tissue/biofluid origin and number of miRNAs investigated would create a more robust conclusion into the effects of AT_2R deficiency on EV characteristics.

4.5.1 Study limitations

The limitations of this study mainly focus on the breadth of the investigation. It would have been beneficial if EVs could have been assessed using basic western blot characterisation, however the issue of EV protein content and antibody optimisation could not be overcome. The panel of miRNAs, if not due to financial and time constraints, would have been ideally expanded or bulk RNA sequencing could have been conducted to identify which miRNAs were present within EVs from AT_2R deficient and wildtype mice. On a similar note, as the data relating to EV cell source was obtained during a two-week exchange placement at Oxford Brookes University, there was a limit to the number of markers that could be optimised during this timeframe. Further optimisation of standard EV surface markers using nano FC would have also been desirable to further characterise EV populations.

4.5.2 Summary

Sex based differences were observed in both AT$_2$R deficient mice in various parts of this investigation, including EV particle size and surface marker expression. Furthermore, differences in EV particle concentration between wildtype and AT$_2$R deficient animals demonstrate a link between RAAS modulation and EV production. It can be concluded that EVs derived from wildtype or AT$_2$R deficient mice have varying characteristics, cargo and surface markers which in turn may alter their overall function. Additional investigations should be carried out into the effects of AT$_2$R deficiency on EV characteristics following experimental stroke.

Chapter 5: *In vitro* optimisation of therapeutic extracellular vesicles

5.1 Introduction

EVs can be produced from almost every cell type in the body and can be considered as potential diagnostic and prognostic markers in disease. As EV research can range from diagnostics to therapeutics, MISEV guidelines have been established to aid in the development of EV related methods, including sample collection, EV isolation and characterisation (Thery et al., 2018, Welsh et al., 2024, Lötvall et al., 2014). EVs can be collected and isolated from a wide variety of bodily fluids or tissues. Examples of the most common methods of EV isolation recognised within MISEV2018 guidelines are ultracentrifugation (UC) and size exclusion chromatography (SEC). UC, long considered the 'gold-standard' method of EV isolation, is a method by which EVs are isolated from biofluids using high speed centrifugation, leading to the separation of EVs from proteins and lipids within the biological sample (Thery et al., 2006). However, with UC isolation, high-speed centrifugation may negatively affect EV structural integrity and EVs may be lost within supernatants (Musante et al., 2013). Such problems led to advancements in EV isolation methods. A quicker, more streamlined method of EV isolation, SEC, can be used in place of UC isolation. Using SEC isolation method, biological fluids are passed through porous SEC columns and small EVs can be eluted from columns into fractions (Boing et al., 2014). SEC isolation can better separate EVs from larger contaminant proteins or lipids compared to UC methods (Izon Science, 2023a, Ter-Ovanesyan et al., 2023). The use of SEC columns allows for the isolation of highly pure EV samples within a quick timeframe (Forteza-Genestra et al., 2020). Other methods for isolating EVs have also been well established, such as precipitation isolation, density gradient centrifugation or immunocapture(García-Romero et al., 2019, Iwai et al., 2016, Paget et al., 2022). Every method of EV isolation has both benefits and drawbacks. The most important feature of any EV isolation method is its ability provide adequate EV yield, as well as generate highly pure EV preparations.

In line with MISEV guidelines, after isolation, EVs should be characterised in multiple ways (Thery et al., 2018). Nanotracking analysis (NTA) relies upon Brownian motion and laser light diffraction to quantify the number and size of isolated particles (Soo et al., 2012). Transmission electron microscopy (TEM) uses transmitted electron beams to create bright field images of EVs that are embedded in grids (Pascucci and Scattini, 2021). TEM

provides information of the EV morphology, such as diameter, circumference, and overall EV dimensions, and can be used in conjunction with NTA data to confirm EV size (Pascucci and Scattini, 2021). A relatively new method in the EV field, nano flow cytometry (nanoFC), is beginning to be adopted as a substitute for NTA. This method works on the principle of flow cytometry, however for small particles such as EVs rather than cells. This method can be extremely powerful in that not only does it provide information into the size and concentration of EVs, but it can also be used to identify distinct EV populations within a sample by using fluorescent antibodies that may bind to unique proteins on the EV surface (Morales-Kastresana et al., 2017). Similarly, super resolution imaging can also provide information about distinct EV populations using similar antibody-EV protein binding. At a protein level, a standard method of identifying key EV surface markers is western blotting. With this, conventional EV markers, such as CD81 and CD63, can be used to positively identify EVs within a sample containing nanoparticles (Arab et al., 2021). As the EV field grows, more and more EV markers are being incorporated into identification guidelines, for example, the inclusion of LAMP1 and Syntenin (Mathieu et al., 2021). Negative control markers should also be used to distinguish between EV and other nanoparticle populations, for example, ApoB and Calnexin are often used to identify lipoprotein or endoplasmic reticulum contaminants from EV samples (Sun et al., 2019).

EVs have been investigated for their possible use as therapeutic delivery vectors. Following regulatory approval, in disease patients, EVs could be rapidly isolated from patient blood samples to provide personalised treatment for disease. Isolated EVs may be loaded with therapeutic compounds and re-delivered to the individual patients. However, the practicalities of such personalised EV therapeutics are uncertain. In order to combat the issues that arise with personalised EV therapies, other methods of creating therapeutic EVs have been widely studied. Exogenous EVs may be engineered to contain therapeutic compounds that may be delivered therapeutically. A common method of producing EVs that contain therapeutics is to design a cell line that over-expresses said therapeutic. This cell line should, in theory, produce EVs that contain high levels of the therapeutic compound. One group enriched the expression of miR-126 within endothelial progenitor cells (EPCs) by treating EPCs with miR-126 mimic and transfection reagents (Wang et al., 2020). A benefit of this type of method is that EV populations may be mass produced and stored for easy access to be used in a clinical setting. Similarly, immortalised cell lines may also be transfected with plasmids to allow for the incorporation of desired genetic

material into cellular DNA. Successfully transfected cells may produce EVs that possess this desired genetic material and may be collected and isolated at a large scale.

EVs isolated from biological samples may be loaded with therapeutic compounds using diffusion incubation or using electroporation. When EVs are incubated with therapeutic compounds, these compounds may be taken up by EVs along the concentration gradient. Building on this principle, electroporation uses a small voltage to increase EV membrane permeability, again allowing compounds to enter the EVs along the concentration gradient. Some studies have suggested that electroporation cargo loading of EVs is greater than diffusion incubation (Kim et al., 2016). Electroporation has also proven effective in loading EVs with drugs such as doxorubicin, whereby one group found that optimisation of electroporation protocols could lead to a 190-fold increase in doxorubicin potency when doxorubicin was loaded into EVs compared to unloaded doxorubicin (Lennaard et al., 2021). Another group used electroporation to load RVG-targeted EVs with siRNA to silence the protease BACE1, a component required for amyloid plaque formation and a potentiator of Alzheimer's pathology. Results demonstrated a significant reduction in BACE1 expression in mouse cortical tissue after systemic administration of BACE1 siRNA loaded EVs (Alvarez-Erviti et al., 2011). Not only does this result demonstrate that EVs can be loaded with therapeutic RNA molecules, but it also shows that systemically administered therapeutically loaded EVs may be used to treat neurological diseases.

The development of a new therapy relies upon *in vitro*, *in vivo* and human experimentation. Provisionally, basic cell assays are conducted to understand the effects of therapeutics on cell survival or viability. This information provides robust understanding on how the therapeutic may act in more complex living systems. Just like with other therapeutics, EVs must also undergo testing using basic cell assays, such as 3-(4,5-Dimethylthiazol-2-yl)-2,5-diphenyltetrazolium bromide (MTT) or Lactate dehydrogenase (LDH) assays. Both MTT and LDH assays are colorimetric assays that rely on conversion tetrazolium salts to formazan crystals. In MTT assays, the intensity of formazan solution is directly proportional to the metabolic activity of cells, and, by proxy, is often linked to cell viability (Berridge et al., 2005). One group investigated the effects of leukaemia cell derived EVs on human astrocyte cultures using MTT, whereby they found that leukaemia cell derived EVs increased viability, proliferation and lifespan of cultured astrocytes (Esmati et al., 2023). In LDH assays, the intensity of red signal is directly proportional to cell membrane damage, and as a result, is often used as a measurement of cell viability (Parhamifar et al., 2013). In a model of *in vitro* hypoxia reperfusion injury, cardiomyocytes treated with human mesenchymal stem cell derived EVs (hMSC-EVs) led to reduced LDH levels

compared to vehicle controls (Yu et al., 2022a). Using this robust assay, the group was able to determine how hMSC-derived EVs directly affected cell viability.

To better understand how EVs function, it may be necessary to identify where EVs locate within a biological system. This is often achieved using fluorescent labels such as PKH or DiR lipophilic dyes (Tian et al., 2022, Wiklander et al., 2015). Labelling EVs with dyes is carried out after EVs have been isolated from samples and can often add time to lengthy EV isolation methods. Alternatively, cell lines can be transfected with plasmids containing fluorescence sequences that are incorporated into the cell line and lead to the production of fluorescently labelled EVs (Wiklander et al., 2015). It should be noted that, depending on plasmid transfection efficiency, the number of fluorescently labelled EVs may vary. When EVs are isolated from a biofluid, depending on the EV isolation method, other lipid particles such as very-low density lipoproteins (VLDL) may also be co-isolated (Yuana et al., 2014). As such the use of lipophilic dyes to label isolated EVs can lead to false fluorescent EV signals, whereby VLDL particles have been successfully labelled with PKH and DiI dyes (Chen et al., 2023). Irrespective of the labelling method, identifying where EVs locate in the body may provide insight into their therapeutic ability.

By creating therapeutically loaded EVs, new methods of treating disease may be established. EVs may be bioengineered on a mass scale for wide clinical use or can be, in theory, be produced as patient-specific therapies. With this, EVs must be subjected to standardised isolation and characterisation methods that are crucial in defining novel EV therapies. EV treatments must undergo rigorous *in vitro* and *in vivo* optimisation to produce safe and efficacious treatments for diseases such as ischaemic stroke.

5.2 Hypotheses and aims

5.2.1 Hypotheses

- EVs can be isolated using different isolation methods.

- EVs can be successfully loaded with desired cargo using electroporation.

- EV isolation methods may result in changes within EV characteristics.

- Ang-(1-9) peptides or Ang-(1-9) peptide-electroporated EVs will improve cell viability within *in vitro* models of ischaemic stroke.

5.2.2 Aims

- Quantify EVs isolated using polyethylene glycol (PEG).

- Quantify PEG isolated EVs after electroporation-mediated cargo loading.

- Optimise electroporation-mediated cargo loading methods.

- Quantify EVs isolated using SEC.

- Quantify SEC isolated EVs after electroporation-mediated cargo loading.

- Understand the effects of PEG and SEC EV isolation methods on EV quantity.

- Characterise SEC isolated EVs.

- Understand the effects of EVs electroporated with different Ang-(1-9) peptides on cell viability.

- Assess the biodistribution of fluorescently labelled EVs and EVs electroporated with fluorescent Ang-(1-9) peptides within cell culture models.

5.3 Methods

Methods used in Chapter 5 can be found in Chapter 2 of this thesis and are outlined below:

2.1.2.8 Historical samples

2.2.1.1 Precipitation isolation

2.2.1.2 Ultracentrifugation isolation

2.2.1.3 Size exclusion chromatography

2.2.1.4 Pierce BCA protein assay

2.2.1.5 Nanoparticle tracking analysis

2.2.1.6 EV electroporation loading

2.2.1.7 PKH26 labelling

2.2.1.9 Transmission electron microscopy of EVs

2.2.2.1 Immortalised cell line maintenance

2.2.2.2 Primary neuronal cell isolation and cultures

2.2.2.3 Cell-derived EVs

2.2.2.4 Oxygen glucose deprivation

2.2.2.5 EV and peptide treatment

2.2.2.6 MTT assay

2.2.2.7 Cell fixation and imaging

2.2.2.8 Immunocytochemistry

2.2.4 Western Blotting

2.2.5 Ang-(1-9) ELISA

2.2.7 Statistical analysis

5.4 Results

5.4.1 Characterisation of PEG isolated EVs

In the preliminary stages of this study, EVs were isolated using Total exosome isolation kit that contained the polyether, polyethylene glycol (PEG) method. PEG is a common method of isolating EVs. EVs were isolated using PEG and were characterised using NTA to assess particle concentration and size. Following PEG isolation, the average EV particle concentration was $2.04 \times 10^{13} \pm 1.54 \times 10^{11}$ p/mL (mean $\pm$ SEM), while the average EV particle size was 92.17 ± 6.22 nm (mean $\pm$ SEM) (Figure 5.1 A & B). The protein content of PEG isolated EVs was assessed using BCA whereby EV protein content was 2744.62 ± 505.14 µg/mL (mean $\pm$ SEM) (Figure 5.2).

Further to individual characterisation, the correlation between EV concentration and EV protein content and EV concentration and EV size were also determined. In instances where protein content could not be established in later stages of this study, particle number was used to provide a relative protein concentration. There was a weak positive correlation between EV concentration and protein content as determined by Pearson r correlation test, though not significant (r value of 0.43; p=0.40) (Figure 5.3 A). There was a weak negative correlation between EV concentration and size as determined by Pearson r correlation test, however, again, not significant (r value of -0.80; p=0.10) (Figure 5.3 B).

A

B
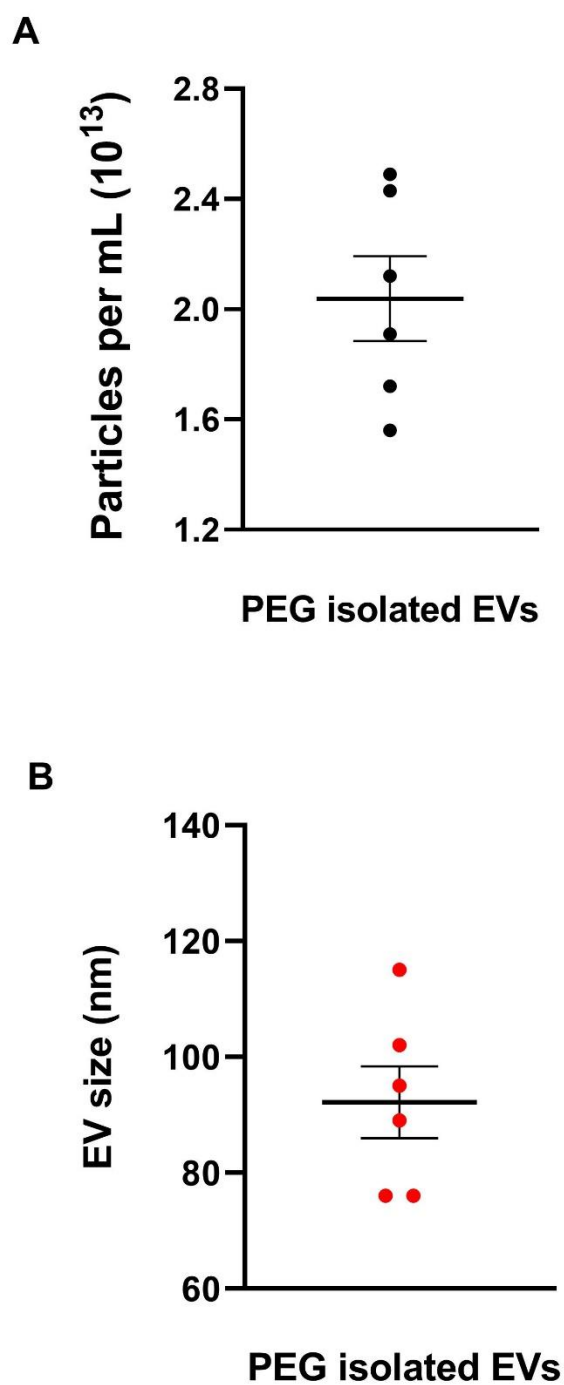
Figure 5.1 Characterisation of PEG-isolated EVs.
SHRSP plasma-derived EV particle concentration (A) and particle size (B) was determined
by NTA (n=6).
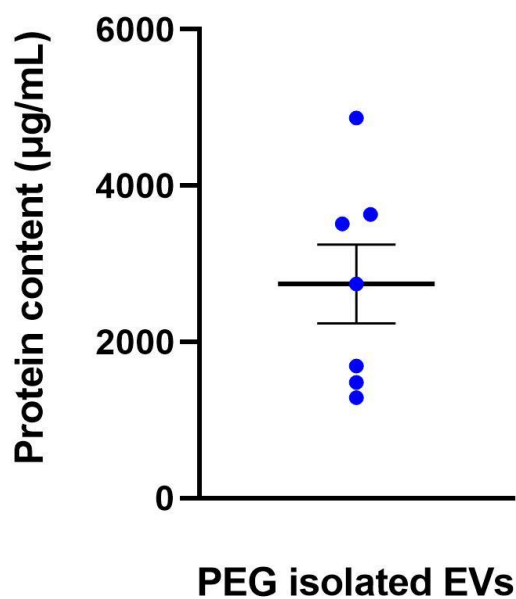
Figure 5.2 Protein concentration of PEG-isolated EVs.
EVs were isolated from SHRSP plasma using PEG and total protein content was
determined by BCA (n=7).
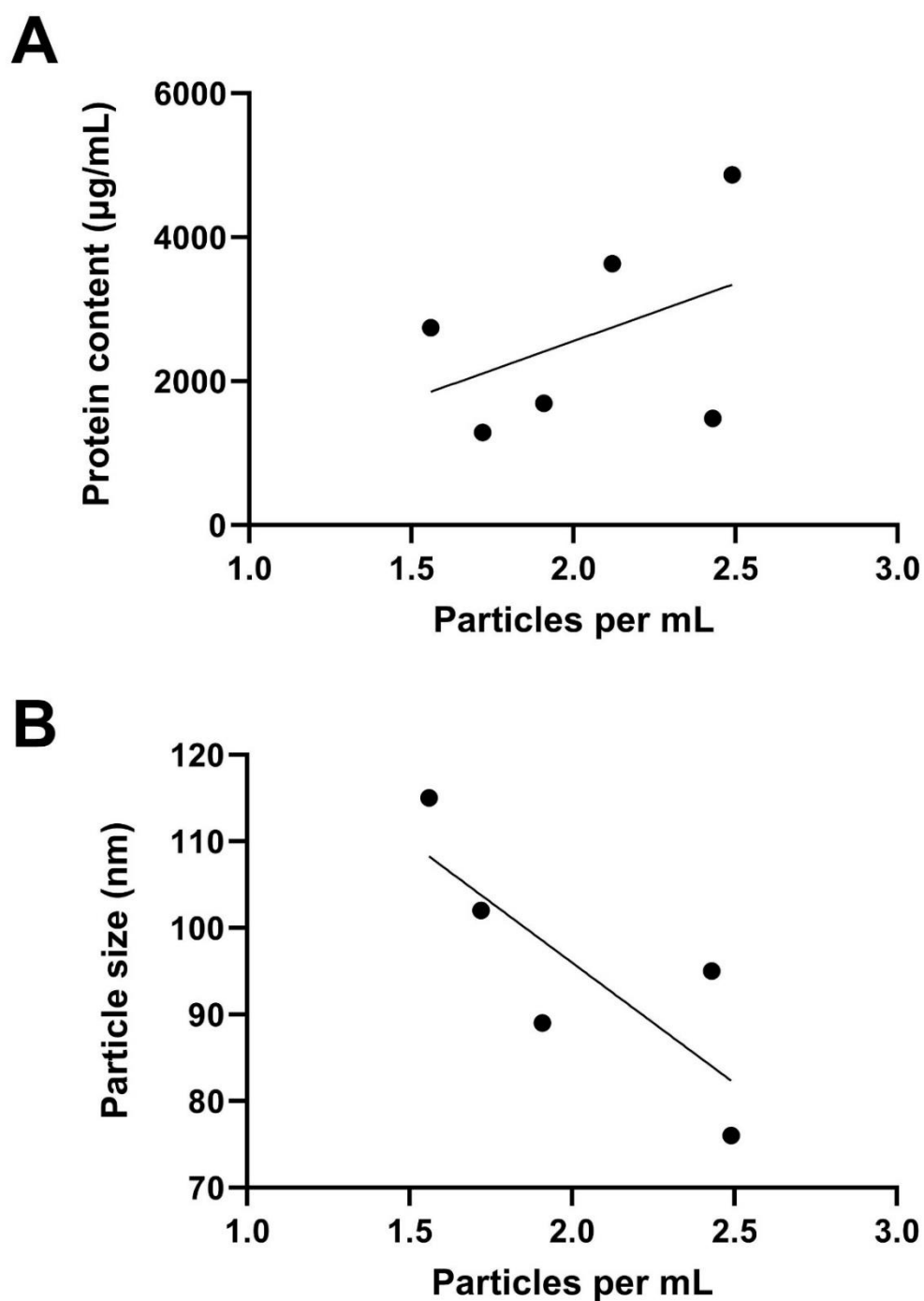
Figure 5.3 Relationship between EV characteristics.
(A) Correlation between SHRSP plasma-derived EV particle concentration and total protein content of EVs (n=6, p>0.05, Pearsons's correlation coefficient). (B) Correlation between SHRSP plasma-derived EV particle concentration and EV particle size (n=5, p>0.05, Pearsons's correlation coefficient).

5.4.2 Effect of EV loading on particle concentration

Therapeutic miRNAs and other peptides can be loaded into EVs via electroporation. As electroporation can reduce membrane integrity, 200, 400 or 600 mV were assessed to determine which electroporation voltage resulted in greater particle concentration following loading. After 200 mV of electroporation, there was no significant difference in EV concentration prior to ($1.31 \times 10^{12} \pm 1.19 \times 10^{11}$ particles) and immediately after electroporation ($8.80 \times 10^{11} \pm 1.40 \times 10^{11}$ particles) (Figure 5.4). After 400 mV of electroporation, there was no significant difference in EV concentration prior to ($1.42 \times 10^{12} \pm 4.98 \times 10^{10}$ particles) and immediately after electroporation ($1.78 \times 10^{12} \pm 3.28 \times 10^{11}$ particles) (Figure 5.5). After 600 mV of electroporation, there was a significant decrease in EV concentration immediately after electroporation ($9.03 \times 10^{11} \pm 1.51 \times 10^{11}$ particles) compared with prior to electroporation ($1.37 \times 10^{12} \pm 1.67 \times 10^{11}$ particles) ($p < 0.01$) (Figure 5.6).

EVs were quantified following electroporation and UC re-isolation to understand whether electroporation voltage led to changes in final EV concentration. There was no difference in EV concentration after electroporation and UC at 200 mV ($4.93 \times 10^9 \pm 6.33 \times 10^8$ particles), 400 mV ($8.93 \times 10^9 \pm 2.57 \times 10^9$ particles) and 600 mV ($7.23 \times 10^9 \pm 1.07 \times 10^9$ particles), though 400 mV provided the greatest number of particles on re-isolation compared to other voltages (Figure 5.7).

Overall, total EV loss from starting concentration to UC re-isolation of electroporated EVs was also determined to understand the efficiency of this method. Compared to starting EV concentration ($1.31 \times 10^{12} \pm 1.19 \times 10^{11}$ particles) final EV concentration was significantly decreased after 200 mV of electroporation and UC re-isolation ($4.93 \times 10^9 \pm 6.33 \times 10^8$ particles) ($p < 0.0001$). Compared to starting EV concentration ($1.42 \times 10^{12} \pm 4.98 \times 10^{10}$ particles) final EV concentration was significantly decreased after 400 mV of electroporation and UC re-isolation ($8.93 \times 10^9 \pm 2.57 \times 10^9$ particles) ($p < 0.0001$). Compared to starting EV concentration ($1.37 \times 10^{12} \pm 1.67 \times 10^{11}$ particles) final EV concentration was significantly decreased after 600 mV of electroporation and UC re-isolation ($7.23 \times 10^9 \pm 1.07 \times 10^9$ particles) ($p < 0.0001$) (Figure 5.8).

As electroporation may decrease the structural integrity of EVs by increasing membrane permeability, high centrifugation speeds may exacerbate EV loss. EVs were either immediately re-isolated using UC after electroporation or, after electroporation, EVs were incubated at 4°C for 24 hours before re-isolation using UC to understand if pausing re-isolation to allow "recovery" may improve final EV concentration. When EVs were

immediately re-isolated via UC after electroporation, final EV concentration was significantly decreased ($3.92x10^9 \pm 7.60x10^8$ particles) compared to the starting EV concentration ($1.41x10^{12} \pm 2.56x10^{11}$ particles) ($p<0.001$). After electroporation, EVs that were incubated at 4°C for 24 hours before re-isolation via UC, led to a significant reduction in final EV concentration ($8.93x10^9 \pm 2.57x10^9$ particles) compared to the starting EV concentration ($1.46x10^{12} \pm 1.33x10^{11}$ particles) ($p<0.01$) (Figure 5.9).
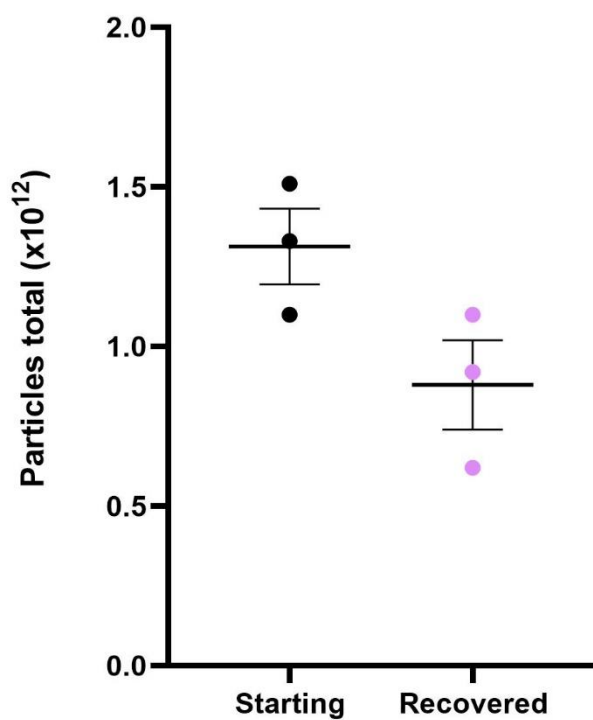
Figure 5.4 Effects of 200mV electroporation on EV concentration.
Prior to UC re-isolation, EV concentration was compared before electroporation (starting) and after EVs were electroporated at 200 mV (recovered). EV concentration was determined by NTA (n=3, p>0.05, paired t-test).
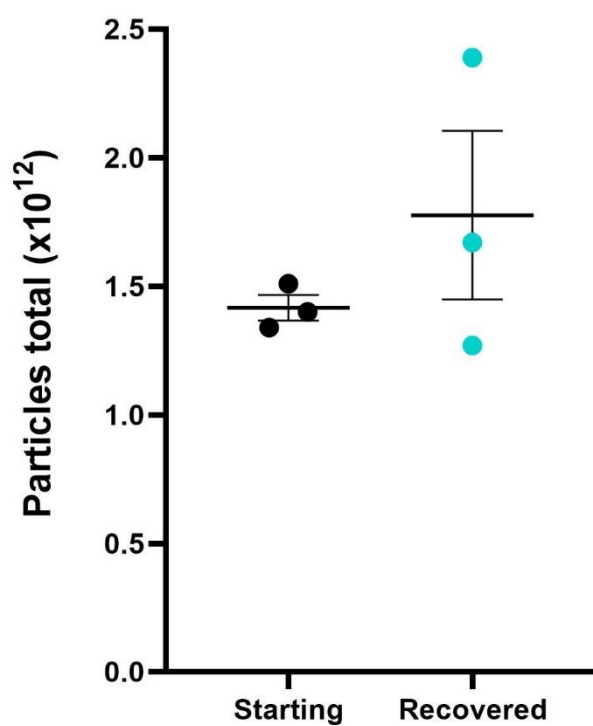
Figure 5.5 Effects of 400mV electroporation on EV concentration.
Prior to UC re-isolation, EV concentration was compared before electroporation (starting) and after EVs were electroporated at 400 mV (recovered) using NTA (n=3, p>0.05, paired t-test).
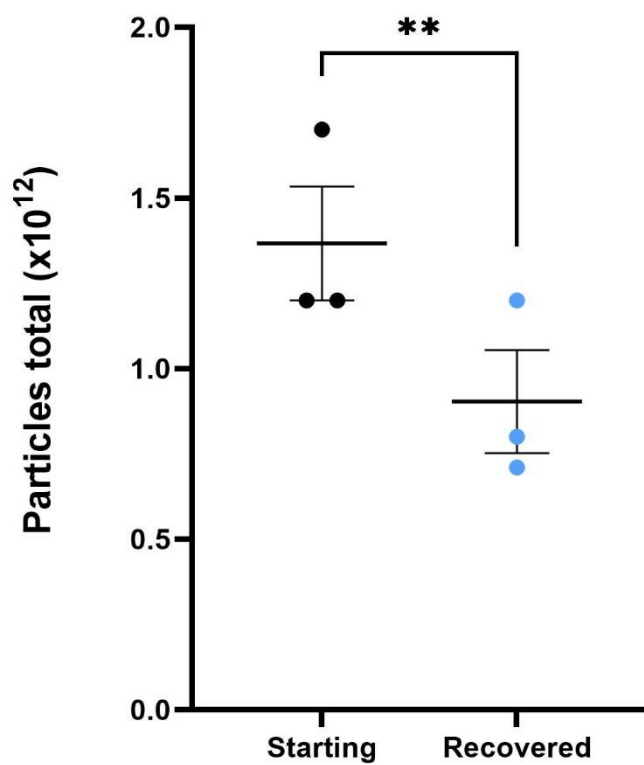
Figure 5.6 Effects of 600 mV electroporation on EV concentration.
Prior to UC re-isolation, EV concentration was compared before electroporation (starting) and after EVs were electroporated at 600 mV (recovered). EV concentration was determined by NTA (n=3, **p≤0.01, paired t-test).
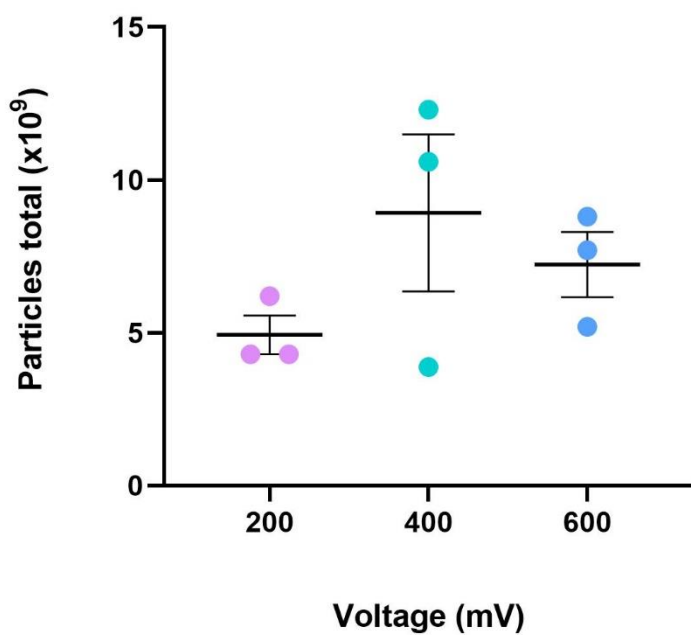
Figure 5.7 Effects of electroporation voltage on EV concentration.
After UC re-isolation, EV concentration was compared after either 200, 400 or 600 mV electroporation loading method. EV concentration was determined by NTA (n=3, p>0.05, One-way ANOVA with post-hoc Tukey's).
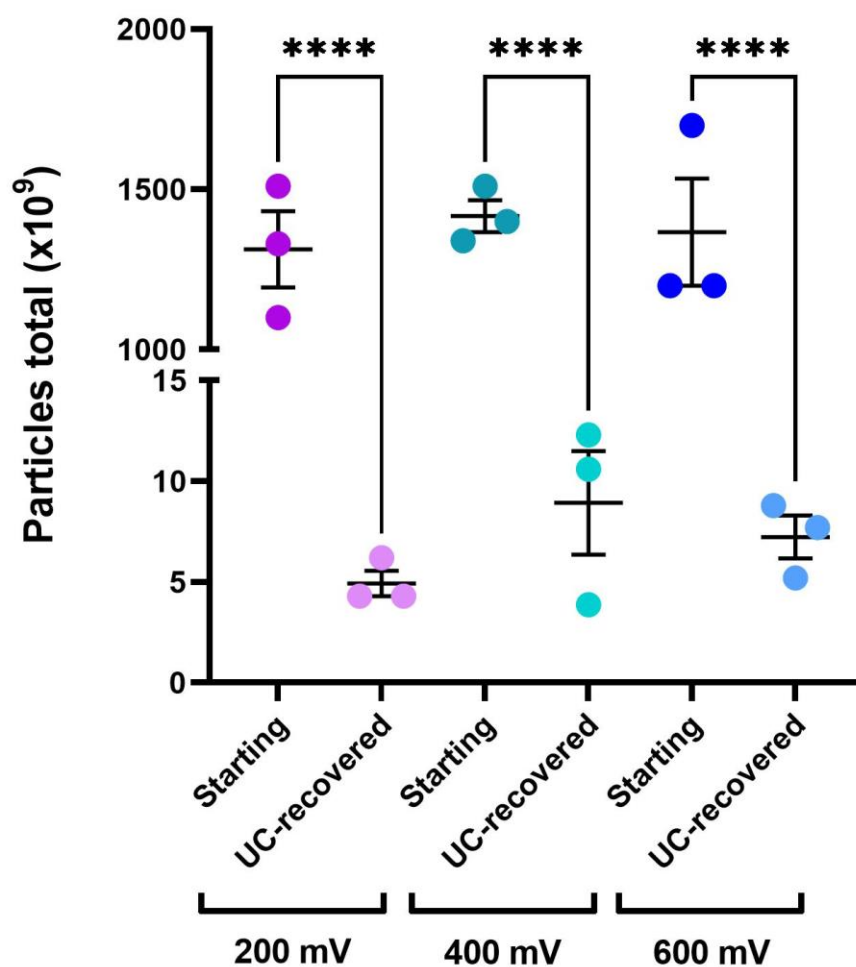
Figure 5.8 Effects of electroporation and UC re-isolation on EV concentration.
Comparison of EV concentration before electroporation (starting) at various voltage and after EVs were re-isolated by UC (UC-recovered). EV concentration was determined by NTA (n=3, **** $p<0.0001$, One-way ANOVA with post-hoc Tukey's).
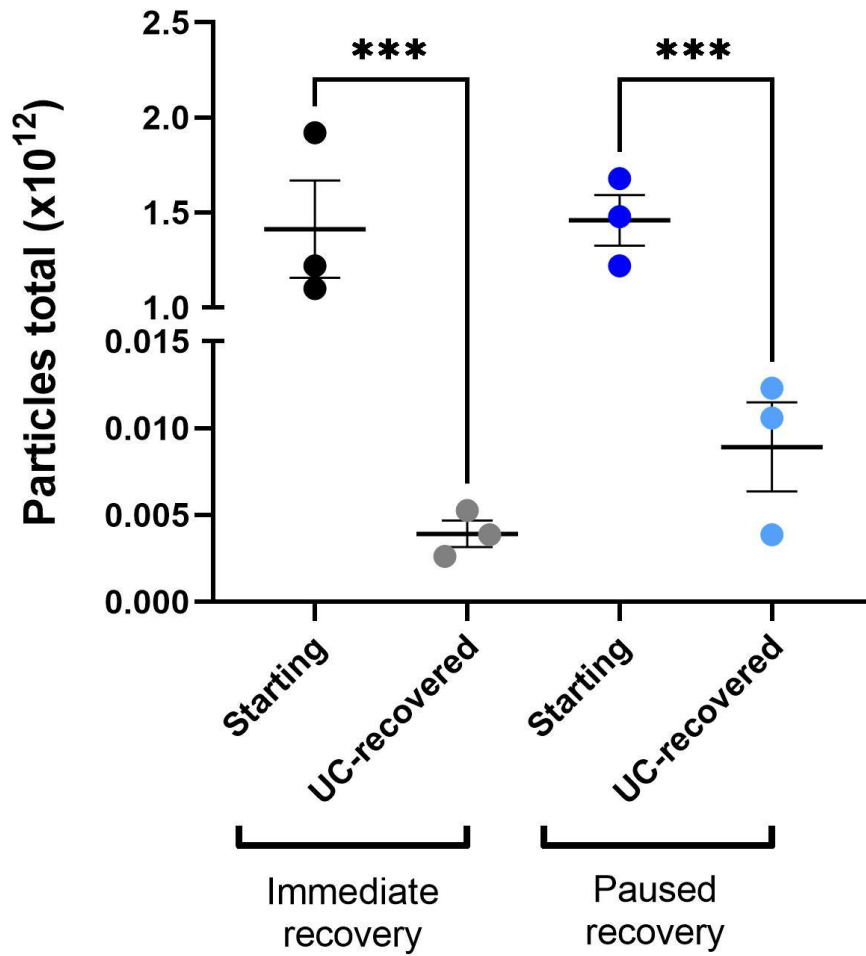
Figure 5.9 Effects of pausing UC re-isolation after electroporation on EV concentration.
Comparison of EV concentration before electroporation (starting) and after EVs were re-isolated by UC (UC-recovered). EVs were either immediately re-isolated after electroporation (immediate recovery) or were re-isolated after a 24-hour pause (paused recovery). EV concentration was determined by NTA (n=3, *** $p<0.001$, One-way ANOVA with post-hoc Tukey's).

5.4.3 Characterisation of SEC isolated EVs

To determine if a different isolation method could combat issues with EV loss after electroporation and UC, size exclusion chromatography (SEC) isolation methods were used in place of UC to re-isolate EVs following electroporation. SEC qEV columns were used to isolate EVs, alongside the automated fraction collector (AFC) from IZON. As per IZON plasma EV isolation methods, users were instructed to pool fractions 1-3 as these fractions contained the greatest number of EVs. To confirm that this these fractions contained the greatest numbers of particles, the concentration of EVs within the void volume and fractions 1 through 5 were analysed using NTA. Fraction 1 contained the greatest number of particles ($9x10^9$ p/mL), followed by fraction 2 ($7.03x10^9$ p/mL). Fraction 3 contained $7.72x10^9$ p/mL while, fraction 4 contained $4.32x10^9$ p/mL. Fraction 5 was also quantified and was found to contain $1.92x10^9$ p/mL. The void volume also contained $3.79x10^9$ p/mL (Figure 5.10).

EVs isolated using SEC were initially characterised using NTA to assess particle concentration and size. The average EV particle concentration was $1.14x10^{13} \pm 9.12x10^{11}$ p/mL (mean $\pm$ SEM), while average EV particle size was 82.54 ± 0.91 nm (mean $\pm$ SEM) (Figure 5.11 A & B). The protein content of SEC isolated EVs was assessed using BCA whereby EV protein content was 784.30 ± 86.87 µg/mL (mean $\pm$ SEM) (Figure 5.12).

Further to individual characterisation of SEC isolated EVs, the correlation between EV concentration and protein content and EV concentration and size were also determined. There was a weak positive correlation between EV concentration and protein content as determined by Pearson r correlation test, though not significant (r value of 0.21; p=0.73) (

A
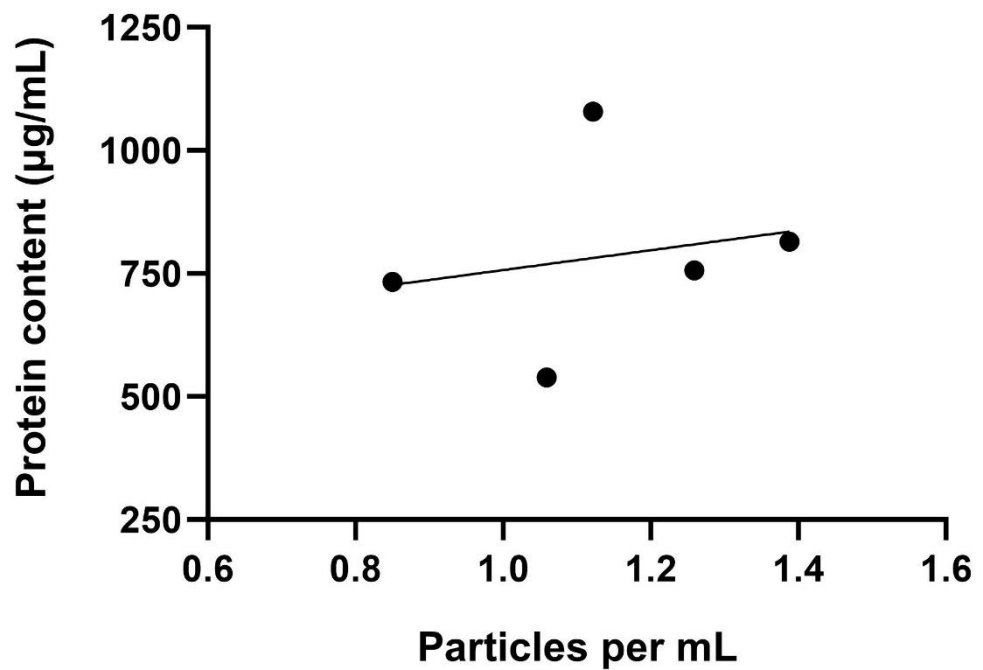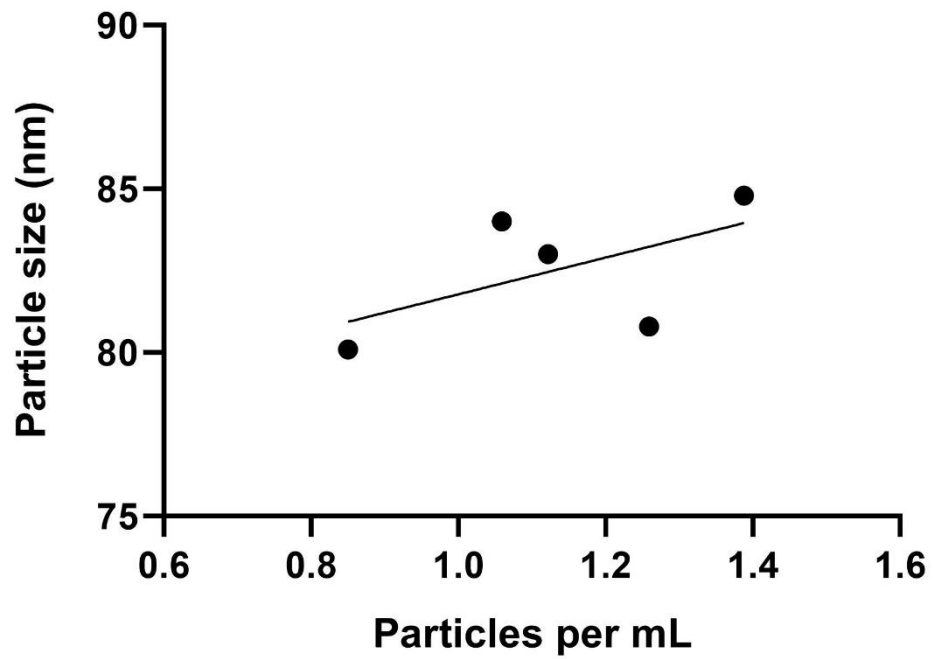
A). There was a weak positive correlation between EV concentration and size as determined by Pearson r correlation test, though not significant (r value of 0.56; p=0.32) (
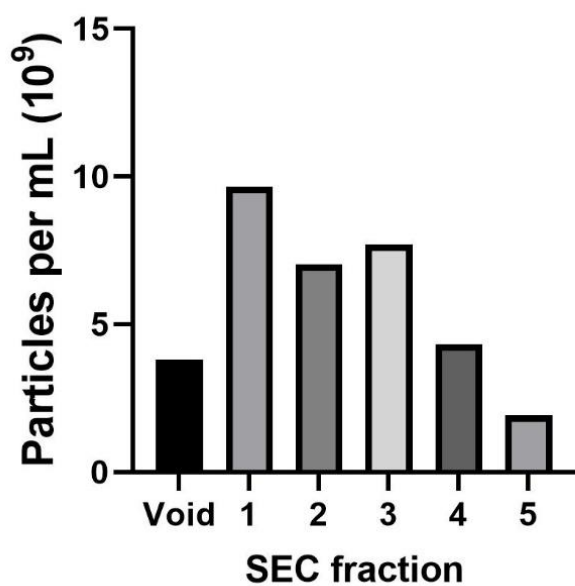
A
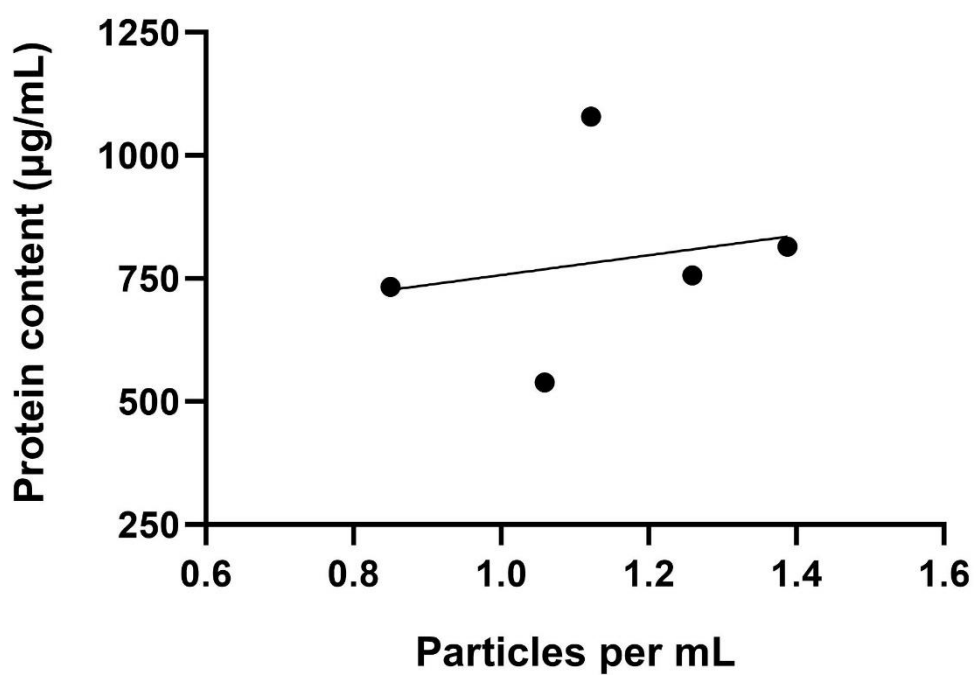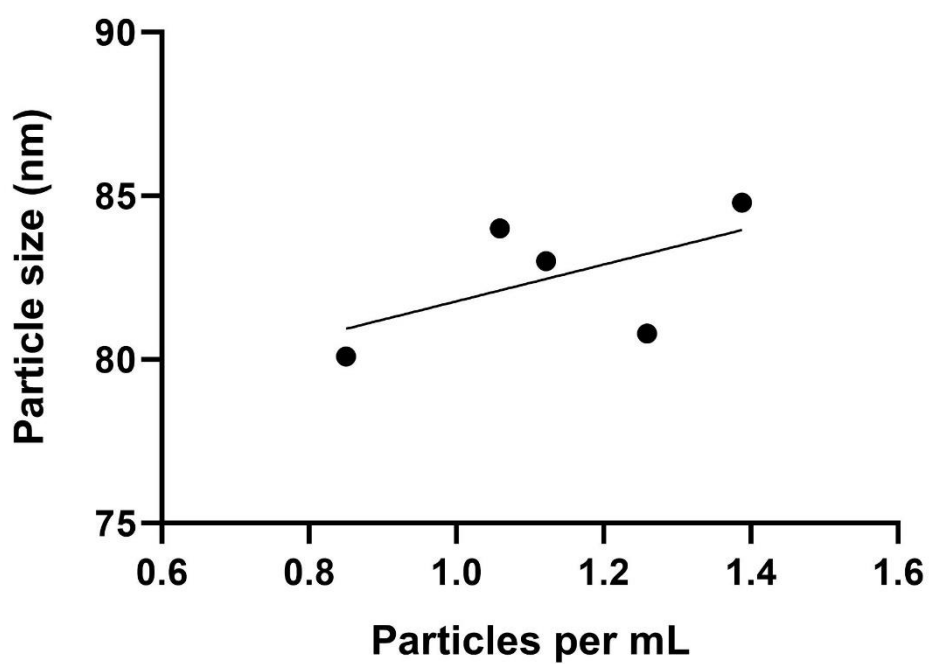
B).

Figure 5.10 Characterisation of SEC fractions.
IZON qEV-35mm SEC columns and IZON AFC were used to isolate SHRSP plasma EVs. SHRSP plasma was passed through SEC columns. Void volume and EVs were collected in individual fractions 1-5. EV concentration was determined by NTA (n=1).
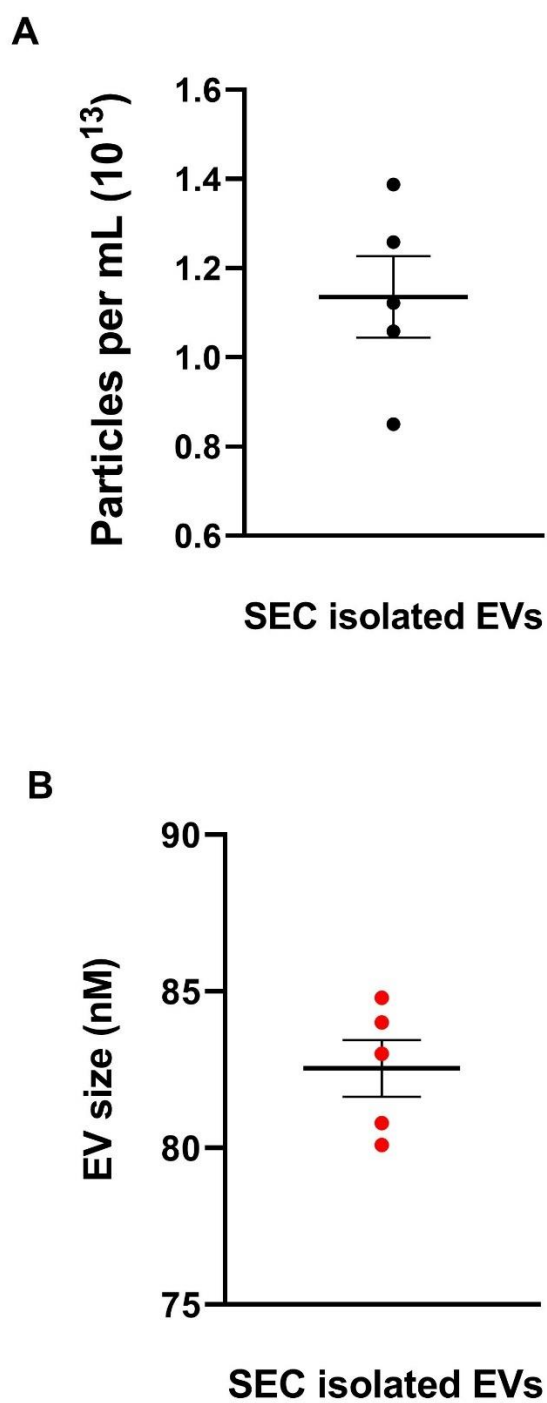
A

B

Figure 5.11 Characterisation of SEC-isolated EVs.
SHRSP plasma-derived EV particle concentration (A) and particle size (B) was determined
by NTA (n=5).
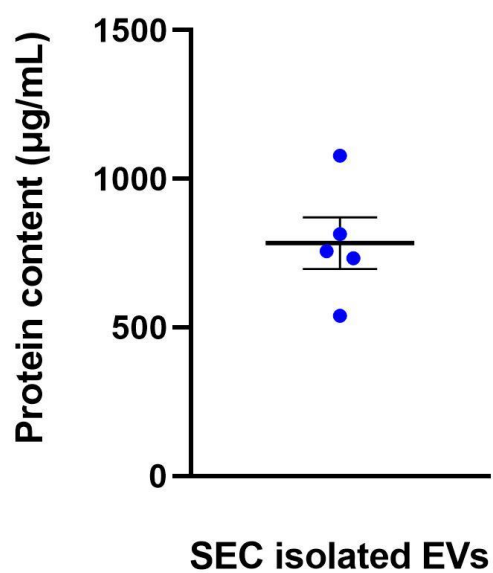
Figure 5.12 Protein content of SEC-isolated EVs.
EVs were isolated from SHRSP plasma using SEC and total protein content was determined by BCA (n=5).

A
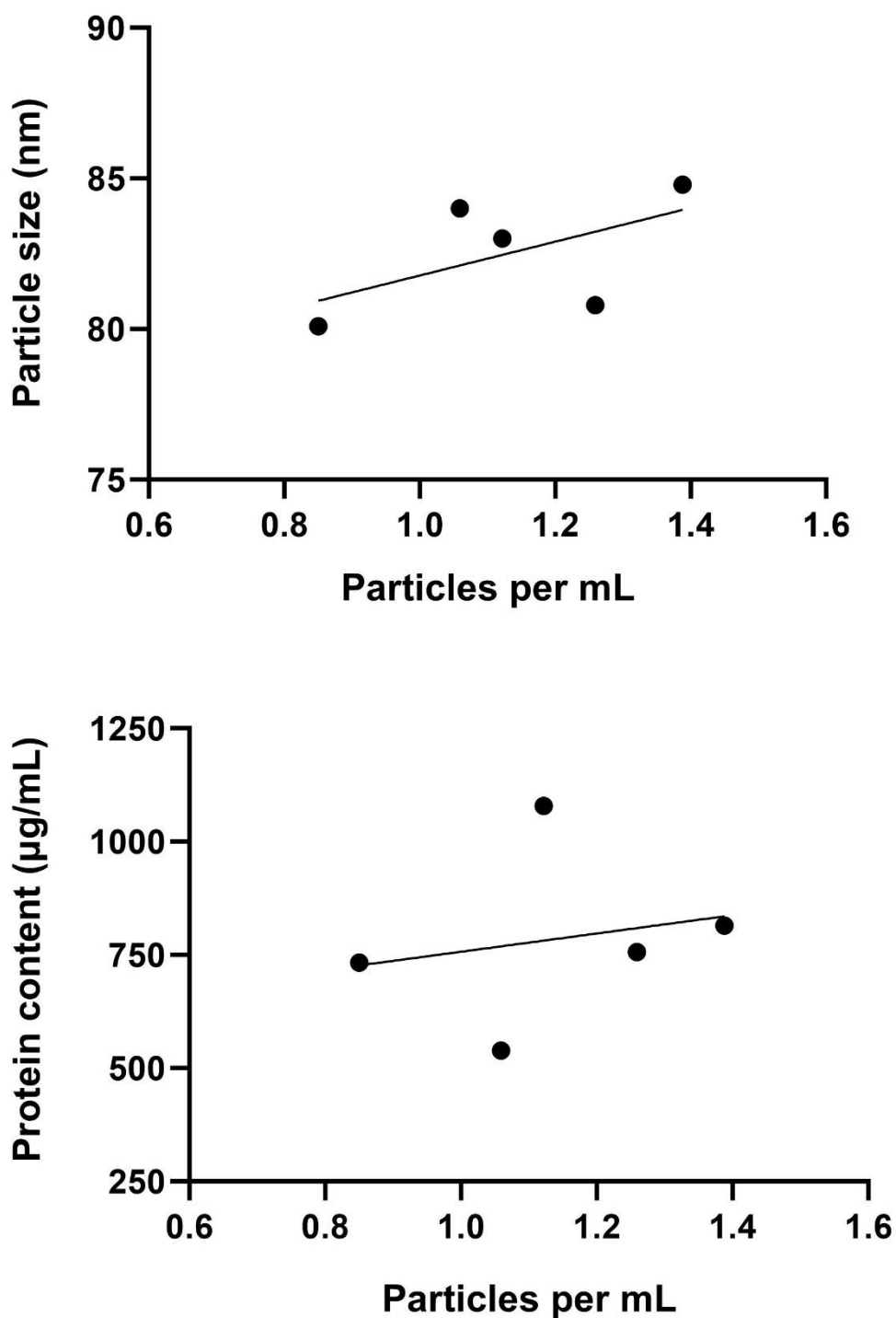
Figure 5.13 Relationship between SEC-isolated EV characteristics.
(A) Correlation between SEC-isolated EV concentration and EV protein content. (B) Correlation between SEC-isolated EV concentration and EV size (n=5, p>0.05, Pearsons's correlation coefficient).

5.4.4 The use of SEC EV isolation after electroporation

To assess whether SEC EV isolation after electroporation led to a greater final EV concentration, EVs were firstly isolated from SHRSP plasma using SEC and were electroporated at 400mV. EVs were then re-isolated using SEC. After electroporation and SEC re-isolation the final EV concentration was significantly reduced ($4.45x10^{11} \pm 1.68x10^{11}$ particles; mean $\pm$ SEM) compared to starting EV concentration ($1.37x10^{12} \pm 5.13x10^{10}$ particles; $p<0.05$). Following electroporation and UC re-isolation, final EV concentration was reduced ($8.93 x10^9 \pm 2.57x10^9$ particles) compared to starting EV concentration ($1.42 x10^{12} \pm 4.98x10^{10}$ particles) ($p<0.01$) (Figure 5.14). There was a -0.98-fold change in final EV concentration between UC and SEC, whereby SEC provided a greater final EV concentration compared to UC.
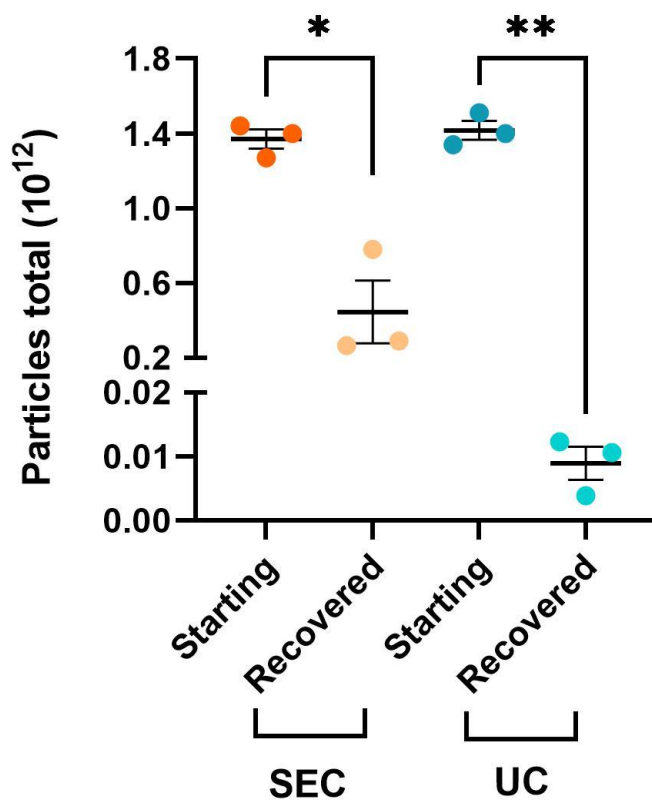
Figure 5.14 Effects of re-isolation method of EV concentration post-electroporation.
Comparison between EV concentration before (starting) and after (recovered)
electroporation using either UC or SEC re-isolation methods. EV concentration was
determined by NTA (n=3, *p<0.05, **p<0.01, paired t-test).

5.4.5 Relationship between EV isolation method and particle concentration

SEC and PEG methods of EV isolation were compared to determine whether these different isolation methods led to changes in EV characteristics. There was no difference in EV concentration between PEG isolated EVs ($1.38 \times 10^{13} \pm 1.48 \times 10^{12}$ p/mL; mean $\pm$ SEM) and SEC isolated EV ($1.29 \times 10^{13} \pm 1.39 \times 10^{12}$ p/mL) (Figure 5.15). There was no difference in EV particle size between PEG isolated EVs (106.60 ± 15.33 nm; mean $\pm$ SEM) and SEC isolated EVs (82.54 ± 0.91 nm) (Figure 5.16). EV protein content was increased in PEG isolated EVs (2744.62 ± 505.14 µg/mL; mean $\pm$ SEM) compared to SEC isolated EVs (784.27 ± 86.87 µg/mL; $p < 0.01$) (Figure 5.17).
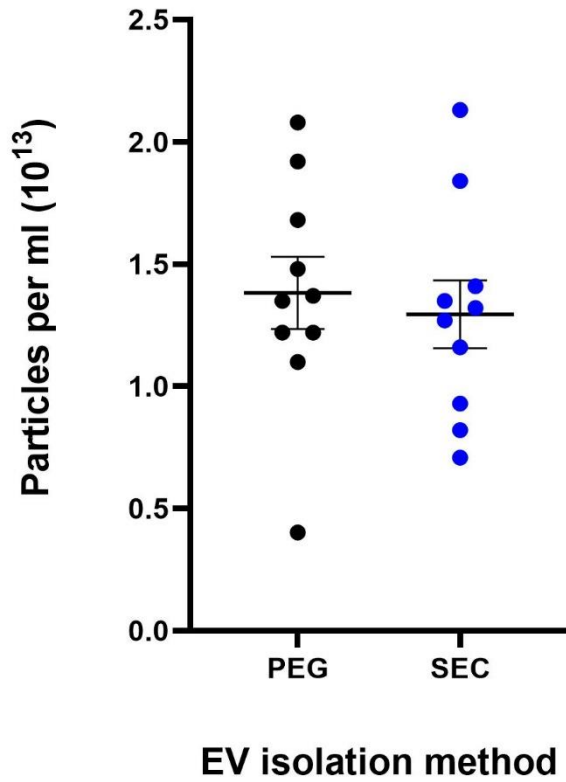
Figure 5.15 Effects of PEG or SEC isolation methods on EV concentration.
EV were isolated from SHRSP plasma using either PEG or SEC. EV particle concentration as determined by NTA (n=10, p>0.05, Welch's t-test).
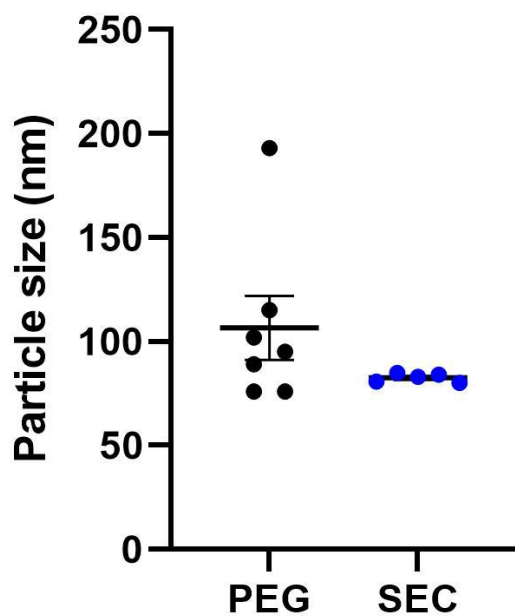
Figure 5.16 Effects of PEG or SEC isolation methods on EV size.
EV were isolated from SHRSP plasma using either PEG or SEC. EV particle size as determined by NTA (n=5-7, p>0.05, Welch's t-test).
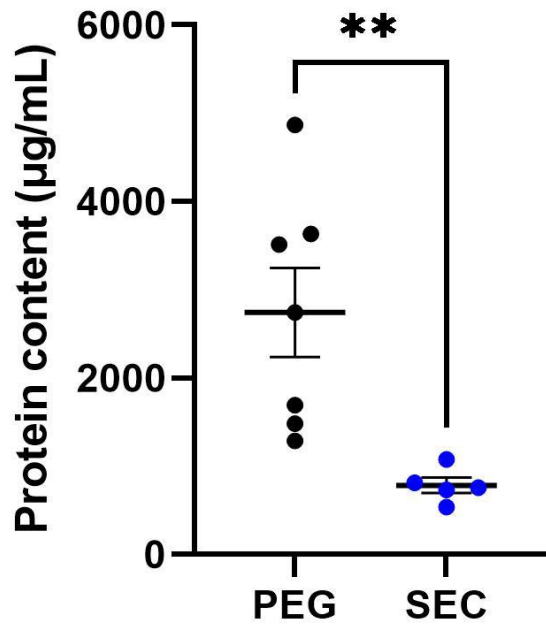
Figure 5.17 Effects of PEG or SEC isolation methods on EV protein content.
EV were isolated from SHRSP plasma using either PEG or SEC. EV protein content as determined by BCA (n=5-7, p<0.01, Welch's t-test).

5.4.6 Western blot characterisation of EVs

In line with standard EV characterisation methods, western blotting was used to identify the presence of common EV marker within EV samples derived from SHRSP plasma. EV markers Annexin XI, TSG101, CD81 and CD63 were assessed in EV samples isolated using SEC. Banding was observed in all markers at their respective molecular weights (Figure 5.18).
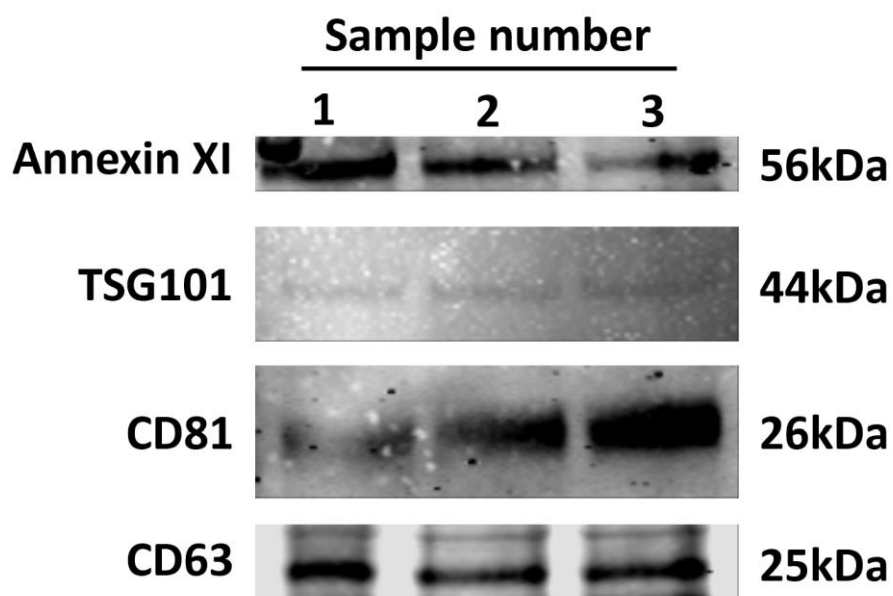
Figure 5.18 Characterisation of common EVs markers.
Western blot images show bands corresponding to EV markers Annexin XI, TSG101,
CD81, and CD63 from SHRSP plasma-derived EV lysates (Samples 1, 2, and 3).
Molecular weight in kilo Dalton (kDa) of each band are shown on the right-hand side of
the image. Samples were loaded equally for each marker (10-30 µg). Loading control
absent as no appropriate loading control exists for extracellular vesicles (n=3).

5.4.7 TEM characterisation of electroporated EVs

As electroporation may alter the structural integrity of EVs, transmission Electron Microscopy (TEM) was carried out on electroporated EV samples to understand whether electroporation led to changes within overall EV morphology. Unloaded control EVs (U-EVs) and EVs that were electroporated with Ang-(1-9) peptide (A-EVs) or *Cel-miR-39* mimic miRNA (C-EVs) were imaged (Figure 5.19). There was no difference in EV diameter between unloaded controls or electroporated samples. The average diameter of U-EVs was 75.98 ± 8.33 nm (mean ± SEM), while A-EVs had an average diameter of 75.98 ± 8.33 nm, and C-EVs had an average diameter of 70.15 ± 6.43 nm (Figure 5.20).
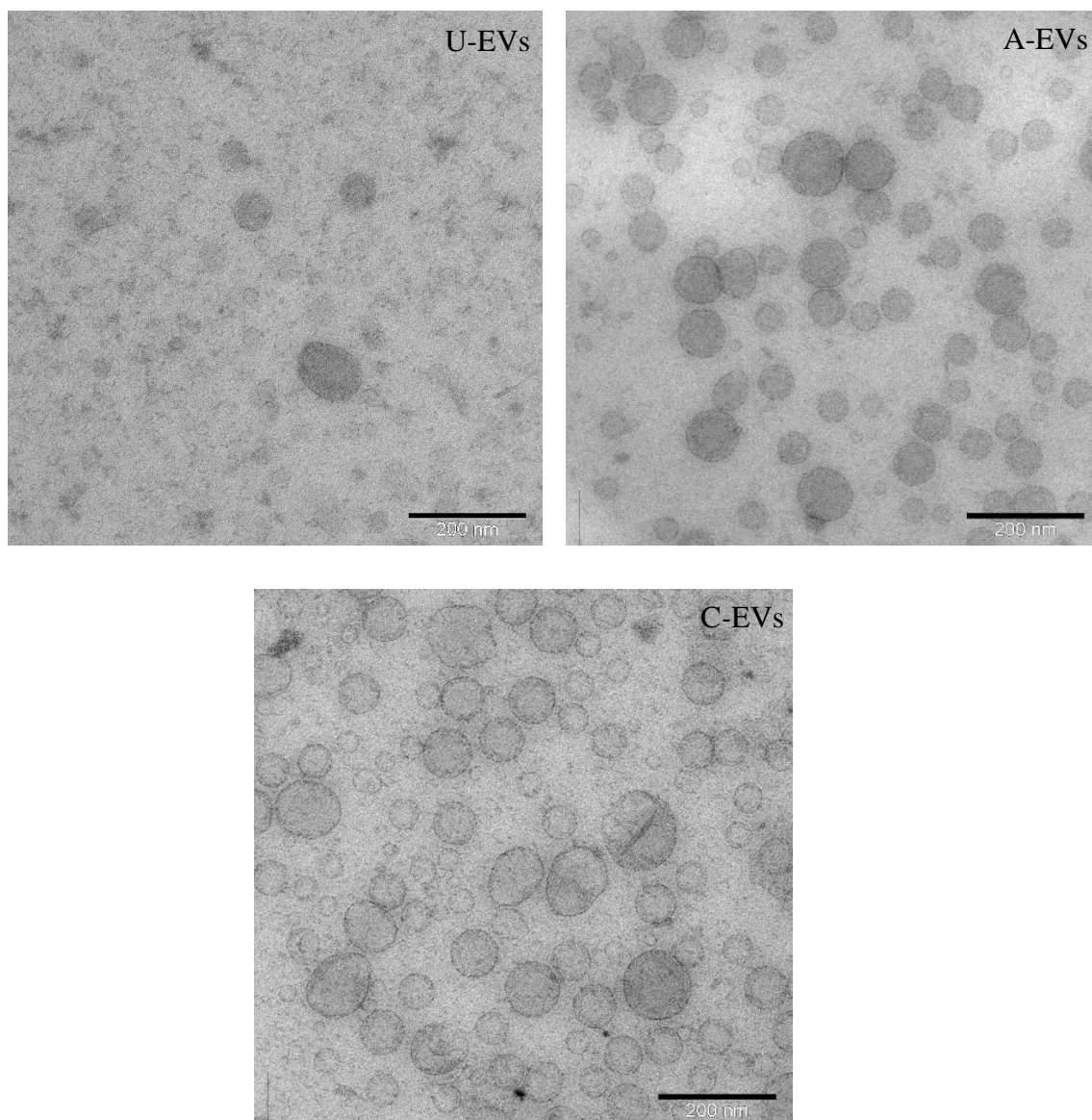
Figure 5.19 TEM analysis of electroporated EVs.
Representative image of unloaded control EVs (U-EVs) or EVs were electroporated with either Ang-(1-9) peptide (A-EVs) or *Cel-miR-39* mimic miRNA (C-EVs) were imaged using TEM. Electroporated EVs were mounted and imaged by the University of Glasgow microscopy department. Scale bar 200nm.
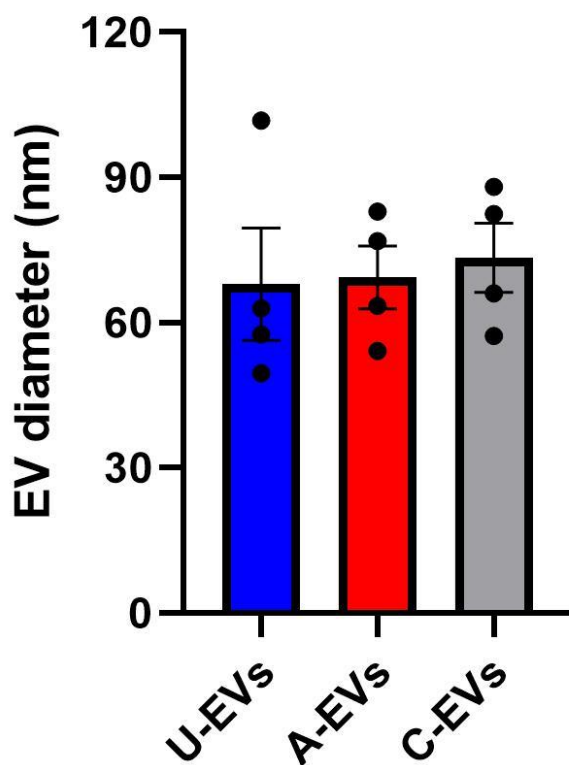
Figure 5.20 Effects of electroporation on EV diameter.
EVs were either unloaded (U-EVs) or electroporated with either Ang-(1-9) peptide (A-EVs) or *Cel-miR-39* mimic miRNA (C-EVs). Electroporated EVs were mounted and imaged using TEM by the University of Glasgow microscopy department. EV diameter was determined using Fiji image-J software (n=4, $p>0.05$, One-way ANOVA with post-hoc Tukey's).

5.4.8 Assessment of Ang (1-9) peptide treatment on primary neuronal cell viability

To understand whether Ang-(1-9) peptide affects primary neuronal cell viability under normal and OGD culture conditions, MTT assays was carried out. Once matured, primary neuronal cells were incubated with 1-, 5-, 10-, and 20-µM of Ang-(1-9) peptide for 24 hours. Under normal culture conditions, relative to untreated control (baseline 100 ± 0.00 %, cell viability; mean $\pm$ SEM), 1 µM (98.83 ± 4.49 %), 5 µM (97.96 ± 5.91 %), 10 µM (91.66 ± 6.20 %) and 20 µM (77.29 ± 12.51 %) Ang-(1-9) concentrations did not affect primary neuronal cell viability (Figure 5.21). Within the OGD model, once mature and confluent, primary neuronal cells were incubated with 1-, 5-, 10, and 20-µM of Ang-(1-9) peptide for 18 hours during the reperfusion stage after OGD. Relative to untreated control (baseline 100 ± 0.00 %, cell viability), 1 µM (95.33 ± 3.75 %), 5 µM (83.48 ± 10.67 %), 10 µM (81.22 ± 11.80 %) and 20 µM (66.76 ± 12.73 %) Ang-(1-9) concentrations did not affect primary neuronal cell viability (Figure 5.22).

Figure 5.21 Effects of Ang-(1-9) peptide on normal cell culture conditions.
Effects of Ang (1-9) on primary neuronal cell viability. Primary neuronal cells were plated at 1.2×10^6 cells/mL and were matured for 8 days before peptide treatment. Cells were treated with, 5, 10 or 20μM Ang-(1-9) peptide. Cell viability was determined using MTT assay (n=4, p>0.05, One-way ANOVA with post hoc Tukey's).
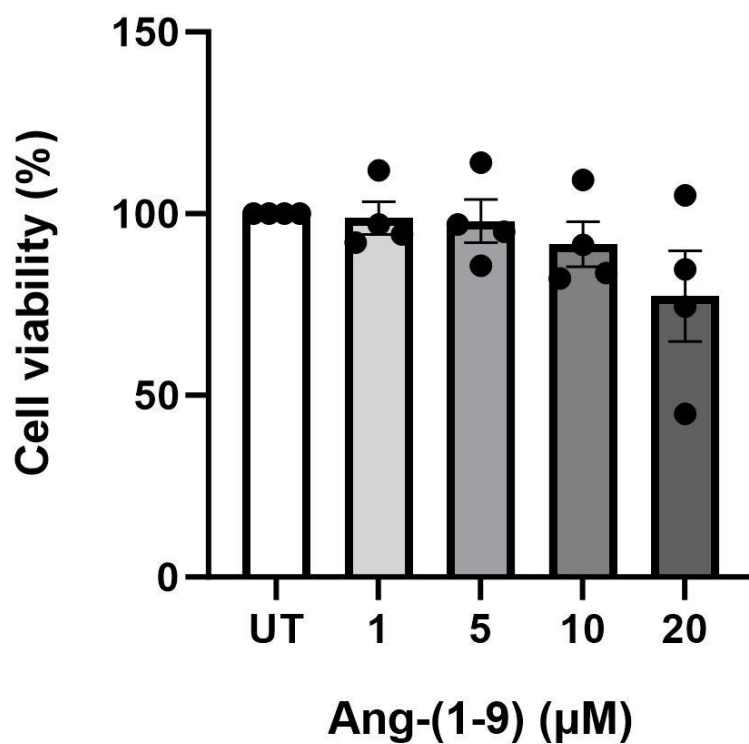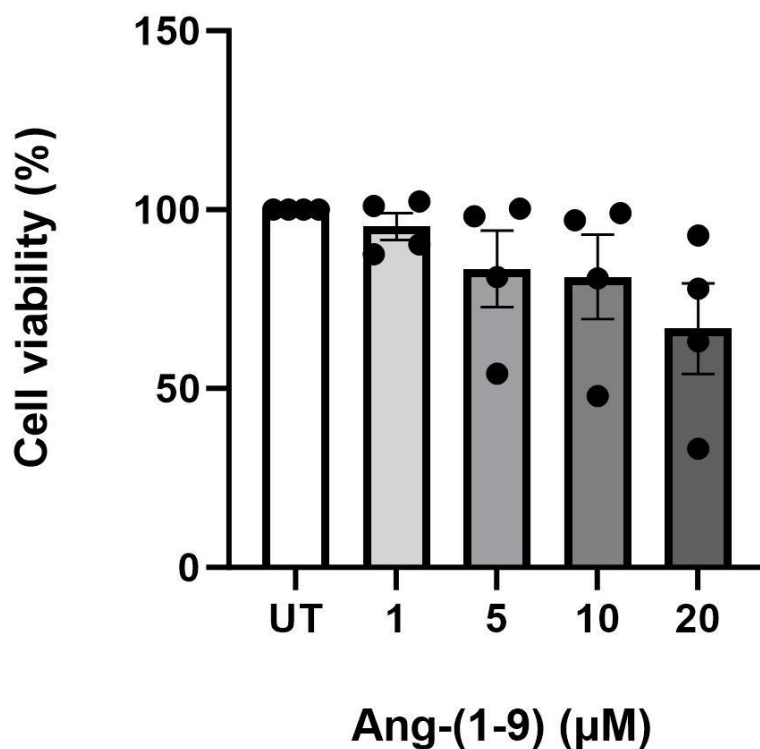
Figure 5.22 Effects of Ang-(1-9) peptide on OGD cell culture conditions.
Effects of Ang (1-9) on primary neuronal cell viability. Primary neuronal cells were plated at 1.2×10^6 cells/mL and were matured for 8 days before OGD. Cells were treated with, 5, 10 or 20μM Ang-(1-9) peptide during the reperfusion stage. Cell viability was determined using MTT assay (n=4, p>0.05, One-way ANOVA with post hoc Tukey's).

5.4.9 Effect of EVs electroporated with Ang-(1-9) peptides on primary neuronal cell viability

EVs were electroporated with Ang-(1-9) or 5-FAM- Ang-(1-9) before assessing their effects on primary neuronal cells viability under normal and OGD culture conditions. Under normal culture conditions, compared to untreated control (100 ± 0.00 %, cell viability; mean $\pm$ SEM), unloaded EVs at a concentration of $5x10^8$ particles per mL (p/mL) (106.90 ± 5.95 %), $5x10^9$ p/mL (93.58 ± 4.63 %), and $5x10^{10}$ p/mL (74.42 ± 16.16 %) did not affect cell viability. When compared to untreated control (100 ± 0.00 %), Ang-(1-9) electroporated EVs at a concentration of $5x10^8$ p/mL (86.60 ± 8.84 %), $5x10^9$ p/mL (82.67 ± 18.68 %), and $5x10^{10}$ p/mL (81.43 ± 14.46 %) Ang-(1-9) did not change cell viability. Similarly, compared to unloaded EVs (100 ± 0.00 %), 5-FAM-Ang-(1-9) electroporated EVs at a concentration of $5x10^8$ p/mL (79.49 ± 17.19 %), $5x10^9$ p/mL (82.61 ± 12.38 %), and $5x10^{10}$ p/mL (69.49 ± 13.03 %) did not affect cell viability (Figure 5.23).

Within the OGD model, compared to untreated control (100 ± 0.00 %, cell viability), unloaded EVs at a concentration of $5x10^8$ p/mL (107.90 ± 3.36 %), $5x10^9$ p/mL (93.83 ± 9.34 %), and $5x10^{10}$ p/mL (102.5 ± 2.80 %) did not result in any significant changes in cell viability. Compared to untreated control (100 ± 0.00 %), Ang-(1-9) electroporated EVs at a concentration of $5x10^8$ p/mL (89.79 ± 12.15%), $5x10^9$ p/mL (102.00 ± 2.61 %), and $5x10^{10}$ p/mL (96.37 ± 8.19 %) did not affect cell viability. Similarly, compared to unloaded EVs (100 ± 0.00 %), 5-FAM-Ang-(1-9) electroporated EVs at a concentration of $5x10^8$ p/mL (96.92 ± 11.02 %), $5x10^9$ p/mL (74.65 ± 12.14 %), and $5x10^{10}$ p/mL (71.11 ± 11.06 %) did not change cell viability (Figure 5.24).

Figure 5.23 Effects of electroporated EVs on normal cell culture conditions.
Primary neuronal cells were plated at 1.2×10^6 cells/mL and were matured for 8 days before EV treatment. Cells were treated with 5×10^8, 5×10^9 and 5×10^{10} p/mL of unloaded EVs or Ang-(1-9) or 5-FAM-Ang-(1-9) electroporated EVs. Cell viability was determined using MTT assay (n=4, p>0.05, One-way ANOVA with post hoc Tukey's).
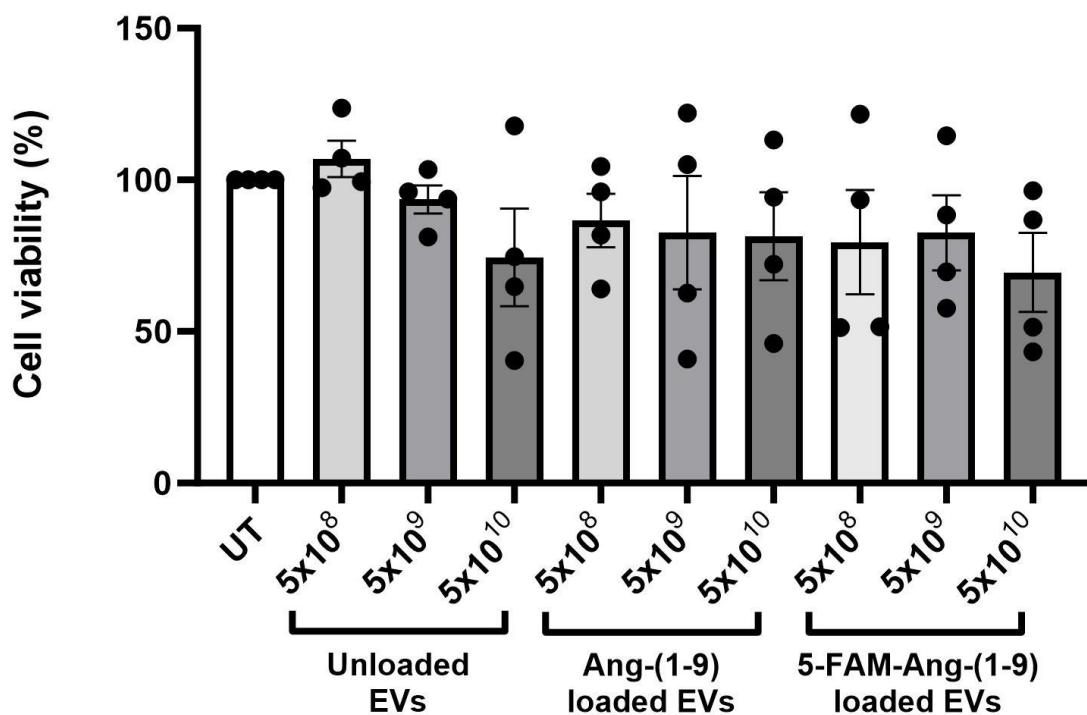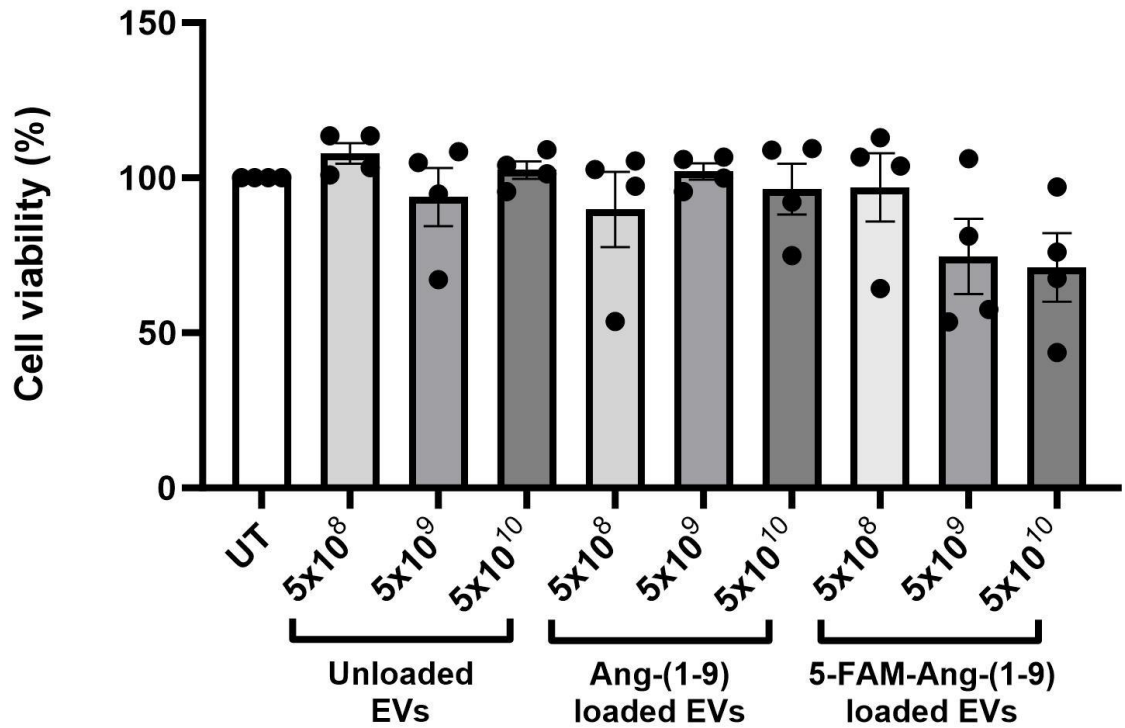
Figure 5.24 Effects of electroporated EVs on OGD cell culture conditions.
Primary neuronal cells were plated at 1.2×10^6 cells/mL and were matured for 8 days before OGD. Cells were treated with 5×10^8, 5×10^9 and 5×10^{10} p/mL of unloaded EVs or Ang-(1-9) or 5-FAM-Ang-(1-9) electroporated EVs during the reperfusion stage. Cell viability was determined using MTT assay (n=4, p>0.05, One-way ANOVA with post hoc Tukey's)

5.4.10 ICC of 5-FAM-Ang-(1-9) electroporated EV treatment on B50 and GPNT cells

To better illustrate the distribution of Ang-(1-9) peptide within cell cultures, B50 and GPNT cells were treated with $5x10^9$ p/mL of 5-FAM-Ang-(1-9) electroporated EVs and were imaged at various incubation periods. At 3-, 6- and 18-hours of incubation with $5x10^9$ p/mL of 5-FAM-Ang-(1-9) electroporated EVs, no fluorescence signal was observed in either B50 (Figure 5.25) or GPNT (Figure 5.26) cells.

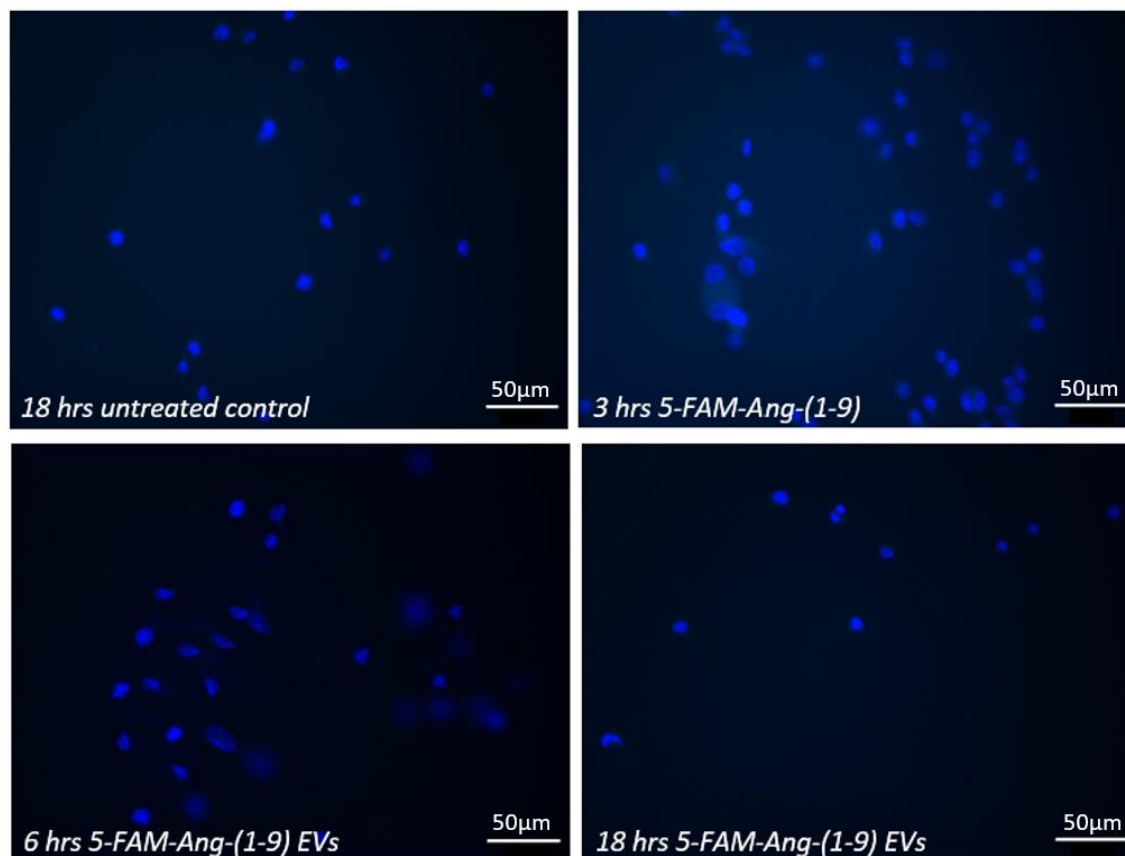**Figure 5.25 Immunofluorescence of 5-FAM-Ang-(1-9) electroporated EVs in B50 cells.**

Representative image of B50 rat neuronal cells treated with $5x10^9$ EV electroporated with 5-FAM-Ang-(1-9) peptide for 3-, 6- and 18-hours. B50s were grown to a density of $0.5x10^5$ cells/well. Cells were imaged using fluorescence microscope at 40X magnification. Nuclear staining is shown by DAPI (blue) (n=3, replicate=2).

Figure 5.26 Immunofluorescence of 5-FAM-Ang-(1-9) electroporated EVs in GPNT cells.
Representative image of GPNT rat cerebral endothelial cells treated with $5x10^9$ EVs electroporated with 5-FAM-Ang-(1-9) peptide for 3-, 6- and 18-hours. GPNTs were grown to a density of $0.5x10^5$ cells/well. Cells were imaged using fluorescence microscope at 40X magnification. Nuclear staining is shown by DAPI (blue) (n=3, replicate=2).
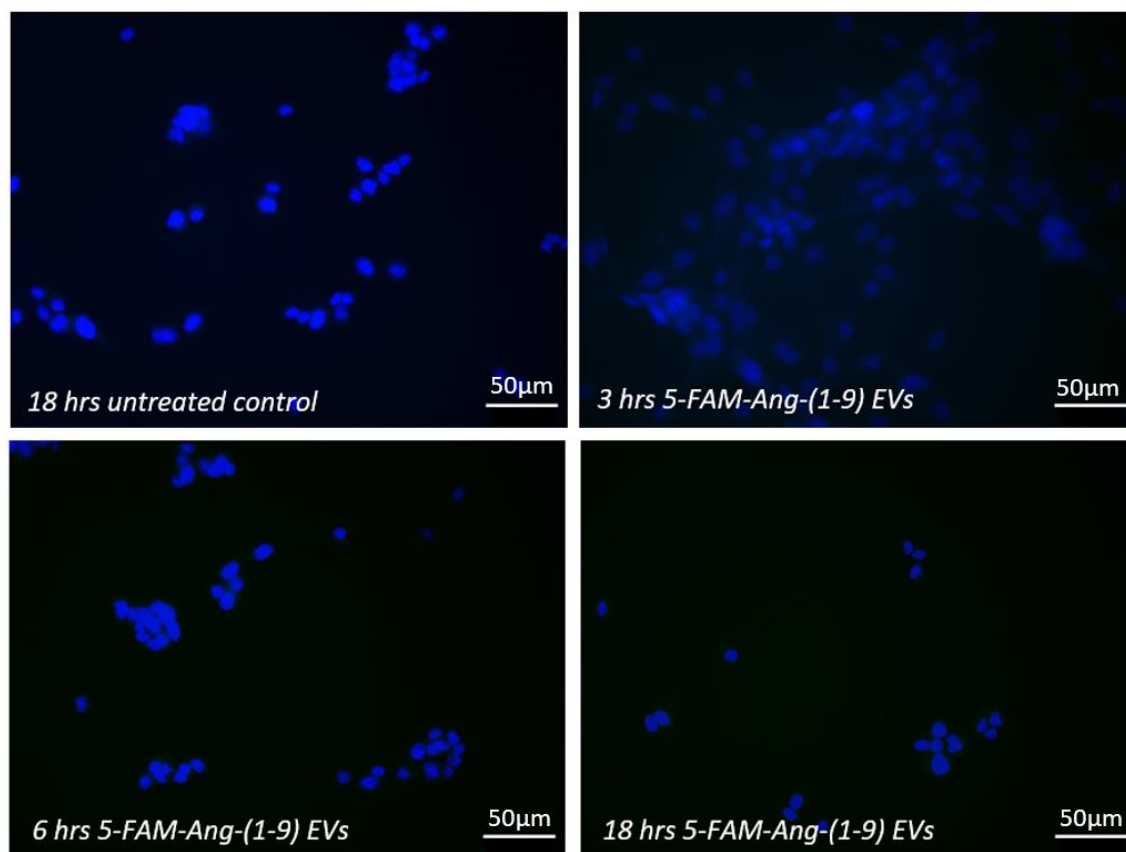
5.4.11 ICC of 1μM 5-FAM-Ang-(1-9) treatment on B50 and GPNT cells

As 5-FAM-Ang-(1-9) electroporated EVs did not provide a fluorescent signal, B50 and GPNT cells were treated with 1μM 5-FAM-Ang-(1-9) peptide to understand its bioactivity. Success of peptide uptake was assessed by fluorescence microscopy. After incubation, no fluorescence signal was observed after 48 hours incubation in either B50 cells (Figure 5.27 A) or GPNT cells (Figure 5.27 B).
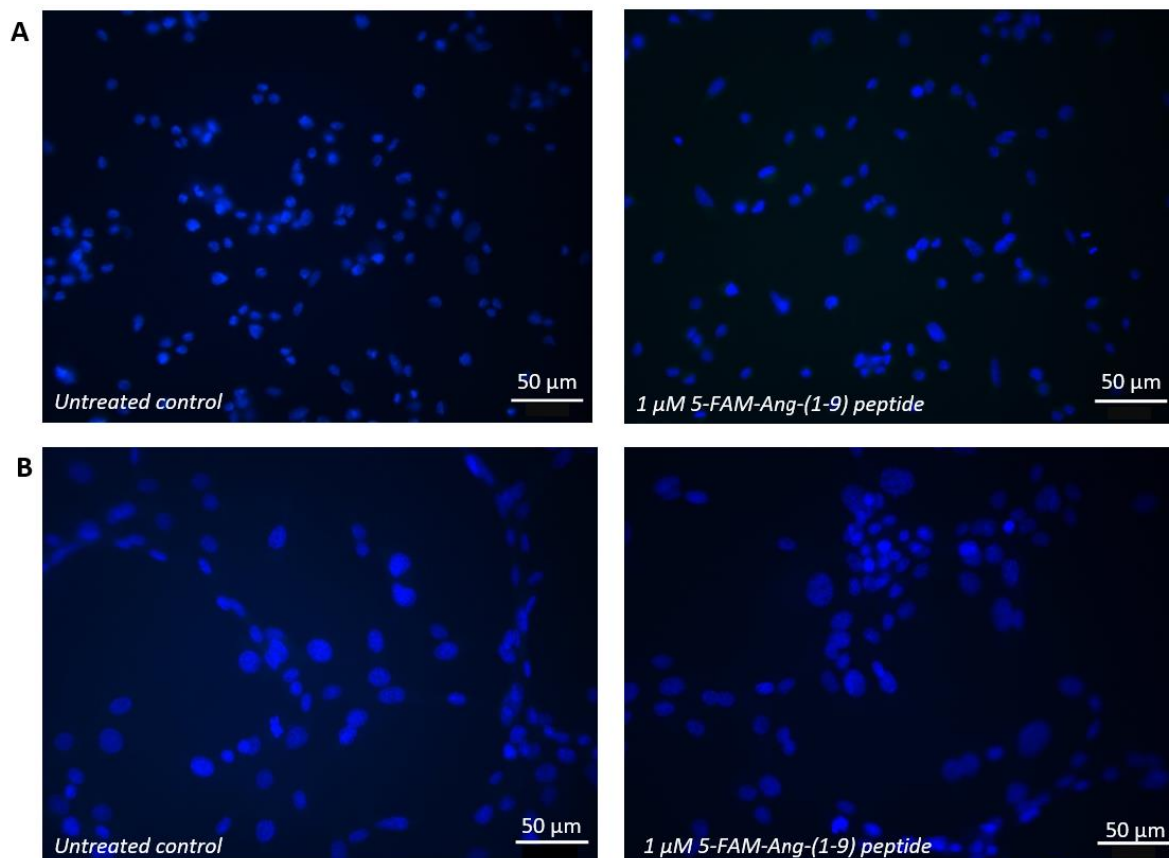
Figure 5.27 Immunofluorescence of 1µM 5-FAM-Ang-(1-9) peptide in B50 and GPNT cells.
Representative image of B50 rat neuronal cells (A) and GPNT rat cerebral endothelial cells (B) were treated with 1µM of 5-FAM-Ang-(1-9) peptide for 48 hours. Cells were grown to a density of 0.5×10^5 cells/well before treatment. Cells were imaged using fluorescence microscope at 40X magnification. Nuclear staining is shown by DAPI (blue) (n=3, replicate=2).

5.4.12 Cell-derived EVs treatment of recipient cells

As treatment with 5-FAM-Ang-(1-9) electroporated EVs nor 5-FAM-Ang-(1-9) peptide did not result in fluorescence signal, cell-derived EVs were assessed for their peptide uptake ability. B50s and GPNTs were treated with 1µM 5-FAM-Ang-(1-9) peptide for 48 hours and EVs were isolated from culture media. These EVs were then used to treat recipient B50 and GPNT cells. Cell-derived EV treatment did not deliver a fluorescence signal in either B50 (Figure 5.28 A) or GPNT (Figure 5.28 B) cells.
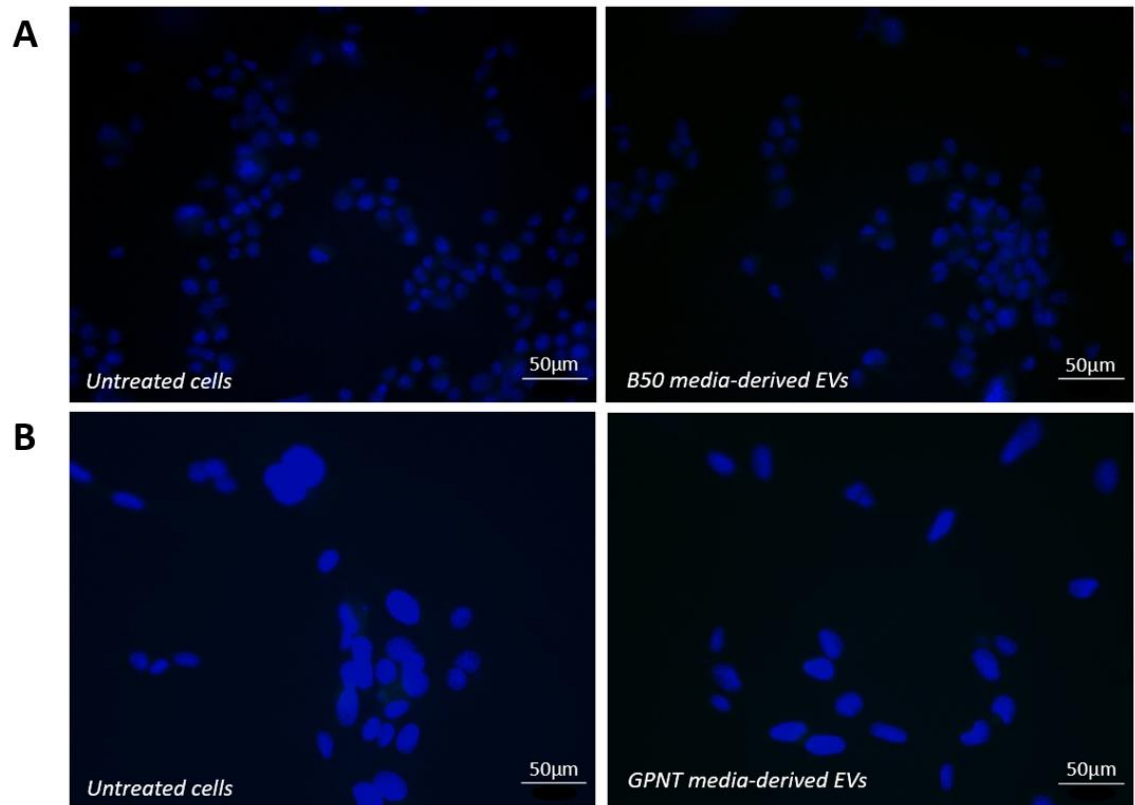
Figure 5.28 Immunofluorescence cell derived EVs on recipient cells.
Representative image of B50 rat neuronal cells (A) and GPNT rat cerebral endothelial cells
(B) were treated with $5x10^9$ of cell-derived EVs following 1µM 5-FAM-Ang-(1-9) peptide
treatment for 18 hours. All cells were grown to a density of $0.5x10^5$ cells/well prior to
treatment. Recipient cells were imaged using fluorescence microscope at 40X
magnification. Nuclear staining is shown by DAPI (blue) (n=3, replicate=2).

5.4.13 5-FAM-Ang-(1-9) treatment of B50 and primary neuronal cells

Previously it was found that fluorescence signal could not be observed when GPNTs and B50 cells were treated with 1µM 5-FAM-Ang-(1-9) peptide, as such B50 cells were treated with a range of 5-FAM-Ang-(1-9) peptide concentrations. Success of peptide uptake was assessed by fluorescence microscopy. After incubation for 48 hrs, no fluorescence was seen in B50 cells treated with 10 µM of 5-FAM-Ang-(1-9) peptide (Figure 5.29 B). Faint fluorescence signals were observed predominantly at 20 and 40 µM (Figure 5.29 C & D). 40 µM of 5-FAM-Ang-(1-9) peptide provided the greatest fluorescent signal within B50 cells, though overall faint (Figure 5.29 D).

As B50 cell lines did not provide significant fluorescence signal of treatment with various 5-FAM-Ang-(1-9) concentrations, SHRSP neonatal primary neuronal cells were treated with 5-FAM-Ang-(1-9). After incubation for 48 hrs fluorescence signal was observed at 10, 20 and 40 µM 5-FAM-Ang-(1-9) peptide treatment (Figure 5.30 B, C and D). 40 µM provided the most intense fluorescence signal (Figure 5.30 D), whereas 10 µM provided the weakest fluorescence signal (Figure 5.30 B).
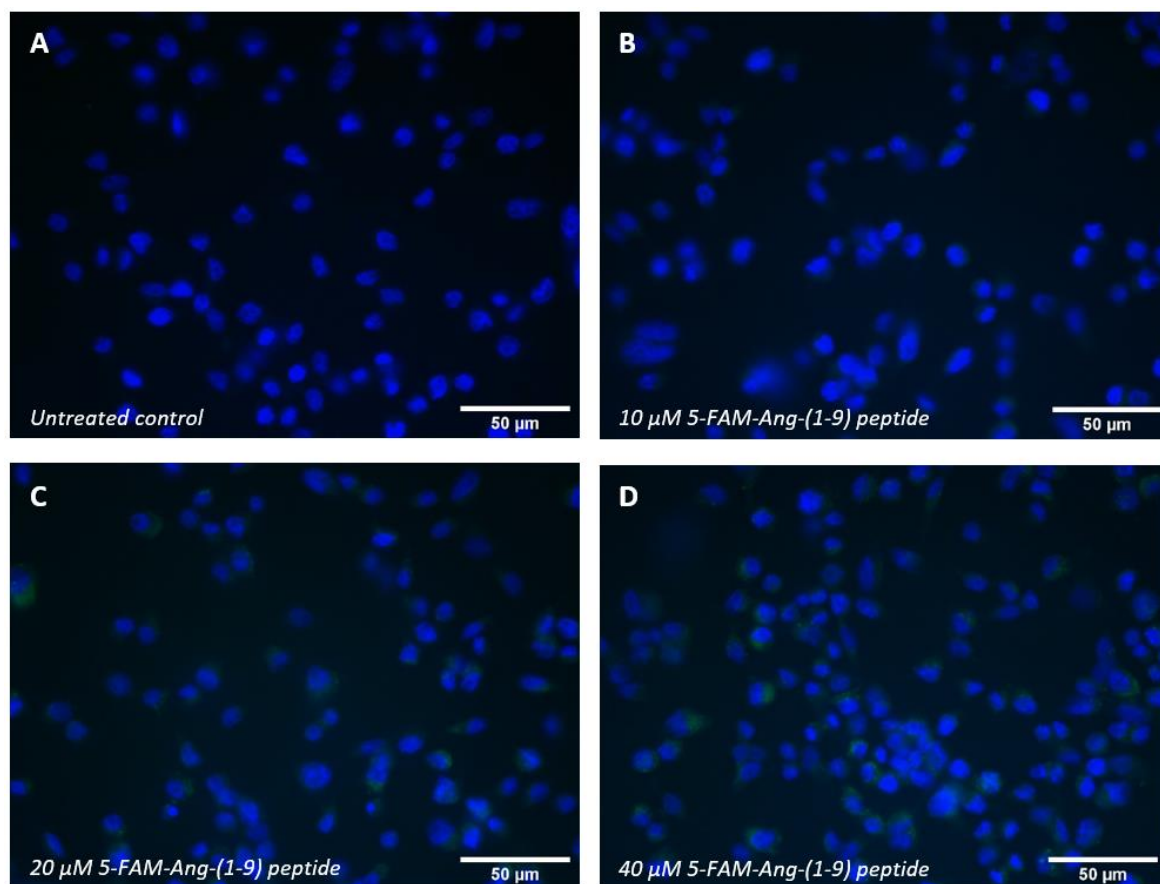
Figure 5.29 Immunofluorescence of 5-FAM-Ang-(1-9) peptide concentrations on B50 cells.
Representative image of B50 rat neuronal cells treated as follows: untreated (A), 10 µM (B), 20 µM (C) and 40 µM (D) of 5-FAM-Ang-(1-9) peptide. Cells were incubated with 5-FAM-Ang-(1-9) peptide after 48 hours incubation. B50s were grown to a density of 0.5×10^5 cells/well prior to treatment. Cells were imaged using fluorescence microscope at 40X magnification. Nuclear staining is shown by DAPI (blue) while 5-FAM-Ang-(1-9) peptide is shown in green (n=3, replicate=2).
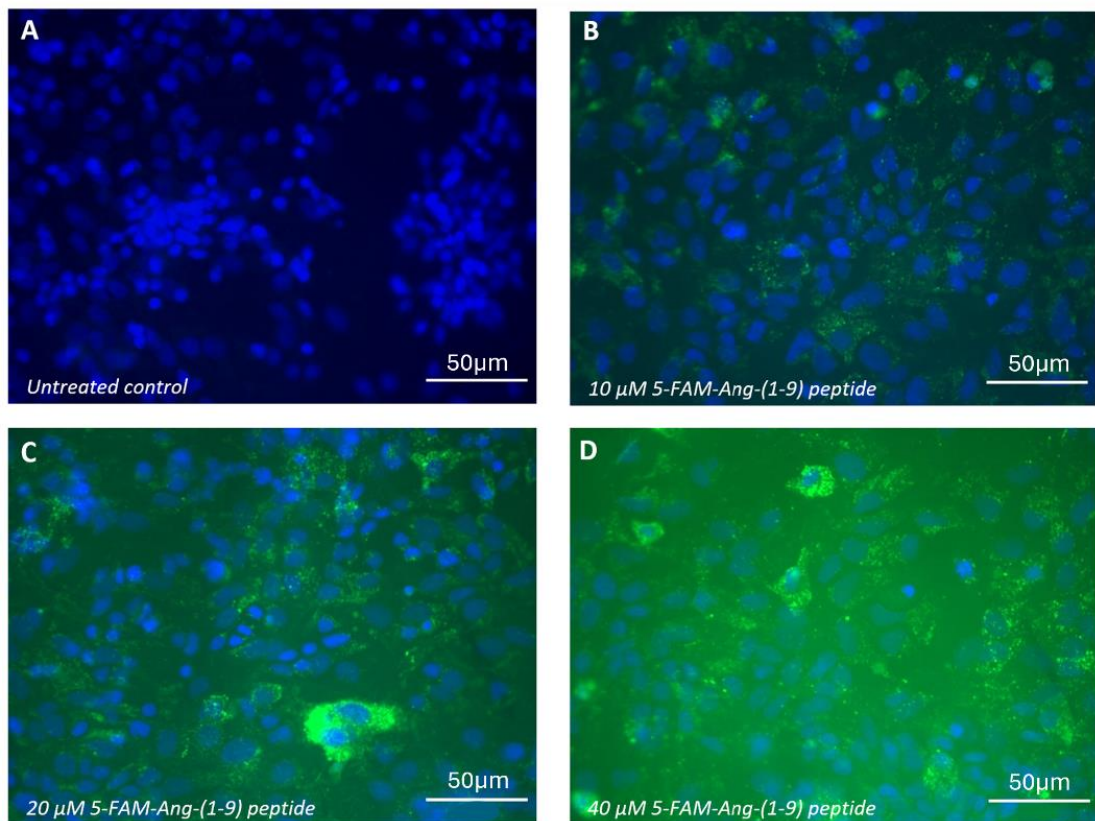
Figure 5.30 Immunofluorescence of 5-FAM-Ang-(1-9) peptide concentrations on SHRSP primary neuronal cells.
Representative image of SHRSP primary neuronal cells treated as follows: untreated (A), 10 µM (B), 20 µM (C) and 40 µM (D) of 5-FAM-Ang-(1-9) peptide. Cells were incubated with 5-FAM-Ang-(1-9) peptide after 48 hours incubation. Primary neuronal cells were plated at 1.2×10^6 cell/mL and were matured for 8 days prior to peptide treatment. Cells were imaged using fluorescence microscope at 40X magnification. Nuclear staining is shown by DAPI (blue) while 5-FAM-Ang-(1-9) peptide is shown in green (n=3, replicate=2).

5.4.14 Labelling of EVs with PKH26 dye in GPNTs and primary neuronal cells

EVs were labelled with lipophilic dye PKH26 in order to assess distribution within cell cultures. PKH26 labelling of EVs was assessed using microscopy whereby PKH26 dyed EVs appeared red in colour. Fluorescence signal varied in both GPNTs (Figure 5.31) and primary neuronal cell cultures (Figure 5.32) at 6- and 18-hour timepoints. In most cases, fluorescence signal was aggregated and not reproducible in both cell types.
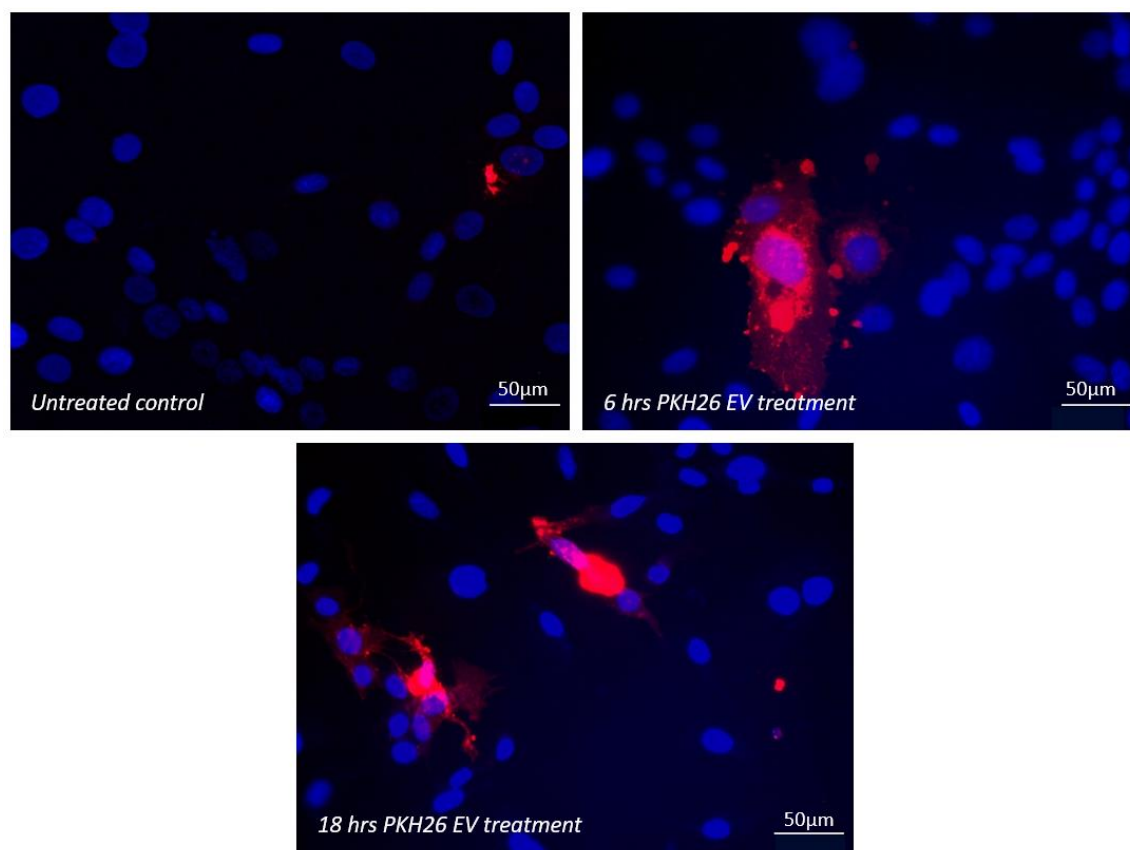
Figure 5.31 PKH26 labelled EVs distribution in GPNT cells.
Representative image of GPNT cells were treated with PKH26 labelled EVs at a concentration of $5x10^9$ particles after 6 hrs or 18 hrs incubation. GPNTs were grown to a density of $1x10^5$ cells/well prior to treatment. A total of 300µg of EVs were labelled with diluted PKH26 (1: 250; label: diluent). Cells were imaged using fluorescence microscope at 40X magnification. Nuclear staining is shown by DAPI (blue) while lipophilic dye PHK26 is shown in red (n=3).
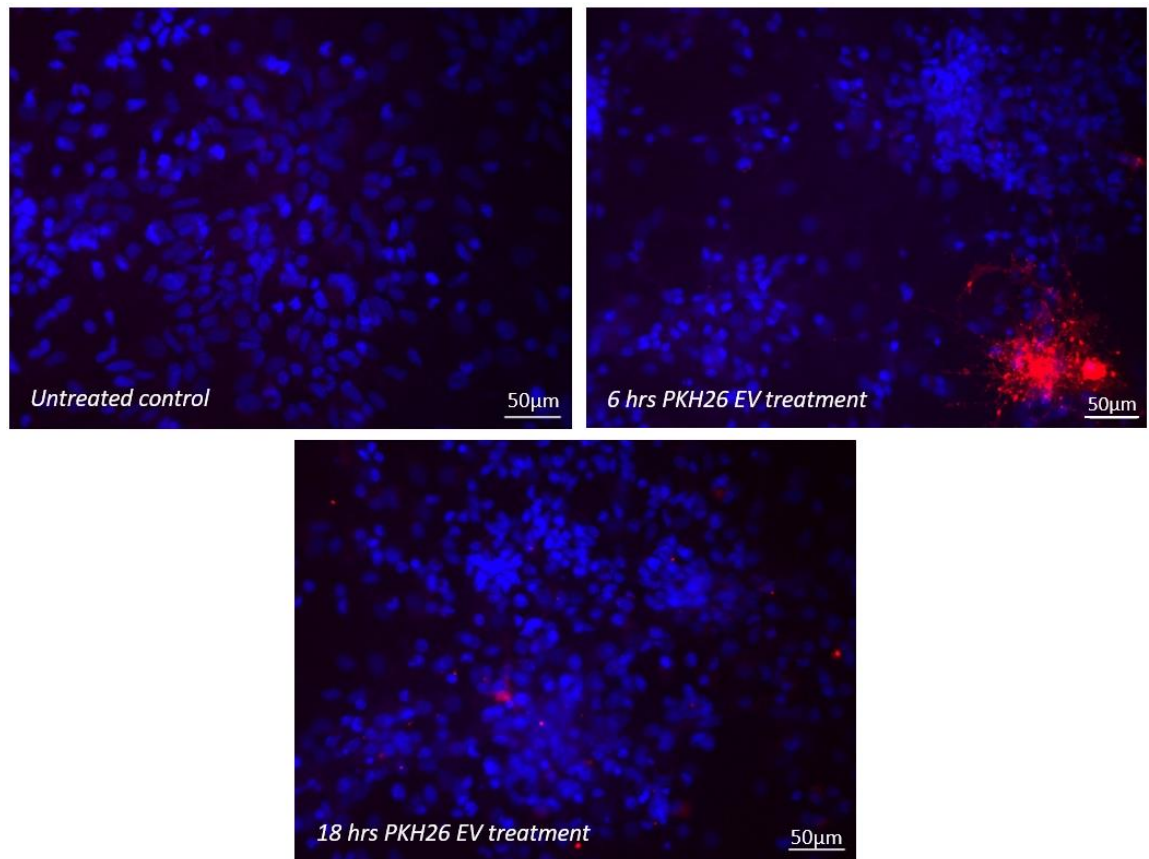
Figure 5.32 KH26 labelled EVs distribution in primary neuronal cells.
Representative image of primary neuronal cells treated with PKH26 labelled EVs at a concentration of 5×10^9 particles after 6 hrs or 18 hrs incubation. Primary neuronal cells were plated at 1.2×10^6 cells/mL and were matured for 8 days prior to EV treatment. A total of 300µg of EVs were labelled with diluted PKH26 (1: 250; label: diluent). Cells were imaged using fluorescence microscope at 40X magnification. Nuclear staining is shown by DAPI (blue) while lipophilic dye PHK26 is shown in red (n=3)

5.5 Discussion

In this chapter circulating EVs were isolated from SHRSP plasma using different methods and were characterised using standard EV characterisation methods. EV loading through electroporation led to significant loss in final EV concentration, however optimisation of EV electroporation and re-isolation methods improved final EV concentration. In cells treated with either Ang-(1-9) peptide or Ang-(1-9) peptide electroporated EVs cell viability was not affected. Only primary neuronal cells led to fluorescence signal after treatment with 5-FAM-Ang-(1-9) peptide. Lipophilic EV membrane dye led to variable results in all cell types.

Statistically there was no correlation between EV particle concentration and EV protein content. As EV protein content could not be determined by BCA following electroporation, EV particle concentration was used as an estimate for EV protein content in later experiments. In terms of EV protein content, the expression of EV tetraspanin CD63, as determined by western blot, has been shown to be correlated with EV protein content, but was not correlated to the concentration of EVs (Brennan et al., 2020). These findings further demonstrate that EV characteristics can vary and that these characteristic variances may relate to overall function. Similarly, EV particle size was also not correlated with EV particle concentration. This lack of correlation between EV concentration and size or protein content may be related to heterogenous EV populations. EV heterogeneity has been widely observed within the field as EV populations contain vesicles of various sizes. Research into EV heterogeneity has recently identified a link between ESCRT secretory mechanisms and EV heterogeneity (Colombo et al., 2013). In terms of heterogeneity, there may be many billions of EVs that vary in diameter which may lead to variable protein content. It is also important to consider that circulating plasma EVs samples contain EVs from many different regions of the body, further compounding the issue of EV heterogeneity. It would be interesting to compare tissue specific EVs to understand whether a single origin EV population is heterogeneous.

Loading EVs using electroporation is an easy method of introducing compounds into EVs, that, when delivered therapeutically, may lead to improvements post-stroke. In this study it was found that high electroporation voltages led to reduction in EV concentration. When cells are electroporated at ever increasing voltages, the number of nanopores within cell membranes have been shown to increase (Beebe et al., 2012). When voltages are applied to EVs a decrease in membrane integrity may occur. If the EV membrane is disrupted by high voltages, beyond the point of reformation, it may explain the reduction in EV

concentration experienced post-electroporation. One study found that electroporation of EVs with 10 pulses at 1000V led to a significant reduction in EV number compared to non-electroporated controls (Pomatto et al., 2019). Further, after electroporation EVs were re-isolated using UC, which uses high levels of centrifugal force to purify EV samples from electroporation buffers. One could theorise that this extreme centrifugal force may also lead to particle membrane rupture and subsequently, reduced final EV concentration. It is therefore plausible that electroporation and UC re-isolation may be responsible for the substantial reduction in EV concentration observed in this protocol.

In order to improve the concentration of electroporated EVs, an alternative to UC re-isolation was investigated, which led to the conclusion that SEC re-isolation led to an increased concentration of EVs compared to UC re-isolation. This increase in EV concentration after changing isolation method may be supported by other groups, whereby the concentration of cell media derived EVs was found to be greater with SEC isolation compared to UC isolation (Benedikter et al., 2017). Additionally, an incubation period was added to the method between electroporation and re-isolation in line with an observed trend towards improved final EV concentration compared to EVs that were immediately re-isolated. One may speculate that incubation of EVs within their trehalose electroporation buffer may promote EV membrane recovery and in turn may improve final EV concentration after re-isolation. Indeed, one group previously noted that trehalose, a common electroporation buffer, led to an improvement in EV structural integrity after electroporation (Hood et al., 2014). Further, with regards to electroporation, one group found that, depending on the buffer and voltage used for electroporation, the percentage EV recovery was approximately between 1% and 25% (Lennaard et al., 2021). These EV recovery figures are comparable to the EV recovery experienced in this investigation, whereby after electroporation and SEC re-isolation EV recovery was approximately 10%. However, Lenaard's results also identify the importance of the buffer used for the success of EV loading. For example, the group found that electroporating EVs in 50mM of Trehalose buffer, the same electroporation buffer and concentration used in this investigation, that EV uptake of doxorubicin was lower compared to other electroporation buffers such as those containing potassium hydrogen phosphate, sucrose and magnesium chloride (Lennaard et al., 2021). It should therefore be considered that an alternative electroporation buffer may improve EV cargo uptake.

Several groups have identified differences in EV concentration between EV isolation methods. For example, investigating different isolation methods including ExoQuick precipitation, IZON qEV1 and qEV2 SEC columns and UC it was found that ExoQuick

isolation provided the greatest yield of human plasma derived EVs, followed closely by IZON qEV1 SEC column isolation which led to similar EV yields (Brennan et al., 2020). SHRSP plasma EV concentration did not differ between PEG and SEC isolation methods. This may be due to the nature of PEG precipitation, whereby particles other than EVs may be isolated from samples, such as lipoproteins, that may be subsequently detected by NTA quantification. As SEC isolation can remove these contaminants it is widely accepted that this method of isolation provides a purer EV sample compared to PEG isolation methods (Forteza-Genestra et al., 2020). An example of sample purity can be related to lower total EV protein content. In this investigation, total protein content was significantly reduced when EVs were isolated using SEC compared to PEG, a finding also observed in a comparable study (Gamez-Valero et al., 2016). Using PEG EV isolation, other proteins may be co-precipitated with EVs to provide a greater protein yield. Combined, it may be concluded that the particle concentration obtained after SEC isolation may better represent the true number of EVs within isolated samples compared to their PEG isolated counterparts.

It is also important to note that disease state may alter EV concentrations, irrespective of isolation method. For example, plasma derived EV concentrations have been shown to be decreased in patients with Alzheimer's, Lewy body dementia and frontotemporal dementia (Longobardi et al., 2021). With this in mind, all EVs isolated in this project were derived from SHRSP, a well-established model of essential hypertension and cerebral small vessel disease (Yamori et al., 1974, Hannawi et al., 2021b). It should be considered that the SHRSP may possess higher concentrations of circulating plasma EVs compared to healthy control animals. Therefore, the incorporation of control normotensive model such as WKY rats may act as a valuable comparator. Interestingly, one group did not identify any difference in serum-derived EV concentration between WKY and SHRSPs, however that is not to say that plasma derived EVs concentrations may not differ between strains (van Kralingen et al., 2019). It can be concluded that several compounding factors may affect basic EV characteristics, such as particle concentration.

Western blotting can identify EV-specific proteins required for EV characterisation, for example for the presence of common markers such as TSG101, CD81 and CD63, all of which have been confirmed during this investigation and others (Lee et al., 2019, Martinez-Greene et al., 2021). These findings demonstrate that some EV-specific markers are conserved in various EV populations. Just as EV isolation method may result in changes in EV concentration, so too isolation method may be linked with differences in EV marker expression. For example, EVs isolated using ExoQuick precipitation, UC and

cushion-UC led to EVs containing greater levels of CD63 compared to SEC qEV1 and qEV2 columns as determined by western blot (Brennan et al., 2020). Similarly, using flow cytometry it was found that SEC isolation led to greater numbers of CD63^{+} and CD81^{+} EVs compared to PEG isolated EVs, while there was no difference in the number of CD9^{+} EVs between isolation methods (Gamez-Valero et al., 2016). Further, the number of CD9^{+} and CD81^{+} EVs was increased following UC isolation compared to precipitation, acoustic trapping, SEC and immunoaffinity capture isolation, as determined by protein array (Paget et al., 2022). Unfortunately, in this investigation CD9 could not be identified in SHRSP plasma EV samples using conventional western blotting. With the above studies in mind, the lack of CD9 protein expression in SEC EV samples could be linked to the isolation method. However, the lack of CD9 expression by western blot may be more easily explained by poor cross reactivity of the humanised antibody with rat species, or perhaps SHRSP plasma derived EVs may possess very little CD9. Ideally, further optimisation of western blotting antibodies or purification of EV sample using immunoprecipitation or targeted proteomics may be used to identify whether or not SHRSP plasma derived EVs possess CD9.

With regards to isolation methods, commercially available SEC EV isolation equipment may be an extremely useful tool when developing novel EV therapies due to their ease of use and high-throughput potential. In this investigation IZON SEC isolation methods were used. EVs were isolated from plasma using the standard protocol set out by the company IZON for SEC isolation using the IZON AFC. With this, IZON advised that the void volume should be discarded. However, it was found that there was a large number of particles present in the void volume, comparable to that of fraction 4. The presence of a large number of particles within the void volume was also observed by another group within SCMH. As a result, the void volume and fractions 1-4 were pooled to provide the isolated EV sample. In recent months, IZON has further developed the SEC AFC EV isolation protocol to reduce the volume of void that should be discarded. This change in protocol confirms our previous conclusion that the void volume contained a large number of EVs and should be pooled with collected fractions to prevent particle loss. A benefit of using commercialised products is that methods and equipment are constantly being optimised and upgraded, providing the most up-to-date EV isolation method. Unfortunately, frequent upgrades may introduce variability in methodology, and in most cases cannot be immediately introduced into ongoing experimentation. For example, an upgraded generation 2 version of qEV original columns was made available to purchase halfway into this investigation. The generation 1 qEV original columns used in this study

will be discontinued in late 2023 and after which time only generation 2 columns will be available to purchase (IZON Science, 2023b). To reduce SEC EV isolation variability, it was decided not to upgrade to the generation 2 qEV original columns in the middle of the investigation, however upgrading columns may have provided higher quality EV samples.

Levels of LDH were measured to provide an insight into the effects of electroporated EVs on cell survival. Under normal culture conditions, the level of cell death was high, and in some cases, was higher than cells that had undergone OGD. As such the decision was made to change the cell viability assay from LDH to MTT as it was more reliable and representative of expected cell death following OGD. Perhaps cells under normal conditions may have become over-confluent which may lead to detachment and subsequent cell death. Cells subjected to OGD treatment had multiple changes to cell media that may have removed free-floating and toxic metabolites from cell media, that may reduce the observed percentage cell death in LDH assays. Removal of initial media may influence levels of cell viability. In turn as percentage cell death in the OGD groups appeared low, it may be difficult to identify changes in cell viability using LDH assay. Primary neuronal cell cultures may also contain other cell or tissue contaminants due to brain sectioning methods which may require different growth conditions from neuronal cells and as such may die, leading to elevated levels of cell death. Primary neuronal cells were observed to shed more cellular debris compared to conventional cell lines. Further, primary cells are liable to clumping, which may cause variability in cell viability between samples.

All cell viability assays were carried out using MTT for most experiments in this study as, relative to normal culture conditions, OGD resulted in a uniform 25% reduction in cell viability within untreated cells. When Ang-(1-9) peptide was applied to primary neuronal cells under normal and OGD culture conditions at increasing concentrations, there was no significant reduction in cell viability. Similarly, Ang-(1-9) electroporated EVs, when applied to primary neuronal cells, did not affect cell viability. Together these findings suggest that Ang-(1-9) does not significantly affect cell viability in either normal culture conditions or OGD. Ang-(1-9) is a functional ligand of the Angiotensin II type 2 receptor (AT$_2$R) and clinically the use of angiotensin receptor blockers (ARBs) have been shown to reduce left ventricular hypertrophy (Ocaranza et al., 2014, Verdecchia et al., 2009). In humans the dose of ARBs varies depending on the drug used, for example, the maximum daily dose for Candesartan is 32 mg, while the maximum daily dose of Eprosartan is 900mg (Joint Formulary Committee British National Formulary, 2023a, Joint Formulary Committee British National Formulary, 2023b). As Ang-(1-9) is not clinically used, a

range of 0-20 μM was assessed *in vitro*. Given the wide dose range, it was expected that the IC50 value or toxic concentration may have been observed, however this was not the case. Further *in vitro* study into the therapeutic dose of Ang-(1-9) peptide needs to be carried out. One must also be mindful of the concentration of Ang-(1-9) that may be delivered using EV therapies and should consider whether or not the concentration of EVs required to deliver the desired therapeutic dose of Ang-(1-9) is clinically feasible.

Biodistribution of therapeutic EVs may be important in understanding their role within the living system. *In vitro*, B50 cells were treated with fluorescent 5-FAM-Ang-(1-9) electroporated EVs, 5-FAM-Ang-(1-9) peptide and cell-derived EVs, all of which did not lead to fluorescent signal. However, when 5-FAM-Ang-(1-9) peptide was applied to primary isolated neuronal cells an intense fluorescence was observed. One may speculate that, primary neuronal cell may express greater 5-FAM-Ang-(1-9) receptor, AT_2R, compared to B50 or GPNT cell lines (McFall, 2020). Although not pertinent to the overall research question, qPCR analysis may have been able to definitively identify changes in AT_2R expression between immortalised cell lines and isolated cells. Lack of fluorescence in EV treated B50s may also suggest that the fluorescent FAM attached to Ang-(1-9) peptide may sterically hinder the uptake of Ang-(1-9) peptide into the EVs. To further investigate this point, a highly sensitive ELISA could be carried out to determine whether 5-FAM interferes with Ang-(1-9) EV loading. In a similar vein, B50 cells may not easily package 5-FAM-Ang-(1-9), as shown by little to no fluorescence after peptide treatment, and as such may not be able to produce cell derived EVs that contain 5-FAM-Ang-(1-9). PKH26 lipophilic labelling of EVs did not produce reproducibly labelled EVs, and, like other studies, demonstrated clear aggregation (Puzar Dominkus et al., 2018). In order to produce a more homogeneous, fluorescent EV population, plasmids may be used in future studies to create transfected cell lines to produce fluorescent EVs.

5.5.1 Limitations

The presence of Ang-(1-9) within electroporated EVs could not be confirmed in this investigation and the uptake of *Cel-miR-39* mimic miRNA was used as a proof of concept for electroporation loading of EVs and subsequent cargo quantification. An Ang-(1-9) ELISA was carried out in the later stages of this investigation; however, this was not successful. As the standards in the assay also did not undergo a colour change it could be theorised that the reagents in the kit, bought prior to the COVID pandemic, had expired. One may speculate that there may have been issues with species detection, however as per

the manufacturers data sheet, the ELISA should have been able to detect human, rat and mouse Ang-(1-9) while the Ang-(1-9) peptide fragment used during electroporation was conserved between humans, rats, mice and canines (MyBioSource, 2023). As Ang-(1-9) is a relatively novel peptide, there are very few quantification methods. Alternative ELISA kits may have provided more success in determining the concentration of Ang-(1-9) in EV samples. Additional quantification methods for future studies may include the use of antibodies against Ang-(1-9) that may be used in western blotting or flow cytometry.

In this study, many western blot antibodies for EV markers were assessed to characterise EVs, however only a few could be optimised during this investigation. On many occasions, EV protein content was too low for experimentation. The minimum EV protein content required for western blotting was 30 µg per sample. Additionally, when antibody concentrations were increased to compensate for low protein content, a high level of non-specific binding was observed. It would be interesting to understand the expression profile of numerous EV markers within the SHRSP plasma EV population to understand how they may differ from control models. It may also be beneficial to identify differences in EV markers after EVs were isolated using different methods. With this EVs isolated from plasma may express tetraspanins differently, which may influence EV targeting abilities in later stages of this investigation. The addition of negative control markers may also be useful to provide an insight into EV sample purity. Although not carried out in this investigation, quantification of EV markers may be achieved by normalising total EV stain relative to marker staining.

Biodistribution assessments in this investigation were largely unremarkable. PKH26 lipophilic dye was used to understand EV biodistribution, with varying success between studies. In this study, results could not be easily reproduced in all cell types used at all time points. This may be a result of EV or lipophilic dye aggregation. Further, this labelling method utilised UC as a re-isolation method after the EV dying process, which has previously been shown to cause issues with EV aggregation (Linares et al., 2015). Perhaps if a different re-isolation method were used, for example using an isolation method that does not cause EV aggregation, PKH26 labelling might have been more successful. Likewise, alternative methods of producing fluorescent EVs such as using reporter systems to create fluorescent EVs would most likely have been more successful in assessing biodistribution (Lai et al., 2014). However, use of such systems in this study would detract from the overall purpose of using SHRSP-derived EVs therapeutically. Further biodistribution investigation with 5-FAM-Ang-(1-9) treatment demonstrated little to no fluorescence in conventional cell lines. However, primary neuronal cells were shown to

fluoresce after 5-FAM-Ang-(1-9) treatment. Following 5-FAM-Ang-(1-9) treatment, primary neuronal cell-derived EVs were not produced in this experiment. Carrying out this additional investigation may determine whether primary neuronal cells could produce EVs that contained 5-FAM-Ang-(1-9). If primary neuronal cells were able to uptake, package and secrete EVs containing 5-FAM-Ang-(1-9), biodistribution and quantification of fluorescence may have been useful in models of ischaemic stroke. Many of these preliminary experiments occurred in the early stage of return to laboratory work during the COVID pandemic when the number of animals available for experimentation was significantly reduced. As the use of 5-FAM-Ang-(1-9) to assess biodistribution remained mostly unsuccessful, combined with the issue of animal availability, the decision was made to move on from 5-FAM-Ang-(1-9) or PKH26 biodistribution assessment to the therapeutic potential of Ang-(1-9).

5.5.2 Summary

Circulating EVs were isolated from SHRSP plasma samples using optimised isolation methods and were characterised using conventional EV guideline methods. The protective benefit of Ang-(1-9) peptide treatment and treatment with EVs electroporated with Ang-(1-9) peptides were not obvious *in vitro*; however, data revealed that Ang-(1-9) peptide delivered on or within EVs did not cause substantial cellular toxicity. As such the potential benefits of Ang-(1-9) electroporated EVs within a whole living system required investigation. Initial uptake of fluorescent forms of Ang-(1-9) peptide into isolated primary neuronal cells emphasised the need to further understand the effects of EVs electroporated with Ang-(1-9) peptide *in vivo*.

Chapter 6 Optimisation of therapeutic extracellular vesicles

6.1 Introduction

Therapeutic EVs may be administered through topical application, injection directly into the desired tissue, intravenous or intranasal delivery (Guo et al., 2017b, Potz et al., 2018, Wiklander et al., 2015, Driedonks et al., 2022). Intravenous administration is the most common method of delivering therapeutic EVs across a number of different disease models, including cerebrovascular disease. In preclinical models, MSC-EVs were administered intravenously to APP/PS1 Alzheimer disease (AD) mice which improved function and morphology of hippocampal neurons, while MSC-EVs administered intravenously to Wistar rats 24-hours following tMCAO improved neurological outcomes, reduced infarct volume and increased levels of neurogenesis post-stroke (Wang et al., 2021, Xin et al., 2013).

Therapeutic EVs may lack efficacy in treating site-specific diseases. After intravenous administration, EVs can accumulate systemically throughout the body rather than localise to desired sites (Wiklander et al., 2015). HEK293T derived EVs were labelled with near-infrared fluorescent dye, DiR, and were intravenously injected into NMRI mice. Twenty-four hours later, EV distribution within organs was assessed using IVIS *in vivo* and *ex vivo* imaging. At various concentrations, DiR-labelled EVs were found to accumulate within the lung, liver, spleen, pancreas, gastrointestinal tract, and kidneys (Wiklander et al., 2015). Therefore, to improve delivery of therapeutic compounds to the brain, alternative methods of administration may be more beneficial. With regards to disease that affect the brain, delivery of therapeutic compounds to the brain remains challenging due to the presence of the blood brain barrier (BBB) (Pardridge, 2012). Intranasal administration of therapeutic compounds, including EVs, has the potential to reduce the invasiveness of stroke therapies. Once in the nasal cavity therapeutic compounds can bypass the BBB by entering the brain directly though the olfactory trigeminal nerve pathways (Illum, 2003, Ahmad et al., 2017). Studies have assessed the effectiveness of intranasal delivery of therapeutic EVs on outcomes in cerebrovascular disease. In mouse models of hippocampal and cortical traumatic brain injury (TBI), C57BL/6 mice were subjected to hippocampal brain injury before being treated with human MSC-EVs intranasally. MSC-EV treatment following TBI improved neurological and behavioural outcomes to levels similar of uninjured control mice, while lesion volume was reduced in the hippocampal injury TBI model following

MSC-EV treatment compared to untreated controls (Leon-Moreno et al., 2020). In Wistar rat models of Parkinson's disease, intranasal delivery of stem cells from human exfoliated deciduous teeth culture derived EVs led to improvement in spatial learning and memory along with gaiting (Narbute et al., 2021). When MSC-EVs were delivered intranasally to 3xTg mouse model of AD, EVs were found to accumulate within the brain. MSC-EV treatment also reduced proinflammatory microglial cell activation and improved dendritic cell integrity (Losurdo et al., 2020). Another study investigated gold labelled EV accumulation within the brain of ET-1 MCAO C57BL/6 mice following either intranasal or intravenous administration. Using flame atomic absorption spectroscopy, it was found that EV accumulation within the brain was greater following intranasal delivery compared to intravenous delivery, while *ex vivo* analysis identified increased gold labelled EV accumulation within the stroke region of the brain 24-hours post-intranasal delivery (Betzer et al, 2017).

In order to enhance EV delivery to- and accumulation within- specific organs of the body, EVs may be combined with targeting molecules. One method of improving EV delivery towards the brain may include using Rabies Virus Glycoprotein (RVG) peptide as a targeting mechanism. RVG can bind neuronal nicotinic acetylcholine receptor subunit beta-2 (CHRNB2) which is expressed within the brain, most abundantly within the cerebral cortex (Uhlen et al., 2015). Using a direct incubation method to bind RVG to EVs, RVG joined to a CP05 linker peptide can recognise and bind to CD63 tetraspanin on the surface of EVs (Gao et al., 2018) (Figure 6.1). Using a common EV bioengineering method, cell lines may be transfected with plasmids containing an RVG sequence to produce cell-derived RVG-EVs (Alvarez-Erviti et al., 2011, Wiklander et al., 2015).

Intravenous tail vein injection of RVG targeted GAPDH siRNA loaded EVs has been shown to increased GAPDH mRNA expression within striatum, midbrain and cortex, while RVG targeted EVs led to a reduction in GAPDH mRNA expression solely within the brain and not in other peripheral organs (Alvarez-Erviti et al., 2011). In a photothrombotic preclinical model of stroke, intravenous tail vein injection of RVG targeted EVs containing nerve growth factor (NGF) led to significant upregulation of NGF mRNA in the ipsilateral cortex compared to non-targeted EVs containing NGF (Yang et al., 2020a). Further, in 3xTg-AD mice models, intranasally administered RVG targeted EVs containing the reactive oxygen species responsive polymer BA-PDMAEMA (BAP) combined with BACE1 and Caspase-3 siRNAs (BAP siRNAs), led to reduced BACE1 and Aβ42 expression in whole brain tissue compared to non-targeted EVs containing BAP siRNAs (Li et al., 2023a). In mouse models of Parkinson's disease, intravenously administered

RVG targeted EVs containing anti-alpha-synuclein minicircles (shRNA-MC) downregulated alpha-synuclein within the midbrain, cortex, and spinal cord (Izco et al., 2023). Similarly, IVIS *ex vivo* imaging determined that intravenously injected DiR-labelled RVG targeted EVs accumulated within the brain, but not other peripheral organs, of C57BL/6 mice compared to DiR-labelled untargeted control EVs by 72 hours post-EV administration (Haroon et al., 2023).

Through use of targeting peptides, such as RVG, EVs may be delivered to specific sites within the body. With this, EV cargo delivery to desired sites may be improved which in turn may enhance the therapeutic capacity of EVs. By combining intranasal delivery method of EVs with RVG targeting, novel non-invasive therapies for neurological and cerebrovascular diseases may be developed.
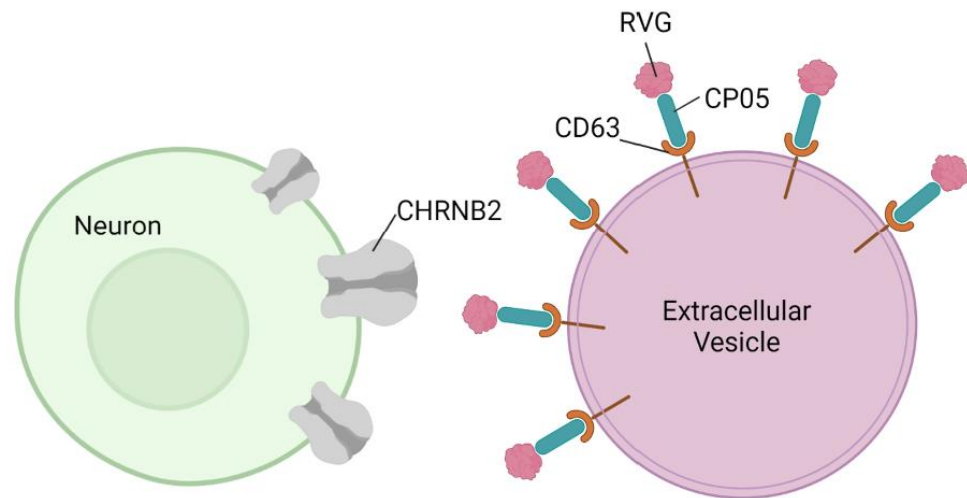

Figure 6.1 Mechanisms of EV targeting using RVG-CP05 targeting.
(A) Amino acid sequence of CP05-RVG targeting peptide. (B) Illustration of the principles of EV targeting whereby the EV tetraspanin CD63 acts as an anchor and is bound by linker peptide CP05 that is conjugated to RVG. RVG binds CHRNB on neuronal cells. Figure created in Bio Render.

6.2 Hypotheses and Aims

6.2.1 Hypotheses

- EVs derived from plasma of SHRSPs will possess required anchor tetraspanins for RVG conjugation and primary neuronal cells isolated from SHRSPs will possess RVG receptors.

- Loaded, RVG-targeted EVs will increase EV cargo uptake *in vitro.*

- Intranasal delivery of loaded EVs will result in EV cargo uptake within brain tissues.

- Loaded, RVG-targeted EVs will increase EV cargo uptake within brain tissues.

6.2.2 Aims

- Identify the presence of receptor(s) required for RVG targeting of therapeutic EVs.

- Determine if RVG targeting improves EV-cargo uptake *in vitro.*

- Determine if intranasal delivery of EVs leads to EV cargo delivery to the brain.

- Determine if RVG targeting improves EV-cargo uptake *in vivo.*

6.3 Methods

Methods used in Chapter 6 can be found in Chapter 2 of this thesis and are outlined below:

2.1.2.4 RVG (+/-) Cel-miR-39 mimic miRNA electroporated EV treatment

2.1.2.7 Tissue collection

2.1.2.8 Historical samples

2.2.1.3 Size exclusion chromatography

2.2.1.5 Nanoparticle tracking analysis

2.2.1.6 EV electroporation loading

2.2.1.8 RVG-CP05 EV targeting

2.2.2.1 Immortalised cell line maintenance

2.2.2.2 Primary neuronal cell isolation and cultures

2.2.2.5 EV and peptide treatment

2.2.2.6 MTT assay

2.2.2.7 Cell fixation and imaging

2.2.3.1 RNA extraction

2.2.3.2 Nanodrop quantification

2.2.3.3 miRNA reverse transcription

2.2.3.5 Quantitative real-time polymerase chain reaction

2.2.4 Western Blotting

2.2.7 Statistical analysis

6.4 Results

6.4.1 Mechanisms of RVG-CP05 targeting of EVs in SHRSP primary neuronal cells

B50 rat neuronal cells and primary isolated neuronal cells are commonly used within the laboratory to model the brain *in vitro*. The expression levels of RVG receptor, *CHRNB2*, was determined in order to understand the potential mechanisms of RVG-CP05 targeting of EVs towards neuronal cells. *CHRNB2* was expressed at the gene level in both B50 rat neuronal cells (13.16 ± 0.06; dCT $\pm$ SEM) (1 ± 0.04; RQ $\pm$ RQ$_{max}$) and primary isolated neuronal cells (8.85 ± 0.18 dCT $\pm$ SEM) (19.86 ± 2.68; RQ $\pm$ RQ$_{max}$) with the expression of *CHRNB2* being greater in the primary neuronal cells ($p<0.001$) (Figure 6.2).

CHRNB2 protein expression within primary neuronal cells was further confirmed using immunocytochemistry (ICC) (Figure 6.3). From these combined results it was determined that cell experiments investigating the potential of RVG targeted EVs should be carried out in primary isolated neuronal cells.

SHRSP plasma-derived EVs were investigated for the presence of the RVG-CP05 anchor tetraspanin, CD63. Western blot analysis determined that EVs derived from the plasma of SHRSPs possessed CD63 (Figure 6.4).
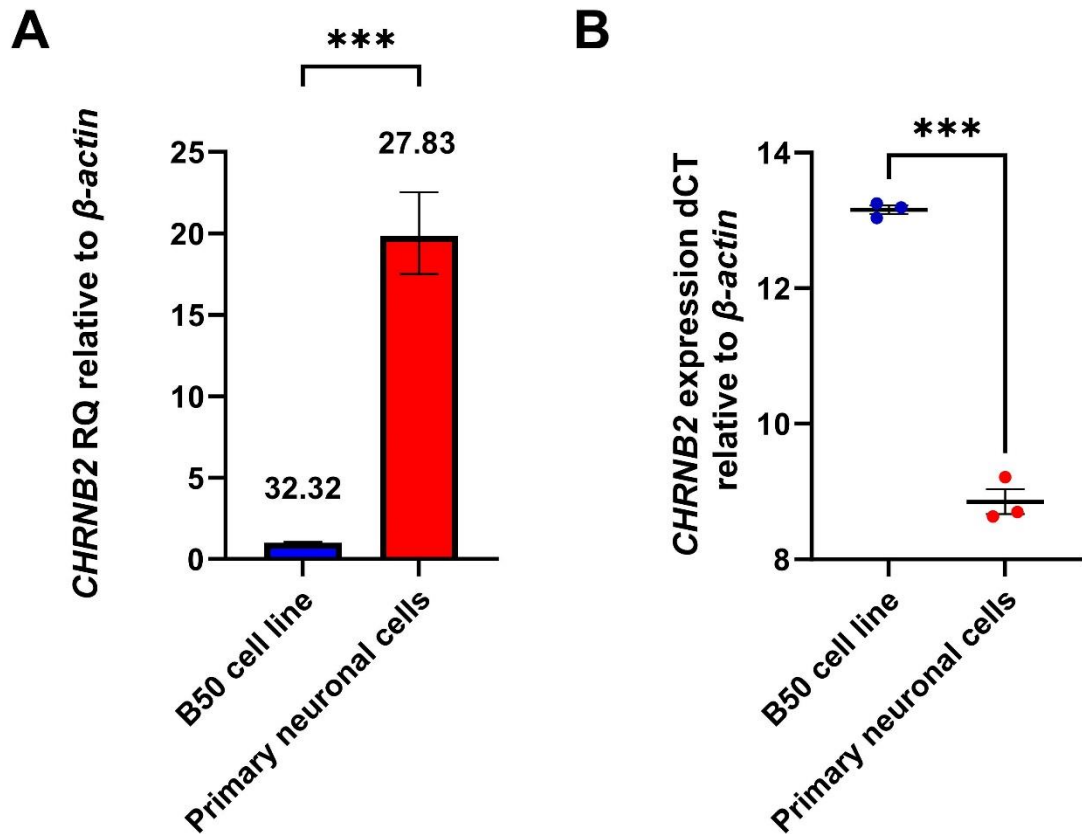
Figure 6.2 Identification of key components required for RVG-CP05 EV targeting.
qPCR of *CHRNB2* expression was performed from RNA of B50 neuronal cell lines and primary neuronal cells isolated from brains of gestational day 18 SHRSP neonates. A) relative quantity (RQ) value demonstrates relative change in gene expression and error bars represent $RQ_{min/max}$. Numbers above each bar denotes average CT value for each cell line. B) delta cycle threshold (dCT) demonstrates relative gene expression and error bars represent standard error of the mean (SEM). (n=3, ***p≤0.001, Welch's t-test).
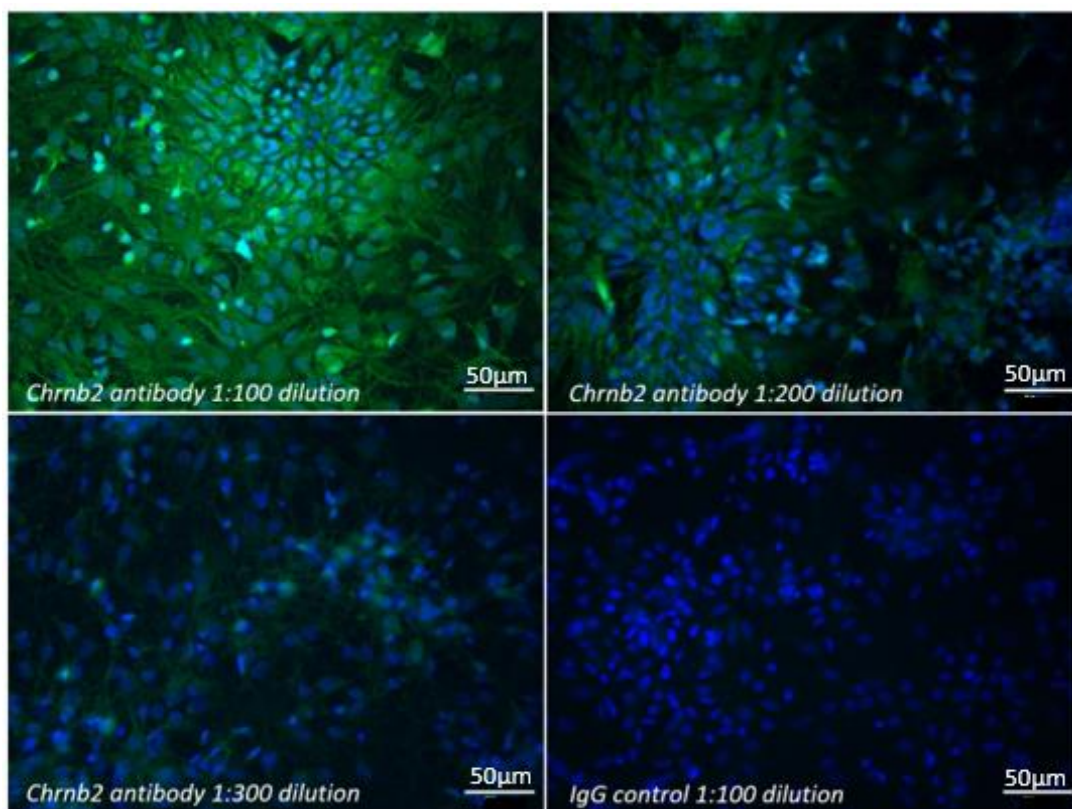
Figure 6.3 Representative image of CHRNB2 ICC staining in primary neuronal cells.
CHRNB2 expression within cultured primary isolated neuronal cells and was analysed
using ICC. CHRNB2 is shown in green whereas nuclear (DAPI) staining is shown in blue.
Scale bar represents 50µm

Figure 6.4 Characterisation of CD63 EVs markers.
Western blot image shows a band corresponding to CD63 from SHRSP plasma-derived EV lysates (Samples 1, 2, and 3). Molecular weight in kilo Dalton (kDa) of each band are shown on the right-hand side of the image. Samples were loaded equally for each marker (30 µg). Loading control was not included as bands were not quantified (n=3).

6.4.2 Intranasal delivery of *Cel-miR-39 mimic* loaded EVs in SHRSPs

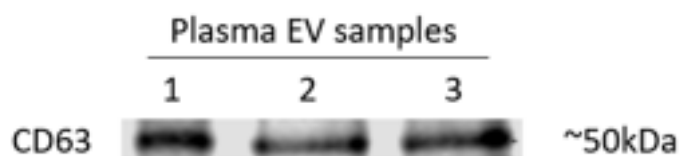To assess whether EV cargo could be successfully delivered using a non-invasive nose-to-brain method, EVs were intranasally delivered to ~18-week-old male SHRSPs. SHRSPs were weighed prior to EV administration. EVs were administered on day one and two in the morning and afternoon and organs and plasma were collected on day four (Figure 6.5). Following intranasal EV treatment, brains were harvested to determine the levels of EV cargo, *Cel-miR-39*, rostrocaudally to determine expression throughout the brain (Figure 6.6). There was no significant difference in SHRSP body weight between the control EV group (280.67 ± 15.51 g; mean $\pm$ SEM), 1×10^{11} *Cel-miR-39* loaded EV group (262.00 ± 11.27 g), 2.5×10^{11} *Cel-miR-39* loaded EV group (319.67 ± 3.48 g) and 5×10^{11} *Cel-miR*-39 loaded EV group (285.00 ± 20.60 g) (

Figure 6.7).

Cel-miR-39 expression was similar between 1×10^{11} of unloaded control EVs, and 1-, 2.5- and 5×10^{11} of *Cel-miR-39* loaded EVs within the olfactory bulb (Figure 6.8), brain section 1 (Figure 6.9), brain section 2 (Figure 6.10) and brain section 3 (Figure 6.11). In brain section 4, *Cel-miR-39* expression was increased with 2.5×10^{11} *Cel-miR-39* loaded EVs (5.41 ± 0.69; dCT $\pm$ SEM) (5.02 ± 0.12; RQ $\pm$ RQ$_{max}$) compared to 5×10^{11} *Cel-miR-39* loaded EVs (8.67 ± 0.71; dCT $\pm$ SEM) (0.52 ± 0.26; RQ $\pm$ RQ$_{max}$) ($p < 0.05$) (Figure 6.12).

To assess whether EV delivered intranasally also led to EV cargo delivery to periphery of SHRSPs, lung, liver, kidney, spleen and plasma were collected, and *Cel-miR-39* expression was determined using qPCR. Within the lung (Figure 6.13), liver (Figure 6.15), kidney (Figure 6.16) and spleen (Figure 6.17) *Cel-miR-39* expression was similar between unloaded control EVs and *Cel-miR-39* loaded EV groups. Within plasma samples, Cel-miR-39 expression was significantly increased following 2.5×10^{11} *Cel-miR-39* loaded EVs (-3.99 ± 0.46; dCT $\pm$ SEM) (9.06 ± 3.41; RQ $\pm$ RQ$_{max}$) compared to 1×10^{11} *Cel-miR-39* loaded EVs (-1.07 ± 0.32; dCT $\pm$ SEM) (1.20 ± 0.30; RQ $\pm$ RQ$_{max}$) ($p < 0.05$) (Figure 6.17).
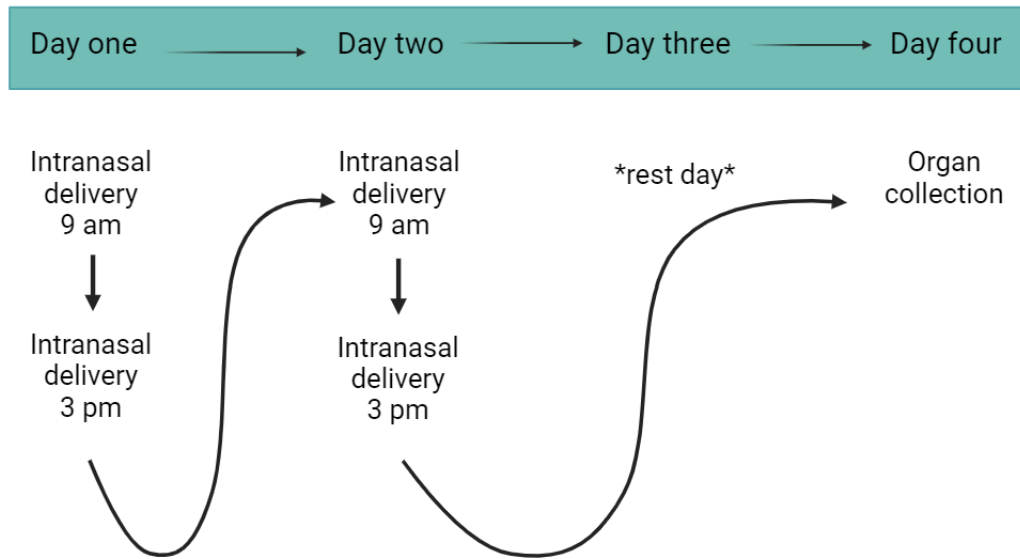
Figure 6.5 Intranasal delivery time frame.
EVs were delivered on four occasions in 48 µL volumes. EVs were delivered to SHRSPs at 9am and 3pm on days one and two. On day three no EVs were administered to SHRSPs. On day 4 SHRSPs were humanely culled, and organs and blood were collected. Figure created in BioRender.
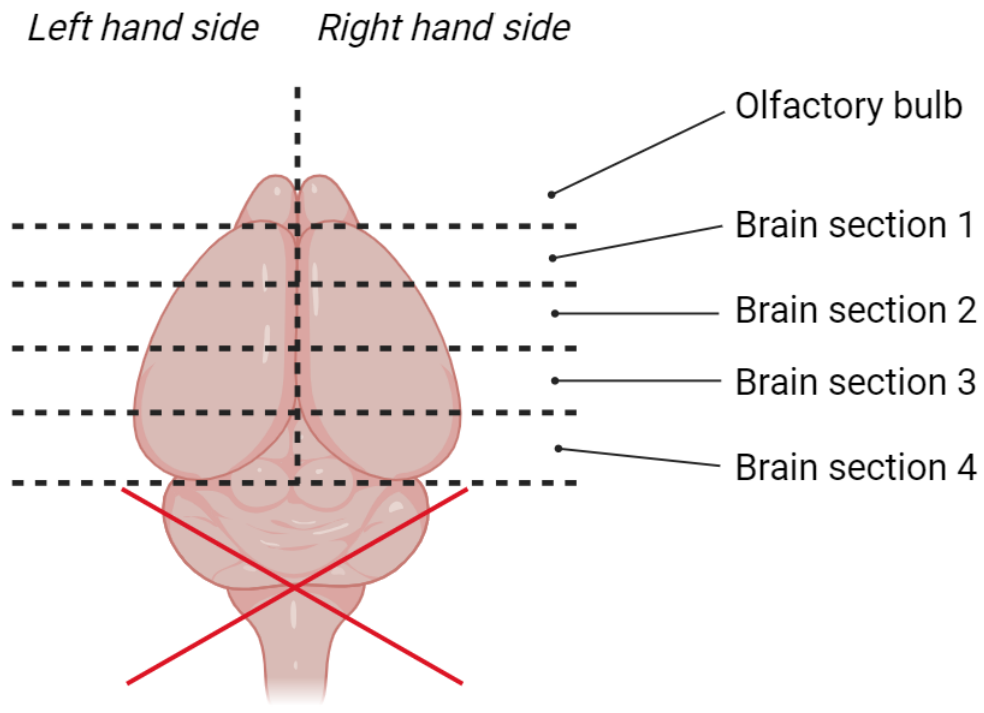
Figure 6.6 llustration of rostocaudal brain section technique.
SHRSP rat brain were removed from the skull and sectioned into left and right hemispheres. Left and right hemispheres were then further section from olfactory bulb at the front to brain section 4 at the back, forming 10 separate brain sections. Cerebellum was discarded. Figure created in Bio Render.
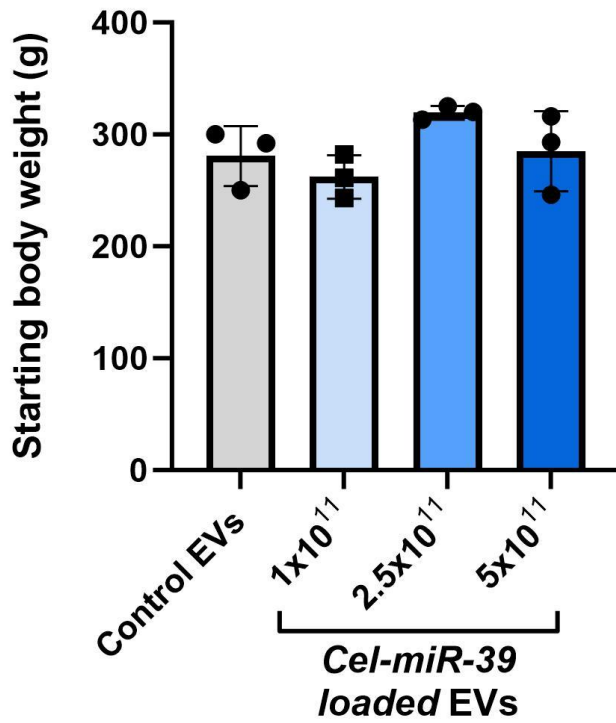
Figure 6.7 Body weight of SHRSPs prior to *Cel-miR-39* loaded EV treatment.
SHRSPs of approximately 18 weeks old were weighed prior to EV treatment. SHRSPs
were administered with unloaded EVs (Control-EVs) or 1-, 2.5- or 5-x10^{11} *Cel-miR-39*
mimic miRNA loaded EVs. Weight in grams (g) (n=3, p>0.05, Brown-Forsythe and Welch
ANOVA with post-hoc Dunnett's T3 multiple comparison).

Figure 6.8 Effects of intranasally delivery method on EV cargo uptake within olfactory bulb of SHRSP brain.
qPCR was performed to assess the expression of *Cel-miR-39* within olfactory bulb from 18-week-old male SHRSP rats after intranasal delivery of unloaded control EVs or *Cel-miR-39* loaded EVs. *Cel-miR-39* miRNA expression was normalised to U87 housekeeper (mean CT value found in black box in top right). A) Relative Quantity (RQ) is accompanied by error bars denoting RQ min/max with average CT value displayed above bars and B) Delta cycle threshold (dCT) with error bars representing standard error of the mean (SEM) (n=3, $p > 0.05$, Brown-Forsythe and Welch ANOVA with post-hoc Dunnett's T3 multiple comparison).

Figure 6.9 Effects of intranasally delivery method on EV cargo uptake within brain section 1 of SHRSP brain.

qPCR was performed to assess the expression of *Cel-miR-39* within brain section 1 from 18-week-old male SHRSP rats after intranasal delivery of unloaded control EVs or *Cel-miR-39* loaded EVs. *Cel-miR-39* miRNA expression was normalised to U87 housekeeper (mean CT value found in black box in top right). A) Relative Quantity (RQ) is accompanied by error bars denoting RQ min/max with average CT value displayed above bars and B) Delta cycle threshold (dCT) with error bars representing standard error of the mean (SEM) (n=3, $p > 0.05$, Brown-Forsythe and Welch ANOVA with post-hoc Dunnett's T3 multiple comparison).
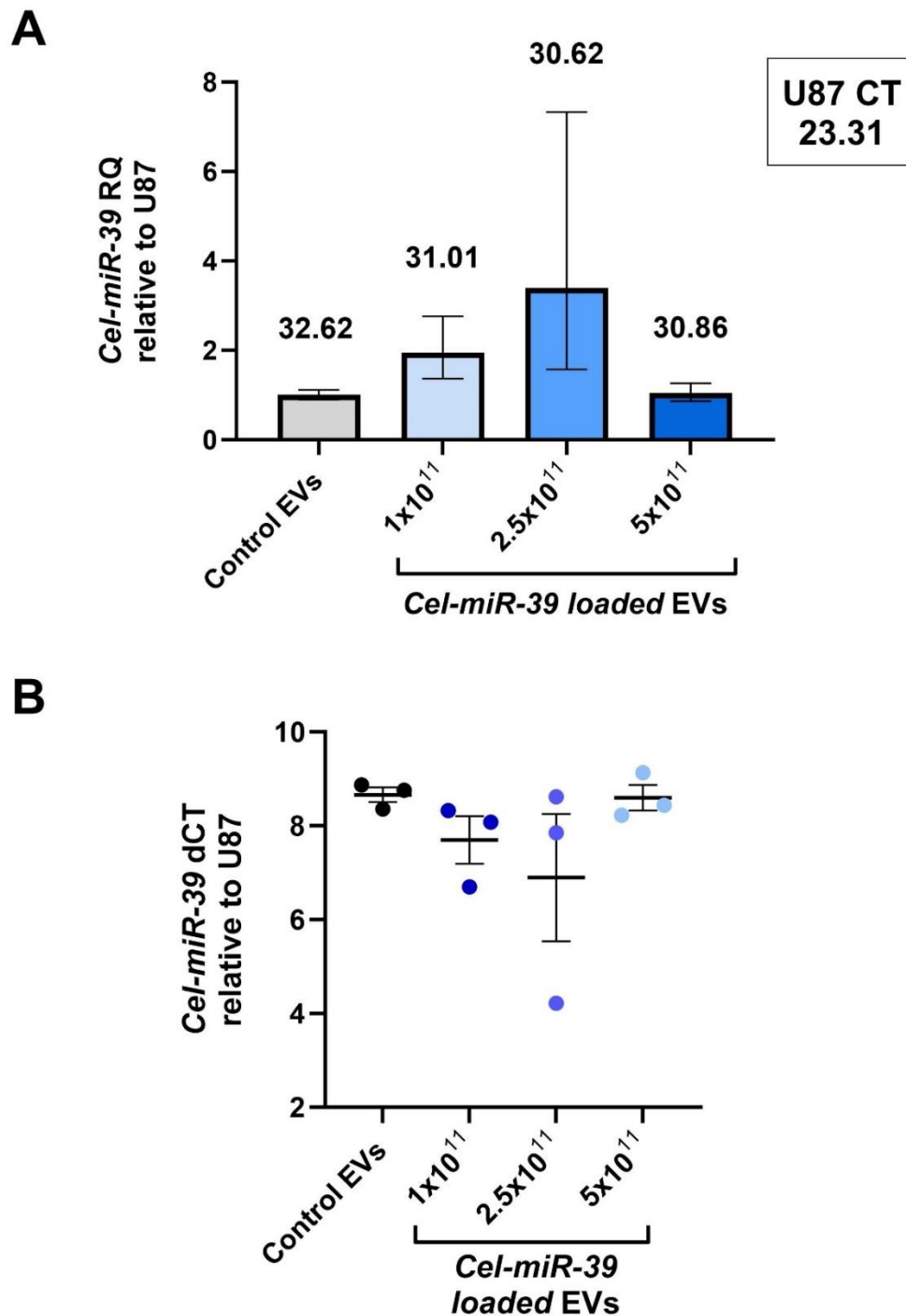
Figure 6.10 Effects of intranasally delivery method on EV cargo uptake within brain section 2 of SHRSP brain.
qPCR was performed to assess the expression of *Cel-miR-39* within brain section 2 from 18-week-old male SHRSP rats after intranasal delivery of unloaded control EVs or *Cel-miR-39* loaded EVs. *Cel-miR-39* miRNA expression was normalised to U87 housekeeper (mean CT value found in black box in top right). A) Relative Quantity (RQ) is accompanied by error bars denoting RQ min/max with average CT value displayed above bars and B) Delta cycle threshold (dCT) with error bars representing standard error of the mean (SEM) (n=3, $p>0.05$, Brown-Forsythe and Welch ANOVA with post-hoc Dunnett's T3 multiple comparison).
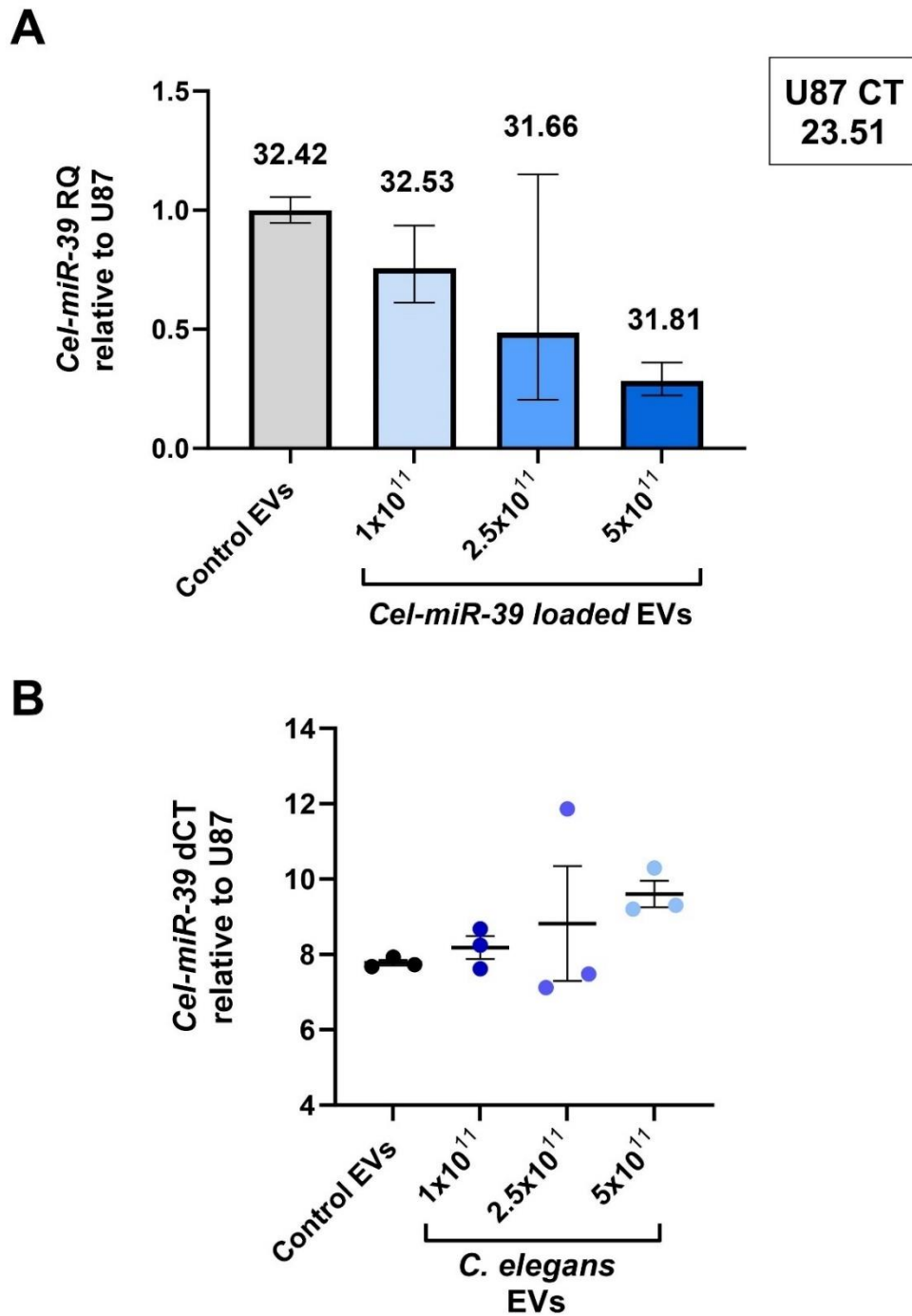
A

B

Figure 6.11 Effects of intranasally delivery method on EV cargo uptake within brain section 3 of SHRSP brain.

qPCR was performed to assess the expression of *Cel-miR-39* within brain section 3 from 18-week-old male SHRSP rats after intranasal delivery of unloaded control EVs or *Cel-miR-39* loaded EVs. *Cel-miR-39* miRNA expression was normalised to U87 housekeeper (mean CT value found in black box in top right). A) Relative Quantity (RQ) is accompanied by error bars denoting RQ min/max with average CT value displayed above bars and B) Delta cycle threshold (dCT) with error bars representing standard error of the mean (SEM) (n=3, p>0.05, Brown-Forsythe and Welch ANOVA with post-hoc Dunnett's T3 multiple comparison).
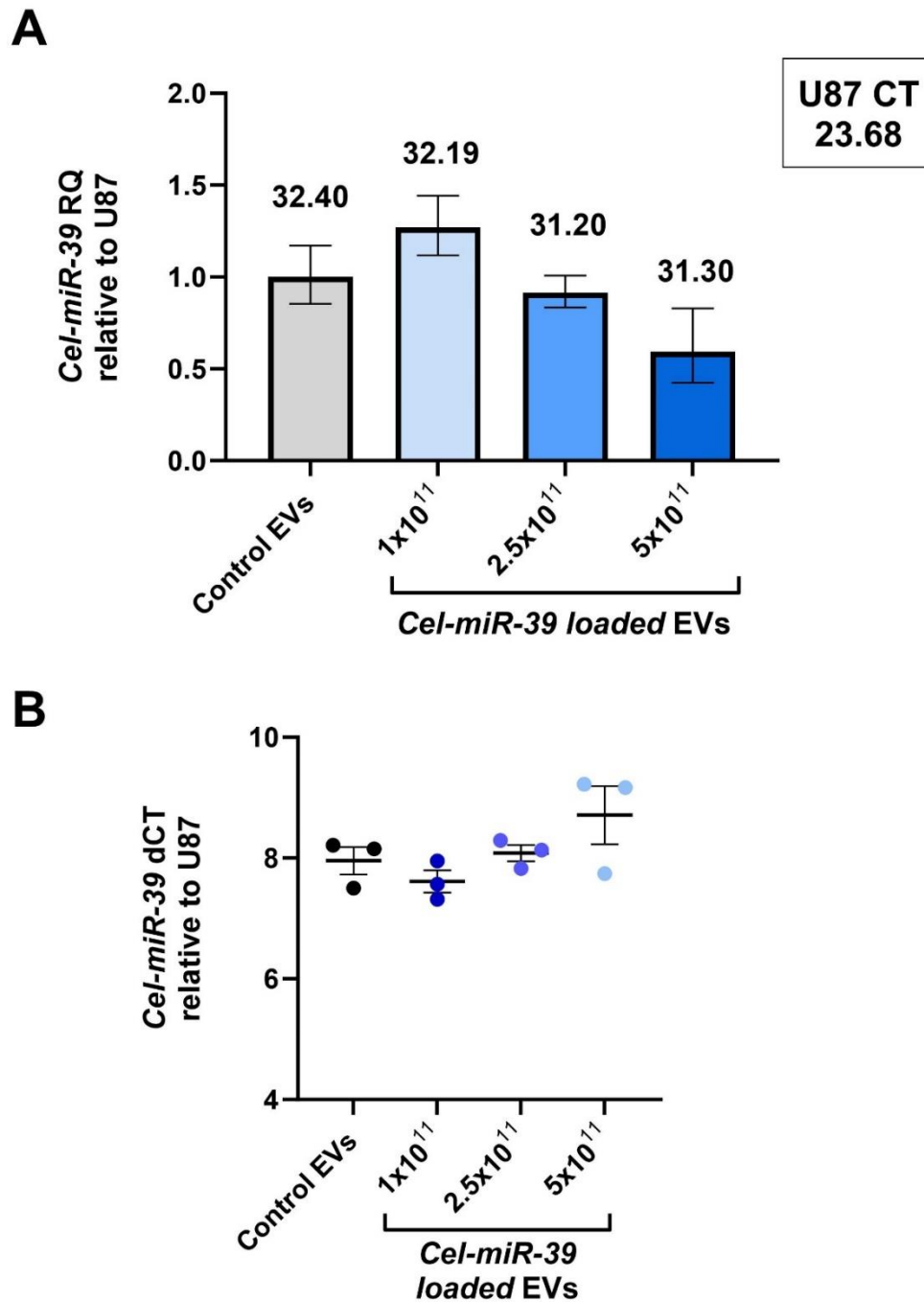
Figure 6.12 Effects of intranasally delivery method on EV cargo uptake within brain section 4 of SHRSP brain.
qPCR was performed to assess the expression of *Cel-miR-39* within brain section 4 from 18-week-old male SHRSP rats after intranasal delivery of unloaded control EVs or *Cel-miR-39* loaded EVs. *Cel-miR-39* miRNA expression was normalised to U87 housekeeper (mean CT value found in black box in top right). A) Relative Quantity (RQ) is accompanied by error bars denoting RQ min/max with average CT value displayed above bars and B) Delta cycle threshold (dCT) with error bars representing standard error of the mean (SEM) (n=3, *p<0.05, Brown-Forsythe and Welch ANOVA with post-hoc Dunnett's T3 multiple comparison).

Figure 6.13 Effects of intranasally delivery method on EV cargo uptake within the lung of SHRSPs.

qPCR was performed to assess the expression of *Cel-miR-39* within the lung of 18-week-old male SHRSP rats after intranasal delivery of unloaded control EVs or *Cel-miR-39* loaded EVs. *Cel-miR-39* miRNA expression was normalised to U87 housekeeper (mean CT value found in black box in top right). A) Relative Quantity (RQ) is accompanied by error bars denoting RQ min/max with average CT value displayed above bars and B) Delta cycle threshold (dCT) with error bars representing standard error of the mean (SEM) (n=3, $p > 0.05$, Brown-Forsythe and Welch ANOVA with post-hoc Dunnett's T3 multiple comparison).
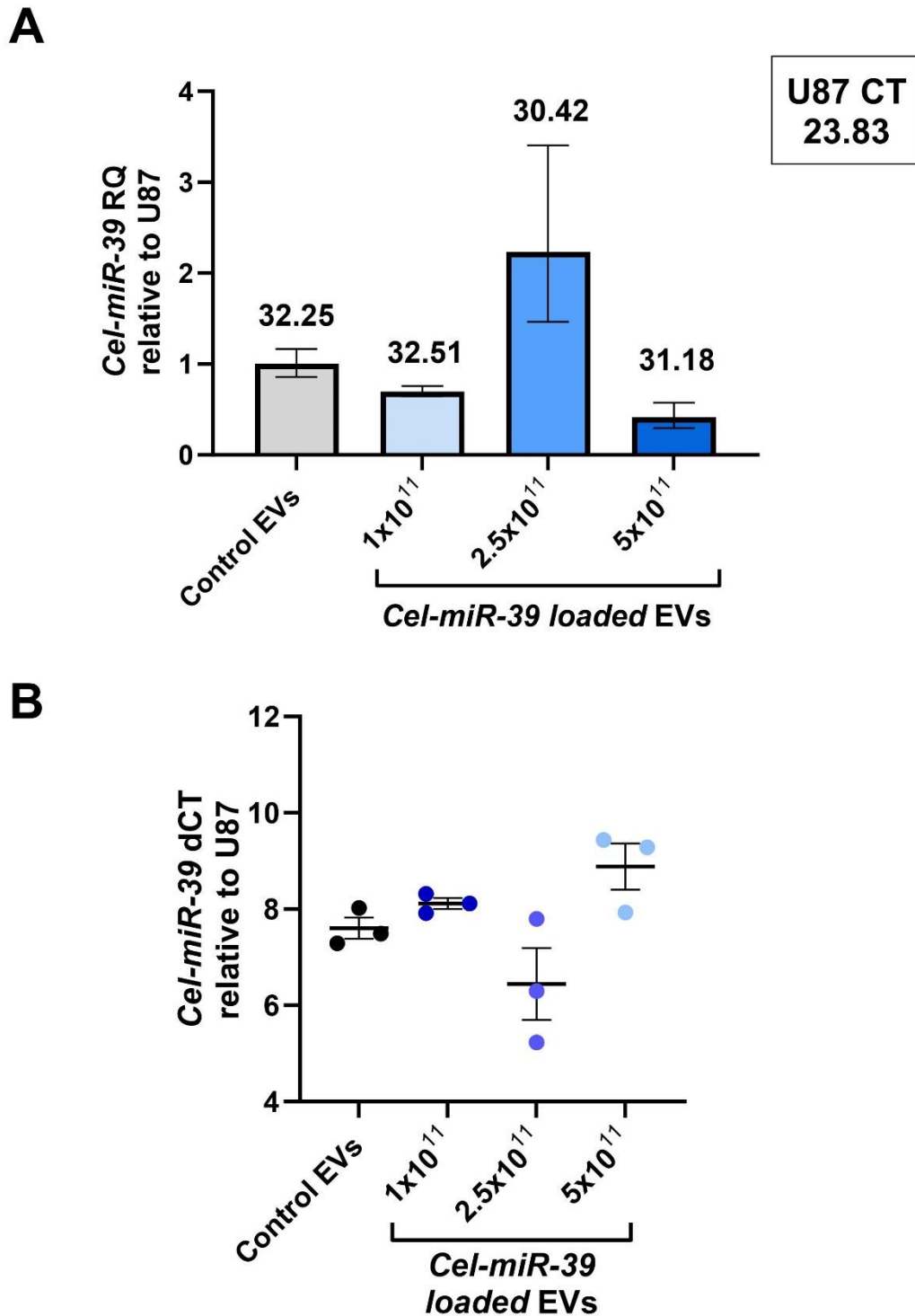
Figure 6.14 Effects of intranasally delivery method on EV cargo uptake within the liver of SHRSPs.

qPCR was performed to assess the expression of *Cel-miR-39* within the liver of 18-week-old male SHRSP rats after intranasal delivery of unloaded control EVs or *Cel-miR-39* loaded EVs. *Cel-miR-39* miRNA expression was normalised to U87 housekeeper (mean CT value found in black box in top right). A) Relative Quantity (RQ) is accompanied by error bars denoting RQ min/max with average CT value displayed above bars and B) Delta cycle threshold (dCT) with error bars representing standard error of the mean (SEM) (n=3, p>0.05, Brown-Forsythe and Welch ANOVA with post-hoc Dunnett's T3 multiple comparison).
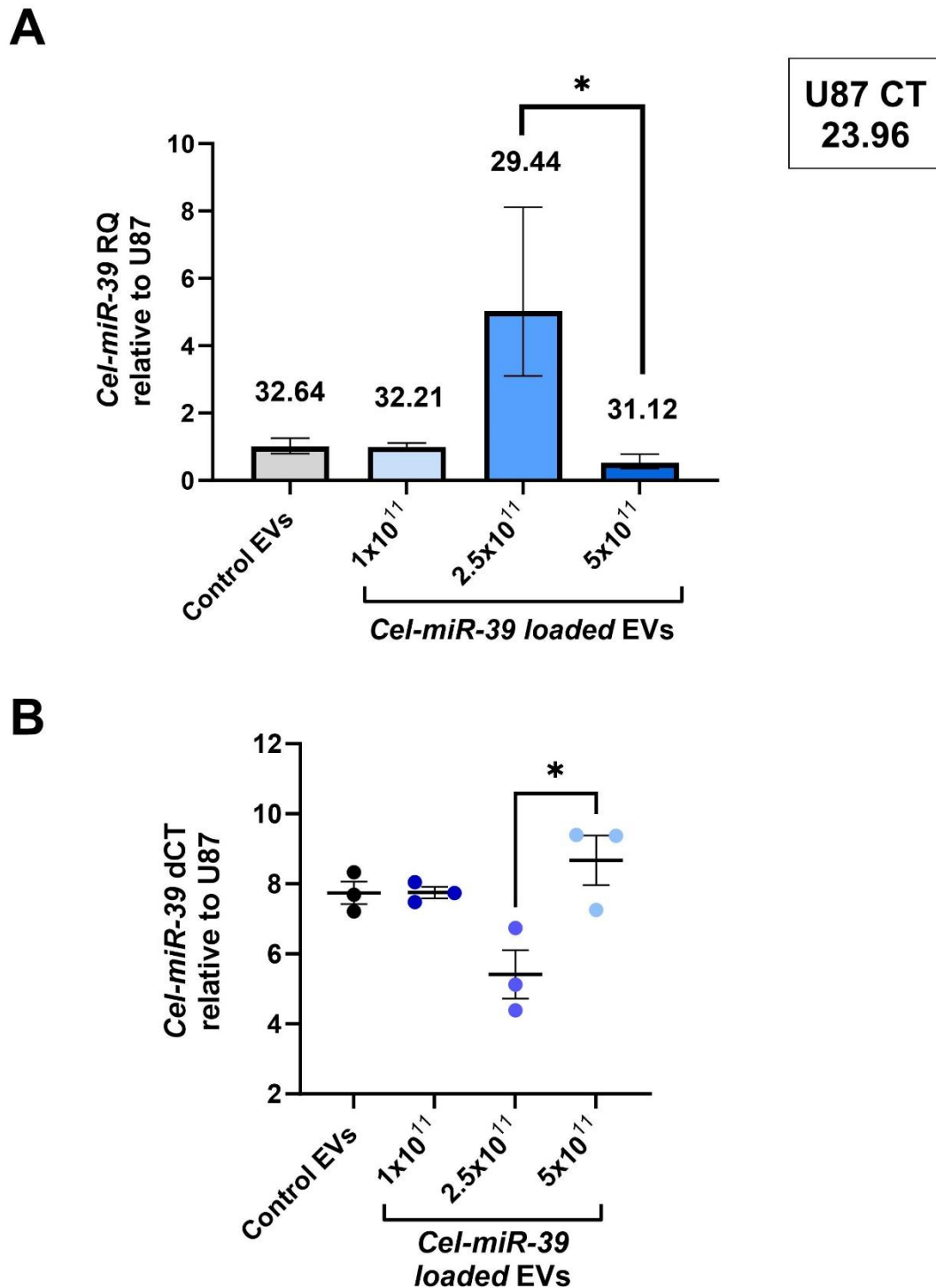
A
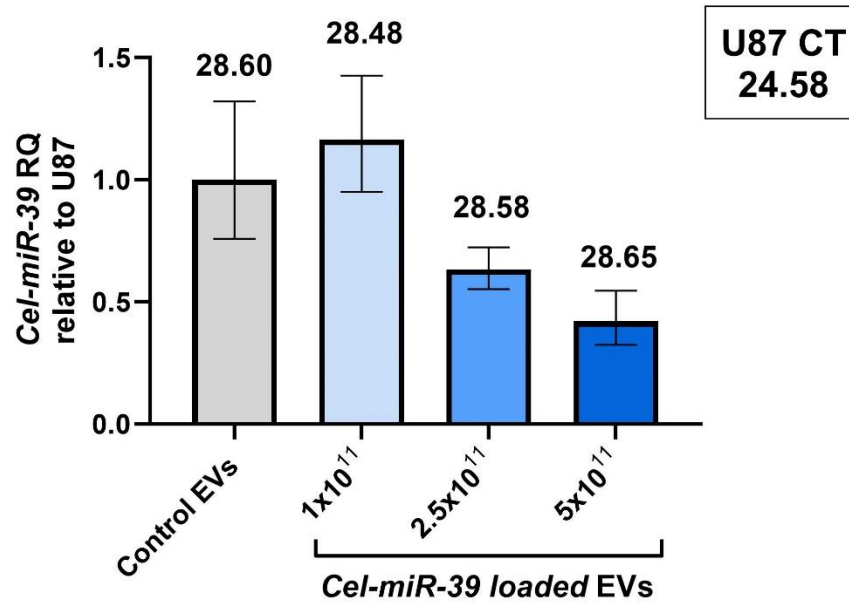
B
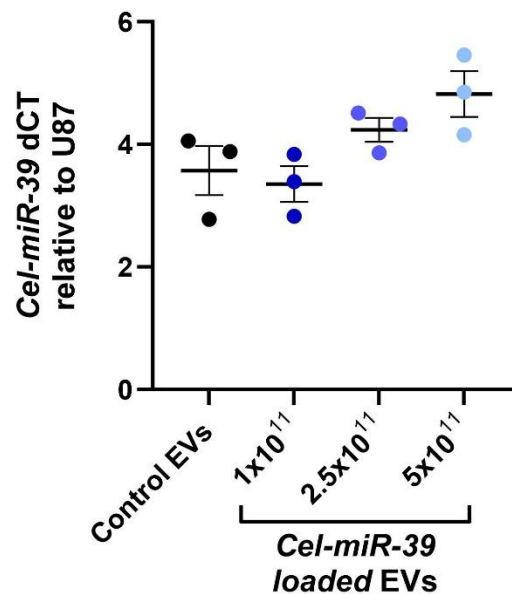
Figure 6.15 Effects of intranasally delivery method on EV cargo uptake within the kidney of SHRSPs.
qPCR was performed to assess the expression of *Cel-miR-39* within the kidney of 18-week-old male SHRSP rats after intranasal delivery of unloaded control EVs or *Cel-miR-39* loaded EVs. *Cel-miR-39* miRNA expression was normalised to U87 housekeeper (mean CT value found in black box in top right). A) Relative Quantity (RQ) is accompanied by error bars denoting RQ min/max with average CT value displayed above bars and B) Delta cycle threshold (dCT) with error bars representing standard error of the mean (SEM) (n=3, p>0.05, Brown-Forsythe and Welch ANOVA with post-hoc Dunnett's T3 multiple comparison).
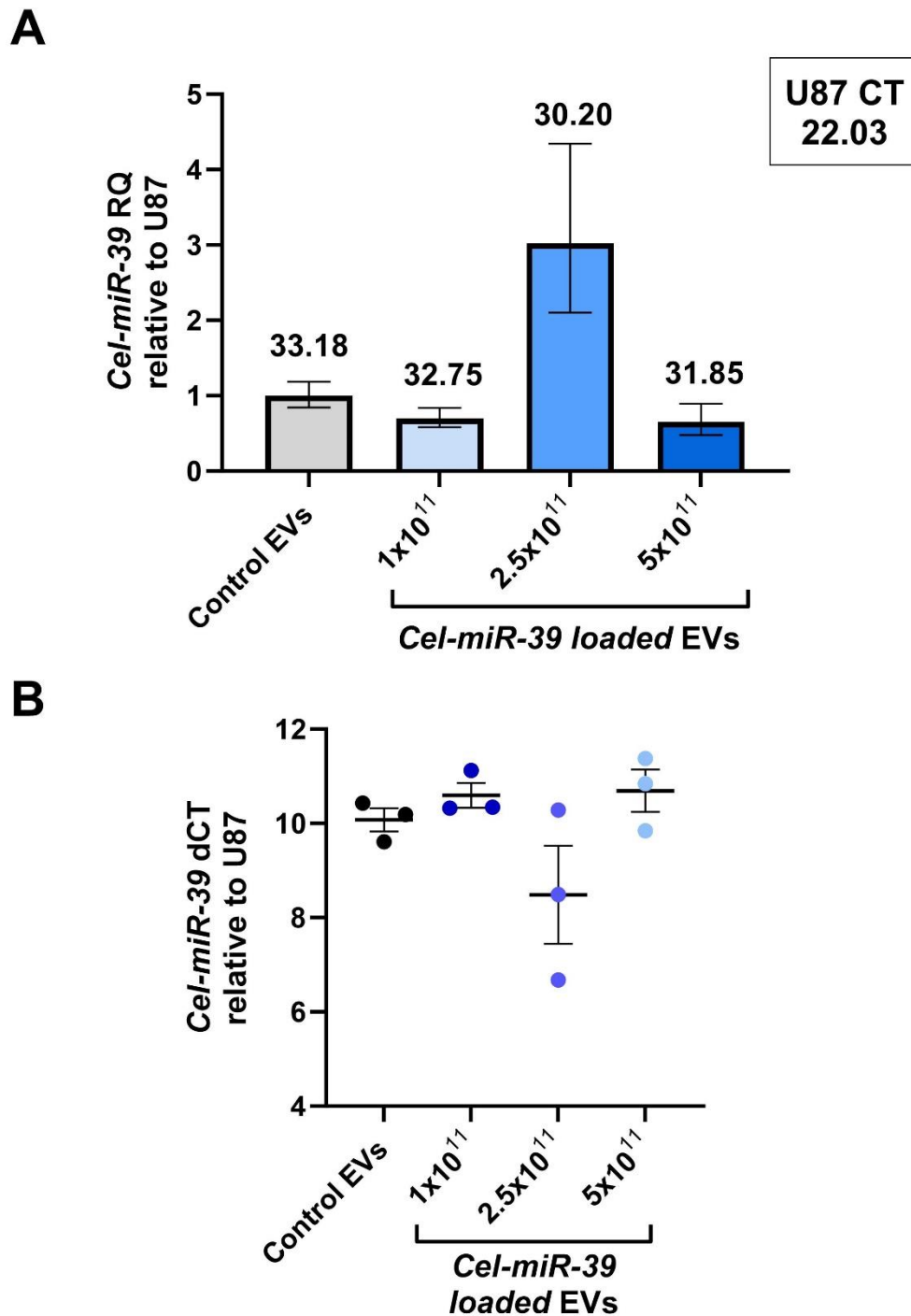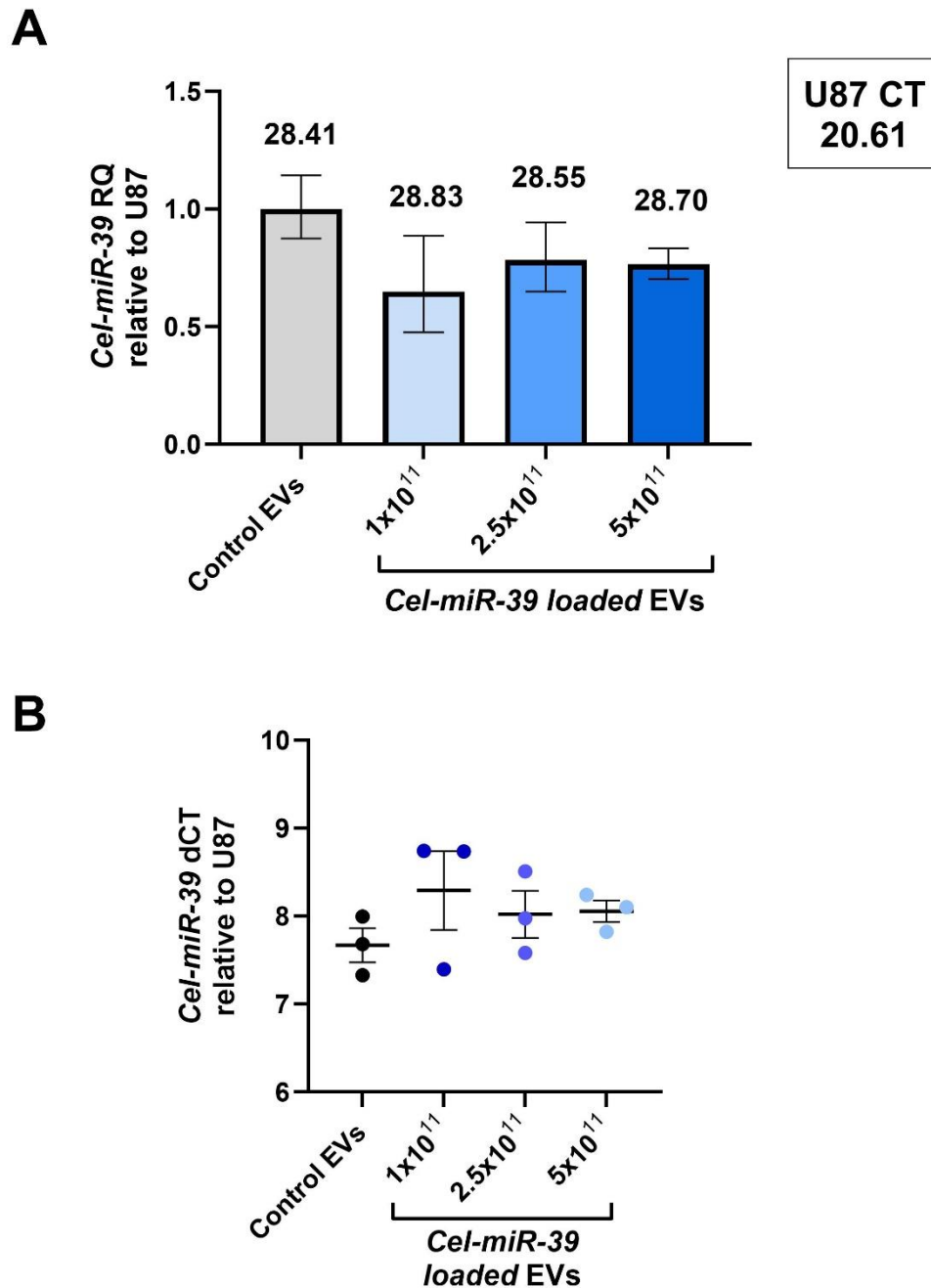
Figure 6.16 Effects of intranasally delivery method on EV cargo uptake within the spleen of SHRSPs.
qPCR was performed to assess the expression of *Cel-miR-39* within the spleen of 18-week-old male SHRSP rats after intranasal delivery of unloaded control EVs or *Cel-miR-39* loaded EVs. *Cel-miR-39* miRNA expression was normalised to U87 housekeeper (mean CT value found in black box in top right). A) Relative Quantity (RQ) is accompanied by error bars denoting RQ min/max with average CT value displayed above bars and B) Delta cycle threshold (dCT) with error bars representing standard error of the mean (SEM) (n=3, p>0.05, Brown-Forsythe and Welch ANOVA with post-hoc Dunnett's T3 multiple comparison).
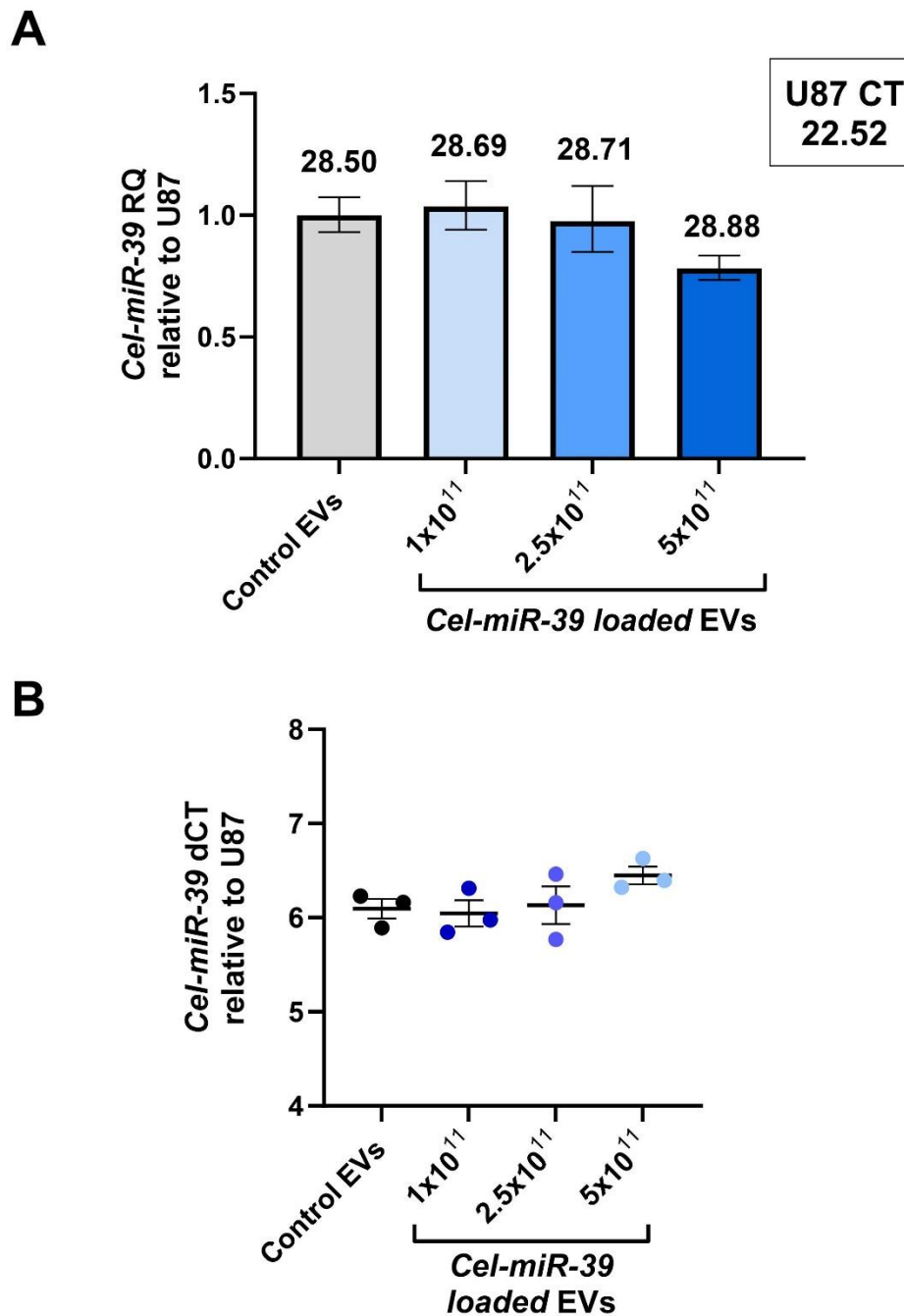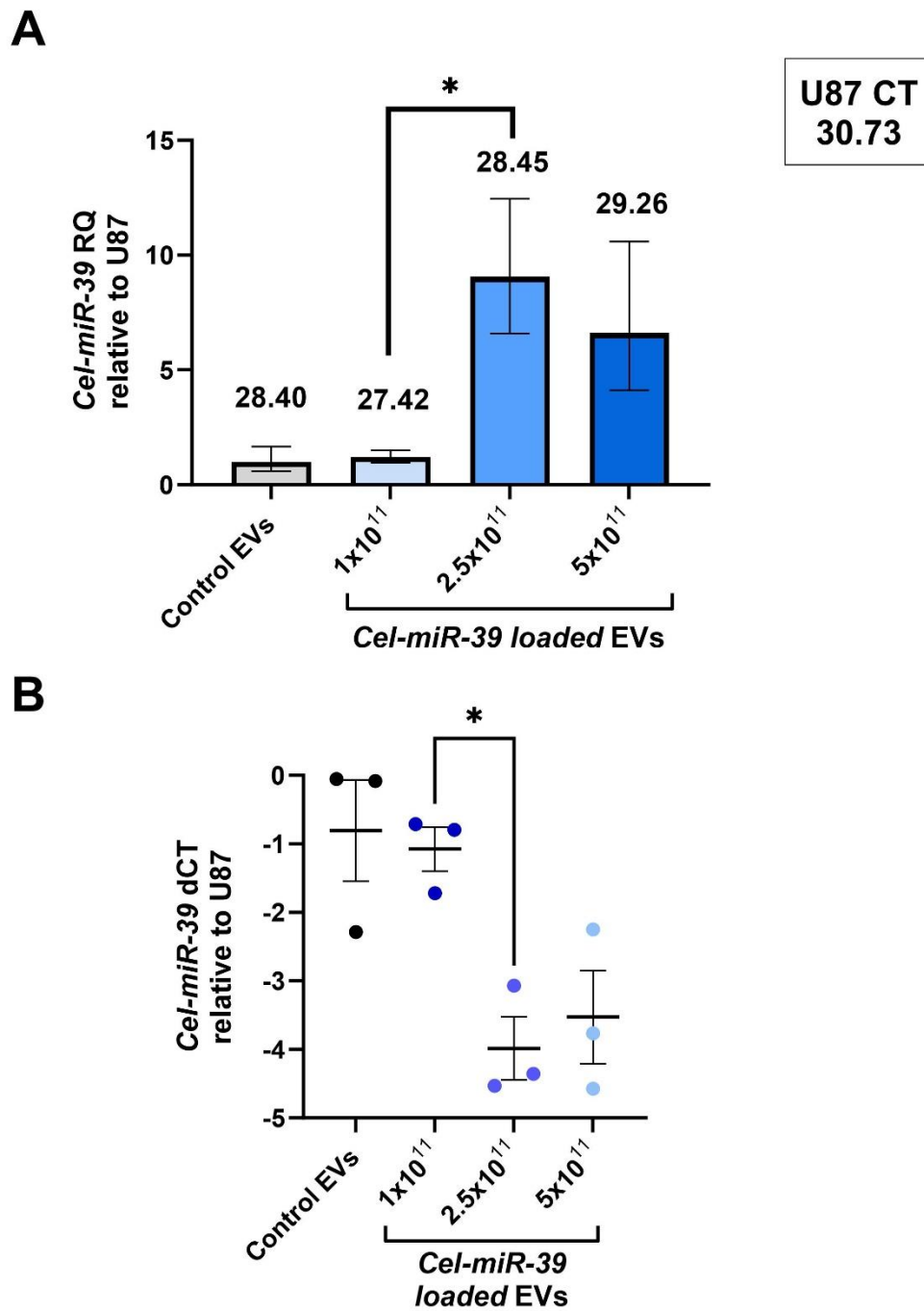
Figure 6.17 Effects of intranasally delivery method on EV cargo uptake within plasma of SHRSPs.

qPCR was performed to assess the expression of *Cel-miR-39* within plasma of 18-week-old male SHRSP rats after intranasal delivery of unloaded control EVs or *Cel-miR-39* loaded EVs. *Cel-miR-39* miRNA expression was normalised to U87 housekeeper (mean CT value found in black box in top right). A) Relative Quantity (RQ) is accompanied by error bars denoting RQ min/max with average CT value displayed above bars and B) Delta cycle threshold (dCT) with error bars representing standard error of the mean (SEM) (n=3, *p<0.05, Brown-Forsythe and Welch ANOVA with post-hoc Dunnett's T3 multiple comparison).

6.4.3 EV concentrations after RVG targeting.

As previously shown in chapter 5, electroporation can lead to a reduction in EV concentration. RVG targeting of loaded EVs was investigated to determine if the process of targeting EVs led to further reduction in EV concentrations. EV concentration was reduced though not significantly between SEC-isolated plasma EVs ($8.35 \times 10^{12} \pm 2.01 \times 10^{12}$ p/mL; mean $\pm$ SEM) and *Cel-miR-39* loaded EVs ($5.17 \times 10^{12} \pm 1.14 \times 10^{12}$ p/mL). However, EV concentration was further reduced following RVG-targeting of *Cel-miR-39* loaded EVs ($1.95 \times 10^{12} \pm 9.34 \times 10^{11}$ p/mL), ultimately leading to a significant reduction in EV concentrations compared to un-electroporated SEC-isolated plasma EVs ($p < 0.05$) (Figure 6.18).
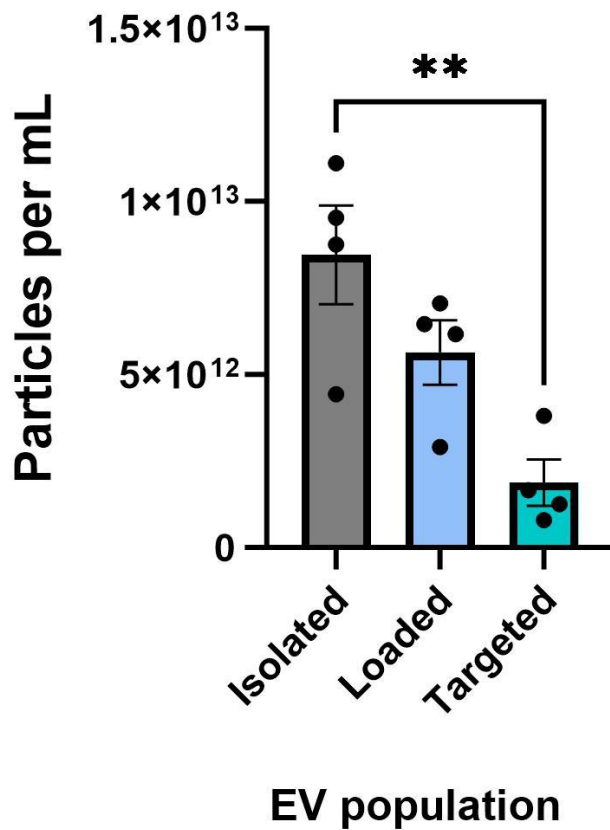
Figure 6.18 The effects of EV loading and targeting on EV concentration.
EVs were isolated from plasma of SHRSP via SEC and initial concentration was
determined using NTA (Isolated). EVs were then loaded with *Cel-miR-39* mimic miRNA
using electroporation before re-isolating via SEC and determining EV concentration using
NTA (Loaded). Loaded EVs were then conjugated with RVG-CP05 targeting peptide
before re-isolating via SEC and determining EV concentration using NTA (Targeted). EV
concentrations were then compared between isolated, loaded and targeted groups (n=3,
**p<0.01, One way-ANOVA with post-hoc Tukey's multiple comparison correction).

6.4.4 Effects of RVG EV targeting on primary neuronal cell viability

Primary neuronal cells were treated with RVG targeted EVs electroporated with Ang-(1-9) or *Cel-miR-39* mimic miRNA to assess their effects on cell viability. Primary neuronal cells were treated with 1×10^8, 4×10^8 and 1×10^9 p/mL of RVG electroporated/loaded EVs for 24 hours prior to MTT assay. The effect of RVG targeted EV treatment on cell death was calculated relative to cell death of non-targeted EV treatment at the same concentration.

Cel-miR-39 loaded RVG targeted EVs 1×10^8 p/mL (100.89 ± 3.06 % cell viability; mean $\pm$ SEM) did not affect cell viability compared to 1×10^8 p/mL non-targeted *Cel-miR-39* loaded EVs ($100.00 \pm 0.00\%$) (Figure 6.19 A). *Cel-miR-39* loaded RVG targeted EVs 4×10^8 p/mL (93.16 ± 1.74) decreased cell viability compared to 4×10^8 p/mL non-targeted *Cel-miR-39* loaded EVs ($100.00 \pm 0.00\%$; $p<0.01$) (Figure 6.19 B). *Cel-miR-39* loaded RVG targeted EVs 1×10^9 p/mL (107.10 ± 3.87) did not affect cell death compared to 1×10^9 p/mL non-targeted *Cel-miR-39* loaded EVs (100.00 ± 0.00 %) (Figure 6.19 C).

Ang-(1-9) electroporated RVG targeted EVs 1×10^8 p/mL (104.48 ± 7.91 %) did not affect cell viability compared to 1×10^8 p/mL non-targeted Ang-(1-9) electroporated EVs ($100.00 \pm 0.00\%$) (Figure 6.20 A). Ang-(1-9) electroporated RVG targeted EVs 4×10^8 p/mL (95.34 ± 4.43 %) did not affect cell viability compared to 4×10^8 p/mL non-targeted Ang-(1-9) electroporated EVs ($100.00 \pm 0.00\%$) (Figure 6.20 B). Ang-(1-9) electroporated RVG targeted EVs 1×10^9 p/mL decreased cell viability (75.68 ± 4.91 %) compared to 1×10^9 p/mL non-targeted Ang-(1-9) electroporated EVs ($100.00 \pm 0.00\%$; $p<0.05$) (Figure 6.20 C).
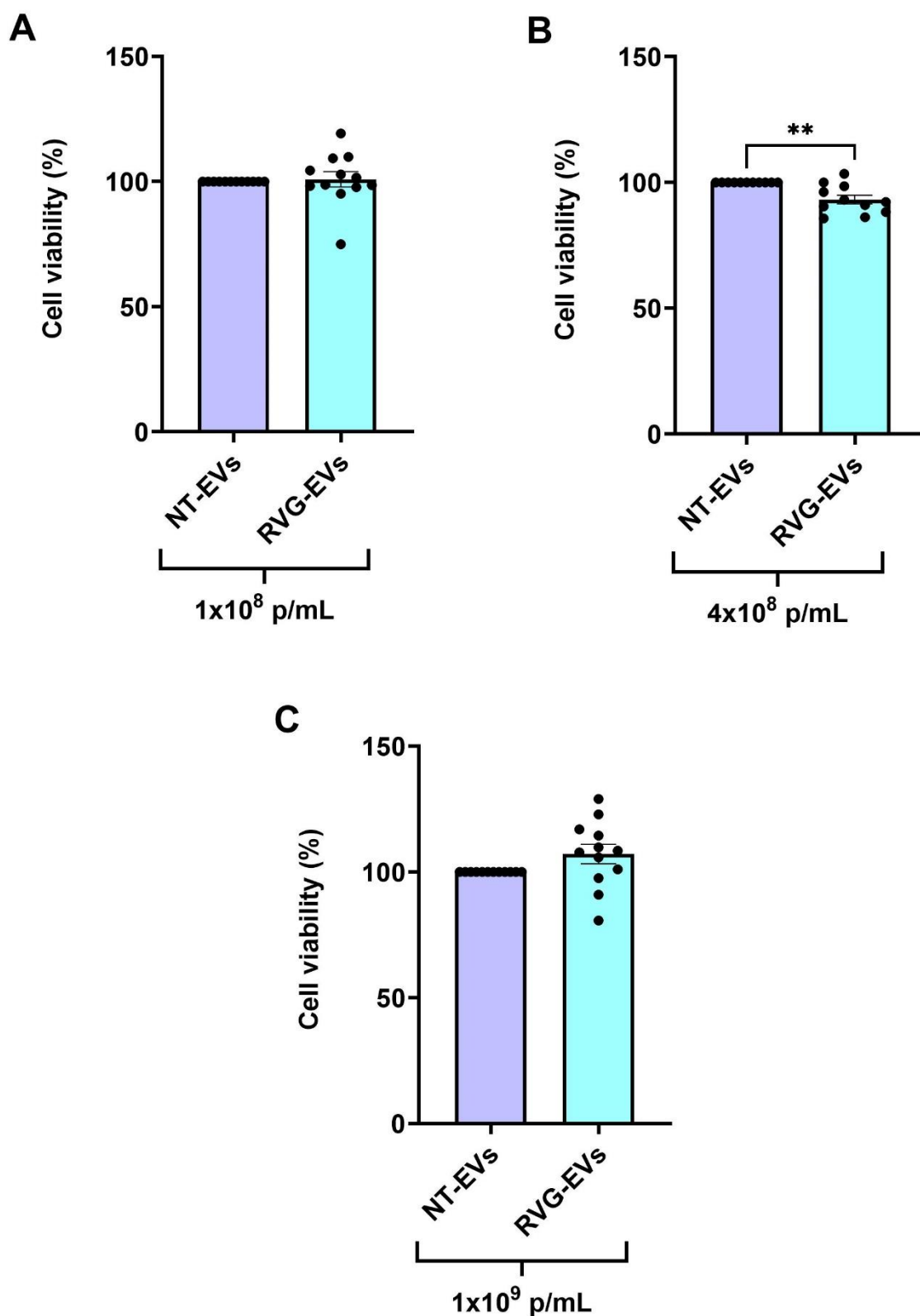
Figure 6.19 Effects of *Cel-miR-39* loaded RVG targeted EVs on primary neuronal cell viability.
Primary neuronal cells were plated at 1.2×10^6 cells/mL and were matured for 8 days before EV treatment. Cells were treated with A) 1×10^8, B) 4×10^8 and C) 1×10^9 p/mL of non-targeted *Cel-miR-39* loaded EVs or RVG-targeted *Cel-miR-39* loaded EVs Cell viability was determined using MTT assay (n=4, replicate=3, *p<0.05, Welch's t-test).
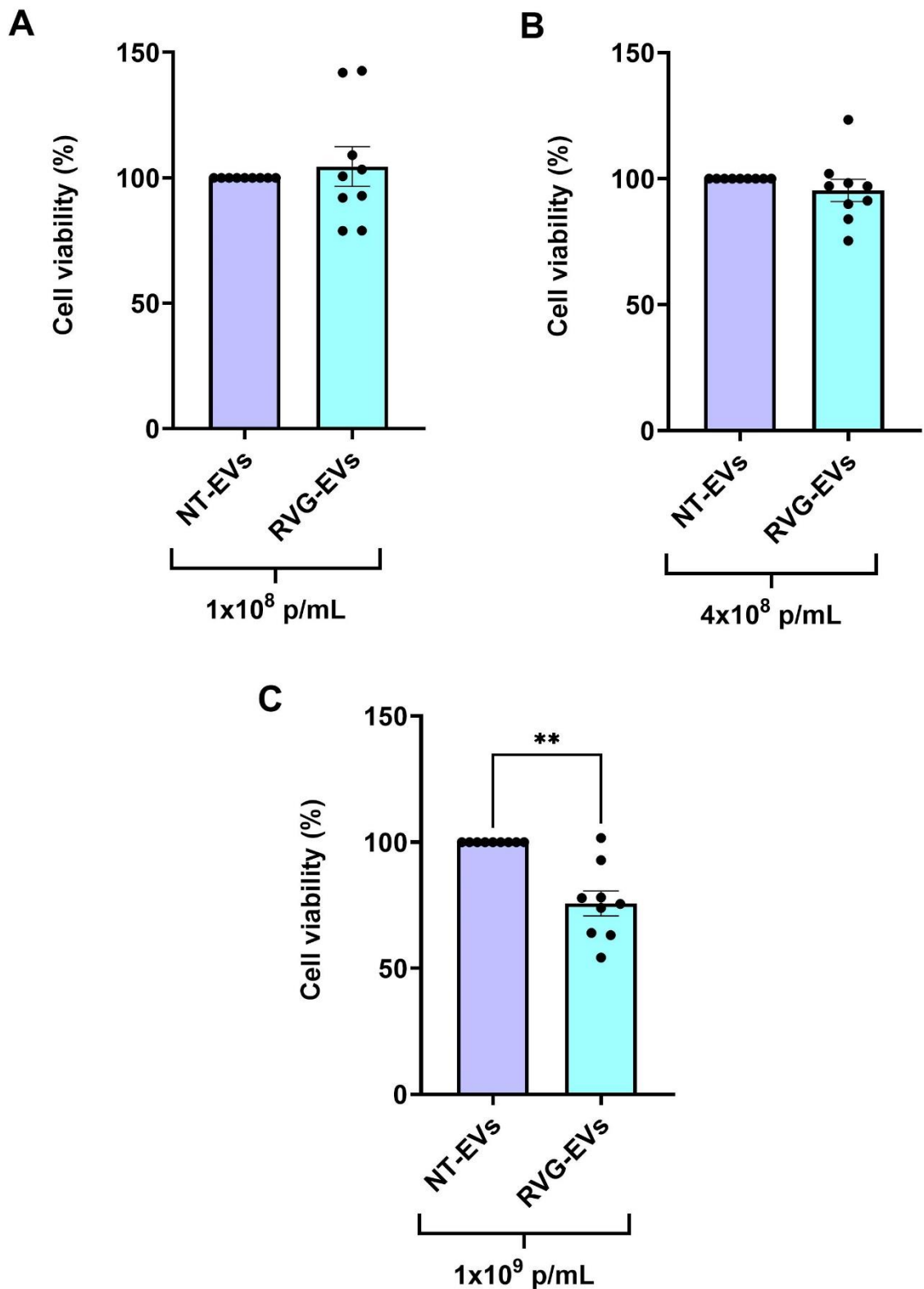
Figure 6.20 Effects of Ang-(1-9) electroporated RVG targeted EVs on primary neuronal cell viability.
Primary neuronal cells were plated at 1.2×10^6 cells/mL and were matured for 8 days before EV treatment. Cells were treated with A) 1×10^8, B) 4×10^8 and C) 1×10^9 p/mL of non-targeted Ang-(1-9) electroporated EVs or RVG-targeted Ang-(1-9) electroporated EVs. Cell viability was determined using MTT assay (n=3, replicate=3, *$p < 0.05$, Welch's t-test).

6.4.5 Effects of RVG-targeting in SHRSP primary neuronal cells

In order to assess whether RVG-CP05 targeting improved EV cargo delivery, primary neuronal cells were treated with $1x10^8$, $4x10^8$ or $1x10^9$ p/mL of non-targeted *Cel-miR-39* loaded EVs (NT-EVs) or RVG-targeted *Cel-miR-39* loaded EVs (RVG-EVs). The cellular expression of *Cel-miR-39* was assessed using qPCR at a 4- or 18-hour timepoint. At both 4- and 18-hour timepoints there was no difference in *Cel-miR-39* expression between RVG-EVs and NT-EVs at any concentration. Increasing concentration of *Cel-miR-39* loaded EVs did not show a concentration dependent effect in *Cel-miR-39* uptake in primary neuronal cells at either 4- or 18-hours (Figure 6.21 & Figure 6.22).
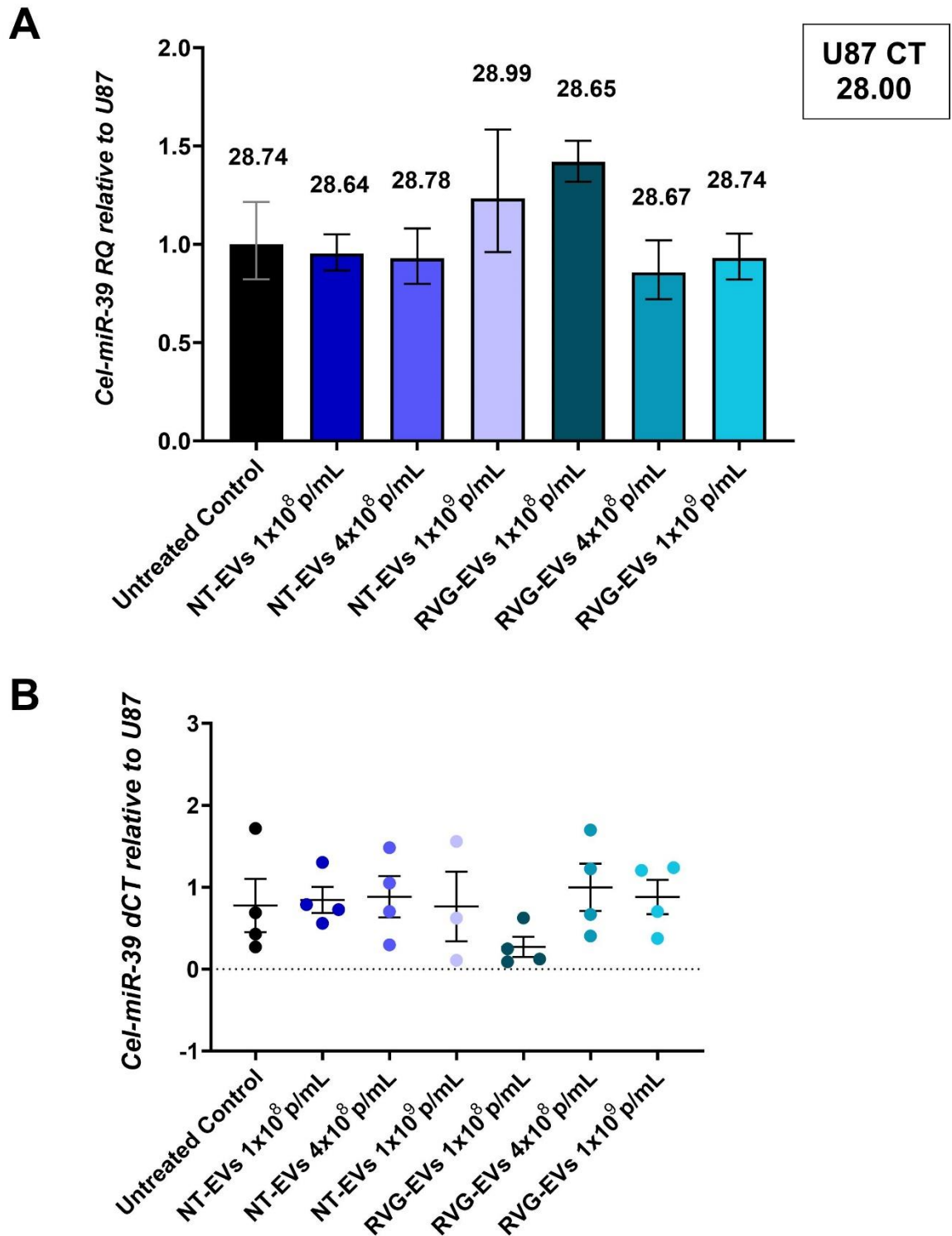
Figure 6.21 Effects of RVG-targeting on EV cargo uptake *in vitro*.
qPCR was carried out to assess the expression of *Cel-miR-39* in primary isolated neuronal
cells following 4 hours treatment with non-targeted, *Cel-miR-39*-loaded EVs (NT-EVs)
and RVG-targeted, *Cel-miR-39*-loaded EVs (RVG-EVs) treatment. MiRNA expression
was normalised to U87 housekeeper (mean CT value found in black box in top right). A)
Delta cycle threshold (dCT) demonstrated the abundance of miRNAs and error bars
represent standard error of the mean (SEM) with average CT value displayed above bars.
B) Relative Quantity (RQ) is accompanied by error bars denoting RQ min/max.
(n=3-4, p>0.05, Brown-Forsythe and Welch ANOVA with post-hoc Dunnett's T3 multiple
comparison).
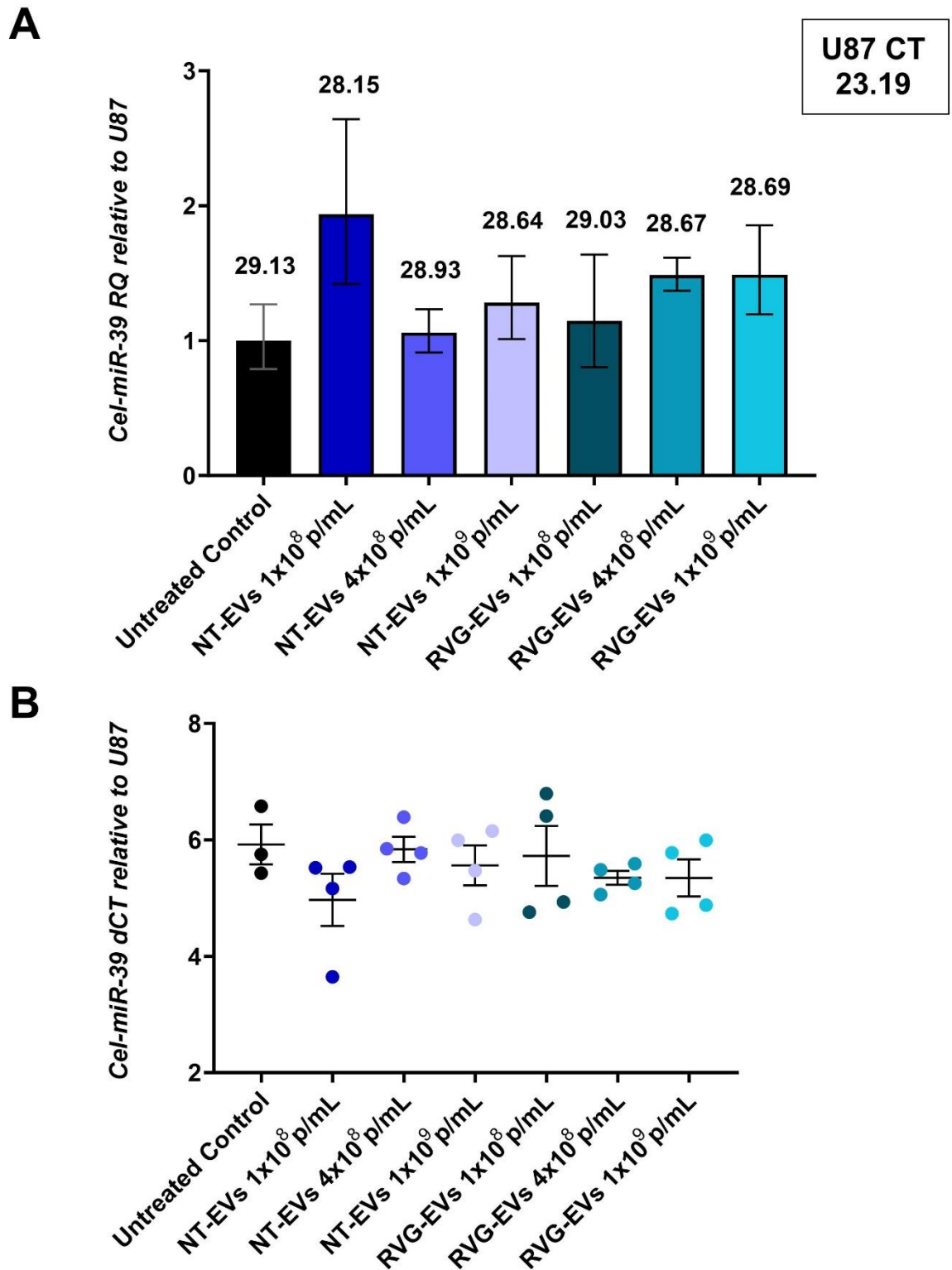
Figure 6.22 Effects of RVG-targeting on EV cargo uptake *in vitro*.
qPCR was carried out to assess the expression of *Cel-miR-39* in primary isolated neuronal cells following 18 hours treatment with non-targeted, *Cel-miR-39*-loaded EVs (NT-EVs) and RVG-targeted, *Cel-miR-39*-loaded EVs (RVG-EVs) treatment. MiRNA expression was normalised to U87 housekeeper (mean CT value found in black box in top right). A) Delta cycle threshold (dCT) demonstrated the abundance of miRNAs and error bars represent standard error of the mean (SEM) with average CT value displayed above bars. B) Relative Quantity (RQ) is accompanied by error bars denoting RQ min/max. (n=3-4, p>0.05, Brown-Forsythe and Welch ANOVA with post-hoc Dunnett's T3 multiple comparison).

6.4.6 Intranasal delivery of RVG targeted *C. elegans miRNA-39 mimic*-loaded EVs in SHRSPs

In order to determine how efficient RVG targeting of EVs may be *in vivo*, $1x10^{11}$ RVG-targeted *Cel-miR-39* loaded EVs were delivered intranasally to ~18-week-old male SHRSPs. The concentration of RVG targeted *Cel-miR-39* loaded EVs was determined from previous *Cel-miR-39* intranasal biodistribution study, whereby $2.5x10^{11}$ particles was determined to be the concentration of preference as it was sufficient enough to be detected within the brain (Figure 6.8 through Figure 6.12). However, as a result of EV loss after RVG targeting, the maximum concentration of RVG targeted *Cel-miR-39* EVs had to be lowered to $1x10^{11}$.

EVs were delivered on days one and two and organs and plasma were collected on day four (Figure 6.5 & Figure 6.6) brains were sectioned rostrocaudally 72 hours after EV delivery and the expression of *Cel-miR-39* expression within brain sections were assessed using qPCR. In all brain sections and the lungs, *Cel-miR-39* expression was upregulated in both NT-EVs and RVG-EVs compared to unloaded control EVs (U-EVs). However, there was no difference in *Cel-miR-39* expression between NT-EVs and RVG-EVs in all brain tissues and the lungs (Figure 6.24 to Figure 6.29).
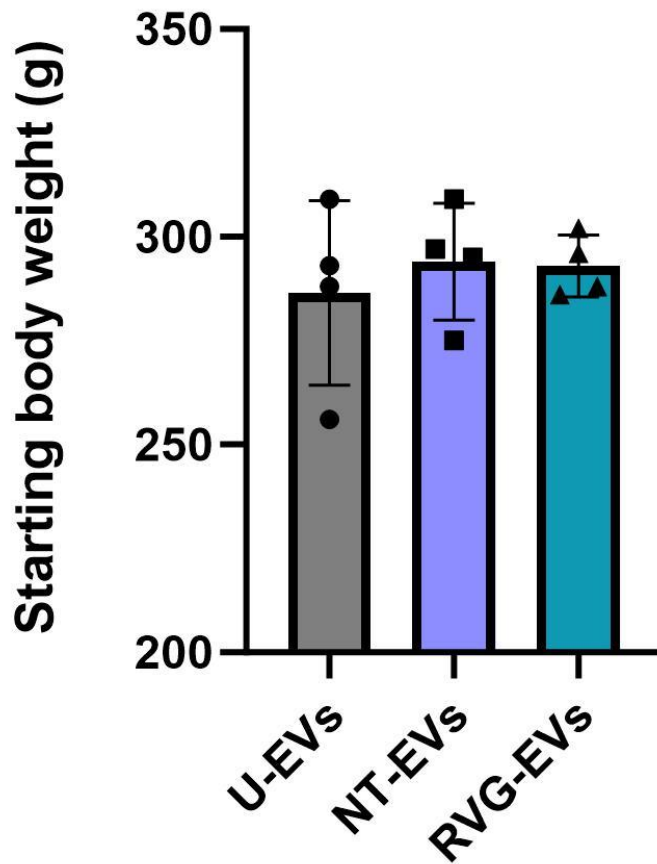
Figure 6.23 Body weight of SHRSPs prior to EV targeting treatment.
SHRSPs of approximately 18 weeks old were weighed prior to targeting EV treatments.
SHRSPs were administered either unloaded EVs (U-EVs), non-targeted *Cel-miR-39* mimic
miRNA loaded EVs (NT-EVs) or RVG-targeted *Cel-miR-39* mimic miRNA loaded EVs
(RVG-EVs). Weight in grams (g) (n=3, p>0.05, Brown-Forsythe and Welch ANOVA with
post-hoc Dunnett's T3 multiple comparison).

Figure 6.24 *Cel-miR-39* uptake in the olfactory bulb following intranasal delivery of RVG- targeted *Cel-miR-39* loaded EVs.
qPCR was performed to assess the expression of *Cel-miR-39* within the olfactory bulb of 18-week-old male SHRSP rats following unloaded (U-EVs), non-targeted (NT-EVs) and RVG-targeted (RVG-EVs) EV treatment. MiRNA expression was normalised to U87 housekeeper (mean CT value found in black box in top right). A) Relative Quantity (RQ) is accompanied by error bars denoting RQ min/max with average CT value displayed above bars and B) Delta cycle threshold (dCT) with error bars representing standard error of the mean (SEM) (n=3-4, **p<0.01, ****P<0.0001, Brown-Forsythe and Welch ANOVA with post-hoc Dunnett's T3 multiple comparison).

A

U87 CT
26.07

B
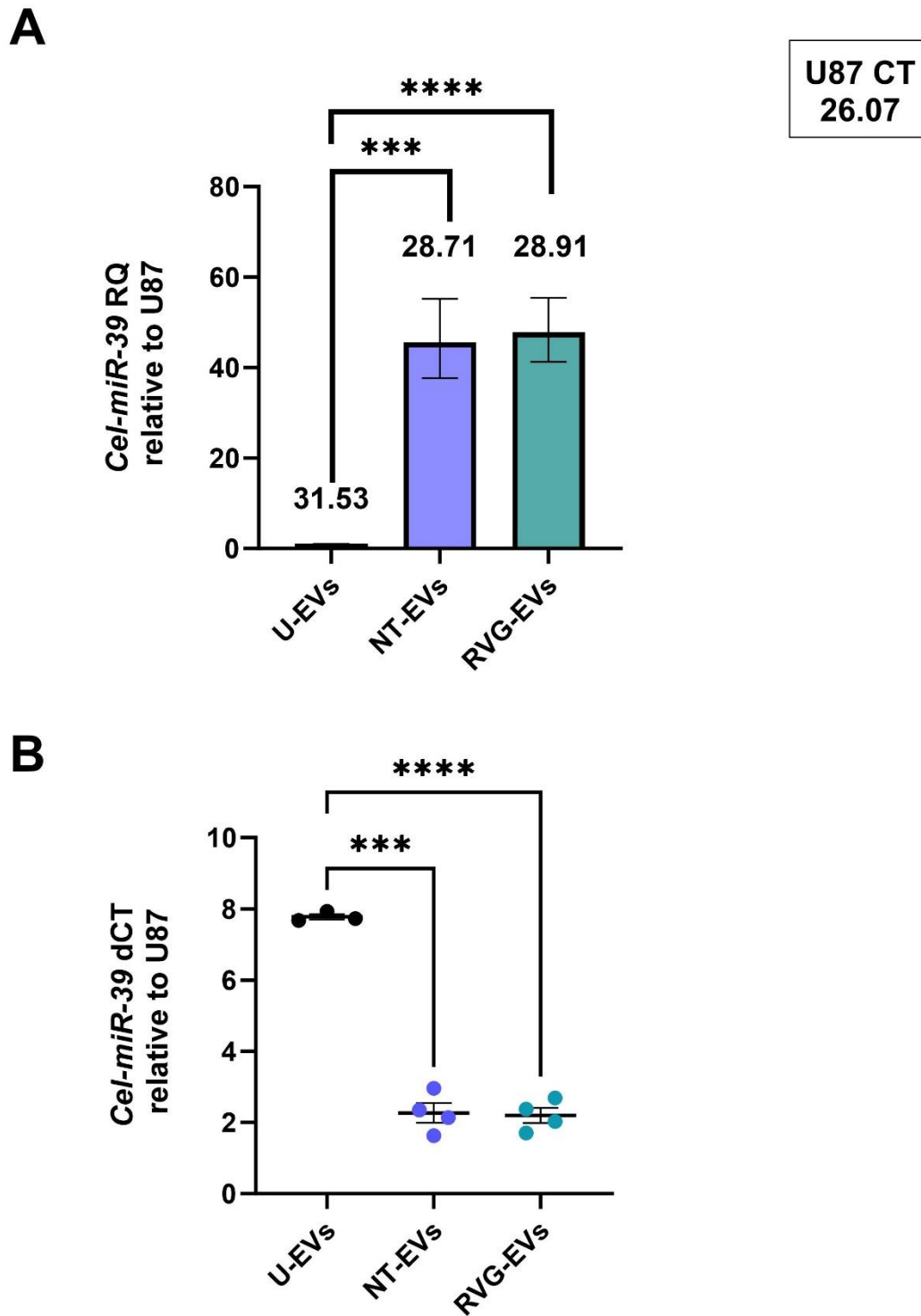
Figure 6.25 *Cel-miR-39* uptake in brain section 1 following intranasal delivery of RVG- targeted *Cel-miR-39* loaded EVs.
qPCR was performed to assess the expression of *Cel-miR-39* within brain section 1 of 18-week-old male SHRSP rats following unloaded (U-EVs), non-targeted (NT-EVs) and RVG-targeted (RVG-EVs) EV treatment. MiRNA expression was normalised to U87 housekeeper (mean CT value found in black box in top right). A) Relative Quantity (RQ) is accompanied by error bars denoting RQ min/max with average CT value displayed above bars and B) Delta cycle threshold (dCT) with error bars representing standard error of the mean (SEM) (n=3-4, ***p<0.001, ****P<0.0001, Brown-Forsythe and Welch ANOVA with post-hoc Dunnett's T3 multiple comparison).

A
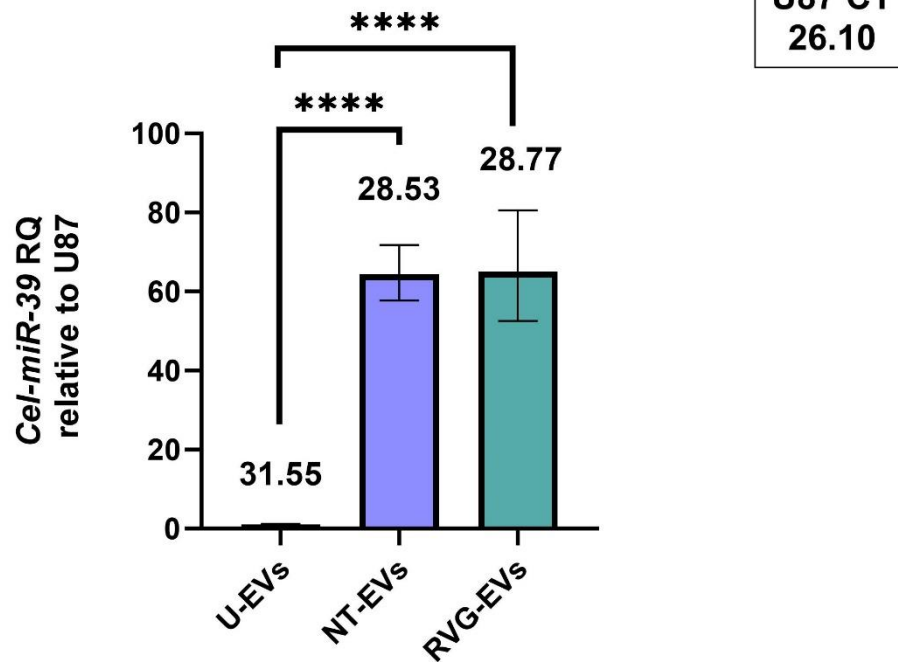
B
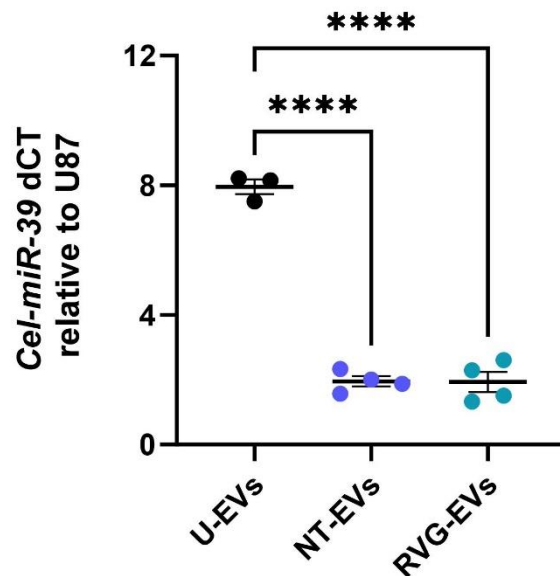
Figure 6.26 *Cel-miR-39* uptake in brain section 2 following intranasal delivery of RVG- targeted *Cel-miR-39* loaded EVs.
qPCR was performed to assess the expression of *Cel-miR-39* within brain section 2 of 18-week-old male SHRSP rats following unloaded (U-EVs), non-targeted (NT-EVs) and RVG-targeted (RVG-EVs) EV treatment. MiRNA expression was normalised to U87 housekeeper (mean CT value found in black box in top right). A) Relative Quantity (RQ) is accompanied by error bars denoting RQ min/max with average CT value displayed above bars and B) Delta cycle threshold (dCT) with error bars representing standard error of the mean (SEM) (n=3-4, ****P<0.0001, Brown-Forsythe and Welch ANOVA with post-hoc Dunnett's T3 multiple comparison).

A

**U87 CT
26.00**

B
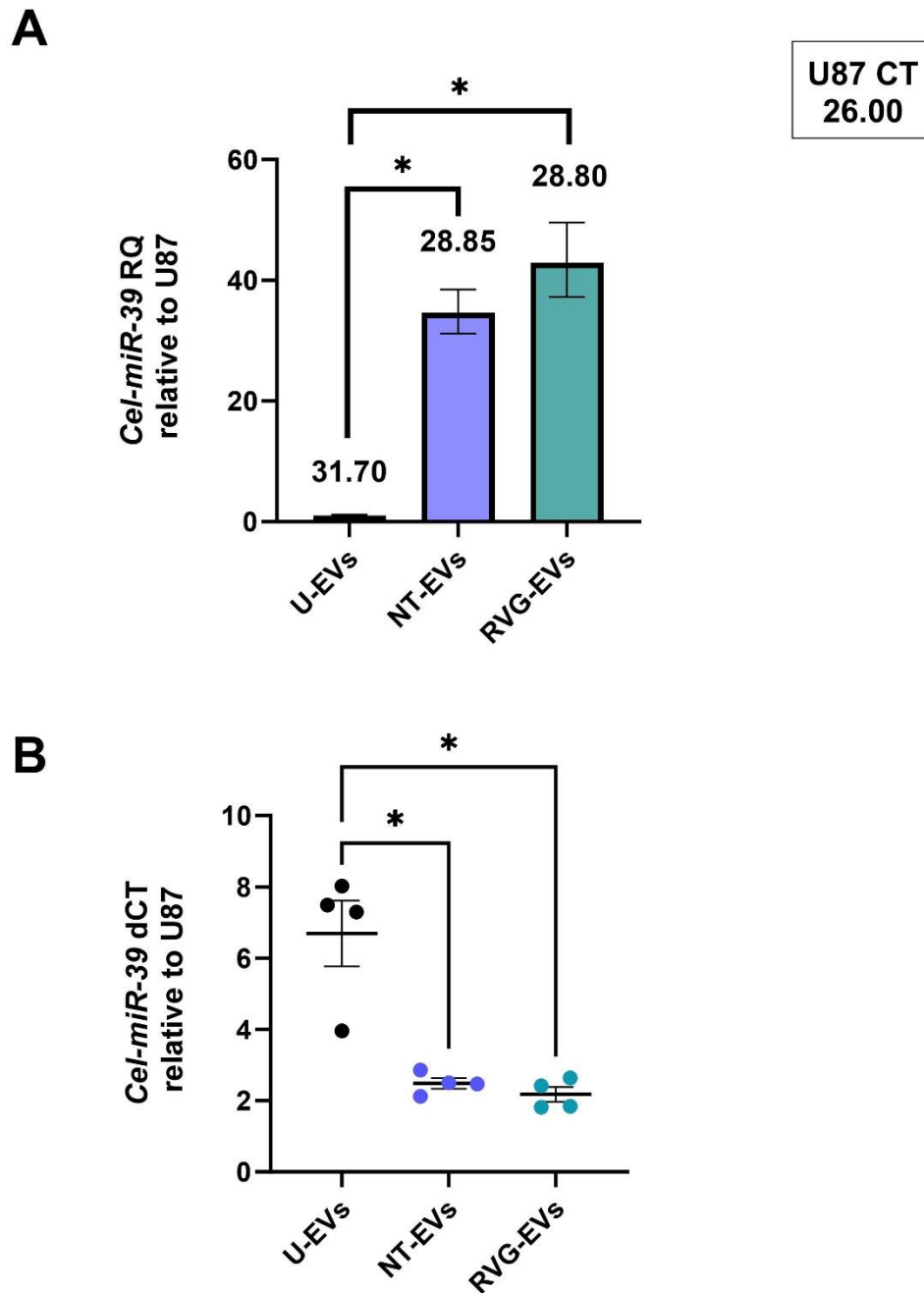
Figure 6.27 *Cel-miR-39* uptake in brain section 3 following intranasal delivery of RVG- targeted *Cel-miR-39* loaded EVs.
qPCR was performed to assess the expression of *Cel-miR-39* within brain section 3 of 18-week-old male SHRSP rats following unloaded (U-EVs), non-targeted (NT-EVs) and RVG-targeted (RVG-EVs) EV treatment. MiRNA expression was normalised to U87 housekeeper (mean CT value found in black box in top right). A) Relative Quantity (RQ) is accompanied by error bars denoting RQ min/max with average CT value displayed above bars and B) Delta cycle threshold (dCT) with error bars representing standard error of the mean (SEM) (n=4, *p<0.05, Brown-Forsythe and Welch ANOVA with post-hoc Dunnett's T3 multiple comparison).
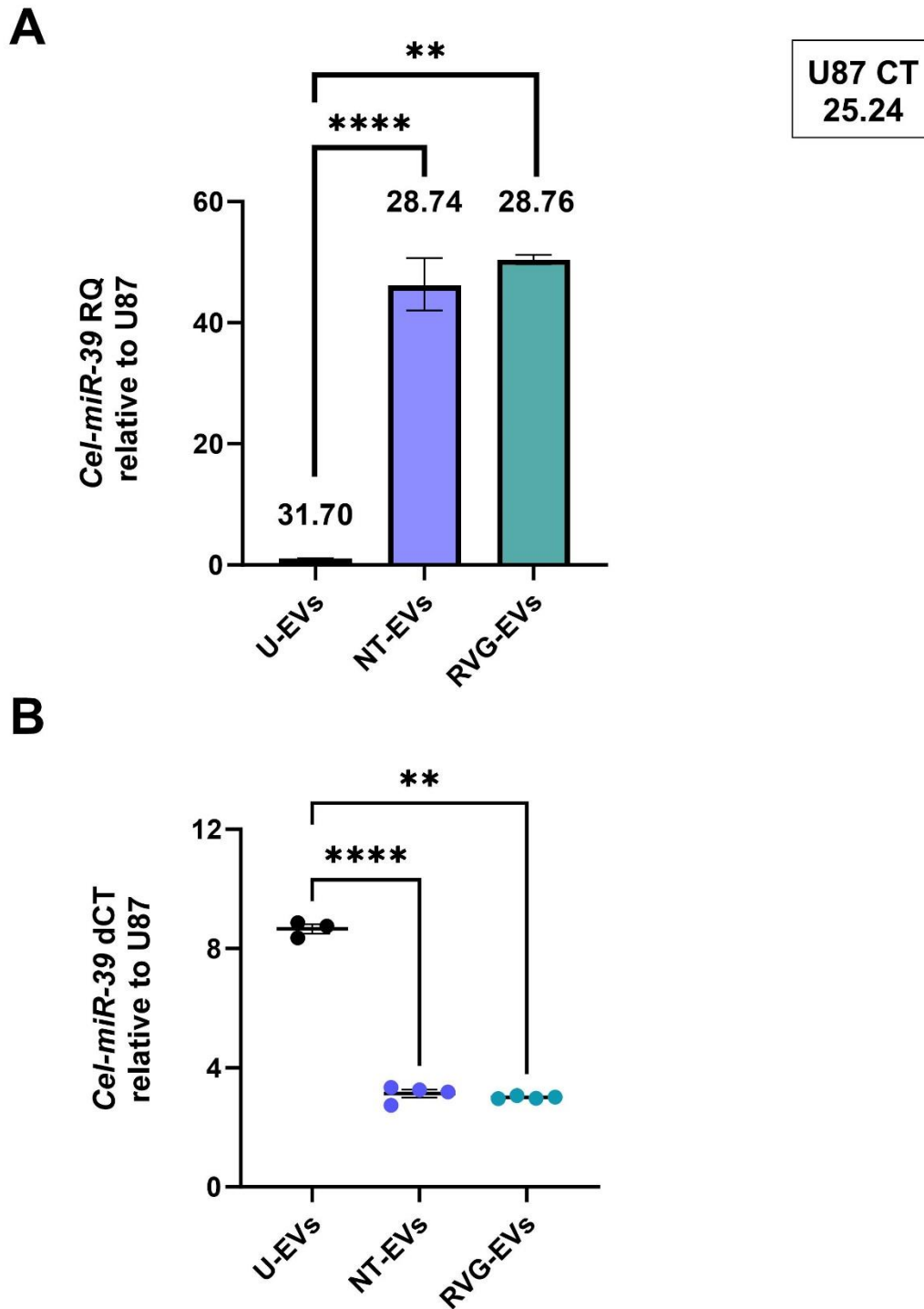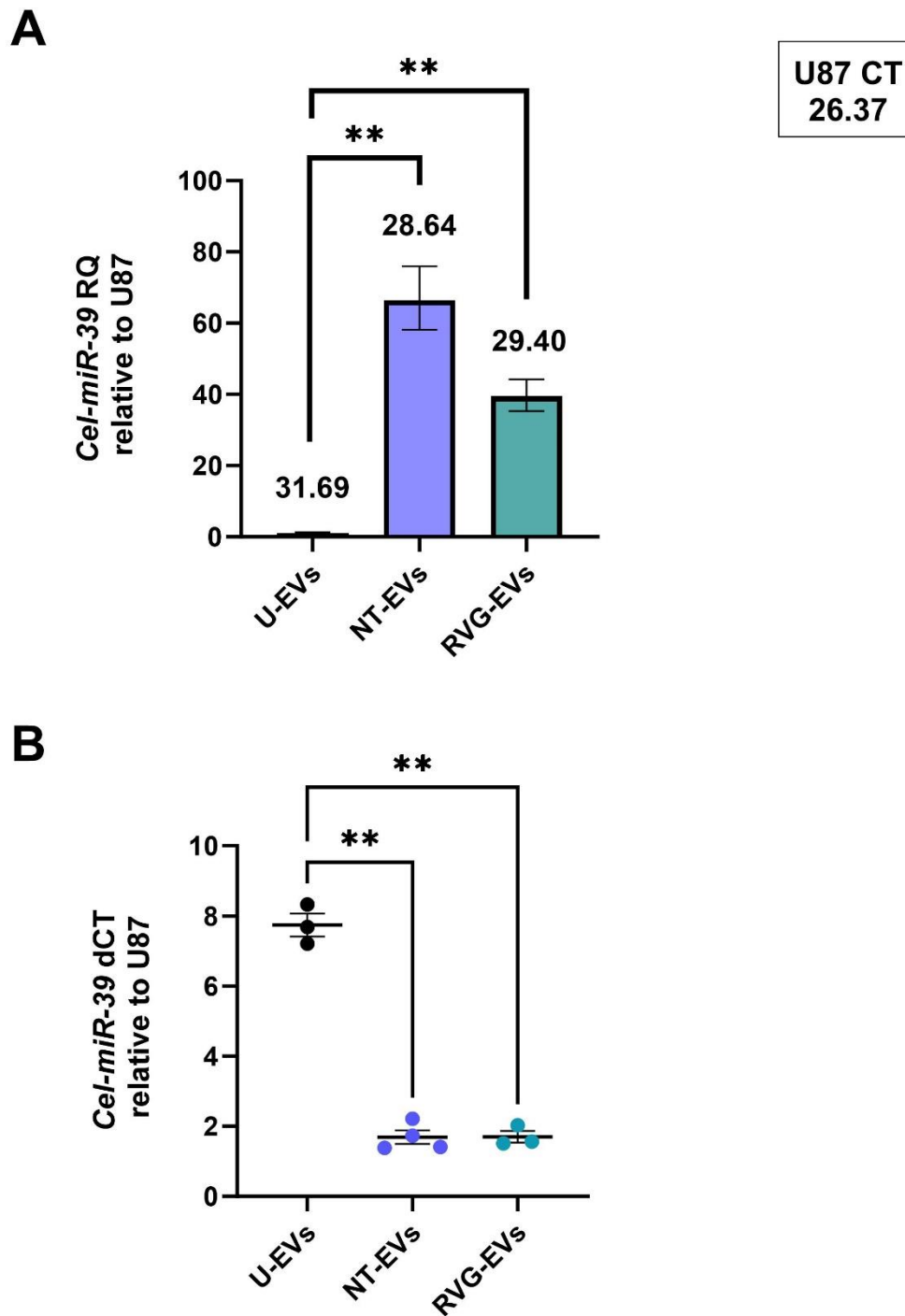
Figure 6.28 *Cel-miR-39* uptake in brain section 4 following intranasal delivery of RVG- targeted *Cel-miR-39* loaded EVs.
qPCR was performed to assess the expression of *Cel-miR-39* within brain section 4 of 18-week-old male SHRSP rats following unloaded (U-EVs), non-targeted (NT-EVs) and RVG-targeted (RVG-EVs) EV treatment. MiRNA expression was normalised to U87 housekeeper (mean CT value found in black box in top right). A) Relative Quantity (RQ) is accompanied by error bars denoting RQ min/max with average CT value displayed above bars and B) Delta cycle threshold (dCT) with error bars representing standard error of the mean (SEM) (n=3-4, **p<0.01, Brown-Forsythe and Welch ANOVA with post-hoc Dunnett's T3 multiple comparison).

A

B
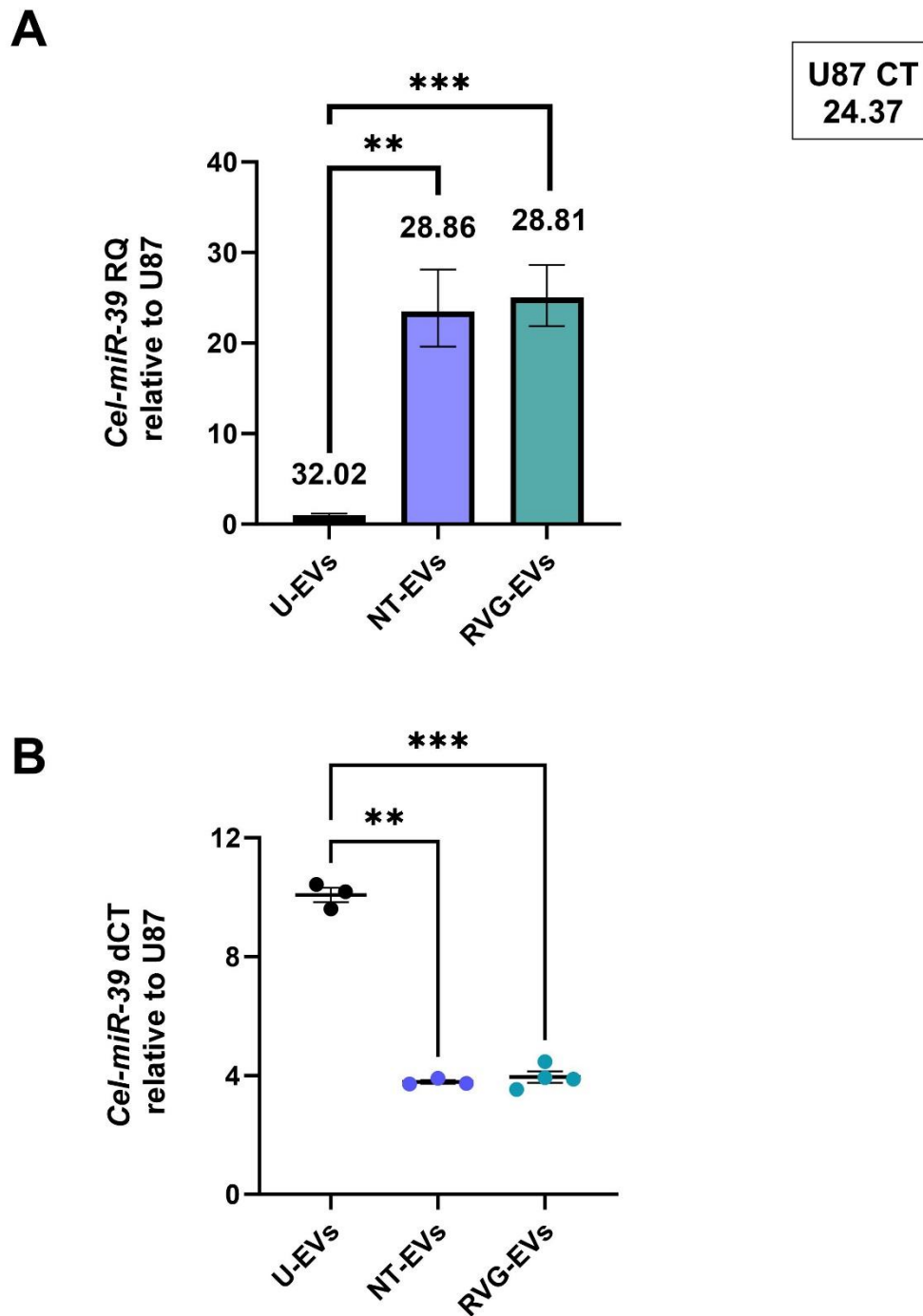
Figure 6.29 *Cel-miR-39* uptake in the lung following intranasal delivery of RVG-targeted *Cel-miR-39* loaded EVs.

qPCR was performed to assess the expression of *Cel-miR-39* within the lung of 18-week-old male SHRSP rats following unloaded (U-EVs), non-targeted (NT-EVs) and RVG-targeted (RVG-EVs) EV treatment. MiRNA expression was normalised to U87 housekeeper (mean CT value found in black box in top right). A) Relative Quantity (RQ) is accompanied by error bars denoting RQ min/max with average CT value displayed above bars and B) Delta cycle threshold (dCT) with error bars representing standard error of the mean (SEM) (n=3-4, **p<0.01, ***P<0.001 Brown-Forsythe and Welch ANOVA with post-hoc Dunnett's T3 multiple comparison).

6.4.7 Understanding baseline *Cel-miR-39* expression

Cel-miR-39 amplification was observed in untreated and water controls in numerous experiments throughout this investigation. To understand if concentration of *Cel-miR-39* primer would affect background *Cel-miR-39* amplification, *Cel-miR-39* primer volumes were added to qPCR containing water samples. There was no obvious relationship between CT value and concentration of *Cel-miR-39* primer. CT values ranged from 30.01 to 35.05 between primer volumes of 0.25-2.50 µL (Figure 6.30).
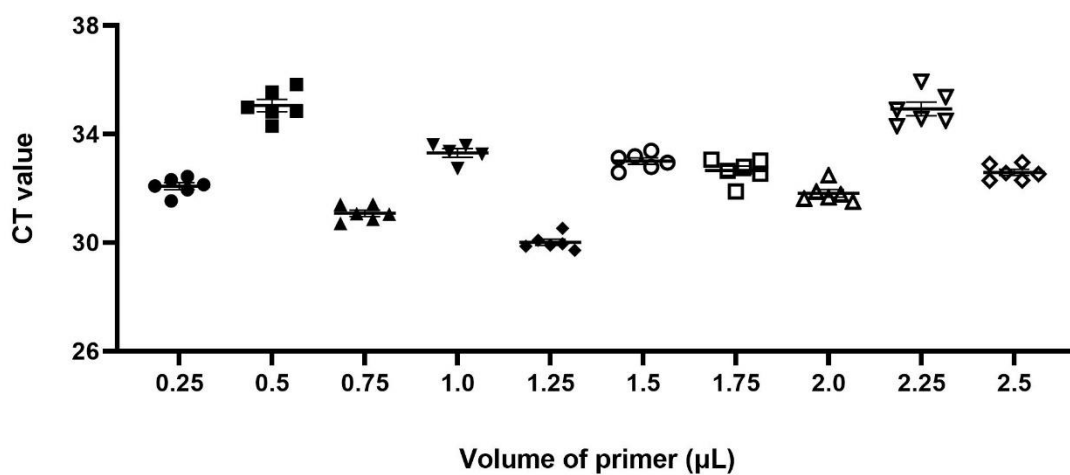
Figure 6.30 Dimerisation of *Cel-miR-39* mimic mRNA.
Water samples were added in place of miRNA. Cycle threshold (CT) demonstrated the abundance of *Cel-miR-39* expression while error bars represent standard error of the mean (SEM) (n=3, replicate=2).

6.5 Discussion

The use of RVG as a targeting peptide was investigated to understand its effects on EV delivery to neurons of the brain. Primary neuronal cells were found to express the receptor for RVG-CP05 peptide, while SHRSP plasma derived EVs were found to possess CD63, the tetraspanin onto which RVG-CP05 binds. In primary neuronal cell cultures, addition of RVG-CP05 to *Cel-miR-39* loaded EVs did not affect cell viability. *Cel-miR-39* levels were unchanged in primary neuronal cell cultures following 4- or18-hours incubation with RVG targeted, *Cel-miR-39* mimic miRNA loaded EVs, RVG-EVs compared to non-targeted, *Cel-miR-39* mimic miRNA loaded EVs, NT-EVs. Intranasal delivery of *Cel-miR-39* mimic miRNA loaded EVs revealed that, although not significant, 2.5×10^{11} particles increase *Cel-miR-39* expression within all regions of the brain. *Cel-miR-39* expression within the plasma was significantly increased following intranasal delivery of 2.5×10^{11} *Cel-miR-39* mimic miRNA loaded EVs, but not in other peripheral organs. Intranasal delivery of RVG-EVs did not improve *Cel-miR-39* EV cargo uptake compared to NT-EV. Within the RVG-EV targeting study, both NT-EVs and RVG-EVs led to increased *Cel-miR-39* levels in all brain sections and lung compared to unloaded-EVs (U-EVs).

In this study, intranasal delivery of EVs led to increased accumulation of EV cargo within brain tissue, and in the lungs. Similar findings were uncovered when C57BL/6 mice subjected to ET-1 MCAO were administered gold-labelled exosomes intranasally, whereby they found that EVs accumulated within the brain, lung and spleen following stroke delivery (Betzer et al., 2017). Intranasal delivery of EVs in rodents requires the animal to be placed in a supine position. In this position, solutions containing EVs may remain in the nasal cavity, allowing EVs to transverse the olfactory trigeminal nerve pathway to enter the brain, or EVs solutions may flow down into the larynx and into the lungs (Illum, 2003, Ahmad et al., 2017). In some cases, EV administration to the lungs is best facilitated through intranasal delivery, for example, human umbilical cord derived MSCs were delivered to rodent models of bronchopulmonary dysplasia rats intranasally which led to improved lung alveolarisation and vascularisation (Moreira et al., 2020). Intranasal delivery of substances to the lungs is generally achieved by using greater volumes than those used in delivering substances to the brain. In this study, EV cargo was detected at high level in the plasma of SHRSPs following intranasal delivery of *Cel-miR-39* loaded EVs. It has been well established that drugs may pass through the lungs into the blood stream (Labiris and Dolovich, 2003). With this in mind, if the EV solution delivered intranasally to these SHRSPs entered into the lungs, EVs or indeed the EV cargo, may

have entered into the blood stream and resultantly was detectable within plasma samples. Following intranasal delivery EVs may also be retained within the nasal cavity (Driedonks et al., 2022). Although not assessed in this investigation, tissue from the nasal cavity or nasal lavage could have been carried out to determine whether *Cel-miR-39* loaded EVs were retained within the nasal cavity.

A notable study utilised palmitoylated EGFP-Nanoluciferase (PalmGRET) reporter while assessing EV accumulation within the organs of male pig-tailed macaques after either intranasal or intravenous administration using *in vivo* imaging (Driedonks et al., 2022). Nanoluciferase signal, indicative of EV accumulation, was detected in the liver, lungs, and spleen after intravenous injection, however following intranasal administration of PalmGRET EVs, little to no nLuc signal was detected in these organs. It also found that intranasal administration of PalmGRET EVs to Balb/cJ mice led to increased EV accumulation within the nasal cavity and the lungs, while intravenous administration of PalmGRET reporter EVs led to accumulation within the liver. Nanoluciferase signal was also assessed within mouse tissue homogenates, whereby intravenous administration provided a greater nanoluceiferase signal, more so than intranasal delivery, within the liver, spleen, kidney colon and brain (Driedonks et al., 2022). These findings corroborated those found within this investigation, whereby following intranasal delivery of EVs, EVs or indeed EV cargo, could be detected in both the brain and lungs in small rodent models. However, this group evaluated EV biodistribution using fluorescence, while in this thesis EV biodistribution study, EV cargo delivery was used as a proxy for EV biodistribution. Importantly, the accumulation of EVs was assessed by this group at a relatively short time frame 10-40 minutes following intranasal or intravenous injection (Driedonks et al., 2022). In this thesis biodistribution study, EV cargo delivery was assessed on day four following intranasal administration of *Cel-miR-39* mimic miRNA loaded EVs. One may speculate that assessment of EV accumulation or cargo distribution at a shorter timeframe may influence cargo expression within the organs investigated. The average of miRNA half-life has been theorised to be 119 hours, which is approximately 5 days (Gantier et al., 2011). Based on this figure, the expression of *Cel-miR-39* may be significantly reduced at the day-four assessment timepoint compared to more acute assessment timepoints. While a similar concentration of EVs was used in this experiment and the biodistribution study in this thesis (1.5×10^{11} of PalmGRET EVs and $1-5 \times 10^{11}$ *Cel-miR-39* loaded EVs), there is a noticeable difference in rodent species used to assess EV biodistribution. Rats weigh approximately 10 times more than mice, however between studies these rodents received a very similar dose of EVs. Therefore, the number of EVs per unit weight was much greater

in mouse species compared to rats. This highlights technical differences between studies, however similar biological conclusions can be drawn.

Further differences in EV accumulation between rodent models and non-human primates has also been observed, the latter being more directly translatable to human physiology (Driedonks et al., 2022). These findings may introduce a degree of doubt to intranasal EV delivery methods in higher primates and in turn their use as a non-invasive post-stroke treatment in humans. Intranasal administration of therapeutics, such as the annual flu vaccine, has proven effective in delivery therapeutics and conveying protection against influenza (Centers for Disease Control and Prevention, 2022a). Despite their possible role as a therapeutic vector, EVs do not possess site-specific cargo delivery mechanisms. As a result, the use of targeting molecules may vastly improve EV cargo delivery to desired organs.

The basis of the targeting method used in this thesis was derived from a high-profile paper that found success in targeting EVs to the brain using RVG-CP05 peptide (Gao et al., 2018). Within this paper, phage display was used to identify display peptides that were able to bind to EV membrane domains. The peptide CP05 was found to bind CD63 with strong affinity. To assess brain targeting, CP05 was linked to RVG to form EXO_{RVG} and were administered to C57BL/6 mice through intravenous injection. EXO_{RVG} accumulated within the brain significantly more than non-targeted EXO (Gao et al., 2018). With this successful method in mind, the method was further adapted for study in this thesis. Despite using the same linker and targeting peptides published in the above paper, RVG targeting of EVs did not improve EV cargo delivery to the brain compared to non-target EVs in this investigation. Following loading of EVs using electroporation, EV protein content could not be determined using conventional BCA. Therefore, starting EV protein content and corresponding EV particle concentration were used to estimate EV protein content following EV loading. As such the EV protein content required to bind CP05-RVG, as determined by the original protocol, may have ultimately been inaccurate. EVs should have been incubated with CP05-RVG at a 1:1 ratio (30 µg: 30 µg). If the estimated EV protein content was higher than 30 µg, then there would be a greater proportion of EVs to CP05-RVG, and as such fewer EVs coated in CP05-RVG. As the number of particles was used as a measurement of targeted EVs for delivery to SHRSPs, the issue of inaccurate protein content estimation could be masked. RVG targeted EVs were also delivered to SHRSPs rather than C57BL/6 mice in this RVG biodistribution investigation. In theory, a larger concentration of EVs, equivalent to EV protein content, could have been delivered to SHRSPs to compensate for the increased body weight of rats, however in reality, loss of

EVs through the isolation, loading and targeting method meant increasing the number of RVG targeted EVs was not possible. Although, it has previously been found that smaller doses of EVs may be more beneficial in stroke than larger doses of EVs (Otero-Ortega et al., 2020). Perhaps a reduced RVG-EV dose may be more beneficial in experimental stroke models, however, was not examined within this investigation.

With regard to differing rodent species between this study and the study on which this targeting project was based upon, BLAST analysis revealed that the amino acid sequence of CD63 is conserved between mice and rats, and so, binding ability of CP05 to CD63 should be consistent between species. EXO_{RVG} were not present within the lungs of C57BL/6 mice following intravenous injection, however RVG-targeted EV cargo was present in the lungs of SHRSPs following intranasal administration. As previously discussed, due to the nature of intranasal administration of EVs to rodents, EVs may subsequently be found within the lungs. The differences in administration route may account for differences in targeted EV accumulation/cargo delivery within the lungs. However, various papers have published conflicting findings on the accumulation of intravenously administered EVs found within the lungs (Driedonks et al., 2022, Yu et al., 2022b).

In this RVG biodistribution study, there was no difference in EV cargo delivery to the olfactory bulb and brain sections one through four. In another study, intravenous injection of 200 µg of circular RNA DYM (CircDYM) DiR labelled RVG-EVs were successfully delivered to the brain and other organs of C57BL/6 mice as determined by qPCR (Yu et al., 2022b). Interestingly, when analysing the relative fluorescence provided by these DiR labelled EVs, RVG targeted EVs significantly accumulated within brain tissue only and not in other organs. Conversely, C57BL/6 mice with established melanoma were intravenously injected with $1x10^{10}$ particles per gram of DiR labelled RVG-EVs or DiR non-targeted control EVs. DiR labelled RVG-EVs provided significantly higher fluorescent signal in both the brain and heart of these mice compared to DiR untargeted EVs (Wiklander et al., 2015). The success of EV targeting using RVG peptides can be assessed and documented using EV accumulation (determined by *in vivo/ex vivo* imaging) and EV cargo delivery (determined by qPCR) as discussed above. However, it is important to note that these two methods of determining RVG-EV targeting success are very different. Accumulation of RVG-EVs as determined by imaging allows for spatial and temporal assessment of EV biodistribution, however, cargo delivery assesses the release or uptake of cargo from RVG-EV. Both methods may have their drawback, for example, limited fluorescent signal or cargo degradation. With the observed difference in RVG-EV

targeting success between labelling and cargo delivery methods, it would be interesting to carry out *in vivo* imaging to determine the biodistribution of labelled RVG-EVs following intranasal administration to SHRSPs. Studies discussed in this section also used different methods of producing RVG targeted EVs, for example, the use of RVG peptides joined to linkers that bind surface tetraspanins, or the production of RVG targeted EVs through transfection of cell lines with plasmids (Wiklander et al., 2015, Yu et al., 2022b, Gao et al., 2018). With this in mind, further studies must be carried out to identify which methods of RVG-mediated EV targeting may be most successful.

The studies discussed above also identify the importance of the therapeutic window for RVG-EV treatment. In this RVG biodistribution investigation, *in vitro* investigation of RVG-EV cargo delivery did not show any clear superiority. However, various groups have assessed RVG targeting success at different assessment timepoints which in turn may influence EV accumulation and clearance patterns. Phagocytic immune cells have been shown to clear EVs rapidly within circulation, while studies have shown that EVs delivered in multiple doses over various time periods lead to heightened immune-mediated EV clearance (Robbins and Morelli, 2014, Nguyen et al., 2022, Driedonks et al., 2022). It is therefore theorised that the effectiveness of RVG-EVs to deliver internalised cargo may be time dependent and was not captured at the timepoints included in this investigation. As mentioned previously, one theory may be that EV cargo uptake may also be attributed to the half-life of EV cargo, as such, irrespective of RVG targeting, EV cargo delivery may be limited by miRNA cargo half-life (Gantier et al., 2011). Immune cell clearance of EVs may also limit the delivery of therapeutic EVs, irrespective of the presence of RVG targeting peptide, indeed one study determined the half-life of therapeutic EVs delivered intravenously to be approximately 40 minutes depending on EV concentration (Driedonks et al., 2022). Between methods by which RVG-EVs are created to therapeutic window of RVG-EV delivery, there are various factors that may contribute to the effectiveness of targeted EV delivery. As such further optimisation of EV targeting methods must be carried out in order to improved therapeutic EV delivery to the brain for possible use in neurological and cerebrovascular diseases.

The presence of EV tetraspanins can be influenced by a number of different factors such as species, biofluid and the cytoplasmic pH of parental cells from which they are derived (Sivanantham and Jin, 2022). RVG targeting in this investigation is dependent on the linker peptide, CP05, binding to CD63 EV tetraspanin (Gao et al., 2018). However, the abundance of CD63 in EV populations can vary between the bio fluid, disease state and even species from which EVs are isolated (Karimi et al., 2022, Akbar et al., 2022, Zhao et

al., 2020). In turn this may limit the binding of CP05-RVG to CD63 on the surface of EVs, and thus may reduce the targeting ability of RVG-EVs. The CD63 tetraspanin possesses four individual transmembrane domains through the phospholipid bilayer of EVs, where both the N and C termini of CD63 are found intraluminally (The UniProt Consortium, 2023). Resultantly, the CP05 linker joined to RVG must bind to all or at least a portion of the extraluminal region of the CD63. As such there may be limited interaction between CP05 and CD63 that in turn may limit the ability of CP05-RVG to effectively label EVs and subsequently target EVs to the brain. As an alternative, the N or C terminus of CD63 may also be truncated, leading to the formation of CD63 with an extraluminal N or C terminus, that can act as a secure anchor for EV targeting molecules to bind (Curley et al., 2020).

6.5.1 Study limitations.

Background *Cel-miR-39* expression has been observed in water samples in RT-PCRs carried out by multiple groups in the department. CT values were observed for water controls taken from RT-PCR plates for *Cel-miR-39* RT primer, however water controls added to the qPCR plate provided undetermined CT values for *Cel-miR-39* TM primer, as expected. These findings suggest that, during the amplification stage of RT-PCR, the RT *Cel-miR-39* primer may dimerise, or an artefact of the RT primer may form during the RT stage or that there may be environmental contamination. The conclusion that the primer was dimerising was also supported by the fact that CT values for *Cel-miR-39* expression was not correlated to the volume of primer used. Reagent and primer contamination was initially suspected as the cause of CT value in *Cel-miR-39* water controls during the RT-stage, however new reagents and primers were used in these experiments. *Cel-miR-39* mimic miRNA has been widely used throughout the department for several years. In an attempt to determine if there could be environmental contamination of *Cel-miR-39* mimic miRNA, all surfaces were cleaned with RNase Zap, sterile fume hoods were used for the preparation of RT-PCR and qPCR, different lab benches were also used. Unfortunately, changing the environment did not resolve the issue. Further, when a *Cel-miR-39* mimic miRNA plate was set up on an entirely different laboratory level, *Cel-miR-39* was still detected within RT-PCR water controls. Other mimic miRNAs were also investigated for their use in place of *Cel-miR-39* however similar RT-water presence was reported. As this issue had no immediate remedy, it was accepted that there was a certain level of background *Cel-miR-39* primer dimerisation, which consequently could affect results of

any experiment investigating *Cel-miR-39* expression through qPCR. It is important to note that CT values for water controls of *Cel-miR-39* RT plates were approximately 35-38 cycles. In most cases where *Cel-miR-39* mimic miRNA expression was expected, CT values were several cycles smaller, approximately 24-32 cycles. The difference in CT values was clear enough to delineate between background dimerisation/contamination and *Cel-miR-39* mimic miRNA expression as a result of loaded EV treatment. Alternative, endogenous miRNAs may be investigated for their use in future as a quantitative measure of EV cargo, however this introduces further experimental issues such as the potential beneficial effects of these endogenous miRNAs relative to therapeutically loaded EVs. Additionally, EVs may already contain certain miRNAs and as such loading of EVs with this miRNA may not represent the concentration of miRNA loaded into EVs and in turn affect outcomes of the experiment. It should be noted that loaded EVs undergo two SEC steps that could potentially remove environmental *Cel-miR-39*, whereas unloaded EVs (U-EVs) only undergo one SEC step during initial isolation from plasma. SEC isolation of EVs has been shown to reduce the abundance of short RNA fragments, including miRNA, from human serum samples (Buschmann et al., 2018). Resultantly, U-EVs that had only undergone one round of SEC isolation may, in some cases, possess greater levels of background *Cel-miR-39* miRNA than *Cel-miR-39*-loaded EVs.

Within the RVG targeting EV study, EV administration and brain sectioning were carried out by one investigator. Despite this, section sizes can vary between SHRSPs brains. SHRSPs used in these studies ranged 270-320g and were approximately 18 weeks of age. Animals were randomly assigned to treatment groups to reduce the bias and there was no difference in body weight between experimental groups. In order to reduce the number of animals used in scientific research, in line with National Centre for the Replacement, Refinement and Reduction of Animals in Research, within the optimal EV concentration study there was only one unloaded control EV population (1×10^{11} U-EVs) matched with the lowest concentration of therapeutic EVs, as opposed to three individual unloaded EV control groups (1-, 2.5- and 5×10^{11} EVs). The premise of this study was to better understand the concentration at which *Cel-miR-39* expression was detectable in brain tissue after intranasal delivery of *Cel-miR-39* loaded EVs and as such the addition of at least six further animals to create two extra control groups was not deemed necessary in this study.

The success of RVG-CP05 conjugation could not be determined in this investigation. Other studies have been able to quantify RVG-EV conjugation using flow cytometry through use of rhodamine labelled CP05 peptide and PKH67 labelled EVs (Gao et al.,

2018). As the CP05 linker in this investigation was not labelled and labelling of EVs with PKH dyes previously proved to be unreliable, this flow cytometry method of determining RVG-EV conjugation could not be used in this investigation. Further studies with labelled CP05 and labelled loaded EVs may be carried out in future to determine whether EVs were bound by CP05-RVG.

6.6 Summary

RVG targeting was assessed to determine if EV cargo uptake in cells and in the brain was improved after targeting. *In vitro* delivery of RVG targeted and non-targeted EVs demonstrated no clear superiority in EV cargo uptake. Intranasal EV delivery methods were successful in delivering EV cargo *in vivo*, however RVG targeting did not increase EV cargo uptake. RVG targeting of EVs requires further optimisation in order to assess its in improving EV therapies. Nevertheless, EV cargo can be delivered to the brain using non-invasive intranasal delivery methods and as such may be beneficial in the development of novel stroke treatments.

Chapter 7 Effects of extracellular vesicles following experimental stroke

7.1 Introduction

Ischaemic stroke in rodent models can be achieved in various ways, however the most common method is intraluminal filament-mediated occlusion of the middle cerebral artery (MCAO). Using this method, a microfilament is inserted into the common carotid artery and is advanced to the opening of the middle cerebral artery (MCA) blocking blood flow to areas of the brain supplied by this major cerebral vessel (Longa et al., 1989). However, there are many serious side effects of this surgery such as insufficient occlusion or damage to surrounding arteries which in turn may lead to haemorrhage (Laing et al., 1993). MCAO can be transient (tMCAO), mimicking the reperfusion that occurs either naturally or through intervention in stroke patients, or it can be permanent (pMCAO), representing more severe cases of stroke. MCAO can vary between rodent models, mainly due to a variety of reasons including; animal size, strain, sex, and presence of co-morbidities, and require optimisation in order for success (Liu et al., 2022b). After optimisation post-tMCAO mortality rates can be challenging, especially in models with additional co-morbidities. Optimising robust experimental stroke models furthers research into new therapies that may improve functional outcomes post-stroke.

Modulation of the RAAS, more specifically agonism and antagonism of aspects of the RAAS, has been identified as a potential treatment for stroke. Agonism of the MasR by AVE0991 has been shown to decrease neuronal cell death following oxygen glucose deprivation in *in vitro* models of ischaemic stroke. When AVE0991 was combined with a MasR antagonist A-779 this neuroprotective effect was abolished (Lee et al., 2015). Following tMCAO, C57BL/6 mice treated with the AT_2R agonist CGP42112 demonstrated improved neurological and behavioural outcomes and reduced total infarct volume compared to controls (Lee et al., 2012). CGP42112 delivered to SHRs post-stroke led to reduced infarct volumes, however, when CGP42112 was combined with the AT_2R antagonist PD123319, this reduction in infarct volume was nullified (McCarthy et al., 2009, McCarthy et al., 2012). Increased endogenous levels of Angiotensin Converting Enzyme (ACE) 2, ACE2 and Angiotensin-(1-7) [Ang-(1-7)] in the brain in an experimental model of ischaemic stroke have been reported following administration of the ACE inhibitor captopril (Tao et al., 2018). These findings highlight the potential importance of the counter-regulatory axis of the RAAS as a target for stroke therapies.

Recent research in the counter-regulatory axis of RAAS has focused on the AT_2R agonist, C21, and the peptide Ang-(1-7) which is the functional ligand of MasR (Souza-Silva et al., 2024, Chen et al., 2024, Farooqui and Banday, 2024, Sheng et al., 2024). Following tMCAO, C21 treatment led to improvement in passive avoidance outcomes in SHRs (Ahmed et al., 2018). In a follow-on study, Wistar rats were treated with C21 after distal MCAO, and improvements in Bederson neurological score were observed (Ahmed et al., 2019). In models of ET1-MCAO, C21 led to significant improvement in Bederson score and Garcia neurological score post-stroke (Bennion et al., 2018a). Therapeutic delivery of C21 has also been shown to reduce infarct volume in various models of experimental stroke (Alhusban et al., 2015, Bennion et al., 2017, Bennion et al., 2018a, Fouda et al., 2017, Joseph et al., 2014, McCarthy et al., 2014, Min et al., 2014, Shan et al., 2018). In terms of mechanistic effect, C21 treatment can directly affect RAAS modulation by reducing AT_1R expression in male Wistar rats post-stroke (Alhusban et al., 2015). Additionally, C21 has been shown to alter immune responses post-stroke whereby C21 has been linked to: increased anti-inflammatory IL-10 concentrations (Alhusban et al., 2015), reduced levels of proinflammatory TNFα (Fouda et al., 2017) and reduced expression of CCL2 and CCR2, central in monocyte recruitment (Joseph et al 2014) in experimental models of stroke. C21 treatment has also led to increased protective eNOS and decreased inflammation-stimulating iNOS expression post-stroke (Alhusban et al., 2015). Together these findings demonstrate AT_2R stimulation leads to changes in neurological outcomes, infarct volume, inflammation and reactive oxygen species, which in turn may be beneficial post-stroke.

The ACE2/Ang-(1-7)/MasR axis has been extensively studied in both cardiac and cerebral ischaemia. It has been found that, following cerebral ischaemia, circulating levels of Ang-(1-7), MasR and ACE2 are increased in rats following experimental stroke (Lu et al., 2013), demonstrating that stroke leads to changes within key components of the counter-regulatory axis of the RAAS. Research has shown that Wistar subjected to tMCAO followed by Ang-(1-7) treatment decreased post-stroke final lesion (Arroja et al., 2019), while Ang-(1-7) treatment has also been shown to decrease levels of apoptosis in human brain vascular smooth muscle cells *in vitro* (Bihl et al., 2015), thus suggesting a link between Ang-(1-7) and cell survival. Ang-(1-7) treatment has also led to increased angiogenesis via Mas/eNOS-dependent pathway in preclinical models of pMCAO, further strengthening the idea that Ang-(1-7) may play a role in restoring the neurovascular unit post-stroke (Jiang et al., 2014). In terms of immune response, endogenous Ang-(1-7) concentration was reduced within the rostral ventrolateral medulla of Sprague-Dawley rats

post-stroke, leading to increased inflammatory response (Chang, 2014). Ang-(1-7) treatment dampened NOS species, cytokine profiles and chemoattractants within brain tissue of Sprague-Dawley rats following ET-1-MCAO (Regenhardt et al., 2013). Overall, stimulation of the MasR within the counter-regulatory axis of RAAS, has demonstrated similar neuroprotective qualities as AT_2R stimulation post-stroke.

As Ang-(1-7), which can also be derived from Ang-(1-9) as well as Ang II, has proven beneficial post-stroke, it has been proposed that Ang-(1-9) could be neuroprotective post-stroke. Unlike Ang-(1-7) which binds MasR, Ang-(1-9) is a functional ligand of the AT_2R and may play a protective role in cardiovascular disease (Flores-Muñoz et al., 2011, Flores-Muñoz et al., 2012, Cha et al., 2018, Ocaranza et al., 2006). The importance of the AT_2R in post-stroke outcome has been demonstrated in Agtr2 deficient mice, whereby Agtr2 deficiency led to increased infarct volume compared to wild-type mice post-stroke (Iwai et al., 2004, Iwanami et al., 2011). Although less is known about the therapeutic potential of Ang-(1-9) in ischaemic stroke, administration of this peptide in cardiac ischaemia models has provided evidence that it has potential to be therapeutic. Ang-(1-9) treatment led to decreased hypertrophy in cardiomyocytes and reduce cardiac fibrosis *in vivo* (Flores-Muñoz et al., 2012). Additionally, Ang-(1-9) has been shown to reduce levels of apoptosis within the lungs and reduce circulating proinflammatory cytokines/chemokines in rodent models of pulmonary arterial hypertension (Cha et al., 2018). In Sprague-Dawley rats subjected to myocardial infarction, circulating Ang-(1-9) levels and ACE2 activity were elevated after Enalapril (ACE inhibitor) treatment, while Ang-(1-7) concentrations were unchanged, suggesting Ang-(1-9) production through the catalysis of Ang II by ACE2 may be pertinent in preventing heart failure (Ocaranza et al., 2006). Therefore, increasing evidence in other CVDs supports the hypothesis that Ang-(1-9) may also play a protective role in experimental models of ischaemic stroke.

7.2 Hypotheses and aims

7.2.1 Hypotheses

- Experimental stroke occlusion duration will affect gene expression within brain tissue of male SHRSPs.

- Reperfusion duration will affect gene expression within brain tissue of male SHRSPs following experimental stroke.

- Therapeutic Ang-(1-9) EV treatment will alter gene expression within brain tissues of male SHRSPs following experimental stroke.

7.2.2 Aims

- Assess changes in gene expression in brain tissues of male SHRSPs at various occlusion durations of experimental stroke.

- Assess changes in gene expression in brain tissues of male SHRSPs at different reperfusion timepoints after experimental stroke.

- Determine whether therapeutic Ang-(1-9) EV treatment leads to changes in gene expression in brain tissues of male SHRSPs following experimental stroke.

7.3 Methods

Methods used in Chapter 7 can be found in Chapter 2 of this thesis and are outlined below:

2.1.2.1 Tail cuff plethysmography

2.1.2.2 Antihypertensive treatment

2.1.2.3 Burrhole and tMCAO surgery

2.1.2.5 Ang-(1-9) electroporated EV treatment

2.1.2.6 Neurological deficit score

2.1.2.7 Tissue collection

2.1.2.8 Historical samples

2.2.1.3 Size exclusion chromatography

2.2.1.5 Nanoparticle tracking analysis

2.2.1.6 EV electroporation loading

2.2.3.1 RNA extraction

2.2.3.2 Nanodrop quantification

2.2.3.4 cDNA synthesis

2.2.3.5 Quantitative real-time polymerase chain reaction

2.2.7 Statistical analysis

7.4 Results

7.4.1 Effects of stroke duration on gene expression in following tMCAO

In order to determine if stroke duration led to changes in gene expression within the brain, SHRSPs of approximately 18 weeks of age were subjected to tMCAO of 10- or 30-minutes duration and reperfusion was allowed for 1.5 hours post-stroke. Brains were sectioned into ipsi- and contra-lateral hemispheres before being further sectioned into infarct zone, peri-infarct zone, and remaining tissue. Within the contralateral zone, brain sections were taken that were representative of the location of ipsilateral infarct zone, peri-infarct zone, and remaining tissue.

VEGFA and VEGFB, influence vascular endothelial cell proliferation, migration and angiogenesis and are important factors in the brain post-stroke (Shibuya, 2011). The expression of VEGF has been shown to be altered following stroke, for example, serum VEGFA concentration were elevated in ischaemic and haemorrhagic stroke patients during the early subacute phase following stroke (Babkina et al., 2022). Further the administration of VEGF has proven beneficial post-stroke, wherein C57BL/6 mice treated with VEGFB following tMCAO showed reduced extravasation, indicative of blood brain barrier (BBB) integrity, and improved neurological outcome post-stroke (Jean LeBlanc et al., 2018).

Within the counter-regulatory axis of the RAAS, the G protein coupled receptor MasR, encoded by the Mas1 gene, is bound by Ang-(1-7) to stimulate vasodilation, influence sodium and water handling and nitric oxide release (Simões e Silva et al., 2013). The MasR agonist, Ang-(1-7), is produced by the breakdown of Ang II by ACE2. Preclinically, Sprague-Dawley rats subjected to ET-1 MCAO followed by intracerebroventricular delivery of Ang-(1-7) reduced infarct volume and improved neurological outcomes (Regenhardt et al., 2013). Concentration of Ang-(1-7), Mas1 and Ace2 expression were increased in the cerebral ischaemic cortex of Sprague-Dawley rats following pMCAO (Lu et al., 2013).

Runt-related transcription factor (RUNX) family transcription factor 1, RUNX1, heterodimerises with core binding factor β (CBFβ), following which RUNX1 may bind to DNA (Warren et al., 2000). RUNX1 regulates genes associated with haematopoiesis and mutations within RUNX1 gene are associated with leukaemia (Ichikawa et al., 2013). RUNX1 has also proven crucial for neuronal cell growth, whereby, treatment with RUNX1 inhibitor RO5-3335 prevented proliferation of C57BL/6J mice neurosphere cultures

(Logan et al., 2015). In Sprague-Dawley rats subjected to intracranial haemorrhage, miRNA-18 was found to target RUNX1 which was subsequently associated with increased cerebral injury and increased BBB permeability, due to reduced expression of tight junction proteins (Ren et al., 2021). Therefore, the expression of VEGFA, VEGFB, Mas1, RUNX1 and ACE2 were assessed in brain tissue following tMCAO.

VEGFA expression was similar in all brain regions within both the ipsi- and contra-lateral hemisphere at both 10- and 30-minute occlusion duration plus 1.5 hours of reperfusion. (Figure 7.1). VEGFB expression was comparable in all brain regions within both the ipsi- and contra-lateral hemispheres at both 10- and 30-minute occlusion duration plus 1.5 hours of reperfusion (Figure 7.2). Mas1 expression was comparable in all brain regions within the ipsilateral hemisphere at both 10- and 30-minute occlusion duration plus 1.5 hours of reperfusion (Figure 7.3 A). Mas1 expression was similar between brain regions in both sham animals and animals that had undergone 10 minutes of occlusion plus 1.5 hours of reperfusion (Figure 7.3 B). Within the remaining tissue (8.42 ± 0.45; dCT $\pm$ SEM) of the contralateral hemisphere following 30 minutes of tMCAO plus 1.5 hours of reperfusion, Mas1 expression was downregulated compared to the infarct zone (4.08 ± 0.31, $p<0.01$) (Figure 7.3 B). ACE2 expression was comparable in all brain regions within both the ipsi- and contra-lateral hemisphere at both 10- and 30-minute occlusion duration plus 1.5 hours of reperfusion. (Figure 7.4). RUNX1 expression was similar in all brain regions within both the ipsi- and contra-lateral hemispheres at both 10- and 30-minute occlusion duration plus 1.5 hours of reperfusion. (Figure 7.5).

Figure 7.1 Effects of stroke duration and VEGFA expression.
qPCR for VEGFA expression in the ipsilateral (A) and contralateral (B) brain tissue after experimental stroke at either 10- or 30-minute occlusion duration. VEGFA expression was normalised to UBC housekeeper. Brain tissue analysed included infarcted zone (infarct), peri-infarct zone (peri-infarct), and remaining tissue (remainder). Delta cycle threshold (dCT) demonstrated the abundance of gene expression and error bars represent standard error of the mean (n=3, p>0.05, Repeated measures ANOVA with post-hoc Tukey's multiple comparison correction).

Figure 7.2 Effects of stroke duration and VEGFB expression.
qPCR for VEGFB expression in the ipsilateral (A) and contralateral (B) brain tissue after experimental stroke at either 10- or 30-minute occlusion duration. VEGFB expression was normalised to UBC housekeeper. Brain tissue analysed included infarcted zone (infarct), peri-infarct zone (peri-infarct), and remaining tissue (remainder). Delta cycle threshold (dCT) demonstrated the abundance of gene expression and error bars represent standard error of the mean (n=3, p>0.05, Repeated measures ANOVA with post-hoc Tukey's multiple comparison correction).

Figure 7.3 Effects of stroke duration and Mas1 expression.
qPCR for Mas1 expression in the ipsilateral (A) and contralateral (B) brain tissue after experimental stroke at either 10- or 30-minute occlusion duration. Mas1 expression was normalised to UBC housekeeper. Brain tissue analysed included infarcted zone (infarct), peri-infarct zone (peri-infarct), and remaining tissue (remainder). Delta cycle threshold (dCT) demonstrated the abundance of gene expression and error bars represent standard error of the mean (n=3, **p<0.01, Repeated measures ANOVA with post-hoc Tukey's multiple comparison correction).

Figure 7.4 Effects of stroke duration and ACE2 expression.
qPCR for ACE2 expression in the ipsilateral (A) and contralateral (B) brain tissue after experimental stroke at either 10- or 30-minute occlusion duration. ACE2 expression was normalised to UBC housekeeper. Brain tissue analysed included infarcted zone (infarct), peri-infarct zone (peri-infarct), and remaining tissue (remainder). Delta cycle threshold (dCT) demonstrated the abundance of gene expression and error bars represent standard error of the mean (n=3, p>0.05, Repeated measures ANOVA with post-hoc Tukey's multiple comparison correction).

Figure 7.5 Effects of stroke duration and RUNX1 expression.
qPCR for RUNX1 expression in the ipsilateral (A) and contralateral (B) brain tissue after experimental stroke at either 10- or 30-minute occlusion duration. RUNX1 expression was normalised to UBC housekeeper. Brain tissue analysed included infarcted zone (infarct), peri-infarct zone (peri-infarct), and remaining tissue (remainder). Delta cycle threshold (dCT) demonstrated the abundance of gene expression and error bars represent standard error of the mean (n=3, p>0.05, Repeated measures ANOVA with post-hoc Tukey's multiple comparison correction).

7.4.2 Effects of reperfusion duration following tMCAO on gene expression

To identify if reperfusion time post-stroke leads to changes in gene expression within the brain, SHRSPs of approximately 18 weeks of age were subjected to tMCAO of 10-minute duration and reperfusion was allowed for 1.5- or 4-hours post-stroke. Gene expression was unaltered following 10 minutes of occlusion followed by either 1.5- or 4- hours of reperfusion post-stroke. VEGFA expression was similar in all brain regions within both the ipsi- and contra-lateral hemisphere following 10 minutes of occlusion plus either 1.5- or 4-hours reperfusion post-stroke (Figure 7.6). VEGFB expression was similar in all brain regions within both the ipsi- and contra-lateral hemisphere following 10 minutes of occlusion plus either 1.5- or 4-hours reperfusion post-stroke (Figure 7.7). Mas1 expression was similar in all brain regions within both the ipsi- and contra-lateral hemisphere following 10 minutes of occlusion plus either 1.5- or 4-hours reperfusion post-stroke (Figure 7.8). ACE2 expression was similar in all brain regions within the ipsilateral hemisphere following 10 minutes of occlusion plus either 1.5- or 4-hours reperfusion post-stroke (Figure 7.9 A). ACE2 expression was similar within all brain regions following 10 minutes occlusion plus 1.5 hours of reperfusion compared to non-stroke controls (Figure 7.9 B). ACE2 expression was downregulated in the peri-infarct zone of the contralateral hemisphere 10 minutes occlusion plus 4 hours of reperfusion (4.76 ± 0.15; $p<0.05$) compared to 10 minutes occlusion plus 1.5 hours of reperfusion (3.77 ± 0.20) (Figure 7.9 B). RUNX1 expression was similar in all brain regions within both the ipsi- and contra-lateral hemisphere following 10 minutes of occlusion plus either 1.5- or 4-hours reperfusion post-stroke (Figure 7.10).
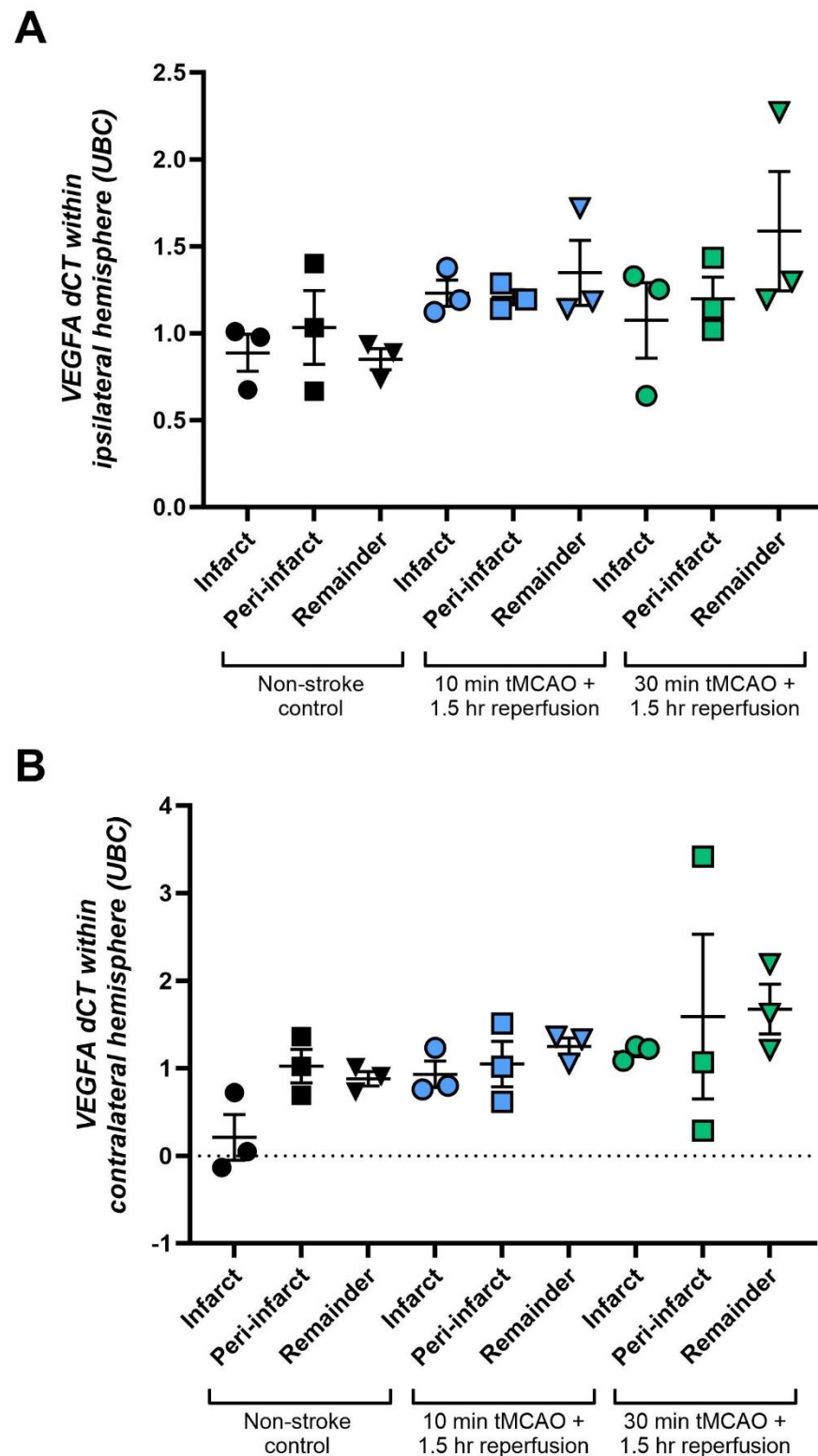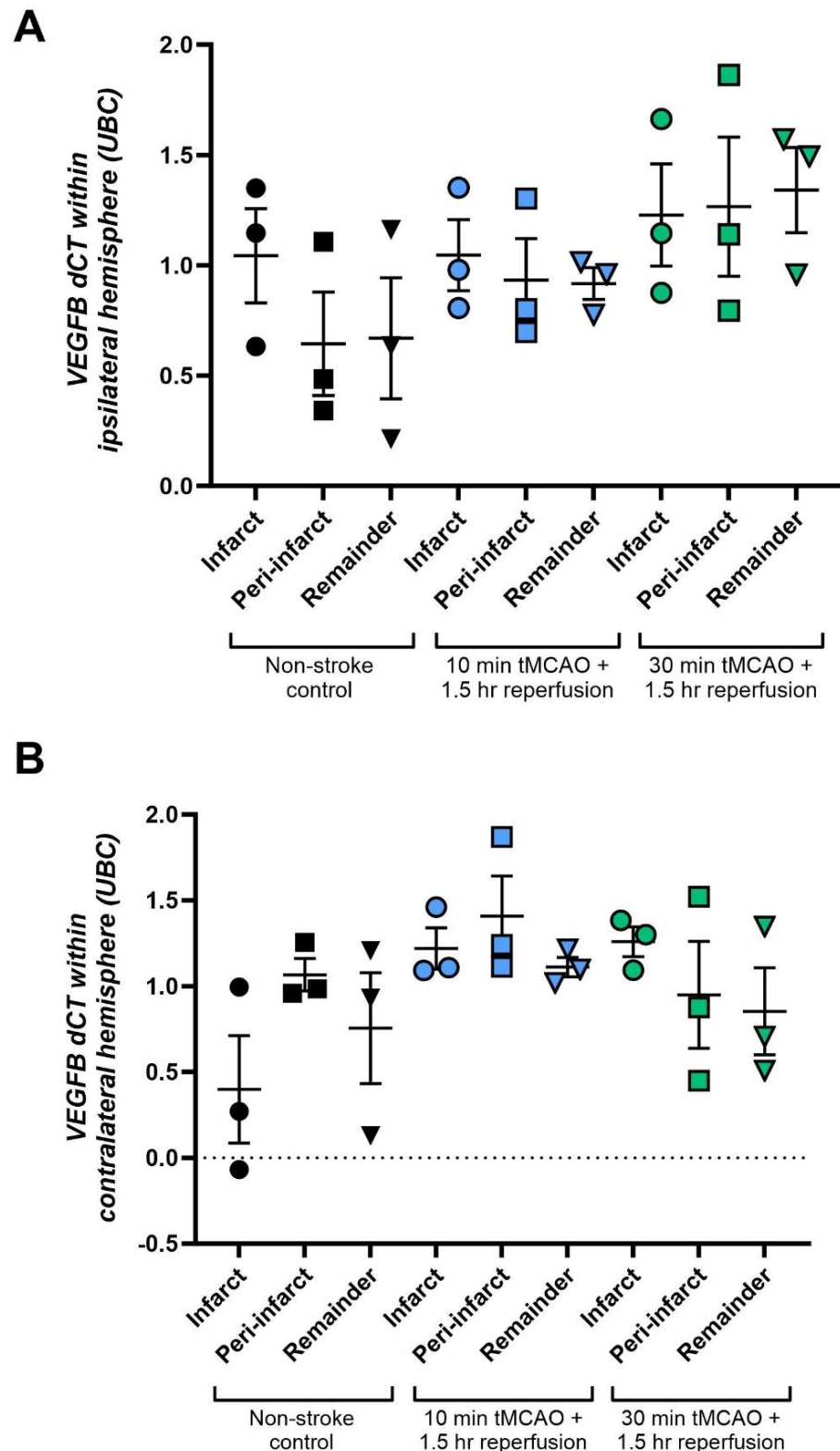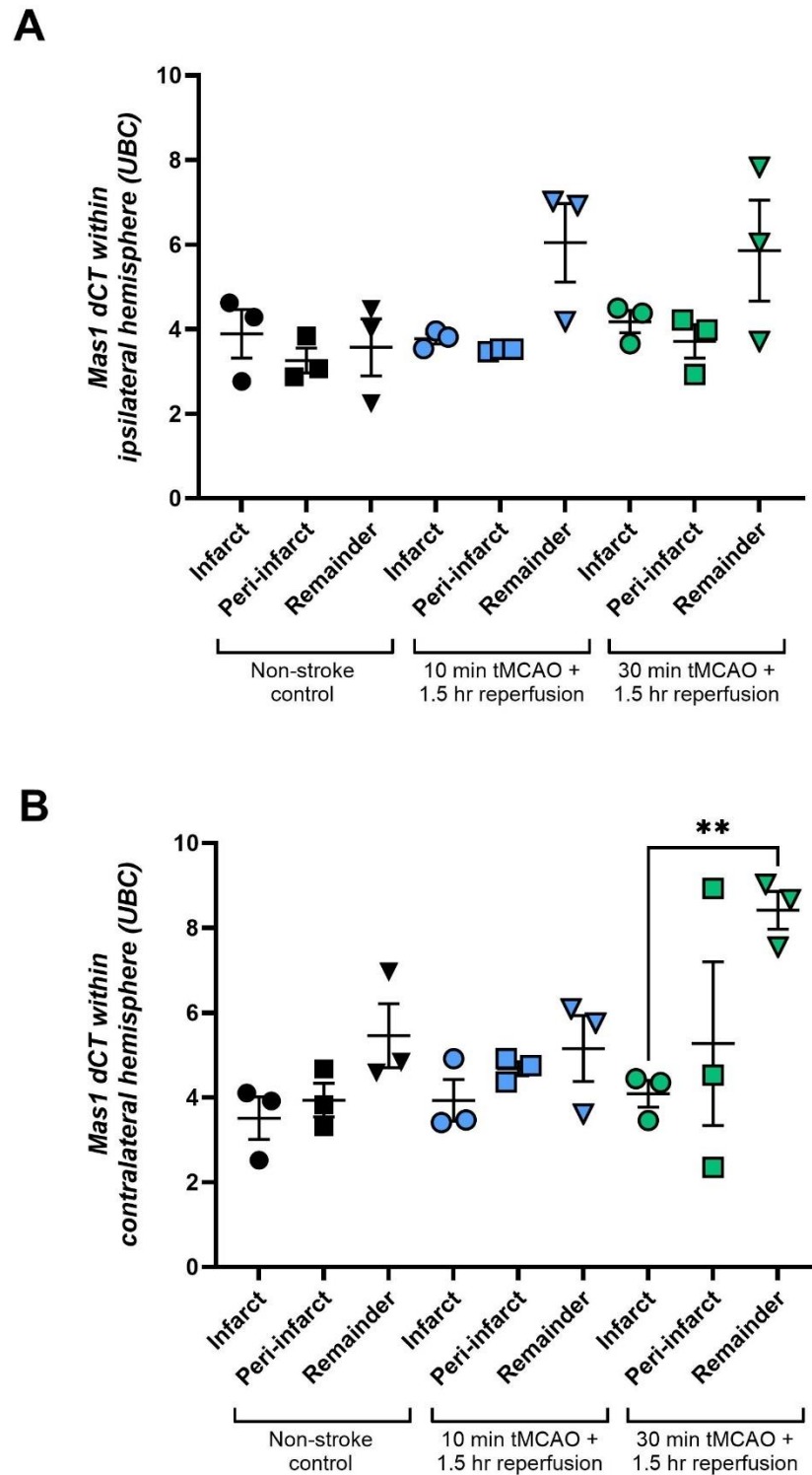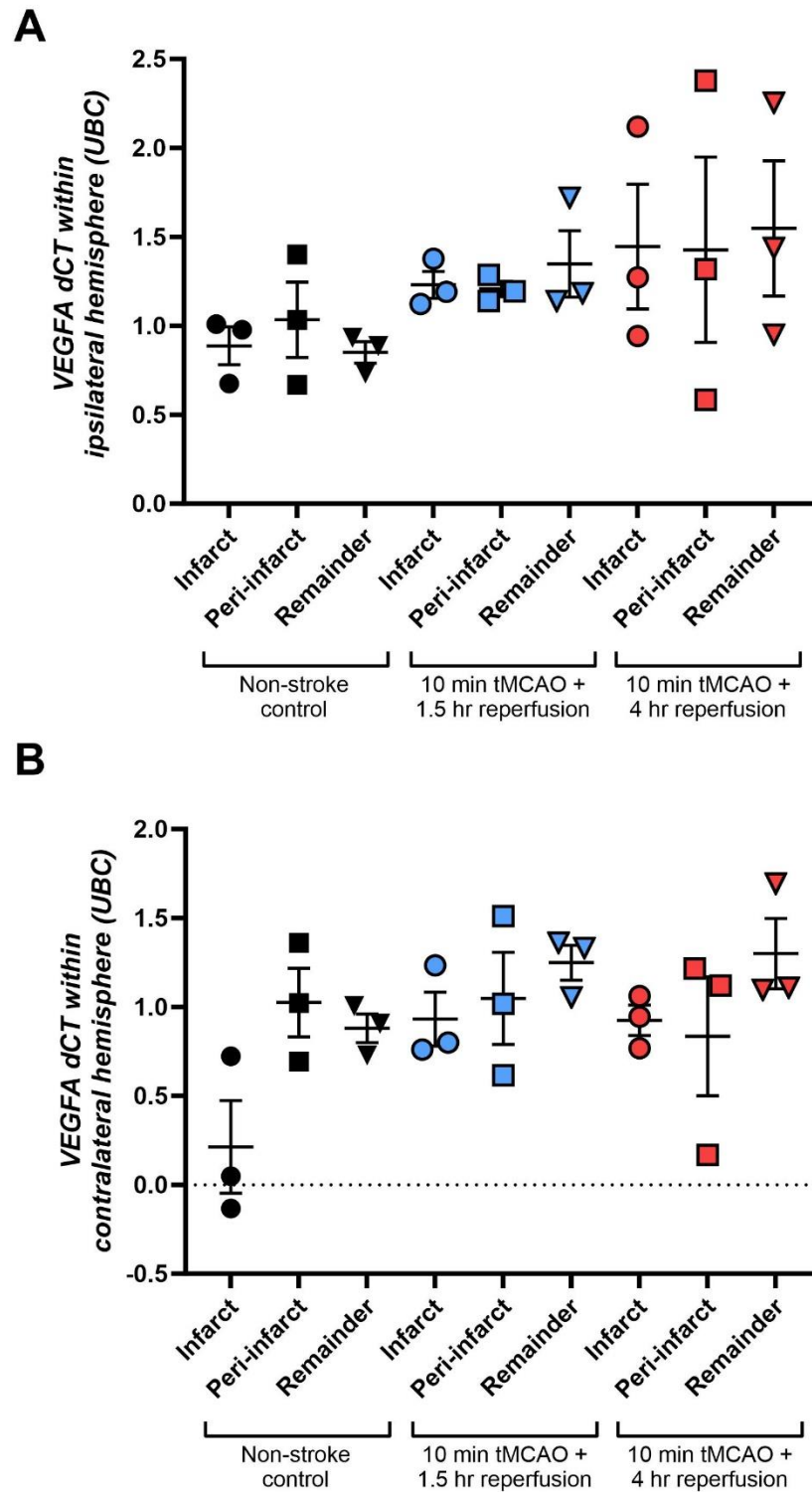
Figure 7.6 Effects of reperfusion time and VEGFA expression.
qPCR for VEGFA expression in the ipsilateral (A) and contralateral (B) brain tissue after experimental stroke after 1.5- or 4-hours reperfusion duration. VEGFA expression was normalised to UBC housekeeper. Brain tissue analysed included infarcted zone (infarct), peri-infarct zone (peri-infarct), and remaining tissue (remainder). Delta cycle threshold (dCT) demonstrated the abundance of gene expression and error bars represent standard error of the mean (n=3, p>0.05, Repeated measures ANOVA with post-hoc Tukey's multiple comparison correction).
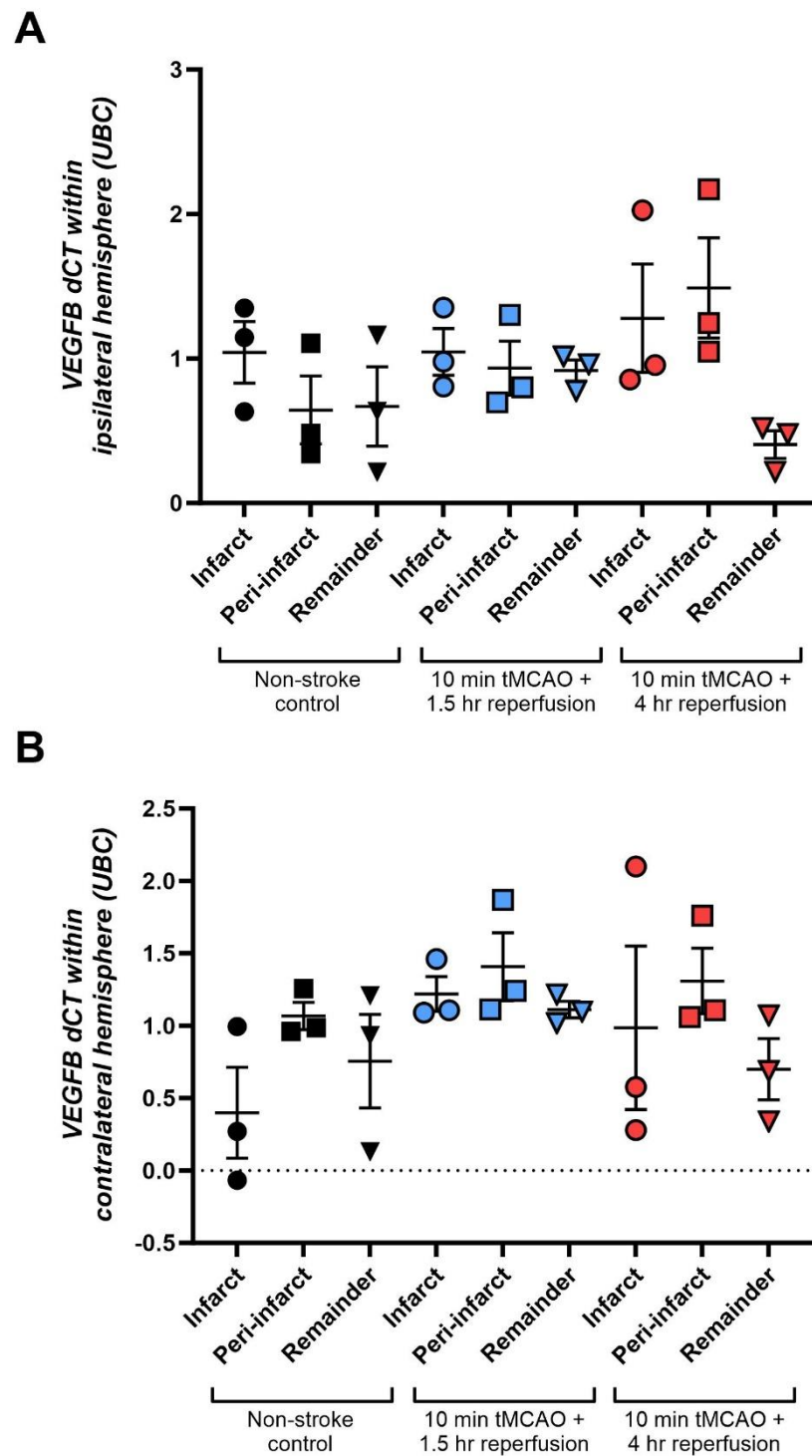
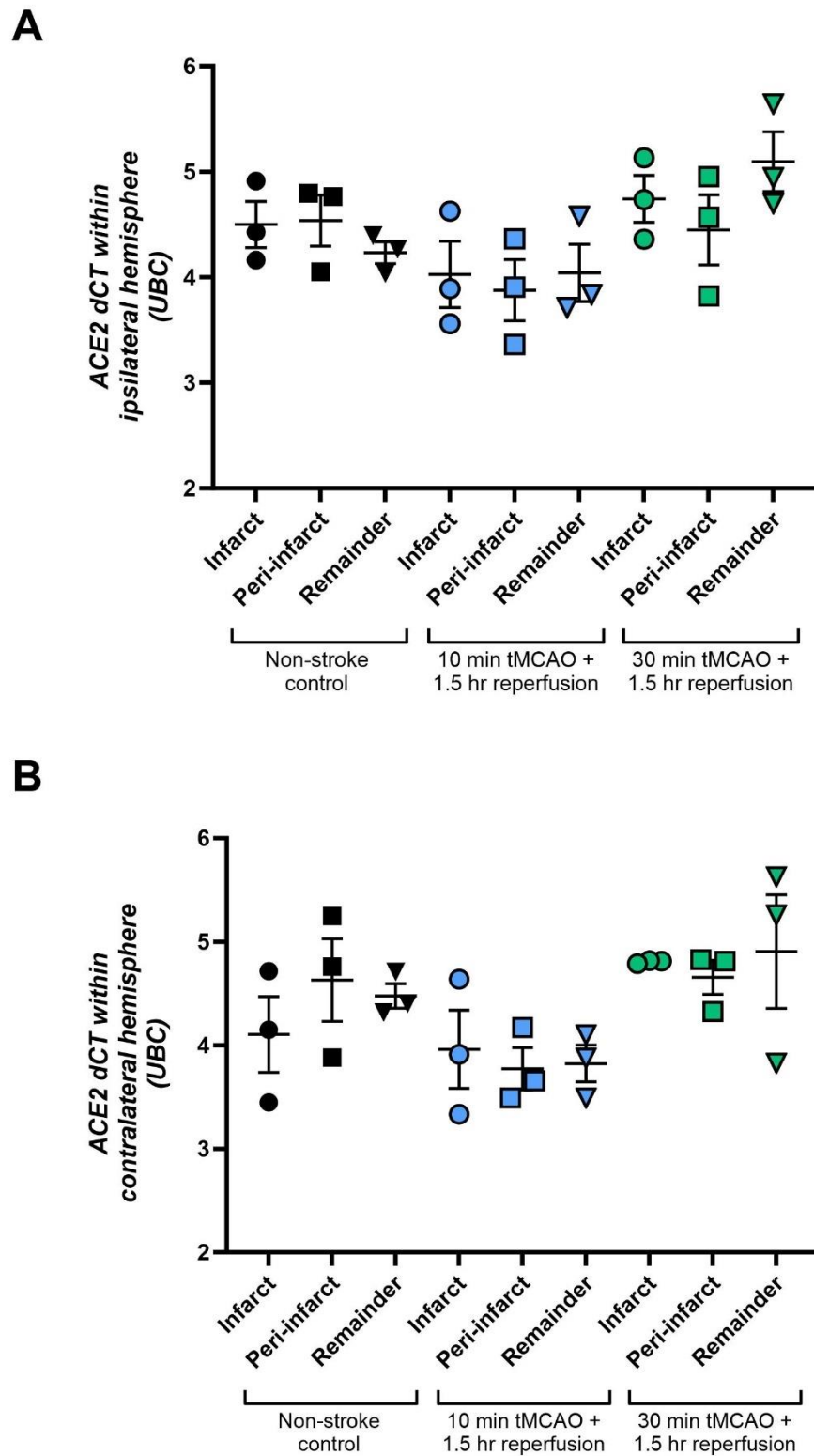**Figure 7.7 Effects of reperfusion time and VEGFB expression.**
qPCR for VEGFB expression in the ipsilateral (A) and contralateral (B) brain tissue after experimental stroke after 1.5- or 4-hours reperfusion duration. VEGFB expression was normalised to UBC housekeeper. Brain tissue analysed included infarcted zone (infarct), peri-infarct zone (peri-infarct), and remaining tissue (remainder). Delta cycle threshold (dCT) demonstrated the abundance of gene expression and error bars represent standard error of the mean (n=3, p>0.05, Repeated measures ANOVA with post-hoc Tukey's multiple comparison correction).
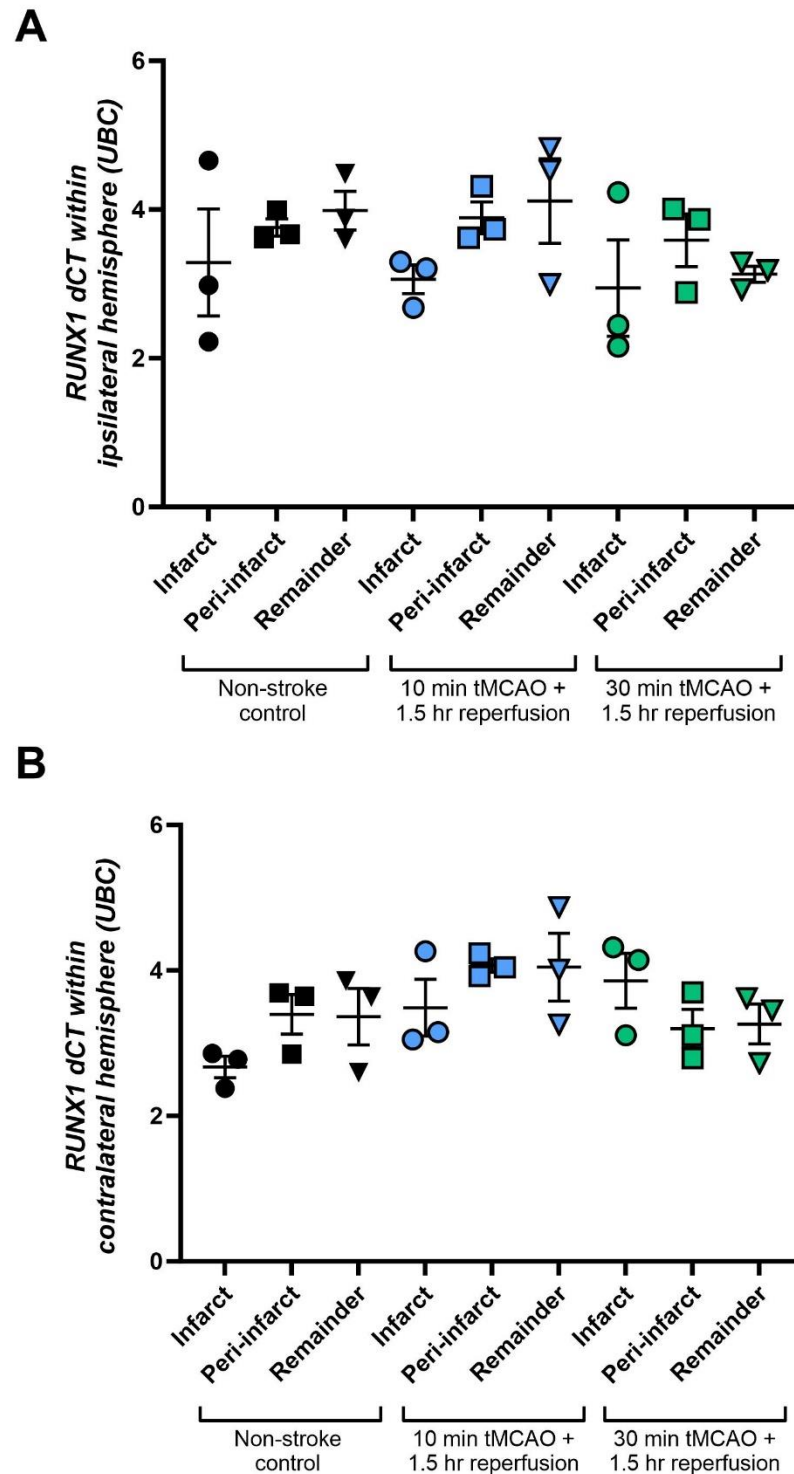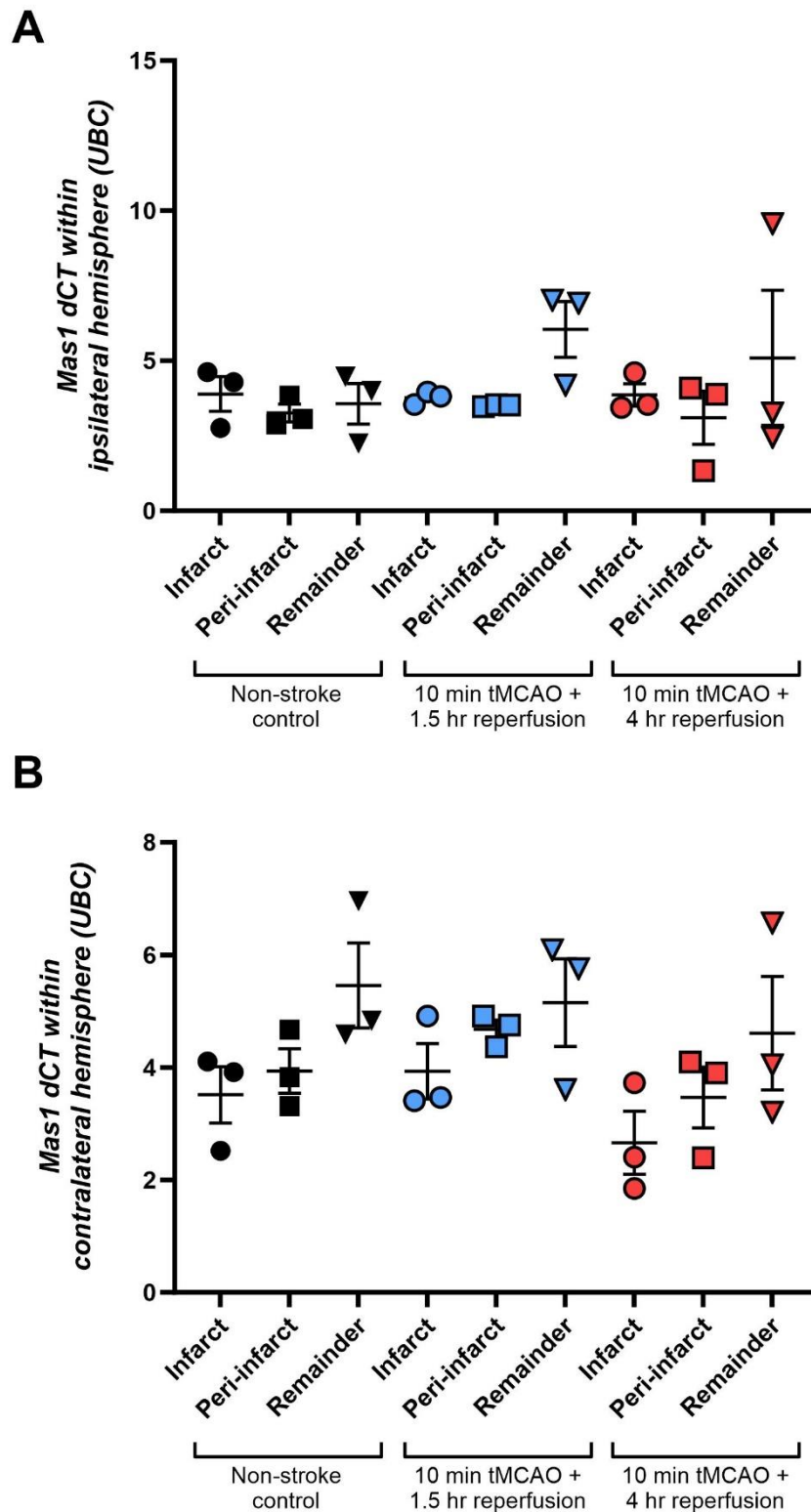
Figure 7.8 Effects of reperfusion time and Mas1 expression.
qPCR for Mas1 expression in the ipsilateral (A) and contralateral (B) brain tissue after experimental stroke after 1.5- or 4-hours reperfusion duration. Mas1 expression was normalised to UBC housekeeper. Brain tissue analysed included infarcted zone (infarct), peri-infarct zone (peri-infarct), and remaining tissue (remainder). Delta cycle threshold (dCT) demonstrated the abundance of gene expression and error bars represent standard error of the mean (n=3, p>0.05, Repeated measures ANOVA with post-hoc Tukey's multiple comparison correction).
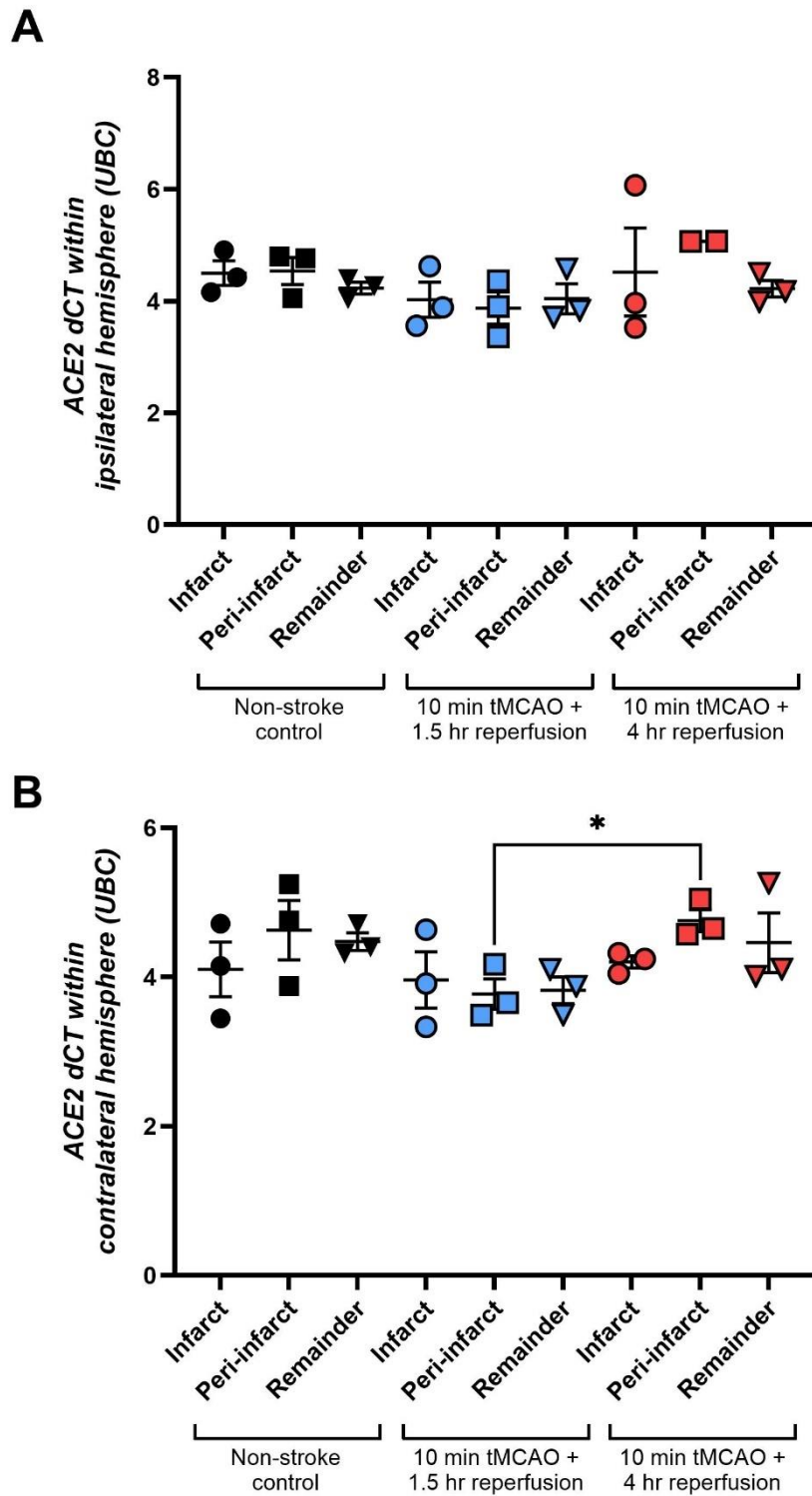
Figure 7.9 Effects of reperfusion time and ACE2 expression.
qPCR for ACE2 expression in the ipsilateral (A) and contralateral (B) brain tissue after experimental stroke after 1.5- or 4-hours reperfusion duration. ACE2 expression was normalised to UBC housekeeper. Brain tissue analysed included infarcted zone (infarct), peri-infarct zone (peri-infarct), and remaining tissue (remainder). Delta cycle threshold (dCT) demonstrated the abundance of gene expression and error bars represent standard error of the mean. Outliers were identified using ROUT test at an aggressive value of Q=1%. (n=2-3, p>0.05, Repeated measures ANOVA with post-hoc Tukey's multiple comparison correction or mixed effects ANOVA with post-hoc Tukey's multiple comparison correction).

Figure 7.10 Effects of reperfusion time and RUNX1 expression.
qPCR for RUNX1 expression in the ipsilateral (A) and contralateral (B) brain tissue after experimental stroke after 1.5- or 4-hours reperfusion duration. RUNX1 expression was normalised to UBC housekeeper. Brain tissue analysed included infarcted zone (infarct), peri-infarct zone (peri-infarct), and remaining tissue (remainder). Delta cycle threshold (dCT) demonstrated the abundance of gene expression and error bars represent standard error of the mean (n=3, p>0.05, Repeated measures ANOVA with post-hoc Tukey's multiple comparison correction).

7.4.3 Effects of tMCAO on functional outcomes

To better reflect the drug regime of a patient at a higher risk of stroke occurrence, SHRSPs were prophylactically treated with antihypertensives for 2 weeks prior to stroke surgery in line with established protocols for SHRSP models (Koh-Tan et al., 2009). To achieve a reduction in blood pressure, hydralazine hydrochloride (16 mg/kg/day) and hydrochlorothiazide (16 mg/kg/day) were administered orally within additional wet food. Mean systolic blood pressure was reduced from 207.6 ± 2.1 mmHg (mean $\pm$ SEM) to 184.1 ± 3.1 mmHg following antihypertensive treatment ($p<0.0001$) (Figure 7.11).

Preliminary stroke surgeries were accompanied with a 10-day post-stroke assessment period. The number of sham and tMCAO surgeries, along with the survival time post-surgery are outlined in Table 7.1. Generally, two stroke surgeries were conducted per surgical day, one tMCAO and one sham surgery. Initially four animals successfully underwent either tMCAO or sham surgery and survived 10 days following surgery. However, after this point, all animals undergoing tMCAO had a significant decline in their health meaning that they were humanely killed prior to the 10-day assessment timepoint, with most needing to be humanely killed 24-48 hours following tMCAO resulting in group sizes which were not statistically powered. To note, only two animal died overnight following tMCAO surgery. Of the four animals that successfully made it to the 10-day assessment time point, changes in body weight were observed as a measure of stroke outcome. From the data provided there was a trend towards a sharp decline in body weight post-stroke compared to sham controls (Figure 7.12).

To assess the neurological and motor deficits associated with stroke, animals were assessed using a 30-point neuroscore at baseline, days 3, 7 and 10 post-surgery. As expected, there was a trend towards a decline in neuroscore on day 3 post-surgery in stroke animals. After day 3 there was a trend towards an improvement in neuroscore at days 7 and 10 post-surgery in stroke animals. There was a trend towards maintained neuroscore in sham animals at all assessment timepoint post-surgery (Figure 7.13).
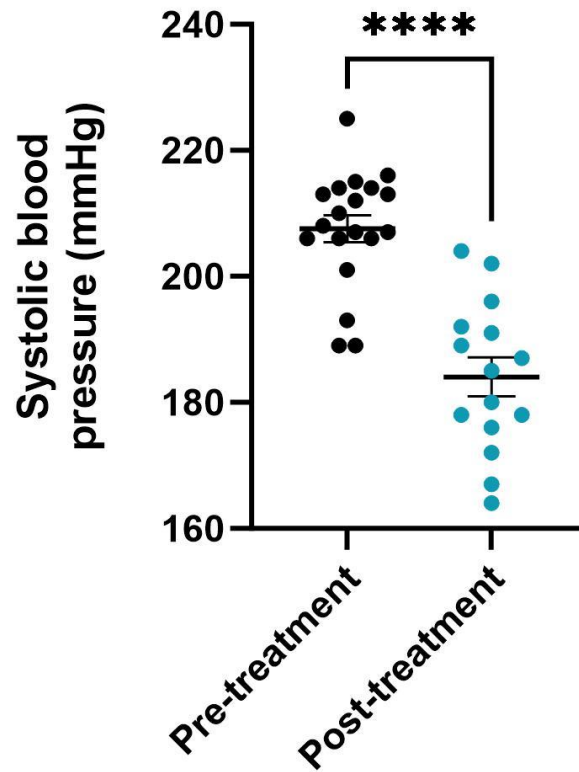
Figure 7.11 Effects of antihypertensive treatment on SHRSP systolic blood pressure. Systolic blood pressure was measured in ~18-week-old male SHRSPs using tail cuff plethysmography (mmHg). Animals were allowed two acclimatisation sessions with the apparatus. Graph depicts systolic blood pressure before and after 2-week antihypertensive treatment. Error bars denote SEM of systolic blood pressure (n=15-19).

Table 7.1 Effects of tMCAO on survival time.
SHRSPs of approximately 18 weeks in age were subjected to tMCAO or sham surgery with burrhole surgery. Post-tMCAO animals were treated with vehcole control of Angiotenin-(1-9) electroporated EVs. The duration of survial ranged from 24 hours to 10 days post-surgery depending on experimental end-point. Anaesthetic

Animal ID	Surgery type	Survival time post-stroke	Reason for death
C1910	Sham + burrhole	10 days	Completion to 10-day timepoint
C1911	tMCAO + burrhole	48 hours	Animal exceeded humane endpoints and was humanely killed
C1913	tMCAO + burrhole	10 days	Completion to 10-day timepoint
C1940	tMCAO + burrhole	10 days	Completion to 10-day timepoint
C1941	tMCAO + burrhole	N/A	Death due to anaesthetic
C1942	Sham + burrhole	10 days	Completion to 10-day timepoint
C1949	tMCAO + burrhole	24 hours	Animal exceeded humane endpoints and was humanely killed
C1950	tMCAO + burrhole	N/A	Found dead overnight
C1965	tMCAO + burrhole	24 hours	Animal exceeded humane endpoints and was humanely killed
C1966	tMCAO + burrhole	N/A	Found dead overnight
C1967	Sham + burrhole	24 hours	Animal exceeded humane endpoints and was humanely killed
C1968	Sham + burrhole	8 days	Completion to 8-day modified timepoint
C1969	Sham + burrhole	8 days	Completion to 8-day modified timepoint
C1970	tMCAO + burrhole	24 hours	Completion to 24 hour modified timepoint
C1971	tMCAO + burrhole	24 hours	Completion to 24 hour modified timepoint
C2004	Sham + burrhole	24 hours	Completion to 24 hour modified timepoint
C2005	Sham + burrhole	24 hours	Completion to 24 hour modified timepoint
C2006	tMCAO + burrhole	24 hours	Completion to 24 hour modified timepoint
C2007	tMCAO + burrhole	24 hours	Completion to 24 hour modified timepoint
C2016	tMCAO + burrhole	24 hours	Completion to 24 hour modified timepoint
C2017	tMCAO + burrhole	24 hours	Completion to 24 hour modified timepoint
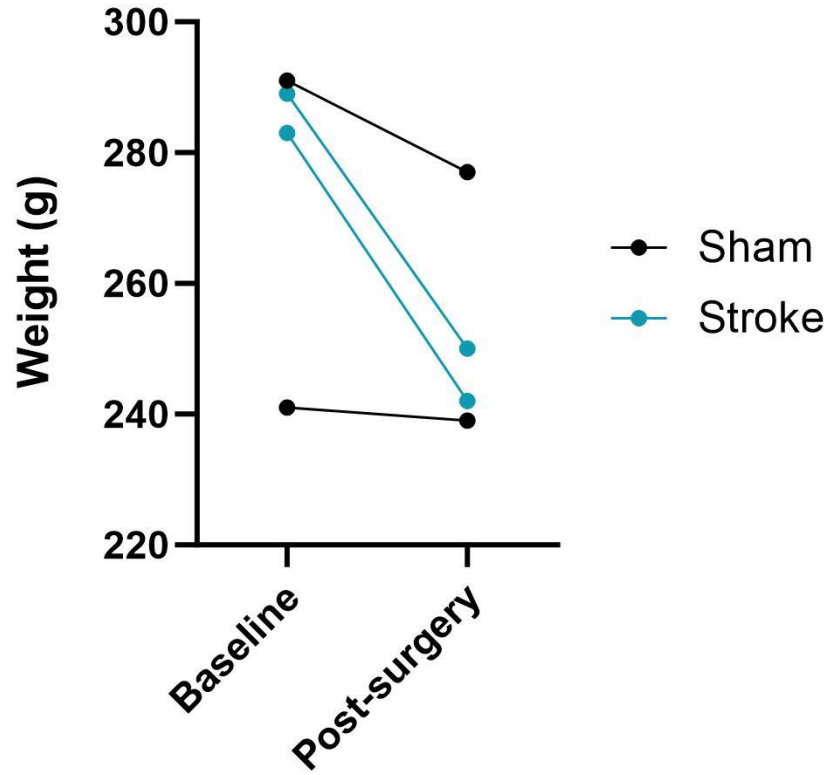
Figure 7.12 Effects of burr hole and tMCAO on SHRSP weight loss.
Body weight of SHRSPs was measured before and 10 days after either sham or tMCAO surgery. Graph represents individual animals including those that underwent sham and stroke surgery while the trendline demonstrates changes in weight at each timepoint after surgery (n=2).
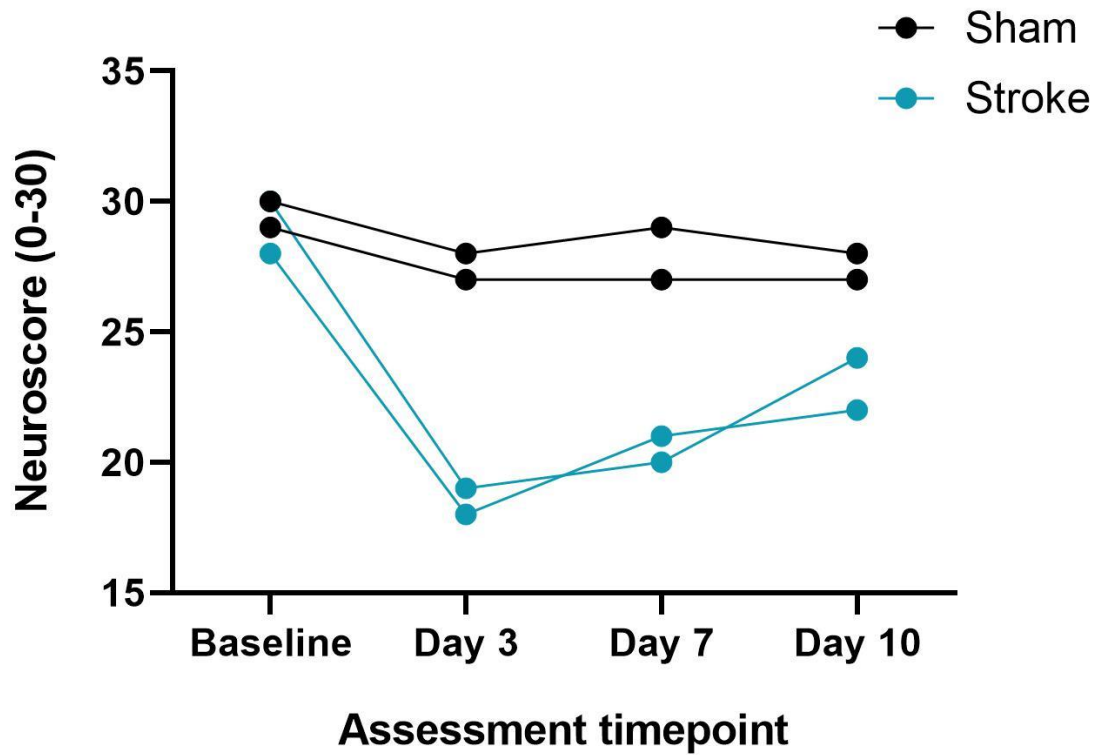
Figure 7.13 Effects of burr hole and tMCAO surgery on neuroscore.
Neuroscoring (no deficit = 30) was performed at baseline and days 3, 7 and 10 post-tMCAO. Neuroscore points represent individual animals including those that underwent sham and stroke surgery. Trendline demonstrates changes in neuroscore at each timepoint after surgery (n=2).

7.4.4 Distribution of body weight between treatment groups prior to experimental stroke surgery

Prior to EV treatment SHRSP body weight was assessed to ensure body weight was similar between groups. There was no difference in mean body weight between sham (292.0 ± 6.7 g; mean weight $\pm$ SEM), vehicle treated (283.0 ± 9.1 g), or Ang-(1-9) loaded EV treated (287.5 ± 7.5 g) animals (Figure 7.14).
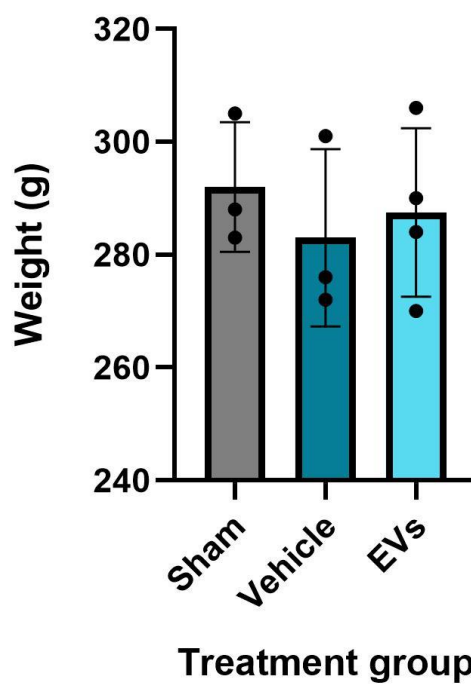
Figure 7.14 Weight distribution within treatment groups before experimental stroke. Body weight of SHRSPs was measured prior to either sham or tMCAO surgery. Graph represents mean body weight of animals that underwent sham and stroke surgery that were ultimately assigned to EV or vehicle treatment. Error bars donate SEM (n=3-4, p>0.05, One-way AVOVA with post-hoc Dunnett's multiple comparison correction).

7.4.5 Expression of housekeeping genes after intranasal delivery of Ang-(1-9) loaded EVs in experimental stroke models

Ang-(1-9) electroporated EVs [Ang-(1-9) EVs] treatment was assessed to determine whether Ang-(1-9) may alter gene expression following tMCAO. Following tMCAO, a total of 2.5×10^{10} of Ang-(1-9) EVs or equivalent volume of vehicle (48 µL of PBS) was administered intranasally to tMCAO rats on one occasion following tMCAO. Twenty-four hours following tMCAO surgery, animals were humanely killed and brain tissue was collected, as documented in depth in the methods chapter. Using qPCR, a stable housekeeping gene was established from a bank of possible genes in order to determine changes in gene expression post-stroke after Ang-(1-9) EV treatment. Samples were grouped into brain region and treatment to create six subgroups: ipsi- and contra-lateral infarct zone, peri-infarct zone and remaining brain tissue.

The CT ± SD values of individual subgroups for β-actin expression were: ipsilateral infarct zone 25.15 ± 1.11, ipsilateral peri-infarct zone 24.28 ± 0.35, ipsilateral remaining tissue 24.55 ± 0.38, contralateral infarct zone 24.80 ± 0.35, contralateral peri-infarct zone 24.68 ± 0.23, and contralateral remaining tissue 25.06 ± 0.38 (Figure 7.15 A). β-actin provided an overall mean CT value of 24.75 across all samples with a standard deviation of 0.60 (Figure 7.15 B).

The CT ± SD values of individual subgroups for B2M expression were as follows: ipsilateral infarct zone 27.45 ± 0.85, ipsilateral peri-infarct zone 27.72 ± 0.48, ipsilateral remaining tissue 27.41 ± 0.61, contralateral infarct zone 27.81 ± 0.67, contralateral peri-infarct zone 28.02 ± 0.42, and contralateral remaining tissue 27.32 ± 0.47 (Figure 7.16 A). B2M provided an overall mean CT value of 27.61 across all samples with a standard deviation of 0.62 (Figure 7.16 B).

The CT ± SD values of individual subgroups for UBC expression were: ipsilateral infarct zone 30.91 ± 1.27, ipsilateral peri-infarct zone 30.68 ± 0.59, ipsilateral remaining tissue 30.47 ± 0.57, contralateral infarct zone 30.84 ± 0.64, contralateral peri-infarct zone 31.00 ± 0.57, and contralateral remaining tissue 30.56 ± 0.52 (Figure 7.17 A). UBC provided an overall mean CT value of 30.74 across all samples with a standard deviation of 0.73 (Figure 7.17 B).

The CT ± SD values of individual subgroups for GAPDH expression were: ipsilateral infarct zone 28.55 ± 1.40, ipsilateral peri-infarct zone 27.88 ± 0.73, ipsilateral remaining tissue 28.30 ± 0.58, contralateral infarct zone 28.08 ± 0.62, contralateral peri-infarct zone 28.09 ± 0.62, and contralateral remaining tissue 28.03 ± 0.60 (Figure 7.18 A). GAPDH

provided an overall mean CT value of 28.15 across all samples with a standard deviation of 0.81 (Figure 7.18 B).

The CT ± SD values of individual subgroups for HPRT1 expression were: ipsilateral infarct zone 30.93 ± 1.58, ipsilateral peri-infarct zone 30.16 ± 0.77, ipsilateral remaining tissue 30.39 ± 0.59, contralateral infarct zone 30.39 ± 0.67, contralateral peri-infarct zone 30.49 ± 0.77, and contralateral remaining tissue 30.24 ± 0.68 (Figure 7.19 A). HPRT1 provided an overall mean CT value of 30.43 across all samples with a standard deviation of 0.90 (Figure 7.19 B).

Overall, β-actin provided the smallest standard deviation from mean CT value and so was chosen as the housekeeping gene required to quantify the expression of genes of interest.

A

B

Figure 7.15 Assessment of β-actin as a stable housekeeping gene in brain tissues after intranasal delivery of EV post-tMCAO.
qPCR for β-actin expression in the ipsilateral and contralateral brain tissue after experimental stroke and therapeutic Ang-(1-9) EV treatment. Cycle threshold (CT) demonstrated the abundance of gene expression. (A) Brain tissue analysed included infarcted zone (infarct), peri-infarct zone (peri-infarct), and remaining tissue (remainder). Error bars represent standard error of the mean (SEM, n=3-4per treatment group). (B) Individual samples were grouped to demonstrate variation in dCT between samples. Error bars denote standard deviation (SD, n=3-4 per treatment group).

Figure 7.16 Assessment of B2M as a stable housekeeping gene in brain tissues after intranasal delivery of EV post-tMCAO.
qPCR for B2M expression in the ipsilateral and contralateral brain tissue after experimental stroke and therapeutic Ang-(1-9) EV treatment. Cycle threshold (CT) demonstrated the abundance of gene expression. (A) Brain tissue analysed included infarcted zone (infarct), peri-infarct zone (peri-infarct), and remaining tissue (remainder). Error bars represent standard error of the mean (SEM, n=3-4per treatment group). (B) Individual samples were grouped to demonstrate variation in dCT between samples. Error bars denote standard deviation (SD, n=3-4 per treatment group).
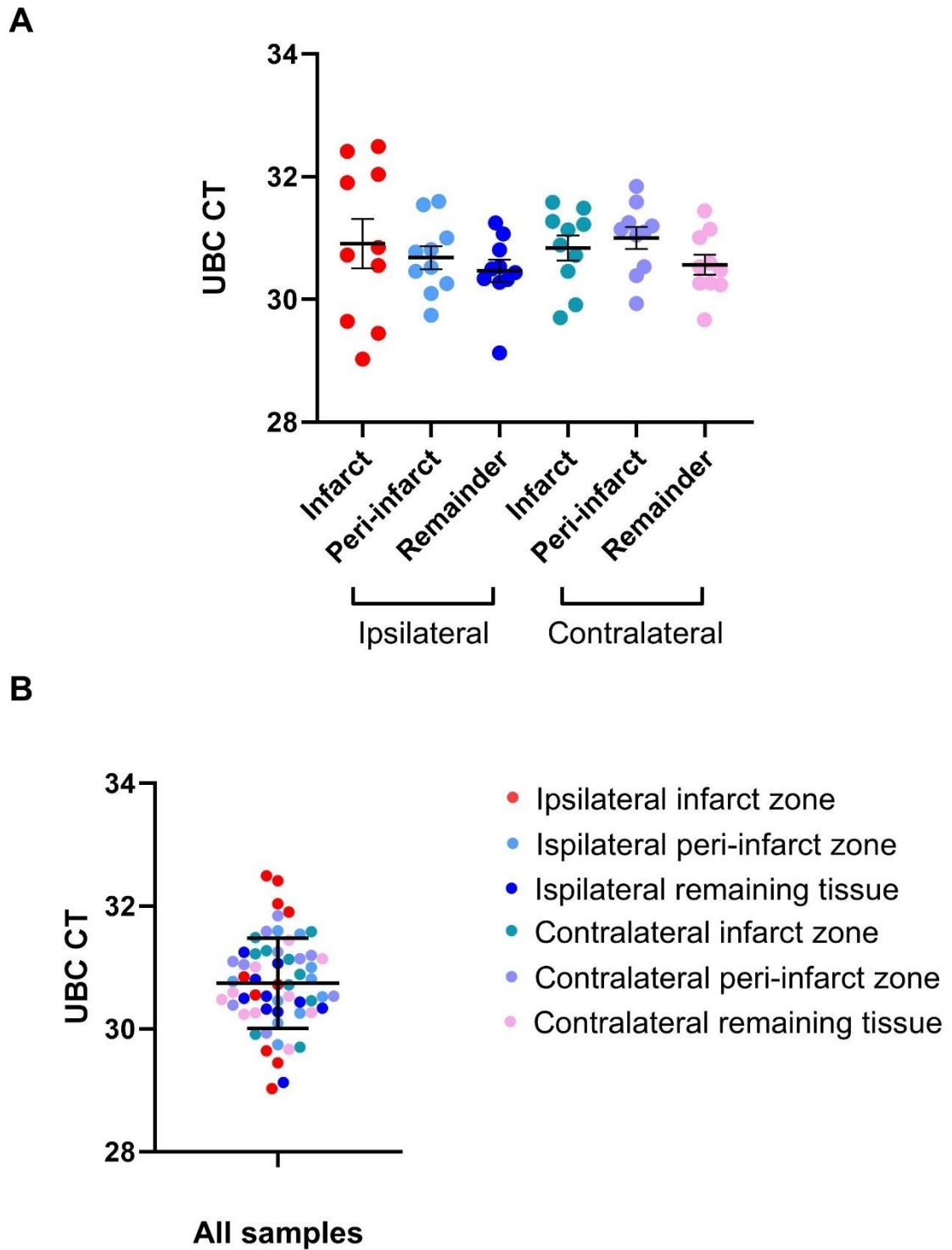
Figure 7.17 Assessment of UBC as a stable housekeeping gene in brain tissues after intranasal delivery of EV post-tMCAO.
qPCR for UBC expression in the ipsilateral and contralateral brain tissue after experimental stroke and therapeutic Ang-(1-9) EV treatment. Cycle threshold (CT) demonstrated the abundance of gene expression. (A) Brain tissue analysed included infarcted zone (infarct), peri-infarct zone (peri-infarct), and remaining tissue (remainder). Error bars represent standard error of the mean (SEM, n=3-4per treatment group). (B) Individual samples were grouped to demonstrate variation in dCT between samples. Error bars denote standard deviation (SD, n=3-4 per treatment group).

Figure 7.18 Assessment of GAPDH as a stable housekeeping gene in brain tissues after intranasal delivery of EV post-tMCAO.
qPCR for GAPDH expression in the ipsilateral and contralateral brain tissue after experimental stroke and therapeutic Ang-(1-9) EV treatment. Cycle threshold (CT) demonstrated the abundance of gene expression. (A) Brain tissue analysed included infarcted zone (infarct), peri-infarct zone (peri-infarct), and remaining tissue (remainder). Error bars represent standard error of the mean (SEM, n=3-4per treatment group). (B) Individual samples were grouped to demonstrate variation in dCT between samples. Error bars denote standard deviation (SD, n=3-4 per treatment group).
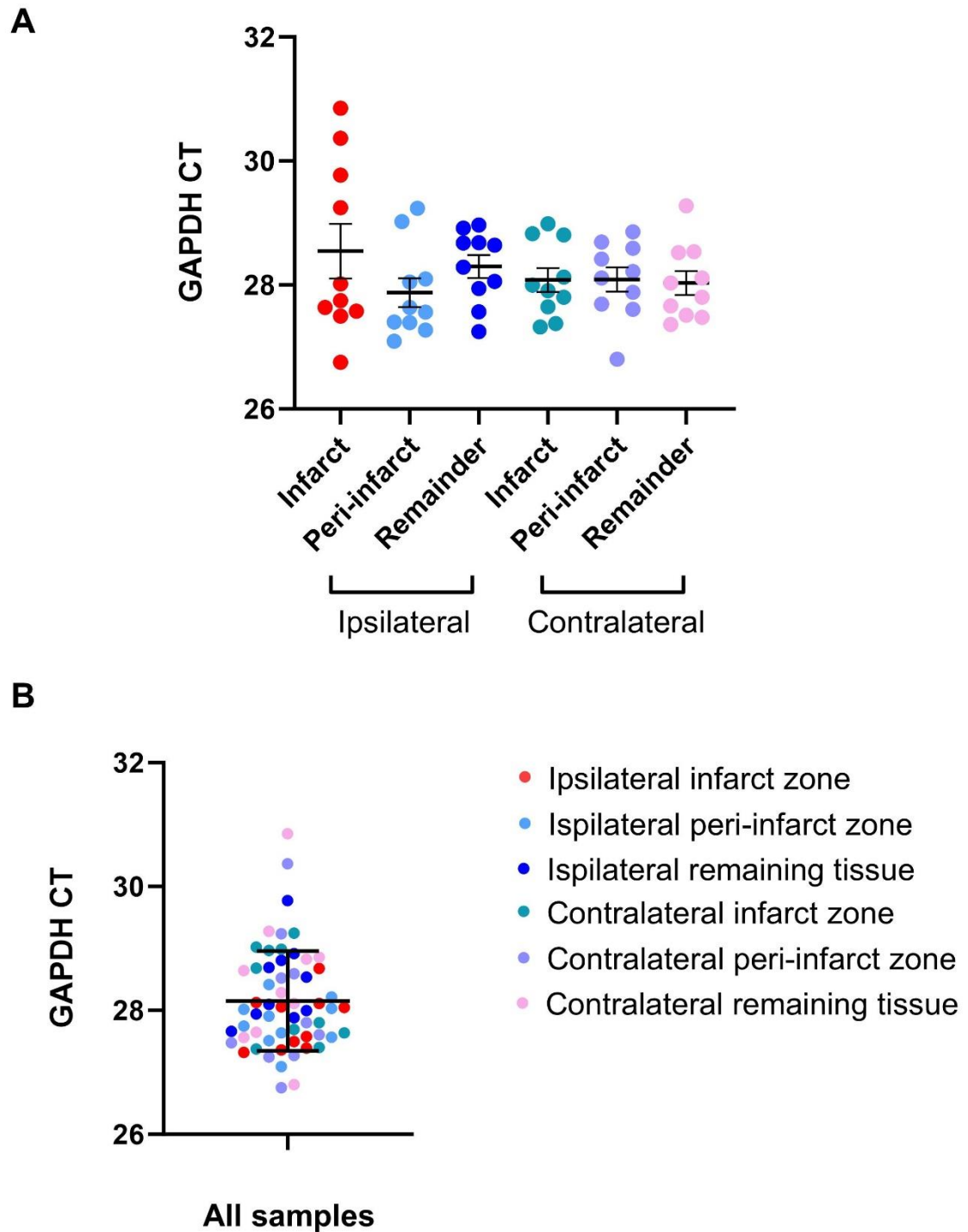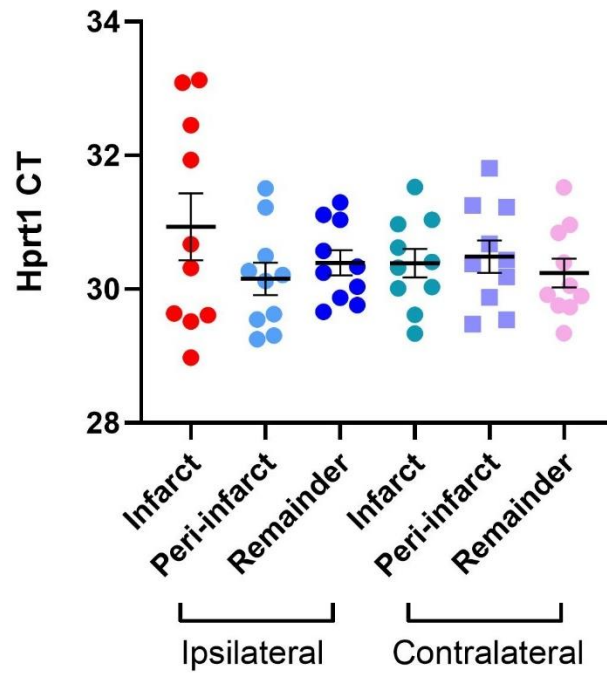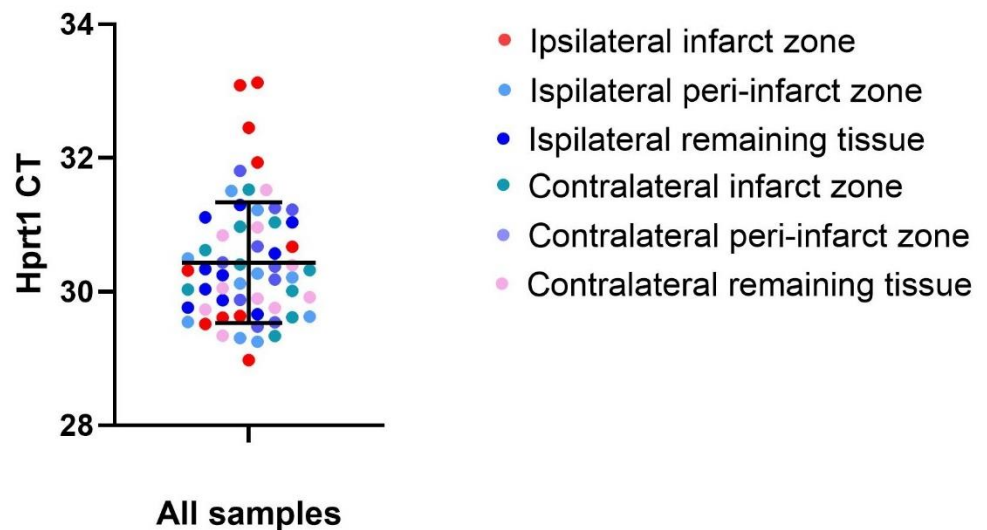
Figure 7.19 Assessment of Hprt1 as a stable housekeeping gene in brain tissues after intranasal delivery of EV post-tMCAO.
qPCR for Hprt1 expression in the ipsilateral and contralateral brain tissue after experimental stroke and therapeutic Ang-(1-9) EV treatment. Cycle threshold (CT) demonstrated the abundance of gene expression. (A) Brain tissue analysed included infarcted zone (infarct), peri-infarct zone (peri-infarct), and remaining tissue (remainder). Error bars represent standard error of the mean (SEM, n=3-4per treatment group). (B) Individual samples were grouped to demonstrate variation in dCT between samples. Error bars denote standard deviation (SD, n=3-4 per treatment group).

7.4.6 Effects of intranasal delivery of Ang-(1-9) loaded EVs on the expression of RAAS-specific genes after experimental stroke

ACE is a key component of the RAAS and is responsible for the conversion of Ang I to vasoconstrictive Ang II. Preventing the conversion of Ang I to Ang II by ACE or activation of receptors of the counterregulatory axis of RAAS, such as MasR or AT_2R, has proven beneficial in stroke (Bennion et al., 2017, Regenhardt et al., 2014, Liu et al., 2023). Therefore, the expression of ACE, ACE2 and Mas1 was assessed in brain tissue following tMCAO with or without Ang-(1-9) EV intervention. The expression of ACE and Mas1 were consistent between groups in the infarct zone, peri-infarct zone, and remaining tissue in both ipsi- and contra-lateral hemispheres (Figure 7.20 & Figure 7.22).

ACE2 expression was similar between groups within the infarct and peri-infarct zone within of both the ipsilateral hemisphere (Figure 7.21 A). ACE2 expression was downregulated after Ang-(1-9) EV treatment (7.69 ± 0.15, p<0.01) compared to Sham control (5.36 ± 0.05) within the ipsilateral remaining tissue (Figure 7.21 A). ACE2 expression was similar between groups within the contralateral hemispheres (Figure 7.21 B).
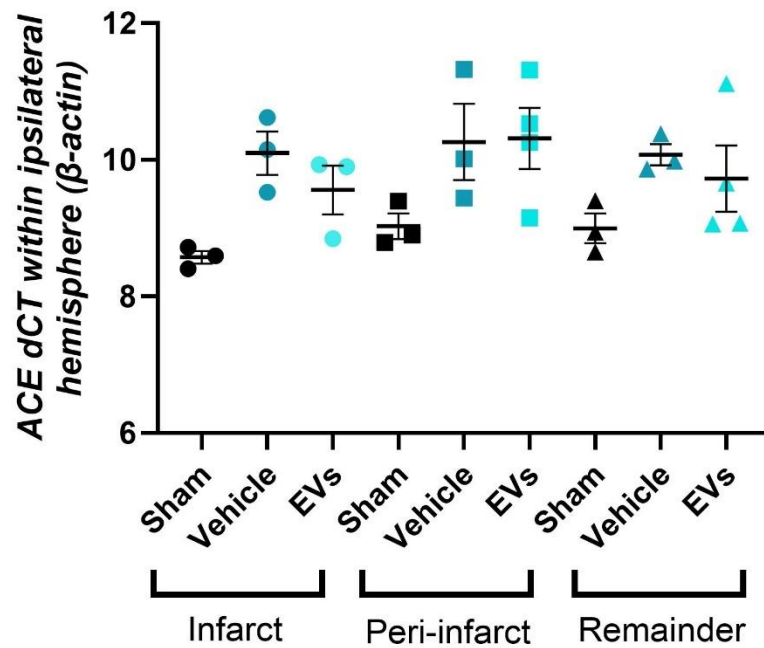
Figure 7.20 Expression of ACE in brain tissues after intranasal delivery of EV post-tMCAO.
qPCR for ACE expression in the infarct, peri-infarct and remaining tissue of the (A) ipsilateral and (B) contralateral hemispheres after experimental stroke. ACE expression was normalised to β-actin housekeeper. Delta cycle threshold (dCT) demonstrated the abundance of gene expression and error bars represent standard error of the mean (n=3-4, $p>0.05$, Brown-Forsythe and Welch ANOVA with post-hoc Dunnett's T3 multiple comparison).
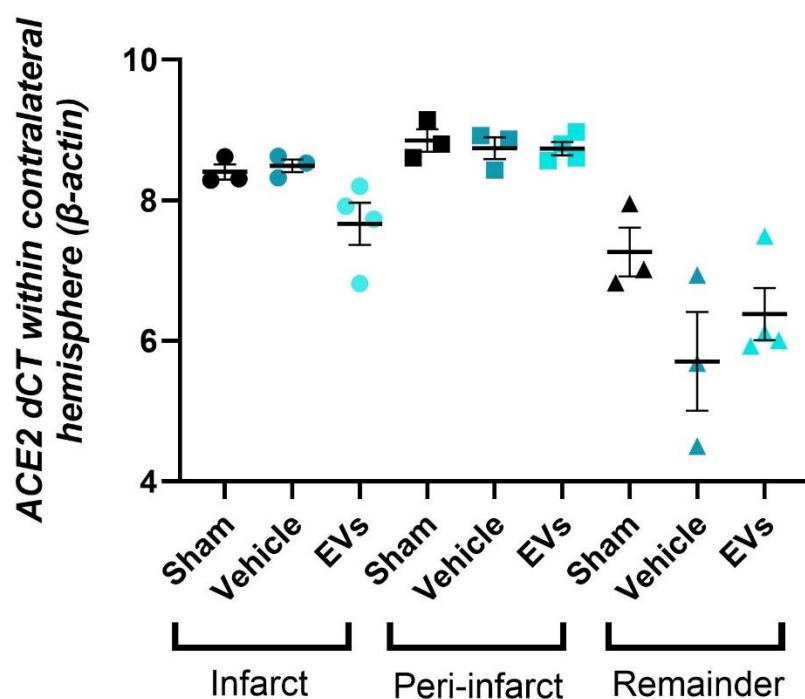
Figure 7.21 Expression of ACE2 in brain tissues after intranasal delivery of EV post-tMCAO.
qPCR for ACE2 expression in the infarct, peri-infarct and remaining tissue of the (A) ipsilateral and (B) contralateral hemispheres after experimental stroke. ACE2 expression was normalised to β-actin housekeeper. Delta cycle threshold (dCT) demonstrated the abundance of gene expression and error bars represent standard error of the mean (n=3-4, ***p<0.001, Brown-Forsythe and Welch ANOVA with post-hoc Dunnett's T3 multiple comparison).

A

B

Figure 7.22 Expression of Mas1 in brain tissues after intranasal delivery of EV post-tMCAO.
qPCR for Mas1 expression in the infarct, peri-infarct and remaining tissue of the (A) ipsilateral and (B) contralateral hemispheres after experimental stroke. Mas1 expression was normalised to β-actin housekeeper. Delta cycle threshold (dCT) demonstrated the abundance of gene expression and error bars represent standard error of the mean (n=3-4, $p > 0.05$, Brown-Forsythe and Welch ANOVA with post-hoc Dunnett's T3 multiple comparison).

7.4.7 Effects of intranasal delivery of Ang-(1-9) loaded EVs on the expression of brain-specific genes after experimental stroke

Brain derived neurotrophic factor, BDNF, is a neurotrophic factor that affects neuronal cell growth, differentiation, survival, and function (Zigova et al., 1998, Huang and Reichardt, 2001). BDNF expression has been found to be significantly reduced in serum samples of acute ischaemic stroke patients on the day of hospital administration compared to healthy control samples (Chaturvedi et al., 2020). Intravenous delivery of BDNF to Wistar rats following photothrombotic ischaemia led to increased neurogenesis and improved functional outcomes 6 weeks post-ischaemic insult (Schäbitz et al., 2007). The BBB is mainly composed of endothelial cells which are tightly held together by tight junctions that are composed of transmembrane proteins such as claudins (Daneman and Prat, 2015). Claudin-5 deficiency in mice leads to increased BBB permeability to small molecules and death within 10 hours of birth, demonstrating the importance of Claudin-5 in BBB integrity and survival (Nitta et al., 2003). Due to the importance of both BDNF and Claudin-5 within the stroke brain, the expression of both was assessed in brain tissue following tMCAO with or without Ang-(1-9) EV intervention. The expression of BDNF and Claudin-5 were consistent between groups in the infarct zone, peri-infarct zone, and remaining tissue in both ipsi- and contra-lateral hemispheres (Figure 7.23 & Figure 7.24).
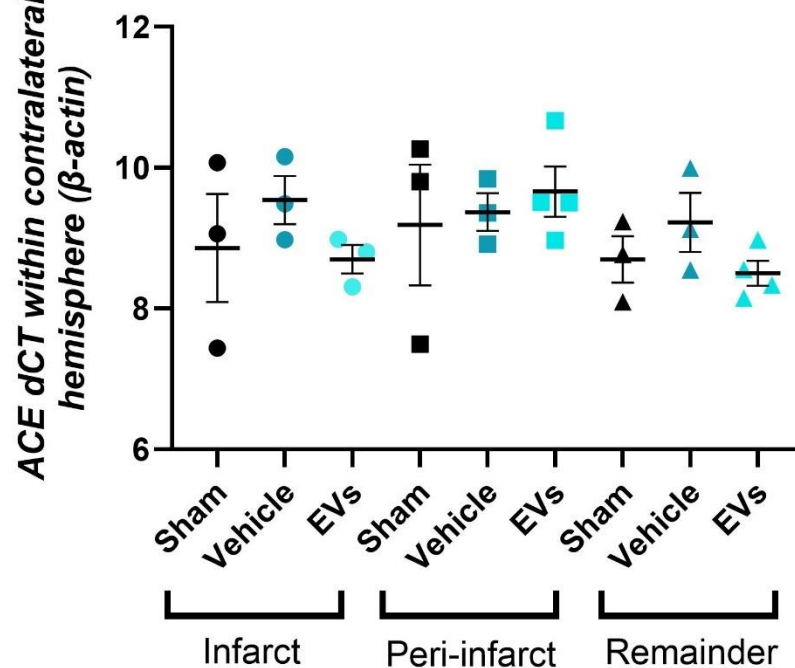
A

B

Figure 7.23 Expression of BDNF in brain tissues after intranasal delivery of EV post-tMCAO.
qPCR for BDNF expression in the infarct, peri-infarct and remaining tissue of the (A) ipsilateral and (B) contralateral hemispheres after experimental stroke. BDNF expression was normalised to β-actin housekeeper. Delta cycle threshold (dCT) demonstrated the abundance of gene expression and error bars represent standard error of the mean (n=3-4, $p > 0.05$, Brown-Forsythe and Welch ANOVA with post-hoc Dunnett's T3 multiple comparison).
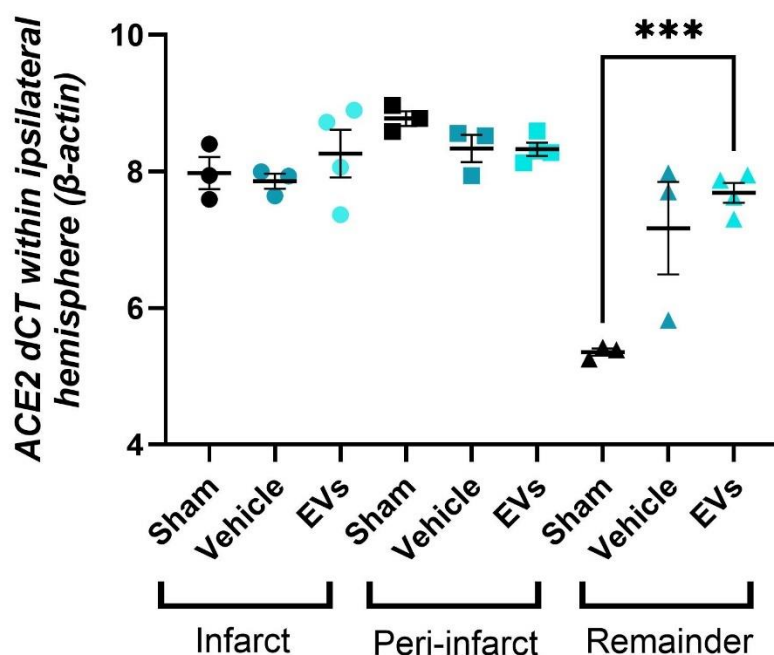
A

B

Figure 7.24 Expression of Claudin-5 in brain tissues after intranasal delivery of EV post-tMCAO.
qPCR for Claudin-5 expression in the infarct, peri-infarct and remaining tissue of the (A) ipsilateral and (B) contralateral hemispheres after experimental stroke. Claudin-5 expression was normalised to β-actin housekeeper. Delta cycle threshold (dCT) demonstrated the abundance of gene expression and error bars represent standard error of the mean (n=3-4, p>0.05, Brown-Forsythe and Welch ANOVA with post-hoc Dunnett's T3 multiple comparison).
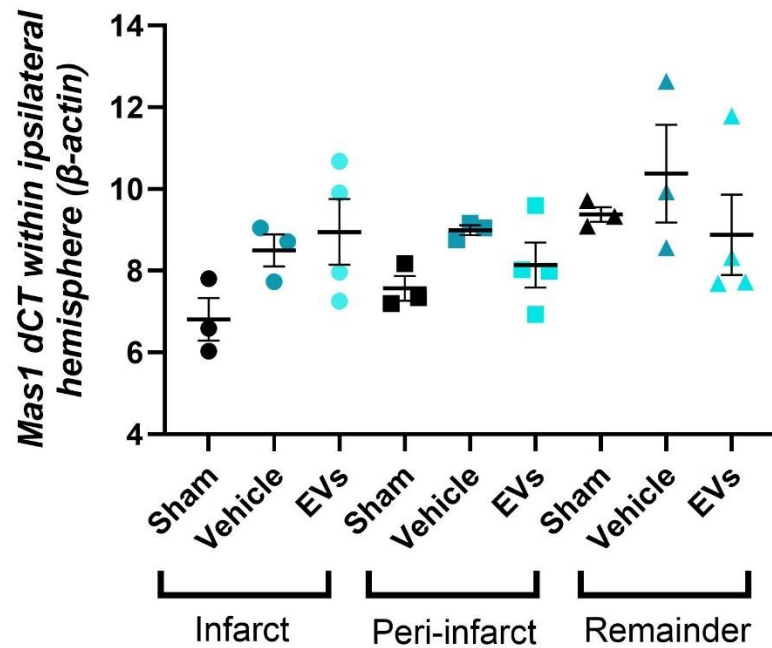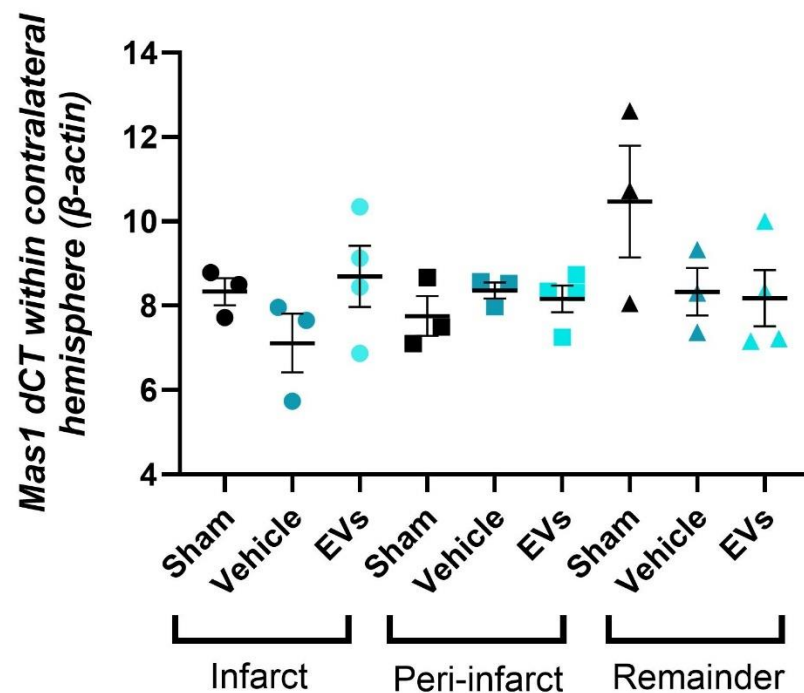
7.4.8 Effects of intranasal delivery of Ang-(1-9) loaded EVs on the expression of growth factor-specific genes after experimental stroke

Growth factors such as VEGF and TGF may regulate and enable angiogenesis, and as a result may play an important role in post-stroke recovery (James et al., 2009, Ferrari et al., 2009). The expression of both was assessed in brain tissue following tMCAO with or without EV intervention. The expression of TGFα (Figure 7.25) and VEGFA (Figure 7.27) was constant between groups in the infarct zone, peri-infarct zone, and remaining brain tissue in both ipsi- and contra-lateral hemispheres.

Compared to the sham control (6.22 ± 0.30; dCT $\pm$ SEM) of the ipsilateral infarct zone, TGFβ1 was upregulated following vehicle treatment (4.30 ± 0.27; $p < 0.05$) (Figure 7.26 A). Compared to the sham control (6.55 ± 0.21) of the ipsilateral peri-infarct zone, TGFβ1 was upregulated following Ang-(1-9) EV treatment (4.95 ± 0.23; $p < 0.05$) (Figure 7.26 A). Vehicle and Ang-(1-9) treatment did not affect TGFβ1 expression between groups within the contralateral hemisphere (Figure 7.26 B).

Within the infarct and peri-infarct zone of the ipsilateral hemisphere VEGFB expression was similar between groups (Figure 7.28 A). Compared to the sham control of the ipsilateral remaining zone (5.27 ± 0.15), VEGFB was downregulated following Ang-(1-9) EV treatment (6.48 ± 0.21; $p < 0.05$) (Figure 7.28 A). VEGFB expression was similar between groups within the contralateral hemisphere (Figure 7.28 B).
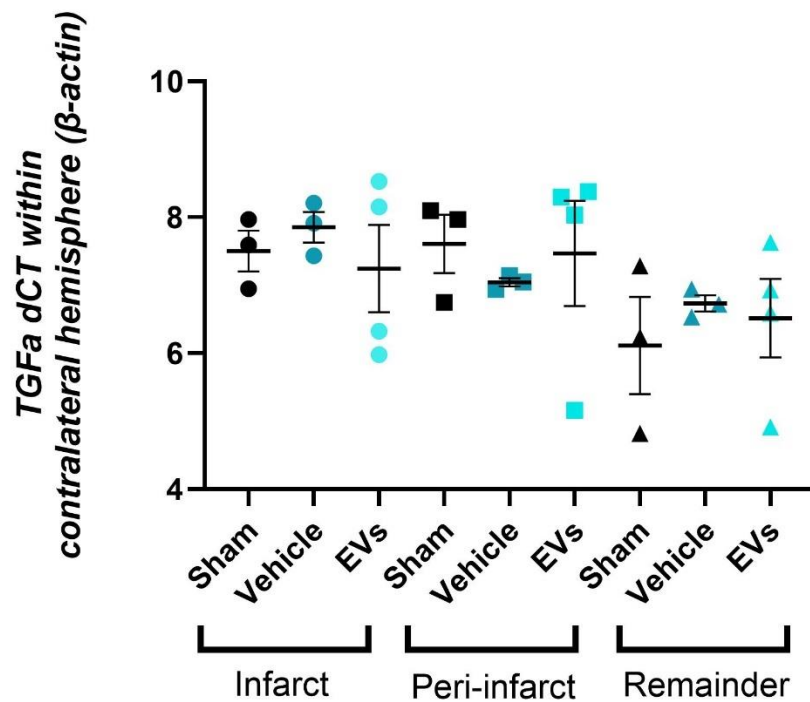
Figure 7.25 Expression of TNFα in brain tissues after intranasal delivery of EV post-tMCAO.
qPCR for TNFα expression in the infarct, peri-infarct and remaining tissue of the (A) ipsilateral and (B) contralateral hemispheres after experimental stroke. TNFα expression was normalised to β-actin housekeeper. Delta cycle threshold (dCT) demonstrated the abundance of gene expression and error bars represent standard error of the mean (n=3-4, p>0.05, Brown-Forsythe and Welch ANOVA with post-hoc Dunnett's T3 multiple comparison).

Figure 7.26 Expression of TGFβ1 in brain tissues after intranasal delivery of EV post-tMCAO.

qPCR for TGFβ1 expression in the infarct, peri-infarct and remaining tissue of the (A) ipsilateral and (B) contralateral hemispheres after experimental stroke. TGFβ1 expression was normalised to β-actin housekeeper. Delta cycle threshold (dCT) demonstrated the abundance of gene expression and error bars represent standard error of the mean (n=3-4, *p<0.05, Brown-Forsythe and Welch ANOVA with post-hoc Dunnett's T3 multiple comparison).

A

B

Figure 7.27 Expression of VEGFA in brain tissues after intranasal delivery of EV post-tMCAO.
qPCR for VEGFA expression in the infarct, peri-infarct and remaining tissue of the (A) ipsilateral and (B) contralateral hemispheres after experimental stroke. VEGFA expression was normalised to β-actin housekeeper. Delta cycle threshold (dCT) demonstrated the abundance of gene expression and error bars represent standard error of the mean (n=3-4, $p > 0.05$, Brown-Forsythe and Welch ANOVA with post-hoc Dunnett's T3 multiple comparison).
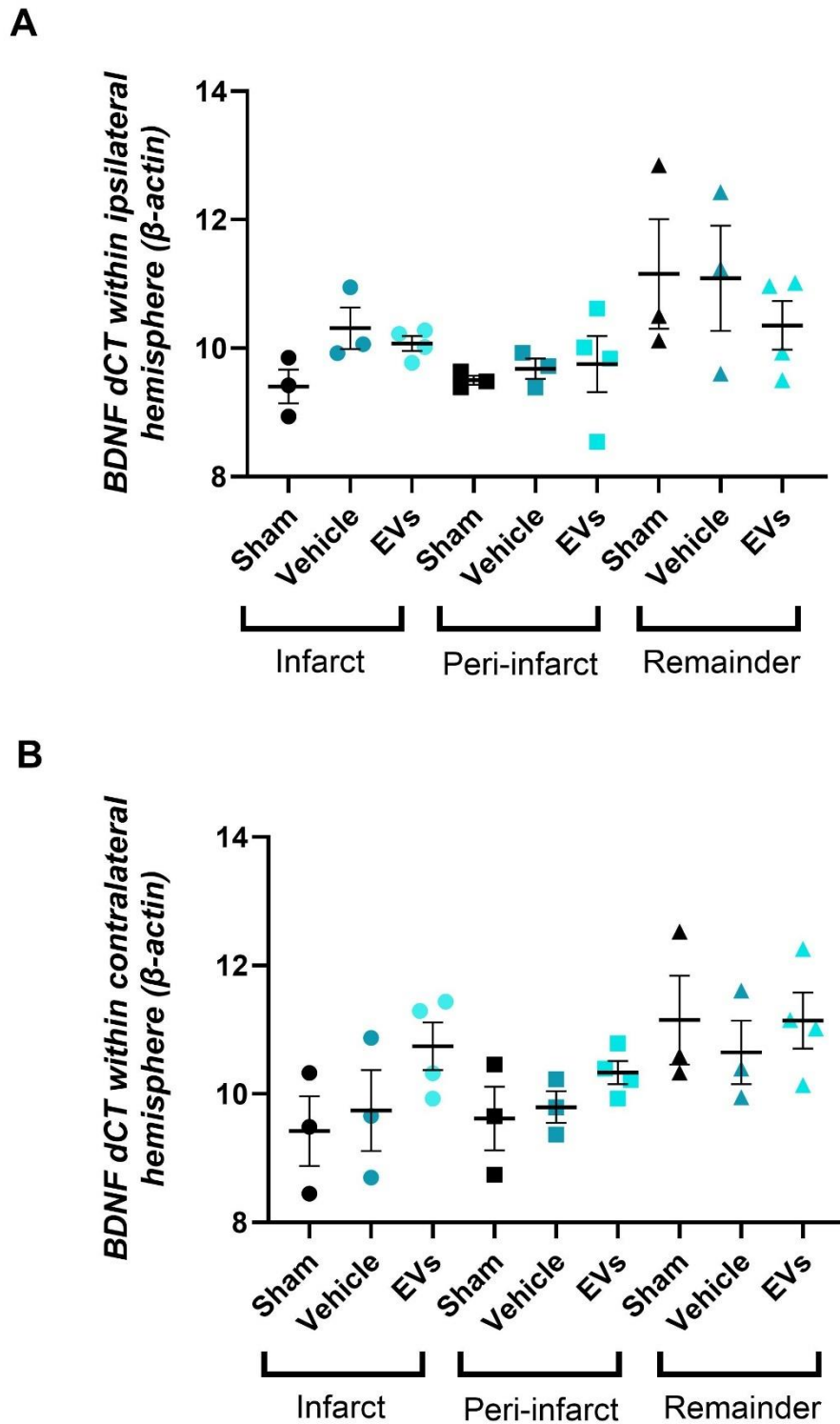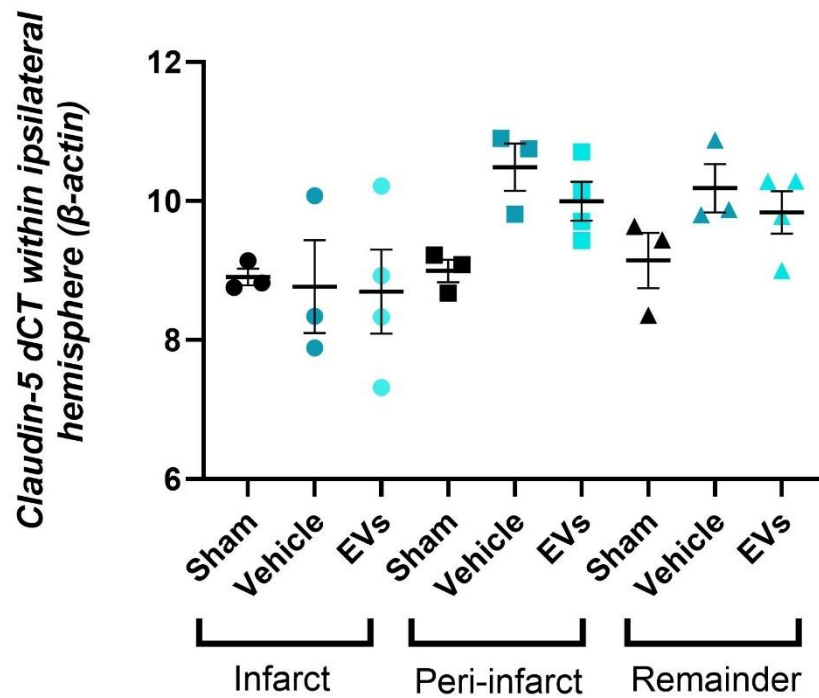
Figure 7.28 Expression of VEGFB in brain tissues after intranasal delivery of EV post-tMCAO.
qPCR for VEGFB expression in the infarct, peri-infarct and remaining tissue of the (A) ipsilateral and (B) contralateral hemispheres after experimental stroke. VEGFB expression was normalised to β-actin housekeeper. Delta cycle threshold (dCT) demonstrated the abundance of gene expression and error bars represent standard error of the mean (n=3-4, *p<0.05, Brown-Forsythe and Welch ANOVA with post-hoc Dunnett's T3 multiple comparison).
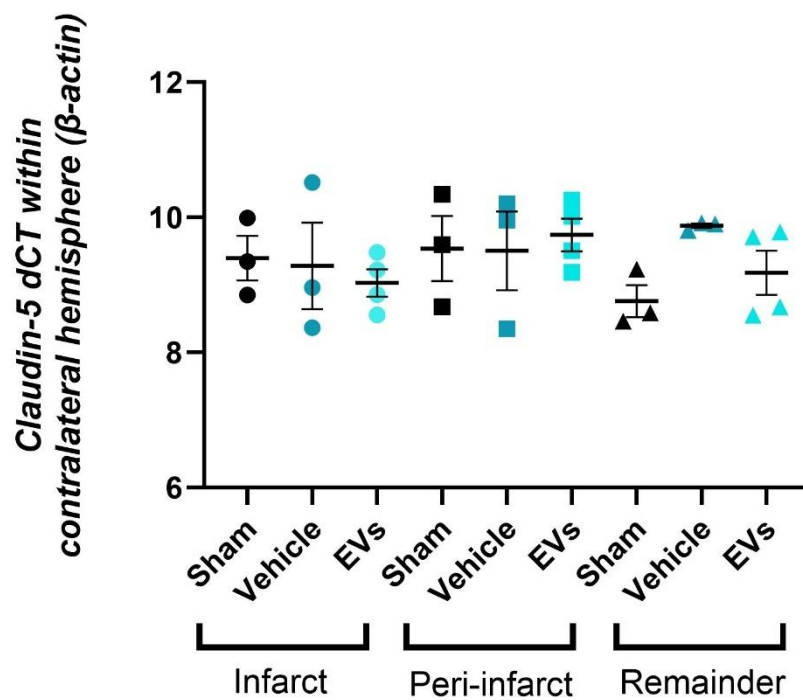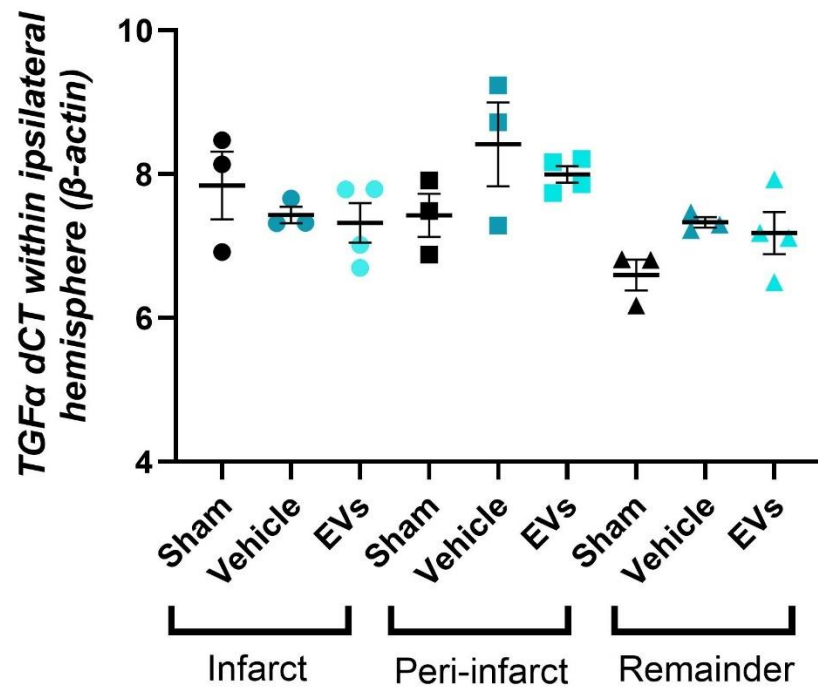
7.4.9 Effects of intranasal delivery of Ang-(1-9) loaded EVs on the expression of inflammation-specific genes after experimental stroke

Neuroinflammation in the acute phase post-stroke leads to immune cell infiltration, increased release of reactive oxygen species and decreased BBB integrity (Iadecola et al., 2020, Hernandes et al., 2022). Following the activation of resident immune cells, additional immune cell recruitment is facilitated by transcription factor activation and cytokine signalling (Smith et al., 2012, Xiong et al., 2016). IL-1 family of cytokines is comprised of IL-1 alpha (IL-1α), IL-1beta (IL-1β) and IL-1 receptor antagonist (IL-1RN) (Sims and Smith, 2010). In preclinical models of stroke, C57BL/6J mice treated with cytokine IL-1α demonstrated reduced infarct volume and improved neurological outcomes 3 days post-common carotid and middle cerebral artery occlusion (Salmeron et al., 2019). IL-1RN, dampens pro-inflammatory properties of IL-1α and IL-1β, especially in the acute phase of inflammation (National Institutes for Health, 2023). In the SCIL-STROKE clinical trial, IL-1RN, also known as IL-1Ra, delivered subcutaneously to ischaemic stroke patients led to reduced plasma levels of pro-inflammatory IL-6 and C-reactive protein (Smith et al., 2018). Wistar rats subjected to tMCAO followed by IL-1Ra treatment showed reduced infarct volume 24 hours post stroke, and improved neurological outcome up to 14 days post-stroke (Pradillo et al., 2017).

Tumour necrosis factor, TNF, binds to TNF receptors to activate downstream signalling pathways that influence cell proliferation, survival, migration, angiogenesis and apoptosis, and as such is implicated in stroke pathology (Wang and Lin, 2008). TNF-alpha, TNFα, delivered via intracerebroventricular injection to spontaneously hypertensive rats prior to pMCAO, led to increased infarct volume and reduced neurological score, while anti-TNF antibodies delivered by intracerebroventricular injection prior to pMCAO led to reduced infarct volume (Barone et al., 1997).

NFκB, regulates inflammation genes and the activation of immune cells through stimulation of canonical and alternative signalling pathways (Oeckinghaus and Ghosh, 2009). Following experimental tMCAO, Sprague-Dawley rats demonstrated increased NFκB DNA binding activity in the ischaemic cortex and striatum post-stroke (Stephenson et al., 2000). As IL-1α, IL-1RN, TNF and NFκB may contribute to stroke pathology and post-stroke recovery, the expression of these cytokines and transcription factors was assessed in brain tissue following tMCAO with or without Ang-(1-9) EV intervention. IL-1α and NFκB expression remained constant between groups in the infarct zone, peri-infarct

zone and remaining tissue in both ipsi- and contra-lateral hemispheres (Figure 7.29 & Figure 7.31).

Within the ipsilateral hemisphere, IL-1RN was upregulated in vehicle controls of the peri-infarct zone (8.53 ± 0.23; $p<0.05$) and the remaining tissue (7.83 ± 0.16; $p<0.05$) compared to sham controls (Figure 7.30 A). IL-1RN expression was comparable between in the contralateral hemisphere (Figure 7.30 B).

TNF was upregulated in Ang-(1-9) EV treatment (8.22 ± 0.20; $p<0.01$) compared to sham controls (10.19 ± 0.20) within the remaining tissue of the ipsilateral hemisphere (Figure 7.32 A). There was no difference in TNF expression between groups in the contralateral hemisphere (Figure 7.32 C).
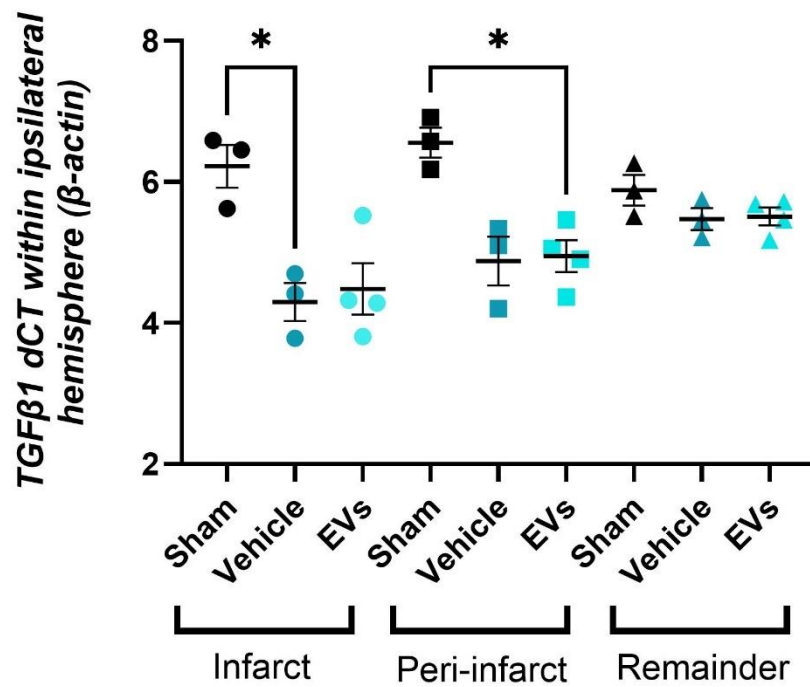
A
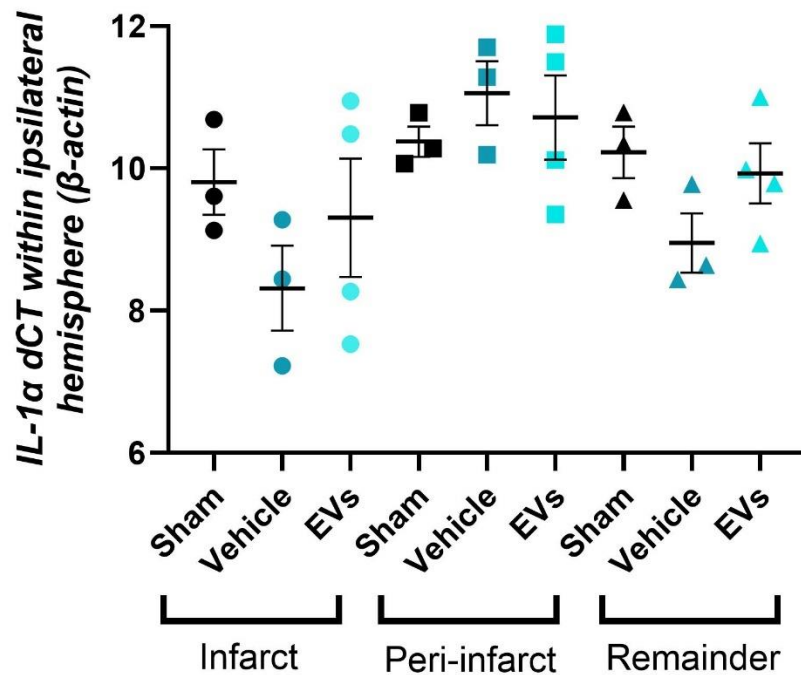
B
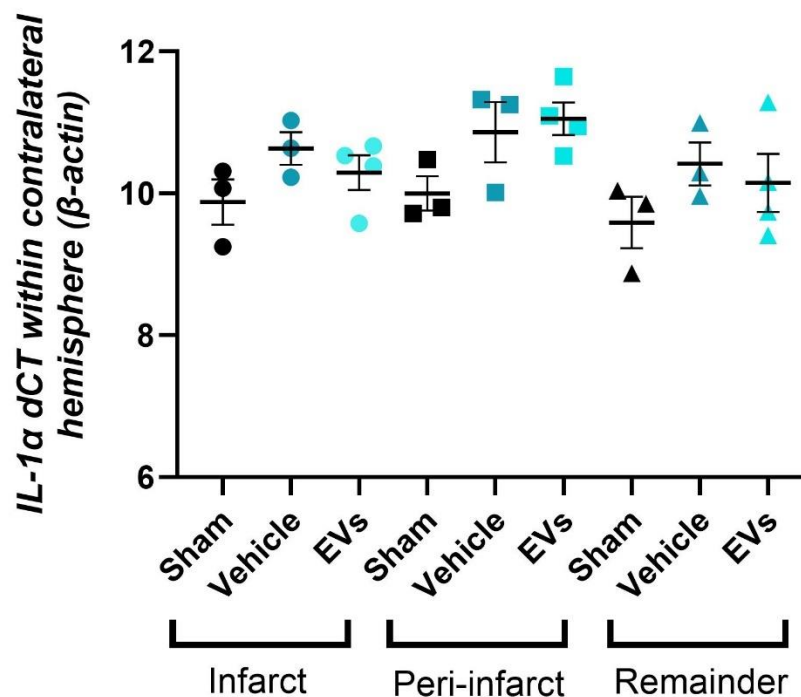
Figure 7.29 Expression of IL-1α in brain tissues after intranasal delivery of EV post-tMCAO.
qPCR for IL-1α expression in the infarct, peri-infarct and remaining tissue of the (A) ipsilateral and (B) contralateral hemispheres after experimental stroke. IL-1α expression was normalised to β-actin housekeeper. Delta cycle threshold (dCT) demonstrated the abundance of gene expression and error bars represent standard error of the mean (n=3-4, p>0.05, Brown-Forsythe and Welch ANOVA with post-hoc Dunnett's T3 multiple comparison).
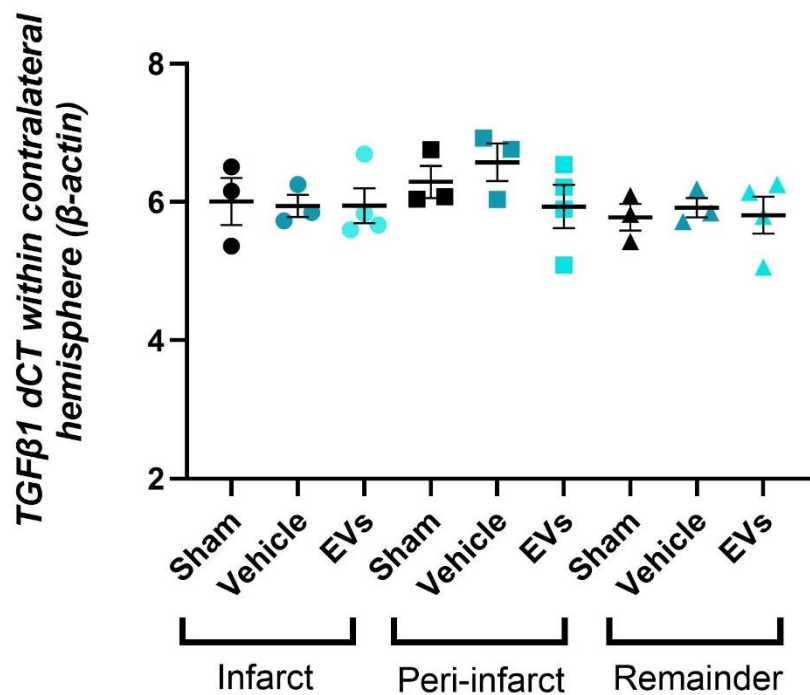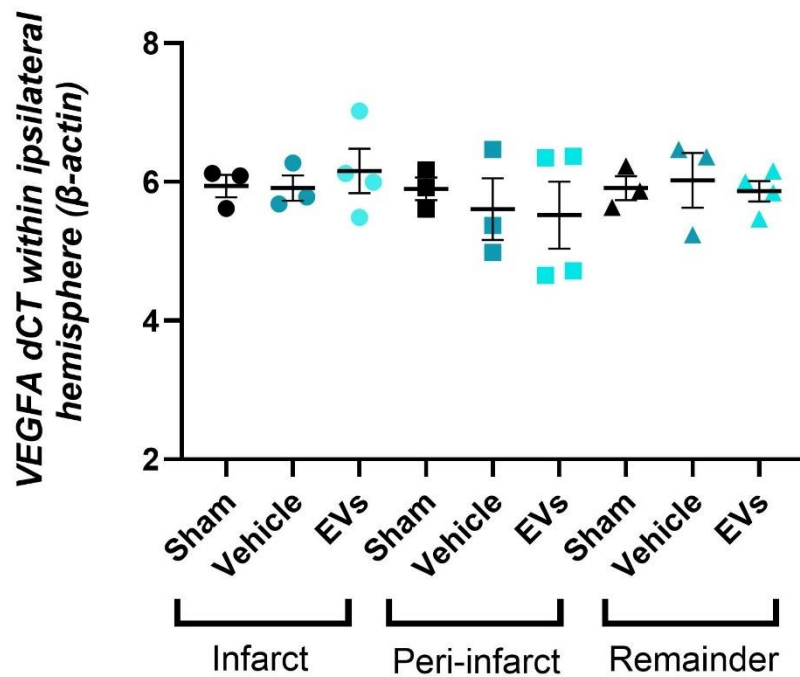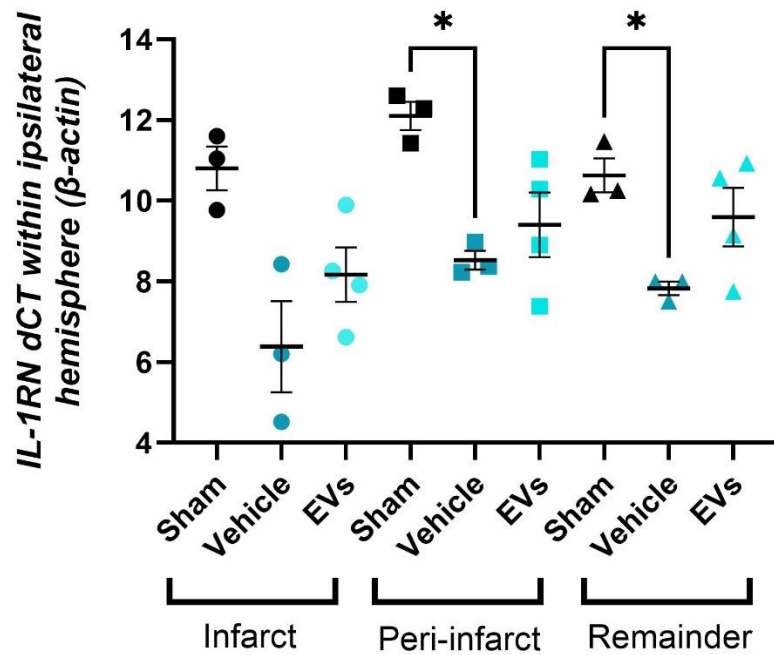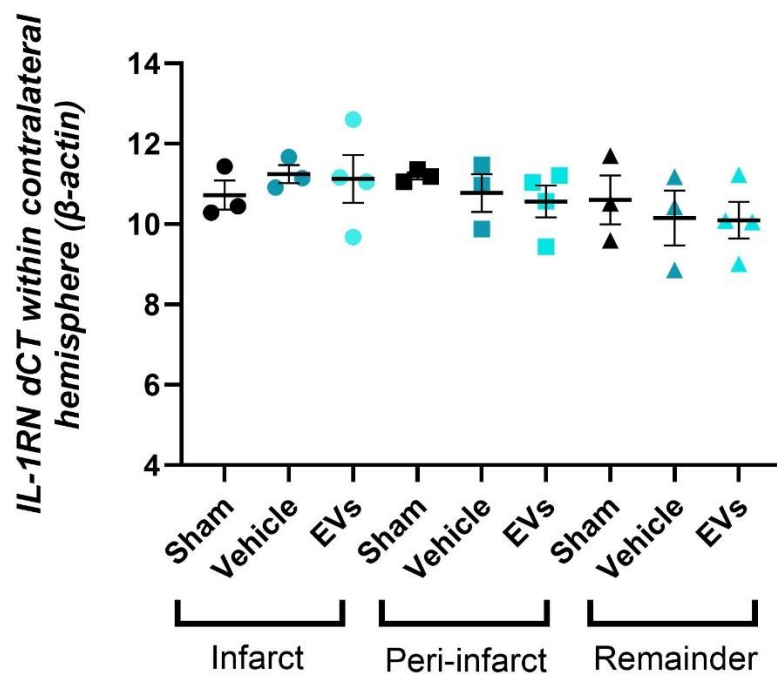
Figure 7.30 Expression of IL-1RN in brain tissues after intranasal delivery of EV post-tMCAO.
qPCR for IL-1RN expression in the infarct, peri-infarct and remaining tissue of the (A) ipsilateral and (B) contralateral hemispheres after experimental stroke. IL-1RN expression was normalised to β-actin housekeeper. Delta cycle threshold (dCT) demonstrated the abundance of gene expression and error bars represent standard error of the mean (n=3-4, $*p<0.05$, Brown-Forsythe and Welch ANOVA with post-hoc Dunnett's T3 multiple comparison).
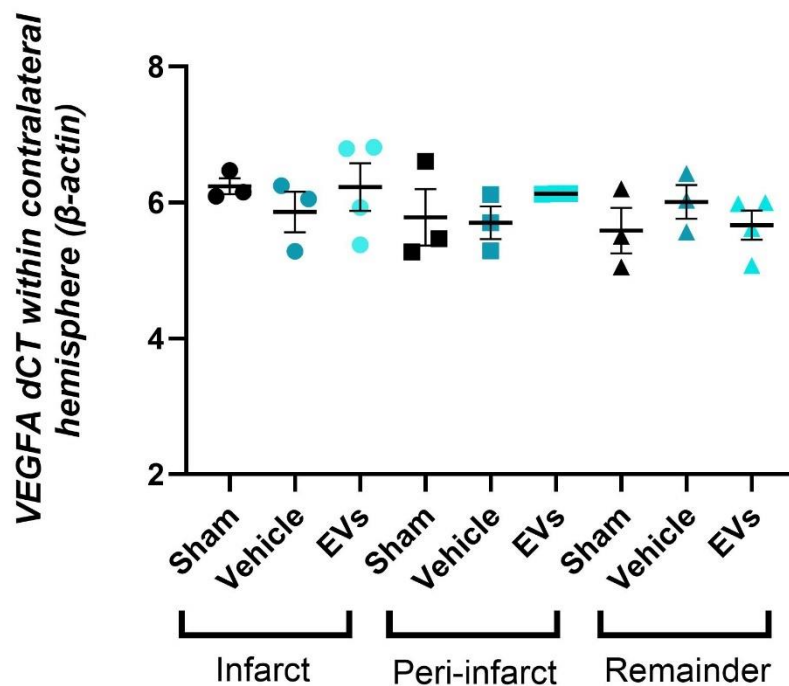
A

B
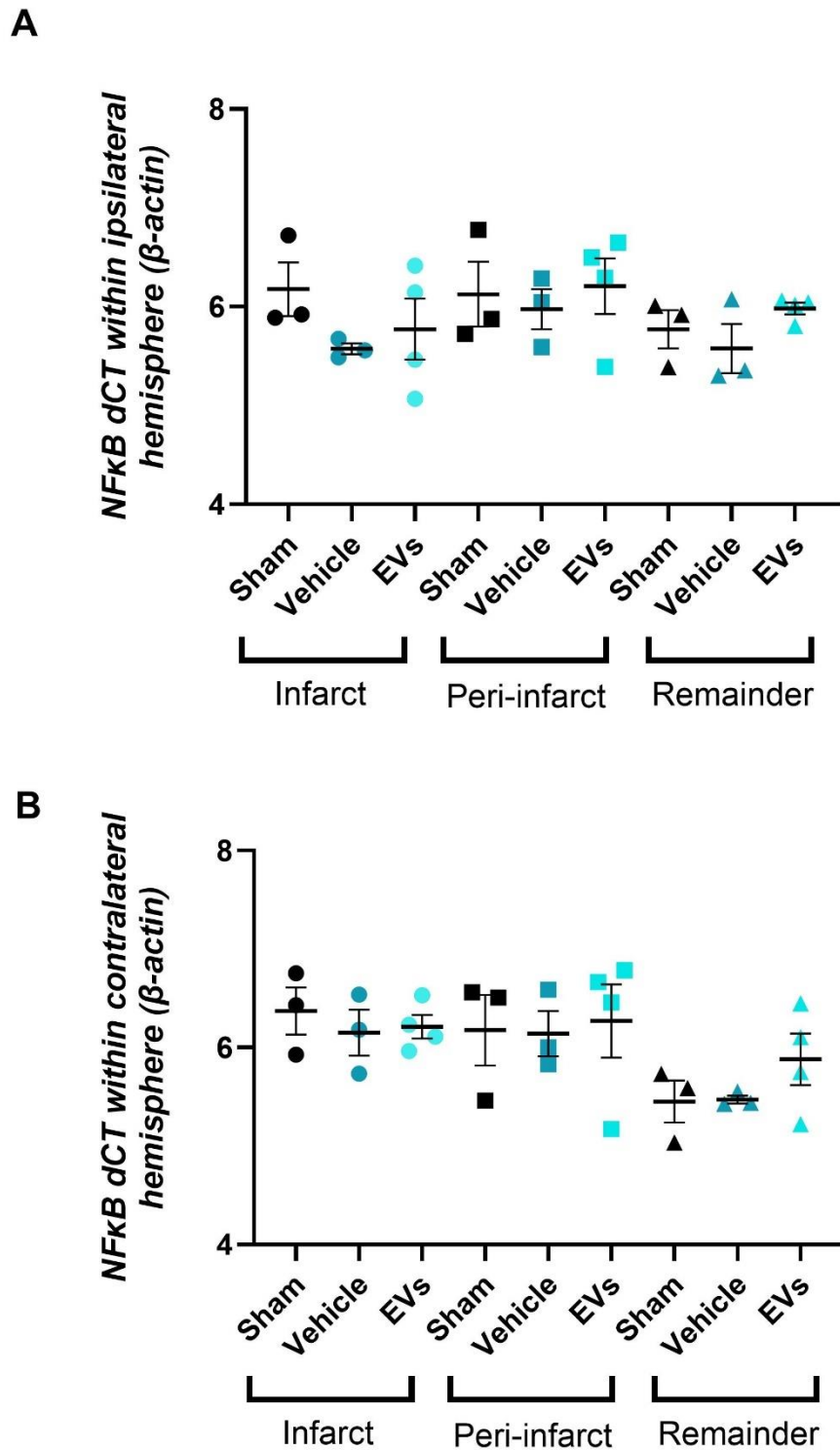
Figure 7.31 Expression of NFκB in brain tissues after intranasal delivery of EV post-tMCAO.
qPCR for NFκB expression in the infarct, peri-infarct and remaining tissue of the (A) ipsilateral and (B) contralateral hemispheres after experimental stroke. NFκB expression was normalised to β-actin housekeeper. Delta cycle threshold (dCT) demonstrated the abundance of gene expression and error bars represent standard error of the mean (n=3-4, p>0.05, Brown-Forsythe and Welch ANOVA with post-hoc Dunnett's T3 multiple comparison).
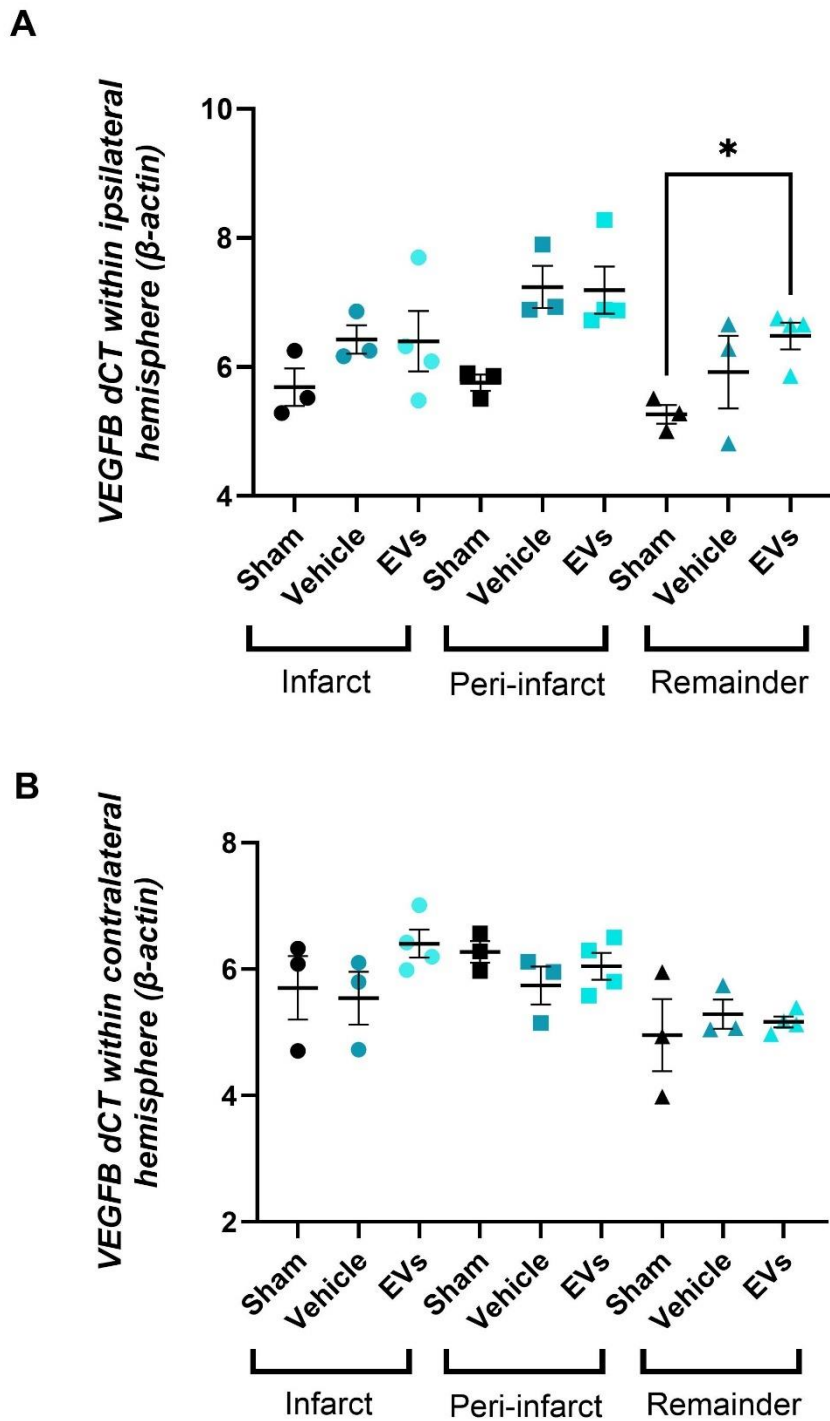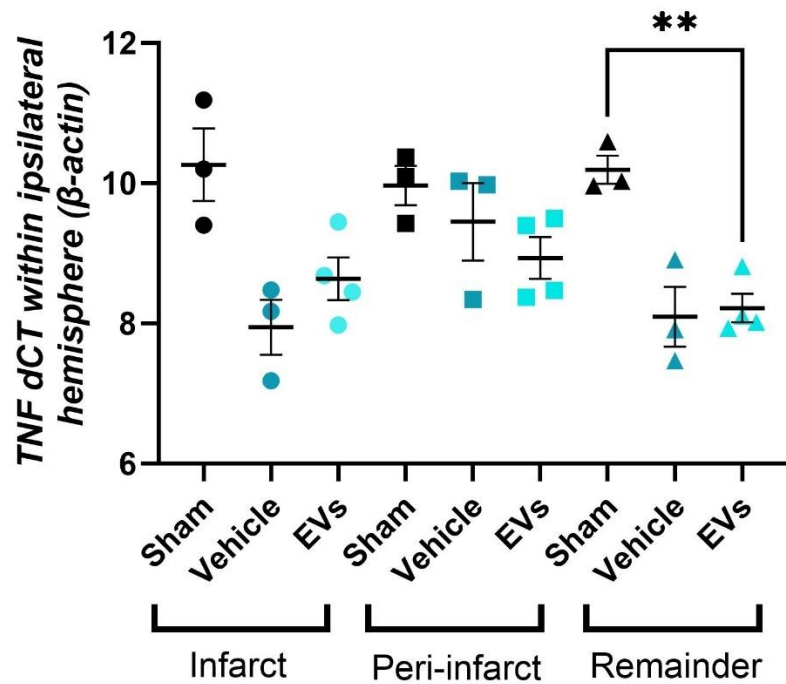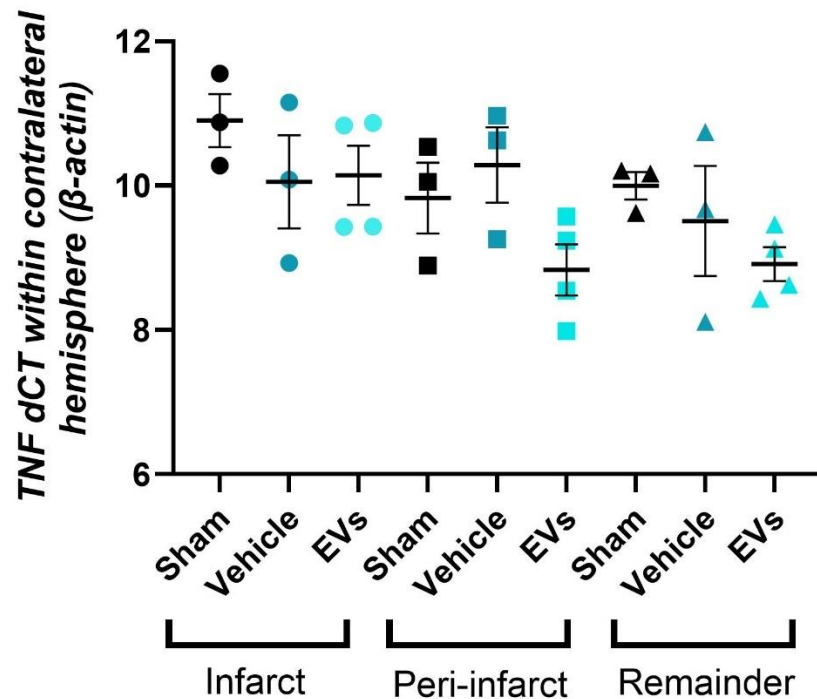
Figure 7.32 Expression of TNF in brain tissues after intranasal delivery of EV post-tMCAO.
qPCR for TNF expression in the infarct, peri-infarct and remaining tissue of the (A) ipsilateral and (B) contralateral hemispheres after experimental stroke. Delta cycle threshold (dCT) demonstrated the abundance of gene expression and error bars represent standard error of the mean (n=3-4, *p<0.05, Brown-Forsythe and Welch ANOVA with post-hoc Dunnett's T3 multiple comparison).

7.4.10 Effects of intranasal delivery of Ang-(1-9) loaded EVs on RUNX1 expression after experimental stroke

As previously discussed, RUNX1 may play a protective role within the brain post-stroke and as such the expression of RUNX1 was assessed in brain tissue following tMCAO with or without Ang-(1-9) EV intervention. There was no difference in RUNX1 expression between groups between the ipsi- and contra-later hemispheres (Figure 7.33 A & B).

A
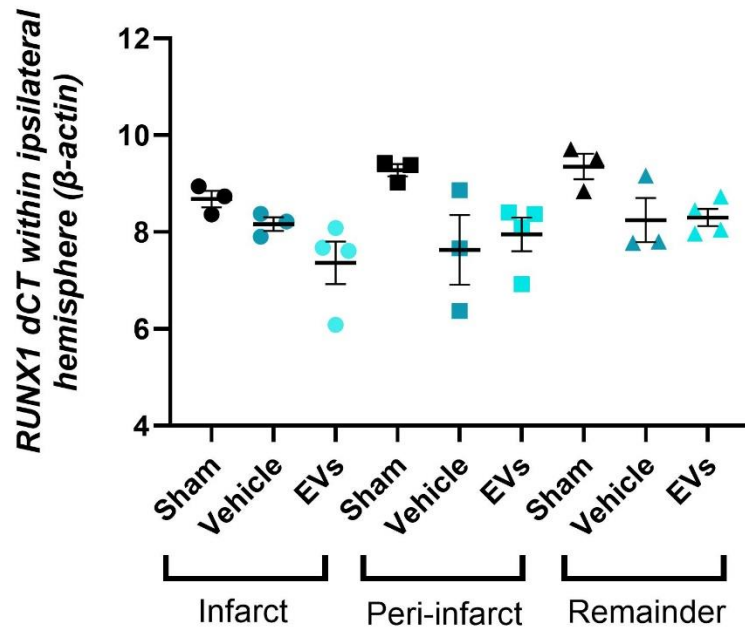
B
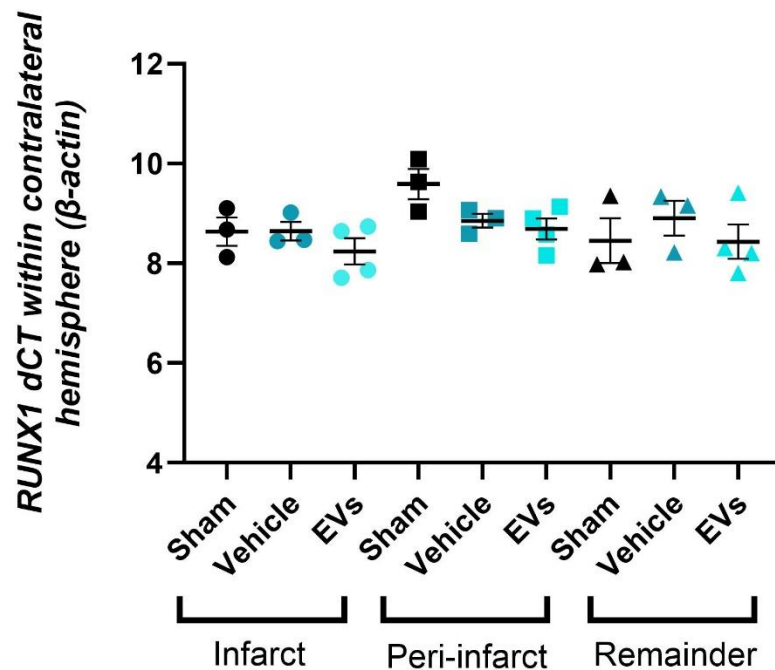
Figure 7.33 Expression of RUNX1 in brain tissues after intranasal delivery of EV post-tMCAO.
qPCR for RUNX1 expression in the infarct, peri-infarct and remaining tissue of the (A) ipsilateral and (B) contralateral hemispheres after experimental stroke. RUNX1 expression was normalised to β-actin housekeeper. Delta cycle threshold (dCT) demonstrated the abundance of gene expression and error bars represent standard error of the mean (n=3-4, *$p<0.05$, Brown-Forsythe and Welch ANOVA with post-hoc Dunnett's T3 multiple comparison).

7.5 Discussion

The length of occlusion time and reperfusion time did not alter VEGFA, VEGFB, ACE2, Mas1 or RUNX1 expression following tMCAO. A stable housekeeper was difficult to establish in brain tissue following tMCAO with or without Ang-(1-9) EV treatment, while β-actin provided the smallest standard deviation from mean CT value. The expression of ACE, BDNF, Claudin-5, TGFα, VEGFA, IL-1α, NFκB were unaltered following tMCAO with or without Ang-(1-9) EV treatment. Compared to sham control, stroke with vehicle treatment led to: downregulation of ACE2 in the remaining tissue of the ipsilateral hemisphere, upregulation of TGFβ1 in the infarct and peri-infarct zone of the ipsilateral hemisphere, downregulation of VEGFB in the peri-infarct zone of the ipsilateral hemisphere, upregulation of IL-1RN in the infarct and peri-infarct zone of the ipsilateral hemisphere, upregulation of TNF in the remaining zone of the ipsilateral hemisphere, and upregulation of RUNX1 in the peri-infarct zone of the ipsilateral hemisphere. Compared to sham control, Ang-(1-9) EV treatment following stroke led to: downregulation of ACE2 in the remaining tissue of the ipsilateral hemisphere, downregulation of Mas1 in the infarct zone of the ipsilateral hemisphere, upregulation of TGFβ1 in the infarct and peri-infarct zone of the ipsilateral hemisphere, downregulation of VEGFB in the peri-infarct zone of the ipsilateral hemisphere, upregulation of IL-1RN in the peri-infarct zone of the ipsilateral hemisphere, and upregulation of TNF in the remaining zone of the ipsilateral hemisphere.

Experimental stroke in animal models with stroke-related co-morbidities, such as hypertension or age, can influence post-stroke outcomes, including post-stroke morbidity. In order to better represent the population of individuals who may also experience co-morbidities of stroke, such as those who are hypertensive and are taking antihypertensive agents or those who have a clinical history of stroke and are prescribed antihypertensives to reduce stroke risk, the decision was made to treat SHRSPs with antihypertensives for two weeks prior to- and following experimental stroke surgery (Aiyagari and Gorelick, 2009, PROGRESS Collaborative Group, 2001). Hydralazine hydrochloride is an inositol triphosphate inhibitor that prevents calcium release from smooth muscle cell sarcoplasmic reticulum, while hydrochlorothiazide is a thiazide diuretic that inhibits sodium chloride co-transporter in the distal convoluted tubule which reduces water reabsorption and ultimately reduces blood pressure (Ellershaw and Gurney, 2001, Herman et al., 2023). Both antihypertensives were chosen as suitable blood pressure reducing agents as they would effectively reduce blood pressure without directly affecting the RAAS. As such modulation of the RAAS using Ang-(1-9) would not be impacted by the use of these antihypertensive

agents. The concentration of antihypertensive medications required to reduce blood pressure within SHRSPs, a dose of 16 mg/kg/day given orally, was determined by previous research within the University of Glasgow (Koh-Tan et al., 2009). After two-weeks of treatment, mean systolic blood pressure of the SHRSPs was significantly reduced. In a related study, SHRSPs were treated with either hydralazine plus hydrochlorothiazide at 6-10 weeks of age and systolic blood pressure was assessed at 17 weeks of age. It was found that hydralazine plus hydrochlorothiazide (198 mmHg) reduced mean systolic blood pressure compared to untreated controls (217 mmHg) (Traub et al., 1995), which is comparable to the results in the studies presented here. Antihypertensive treatment commenced at approximately 16 weeks and continued for two weeks, until the age of approximately 18 weeks. Depending on the experiment, animals were monitored for up to 10 days following experimental stroke surgery to an approximate final age of 20 weeks. The age at which rats undergo experimental stroke surgery can influence infarct size, for example, following photothrombotic stroke, Fisher rats of 20 months of age have very similar infarct volumes to those who undergo stroke surgery at 27 months of age by day 7 post-stroke. However, compared to rats of 4 months in age, infarct volume continued to grow within 20- and 27-month-old rats up to 7 days post-stroke (Kharlamov et al., 2000). Various publications have proven that experimental stroke surgery conducted on SHRSPs at the age of 18 weeks enables the formation of cerebral infarct, and so SHRSP rats approximately 4.5 months in age, the equivalent of 18 weeks, were subjected to tMCAO to mimic ischaemic stroke *in vivo* (van Kralingen et al., 2019, McGill et al., 2005, Yao et al., 2015).

The animals used in this experiment were initially severely hypertensive prior to treatment with a mean systolic blood pressure of 207.6 mmHg. Research conducted almost 30 years ago at the University of Glasgow found that untreated SHRSPs of 16 weeks of age, the same age as those in this investigation before commencement of antihypertensive treatment, had a mean systolic blood pressure of 180 mmHg (Davidson et al., 1995). In this investigation, even after two weeks of antihypertensive treatment, mean systolic blood pressure was greater than that observed in this previous research conducted 27 years ago. The gradual increase in mean systolic blood pressure of SHRSPs housed at the University of Glasgow may be the cause of the increased mortality observed after experimental stroke in SHRSPs in more recent years. This drift in systolic blood pressure may be a result of inbreeding of extremely hypertensive animals or introduction of random single nucleotide polymorphisms (SNPs) that may exacerbate hypertension. It should be noted that tail cuff plethysmography is no longer conducted on rats prior to breeding, and so the degree of

hypertension in breeding animals is unknown. Further, SHRSP genomes were not studied in this investigation to determine whether SNPs have been introduced into this strain that contributes to hypertension. It would be in the interest of those using SHRSPs as a model of comorbidity in stroke to stratify breeding SHRSPs by blood pressure and presence of SNPs. Mean systolic blood pressure has been shown to increase after acute ischaemic stroke (Alhusban et al., 2015). Increased pressure within vessels of the brain can be damaging to cells, which can lead to increased cell death. It is theorised that due to severe hypertension in SHRSPs prior to experimental stroke surgery leading to damage within cerebral vasculature and exacerbated hypertension post-stroke, the higher mortality rates observed in this investigation may be linked to hypertension. Indeed, a largescale multinational screening campaign evaluating over 2.5 million participants who had prior clinical history of stroke, identified a strong positive association with stroke mortality and mean systolic blood pressure, whereby high blood pressure was correlated with stroke mortality (Lin et al., 2022). Additionally, untreated hypertension has been linked to a 2-fold increase in hospital deaths following stroke (King et al., 2023). One theory is that the negative impact of cerebral oedema following ischaemic stroke may be exacerbated by increase cerebral blood pressure as a result of hypertension, which may ultimately compress the brain stem leading to death. In terms of pathology, post-mortem assessment of brain tissue from the perifocal zone of the ischaemic infarct region of the middle cerebral artery of ischaemic stroke patients with clinical history of hypertension noted increased arterial wall thickness and decreased luminal area compared to comparative brain tissue from non-hypertensive controls (Gychka et al., 2020).

Although the data regarding changes in body weight after experimental stroke is not statistically powered, a clear decreasing trend in body weight can be observed in SHRSPs that had been subjected to experimental stroke compared to sham controls. This is a recognised adverse effect after experimental stroke in preclinical studies and reflects what is seen clinically. Similar findings have been observed in other preclinical models of ischaemic stroke and in humans (Ahmed et al., 2019, Ishrat et al., 2019, Iwanami et al., 2011). The overall health of the animal declines rapidly within the acute phase post-stroke and as the health of the animal improves, body weight begins to normalise to baseline levels. Weight loss remains a common issue in patients post-stroke and in part has been linked to muscle wastage due to hemiparesis (Scherbakov et al., 2019). Additional data showed a clear trend in neuroscore after experimental stroke, whereby the most severe reduction in neuroscore is seen at acute timepoints post-stroke, with gradual improvements seen over time. Another factor that may negatively influence neuroscore in the acute post-

stroke include brain swelling and oedema, which are maximal during the acute phase (Liebeskind et al., 2019). Again, these findings relate to the severe damage to the brain during ischaemia and gradual activation of repair pathways leading to post-stroke recovery. During the recovery phase, new neuronal connections develop within brain tissues and the formation of neurons has been linked with behaviour recovery (Yan et al., 2023). A sharp decline followed by a gradual increase in neuroscore has been noted after experimental stroke (Bennion et al., 2018b, Ishrat et al., 2019, Ord et al., 2013).

Following tMCAO, gene expression in the ipsilateral hemisphere has been shown to be altered (Buga et al., 2008, Filippenkov et al., 2023). Different lengths of experimental stroke occlusion duration may influence gene expression post-stroke at distinct time-points. The current method, 10 minutes of occlusion stroke duration plus 1.5 hours of reperfusion, was compared to a previous method, 30 minutes of occlusion duration plus 1.5 hours of reperfusion and non-stroke controls. Regions of the brain relative to infarct, peri-infarct and remaining tissue were collected from stroke and non-stroke control animals. Of all genes investigated, only Mas1 was differentially expressed following ischaemic stroke. Mas1 was downregulated after 30 minutes of occlusion within the remaining tissue compared to the infarct region. As Mas1 expression was downregulated in the unaffected remaining tissue of the contralateral hemisphere, one may speculate that downregulation of Mas1 may be compensatory in these brain regions, for example to increase counter-regulatory axis of RAAS in the brain to compensate for reduced cerebral blood flow following stroke.

The length of reperfusion time was assessed to determine changes in the expression of ACE2, Mas1, VEGFA, VEGFB and RUNX1. There were no significant changes in gene expression across brain regions of the ipsi- and contra-lateral hemispheres following 10-minutes of occlusion and 1.5 hours of reperfusion or 10 minutes of occlusion and 4 hours of reperfusion. It is important to remember that lesion volume increases in the hours and days immediately following stroke before gradually subsiding (Schwamm et al., 1998, Sah et al., 2018). Perhaps if the expression of these genes were assessed at various time-point such as 24- 48- or 72 hours post-stroke, changes in gene expression may have been observed. However, issues with maintaining SHRSPs more than 24 hours following tMCAO, an issue that will be discussed later in this chapter, meant that this study was specifically designed to investigate up to 24 hours post-stroke.

In the Ang-(1-9) EV study, initial experimental design included the delivery of therapeutic EVs (1×10^{11} EVs total) four times over a 4-day period and the maintenance of animals to

10 days post-surgery. With this experimental design, presence of stroke-related adverse effects (described in Table 2.1), and, in some cases, mortality rate, was high within the stroke groups despite effective, prophylactic antihypertensive treatment. Post-mortem analysis identified large ischaemic lesion volumes which frequently encompassed the entire ipsilateral hemisphere. It was therefore concluded that despite the technical success of the burr hole and tMCAO surgeries, the short occlusion time of only 10 minutes resulted in very large infarct volume which most probably led to significant brain oedema and compression of the brain, culminating in death. Consequently, the number of animals exceeding the pre-defined humane endpoints within the PPL to be maintained to 10 days post-operatively or unforeseen deaths due to tMCAO surgery led to the implementation of experimental modifications to maximise the remaining time within my PhD studies. As opposed to assessing infarct size and neurological outcome up to day 10 post-stroke and expression of RAAS-related genes at 10-days post-stroke, the decision was made to assess the expression of RAAS-related genes at an acute time frame of 24 hours post-stroke, therefore circumventing issues with stroke associated adverse effects or mortality. By altering the length of time animals were maintained following stroke surgery, and in line with the standard EV dosing regimen, discussed in depth within the methods chapter and the *in vivo* optimisation chapter, animals were administered with 2.5×10^{10} Ang-(1-9) EVs, as opposed to 1×10^{11} Ang-(1-9) EVs, three hours following tMCAO and were humanely killed 24 hours following tMCAO.

Delivery of Ang-(1-9) EVs led to direct changes in ACE2, Mas1, TGFβ1, VEGFB, TNF and IL-1RN expression 24 hours after experimental stroke compared to either sham controls or vehicle treatment. There was no significant difference in ACE expression after Ang-(1-9) EV treatment following tMCAO, however, there were identifiable trends in this data. For example, within both the infarct and remaining tissue of the ipsilateral hemisphere, ACE expression trended towards downregulation after vehicle treatment compared to sham control. Interestingly however, following Ang-(1-9) EV treatment, ACE expression trended towards upregulation relative to the vehicle control, suggesting that Ang-(1-9) EV treatment may restore ACE expression to levels similar to that of the sham control. Perhaps the presence of Ang-(1-9) delivered by EVs leads to the upregulation of ACE to enable the conversion of Ang-(1-9) into Ang-(1-7) which may in turn stimulate the MasR and activate protective downstream mechanisms of the counter-regulatory axis of RAAS. Or, alternatively, increased ACE expression may lead to increased conversion of vasoconstrictive Ang II which binds to the AT_1R to stimulate the classical axis of RAAS. It is important to note that Mas1 expression was downregulated within the ipsilateral infarct

zone following Ang-(1-9) EV treatment post-stroke. In the peri-infarct zone of the ipsilateral hemisphere, Mas1 expression trended towards downregulation following vehicle treatment compared to the sham control, however Ang-(1-9) EV treatment again appeared to restore Mas1 expression similar to that of the sham control. Mas1 expression has been shown to be downregulated in Sprague-Dawley rat heart tissue following myocardial infarction, and in the brain peri-infarct zone of Wistar rats following tMCAO (Zhou et al., 2022, Arroja et al., 2019). One hypothesis may be that decreased Mas1 expression may lead to activation of the classical RAAS within the brain and may increase local blood pressure in the brain, perhaps to compensate for poor cerebral flow following ischaemic stroke. In order to confirm this theory additional genes would need to be investigated further, as well as monitoring of cerebral blood flow. MasR is known to form a heterodimer with AT_2R, perhaps, this observed downregulation of Mas1, may be due to dimerisation or indeed increased stimulation of the AT_2R (Leonhardt et al., 2017). It is important to mention that, although qPCR was carried out to investigate the expression of Agtr1a and Agtr2 in this study, variability was extremely high within groups and the majority of replicates provided undetermined values. Similarly, cerebral blood flow assessment was not able to be conducted on these animals due to the acute assessment time-point. If this study were to be continued, later time points may also be assessed to determine dynamic changes in cerebral blood flow.

ACE2 expression was downregulated in the remaining tissue of the ipsilateral hemisphere following vehicle treatment and to a greater extent following Ang-(1-9) EV treatment. A similar study found that Wistar subjected to tMCAO and treated with aCSF showed a trend towards decreased expression of ACE2 within the peri-infarct zone by 24 hours post-stroke (Arroja et al., 2019). One may postulate that as blood flow and glucose availability to the ischaemic penumbra can be significantly depressed following stroke, cells within the penumbra may be metabolically compromised, for example have impaired oxidative metabolism or reduced ATP availability, compensatory cellular mechanisms may result in reduced expression of certain genes (Belayev et al., 1997, Sims and Muyderman, 2010). Perhaps delivery of Ang-(1-9) EVs signalled to regulators of the ACE2 gene to suppress expression of ACE2, as local concentrations of Ang-(1-9) were temporally sufficient. Interestingly, ACE2 expression within the contralateral reaming tissue trended towards increased expression within vehicle and Ang-(1-9) EV treatment following stroke. Similarly, within the infarct region of the contralateral hemisphere ACE2 expression trended towards upregulation relative to sham control following Ang-(1-9) EV treatment. One may speculate that this trend towards an increase in ACE2 within the contralateral

tissue may lead to downstream activation of the protective counter-regulatory axis of the RAAS. However, further study must be conducted to build on this hypothesis.

Although most information relating to the expression of the angiogenic growth factor, VEGF, after RAAS modulation relate to myocardial infarction, it provides great insight into potential role of the RAAS and VEGF in cerebral ischaemia. Antagonism of the MasR via A779 has been shown to reduce VEGF-D expression in cardiac tissue of Sprague-Dawley rats that were subjected to myocardial infarction (Zhao et al., 2013). These findings suggest that by inhibiting the counter-regulatory axis of the RAAS, specifically through antagonism of the MasR, VEGF-D-dependent angiogenesis may be reduced. While VEGFA expression was similar between brain regions, hemispheres and treatment groups, VEGFB expression was downregulated in the peri-infarct zone of the ipsilateral hemisphere following stroke, irrespective of treatment group, compared to sham control. When compared to vehicle and Ang-(1-9) treatment of the contralateral hemisphere of the peri-infarct zone, vehicle, and Ang-(1-9) EV treatment within the ipsilateral hemisphere was downregulated. Similar trends in VEGFB expression were observed in the remaining tissue. As there was no significant difference or clear trend in VEGFB expression between Ang-(1-9) EV or vehicle treatment between brain regions and hemispheres, Ang-(1-9) does not appear to influence the expression of VEGFB post-stroke. However, as there are different isoforms of VEGF it would be interesting to understand how RAAS modulation through Ang-(1-9) may relate to other mechanisms of VEGF-mediated angiogenesis. As a result of these findings, it has been theorised that angiogenesis may be potentiated by isoforms that were not investigated. One study has suggested that VEGFB plays a more important role in cell survival than angiogenesis (Zhang et al., 2009). Downregulation of VEGFB suggests that delivery of Ang-(1-9) to stimulate the counter-regulatory axis of RAAS may suppress VEGFB-mediated angiogenesis or perhaps cell survival within the remaining ipsilateral tissue. Indeed, delivery of Ang II to C57BL/6 mice has been shown to increase VEGF concentrations and angiogenesis in Matrigel plugs, a cold liquid that solidifies under the skin following subcutaneous injection, through AT_1R activation, while blocking AT_2R using PD123319 antagonist enhanced VEGF expression (Tamarat et al., 2002). With this in mind, activation of AT_2R by Ang-(1-9) may suppress VEGF expression and prevent fibrosis following stroke.

Within the infarct and peri-infarct zone of the ipsilateral hemisphere TGFβ1 was significantly upregulated following vehicle treatment and Ang-(1-9) EV treatment. Clinically, TGFβ1 has previously been shown to be upregulated in the ischaemic penumbra of patients who had died due to ischaemic stroke (Krupinski et al., 1996). Additionally,

plasma levels of TGFβ1 have been found to be altered following intercranial haemorrhage (ICH), whereby some patients experience increased TGFβ1 levels and others experience low TGFβ1 levels (Taylor et al., 2017). Interestingly, ICH patients that have higher plasma TGFβ1 levels have been shown to correlate with better clinical outcomes and fewer deaths by 90 days post-stroke (Taylor et al., 2017). Preclinically, TGFβ1 treatment has been shown to improve functional outcomes in mice following ICH, while proinflammatory IL-6 was downregulated in cultured microglia cells following TGFβ1 treatment (Taylor et al., 2017). Mechanistically, TGFβ1 can influence cell differentiation and alter the expression of proinflammatory cytokines such as interferon-γ (IFNγ) (Takaki et al., 2006). TGFβ1 can be described as an anti-inflammatory cytokine and can suppress T cell proliferation and macrophage activation (Takaki et al., 2006). Therefore, upregulation of TGFβ1 within the brain tissue following ischaemic stroke irrespective of treatment, may prevent neuroinflammation and may ultimately be beneficial post-stroke. It would be interesting, however, to profile additional cytokines to determine whether Ang-(1-9) EVs delivered post-stroke may influence their expression.

There was no significant difference in IL-1α expression after Ang-(1-9) EV treatment following tMCAO, however, there were identifiable trends in this data. For example, within both the infarct and remaining tissue of the ipsilateral hemisphere, IL-1α expression trended towards upregulation after vehicle treatment compared to sham control. Interestingly however, following Ang-(1-9) EV treatment, IL-1α expression trended towards downregulation relative to the vehicle control, suggesting that Ang-(1-9) EV treatment restores IL-1α expression to levels similar to that of the sham control. The potential reduction in IL-1α as a result of Ang-(1-9) EV treatment may lead to decreased immune cell activation and signalling; however further study must be conducted in order to confirm this hypothesis. Within the infarct, peri-infarct and remaining tissue IL-1α expression trended towards downregulation in both vehicle and Ang-(1-9) EV treated stroke animals compared to sham controls. It may be speculated that localised reduction in IL-1α expression within the unaffected hemisphere of the brain may prevent IL-1α-mediated proinflammatory signalling, subsequent immune cell activation and resultant neuroinflammation in healthy brain tissue. IL-1 antagonism is known to reduce blood pressure within obese patients (Urwyler et al., 2020), while Wistar rats subjected to tMCAO followed by IL-1Ra treatment showed reduced infarct volume and improved neurological outcomes (Pradillo et al., 2017). IL-1 receptor antagonist, IL-1RN, was upregulated following vehicle treatment compared to sham control in the infarct zone of the ipsilateral hemisphere, while IL-1RN expression was similar to sham control following

Ang-(1-9) EV treatment. One may postulate that IL-1RN expression was upregulated to compete with IL-1α, preventing IL-1α binding to the IL-1 receptor and stimulating downstream proinflammatory pathways. It may be postulated that downregulation of IL-1α expression, perhaps through upregulation of IL-1RN by use of Ang-(1-9) may create a negative feedback look that may positively impact post-stroke outcomes.

TNF was upregulated in the remaining tissue of the ipsilateral hemisphere following stroke. Aside from its pro-inflammatory and pro-apoptosis roles, TNF can activate immune cells, such as dendritic cells, which subsequently prime other immune cells such as T cells (Jonuleit et al., 1997). The number of regulatory T cells within circulation has been linked to improved functional outcomes in ischaemic stroke patients (Santamaría-Cadavid et al., 2020). One may therefore speculate that this increase in TNF expression may not solely be linked to the pro-inflammatory cascade but may prime immune cells that can protect the brain following stroke. In future studies it would be interesting to carry out histology on brain sections following stroke and Ang-(1-9) EV treatment to identify whether these changes in cytokine expression may also relate to immune cell number and or infiltration.

Most research into the function of RUNX1 relates to cancer and cardiovascular disease, rather than cerebrovascular disease. In *this* study, RUNX1 expression was upregulated within peri-infarct zone of the ipsilateral hemispheres after vehicle treatment, but not Ang-(1-9) EV treatment, suggesting that Ang-(1-9) treatment may normalise RUNX1 expression similar to that of sham control. Adding to this, it may be theorised that Ang-(1-9) EV treatment may improve neuronal cell differentiation within the peri-infarct zone by increasing RUNX1 expression. This theory is supported by previous research that found disruption of RUNX1 signalling led to reduced neuronal stem or progenitor cell proliferation *in vitro* (Logan et al., 2015). In mouse models of ischaemic heart injury, RUNX1 expression was upregulated in C57BL/6 mice following myocardial infarction (McCarroll et al., 2018). As such, RUNX1 may also have beneficial roles following cerebral ischaemia that may be linked to Ang-(1-9).

7.5.1 Study limitations

The data provided for animals that had undergone stroke and were able to be maintained to 10-days post-surgery was too small to derive any statistical significance, though trends in data can be observed. Due to experimental modifications, lack of animal availability and limited time remaining in my PhD studies, the group sizes within the study investigating

the effects of therapeutic Ang-(1-9) EVs were small, treatment groups were limited to three or four animals, however significance could be drawn from this data. If animal availability was not a major issue, it may have been beneficial to add an additional treatment group, or substitute vehicle control for unloaded EV control to assess their effect on gene expression post-stroke. Unloaded EVs isolated from bone marrow derived dendritic cells were applied to B16 melanoma cell lines and led to increased T cell response and reduced tumour growth, while EVs loaded with antibodies targeting checkpoint inhibitor and its ligand programmed cell death protein 1 or programmed death ligand 1, compounded this increased T cell response and reduced tumour cell growth (Veerman et al., 2023). Such studies demonstrate the therapeutic effect of unloaded EVs in disease and emphasise the importance of including unloaded EV controls in future studies. Additional EV concentrations could have been assessed to determine their effects on gene expression. If animal mortality and availability was not an issue in this investigation, the number of animals being maintained to 10-days would have been greater and the effects of Ang-(1-9) EVs on neuroscore and cognition assessment post-stroke, infarct volume and the expression of RAAS related gene could have been assessed at a later stage post-stroke.

Within the study assessing the effects of post-stroke reperfusion time on gene expression, only two reperfusion time-points (1.5- and 4-hours) were assessed, along with representative tissues from non-stroke control animals. A third reperfusion timepoint, 24-hours, was also investigated; however, a stable housekeeping gene could not be established within this group and so was omitted from further qPCR analysis. As mentioned, animals that had undergone 10 minutes of occlusion displayed an infarct volume that, in most cases, spanned the entire ipsilateral hemisphere. The cell death within the infarct region may be attributed to issues of establishing a stable housekeeper for the 24-hour timepoint. Again, assessing the effects of longer stroke time points on gene expression would have been beneficial. However, as previously noted, animals that had undergone 10 minutes of occlusion had large infarct volumes. It can therefore be theorised that animals subjected to a 30-minute occlusion period may have even larger infarct volumes which in turn may lead to greater neuronal cell death and subsequent issues with housekeeping gene stability. Additionally, with such a large infarct volume after only 10 minutes of occlusion in the SHRSP model, one may question whether elongation of the occlusion time is required when shorter occlusion timepoints already result in all-encompassing hemisphere lesions.

Throughout this thesis a stable housekeeper was defined as a gene that was constitutively detected that provided an average CT across samples with a SD of <0.5. Within the Ang-(1-9) EV study, it was difficult to establish a stable housekeeper. Several housekeeping

genes were assessed for their stability and PCR/qPCR plates were repeated to improve SD within housekeeping genes. Despite the range of possible housekeeper genes assessed and repetition of both cDNA and qPCR, a SD of <0.5 could not be established. Within most housekeeping genes the infarct zone provided the most variable CT value and in turn related to large SD values. As previously reported, 10 minutes of occlusion led to large lesion volumes and the cell death within this area at 24h reperfusion would be significant in hypertensive animals, therefore the expression of any gene, be it a housekeeper or gene of interest, may be variable. Additionally, lesion size may vary between animals which may influence variability in housekeeping genes between animals. As β-actin provided a SD value closest to 0.5, this housekeeping gene was used to assess changes in gene expression after Ang-(1-9) EV treatment in experimental models of stroke. If time and animal availability were not limiting factors in this experiment, additional animals would be added to groups to ensure the study was significantly powered. To achieve 80% power to detect a change in dCT of 1.25 at a significance level of 0.05 and a SD of 0.60, approximately 4 animals would be required per group. With this increase in animal number variability between samples CT values and resultantly dCT SD may also be reduced.

The relative changes in gene expression identified in this study is representative of changes within mRNA, not enzymatic or protein activity. Further enzymatic assays should be conducted to determine whether Ang-(1-9) delivered using EVs relates to changes in ACE and ACE2 activity within brain tissue after experimental intervention. The expression of IL-10, IL-6, Agtr1a and Agtr2 could not be established using conventional mRNA expression. Additional methods such as western blotting could be carried out to provide information on levels of protein expression and thus relative gene expression. Micro-array analysis and RNA-Seq techniques may also be able to provide information into gene expression.

7.5.2 Summary

The length of stroke affected the expression of Mas1 within the contralateral unaffected hemisphere following 30 minutes of occlusion. Reperfusion duration following tMCAO did not affect gene expression following either 1.5- or 4- hours of reperfusion. Interestingly, Ang-(1-9) EVs delivered intranasally after experimental ischaemic stroke led to changes within gene expression, such as those associated with growth, immune response and the RAAS. Ang-(1-9) EV treatment, in several cases led to trends in gene expression similar to that of sham animals, suggesting a possible restorative effect of Ang-(1-9).

Further studies into the mechanisms of how Ang-(1-9) may influence these genes should be conducted to better understand the potential therapeutic role of Ang-(1-9) following ischaemic stroke.

Chapter 8 General discussion

Several clinical studies have been conducted to better understand the risks of stroke and application of novel clinical interventions in treating ischaemic stroke. Unfortunately, despite these studies, there are few drugs discovered that can reduce post-stroke tissue damage and resultant death or disability. This thesis investigated the synergy between a well understood, deeply studied pathway, the RAAS, and a novel drug delivery system, EVs, in preclinical models of ischaemic stroke. The hypothesis of this thesis was that AT_2R stimulation by the novel peptide Ang-(1-9) could be neuroprotective post-stroke. This hypothesis was based on evidence, discussed in detail in chapter 3 of this thesis, suggesting that stimulation of the receptors and downstream pathways of the counter-regulatory axis of the RAAS may be neuroprotective post-stroke.

In this thesis peer-reviewed published data was systematically compared to determine the benefits of RAAS targeting interventions, whereby most studies identified its benefit in preclinical models of stroke. Additionally, this thesis demonstrates that alteration of the RAAS by means of genetic AT_2R deficiency may lead to changes in EV characteristics, while this study also brought to light differences in EV characteristics between sexes in these animals. The EV isolation method was found to affect EV concentration, which is supported by past and current literature (Thery et al., 2006, Musante et al., 2013, Thery et al., 2018, 2022, Ter-Ovanesyan et al., 2023, Izon Science, 2023a). Ang-(1-9) peptide and electroporated EVs did not lead to significant changes in cell viability, supporting its use in further *in vivo* studies. Intranasal delivery of EVs prove beneficial in delivering internalised EV cargo to the brain, while RVG targeting of EVs delivered intranasally did not improve EV cargo uptake. The in vivo study investigated the potential therapeutic ability of EVs electroporated with Ang-(1-9) in preclinical tMCAO rodent models. The expected output of this experiment was to assess neurological outcomes, infarct volume and gene expression. However, due to issues with animal mortality, only gene expression analysis could be conducted. Intranasal delivery of Ang-(1-9) EV post-stroke led to changes in genes relating to the RAAS, growth and inflammation. EV mediated delivery of Ang-(1-9) downregulated the genes encoding MasR and ACE2, components of the counter-regulatory axis of the RAAS, while appearing to normalise the expression of genes relating to BBB integrity and inflammation. As such intranasal delivery of Ang-(1-9) by EVs, led to EV cargo delivery to the brain and subsequent alteration of gene expression within the brain of a rodent ischaemic stroke model.

The benefit of systematically reviewing data related to the effects of RAAS targeting interventions in preclinical models of stroke is that it allows for direct comparison between studies assessing similar functional outcomes. In doing so, the benefits of RAAS targeting interventions in stroke were uncovered and ultimately supported the hypothesis of this thesis whereby AT$_2$R stimulation would lead to better post-stroke outcomes. An interesting finding of this investigation revealed that AT$_2$R deficiency led to changes in EV characteristics, which to date, has never been previously studied. This study also highlighted the paucity in studies characterising EVs in female subjects and subsequently the need to increase the numbers of female subjects included in scientific research. Moreover, this investigation also highlights the need for standardising cell specific EV markers. The prospect of targeting EVs to the brain is important in maximising EV cargo delivery. Although RVG targeting did not improve EV cargo delivery to the brain in this investigation, others have demonstrated its success in trafficking EVs to the brain (Alvarez-Erviti et al., 2011, Haroon et al., 2023, Gao et al., 2018). In future other targeting molecules such as T7 or c(RGDyK) peptides may also be considered when attempting to target EVs to the brain (Kim et al., 2020, Tian et al., 2018).

To date, there have been no published studies investigating the role of Ang-(1-9) in ischaemic stroke models, however, several studies have investigated Ang-(1-7) in preclinical models of stroke (Arroja et al., 2019, Bennion et al., 2018b, Jiang et al., 2014, Kuipers et al., 2020, Regenhardt et al., 2013). Ang-(1-9) is preferentially broken down by NEP to Ang-(1-7). It is therefore worth considering whether Ang-(1-9) delivered through EVs might be broken down to Ang-(1-7). Consequently, the expected AT$_2$R mediated neuroprotective effects of Ang-(1-9) EV, may be, in reality, caused by MasR activation. If animal mortality were not an issue in this investigation, levels of Ang-(1-7) and Ang-(1-9) within brain tissue and circulation could have been determined, along with cognate receptor expression, to fully understand the protective mechanisms of Ang-(1-9) in stroke, for example by use of LCMS or newly developed Ang-(1-9) antibodies. Further Ang-(1-9) EVs could have been administered in conjunction with the MasR antagonist, for example PD123319 or A779, to better understand the potential therapeutic effects of Ang-(1-9) stimulation of the AT$_2$R in stroke. Alternatively, AT$_2$R antagonists may also be used to demonstrate that Ang-(1-9) effects are mediated through the AT$_2$R.

Upon isolation from biofluid or tissue, EVs may be used as biomarkers or may be applied therapeutically, however they are more commonly investigated for their biomarker potential (Kumar et al., 2024, Irmer et al., 2023, Klyachko et al., 2020). EV derived miRNAs have been established as biomarkers in many diseases including cancer and

stroke (Jiang et al., 2022, Bang et al., 2023, Fullerton et al., 2023). EVs isolated from the blood of acute ischaemic stroke patients have shown enrichment of miRNA-134 and miRNA-223 which are correlated to worse NIHSS, infarct volume and prognosis (Zhou et al., 2018, Chen et al., 2017). Similarly, EVs derived from the serum of acute ischaemic stroke patients are also enriched in miRNA-9 and miR-124 which are correlated to increased pro-inflammatory serum IL-6 concentrations, suggesting a relationship between EVs miRNAs and neuroinflammation (Ji et al., 2016). EV miRNAs may also be used to diagnose stages of stroke, whereby EVs enriched in miRNA-21 and miRNA-30a were used to distinguish between the hyperacute phase, acute phase, subacute phase, and recovery phase of ischaemic stroke patients, potentially enabling better satisfaction of stroke patients after hospital admission (Wang et al., 2018). As EV miRNA cargo has been correlated with severity, infarct volume and prognosis, EVs have real potential to be used in clinical practice.

8.1 Future perspectives

EVs in clinical practice, aside from as biomarkers in disease, would most probably be used in personalised medicine. For example, EVs could be isolated from a patient and may be loaded with therapeutic compounds, or cells isolated from the patient may be cultured and in turn EVs may be isolated from these cells. Isolation of EVs from patient cell culture would be a lengthy process, and in diseases where time is a limiting factor, other synthetic lipid based nanoparticles may be more appropriate for use, for example liposomes. Liposomes, like EVs, are circular lipid bilayers that may be used to store internal cargo and have previously been assessed in ischaemic models (Zahednezhad et al., 2019, Campos-Martorell et al., 2016, Fukuta et al., 2015). Liposomes may be recognised by the host immune system leading to allergic responses, and like EVs, may be cleared from the body (Ishida et al., 2006, Driedonks et al., 2022). Liposomes, however, have one benefit over EVs in that their fundamental components and content can be controlled and subsequently regulated. In 1995 the US Food and Drug Administration (FDA) approved the use of Doxil, the first-of-its-kind, injectable liposome containing the anti-cancer drug doxorubicin (Barenholz, 2012). From 1995 to 2024, very few liposome products were approved by the FDA and European Medicines Agency, although most that have been approved are indicated for use in cancer (Liu et al., 2022a). Most recently, in February of 2024, the FDA approved the liposome irinotecan for first-line treatment for metastatic pancreatic

adenocarcinoma following the success of the NAPOLI3 clinical trial (US Food and Drug Administration, 2024).

Unfortunately, to date there is no EV based therapeutic licenced for use. Although in October of 2021, under EMA designation EU/3/21/2508, EVs have been given orphan designation, to be used under rare and strict circumstances, to prevent bronchopulmonary dysplasia (European Medicine Agency, 2021). According to clicialtrials.gov, there are 2 active fully recruited EV studies ongoing in 2024, one looking at EV biomarkers in stroke, and the other looking at EVs in wound healing. The safety and use of liposomes in disease has been established, mainly as liposomes have been studied longer than EVs. However, liposomes lack the targeting efficacy that EVs possess. Therefore, some groups have combined both EVs and liposome nanoparticles to form EV-liposome hybrid particles that share the beneficial properties of EVs and liposomes(Lin et al., 2018, Evers et al., 2022). A large amount of exciting preclinical research will need to be conducted prior to clinical trial assessment of EV-liposome hybrids in disease.

With preclinical research in mind, given the overwhelmingly neuroprotective effects of the small molecule C21 determined in the systematic review chapter of this thesis, a new research avenue may have been identified (Ahmed et al., 2018, Alhusban et al., 2015, Bennion et al., 2018a, Eldahshan et al., 2019, Eldahshan et al., 2021, Fouda et al., 2017, Jackson et al., 2020, Joseph et al., 2014, McCarthy et al., 2014, Min et al., 2014, Schwengel et al., 2016, Shan et al., 2018). Research into the effects of small molecules in preclinical stroke models is limited(Wu et al., 2023). Encapsulating small molecules in EVs or liposomes may improve brain-specific targeting and molecule delivery, which is an exciting prospect. On a similar note, with better understanding of stroke pathology over the course of this thesis, it may also be interesting to determine the therapeutic potential of EVs or EV-liposome hybrids loaded with glutamate receptor inhibitors post-stroke, as excitotoxicity is the premier cause of damage to the brain following stroke (Belov Kirdajova et al., 2020, Wetterling et al., 2016). Investigators have shown the neuroprotective qualities of glutamate receptor inhibitors post-stroke, however to date, no study has assessed the therapeutic potential of EV or liposome mediated delivery of glutamate receptor inhibitors post-stroke (Hakon et al., 2024). Considering the success of both small molecules in activating the AT_2R and glutamate receptor inhibitors in preclinical models, the prospect of investigating the potential of EVs or EV-liposome hybrids in stroke is intriguing.

8.2 Concluding remarks

In conclusion, the data compiled in this thesis support the hypothesis that RAAS targeting interventions, for example Ang-(1-9), may be beneficial in treating ischaemic stroke. These results may be combined with published literature to expand upon the potential neuroprotective benefits of RAAS targeting interventions in stroke. The results of this thesis support the use of EVs as a reliable delivery vector for potential therapeutics, not solely in ischaemic stroke, but in all other diseases. Future work will continue to focus on EV or EV-liposome hybrid mediated delivery of potential therapeutic compounds or molecules that may be neuroprotective post-stroke.

References

ABADIR, P. M., CAREY, R. M. & SIRAGY, H. M. 2003. Angiotensin AT2 Receptors Directly Stimulate Renal Nitric Oxide in Bradykinin B2-Receptor–Null Mice. *Hypertension,* 42**,** 600-604.

ADAMCOVA, M., KAWANO, I. & SIMKO, F. 2021. The Impact of microRNAs in Renin-Angiotensin-System-Induced Cardiac Remodelling. *Int J Mol Sci,* 22.

ADMYRE, C., JOHANSSON, S. M., QAZI, K. R., FILÉN, J.-J., LAHESMAA, R., NORMAN, M., NEVE, E. P. A., SCHEYNIUS, A. & GABRIELSSON, S. 2007. Exosomes with Immune Modulatory Features Are Present in Human Breast Milk1. *The Journal of Immunology,* 179**,** 1969-1978.

AHMAD, E., FENG, Y., QI, J., FAN, W., MA, Y., HE, H., XIA, F., DONG, X., ZHAO, W., LU, Y. & WU, W. 2017. Evidence of nose-to-brain delivery of nanoemulsions: cargoes but not vehicles. *Nanoscale,* 9**,** 1174-1183.

AHMED, H. A., ISHRAT, T., PILLAI, B., BUNTING, K. M., VAZDARJANOVA, A., WALLER, J. L., ERGUL, A. & FAGAN, S. C. 2019. Angiotensin receptor (AT2R) agonist C21 prevents cognitive decline after permanent stroke in aged animals-A randomized double- blind pre-clinical study. *Behavioural brain research,* 359**,** 560-569.

AHMED, H. A., ISHRAT, T., PILLAI, B., FOUDA, A. Y., SAYED, M. A., ELDAHSHAN, W., WALLER, J. L., ERGUL, A. & FAGAN, S. C. 2018. RAS modulation prevents progressive cognitive impairment after experimental stroke: a randomized, blinded preclinical trial. *Journal of neuroinflammation,* 15**,** 229.

AIYAGARI, V. & GORELICK, P. B. 2009. Management of Blood Pressure for Acute and Recurrent Stroke. *Stroke,* 40**,** 2251-2256.

AKBAR, N., BRAITHWAITE, A. T., CORR, E. M., KOELWYN, G. J., VAN SOLINGEN, C., COCHAIN, C., SALIBA, A.-E., CORBIN, A., PEZZOLLA, D., MØLLER JØRGENSEN, M., BÆK, R., EDGAR, L., DE VILLIERS, C., GUNADASA-ROHLING, M., BANERJEE, A., PAGET, D., LEE, C., HOGG, E., COSTIN, A., DHALIWAL, R., JOHNSON, E., KRAUSGRUBER, T., RIEPSAAME, J., MELLING, G. E., SHANMUGANATHAN, M., OXFORD ACUTE MYOCARDIAL INFARCTION, S., BOCK, C., CARTER, D. R. F., CHANNON, K. M., RILEY, P. R., UDALOVA, I. A., MOORE, K. J., ANTHONY, D. C. & CHOUDHURY, R. P. 2022. Rapid neutrophil mobilization by VCAM-1+ endothelial cell-derived extracellular vesicles. *Cardiovascular Research,* 119**,** 236-251.

AKERS, J. C., RAMAKRISHNAN, V., YANG, I., HUA, W., MAO, Y., CARTER, B. S. & CHEN, C. C. 2016. Optimizing preservation of extracellular vesicular miRNAs derived from clinical cerebrospinal fluid. *Cancer Biomark,* 17**,** 125-32.

AL SHOYAIB, A., ARCHIE, S. R. & KARAMYAN, V. T. 2019. Intraperitoneal Route of Drug Administration: Should it Be Used in Experimental Animal Studies? *Pharm Res,* 37**,** 12.

ALBELDA, S. M., OLIVER, P. D., ROMER, L. H. & BUCK, C. A. 1990. EndoCAM: a novel endothelial cell-cell adhesion molecule. *J Cell Biol,* 110**,** 1227-37.

ALBERS, G. W., MARKS, M. P., KEMP, S., CHRISTENSEN, S., TSAI, J. P., ORTEGA-GUTIERREZ, S., MCTAGGART, R. A., TORBEY, M. T., KIM-TENSER, M., LESLIE-MAZWI, T., SARRAJ, A., KASNER, S. E., ANSARI, S. A., YEATTS, S. D., HAMILTON, S., MLYNASH, M., HEIT, J. J., ZAHARCHUK, G., KIM, S., CARROZZELLA, J., PALESCH, Y. Y., DEMCHUK, A. M., BAMMER, R., LAVORI, P. W., BRODERICK, J. P. & LANSBERG, M. G. 2018. Thrombectomy for Stroke at 6 to 16 Hours with Selection by Perfusion Imaging. *N Engl J Med,* 378**,** 708-718.

ALHUSBAN, A., FOUDA, A. Y., BINDU, P., ISHRAT, T., SOLIMAN, S. & FAGAN, S. C. 2015. Compound 21 is pro-angiogenic in the brain and results in sustained recovery after ischemic stroke. *Journal of hypertension,* 33**,** 170-80.

ALLEN, C. L. & BAYRAKTUTAN, U. 2009. Oxidative stress and its role in the pathogenesis of ischaemic stroke. *Int J Stroke,* 4**,** 461-70.

ALVAREZ-ERVITI, L., SEOW, Y., YIN, H., BETTS, C., LAKHAL, S. & WOOD, M. J. 2011. Delivery of siRNA to the mouse brain by systemic injection of targeted exosomes. *Nat Biotechnol,* 29**,** 341-5.

AMERICAN STROKE ASSOCIATION. 2023a. *About Stroke* [Online]. Available: https://www.stroke.org/en/about-stroke#:~:text=Stroke%20is%20a%20disease%20that,or%20bursts%20(or%20rupt ures [Accessed 31.10.2023 2023].

AMERICAN STROKE ASSOCIATION. 2023b. *Hemorrhagic Stroke* [Online]. Available: https://www.stroke.org/en/about-stroke/types-of-stroke/hemorrhagic-strokes-bleeds [Accessed 31.10.2023 2023].

AMERICAN STROKE ASSOCIATION. 2023c. *Ischemic Stroke (clots)* [Online]. Available: https://www.stroke.org/en/about-stroke/types-of-stroke/ischemic-stroke-clots [Accessed 31.10.2023 2023].

AMIRIFAR, L., SHAMLOO, A., NASIRI, R., DE BARROS, N. R., WANG, Z. Z., UNLUTURK, B. D., LIBANORI, A., IEVGLEVSKYI, O., DILTEMIZ, S. E., SANCES, S., BALASINGHAM, I., SEIDLITS, S. K. & ASHAMMAKHI, N. 2022. Brain-on-a-chip: Recent advances in design and techniques for microfluidic models of the brain in health and disease. *Biomaterials,* 285**,** 121531.

ANAND, S., SAMUEL, M., KUMAR, S. & MATHIVANAN, S. 2019. Ticket to a bubble ride: Cargo sorting into exosomes and extracellular vesicles. *Biochimica et Biophysica Acta (BBA) - Proteins and Proteomics,* 1867**,** 140203.

ANDERSON, C. S., HUANG, Y., LINDLEY, R. I., CHEN, X., ARIMA, H., CHEN, G., LI, Q., BILLOT, L., DELCOURT, C., BATH, P. M., BRODERICK, J. P., DEMCHUK, A. M., DONNAN, G. A., DURHAM, A. C., LAVADOS, P. M., LEE, T.-H., LEVI, C., MARTINS, S. O., OLAVARRIA, V. V., PANDIAN, J. D., PARSONS, M. W., PONTES-NETO, O. M., RICCI, S., SATO, S., SHARMA, V. K., SILVA, F., SONG, L., THANG, N. H., WARDLAW, J. M., WANG, J.-G., WANG, X., WOODWARD, M., CHALMERS, J., ROBINSON, T. G., ANDERSON, C. S., HUANG, Y., LINDLEY, R. I., CHEN, X., ARIMA, H., CHEN, G., LI, Q., BILLOT, L., DELCOURT, C., BATH, P. M., BRODERICK, J. P., DEMCHUK, A. M., DONNAN, G. A., DURHAM, A. C., LAVADOS, P. M., LEE, T.-H., LEVI, C., MARTINS, S. O., OLAVARRIA, V. V., PANDIAN, J. D., PARSONS, M. W., PONTES-NETO, O. M., RICCI, S., SATO, S., SHARMA, V. K., SILVA, F., SONG, L., THANG, N. H., WARDLAW, J. M., WANG, J.-G., WANG, X., WOODWARD, M., CHALMERS, J., ROBINSON, T. G., KIM, J. S., STAPF, C., SIMES, R. J., HANKEY, G. J., SANDERCOCK, P., BOUSSER, M.-G., WONG, K. S. L., SCARIA, A., HIRAKAWA, Y., MOULLAALI, T. J., CARCEL, C., GORDON, P., FUENTES-PATARROYO, S. X., BENITO, D., CHEN, R., CAO, Y., KUNCHOK, A., WINTERS, S., COUTTS, S., YOSHIMURA, S., YOU, S., YANG, J., WU, G., ZHANG, S., MANNING, L., MISTRI, A., HAUNTON, V., MINHAS, J., MALAVERA, A., LIM, J., LIU, L., KUMAR, N. N., et al. 2019. Intensive blood pressure reduction with intravenous thrombolysis therapy for acute ischaemic stroke (ENCHANTED): an international, randomised, open-label, blinded-endpoint, phase 3 trial. *The Lancet,* 393**,** 877-888.

ANDERSON, C. S., ROBINSON, T., LINDLEY, R. I., ARIMA, H., LAVADOS, P. M., LEE, T.-H., BRODERICK, J. P., CHEN, X., CHEN, G., SHARMA, V. K., KIM, J. S., THANG, N. H., CAO, Y., PARSONS, M. W., LEVI, C., HUANG, Y., OLAVARRÍA, V. V., DEMCHUK, A. M., BATH, P. M., DONNAN, G. A.,

MARTINS, S., PONTES-NETO, O. M., SILVA, F., RICCI, S., ROFFE, C., PANDIAN, J., BILLOT, L., WOODWARD, M., LI, Q., WANG, X., WANG, J. & CHALMERS, J. 2016. Low-Dose versus Standard-Dose Intravenous Alteplase in Acute Ischemic Stroke. *New England Journal of Medicine,* 374**,** 2313-2323.

ANDERSON, W. P., JOHNSTON, C. I. & KORNER, P. I. 1979. Acute renal haemodynamic and renin-angiotensin system responses to graded renal artery stenosis in the dog. *J Physiol,* 287**,** 231-45.

ANTONIOU, A., AUDERSET, L., KAURANI, L., SEBASTIAN, E., ZENG, Y., ALLAHHAM, M., CASES-CUNILLERA, S., SCHOCH, S., GRUENDEMANN, J., FISCHER, A. & SCHNEIDER, A. 2023. Neuronal extracellular vesicles and associated microRNAs induce circuit connectivity downstream BDNF. *Cell Rep,* 42**,** 112063.

ARAB, T., MALLICK, E. R., HUANG, Y., DONG, L., LIAO, Z., ZHAO, Z., GOLOLOBOVA, O., SMITH, B., HAUGHEY, N. J., PIENTA, K. J., SLUSHER, B. S., TARWATER, P. M., TOSAR, J. P., ZIVKOVIC, A. M., VREELAND, W. N., PAULAITIS, M. E. & WITWER, K. W. 2021. Characterization of extracellular vesicles and synthetic nanoparticles with four orthogonal single-particle analysis platforms. *J Extracell Vesicles,* 10**,** e12079.

ARAC, A., GRIMBALDESTON, M. A., GALLI, S. J., BLISS, T. M. & STEINBERG, G. K. 2019. Meningeal Mast Cells as Key Effectors of Stroke Pathology. *Front Cell Neurosci,* 13**,** 126.

ARMSTRONG, E. J., CHEN, D. C., SINGH, G. D., AMSTERDAM, E. A. & LAIRD, J. R. 2015. Angiotensin-converting enzyme inhibitor or angiotensin receptor blocker use is associated with reduced major adverse cardiovascular events among patients with critical limb ischemia. *Vasc Med,* 20**,** 237-44.

ARNESEN, T. & NORD, E. 1999. The value of DALY life: problems with ethics and validity of disability adjusted life years. *Bmj,* 319**,** 1423-5.

ARROJA, M. M. C., REID, E., ROY, L. A., VALLATOS, A. V., HOLMES, W. M., NICKLIN, S. A., WORK, L. M. & MCCABE, C. 2019. Assessing the effects of Ang-(1-7) therapy following transient middle cerebral artery occlusion. *Scientific reports,* 9**,** 3154.

AUBER, M. & SVENNINGSEN, P. 2022. An estimate of extracellular vesicle secretion rates of human blood cells. *Journal of Extracellular Biology,* 1**,** e46.

BABKINA, A. S., YADGAROV, M. Y., OSTROVA, I. V., ZAKHARCHENKO, V. E., KUZOVLEV, A. N., GRECHKO, A. V., LYUBOMUDROV, M. A. & GOLUBEV, A. M. 2022. Serum Levels of VEGF-A and Its Receptors in Patients in Different Phases of Hemorrhagic and Ischemic Strokes. *Current Issues in Molecular Biology* [Online], 44.

BACHSTETTER, A. D. & VAN ELDIK, L. J. 2010. The p38 MAP Kinase Family as Regulators of Proinflammatory Cytokine Production in Degenerative Diseases of the CNS. *Aging Dis,* 1**,** 199-211.

BALLINGER, S. W., PATTERSON, C., YAN, C.-N., DOAN, R., BUROW, D. L., YOUNG, C. G., YAKES, F. M., VAN HOUTEN, B., BALLINGER, C. A., FREEMAN, B. A. & RUNGE, M. S. 2000. Hydrogen Peroxide– and Peroxynitrite-Induced Mitochondrial DNA Damage and Dysfunction in Vascular Endothelial and Smooth Muscle Cells. *Circulation Research,* 86**,** 960-966.

BANG, O. Y., KIM, E. H., OH, M. J., YOO, J., OH, G. S., CHUNG, J. W., SEO, W. K., KIM, G. M., AHN, M. J. & YANG, S. W. 2023. Circulating Extracellular-Vesicle-Incorporated MicroRNAs as Potential Biomarkers for Ischemic Stroke in Patients With Cancer. *J Stroke,* 25**,** 251-265.

BARENHOLZ, Y. 2012. Doxil® — The first FDA-approved nano-drug: Lessons learned. *Journal of Controlled Release,* 160**,** 117-134.

BARONE, F. C., ARVIN, B., WHITE, R. F., MILLER, A., WEBB, C. L., WILLETTE, R. N., LYSKO, P. G. & FEUERSTEIN, G. Z. 1997. Tumor Necrosis Factor-α. *Stroke,* 28**,** 1233-1244.

BEDERSON, J. B., PITTS, L. H., TSUJI, M., NISHIMURA, M. C., DAVIS, R. L. & BARTKOWSKI, H. 1986. Rat middle cerebral artery occlusion: evaluation of the model and development of a neurologic examination. *Stroke,* 17**,** 472-6.

BEEBE, S. J., CHEN, Y. J., SAIN, N. M., SCHOENBACH, K. H. & XIAO, S. 2012. Transient features in nanosecond pulsed electric fields differentially modulate mitochondria and viability. *PLoS One,* 7**,** e51349.

BEKCI, E., GOKMEN, R. C., KANIT, L., GOZEN, O., BALKAN, B., KOYLU, E. O. & KESER, A. 2024. Enhanced Novel Object Recognition and Spatial Memory in Rats Selectively Bred for High Nicotine Preference. *Brain Sciences* [Online], 14.

BELAYEV, L., ZHAO, W., BUSTO, R. & GINSBERG, M. D. 1997. Transient Middle Cerebral Artery Occlusion by Intraluminal Suture: I. Three-Dimensional Autoradiographic Image-Analysis of Local Cerebral Glucose Metabolism—Blood Flow Interrelationships during Ischemia and Early Recirculation. *Journal of Cerebral Blood Flow & Metabolism,* 17**,** 1266-1280.

BELOV KIRDAJOVA, D., KRISKA, J., TURECKOVA, J. & ANDEROVA, M. 2020. Ischemia-Triggered Glutamate Excitotoxicity From the Perspective of Glial Cells. *Front Cell Neurosci,* 14**,** 51.

BENDER, L. M., MORGAN, M. J., THOMAS, L. R., LIU, Z. G. & THORBURN, A. 2005. The adaptor protein TRADD activates distinct mechanisms of apoptosis from the nucleus and the cytoplasm. *Cell Death Differ,* 12**,** 473-81.

BENEDEK, A., MÓRICZ, K., JURÁNYI, Z., GIGLER, G., LÉVAY, G., HÁRSING, L. G., JR., MÁTYUS, P., SZÉNÁSI, G. & ALBERT, M. 2006. Use of TTC staining for the evaluation of tissue injury in the early phases of reperfusion after focal cerebral ischemia in rats. *Brain Res,* 1116**,** 159-65.

BENEDIKTER, B. J., BOUWMAN, F. G., VAJEN, T., HEINZMANN, A. C. A., GRAULS, G., MARIMAN, E. C., WOUTERS, E. F. M., SAVELKOUL, P. H., LOPEZ-IGLESIAS, C., KOENEN, R. R., ROHDE, G. G. U. & STASSEN, F. R. M. 2017. Ultrafiltration combined with size exclusion chromatography efficiently isolates extracellular vesicles from cell culture media for compositional and functional studies. *Sci Rep,* 7**,** 15297.

BENNION, D. M., ISENBERG, J. D., HARMEL, A. T., DEMARS, K., DANG, A. N., JONES, C. H., PIGNATARO, M. E., GRAHAM, J. T., STECKELINGS, U. M., ALEXANDER, J. C., FEBO, M., KRAUSE, E. G., DE KLOET, A. D., CANDELARIO-JALIL, E. & SUMNERS, C. 2017. Post-stroke angiotensin II type 2 receptor activation provides long-term neuroprotection in aged rats. *PloS one,* 12**,** e0180738.

BENNION, D. M., JONES, C. H., DANG, A. N., ISENBERG, J., GRAHAM, J. T., SUMNERS, C., LINDBLAD, L., DOMENIG, O., POGLITSCH, M., WATERS, M. F. & STECKELINGS, U. M. 2018a. Protective effects of the angiotensin II AT2 receptor agonist compound 21 in ischemic stroke: A nose-to-brain delivery approach. *Clinical Science,* 132**,** 581-593.

BENNION, D. M., JONES, C. H., DONNANGELO, L. L., GRAHAM, J. T., ISENBERG, J. D., DANG, A. N., RODRIGUEZ, V., SINISTERRA, R. D. M., SOUSA, F. B., SANTOS, R. A. S. & SUMNERS, C. 2018b. Neuroprotection by post-stroke administration of an oral formulation of angiotensin-(1-7) in ischaemic stroke. *Experimental physiology,* 103**,** 916-923.

BERKHEMER, O. A., FRANSEN, P. S., BEUMER, D., VAN DEN BERG, L. A., LINGSMA, H. F., YOO, A. J., SCHONEWILLE, W. J., VOS, J. A., NEDERKOORN, P. J., WERMER, M. J., VAN WALDERVEEN, M. A., STAALS, J., HOFMEIJER, J., VAN OOSTAYEN, J. A., LYCKLAMA À

NIJEHOLT, G. J., BOITEN, J., BROUWER, P. A., EMMER, B. J., DE BRUIJN, S. F., VAN DIJK, L. C., KAPPELLE, L. J., LO, R. H., VAN DIJK, E. J., DE VRIES, J., DE KORT, P. L., VAN ROOIJ, W. J., VAN DEN BERG, J. S., VAN HASSELT, B. A., AERDEN, L. A., DALLINGA, R. J., VISSER, M. C., BOT, J. C., VROOMEN, P. C., ESHGHI, O., SCHREUDER, T. H., HEIJBOER, R. J., KEIZER, K., TIELBEEK, A. V., DEN HERTOG, H. M., GERRITS, D. G., VAN DEN BERG-VOS, R. M., KARAS, G. B., STEYERBERG, E. W., FLACH, H. Z., MARQUERING, H. A., SPRENGERS, M. E., JENNISKENS, S. F., BEENEN, L. F., VAN DEN BERG, R., KOUDSTAAL, P. J., VAN ZWAM, W. H., ROOS, Y. B., VAN DER LUGT, A., VAN OOSTENBRUGGE, R. J., MAJOIE, C. B. & DIPPEL, D. W. 2015. A randomized trial of intraarterial treatment for acute ischemic stroke. *N Engl J Med,* 372**,** 11-20.

BERRIDGE, M. V., HERST, P. M. & TAN, A. S. 2005. Tetrazolium dyes as tools in cell biology: new insights into their cellular reduction. *Biotechnol Annu Rev,* 11**,** 127-52.

BETZER, O., PERETS, N., ANGEL, A., MOTIEI, M., SADAN, T., YADID, G., OFFEN, D. & POPOVTZER, R. 2017. In Vivo Neuroimaging of Exosomes Using Gold Nanoparticles. *ACS Nano,* 11**,** 10883-10893.

BIHL, J. C., ZHANG, C., ZHAO, Y., XIAO, X., MA, X., CHEN, Y., CHEN, S., ZHAO, B. & CHEN, Y. 2015. Angiotensin-(1-7) counteracts the effects of Ang II on vascular smooth muscle cells, vascular remodeling and hemorrhagic stroke: Role of the NFsmall ka, CyrillicB inflammatory pathway. *Vascul Pharmacol,* 73**,** 115-123.

BIVARD, A., LINCZ, L. F., MAQUIRE, J., PARSONS, M. & LEVI, C. 2017. Platelet microparticles: a biomarker for recanalization in rtPA-treated ischemic stroke patients. *Ann Clin Transl Neurol,* 4**,** 175-179.

BLOCK, C. H., SANTOS, R. A. S., BROSNIHAN, K. B. & FERRARIO, C. M. 1988. Immunocytochemical localization of angiotensin-(1–7) in the rat forebrain. *Peptides,* 9**,** 1395-1401.

BLOOD PRESSURE LOWERING TREATMENT TRIALISTS' COLLABORATION 2021. Pharmacological blood pressure lowering for primary and secondary prevention of cardiovascular disease across different levels of blood pressure: an individual participant-level data meta-analysis. *Lancet,* 397**,** 1625-1636.

BOCK, H. A., HERMLE, M., BRUNNER, F. P. & THIEL, G. 1992. Pressure dependent modulation of renin release in isolated perfused glomeruli. *Kidney Int,* 41**,** 275-80.

BODIGA, V. L. & BODIGA, S. 2013. Renin Angiotensin System in Cognitive Function and Dementia. *Asian Journal of Neuroscience,* 2013**,** 102602.

BOECKH-BEHRENS, T., KLEINE, J., KAESMACHER, J., ZIMMER, C., SCHIRMER, L., SIMON, S. & POPPERT, H. 2017. The CD31 molecule: a possible neuroprotective agent in acute ischemic stroke? *Thromb J,* 15**,** 11.

BOING, A. N., VAN DER POL, E., GROOTEMAAT, A. E., COUMANS, F. A., STURK, A. & NIEUWLAND, R. 2014. Single-step isolation of extracellular vesicles by size-exclusion chromatography. *J Extracell Vesicles,* 3.

BRENNAN, K., MARTIN, K., FITZGERALD, S. P., O'SULLIVAN, J., WU, Y., BLANCO, A., RICHARDSON, C. & MC GEE, M. M. 2020. A comparison of methods for the isolation and separation of extracellular vesicles from protein and lipid particles in human serum. *Sci Rep,* 10**,** 1039.

BROTT, T., ADAMS, H. P., JR., OLINGER, C. P., MARLER, J. R., BARSAN, W. G., BILLER, J., SPILKER, J., HOLLERAN, R., EBERLE, R., HERTZBERG, V. & ET AL. 1989. Measurements of acute cerebral infarction: a clinical examination scale. *Stroke,* 20**,** 864-70.

BUGA, A. M., SASCAU, M., PISOSCHI, C., HERNDON, J. G., KESSLER, C. & POPA-WAGNER, A. 2008. The genomic response of the ipsilateral and contralateral

cortex to stroke in aged rats. *Journal of Cellular and Molecular Medicine,* 12**,** 2731-2753.

BÜHRLE, C. P., HACKENTHAL, E., NOBILING, R., SKØTT, O., BAUMACH, L. & TAUGNER, R. 1987. Tachyphylaxis of juxtaglomerular epithelioid cells to angiotensin II. *Pflügers Archiv,* 410**,** 55-62.

BURKE, J. E. 2018. Structural Basis for Regulation of Phosphoinositide Kinases and Their Involvement in Human Disease. *Mol Cell,* 71**,** 653-673.

BURNEY, S., CAULFIELD, J. L., NILES, J. C., WISHNOK, J. S. & TANNENBAUM, S. R. 1999. The chemistry of DNA damage from nitric oxide and peroxynitrite. *Mutation Research/Fundamental and Molecular Mechanisms of Mutagenesis,* 424**,** 37-49.

BUSCHMANN, D., KIRCHNER, B., HERMANN, S., MÄRTE, M., WURMSER, C., BRANDES, F., KOTSCHOTE, S., BONIN, M., STEINLEIN, O. K., PFAFFL, M. W., SCHELLING, G. & REITHMAIR, M. 2018. Evaluation of serum extracellular vesicle isolation methods for profiling miRNAs by next-generation sequencing. *J Extracell Vesicles,* 7**,** 1481321.

CAMBIER, L., GIANI, J. F., LIU, W., IJICHI, T., ECHAVEZ, A. K., VALLE, J. & MARBÁN, E. 2018. Angiotensin II-Induced End-Organ Damage in Mice Is Attenuated by Human Exosomes and by an Exosomal Y RNA Fragment. *Hypertension,* 72**,** 370-380.

CAMPOS-MARTORELL, M., CANO-SARABIA, M., SIMATS, A., HERNÁNDEZ-GUILLAMON, M., ROSELL, A., MASPOCH, D. & MONTANER, J. 2016. Charge effect of a liposomal delivery system encapsulating simvastatin to treat experimental ischemic stroke in rats. *International Journal of Nanomedicine,* 11**,** 3035-3048.

CAMUSSI, G., DEREGIBUS, M. C., BRUNO, S., CANTALUPPI, V. & BIANCONE, L. 2010. Exosomes/microvesicles as a mechanism of cell-to-cell communication. *Kidney Int,* 78**,** 838-48.

CARMICHAEL, S. T. 2005. Rodent models of focal stroke: size, mechanism, and purpose. *NeuroRx,* 2**,** 396-409.

CATALANOTTO, C., COGONI, C. & ZARDO, G. 2016. MicroRNA in Control of Gene Expression: An Overview of Nuclear Functions. *Int J Mol Sci,* 17.

CENTERS FOR DISEASE CONTROL AND PREVENTION. 2022a. *Live Attenuated Influenza Vaccine [LAIV] (The Nasal Spray Flu Vaccine)* [Online]. Available: https://www.cdc.gov/flu/prevent/nasalspray.htm [Accessed 1122023 2023].

CENTERS FOR DISEASE CONTROL AND PREVENTION. 2022b. *Prevent Stroke: What You Can Do* [Online]. Available: https://www.cdc.gov/stroke/prevention.htm [Accessed 31.10.2023 2023].

CHA, S. A., PARK, B. M., GAO, S. & KIM, S. H. 2013. Stimulation of ANP by angiotensin-(1-9) via the angiotensin type 2 receptor. *Life Sciences,* 93**,** 934-940.

CHA, S. A., PARK, B. M. & KIM, S. H. 2018. Angiotensin-(1-9) ameliorates pulmonary arterial hypertension via angiotensin type II receptor. *Korean J Physiol Pharmacol,* 22**,** 447-456.

CHAN, H. H., COOPERRIDER, J. L., PARK, H. J., WATHEN, C. A., GALE, J. T., BAKER, K. B. & MACHADO, A. G. 2017. Crossed Cerebellar Atrophy of the Lateral Cerebellar Nucleus in an Endothelin-1-Induced, Rodent Model of Ischemic Stroke. *Front Aging Neurosci,* 9**,** 10.

CHANG, A. Y., LI, F. C., HUANG, C. W., WU, J. C., DAI, K. Y., CHEN, C. H., LI, S. H., SU, C. H. & WU, R. W. 2014. Interplay between brain stem angiotensins and monocyte chemoattractant protein-1 as a novel mechanism for pressor response after ischemic stroke. *Neurobiol Dis,* 71**,** 292-304.

CHANG, A. Y. W. 2014. Interplay between brain stem angiotensins and monocyte chemoattractant protein-1 as a novel mechanism for pressor response after ischemic stroke. *Neurobiology of Disease,* 71**,** 292-304.

CHATURVEDI, P., SINGH, A. K., TIWARI, V. & THACKER, A. K. 2020. Brain-derived neurotrophic factor levels in acute stroke and its clinical implications. *Brain Circ,* 6**,** 185-190.

CHEN, C., CAI, N., NIU, Q., TIAN, Y., HU, Y. & YAN, X. 2023. Quantitative assessment of lipophilic membrane dye-based labelling of extracellular vesicles by nano-flow cytometry. *J Extracell Vesicles,* 12**,** e12351.

CHEN, K. H., CHEN, C. H., WALLACE, C. G., YUEN, C. M., KAO, G. S., CHEN, Y. L., SHAO, P. L., CHEN, Y. L., CHAI, H. T., LIN, K. C., LIU, C. F., CHANG, H. W., LEE, M. S. & YIP, H. K. 2016a. Intravenous administration of xenogenic adipose-derived mesenchymal stem cells (ADMSC) and ADMSC-derived exosomes markedly reduced brain infarct volume and preserved neurological function in rat after acute ischemic stroke. *Oncotarget,* 7**,** 74537-74556.

CHEN, L., GONG, P., SU, Y., MENG, L., WANG, M., GAO, W. & LIU, Q. 2024. Angiotensin II type 2 receptor agonist attenuates LPS-induced acute lung injury through modulating THP-1-derived macrophage reprogramming. *Naunyn-Schmiedeberg's Archives of Pharmacology,* 397**,** 99-108.

CHEN, Q., TAKADA, R., NODA, C., KOBAYASHI, S. & TAKADA, S. 2016b. Different populations of Wnt-containing vesicles are individually released from polarized epithelial cells. *Sci Rep,* 6**,** 35562.

CHEN, R., OVBIAGELE, B. & FENG, W. 2016c. Diabetes and Stroke: Epidemiology, Pathophysiology, Pharmaceuticals and Outcomes. *Am J Med Sci,* 351**,** 380-6.

CHEN, Y., SONG, Y., HUANG, J., QU, M., ZHANG, Y., GENG, J., ZHANG, Z., LIU, J. & YANG, G.-Y. 2017. Increased Circulating Exosomal miRNA-223 Is Associated with Acute Ischemic Stroke. *Frontiers in Neurology,* 8.

CHENG, C.-Y., CHEN, S.-H., CHEN, H.-M., LI, C.-J., LIU, T.-Y. & TAN, T.-Y. 2021. Impact of estimated-weight-base dose of alteplase in acute stroke treatment on clinical outcome. *Journal of Clinical Neuroscience,* 85**,** 101-105.

CHIABOTTO, G., GAI, C., DEREGIBUS, M. C. & CAMUSSI, G. 2019. Salivary Extracellular Vesicle-Associated exRNA as Cancer Biomarker. *Cancers (Basel),* 11.

CHOEZOM, D. & GROSS, J. C. 2022. Neutral sphingomyelinase 2 controls exosome secretion by counteracting V-ATPase-mediated endosome acidification. *J Cell Sci,* 135.

CHOW, L. S., RAJAGOPAL, H. & PARAMESRAN, R. 2016. Correlation between subjective and objective assessment of magnetic resonance (MR) images. *Magn Reson Imaging,* 34**,** 820-831.

CLAASSEN, J., THIJSSEN, D. H. J., PANERAI, R. B. & FARACI, F. M. 2021. Regulation of cerebral blood flow in humans: physiology and clinical implications of autoregulation. *Physiol Rev,* 101**,** 1487-1559.

COLOMBO, M., MOITA, C., VAN NIEL, G., KOWAL, J., VIGNERON, J., BENAROCH, P., MANEL, N., MOITA, L. F., THERY, C. & RAPOSO, G. 2013. Analysis of ESCRT functions in exosome biogenesis, composition and secretion highlights the heterogeneity of extracellular vesicles. *J Cell Sci,* 126**,** 5553-65.

COLONNA, M. & BUTOVSKY, O. 2017. Microglia Function in the Central Nervous System During Health and Neurodegeneration. *Annu Rev Immunol,* 35**,** 441-468.

CONKRIGHT, W. R., BECKNER, M. E., SAHU, A., MI, Q., CLEMENS, Z. J., LOVALEKAR, M., FLANAGAN, S. D., MARTIN, B. J., FERRARELLI, F., AMBROSIO, F. & NINDL, B. C. 2022. Men and women display distinct extracellular vesicle biomarker signatures in response to military operational stress. *J Appl Physiol (1985),* 132**,** 1125-1136.

CORDERO, I. 2015. Electrosurgical units - how they work and how to use them safely. *Community Eye Health,* 28**,** 15-6.

COSARDERELIOGLU, C., NIDADAVOLU, L. S., GEORGE, C. J., OH, E. S., BENNETT, D. A., WALSTON, J. D. & ABADIR, P. M. 2020. Brain Renin-Angiotensin System at the Intersect of Physical and Cognitive Frailty. *Front Neurosci,* 14**,** 586314.

COUCH, Y., AKBAR, N., DAVIS, S., FISCHER, R., DICKENS, A. M., NEUHAUS, A. A., BURGESS, A. I., ROTHWELL, P. M. & BUCHAN, A. M. 2017. Inflammatory Stroke Extracellular Vesicles Induce Macrophage Activation. *Stroke,* 48**,** 2292-2296.

CRUPI, R., IMPELLIZZERI, D. & CUZZOCREA, S. 2019. Role of Metabotropic Glutamate Receptors in Neurological Disorders. *Frontiers in Molecular Neuroscience,* 12.

CUI, J., ZHAO, S., LI, Y., ZHANG, D., WANG, B., XIE, J. & WANG, J. 2021. Regulated cell death: discovery, features and implications for neurodegenerative diseases. *Cell Communication and Signaling,* 19**,** 120.

CURLEY, N., LEVY, D., DO, M. A., BROWN, A., STICKNEY, Z., MARRIOTT, G. & LU, B. 2020. Sequential deletion of CD63 identifies topologically distinct scaffolds for surface engineering of exosomes in living human cells. *Nanoscale,* 12**,** 12014-12026.

DACOSTA-AGUAYO, R., GRAÑA, M., FERNÁNDEZ-ANDÚJAR, M., LÓPEZ-CANCIO, E., CÁCERES, C., BARGALLÓ, N., BARRIOS, M., CLEMENTE, I., MONSERRAT, P. T., SAS, M. A., DÁVALOS, A., AUER, T. & MATARÓ, M. 2014. Structural Integrity of the Contralesional Hemisphere Predicts Cognitive Impairment in Ischemic Stroke at Three Months. *PLOS ONE,* 9**,** e86119.

DANEMAN, R. & PRAT, A. 2015. The blood-brain barrier. *Cold Spring Harb Perspect Biol,* 7**,** a020412.

DAVIDSON, A. O., SCHORK, N., JAQUES, B. C., KELMAN, A. W., SUTCLIFFE, R. G., REID, J. L. & DOMINICZAK, A. F. 1995. Blood pressure in genetically hypertensive rats. Influence of the Y chromosome. *Hypertension,* 26**,** 452-9.

DAVIES, M. K., GIBBS, C. R. & LIP, G. Y. 2000. ABC of heart failure. Management: diuretics, ACE inhibitors, and nitrates. *Bmj,* 320**,** 428-31.

DAVIS, C. J., KRAMÁR, E. A., DE, A., MEIGHAN, P. C., SIMASKO, S. M., WRIGHT, J. W. & HARDING, J. W. 2006. AT4 receptor activation increases intracellular calcium influx and induces a non-N-methyl-d-aspartate dependent form of long-term potentiation. *Neuroscience,* 137**,** 1369-1379.

DEACON, R. M. 2013. Measuring motor coordination in mice. *J Vis Exp***,** e2609.

DOEPPNER, T. R., HERZ, J., GÖRGENS, A., SCHLECHTER, J., LUDWIG, A. K., RADTKE, S., DE MIROSCHEDJI, K., HORN, P. A., GIEBEL, B. & HERMANN, D. M. 2015. Extracellular Vesicles Improve Post-Stroke Neuroregeneration and Prevent Postischemic Immunosuppression. *Stem Cells Transl Med,* 4**,** 1131-43.

DOMIŃSKA, K., KOWALSKA, K., HABROWSKA-GÓRCZYŃSKA, D. E., URBANEK, K. A., OCHĘDALSKI, T. & PIASTOWSKA-CIESIELSKA, A. W. 2019. The opposite effects of angiotensin 1-9 and angiotensin 3-7 in prostate epithelial cells. *Biochemical and Biophysical Research Communications,* 519**,** 868-873.

DOOBAY, M. F., TALMAN, L. S., OBR, T. D., TIAN, X., DAVISSON, R. L. & LAZARTIGUES, E. 2007. Differential expression of neuronal ACE2 in transgenic mice with overexpression of the brain renin-angiotensin system. *Am J Physiol Regul Integr Comp Physiol,* 292**,** R373-81.

DRIEDONKS, T., JIANG, L., CARLSON, B., HAN, Z., LIU, G., QUEEN, S. E., SHIRK, E. N., GOLOLOBOVA, O., LIAO, Z., NYBERG, L. H., LIMA, G., PANIUSHKINA, L., GARCIA-CONTRERAS, M., SCHONVISKY, K.,

CASTELL, N., STOVER, M., GUERRERO-MARTIN, S., RICHARDSON, R., SMITH, B., MACHAIRAKI, V., LAI, C. P., IZZI, J. M., HUTCHINSON, E. K., PATE, K. A. M. & WITWER, K. W. 2022. Pharmacokinetics and biodistribution of extracellular vesicles administered intravenously and intranasally to Macaca nemestrina. *J Extracell Biol,* 1.

DURAND, M. J., ZINKEVICH, N. S., RIEDEL, M., GUTTERMAN, D. D., NASCI, V. L., SALATO, V. K., HIJJAWI, J. B., REUBEN, C. F., NORTH, P. E. & BEYER, A. M. 2016. Vascular Actions of Angiotensin 1-7 in the Human Microcirculation: Novel Role for Telomerase. *Arterioscler Thromb Vasc Biol,* 36**,** 1254-62.

EAGLE, A. L., WANG, H. & ROBISON, A. J. 2016. Sensitive Assessment of Hippocampal Learning Using Temporally Dissociated Passive Avoidance Task. *Bio Protoc,* 6.

EGAMI, K., MUROHARA, T., SHIMADA, T., SASAKI, K., SHINTANI, S., SUGAYA, T., ISHII, M., AKAGI, T., IKEDA, H., MATSUISHI, T. & IMAIZUMI, T. 2003. Role of host angiotensin II type 1 receptor in tumor angiogenesis and growth. *J Clin Invest,* 112**,** 67-75.

ELDAHSHAN, W., ISHRAT, T., PILLAI, B., SAYED, M. A., ALWHAIBI, A., FOUDA, A. Y., ERGUL, A. & FAGAN, S. C. 2019. Angiotensin II type 2 receptor stimulation with compound 21 improves neurological function after stroke in female rats: A pilot study. *American Journal of Physiology - Heart and Circulatory Physiology,* 316**,** H1192-H1201.

ELDAHSHAN, W., SAYED, M. A., AWAD, M. E., AHMED, H. A., GILLIS, E., ALTHOMALI, W., PILLAI, B., ALSHAMMARI, A., JACKSON, L., DONG, G., SULLIVAN, J. C., COOLEY, M. A., ELSALANTY, M., ERGUL, A. & FAGAN, S. C. 2021. Stimulation of angiotensin II receptor 2 preserves cognitive function and is associated with an enhanced cerebral vascular density after stroke. *Vascul Pharmacol,* 141**,** 106904.

ELLERSHAW, D. C. & GURNEY, A. M. 2001. Mechanisms of hydralazine induced vasodilation in rabbit aorta and pulmonary artery. *Br J Pharmacol,* 134**,** 621-31.

ENCARNACION, A., HORIE, N., KEREN-GILL, H., BLISS, T. M., STEINBERG, G. K. & SHAMLOO, M. 2011. Long-term behavioral assessment of function in an experimental model for ischemic stroke. *J Neurosci Methods,* 196**,** 247-57.

ENGELHORN, T., GOERIKE, S., DOERFLER, A., OKORN, C., FORSTING, M., HEUSCH, G. & SCHULZ, R. 2004. The angiotensin II type 1-receptor blocker candesartan increases cerebral blood flow, reduces infarct size, and improves neurologic outcome after transient cerebral ischemia in rats. *J Cereb Blood Flow Metab,* 24**,** 467-74.

ESMATI, P. Z., BAHARARA, J., SAHAB-NEGAH, S. & SHAHROKHABADI, K. N. 2023. Leukemia-derived Exosomes Can Induce Responses Related to Tumorigenesis on Non-tumoral Astrocytes. *Appl Biochem Biotechnol*.

EUROPEAN MEDICINE AGENCY. 2021. *EU/3/21/2508 - orphan designation for prevention of bronchopulmonary dysplasia* [Online]. Available: https://www.ema.europa.eu/en/medicines/human/orphan-designations/eu-3-21-2508 [Accessed 25.03.2024 2024].

EVERS, M. J. W., VAN DE WAKKER, S. I., DE GROOT, E. M., DE JONG, O. G., GITZ-FRANÇOIS, J. J. J., SEINEN, C. S., SLUIJTER, J. P. G., SCHIFFELERS, R. M. & VADER, P. 2022. Functional siRNA Delivery by Extracellular Vesicle–Liposome Hybrid Nanoparticles. *Advanced Healthcare Materials,* 11**,** 2101202.

FAROOQUI, Z. & BANDAY, A. A. 2024. Angiotensin 1-7 exerts antioxidant effects, suppresses Mammalian Target of Rapamycin (mTOR) signaling, and inhibits apoptosis in renal proximal tubular cells. *Peptides,* 172**,** 171136.

FATTAH, C., NATHER, K., MCCARROLL, C. S., HORTIGON-VINAGRE, M. P., ZAMORA, V., FLORES-MUNOZ, M., MCARTHUR, L., ZENTILIN, L.,

GIACCA, M., TOUYZ, R. M., SMITH, G. L., LOUGHREY, C. M. & NICKLIN, S. A. 2016. Gene Therapy With Angiotensin-(1-9) Preserves Left Ventricular Systolic Function After Myocardial Infarction. *Journal of the American College of Cardiology,* 68**,** 2652-2666.

FERRARI, G., COOK, B. D., TERUSHKIN, V., PINTUCCI, G. & MIGNATTI, P. 2009. Transforming growth factor-beta 1 (TGF-beta1) induces angiogenesis through vascular endothelial growth factor (VEGF)-mediated apoptosis. *J Cell Physiol,* 219**,** 449-58.

FILIPPENKOV, I. B., REMIZOVA, J. A., DENISOVA, A. E., STAVCHANSKY, V. V., GOLOVINA, K. D., GUBSKY, L. V., LIMBORSKA, S. A. & DERGUNOVA, L. V. 2023. Differential gene expression in the contralateral hemisphere of the rat brain after focal ischemia. *Sci Rep,* 13**,** 573.

FINK, S. L. & COOKSON, B. T. 2005. Apoptosis, pyroptosis, and necrosis: mechanistic description of dead and dying eukaryotic cells. *Infect Immun,* 73**,** 1907-16.

FISHER, M., FEUERSTEIN, G., HOWELLS, D. W., HURN, P. D., KENT, T. A., SAVITZ, S. I. & LO, E. H. 2009. Update of the stroke therapy academic industry roundtable preclinical recommendations. *Stroke,* 40**,** 2244-50.

FLORES-MUÑOZ, M., SMITH, N. J., HAGGERTY, C., MILLIGAN, G. & NICKLIN, S. A. 2011. Angiotensin1-9 antagonises pro-hypertrophic signalling in cardiomyocytes via the angiotensin type 2 receptor. *The Journal of Physiology,* 589**,** 939-951.

FLORES-MUÑOZ, M., WORK, L. M., DOUGLAS, K., DENBY, L., DOMINICZAK, A. F., GRAHAM, D. & NICKLIN, S. A. 2012. Angiotensin-(1-9) attenuates cardiac fibrosis in the stroke-prone spontaneously hypertensive rat via the angiotensin type 2 receptor. *Hypertension,* 59**,** 300-7.

FORTEZA-GENESTRA, M. A., ANTICH-ROSSELLÓ, M., CALVO, J., GAYÀ, A., MONJO, M. & RAMIS, J. M. 2020. Purity Determines the Effect of Extracellular Vesicles Derived from Mesenchymal Stromal Cells. *Cells,* 9.

FOUDA, A. Y., PILLAI, B., FAGAN, S. C., ERGUL, A. & DHANDAPANI, K. M. 2017. Role of interleukin-10 in the neuroprotective effect of the Angiotensin Type 2 Receptor agonist, compound 21, after ischemia/reperfusion injury. *European Journal of Pharmacology,* 799**,** 128-134.

FRANCIS, S. H., BUSCH, J. L., CORBIN, J. D. & SIBLEY, D. 2010. cGMP-dependent protein kinases and cGMP phosphodiesterases in nitric oxide and cGMP action. *Pharmacol Rev,* 62**,** 525-63.

FUJIMURA, M., GASCHE, Y., MORITA-FUJIMURA, Y., MASSENGALE, J., KAWASE, M. & CHAN, P. H. 1999. Early appearance of activated matrix metalloproteinase-9 and blood-brain barrier disruption in mice after focal cerebral ischemia and reperfusion. *Brain Res,* 842**,** 92-100.

FUKUOKA, T., HAYASHI, T., HIRAYAMA, M., MARUYAMA, H., MOGI, M., HORIUCHI, M., TAKAO, M. & TANAHASHI, N. 2015. Platelet–endothelial cell interaction in brain microvessels of angiotensin II type-2 receptor knockout mice following transient bilateral common carotid artery occlusion. *Journal of Thrombosis and Thrombolysis,* 40**,** 401-405.

FUKUTA, T., ISHII, T., ASAI, T., SATO, A., KIKUCHI, T., SHIMIZU, K., MINAMINO, T. & OKU, N. 2015. Treatment of stroke with liposomal neuroprotective agents under cerebral ischemia conditions. *European Journal of Pharmaceutics and Biopharmaceutics,* 97**,** 1-7.

FULLERTON, J. L., COSGROVE, C. C., ROONEY, R. A. & WORK, L. M. 2023. Extracellular vesicles and their microRNA cargo in ischaemic stroke. *The Journal of Physiology,* 601**,** 4907-4921.

GAMEZ-VALERO, A., MONGUIO-TORTAJADA, M., CARRERAS-PLANELLA, L., FRANQUESA, M., BEYER, K. & BORRAS, F. E. 2016. Size-Exclusion

Chromatography-based isolation minimally alters Extracellular Vesicles' characteristics compared to precipitating agents. *Sci Rep,* 6**,** 33641.

GANTEN, D., MARQUEZ-JULIO, A., GRANGER, P., HAYDUK, K., KARSUNKY, K. P., BOUCHER, R. & GENEST, J. 1971. Renin in dog brain. *Am J Physiol,* 221**,** 1733-7.

GANTIER, M. P., MCCOY, C. E., RUSINOVA, I., SAULEP, D., WANG, D., XU, D., IRVING, A. T., BEHLKE, M. A., HERTZOG, P. J., MACKAY, F. & WILLIAMS, B. R. 2011. Analysis of microRNA turnover in mammalian cells following Dicer1 ablation. *Nucleic Acids Res,* 39**,** 5692-703.

GAO, X., RAN, N., DONG, X., ZUO, B., YANG, R., ZHOU, Q., MOULTON, H. M., SEOW, Y. & YIN, H. 2018. Anchor peptide captures, targets, and loads exosomes of diverse origins for diagnostics and therapy. *Science Translational Medicine,* 10**,** eaat0195.

GARCÍA-ROMERO, N., MADURGA, R., RACKOV, G., PALACÍN-ALIANA, I., NÚÑEZ-TORRES, R., ASENSI-PUIG, A., CARRIÓN-NAVARRO, J., ESTEBAN-RUBIO, S., PEINADO, H., GONZÁLEZ-NEIRA, A., GONZÁLEZ-RUMAYOR, V., BELDA-INIESTA, C. & AYUSO-SACIDO, A. 2019. Polyethylene glycol improves current methods for circulating extracellular vesicle-derived DNA isolation. *Journal of Translational Medicine,* 17**,** 75.

GARCIA, P. Y., ROUSSEL, M., BUGNICOURT, J. M., LAMY, C., CANAPLE, S., PELTIER, J., LOAS, G., DERAMOND, H. & GODEFROY, O. 2013. Cognitive impairment and dementia after intracerebral hemorrhage: a cross-sectional study of a hospital-based series. *J Stroke Cerebrovasc Dis,* 22**,** 80-6.

GBD 2019 STROKE COLLABORATORS 2021. Global, regional, and national burden of stroke and its risk factors, 1990-2019: a systematic analysis for the Global Burden of Disease Study 2019. *Lancet Neurol,* 20**,** 795-820.

GELDERBLOM, M., LEYPOLDT, F., STEINBACH, K., BEHRENS, D., CHOE, C.-U., SILER, D. A., ARUMUGAM, T. V., ORTHEY, E., GERLOFF, C., TOLOSA, E. & MAGNUS, T. 2009. Temporal and Spatial Dynamics of Cerebral Immune Cell Accumulation in Stroke. *Stroke,* 40**,** 1849-1857.

GENG, W., TANG, H., LUO, S., LV, Y., LIANG, D., KANG, X. & HONG, W. 2019. Exosomes from miRNA-126-modified ADSCs promotes functional recovery after stroke in rats by improving neurogenesis and suppressing microglia activation. *Am J Transl Res,* 11**,** 780-792.

GHOSSOUB, R., LEMBO, F., RUBIO, A., GAILLARD, C. B., BOUCHET, J., VITALE, N., SLAVÍK, J., MACHALA, M. & ZIMMERMANN, P. 2014. Syntenin-ALIX exosome biogenesis and budding into multivesicular bodies are controlled by ARF6 and PLD2. *Nat Commun,* 5**,** 3477.

GILLIOT, S., SIBON, I., MAS, J. L., MOULIN, T., BÉJOT, Y., CORDONNIER, C., GIROUD, M., ODOU, P., BORDET, R., VIVIEN, D. & LEYS, D. 2018. Influence of on-going treatment with angiotensin-converting enzyme inhibitor or angiotensin receptor blocker on the outcome of patients treated with intravenous rt-PA for ischemic stroke. *J Neurol,* 265**,** 1166-1173.

GLIEM, M., MAUSBERG, A. K., LEE, J. I., SIMIANTONAKIS, I., VAN ROOIJEN, N., HARTUNG, H. P. & JANDER, S. 2012. Macrophages prevent hemorrhagic infarct transformation in murine stroke models. *Ann Neurol,* 71**,** 743-52.

GOLDBERG, M. P. & CHOI, D. W. 1993. Combined oxygen and glucose deprivation in cortical cell culture: calcium-dependent and calcium-independent mechanisms of neuronal injury. *J Neurosci,* 13**,** 3510-24.

GOLDHABER, S. Z., MEYEROVITZ, M. F., GREEN, D., VOGELZANG, R. L., CITRIN, P., HEIT, J., SOBEL, M., WHEELER, H. B., PLANTE, D., KIM, H. & ET AL. 1990. Randomized controlled trial of tissue plasminogen activator in proximal deep venous thrombosis. *Am J Med,* 88**,** 235-40.

GONG, L., CHEN, B., ZHANG, J., SUN, Y., YUAN, J., NIU, X., HU, G., CHEN, Y., XIE, Z., DENG, Z., LI, Q. & WANG, Y. 2020. Human ESC-sEVs alleviate age-related bone loss by rejuvenating senescent bone marrow-derived mesenchymal stem cells. *Journal of Extracellular Vesicles,* 9**,** 1800971.

GONZÁLEZ-MARISCAL, L., BETANZOS, A., NAVA, P. & JARAMILLO, B. E. 2003. Tight junction proteins. *Progress in Biophysics and Molecular Biology,* 81**,** 1-44.

GONZALEZ, L., NOVOA, U., MOYA, J., GABRIELLI, L., JALIL, J. E., GARCÍA, L., CHIONG, M., LAVANDERO, S. & OCARANZA, M. P. 2018. Angiotensin-(1-9) reduces cardiovascular and renal inflammation in experimental renin-independent hypertension. *Biochemical Pharmacology,* 156**,** 357-370.

GOYAL, M., DEMCHUK, A. M., MENON, B. K., EESA, M., REMPEL, J. L., THORNTON, J., ROY, D., JOVIN, T. G., WILLINSKY, R. A., SAPKOTA, B. L., DOWLATSHAHI, D., FREI, D. F., KAMAL, N. R., MONTANERA, W. J., POPPE, A. Y., RYCKBORST, K. J., SILVER, F. L., SHUAIB, A., TAMPIERI, D., WILLIAMS, D., BANG, O. Y., BAXTER, B. W., BURNS, P. A., CHOE, H., HEO, J.-H., HOLMSTEDT, C. A., JANKOWITZ, B., KELLY, M., LINARES, G., MANDZIA, J. L., SHANKAR, J., SOHN, S.-I., SWARTZ, R. H., BARBER, P. A., COUTTS, S. B., SMITH, E. E., MORRISH, W. F., WEILL, A., SUBRAMANIAM, S., MITHA, A. P., WONG, J. H., LOWERISON, M. W., SAJOBI, T. T. & HILL, M. D. 2015. Randomized Assessment of Rapid Endovascular Treatment of Ischemic Stroke. *New England Journal of Medicine,* 372**,** 1019-1030.

GRIENDLING, K. K., SORESCU, D. & USHIO-FUKAI, M. 2000. NAD(P)H oxidase: role in cardiovascular biology and disease. *Circ Res,* 86**,** 494-501.

GROSS, V., SCHUNCK, W. H., HONECK, H., MILIA, A. F., KARGEL, E., WALTHER, T., BADER, M., INAGAMI, T., SCHNEIDER, W. & LUFT, F. C. 2000. Inhibition of pressure natriuresis in mice lacking the AT2 receptor. *Kidney Int,* 57**,** 191-202.

GROZOVSKY, R., GIANNINI, S., FALET, H. & HOFFMEISTER, K. M. 2015. Regulating billions of blood platelets: glycans and beyond. *Blood,* 126**,** 1877-84.

GUO, B. B., BELLINGHAM, S. A. & HILL, A. F. 2015. The neutral sphingomyelinase pathway regulates packaging of the prion protein into exosomes. *J Biol Chem,* 290**,** 3455-67.

GUO, C.-L., LIU, H.-M., LI, B. & LU, Z.-Y. 2023. Angiotensin-(1–9) prevents angiotensin II-induced endothelial apoptosis through CNPY2/PERK pathway. *Apoptosis,* 28**,** 379-396.

GUO, L., ZHANG, Q., MA, X., WANG, J. & LIANG, T. 2017a. miRNA and mRNA expression analysis reveals potential sex-biased miRNA expression. *Sci Rep,* 7**,** 39812.

GUO, S. C., TAO, S. C., YIN, W. J., QI, X., YUAN, T. & ZHANG, C. Q. 2017b. Exosomes derived from platelet-rich plasma promote the re-epithelization of chronic cutaneous wounds via activation of YAP in a diabetic rat model. *Theranostics,* 7**,** 81-96.

GURLEY, C., NICHOLS, J., LIU, S., PHULWANI, N. K., ESEN, N. & KIELIAN, T. 2008. Microglia and Astrocyte Activation by Toll-Like Receptor Ligands: Modulation by PPAR-gamma Agonists. *PPAR Res,* 2008**,** 453120.

GURUNG, S., PEROCHEAU, D., TOURAMANIDOU, L. & BARUTEAU, J. 2021. The exosome journey: from biogenesis to uptake and intracellular signalling. *Cell Communication and Signaling,* 19**,** 47.

GYCHKA, S. G., SHULTS, N. V., NIKOLAIENKO, S. I., MARCOCCI, L., SARIIPEK, N. E., RYBKA, V., MALYSHEVA, T. A., DIBROVA, V. A., SUZUKI, Y. J. & GAVRISH, A. S. 2020. Vasa Vasorum Lumen Narrowing in Brain Vascular Hyalinosis in Systemic Hypertension Patients Who Died of Ischemic Stroke. *International Journal of Molecular Sciences* [Online], 21.

HACHINSKI, V., EINHÄUPL, K., GANTEN, D., ALLADI, S., BRAYNE, C., STEPHAN, B. C. M., SWEENEY, M. D., ZLOKOVIC, B., ITURRIA-MEDINA, Y., IADECOLA, C., NISHIMURA, N., SCHAFFER, C. B., WHITEHEAD, S. N., BLACK, S. E., ØSTERGAARD, L., WARDLAW, J., GREENBERG, S., FRIBERG, L., NORRVING, B., ROWE, B., JOANETTE, Y., HACKE, W., KULLER, L., DICHGANS, M., ENDRES, M. & KHACHATURIAN, Z. S. 2019. Preventing dementia by preventing stroke: The Berlin Manifesto. *Alzheimers Dement,* 15**,** 961-984.

HACKE, W., KASTE, M., BLUHMKI, E., BROZMAN, M., DÁVALOS, A., GUIDETTI, D., LARRUE, V., LEES, K. R., MEDEGHRI, Z., MACHNIG, T., SCHNEIDER, D., VON KUMMER, R., WAHLGREN, N. & TONI, D. 2008. Thrombolysis with Alteplase 3 to 4.5 Hours after Acute Ischemic Stroke. *New England Journal of Medicine,* 359**,** 1317-1329.

HAKON, J., QUATTROMANI, M. J., SJÖLUND, C., TALHADA, D., KIM, B., MOYANOVA, S., MASTROIACOVO, F., DI MENNA, L., OLSSON, R., ENGLUND, E., NICOLETTI, F., RUSCHER, K., BAUER, A. Q. & WIELOCH, T. 2024. Inhibiting metabotropic glutamate receptor 5 after stroke restores brain function and connectivity. *Brain,* 147**,** 186-200.

HALLIWELL, B. 1992. Reactive Oxygen Species and the Central Nervous System. *Journal of Neurochemistry,* 59**,** 1609-1623.

HANNAWI, Y., CACERES, E., EWEES, M. G., POWELL, K. A., BRATASZ, A., SCHWAB, J. M., RINK, C. L. & ZWEIER, J. L. 2021a. Characterizing the Neuroimaging and Histopathological Correlates of Cerebral Small Vessel Disease in Spontaneously Hypertensive Stroke-Prone Rats. *Frontiers in Neurology,* 12.

HANNAWI, Y., CACERES, E., EWEES, M. G., POWELL, K. A., BRATASZ, A., SCHWAB, J. M., RINK, C. L. & ZWEIER, J. L. 2021b. Characterizing the Neuroimaging and Histopathological Correlates of Cerebral Small Vessel Disease in Spontaneously Hypertensive Stroke-Prone Rats. *Front Neurol,* 12**,** 740298.

HANSON, P. I. & CASHIKAR, A. 2012. Multivesicular body morphogenesis. *Annu Rev Cell Dev Biol,* 28**,** 337-62.

HARANHALLI, N., MBABUIKE, N., GREWAL, S. S., HASAN, T. F., HECKMAN, M. G., FREEMAN, W. D., GUPTA, V., VIBHUTE, P., BROWN, B. L., MILLER, D. A., JAHROMI, B. S. & TAWK, R. G. 2020. Topographic correlation of infarct area on CT perfusion with functional outcome in acute ischemic stroke. *Journal of Neurosurgery JNS,* 132**,** 33-41.

HARARI, O. A. & LIAO, J. K. 2010. NF-κB and innate immunity in ischemic stroke. *Annals of the New York Academy of Sciences,* 1207**,** 32-40.

HAROON, K., RUAN, H., ZHENG, H., WU, S., LIU, Z., SHI, X., TANG, Y., YANG, G.-Y. & ZHANG, Z. 2023. Bio-clickable, small extracellular vesicles-COCKTAIL therapy for ischemic stroke. *Journal of Controlled Release,* 363**,** 585-596.

HAROON, K., ZHENG, H., WU, S., LIU, Z., TANG, Y., YANG, G.-Y., LIU, Y. & ZHANG, Z. 2024. Engineered exosomes mediated targeted delivery of neuroprotective peptide NR2B9c for the treatment of traumatic brain injury. *International Journal of Pharmaceutics,* 649**,** 123656.

HEART AND STROKE FOUNDATION OF CANADA. 2023. *Atrial fibrillation* [Online]. Available: https://www.heartandstroke.ca/heart-disease/conditions/atrial-fibrillation#:~:text=Untreated%20atrial%20fibrillation%20puts%20you,the%20grooves%20of%20the%20heart [Accessed 31.10.2023 2023].

HERMAN, L. L., ; , WEBER, P., ; & BASHIR, K. 2023. *Hydrochlorothiazide* [Online]. National Library of Medicine. Available: https://www.ncbi.nlm.nih.gov/books/NBK430766/#:~:text=Go%20to%3A-,Mechanism%20of%20Action,the%20sodium%20in%20the%20kidney. [Accessed].

HERNANDES, M. S., XU, Q. & GRIENDLING, K. K. 2022. Role of NADPH Oxidases in Blood-Brain Barrier Disruption and Ischemic Stroke. *Antioxidants (Basel),* 11.

HIETAMIES, T. M., OSTROWSKI, C., PEI, Z., FENG, L., MCCABE, C., WORK, L. M. & QUINN, T. J. 2018. Variability of functional outcome measures used in animal models of stroke and vascular cognitive impairment – a review of contemporary studies. *Journal of Cerebral Blood Flow & Metabolism,* 38**,** 1872-1884.

HILL, M. D., GOYAL, M., MENON, B. K., NOGUEIRA, R. G., MCTAGGART, R. A., DEMCHUK, A. M., POPPE, A. Y., BUCK, B. H., FIELD, T. S., DOWLATSHAHI, D., VAN ADEL, B. A., SWARTZ, R. H., SHAH, R. A., SAUVAGEAU, E., ZERNA, C., OSPEL, J. M., JOSHI, M., ALMEKHLAFI, M. A., RYCKBORST, K. J., LOWERISON, M. W., HEARD, K., GARMAN, D., HAUSSEN, D., CUTTING, S. M., COUTTS, S. B., ROY, D., REMPEL, J. L., ROHR, A. C., IANCU, D., SAHLAS, D. J., YU, A. Y. X., DEVLIN, T. G., HANEL, R. A., PUETZ, V., SILVER, F. L., CAMPBELL, B. C. V., CHAPOT, R., TEITELBAUM, J., MANDZIA, J. L., KLEINIG, T. J., TURKEL-PARRELLA, D., HECK, D., KELLY, M. E., BHARATHA, A., BANG, O. Y., JADHAV, A., GUPTA, R., FREI, D. F., TARPLEY, J. W., MCDOUGALL, C. G., HOLMIN, S., RHA, J. H., PURI, A. S., CAMDEN, M. C., THOMALLA, G., CHOE, H., PHILLIPS, S. J., SCHINDLER, J. L., THORNTON, J., NAGEL, S., HEO, J. H., SOHN, S. I., PSYCHOGIOS, M. N., BUDZIK, R. F., STARKMAN, S., MARTIN, C. O., BURNS, P. A., MURPHY, S., LOPEZ, G. A., ENGLISH, J. & TYMIANSKI, M. 2020. Efficacy and safety of nerinetide for the treatment of acute ischaemic stroke (ESCAPE-NA1): a multicentre, double-blind, randomised controlled trial. *Lancet,* 395**,** 878-887.

HOFSAESS, U. & KAPFHAMMER, J. P. 2003. Identification of numerous genes differentially expressed in rat brain during postnatal development by suppression subtractive hybridization and expression analysis of the novel rat gene rMMS2. *Molecular Brain Research,* 113**,** 13-27.

HOOD, J. L., SCOTT, M. J. & WICKLINE, S. A. 2014. Maximizing exosome colloidal stability following electroporation. *Anal Biochem,* 448**,** 41-9.

HOOTEN, N., MCFARLAND, M. H., FREEMAN, D. W., MODE, N. A., EZIKE, N., ZONDERMAN, A. B. & EVANS, M. K. 2019. Association of Extracellular Vesicle Protein Cargo with Race and Clinical Markers of Mortality. *Sci Rep,* 9**,** 17582.

HU, H., HU, X., LI, L., FANG, Y., YANG, Y., GU, J., XU, J. & CHU, L. 2022. Exosomes Derived from Bone Marrow Mesenchymal Stem Cells Promote Angiogenesis in Ischemic Stroke Mice via Upregulation of MiR-21-5p. *Biomolecules,* 12.

HU, X., DE SILVA, T. M., CHEN, J. & FARACI, F. M. 2017. Cerebral Vascular Disease and Neurovascular Injury in Ischemic Stroke. *Circ Res,* 120**,** 449-471.

HUANG, E. J. & REICHARDT, L. F. 2001. Neurotrophins: Roles in Neuronal Development and Function. *Annual Review of Neuroscience,* 24**,** 677-736.

HUANG, G., SHI, L. Z. & CHI, H. 2009. Regulation of JNK and p38 MAPK in the immune system: signal integration, propagation and termination. *Cytokine,* 48**,** 161-9.

HUANG, X., YUAN, T., TSCHANNEN, M., SUN, Z., JACOB, H., DU, M., LIANG, M., DITTMAR, R. L., LIU, Y., LIANG, M., KOHLI, M., THIBODEAU, S. N., BOARDMAN, L. & WANG, L. 2013. Characterization of human plasma-derived exosomal RNAs by deep sequencing. *BMC Genomics,* 14**,** 319.

HURTADO, O., DE CRISTÓBAL, J., SÁNCHEZ, V., LIZASOAIN, I., CÁRDENAS, A., PEREIRA, M. P., COLADO, M. I., LEZA, J. C., LORENZO, P. & MORO, M. A. 2003. Inhibition of glutamate release by delaying ATP fall accounts for neuroprotective effects of antioxidants in experimental stroke. *Faseb j,* 17**,** 2082-4.

HURWITZ, S. N., CONLON, M. M., RIDER, M. A., BROWNSTEIN, N. C. & MECKES, D. G., JR. 2016a. Nanoparticle analysis sheds budding insights into genetic drivers of extracellular vesicle biogenesis. *J Extracell Vesicles,* 5**,** 31295.

HURWITZ, S. N., RIDER, M. A., BUNDY, J. L., LIU, X., SINGH, R. K. & MECKES JR, D. G. 2016b. Proteomic profiling of NCI-60 extracellular vesicles uncovers common protein cargo and cancer type-specific biomarkers. *Oncotarget; Vol 7, No 52.*

IADECOLA, C., BUCKWALTER, M. S. & ANRATHER, J. 2020. Immune responses to stroke: mechanisms, modulation, and therapeutic potential. *J Clin Invest,* 130**,** 2777-2788.

ICHIKAWA, M., YOSHIMI, A., NAKAGAWA, M., NISHIMOTO, N., WATANABE-OKOCHI, N. & KUROKAWA, M. 2013. A role for RUNX1 in hematopoiesis and myeloid leukemia. *International Journal of Hematology,* 97**,** 726-734.

ILLUM, L. 2003. Nasal drug delivery--possibilities, problems and solutions. *J Control Release,* 87**,** 187-98.

INGBER, D. E., MADRI, J. A. & FOLKMAN, J. 1986. A Possible Mechanism for Inhibition of Angiogenesis by Angiostatic Steroids: Induction of Capillary Basement Membrane Dissolution*. *Endocrinology,* 119**,** 1768-1775.

IRMER, B., CHANDRABALAN, S., MAAS, L., BLECKMANN, A. & MENCK, K. 2023. Extracellular Vesicles in Liquid Biopsies as Biomarkers for Solid Tumors. *Cancers (Basel),* 15.

ISHIDA, T., ICHIHARA, M., WANG, X., YAMAMOTO, K., KIMURA, J., MAJIMA, E. & KIWADA, H. 2006. Injection of PEGylated liposomes in rats elicits PEG-specific IgM, which is responsible for rapid elimination of a second dose of PEGylated liposomes. *Journal of Controlled Release,* 112**,** 15-25.

ISHRAT, T., FOUDA, A. Y., PILLAI, B., ELDAHSHAN, W., AHMED, H., WALLER, J. L., ERGUL, A. & FAGAN, S. C. 2019. Dose-response, therapeutic time-window and tPA-combinatorial efficacy of compound 21: A randomized, blinded preclinical trial in a rat model of thromboembolic stroke. *Journal of Cerebral Blood Flow and Metabolism,* 39**,** 1635-1647.

IWAI, K., MINAMISAWA, T., SUGA, K., YAJIMA, Y. & SHIBA, K. 2016. Isolation of human salivary extracellular vesicles by iodixanol density gradient ultracentrifugation and their characterizations. *Journal of Extracellular Vesicles,* 5**,** 30829.

IWAI, M., LIU, H.-W., CHEN, R., IDE, A., OKAMOTO, S., SHIUCHI, T., HATA, R., SAKANAKA, M. & HORIUCHI, M. 2004. Possible inhibition of focal cerebral ischemia by angiotensin II type 2 receptor stimulation. *Circulation,* 110**,** 843-848.

IWANAMI, J., MOGI, M., TSUKUDA, K., MIN, L. J., SAKATA, A., JING, F., OHSHIMA, K. & HORIUCHI, M. 2011. Effect of angiotensin II type 2 receptor deletion in hematopoietic cells on brain ischemia-reperfusion injury. *Hypertension,* 58**,** 404-9.

IWATA, M., COWLING, R. T., GURANTZ, D., MOORE, C., ZHANG, S., YUAN, J. X. & GREENBERG, B. H. 2005. Angiotensin-(1-7) binds to specific receptors on cardiac fibroblasts to initiate antifibrotic and antitrophic effects. *Am J Physiol Heart Circ Physiol,* 289**,** H2356-63.

IZCO, M., SCHLEEF, M., SCHMEER, M., CARLOS, E., VERONA, G. & ALVAREZ-ERVITI, L. 2023. Targeted Extracellular Vesicle Gene Therapy for Modulating Alpha-Synuclein Expression in Gut and Spinal Cord. *Pharmaceutics* [Online], 15.

IZON SCIENCE. 2023a. *Extracellular Vesicle Isolation: Why Size Exclusion Chromatography Is on the Rise* [Online]. Available: https://www.izon.com/news/extracellular-vesicle-isolation-why-size-exclusion-chromatography-is-on-the-rise [Accessed 21112023 2023].

IZON SCIENCE. 2023b. *qEVoriginal / 35nm Legacy Column - 5 Pack* [Online]. Available: https://store.izon.com/en-gb/collections/consumables2/products/qevoriginal-35nm-5-pack [Accessed 06092023 2023].

JABBER, H., MOHAMMED, B. & HADI, N. R. 2023. Investigating the renoprotective effect of C21 in male mice with sepsis via modulation of p-AKT/PI3K expression. *J Med Life,* 16**,** 203-209.

JACKSON-COWAN, L., ELDAHSHAN, W., DUMANLI, S., DONG, G., JAMIL, S., ABDUL, Y., ALTHOMALI, W., BABAN, B., FAGAN, S. C. & ERGUL, A. 2021. Delayed Administration of Angiotensin Receptor (AT2R) Agonist C21 Improves Survival and Preserves Sensorimotor Outcomes in Female Diabetic Rats Post-Stroke through Modulation of Microglial Activation. *International journal of molecular sciences,* 22.

JACKSON, L., DONG, G., ALTHOMALI, W., SAYED, M. A., ELDAHSHAN, W., BABAN, B., JOHNSON, M. H., FILOSA, J., FAGAN, S. C. & ERGUL, A. 2020. Delayed Administration of Angiotensin II Type 2 Receptor (AT2R) Agonist Compound 21 Prevents the Development of Post-stroke Cognitive Impairment in Diabetes Through the Modulation of Microglia Polarization. *Translational stroke research,* 11**,** 762-775.

JAMERSON, K., WEBER, M. A., BAKRIS, G. L., DAHLÖF, B., PITT, B., SHI, V., HESTER, A., GUPTE, J., GATLIN, M. & VELAZQUEZ, E. J. 2008. Benazepril plus amlodipine or hydrochlorothiazide for hypertension in high-risk patients. *N Engl J Med,* 359**,** 2417-28.

JAMES, J. M., GEWOLB, C. & BAUTCH, V. L. 2009. Neurovascular development uses VEGF-A signaling to regulate blood vessel ingression into the neural tube. *Development,* 136**,** 833-41.

JEAN LEBLANC, N., GURUSWAMY, R. & ELALI, A. 2018. Vascular Endothelial Growth Factor Isoform-B Stimulates Neurovascular Repair After Ischemic Stroke by Promoting the Function of Pericytes via Vascular Endothelial Growth Factor Receptor-1. *Molecular Neurobiology,* 55**,** 3611-3626.

JENNINGS, R. B., KALTENBACH, J. P. & SMETTERS, G. W. 1957. Ensymatic changes in acute myocardial ischemic injury; glutamic oxaloacetic transaminase, lactic dehydrogenase, and succinic dehydrogenase. *AMA Arch Pathol,* 64**,** 10-6.

JEPPESEN, P. L., CHRISTENSEN, G. L., SCHNEIDER, M., NOSSENT, A. Y., JENSEN, H. B., ANDERSEN, D. C., ESKILDSEN, T., GAMMELTOFT, S., HANSEN, J. L. & SHEIKH, S. P. 2011. Angiotensin II type 1 receptor signalling regulates microRNA differentially in cardiac fibroblasts and myocytes. *Br J Pharmacol,* 164**,** 394-404.

JEWETT, B. E. & THAPA, B. 2022. *Physiology, NMDA Receptor* [Online]. StatPearls [Internet]: National Library of Medicine; National Centre for Biotechnology. Available: https://www.ncbi.nlm.nih.gov/books/NBK519495/ [Accessed 31.10.2023 2023].

JI, Q., JI, Y., PENG, J., ZHOU, X., CHEN, X., ZHAO, H., XU, T., CHEN, L. & XU, Y. 2016. Increased Brain-Specific MiR-9 and MiR-124 in the Serum Exosomes of Acute Ischemic Stroke Patients. *PLoS One,* 11**,** e0163645.

JIANG, T., YU, J.-T., ZHU, X.-C., ZHANG, Q.-Q., TAN, M.-S., CAO, L., WANG, H.-F., LU, J., GAO, Q., ZHANG, Y.-D. & TAN, L. 2014. Angiotensin-(1-7) induces cerebral ischaemic tolerance by promoting brain angiogenesis in a Mas/eNOS-dependent pathway. *British journal of pharmacology,* 171**,** 4222-32.

JIANG, Y.-F., WEI, S.-N., GENG, N., QIN, W.-W., HE, X., WANG, X.-H., QI, Y.-P., SONG, S. & WANG, P. 2022. Evaluation of circulating small extracellular vesicle-derived miRNAs as diagnostic biomarkers for differentiating between different pathological types of early lung cancer. *Scientific Reports,* 12**,** 17201.

JOHNSON, V. E., MEANEY, D. F., CULLEN, D. K. & SMITH, D. H. 2015. Chapter 8 - Animal models of traumatic brain injury. *In:* GRAFMAN, J. & SALAZAR, A. M. (eds.) *Handbook of Clinical Neurology.* Elsevier.

JOINT FORMULARY COMMITTEE BRITISH NATIONAL FORMULARY. 2023a. *Candesartan cilexetil- Indications and dose* [Online]. Available: https://bnf.nice.org.uk/drugs/candesartan-cilexetil/#indications-and-dose [Accessed 06092023 2023].

JOINT FORMULARY COMMITTEE BRITISH NATIONAL FORMULARY. 2023b. *Eprosartan- Indictions and dose* [Online]. Available: https://bnf.nice.org.uk/drugs/eprosartan/#indications-and-dose [Accessed 06092023 2023].

JOKINEN, H., MELKAS, S., YLIKOSKI, R., POHJASVAARA, T., KASTE, M., ERKINJUNTTI, T. & HIETANEN, M. 2015. Post-stroke cognitive impairment is common even after successful clinical recovery. *European Journal of Neurology,* 22**,** 1288-1294.

JONULEIT, H., KÜHN, U., MÜLLER, G., STEINBRINK, K., PARAGNIK, L., SCHMITT, E., KNOP, J. & ENK, A. H. 1997. Pro-inflammatory cytokines and prostaglandins induce maturation of potent immunostimulatory dendritic cells under fetal calf serum-free conditions. *Eur J Immunol,* 27**,** 3135-42.

JOSEPH, J. P., MECCA, A. P., REGENHARDT, R. W., BENNION, D. M., RODRÍGUEZ, V., DESLAND, F., PATEL, N. A., PIOQUINTO, D. J., UNGER, T., KATOVICH, M. J., STECKELINGS, U. M. & SUMNERS, C. 2014. The angiotensin type 2 receptor agonist Compound 21 elicits cerebroprotection in endothelin-1 induced ischemic stroke. *Neuropharmacology,* 81**,** 134-41.

JOUNG, S., FIL, J. E., HECKMANN, A. B., KVISTGAARD, A. S. & DILGER, R. N. 2020. Early-Life Supplementation of Bovine Milk Osteopontin Supports Neurodevelopment and Influences Exploratory Behavior. *Nutrients,* 12.

KANELLOPOULOS, J. M. & DELARASSE, C. 2019. Pleiotropic Roles of P2X7 in the Central Nervous System. *Front Cell Neurosci,* 13**,** 401.

KARIMI, N., DALIRFARDOUEI, R., DIAS, T., LÖTVALL, J. & LÄSSER, C. 2022. Tetraspanins distinguish separate extracellular vesicle subpopulations in human serum and plasma - Contributions of platelet extracellular vesicles in plasma samples. *J Extracell Vesicles,* 11**,** e12213.

KATADA, J. & MAJIMA, M. 2002. AT(2) receptor-dependent vasodilation is mediated by activation of vascular kinin generation under flow conditions. *Br J Pharmacol,* 136**,** 484-91.

KATZMANN, D. J., BABST, M. & EMR, S. D. 2001. Ubiquitin-dependent sorting into the multivesicular body pathway requires the function of a conserved endosomal protein sorting complex, ESCRT-I. *Cell,* 106**,** 145-55.

KAWAI, T., FORRESTER, S. J., O'BRIEN, S., BAGGETT, A., RIZZO, V. & EGUCHI, S. 2017. AT1 receptor signaling pathways in the cardiovascular system. *Pharmacol Res,* 125**,** 4-13.

KHARLAMOV, A., KHARLAMOV, E. & ARMSTRONG, D. M. 2000. Age-dependent increase in infarct volume following photochemically induced cerebral infarction: putative role of astroglia. *J Gerontol A Biol Sci Med Sci,* 55**,** B135-41; discussion B142-3.

KILKENNY, C., BROWNE, W. J., CUTHILL, I. C., EMERSON, M. & ALTMAN, D. G. 2010. Improving bioscience research reporting: the ARRIVE guidelines for reporting animal research. *PLoS Biol,* 8**,** e1000412.

KIM, E. H., WON, J. H., HWANG, I. & YU, J. W. 2013. Cobalt Chloride-induced Hypoxia Ameliorates NLRP3-Mediated Caspase-1 Activation in Mixed Glial Cultures. *Immune Netw,* 13**,** 141-7.

KIM, G., KIM, M., LEE, Y., BYUN, J. W., HWANG, D. W. & LEE, M. 2020. Systemic delivery of microRNA-21 antisense oligonucleotides to the brain using T7-peptide decorated exosomes. *J Control Release,* 317**,** 273-281.

KIM, M. S., HANEY, M. J., ZHAO, Y., MAHAJAN, V., DEYGEN, I., KLYACHKO, N. L., INSKOE, E., PIROYAN, A., SOKOLSKY, M., OKOLIE, O., HINGTGEN, S. D., KABANOV, A. V. & BATRAKOVA, E. V. 2016. Development of exosome-encapsulated paclitaxel to overcome MDR in cancer cells. *Nanomedicine,* 12**,** 655-664.

KING, T. L., TIONG, L. L., ABDUL AZIZ, Z. & LAW, W. C. 2023. Association of underlying untreated cardiovascular risk factors with mortality and functional outcome in ischaemic stroke patients. *Journal of Stroke and Cerebrovascular Diseases,* 32**,** 107230.

KLOK, F. A., PRUSZCZYK, P., KONSTANTINIDES, S. V., ON BEHALF OF THE WORKING GROUP ON PULMONARY, C. & RIGHT VENTRICULAR, F. 2023. Thrombolytic treatment of life-threatening pulmonary embolism in times of alteplase shortage. *European Heart Journal,* 44**,** 1837-1839.

KLYACHKO, N. L., ARZT, C. J., LI, S. M., GOLOLOBOVA, O. A. & BATRAKOVA, E. V. 2020. Extracellular Vesicle-Based Therapeutics: Preclinical and Clinical Investigations. *Pharmaceutics,* 12.

KOEPPEN, M., FEIL, R., SIEGL, D., FEIL, S., HOFMANN, F., POHL, U. & DE WIT, C. 2004. cGMP-Dependent Protein Kinase Mediates NO- but not Acetylcholine-Induced Dilations in Resistance Vessels In Vivo. *Hypertension,* 44**,** 952-955.

KOGA, Y., TSURUMAKI, H., AOKI-SAITO, H., SATO, M., YATOMI, M., TAKEHARA, K. & HISADA, T. 2019. Roles of Cyclic AMP Response Element Binding Activation in the ERK1/2 and p38 MAPK Signalling Pathway in Central Nervous System, Cardiovascular System, Osteoclast Differentiation and Mucin and Cytokine Production. *Int J Mol Sci,* 20.

KOH-TAN, H. H. C., GRAHAM, D., HAMILTON, C. A., NICOLL, G., FIELDS, L., MCBRIDE, M. W., YOUNG, B. & DOMINICZAK, A. F. 2009. Renal and vascular glutathione S-transferase μ is not affected by pharmacological intervention to reduce systolic blood pressure. *Journal of Hypertension,* 27.

KOSAKA, N., IGUCHI, H., YOSHIOKA, Y., TAKESHITA, F., MATSUKI, Y. & OCHIYA, T. 2010. Secretory mechanisms and intercellular transfer of microRNAs in living cells. *J Biol Chem,* 285**,** 17442-52.

KOSUGI, A., SAKAKURA, J., YASUDA, K., OGATA, M. & HAMAOKA, T. 2001. Involvement of SHP-1 tyrosine phosphatase in TCR-mediated signaling pathways in lipid rafts. *Immunity,* 14**,** 669-80.

KOTB, H. G., IBRAHIM, A. H., MOHAMED, E. F., ALI, O. M., HASSANEIN, N., BADAWY, D. & ABDELATTY ALY, E. 2019. The expression of microRNA 146a in patients with ischemic stroke: an observational study. *Int J Gen Med,* 12**,** 273-278.

KRÖTZ, F., ENGELBRECHT, B., BUERKLE, M. A., BASSERMANN, F., BRIDELL, H., GLOE, T., DUYSTER, J., POHL, U. & SOHN, H.-Y. 2005. The Tyrosine Phosphatase, SHP-1, Is a Negative Regulator of Endothelial Superoxide Formation. *Journal of the American College of Cardiology,* 45**,** 1700-1706.

KRUPINSKI, J., KUMAR, P., KUMAR, S. & KALUZA, J. 1996. Increased Expression of TGF-β1 in Brain Tissue After Ischemic Stroke in Humans. *Stroke,* 27**,** 852-857.

KUIPERS, A., MOLL, G. N., LEVY, A., KRAKOVSKY, M. & FRANKLIN, R. 2020. Cyclic angiotensin-(1-7) contributes to rehabilitation of animal performance in a rat model of cerebral stroke. *Peptides,* 123**,** 170193.

KUMAR, M. A., BABA, S. K., SADIDA, H. Q., MARZOOQI, S. A., JEROBIN, J., ALTEMANI, F. H., ALGEHAINY, N., ALANAZI, M. A., ABOU-SAMRA, A.-B., KUMAR, R., AL-SHABEEB AKIL, A. S., MACHA, M. A., MIR, R. & BHAT,

A. A. 2024. Extracellular vesicles as tools and targets in therapy for diseases. *Signal Transduction and Targeted Therapy,* 9**,** 27.

KURIAN, G. A. & PEMAIH, B. 2014. Standardization of in vitro Cell-based Model for Renal Ischemia and Reperfusion Injury. *Indian J Pharm Sci,* 76**,** 348-53.

KWAKKEL, G., KOLLEN, B. J., VAN DER GROND, J. & PREVO, A. J. H. 2003. Probability of Regaining Dexterity in the Flaccid Upper Limb. *Stroke,* 34**,** 2181-2186.

LABAT-GEST, V. & TOMASI, S. 2013. Photothrombotic ischemia: a minimally invasive and reproducible photochemical cortical lesion model for mouse stroke studies. *J Vis Exp*.

LABIRIS, N. R. & DOLOVICH, M. B. 2003. Pulmonary drug delivery. Part I: physiological factors affecting therapeutic effectiveness of aerosolized medications. *Br J Clin Pharmacol,* 56**,** 588-99.

LAGOS, D., POLLARA, G., HENDERSON, S., GRATRIX, F., FABANI, M., MILNE, R. S. B., GOTCH, F. & BOSHOFF, C. 2010. miR-132 regulates antiviral innate immunity through suppression of the p300 transcriptional co-activator. *Nature Cell Biology,* 12**,** 513-519.

LAI, C. P., MARDINI, O., ERICSSON, M., PRABHAKAR, S., MAGUIRE, C., CHEN, J. W., TANNOUS, B. A. & BREAKEFIELD, X. O. 2014. Dynamic biodistribution of extracellular vesicles in vivo using a multimodal imaging reporter. *ACS Nano,* 8**,** 483-494.

LAING, R. J., JAKUBOWSKI, J. & LAING, R. W. 1993. Middle cerebral artery occlusion without craniectomy in rats. Which method works best? *Stroke,* 24**,** 294-7; discussion 297-8.

LANCASTER, M. A., RENNER, M., MARTIN, C.-A., WENZEL, D., BICKNELL, L. S., HURLES, M. E., HOMFRAY, T., PENNINGER, J. M., JACKSON, A. P. & KNOBLICH, J. A. 2013. Cerebral organoids model human brain development and microcephaly. *Nature,* 501**,** 373-379.

LANDEIRA, B. S., SANTANA, T., ARAÚJO, J. A. M., TABET, E. I., TANNOUS, B. A., SCHROEDER, T. & COSTA, M. R. 2018. Activity-Independent Effects of CREB on Neuronal Survival and Differentiation during Mouse Cerebral Cortex Development. *Cereb Cortex,* 28**,** 538-548.

LANSBERG, M. G., O'BRIEN, M. W., TONG, D. C., MOSELEY, M. E. & ALBERS, G. W. 2001. Evolution of Cerebral Infarct Volume Assessed by Diffusion-Weighted Magnetic Resonance Imaging. *Archives of Neurology,* 58**,** 613-617.

LARSSON, S. C., ÅKESSON, A. & WOLK, A. 2015. Primary prevention of stroke by a healthy lifestyle in a high-risk group. *Neurology,* 84**,** 2224-8.

LASSEN, N. A. 1985. Normal average value of cerebral blood flow in younger adults is 50 ml/100 g/min. *J Cereb Blood Flow Metab,* 5**,** 347-9.

LEE, S., BRAIT, V. H., EVANS, M. A., KIM, H. A., WIDDOP, R. E., DRUMMOND, G. R., SOBEY, C. G., JONES, E. S. & ARUMUGAM, T. V. 2012. Neuroprotective effect of an angiotensin receptor type 2 agonist following cerebral ischemia in vitro and in vivo. *Experimental and Translational Stroke Medicine,* 4**,** 16.

LEE, S., EVANS, M. A., CHU, H. X., KIM, H. A., WIDDOP, R. E., DRUMMOND, G. R. & SOBEY, C. G. 2015. Effect of a Selective Mas Receptor Agonist in Cerebral Ischemia In Vitro and In Vivo. *PloS one,* 10**,** e0142087.

LEE, S. S., WON, J. H., LIM, G. J., HAN, J., LEE, J. Y., CHO, K. O. & BAE, Y. K. 2019. A novel population of extracellular vesicles smaller than exosomes promotes cell proliferation. *Cell Commun Signal,* 17**,** 95.

LEGER, M., QUIEDEVILLE, A., BOUET, V., HAELEWYN, B., BOULOUARD, M., SCHUMANN-BARD, P. & FRERET, T. 2013. Object recognition test in mice. *Nat Protoc,* 8**,** 2531-7.

LENNAARD, A. J., MAMAND, D. R., WIKLANDER, R. J., EL ANDALOUSSI, S. & WIKLANDER, O. P. B. 2021. Optimised Electroporation for Loading of Extracellular Vesicles with Doxorubicin. *Pharmaceutics,* 14.

LEON-MORENO, L. C., CASTANEDA-ARELLANO, R., AGUILAR-GARCIA, I. G., DESENTIS-DESENTIS, M. F., TORRES-ANGUIANO, E., GUTIERREZ-ALMEIDA, C. E., NAJAR-ACOSTA, L. J., MENDIZABAL-RUIZ, G., ASCENCIO-PINA, C. R., DUENAS-JIMENEZ, J. M., RIVAS-CARRILLO, J. D. & DUENAS-JIMENEZ, S. H. 2020. Kinematic Changes in a Mouse Model of Penetrating Hippocampal Injury and Their Recovery After Intranasal Administration of Endometrial Mesenchymal Stem Cell-Derived Extracellular Vesicles. *Front Cell Neurosci,* 14**,** 579162.

LEONHARDT, J., VILLELA, D. C., TEICHMANN, A., MÜNTER, L.-M., MAYER, M. C., MARDAHL, M., KIRSCH, S., NAMSOLLECK, P., LUCHT, K., BENZ, V., ALENINA, N., DANIELL, N., HORIUCHI, M., IWAI, M., MULTHAUP, G., SCHÜLEIN, R., BADER, M., SANTOS, R. A., UNGER, T. & STECKELINGS, U. M. 2017. Evidence for Heterodimerization and Functional Interaction of the Angiotensin Type 2 Receptor and the Receptor MAS. *Hypertension,* 69**,** 1128-1135.

LI, C., WANG, C., ZHANG, Y., ALSROUJI, O. K., CHEBL, A. B., DING, G., JIANG, Q., MAYER, S. A., LU, M., KOLE, M. K., MARIN, H. L., ZHANG, L., CHOPP, M. & ZHANG, Z. G. 2021a. Cerebral endothelial cell-derived small extracellular vesicles enhance neurovascular function and neurological recovery in rat acute ischemic stroke models of mechanical thrombectomy and embolic stroke treatment with tPA. *J Cereb Blood Flow Metab,* 41**,** 2090-2104.

LI, J., GENG, X. Y. & CONG, X. L. 2016. PGC-1α ameliorates AngiotensinII-induced eNOS dysfunction in human aortic endothelial cells. *Vascul Pharmacol,* 83**,** 90-7.

LI, J., PENG, H., ZHANG, W., LI, M., WANG, N., PENG, C., ZHANG, X. & LI, Y. 2023a. Enhanced Nose-to-Brain Delivery of Combined Small Interfering RNAs Using Lesion-Recognizing Nanoparticles for the Synergistic Therapy of Alzheimer's Disease. *ACS Applied Materials & Interfaces,* 15**,** 53177-53188.

LI, Q., NIU, X., YI, Y., CHEN, Y., YUAN, J., ZHANG, J., LI, H., XIA, Y., WANG, Y. & DENG, Z. 2023b. Inducible Pluripotent Stem Cell-Derived Small Extracellular Vesicles Rejuvenate Senescent Blood-Brain Barrier to Protect against Ischemic Stroke in Aged Mice. *ACS Nano,* 17**,** 775-789.

LI, R., PENG, C., ZHANG, X., WU, Y., PAN, S. & XIAO, Y. 2017a. Roles of Arf6 in cancer cell invasion, metastasis and proliferation. *Life Sci,* 182**,** 80-84.

LI, S. H., CHEN, L., PANG, X. M., SU, S. Y., ZHOU, X., CHEN, C. Y., HUANG, L. G., LI, J. P. & LIU, J. L. 2017b. Decreased miR-146a expression in acute ischemic stroke directly targets the Fbxl10 mRNA and is involved in modulating apoptosis. *Neurochem Int,* 107**,** 156-167.

LI, S. H., SU, S. Y. & LIU, J. L. 2015. Differential Regulation of microRNAs in Patients with Ischemic Stroke. *Curr Neurovasc Res,* 12**,** 214-21.

LI, X., XIE, X., LIAN, W., SHI, R., HAN, S., ZHANG, H., LU, L. & LI, M. 2018. Exosomes from adipose-derived stem cells overexpressing Nrf2 accelerate cutaneous wound healing by promoting vascularization in a diabetic foot ulcer model. *Experimental & Molecular Medicine,* 50**,** 1-14.

LI, Y. Y., CUI, J. G., DUA, P., POGUE, A. I., BHATTACHARJEE, S. & LUKIW, W. J. 2011. Differential expression of miRNA-146a-regulated inflammatory genes in human primary neural, astroglial and microglial cells. *Neurosci Lett,* 499**,** 109-13.

LI, Z., SONG, Y., HE, T., WEN, R., LI, Y., CHEN, T., HUANG, S., WANG, Y., TANG, Y., SHEN, F., TIAN, H. L., YANG, G. Y. & ZHANG, Z. 2021b. M2 microglial small extracellular vesicles reduce glial scar formation via the miR-124/STAT3 pathway after ischemic stroke in mice. *Theranostics,* 11**,** 1232-1248.

LIEBESKIND, D. S., JÜTTLER, E., SHAPOVALOV, Y., YEGIN, A., LANDEN, J. & JAUCH, E. C. 2019. Cerebral Edema Associated With Large Hemispheric Infarction. *Stroke,* 50**,** 2619-2625.

LIN, Q., YE, T., YE, P., BORGHI, C., CRO, S., DAMASCENO, A., KHAN, N., NILSSON, P. M., PRABHAKARAN, D., RAMIREZ, A., SCHLAICH, M. P., SCHUTTE, A. E., STERGIOU, G., WEBER, M. A., BEANEY, T. & POULTER, N. R. 2022. Hypertension in stroke survivors and associations with national premature stroke mortality: data for 2.5 million participants from multinational screening campaigns. *Lancet Glob Health,* 10**,** e1141-e1149.

LIN, Y., WU, J., GU, W., HUANG, Y., TONG, Z., HUANG, L. & TAN, J. 2018. Exosome–Liposome Hybrid Nanoparticles Deliver CRISPR/Cas9 System in MSCs. *Advanced Science,* 5**,** 1700611.

LINARES, R., TAN, S., GOUNOU, C., ARRAUD, N. & BRISSON, A. R. 2015. High-speed centrifugation induces aggregation of extracellular vesicles. *J Extracell Vesicles,* 4**,** 29509.

LINDVALL, O. & KOKAIA, Z. 2015. Neurogenesis following Stroke Affecting the Adult Brain. *Cold Spring Harb Perspect Biol,* 7.

LISZCZAK, T. M., HEDLEY-WHYTE, E. T., ADAMS, J. F., HAN, D. H., KOLLURI, V. S., VACANTI, F. X., HEROS, R. C. & ZERVAS, N. T. 1984. Limitations of tetrazolium salts in delineating infarcted brain. *Acta Neuropathologica,* 65**,** 150-157.

LIU, H., ZHANG, X., ZHOU, Y., NGUYEN, T. N., ZHANG, L., XING, P., LI, Z., SHEN, H., ZHANG, Y., HUA, W., XU, H., ZHU, X., CHEN, L., ZUO, Q., ZHAO, R., LI, Q., DAI, D., ZHANG, Y., XU, Y., HUANG, Q., LIU, J. & YANG, P. 2023. Association between blood pressure and different antihypertensive drugs with outcome after ischemic stroke: A Mendelian randomization study. *International Journal of Stroke,* 18**,** 1247-1254.

LIU, P., CHEN, G. & ZHANG, J. 2022a. A Review of Liposomes as a Drug Delivery System: Current Status of Approved Products, Regulatory Environments, and Future Perspectives. *Molecules,* 27.

LIU, Z., CHEN, M., DUAN, X., ZHAI, Y., MA, B., DUAN, Z., XU, J. & LIU, H. 2022b. Optimisation of a Mouse Model of Cerebral Ischemia-Reperfusion to Address Issues of Survival and Model Reproducibility and Consistency. *Comput Intell Neurosci,* 2022**,** 7594969.

LLOVERA, G., ROTH, S., PLESNILA, N., VELTKAMP, R. & LIESZ, A. 2014. Modeling stroke in mice: permanent coagulation of the distal middle cerebral artery. *J Vis Exp***,** e51729.

LOGALLO, N., NOVOTNY, V., ASSMUS, J., KVISTAD, C. E., ALTEHELD, L., RØNNING, O. M., THOMMESSEN, B., AMTHOR, K.-F., IHLE-HANSEN, H., KURZ, M., TOBRO, H., KAUR, K., STANKIEWICZ, M., CARLSSON, M., MORSUND, Å., IDICULA, T., AAMODT, A. H., LUND, C., NÆSS, H., WAJE-ANDREASSEN, U. & THOMASSEN, L. 2017. Tenecteplase versus alteplase for management of acute ischaemic stroke (NOR-TEST): a phase 3, randomised, open-label, blinded endpoint trial. *The Lancet Neurology,* 16**,** 781-788.

LOGAN, T. T., RUSNAK, M. & SYMES, A. J. 2015. Runx1 promotes proliferation and neuronal differentiation in adult mouse neurosphere cultures. *Stem Cell Res,* 15**,** 554-564.

LONGA, E. Z., WEINSTEIN, P. R., CARLSON, S. & CUMMINS, R. 1989. Reversible middle cerebral artery occlusion without craniectomy in rats. *Stroke,* 20**,** 84-91.

LONGOBARDI, A., BENUSSI, L., NICSANU, R., BELLINI, S., FERRARI, C., SARACENO, C., ZANARDINI, R., CATANIA, M., DI FEDE, G., SQUITTI, R., BINETTI, G. & GHIDONI, R. 2021. Plasma Extracellular Vesicle Size and

Concentration Are Altered in Alzheimer's Disease, Dementia With Lewy Bodies, and Frontotemporal Dementia. *Frontiers in Cell and Developmental Biology,* 9.

LONGOBARDI, A., NICSANU, R., BELLINI, S., SQUITTI, R., CATANIA, M., TIRABOSCHI, P., SARACENO, C., FERRARI, C., ZANARDINI, R., BINETTI, G., DI FEDE, G., BENUSSI, L. & GHIDONI, R. 2022. Cerebrospinal Fluid EV Concentration and Size Are Altered in Alzheimer's Disease and Dementia with Lewy Bodies. *Cells,* 11.

LORENZ, M., KOSCHATE, J., KAUFMANN, K., KREYE, C., MERTENS, M., KUEBLER, W. M., BAUMANN, G., GOSSING, G., MARKI, A., ZAKRZEWICZ, A., MIÉVILLE, C., BENN, A., HORBELT, D., WRATIL, P. R., STANGL, K. & STANGL, V. 2015. Does cellular sex matter? Dimorphic transcriptional differences between female and male endothelial cells. *Atherosclerosis,* 240**,** 61-72.

LOSURDO, M., PEDRAZZOLI, M., D'AGOSTINO, C., ELIA, C. A., MASSENZIO, F., LONATI, E., MAURI, M., RIZZI, L., MOLTENI, L., BRESCIANI, E., DANDER, E., D'AMICO, G., BULBARELLI, A., TORSELLO, A., MATTEOLI, M., BUFFELLI, M. & COCO, S. 2020. Intranasal delivery of mesenchymal stem cell-derived extracellular vesicles exerts immunomodulatory and neuroprotective effects in a 3xTg model of Alzheimer's disease. *Stem Cells Transl Med,* 9**,** 1068-1084.

LÖTVALL, J., HILL, A. F., HOCHBERG, F., BUZÁS, E. I., DI VIZIO, D., GARDINER, C., GHO, Y. S., KUROCHKIN, I. V., MATHIVANAN, S., QUESENBERRY, P., SAHOO, S., TAHARA, H., WAUBEN, M. H., WITWER, K. W. & THÉRY, C. 2014. Minimal experimental requirements for definition of extracellular vesicles and their functions: a position statement from the International Society for Extracellular Vesicles. *J Extracell Vesicles,* 3**,** 26913.

LÖVBLAD, K. O., BAIRD, A. E., SCHLAUG, G., BENFIELD, A., SIEWERT, B., VOETSCH, B., CONNOR, A., BURZYNSKI, C., EDELMAN, R. R. & WARACH, S. 1997. Ischemic lesion volumes in acute stroke by diffusion-weighted magnetic resonance imaging correlate with clinical outcome. *Ann Neurol,* 42**,** 164-70.

LU, J., JIANG, T., WU, L., GAO, L., WANG, Y., ZHOU, F., ZHANG, S. & ZHANG, Y. 2013. The expression of angiotensin-converting enzyme 2-angiotensin-(1-7)-Mas receptor axis are upregulated after acute cerebral ischemic stroke in rats. *Neuropeptides,* 47**,** 289-95.

LU, J., ZHANG, Y. & SHI, J. 2008. Effects of intracerebroventricular infusion of angiotensin-(1-7) on bradykinin formation and the kinin receptor expression after focal cerebral ischemia-reperfusion in rats. *Brain Research,* 1219**,** 127-135.

MA, C.-Y. & YIN, L. 2016. Neuroprotective effect of angiotensin II type 2 receptor during cerebral ischemia/reperfusion. *Neural Regeneration Research,* 11**,** 1102-1107.

MA, H., MAO, C., HU, Y., WANG, L., GUO, X., LI, L., WANG, F. & GUAN, R. 2023. Angiotensin-(1–9) attenuates adriamycin-induced cardiomyopathy in rats via the angiotensin type 2 receptor. *Molecular and Cellular Biochemistry*.

MA, T. K. W., KAM, K. K. H., YAN, B. P. & LAM, Y.-Y. 2010. Renin–angiotensin–aldosterone system blockade for cardiovascular diseases: current status. *British Journal of Pharmacology,* 160**,** 1273-1292.

MACRAE, I. M. 2011. Preclinical stroke research--advantages and disadvantages of the most common rodent models of focal ischaemia. *Br J Pharmacol,* 164**,** 1062-78.

MAGNUS, T., WIENDL, H. & KLEINSCHNITZ, C. 2012. Immune mechanisms of stroke. *Current Opinion in Neurology,* 25.

MAÏER, B., GORY, B., LAPERGUE, B., SIBON, I., RICHARD, S., KYHENG, M., LABREUCHE, J., DESILLES, J.-P., BLANC, R., PIOTIN, M., MAZIGHI, M., HALIMI, J.-M., REDJEM, H., ESCALARD, S., SMAJDA, S., DELVOYE, F.,

HEBERT, S., OBADIA, M., SABBEN, C., OBADIA, A., RAYNOUARD, I., MORVAN, E., BOURSIN, P., BEN MAACHA, M., CONSOLI, A., WANG, A., MIONE, G., HUMBERTJEAN, L., BONNEROT, M., LACOUR, J.-C., ANXIONNAT, R., TONNELET, R., BRACARD, S., BARREAU, X., MARNAT, G., BERGE, J., LUCAS, L., RENOU, P., DEBRUXELLES, S., POLI, M. & SAGNIER, S. 2022. Effect of Baseline Antihypertensive Treatments on Stroke Severity and Outcomes in the BP TARGET Trial. *Stroke,* 53**,** 1837-1846.

MALININ, N. L., BOLDIN, M. P., KOVALENKO, A. V. & WALLACH, D. 1997. MAP3K-related kinase involved in NF-kappaB induction by TNF, CD95 and IL-1. *Nature,* 385**,** 540-4.

MARELLI-BERG, F. M., CLEMENT, M., MAURO, C. & CALIGIURI, G. 2013. An immunologist's guide to CD31 function in T-cells. *Journal of Cell Science,* 126**,** 2343-2352.

MARKUS, H. S. 2004. Cerebral perfusion and stroke. *Journal of Neurology, Neurosurgery & Psychiatry,* 75**,** 353-361.

MARTINEZ-GREENE, J. A., HERNANDEZ-ORTEGA, K., QUIROZ-BAEZ, R., RESENDIS-ANTONIO, O., PICHARDO-CASAS, I., SINCLAIR, D. A., BUDNIK, B., HIDALGO-MIRANDA, A., URIBE-QUEROL, E., RAMOS-GODINEZ, M. D. P. & MARTINEZ-MARTINEZ, E. 2021. Quantitative proteomic analysis of extracellular vesicle subgroups isolated by an optimized method combining polymer-based precipitation and size exclusion chromatography. *J Extracell Vesicles,* 10**,** e12087.

MARTINEZ, N. J. & GREGORY, R. I. 2013. Argonaute2 expression is post-transcriptionally coupled to microRNA abundance. *Rna,* 19**,** 605-12.

MATEOS, L., PEREZ-ALVAREZ, M. J. & WANDOSELL, F. 2016. Angiotensin II type-2 receptor stimulation induces neuronal VEGF synthesis after cerebral ischemia. *Biochimica et biophysica acta,* 1862**,** 1297-308.

MATHIEU, M., NEVO, N., JOUVE, M., VALENZUELA, J. I., MAURIN, M., VERWEIJ, F. J., PALMULLI, R., LANKAR, D., DINGLI, F., LOEW, D., RUBINSTEIN, E., BONCOMPAIN, G., PEREZ, F. & THERY, C. 2021. Specificities of exosome versus small ectosome secretion revealed by live intracellular tracking of CD63 and CD9. *Nat Commun,* 12**,** 4389.

MATSUO, Y., ONODERA, H., SHIGA, Y., NAKAMURA, M., NINOMIYA, M., KIHARA, T. & KOGURE, K. 1994. Correlation between myeloperoxidase-quantified neutrophil accumulation and ischemic brain injury in the rat. Effects of neutrophil depletion. *Stroke,* 25**,** 1469-75.

MCCARROLL, C. S., HE, W., FOOTE, K., BRADLEY, A., MCGLYNN, K., VIDLER, F., NIXON, C., NATHER, K., FATTAH, C., RIDDELL, A., BOWMAN, P., ELLIOTT, E. B., BELL, M., HAWKSBY, C., MACKENZIE, S. M., MORRISON, L. J., TERRY, A., BLYTH, K., SMITH, G. L., MCBRIDE, M. W., KUBIN, T., BRAUN, T., NICKLIN, S. A., CAMERON, E. R. & LOUGHREY, C. M. 2018. Runx1 Deficiency Protects Against Adverse Cardiac Remodeling After Myocardial Infarction. *Circulation,* 137**,** 57-70.

MCCARTHY, C. A., VINH, A., BROUGHTON, B. R. S., SOBEY, C. G., CALLAWAY, J. K. & WIDDOP, R. E. 2012. Angiotensin II type 2 receptor stimulation initiated after stroke causes neuroprotection in conscious rats. *Hypertension (Dallas, Tex. : 1979),* 60**,** 1531-7.

MCCARTHY, C. A., VINH, A., CALLAWAY, J. K. & WIDDOP, R. E. 2009. Angiotensin AT2 receptor stimulation causes neuroprotection in a conscious rat model of stroke. *Stroke,* 40**,** 1482-9.

MCCARTHY, C. A., VINH, A., WIDDOP, R. E., MILLER, A. A., HALLBERG, A., ALTERMAN, M. & CALLAWAY, J. K. 2014. Direct angiotensin AT2 receptor

stimulation using a novel AT2 receptor agonist, compound 21, evokes neuroprotection in conscious hypertensive rats. *PLoS ONE,* 9**,** e95762.

MCCULLOUGH, J., FROST, A. & SUNDQUIST, W. I. 2018. Structures, Functions, and Dynamics of ESCRT-III/Vps4 Membrane Remodeling and Fission Complexes. *Annual Review of Cell and Developmental Biology,* 34**,** 85-109.

MCFALL, A. 2020. *Modulating the counterregulatory renin angiotensin system axis in experimental ischaemic stroke.* Doctor of Philosophy PhD, University of Glasgow.

MCGILL, J. K., GALLAGHER, L., CARSWELL, H. V. O., IRVING, E. A., DOMINICZAK, A. F. & MACRAE, I. M. 2005. Impaired Functional Recovery After Stroke in the Stroke-Prone Spontaneously Hypertensive Rat. *Stroke,* 36**,** 135-141.

MCKENZIE, A. J., HOSHINO, D., HONG, N. H., CHA, D. J., FRANKLIN, J. L., COFFEY, R. J., PATTON, J. G. & WEAVER, A. M. 2016. KRAS-MEK Signaling Controls Ago2 Sorting into Exosomes. *Cell Rep,* 15**,** 978-987.

MCKITTRICK, C. M., LAWRENCE, C. E. & CARSWELL, H. V. 2015. Mast cells promote blood brain barrier breakdown and neutrophil infiltration in a mouse model of focal cerebral ischemia. *J Cereb Blood Flow Metab,* 35**,** 638-47.

MCMEEKIN, P., WHITE, P., JAMES, M. A., PRICE, C. I., FLYNN, D. & FORD, G. A. 2017. Estimating the number of UK stroke patients eligible for endovascular thrombectomy. *Eur Stroke J,* 2**,** 319-326.

MECCA, A. P., REGENHARDT, R. W., O'CONNOR, T. E., JOSEPH, J. P., RAIZADA, M. K., KATOVICH, M. J. & SUMNERS, C. 2011. Cerebroprotection by angiotensin-(1-7) in endothelin-1-induced ischaemic stroke. *Exp Physiol,* 96**,** 1084-96.

MEDALLA, M., CHANG, W., CALDERAZZO, S. M., GO, V., TSOLIAS, A., GOODLIFFE, J. W., PATHAK, D., DE ALBA, D., PESSINA, M., ROSENE, D. L., BULLER, B. & MOORE, T. L. 2020. Treatment with Mesenchymal-Derived Extracellular Vesicles Reduces Injury-Related Pathology in Pyramidal Neurons of Monkey Perilesional Ventral Premotor Cortex. *J Neurosci,* 40**,** 3385-3407.

MENCK, K., SÖNMEZER, C., WORST, T. S., SCHULZ, M., DIHAZI, G. H., STREIT, F., ERDMANN, G., KLING, S., BOUTROS, M., BINDER, C. & GROSS, J. C. 2017. Neutral sphingomyelinases control extracellular vesicles budding from the plasma membrane. *J Extracell Vesicles,* 6**,** 1378056.

MENDOZA-TORRES, E., RIQUELME, J. A., VIELMA, A., SAGREDO, A. R., GABRIELLI, L., BRAVO-SAGUA, R., JALIL, J. E., ROTHERMEL, B. A., SANCHEZ, G., OCARANZA, M. P. & LAVANDERO, S. 2018. Protection of the myocardium against ischemia/reperfusion injury by angiotensin-(1–9) through an AT2R and Akt-dependent mechanism. *Pharmacological Research,* 135**,** 112-121.

MENS, M. M. J., HESHMATOLLAH, A., FANI, L., IKRAM, M. A., IKRAM, M. K. & GHANBARI, M. 2021. Circulatory MicroRNAs as Potential Biomarkers for Stroke Risk. *Stroke,* 52**,** 945-953.

MILASAN, A., TESSANDIER, N., TAN, S., BRISSON, A., BOILARD, E. & MARTEL, C. 2016. Extracellular vesicles are present in mouse lymph and their level differs in atherosclerosis. *J Extracell Vesicles,* 5**,** 31427.

MILATOVIC, D., MONTINE, T. J. & ASCHNER, M. 2011. Measurement of isoprostanes as markers of oxidative stress. *Methods Mol Biol,* 758**,** 195-204.

MIN, L.-J., MOGI, M., TSUKUDA, K., JING, F., OHSHIMA, K., NAKAOKA, H., KAN-NO, H., WANG, X.-L., CHISAKA, T., BAI, H.-Y., IWANAMI, J. & HORIUCHI, M. 2014. Direct stimulation of angiotensin II type 2 receptor initiated after stroke ameliorates ischemic brain damage. *American Journal of Hypertension,* 27**,** 1036-1044.

MIRABITO, K. M., HILLIARD, L. M., WEI, Z., TIKELLIS, C., WIDDOP, R. E., VINH, A. & DENTON, K. M. 2014. Role of inflammation and the angiotensin type 2

receptor in the regulation of arterial pressure during pregnancy in mice. *Hypertension,* 64**,** 626-31.

MIRO-MUR, F., PEREZ-DE-PUIG, I., FERRER-FERRER, M., URRA, X., JUSTICIA, C., CHAMORRO, A. & PLANAS, A. M. 2016. Immature monocytes recruited to the ischemic mouse brain differentiate into macrophages with features of alternative activation. *Brain Behav Immun,* 53**,** 18-33.

MITTELBRUNN, M., GUTIÉRREZ-VÁZQUEZ, C., VILLARROYA-BELTRI, C., GONZÁLEZ, S., SÁNCHEZ-CABO, F., GONZÁLEZ, M., BERNAD, A. & SÁNCHEZ-MADRID, F. 2011. Unidirectional transfer of microRNA-loaded exosomes from T cells to antigen-presenting cells. *Nat Commun,* 2**,** 282.

MOGI, M., LI, J.-M., IWANAMI, J., MIN, L.-J., TSUKUDA, K., IWAI, M. & HORIUCHI, M. 2006. Angiotensin II Type-2 Receptor Stimulation Prevents Neural Damage by Transcriptional Activation of Methyl Methanesulfonate Sensitive 2. *Hypertension,* 48**,** 141-148.

MORALES-KASTRESANA, A., TELFORD, B., MUSICH, T. A., MCKINNON, K., CLAYBORNE, C., BRAIG, Z., ROSNER, A., DEMBERG, T., WATSON, D. C., KARPOVA, T. S., FREEMAN, G. J., DEKRUYFF, R. H., PAVLAKIS, G. N., TERABE, M., ROBERT-GUROFF, M., BERZOFSKY, J. A. & JONES, J. C. 2017. Labeling Extracellular Vesicles for Nanoscale Flow Cytometry. *Sci Rep,* 7**,** 1878.

MOREIRA, A., WINTER, C., JOY, J., WINTER, L., JONES, M., NORONHA, M., PORTER, M., QUIM, K., CORRAL, A., ALAYLI, Y., SENO, T., MUSTAFA, S., HORNSBY, P. & AHUJA, S. 2020. Intranasal delivery of human umbilical cord Wharton's jelly mesenchymal stromal cells restores lung alveolarization and vascularization in experimental bronchopulmonary dysplasia. *Stem Cells Transl Med,* 9**,** 221-234.

MORGAN, M. J. & LIU, Z.-G. 2011. Crosstalk of reactive oxygen species and NF-κB signaling. *Cell Research,* 21**,** 103-115.

MORI, E., MINEMATSU, K., NAKAGAWARA, J., YAMAGUCHI, T., SASAKI, M. & HIRANO, T. 2010. Effects of 0.6 mg/kg intravenous alteplase on vascular and clinical outcomes in middle cerebral artery occlusion: Japan Alteplase Clinical Trial II (J-ACT II). *Stroke,* 41**,** 461-5.

MUHL, L., HE, L., SUN, Y., ANDALOUSSI MÄE, M., PIETILÄ, R., LIU, J., GENOVÉ, G., ZHANG, L., XIE, Y., LEPTIDIS, S., MOCCI, G., STRITT, S., OSMAN, A., ANISIMOV, A., HEMANTHAKUMAR, K. A., RÄSÄNEN, M., HANSSON, E. M., BJÖRKEGREN, J., VANLANDEWIJCK, M., BLOMGREN, K., MÄKINEN, T., PENG, X. R., HU, Y., ERNFORS, P., ARNOLD, T. D., ALITALO, K., LENDAHL, U. & BETSHOLTZ, C. 2022. The SARS-CoV-2 receptor ACE2 is expressed in mouse pericytes but not endothelial cells: Implications for COVID-19 vascular research. *Stem Cell Reports,* 17**,** 1089-1104.

MUKOYAMA, M., NAKAJIMA, M., HORIUCHI, M., SASAMURA, H., PRATT, R. E. & DZAU, V. J. 1993. Expression cloning of type 2 angiotensin II receptor reveals a unique class of seven-transmembrane receptors. *J Biol Chem,* 268**,** 24539-42.

MURPHY, D. E., DE JONG, O. G., BROUWER, M., WOOD, M. J., LAVIEU, G., SCHIFFELERS, R. M. & VADER, P. 2019. Extracellular vesicle-based therapeutics: natural versus engineered targeting and trafficking. *Experimental & Molecular Medicine,* 51**,** 1-12.

MUSANTE, L., SARASWAT, M., RAVIDA, A., BYRNE, B. & HOLTHOFER, H. 2013. Recovery of urinary nanovesicles from ultracentrifugation supernatants. *Nephrol Dial Transplant,* 28**,** 1425-33.

MYBIOSOURCE. 2023. *Ang1-9 elisa kit :: Angiotensin 1-9 (Ang1-9) ELISA Kit* [Online]. MyBioSource.com. Available: https://www.mybiosource.com/human-mouse-rat-elisa-kits/angiotensin-1-9-ang1-9/2700688 [Accessed 20112023 2023].

NADKARNI, N. A., ARIAS, E., FANG, R., HAYNES, M. E., ZHANG, H. F., MULLER, W. A., BATRA, A. & SULLIVAN, D. P. 2022. Platelet Endothelial Cell Adhesion Molecule (PECAM/CD31) Blockade Modulates Neutrophil Recruitment Patterns and Reduces Infarct Size in Experimental Ischemic Stroke. *The American Journal of Pathology,* 192**,** 1619-1632.

NAITO, M. G., XU, D., AMIN, P., LEE, J., WANG, H., LI, W., KELLIHER, M., PASPARAKIS, M. & YUAN, J. 2020. Sequential activation of necroptosis and apoptosis cooperates to mediate vascular and neural pathology in stroke. *Proceedings of the National Academy of Sciences,* 117**,** 4959-4970.

NARBUTE, K., PILIPENKO, V., PUPURE, J., KLINOVICS, T., AUDERS, J., JONAVICE, U., KRIAUCIUNAITE, K., PIVORIUNAS, A. & KLUSA, V. 2021. Time-Dependent Memory and Gait Improvement by Intranasally-Administered Extracellular Vesicles in Parkinson's Disease Model Rats. *Cell Mol Neurobiol,* 41**,** 605-613.

NATIONAL INSTITUTE FOR HEALTH AND CARE EXCELLENCE. 2022. *Hypertension in adults: diagnosis and management* [Online]. Available: https://www.nice.org.uk/guidance/ng136/resources/hypertension-in-adults-diagnosis-and-management-pdf-66141722710213 [Accessed 31.10.2023 2023].

NATIONAL INSTITUTE FOR HEALTH AND CARE EXCELLENCE. 2023a. *Candesartan cilexetil* [Online]. Available: https://bnf.nice.org.uk/drugs/candesartan-cilexetil/ [Accessed 31.10.2023 2023].

NATIONAL INSTITUTE FOR HEALTH AND CARE EXCELLENCE. 2023b. *Captopril* [Online]. Available: https://bnf.nice.org.uk/drugs/captopril/ [Accessed 31.10.2023 2023].

NATIONAL INSTITUTE FOR HEALTH AND CARE EXCELLENCE. 2023c. *What are strokes and TIAs?* [Online]. Available: https://cks.nice.org.uk/topics/stroke-tia/background-information/definition/#:~:text=Stroke%20is%20a%20clinical%20syndrome,hours%20or%20leads%20to%20death [Accessed 31.10.2023 2023].

NATIONAL INSTITUTE FOR HEALTH AND CARE EXCELLENCE. 2023d. *What are the risk factors?* [Online]. Available: https://cks.nice.org.uk/topics/cvd-risk-assessment-management/background-information/risk-factors-for-cvd/ [Accessed 31.10.2023 2023].

NATIONAL INSTITUTE FOR HEALTH AND CARE EXCELLENCE. 2024a. *Losartan potassium* [Online]. Available: https://bnf.nice.org.uk/drugs/losartan-potassium/ [Accessed 21.02.2024 2024].

NATIONAL INSTITUTE FOR HEALTH AND CARE EXCELLENCE. 2024b. *Valsartan* [Online]. Available: https://bnf.nice.org.uk/drugs/valsartan/ [Accessed 21.02.2024 2024].

NATIONAL INSTITUTES FOR HEALTH. 2023. *IL1RN interleukin 1 receptor antagonist [Homo sapiens (human)]* [Online]. Available: https://www.ncbi.nlm.nih.gov/gene/3557 [Accessed 07012024 2024].

NAVAR, L. G. 2014. Physiology: hemodynamics, endothelial function, renin-angiotensin-aldosterone system, sympathetic nervous system. *J Am Soc Hypertens,* 8**,** 519-24.

NEUHAUS, K. L., FEUERER, W., JEEP-TEBBE, S., NIEDERER, W., VOGT, A. & TEBBE, U. 1989. Improved thrombolysis with a modified dose regimen of recombinant tissue-type plasminogen activator. *J Am Coll Cardiol,* 14**,** 1566-9.

NEWMAN, L. A., MULLER, K. & ROWLAND, A. 2022. Circulating cell-specific extracellular vesicles as biomarkers for the diagnosis and monitoring of chronic liver diseases. *Cell Mol Life Sci,* 79**,** 232.

NGUYEN, D. B., TRAN, H. T., KAESTNER, L. & BERNHARDT, I. 2022. The Relation Between Extracellular Vesicles Released From Red Blood Cells, Their Cargo, and the Clearance by Macrophages. *Front Physiol,* 13**,** 783260.

NISHIMURA, Y., ITO, T. & SAAVEDRA, J. M. 2000. Angiotensin II AT(1) blockade normalizes cerebrovascular autoregulation and reduces cerebral ischemia in spontaneously hypertensive rats. *Stroke,* 31**,** 2478-86.

NITTA, T., HATA, M., GOTOH, S., SEO, Y., SASAKI, H., HASHIMOTO, N., FURUSE, M. & TSUKITA, S. 2003. Size-selective loosening of the blood-brain barrier in claudin-5-deficient mice. *J Cell Biol,* 161**,** 653-60.

NOGUEIRA, R. G., JADHAV, A. P., HAUSSEN, D. C., BONAFE, A., BUDZIK, R. F., BHUVA, P., YAVAGAL, D. R., RIBO, M., COGNARD, C., HANEL, R. A., SILA, C. A., HASSAN, A. E., MILLAN, M., LEVY, E. I., MITCHELL, P., CHEN, M., ENGLISH, J. D., SHAH, Q. A., SILVER, F. L., PEREIRA, V. M., MEHTA, B. P., BAXTER, B. W., ABRAHAM, M. G., CARDONA, P., VEZNEDAROGLU, E., HELLINGER, F. R., FENG, L., KIRMANI, J. F., LOPES, D. K., JANKOWITZ, B. T., FRANKEL, M. R., COSTALAT, V., VORA, N. A., YOO, A. J., MALIK, A. M., FURLAN, A. J., RUBIERA, M., AGHAEBRAHIM, A., OLIVOT, J.-M., TEKLE, W. G., SHIELDS, R., GRAVES, T., LEWIS, R. J., SMITH, W. S., LIEBESKIND, D. S., SAVER, J. L. & JOVIN, T. G. 2017. Thrombectomy 6 to 24 Hours after Stroke with a Mismatch between Deficit and Infarct. *New England Journal of Medicine,* 378**,** 11-21.

NORAMBUENA-SOTO, I., OCARANZA, M. P., CANCINO-ARENAS, N., SANHUEZA–OLIVARES, F., VILLAR-FINCHEIRA, P., LEIVA–NAVARRETE, S., MANCILLA-MEDINA, C., MOYA, J., NOVOA, U., JALIL, J. E., CASTRO, P. F., LAVANDERO, S. & CHIONG, M. 2020. Angiotensin-(1–9) prevents vascular remodeling by decreasing vascular smooth muscle cell dedifferentiation through a FoxO1-dependent mechanism. *Biochemical Pharmacology,* 180**,** 114190.

O'DONNELL, M. J., CHIN, S. L., RANGARAJAN, S., XAVIER, D., LIU, L., ZHANG, H., RAO-MELACINI, P., ZHANG, X., PAIS, P., AGAPAY, S., LOPEZ-JARAMILLO, P., DAMASCENO, A., LANGHORNE, P., MCQUEEN, M. J., ROSENGREN, A., DEHGHAN, M., HANKEY, G. J., DANS, A. L., ELSAYED, A., AVEZUM, A., MONDO, C., DIENER, H.-C., RYGLEWICZ, D., CZLONKOWSKA, A., POGOSOVA, N., WEIMAR, C., IQBAL, R., DIAZ, R., YUSOFF, K., YUSUFALI, A., OGUZ, A., WANG, X., PENAHERRERA, E., LANAS, F., OGAH, O. S., OGUNNIYI, A., IVERSEN, H. K., MALAGA, G., RUMBOLDT, Z., OVEISGHARAN, S., AL HUSSAIN, F., MAGAZI, D., NILANONT, Y., FERGUSON, J., PARE, G. & YUSUF, S. 2016. Global and regional effects of potentially modifiable risk factors associated with acute stroke in 32 countries (INTERSTROKE): a case-control study. *The Lancet,* 388**,** 761-775.

OBAMA, T. & EGUCHI, S. 2014. MicroRNA as a novel component of the tissue renin angiotensin system. *Journal of Molecular and Cellular Cardiology,* 75**,** 98-99.

OCARANZA, M. P., GODOY, I., JALIL, J. E., VARAS, M., COLLANTES, P., PINTO, M., ROMAN, M., RAMIREZ, C., COPAJA, M., DIAZ-ARAYA, G., CASTRO, P. & LAVANDERO, S. 2006. Enalapril attenuates downregulation of Angiotensin-converting enzyme 2 in the late phase of ventricular dysfunction in myocardial infarcted rat. *Hypertension,* 48**,** 572-8.

OCARANZA, M. P., MOYA, J., BARRIENTOS, V., ALZAMORA, R., HEVIA, D., MORALES, C., PINTO, M., ESCUDERO, N., GARCIA, L., NOVOA, U., AYALA, P., DIAZ-ARAYA, G., GODOY, I., CHIONG, M., LAVANDERO, S., JALIL, J. E. & MICHEA, L. 2014. Angiotensin-(1-9) reverses experimental hypertension and cardiovascular damage by inhibition of the angiotensin converting enzyme/Ang II axis. *J Hypertens,* 32**,** 771-83.

OECKINGHAUS, A. & GHOSH, S. 2009. The NF-kappaB family of transcription factors and its regulation. *Cold Spring Harb Perspect Biol,* 1**,** a000034.

OLZINSKI, A. R., MCCAFFERTY, T. A., ZHAO, S. Q., BEHM, D. J., EYBYE, M. E., MANISCALCO, K., BENTLEY, R., FRAZIER, K. S., MILLINER, C. M.,

MIRABILE, R. C., COATNEY, R. W. & WILLETTE, R. N. 2005. Hypertensive target organ damage is attenuated by a p38 MAPK inhibitor: role of systemic blood pressure and endothelial protection. *Cardiovascular Research,* 66**,** 170-178.

ORD, E. N. J., SHIRLEY, R., MCCLURE, J. D., MCCABE, C., KREMER, E. J., MACRAE, I. M. & WORK, L. M. 2013. Combined Antiapoptotic and Antioxidant Approach to Acute Neuroprotection for Stroke in Hypertensive Rats. *Journal of Cerebral Blood Flow & Metabolism,* 33**,** 1215-1224.

OTERO-ORTEGA, L., LASO-GARCÍA, F., FRUTOS, M. C. G., DIEKHORST, L., MARTÍNEZ-ARROYO, A., ALONSO-LÓPEZ, E., GARCÍA-BERMEJO, M. L., RODRÍGUEZ-SERRANO, M., ARRÚE-GONZALO, M., DÍEZ-TEJEDOR, E., FUENTES, B. & GUTIÉRREZ-FERNÁNDEZ, M. 2020. Low dose of extracellular vesicles identified that promote recovery after ischemic stroke. *Stem Cell Res Ther,* 11**,** 70.

PACURARI, M. & TCHOUNWOU, P. B. 2015. Role of MicroRNAs in Renin-Angiotensin-Aldosterone System-Mediated Cardiovascular Inflammation and Remodeling. *Int J Inflam,* 2015**,** 101527.

PAGET, D., CHECA, A., ZÖHRER, B., HEILIG, R., SHANMUGANATHAN, M., DHALIWAL, R., JOHNSON, E., JØRGENSEN, M., BÆK, R., OXFORD ACUTE MYOCARDIAL INFARCTION STUDY (OXAMI)WHEELOCK, C. E., CHANNON, K. M., FISCHER, R., ANTHONY, D. C., CHOUDHURY, R. C. & AKBAR, N. 2022. Comparative and integrated analysis of plasma extracellular vesicle isolation methods in healthy volunteers and patients following myocardial infarction. *Journal of Extracellular Biology* e66.

PARDRIDGE, W. M. 2012. Drug transport across the blood-brain barrier. *J Cereb Blood Flow Metab,* 32**,** 1959-72.

PARHAMIFAR, L., ANDERSEN, H. & MOGHIMI, S. M. 2013. Lactate dehydrogenase assay for assessment of polycation cytotoxicity. *Methods Mol Biol,* 948**,** 13-22.

PASCUCCI, L. & SCATTINI, G. 2021. Imaging extracelluar vesicles by transmission electron microscopy: Coping with technical hurdles and morphological interpretation. *Biochim Biophys Acta Gen Subj,* 1865**,** 129648.

PATERSON, M. R. & KRIEGEL, A. J. 2017. MiR-146a/b: a family with shared seeds and different roots. *Physiol Genomics,* 49**,** 243-252.

PATHAK, A., KUMAR, P., PANDIT, A. K., CHAKRAVARTY, K., MISRA, S., YADAV, A. K. & PRASAD, K. 2018. Is Prevalence of Hypertension Increasing in First-Ever Stroke Patients?: A Hospital-Based Cross-Sectional Study. *Ann Neurosci,* 25**,** 219-222.

PEDRAGOSA, J., SALAS-PERDOMO, A., GALLIZIOLI, M., CUGOTA, R., MIRÓ-MUR, F., BRIANSÓ, F., JUSTICIA, C., PÉREZ-ASENSIO, F., MARQUEZ-KISINOUSKY, L., URRA, X., GIERYNG, A., KAMINSKA, B., CHAMORRO, A. & PLANAS, A. M. 2018. CNS-border associated macrophages respond to acute ischemic stroke attracting granulocytes and promoting vascular leakage. *Acta Neuropathologica Communications,* 6**,** 76.

PERCIE DU SERT, N., HURST, V., AHLUWALIA, A., ALAM, S., AVEY, M. T., BAKER, M., BROWNE, W. J., CLARK, A., CUTHILL, I. C., DIRNAGL, U., EMERSON, M., GARNER, P., HOLGATE, S. T., HOWELLS, D. W., KARP, N. A., LAZIC, S. E., LIDSTER, K., MACCALLUM, C. J., MACLEOD, M., PEARL, E. J., PETERSEN, O. H., RAWLE, F., REYNOLDS, P., ROONEY, K., SENA, E. S., SILBERBERG, S. D., STECKLER, T. & WÜRBEL, H. 2020. The ARRIVE guidelines 2.0: Updated guidelines for reporting animal research*. *Journal of Cerebral Blood Flow & Metabolism,* 40**,** 1769-1777.

PEREIRA, R. M., DOS SANTOS, R. A., TEIXEIRA, M. M., LEITE, V. H., COSTA, L. P., DA COSTA DIAS, F. L., BARCELOS, L. S., COLLARES, G. B. & SIMÕES E

SILVA, A. C. 2007. The renin-angiotensin system in a rat model of hepatic fibrosis: evidence for a protective role of Angiotensin-(1-7). *J Hepatol,* 46**,** 674-81.

PEREZ-HERNANDEZ, D., GUTIERREZ-VAZQUEZ, C., JORGE, I., LOPEZ-MARTIN, S., URSA, A., SANCHEZ-MADRID, F., VAZQUEZ, J. & YANEZ-MO, M. 2013. The intracellular interactome of tetraspanin-enriched microdomains reveals their function as sorting machineries toward exosomes. *J Biol Chem,* 288**,** 11649-61.

PETERS, O., BACK, T., LINDAUER, U., BUSCH, C., MEGOW, D., DREIER, J. & DIRNAGL, U. 1998. Increased formation of reactive oxygen species after permanent and reversible middle cerebral artery occlusion in the rat. *J Cereb Blood Flow Metab,* 18**,** 196-205.

PHILLIPS, D. R., CHARO, I. F., PARISE, L. V. & FITZGERALD, L. A. 1988. The platelet membrane glycoprotein IIb-IIIa complex. *Blood,* 71**,** 831-43.

PHILLIPS, M. I. & FELIX, D. 1976. Specific angiotensin II receptive neurons in the cat subfornical organ. *Brain Research,* 109**,** 531-540.

PISITKUN, T., SHEN, R. F. & KNEPPER, M. A. 2004. Identification and proteomic profiling of exosomes in human urine. *Proc Natl Acad Sci U S A,* 101**,** 13368-73.

POLS, M. S. & KLUMPERMAN, J. 2009. Trafficking and function of the tetraspanin CD63. *Experimental Cell Research,* 315**,** 1584-1592.

POMATTO, M. A. C., BUSSOLATI, B., D'ANTICO, S., GHIOTTO, S., TETTA, C., BRIZZI, M. F. & CAMUSSI, G. 2019. Improved Loading of Plasma-Derived Extracellular Vesicles to Encapsulate Antitumor miRNAs. *Mol Ther Methods Clin Dev,* 13**,** 133-144.

POTZ, B. A., SCRIMGEOUR, L. A., PAVLOV, V. I., SODHA, N. R., ABID, M. R. & SELLKE, F. W. 2018. Extracellular Vesicle Injection Improves Myocardial Function and Increases Angiogenesis in a Swine Model of Chronic Ischemia. *J Am Heart Assoc,* 7.

POWERS, W. J., DERDEYN, C. P., BILLER, J., COFFEY, C. S., HOH, B. L., JAUCH, E. C., JOHNSTON, K. C., JOHNSTON, S. C., KHALESSI, A. A., KIDWELL, C. S., MESCHIA, J. F., OVBIAGELE, B. & YAVAGAL, D. R. 2015. 2015 American Heart Association/American Stroke Association Focused Update of the 2013 Guidelines for the Early Management of Patients With Acute Ischemic Stroke Regarding Endovascular Treatment: A Guideline for Healthcare Professionals From the American Heart Association/American Stroke Association. *Stroke,* 46**,** 3020-35.

POWERS, W. J., RABINSTEIN, A. A., ACKERSON, T., ADEOYE, O. M., BAMBAKIDIS, N. C., BECKER, K., BILLER, J., BROWN, M., DEMAERSCHALK, B. M., HOH, B., JAUCH, E. C., KIDWELL, C. S., LESLIE-MAZWI, T. M., OVBIAGELE, B., SCOTT, P. A., SHETH, K. N., SOUTHERLAND, A. M., SUMMERS, D. V., TIRSCHWELL, D. L. & NULL, N. 2019. Guidelines for the Early Management of Patients With Acute Ischemic Stroke: 2019 Update to the 2018 Guidelines for the Early Management of Acute Ischemic Stroke: A Guideline for Healthcare Professionals From the American Heart Association/American Stroke Association. *Stroke,* 50**,** e344-e418.

PRADILLO, J. M., MURRAY, K. N., COUTTS, G. A., MORAGA, A., OROZ-GONJAR, F., BOUTIN, H., MORO, M. A., LIZASOAIN, I., ROTHWELL, N. J. & ALLAN, S. M. 2017. Reparative effects of interleukin-1 receptor antagonist in young and aged/co-morbid rodents after cerebral ischemia. *Brain, Behavior, and Immunity,* 61**,** 117-126.

PRAKASH, L. D., BALAJI, N., KUMAR, S. S. & KATE, V. 2015. Comparison of electrocautery incision with scalpel incision in midline abdominal surgery – A double blind randomized controlled trial. *International Journal of Surgery,* 19**,** 78-82.

PROGRESS COLLABORATIVE GROUP 2001. Randomised trial of a perindopril-based blood-pressure-lowering regimen among 6,105 individuals with previous stroke or transient ischaemic attack. *Lancet,* 358**,** 1033-41.

PUN, P. B. L., LU, J. & MOOCHHALA, S. 2009. Involvement of ROS in BBB dysfunction. *Free Radical Research,* 43**,** 348-364.

PUZAR DOMINKUS, P., STENOVEC, M., SITAR, S., LASIC, E., ZOREC, R., PLEMENITAS, A., ZAGAR, E., KREFT, M. & LENASSI, M. 2018. PKH26 labeling of extracellular vesicles: Characterization and cellular internalization of contaminating PKH26 nanoparticles. *Biochim Biophys Acta Biomembr,* 1860**,** 1350-1361.

QIAN, Y., SONG, J., OUYANG, Y., HAN, Q., CHEN, W., ZHAO, X., XIE, Y., CHEN, Y., YUAN, W. & FAN, C. 2017. Advances in Roles of miR-132 in the Nervous System. *Front Pharmacol,* 8**,** 770.

QIU, L., CAI, Y., GENG, Y., YAO, X., WANG, L., CAO, H., ZHANG, X., WU, Q., KONG, D., DING, D., SHI, Y., WANG, Y. & WU, J. 2022. Mesenchymal stem cell-derived extracellular vesicles attenuate tPA-induced blood–brain barrier disruption in murine ischemic stroke models. *Acta Biomaterialia,* 154**,** 424-442.

QUESSEVEUR, G., DAVID, D. J., GAILLARD, M. C., PLA, P., WU, M. V., NGUYEN, H. T., NICOLAS, V., AUREGAN, G., DAVID, I., DRANOVSKY, A., HANTRAYE, P., HEN, R., GARDIER, A. M., DÉGLON, N. & GUIARD, B. P. 2013. BDNF overexpression in mouse hippocampal astrocytes promotes local neurogenesis and elicits anxiolytic-like activities. *Transl Psychiatry,* 3**,** e253.

QURESHI, A. I., EZZEDDINE, M. A., NASAR, A., SURI, M. F., KIRMANI, J. F., HUSSEIN, H. M., DIVANI, A. A. & REDDI, A. S. 2007. Prevalence of elevated blood pressure in 563,704 adult patients with stroke presenting to the ED in the United States. *Am J Emerg Med,* 25**,** 32-8.

RÄDLER, J., GUPTA, D., ZICKLER, A. & ANDALOUSSI, S. E. 2023. Exploiting the biogenesis of extracellular vesicles for bioengineering and therapeutic cargo loading. *Mol Ther,* 31**,** 1231-1250.

RAJASHEKHAR, G., KAMOCKA, M., MARIN, A., SUCKOW, M. A., WOLTER, W. R., BADVE, S., SANJEEVAIAH, A. R., PUMIGLIA, K., ROSEN, E. & CLAUSS, M. 2011. Pro-inflammatory angiogenesis is mediated by p38 MAP kinase. *Journal of Cellular Physiology,* 226**,** 800-808.

RAK, J. & GUHA, A. 2012. Extracellular vesicles--vehicles that spread cancer genes. *Bioessays,* 34**,** 489-97.

RAMIREZ, F. D., MOTAZEDIAN, P., JUNG, R. G., DI SANTO, P., MACDONALD, Z. D., MORELAND, R., SIMARD, T., CLANCY, A. A., RUSSO, J. J., WELCH, V. A., WELLS, G. A. & HIBBERT, B. 2017. Methodological Rigor in Preclinical Cardiovascular Studies: Targets to Enhance Reproducibility and Promote Research Translation. *Circ Res,* 120**,** 1916-1926.

RANKIN, J. 1957. Cerebral vascular accidents in patients over the age of 60. II. Prognosis. *Scott Med J,* 2**,** 200-15.

REGENHARDT, R. W., DESLAND, F., MECCA, A. P., PIOQUINTO, D. J., AFZAL, A., MOCCO, J. & SUMNERS, C. 2013. Anti-inflammatory effects of angiotensin-(1-7) in ischemic stroke. *Neuropharmacology,* 71**,** 154-63.

REGENHARDT, R. W., MECCA, A. P., DESLAND, F., RITUCCI-CHINNI, P. F., LUDIN, J. A., GREENSTEIN, D., SUMNERS, C., BANUELOS, C., BIZON, J. L. & REINHARD, M. K. 2014. Centrally administered angiotensin-(1-7) increases the survival of stroke-prone spontaneously hypertensive rats. *Experimental Physiology,* 99**,** 442-453.

REHMAN, A., LEIBOWITZ, A., YAMAMOTO, N., RAUTUREAU, Y., PARADIS, P. & SCHIFFRIN, E. L. 2012. Angiotensin Type 2 Receptor Agonist Compound 21

Reduces Vascular Injury and Myocardial Fibrosis in Stroke-Prone Spontaneously Hypertensive Rats. *Hypertension,* 59**,** 291-299.

REN, S., WU, G., HUANG, Y., WANG, L., LI, Y. & ZHANG, Y. 2021. MiR-18a Aggravates Intracranial Hemorrhage by Regulating RUNX1-Occludin/ZO-1 Axis to Increase BBB Permeability. *Journal of Stroke and Cerebrovascular Diseases,* 30**,** 105878.

RICE, G. I., THOMAS, D. A., GRANT, P. J., TURNER, A. J. & HOOPER, N. M. 2004. Evaluation of angiotensin-converting enzyme (ACE), its homologue ACE2 and neprilysin in angiotensin peptide metabolism. *Biochem J,* 383**,** 45-51.

RIGHT-2 INVESTIGATORS 2019. Prehospital transdermal glyceryl trinitrate in patients with ultra-acute presumed stroke (RIGHT-2): an ambulance-based, randomised, sham-controlled, blinded, phase 3 trial. *Lancet,* 393**,** 1009-1020.

ROBBINS, P. D. & MORELLI, A. E. 2014. Regulation of immune responses by extracellular vesicles. *Nat Rev Immunol,* 14**,** 195-208.

ROSENSTEIN, J. M., MANI, N., SILVERMAN, W. F. & KRUM, J. M. 1998. Patterns of brain angiogenesis after vascular endothelial growth factor administration in vitro and in vivo. *Proc Natl Acad Sci U S A,* 95**,** 7086-91.

ROSSI, R., FITZGERALD, S., MOLINA, S., MEREUTA, O. M., DOUGLAS, A., PANDIT, A., SANTOS, A. M. S., MURPHY, B., ALDERSON, J., BRENNAN, P., POWER, S., O'HARE, A., GILVARRY, M., MCCARTHY, R., PSYCHOGIOS, K., MAGOUFIS, G., TSIVGOULIS, G., NAGY, A., VADÁSZ, Á., SZIKORA, I., JOOD, K., REDFORS, P., NORDANSTIG, A., CEDER, E., DEHLFORS, N., DUNKER, D., TATLISUMAK, T., RENTZOS, A., THORNTON, J. & DOYLE, K. M. 2021. The administration of rtPA before mechanical thrombectomy in acute ischemic stroke patients is associated with a significant reduction of the retrieved clot area but it does not influence revascularization outcome. *J Thromb Thrombolysis,* 51**,** 545-551.

RUTTEN-JACOBS, L. C., LARSSON, S. C., MALIK, R., RANNIKMÄE, K., SUDLOW, C. L., DICHGANS, M., MARKUS, H. S. & TRAYLOR, M. 2018. Genetic risk, incident stroke, and the benefits of adhering to a healthy lifestyle: cohort study of 306 473 UK Biobank participants. *Bmj,* 363**,** k4168.

RUZICKA, M., SKARDA, V. & LEENEN, F. H. H. 1995. Effects of ACE Inhibitors on Circulating Versus Cardiac Angiotensin II in Volume OverloadInduced Cardiac Hypertrophy in Rats. *Circulation,* 92**,** 3568-3573.

SABA, R., SORENSEN, D. L. & BOOTH, S. A. 2014. MicroRNA-146a: A Dominant, Negative Regulator of the Innate Immune Response. *Front Immunol,* 5**,** 578.

SAH, R. G., D'ESTERRE, C. D., HILL, M. D., HAFEEZ, M., TARIQ, S., FORKERT, N. D., FRAYNE, R., DEMCHUK, A. M., GOYAL, M. & BARBER, P. A. 2018. Diffusion-weighted imaging lesion growth occurs despite recanalization in acute ischemic stroke: Implications for future treatment trials. *International Journal of Stroke,* 14**,** 257-264.

SALMERON, K. E., MANISKAS, M. E., EDWARDS, D. N., WONG, R., RAJKOVIC, I., TROUT, A., RAHMAN, A. A., HAMILTON, S., FRASER, J. F., PINTEAUX, E. & BIX, G. J. 2019. Interleukin 1 alpha administration is neuroprotective and neuro-restorative following experimental ischemic stroke. *Journal of Neuroinflammation,* 16**,** 222.

SALOMON, C., DAS, S., ERDBRÜGGER, U., KALLURI, R., KIANG LIM, S., OLEFSKY, J. M., RICE, G. E., SAHOO, S., ANDY TAO, W., VADER, P., WANG, Q. & WEAVER, A. M. 2022. Extracellular Vesicles and Their Emerging Roles as Cellular Messengers in Endocrinology: An Endocrine Society Scientific Statement. *Endocr Rev,* 43**,** 441-468.

SALTER, M. W. & STEVENS, B. 2017. Microglia emerge as central players in brain disease. *Nat Med,* 23**,** 1018-1027.

SAMPAIO, W. O., SOUZA DOS SANTOS, R. A., FARIA-SILVA, R., DA MATA MACHADO, L. T., SCHIFFRIN, E. L. & TOUYZ, R. M. 2007. Angiotensin-(1-7) Through Receptor Mas Mediates Endothelial Nitric Oxide Synthase Activation via Akt-Dependent Pathways. *Hypertension,* 49**,** 185-192.

SANTAMARÍA-CADAVID, M., RODRÍGUEZ-CASTRO, E., RODRÍGUEZ-YÁÑEZ, M., ARIAS-RIVAS, S., LÓPEZ-DEQUIDT, I., PÉREZ-MATO, M., RODRÍGUEZ-PÉREZ, M., LÓPEZ-LOUREIRO, I., HERVELLA, P., CAMPOS, F., CASTILLO, J., IGLESIAS-REY, R. & SOBRINO, T. 2020. Regulatory T cells participate in the recovery of ischemic stroke patients. *BMC Neurology,* 20**,** 68.

SANTOS, R. A., SIMOES E SILVA, A. C., MARIC, C., SILVA, D. M., MACHADO, R. P., DE BUHR, I., HERINGER-WALTHER, S., PINHEIRO, S. V., LOPES, M. T., BADER, M., MENDES, E. P., LEMOS, V. S., CAMPAGNOLE-SANTOS, M. J., SCHULTHEISS, H. P., SPETH, R. & WALTHER, T. 2003. Angiotensin-(1-7) is an endogenous ligand for the G protein-coupled receptor Mas. *Proc Natl Acad Sci U S A,* 100**,** 8258-63.

SANTOS, R. A. S., SAMPAIO, W. O., ALZAMORA, A. C., MOTTA-SANTOS, D., ALENINA, N., BADER, M. & CAMPAGNOLE-SANTOS, M. J. 2018. The ACE2/Angiotensin-(1-7)/MAS Axis of the Renin-Angiotensin System: Focus on Angiotensin-(1-7). *Physiol Rev,* 98**,** 505-553.

SAVER, J. L., ALBERS, G. W., DUNN, B., JOHNSTON, K. C. & FISHER, M. 2009. Stroke Therapy Academic Industry Roundtable (STAIR) Recommendations for Extended Window Acute Stroke Therapy Trials. *Stroke,* 40**,** 2594-2600.

SAVER, J. L., GOYAL, M., BONAFE, A., DIENER, H.-C., LEVY, E. I., PEREIRA, V. M., ALBERS, G. W., COGNARD, C., COHEN, D. J., HACKE, W., JANSEN, O., JOVIN, T. G., MATTLE, H. P., NOGUEIRA, R. G., SIDDIQUI, A. H., YAVAGAL, D. R., BAXTER, B. W., DEVLIN, T. G., LOPES, D. K., REDDY, V. K., DU MESNIL DE ROCHEMONT, R., SINGER, O. C. & JAHAN, R. 2015. Stent-Retriever Thrombectomy after Intravenous t-PA vs. t-PA Alone in Stroke. *New England Journal of Medicine,* 372**,** 2285-2295.

SAVOIA, C., TABET, F., YAO, G., SCHIFFRIN, E. L. & TOUYZ, R. M. 2005. Negative regulation of RhoA/Rho kinase by angiotensin II type 2 receptor in vascular smooth muscle cells: role in angiotensin II-induced vasodilation in stroke-prone spontaneously hypertensive rats. *Journal of Hypertension,* 23.

SCHÄBITZ, W.-R., STEIGLEDER, T., COOPER-KUHN, C. M., SCHWAB, S., SOMMER, C., SCHNEIDER, A. & KUHN, H. G. 2007. Intravenous Brain-Derived Neurotrophic Factor Enhances Poststroke Sensorimotor Recovery and Stimulates Neurogenesis. *Stroke,* 38**,** 2165-2172.

SCHERBAKOV, N., PIETROCK, C., SANDEK, A., EBNER, N., VALENTOVA, M., SPRINGER, J., SCHEFOLD, J. C., VON HAEHLING, S., ANKER, S. D., NORMAN, K., HAEUSLER, K. G. & DOEHNER, W. 2019. Body weight changes and incidence of cachexia after stroke. *J Cachexia Sarcopenia Muscle,* 10**,** 611-620.

SCHLATTER, E., SALOMONSSON, M., PERSSON, A. E. G. & GREGER, R. 1989. Macula densa cells sense luminal NaCl concentration via furosemide sensitive Na+2Cl−K+ cotransport. *Pflügers Archiv,* 414**,** 286-290.

SCHNEIDER, M. & NESHEIM, M. 2004. A study of the protection of plasmin from antiplasmin inhibition within an intact fibrin clot during the course of clot lysis. *J Biol Chem,* 279**,** 13333-9.

SCHRADER, J., LÜDERS, S., KULSCHEWSKI, A., HAMMERSEN, F., PLATE, K., BERGER, J., ZIDEK, W., DOMINIAK, P. & DIENER, H. C. 2005. Morbidity and Mortality After Stroke, Eprosartan Compared with Nitrendipine for Secondary Prevention: principal results of a prospective randomized controlled study (MOSES). *Stroke,* 36**,** 1218-26.

SCHWAMM, L. H., KOROSHETZ, W. J., SORENSEN, A. G., WANG, B., COPEN, W. A., BUDZIK, R., RORDORF, G., BUONANNO, F. S., SCHAEFER, P. W. & GONZALEZ, R. G. 1998. Time Course of Lesion Development in Patients With Acute Stroke. *Stroke,* 29**,** 2268-2276.

SCHWENGEL, K., LUCHT, K., VALERO-ESQUITINO, V., NAMSOLLECK, P., UNGER, T., CLAUSEN, B. H., LAMBERTSEN, K. L., THONE-REINEKE, C., MULLER, S., WIDDOP, R. E., DENTON, K. M., HORIUCHI, M., IWAI, M., BOATO, F., DAHLOF, B., HALLBERG, A. & STECKELINGS, U. M. 2016. Angiotensin AT2-receptor stimulation improves survival and neurological outcome after experimental stroke in mice. *Journal of Molecular Medicine,* 94**,** 957-966.

SEKERDAG, E., SOLAROGLU, I. & GURSOY-OZDEMIR, Y. 2018. Cell Death Mechanisms in Stroke and Novel Molecular and Cellular Treatment Options. *Curr Neuropharmacol,* 16**,** 1396-1415.

SEPÚLVEDA-RIVAS, S., LEAL, M. S., PEDROZO, Z., KOGAN, M. J., OCARANZA, M. P. & MORALES, J. O. 2021. Nanoparticle-Mediated Angiotensin-(1-9) Drug Delivery for the Treatment of Cardiac Hypertrophy. *Pharmaceutics* [Online], 13.

SHAN, B. S., MOGI, M., IWANAMI, J., BAI, H. Y., KAN-NO, H., HIGAKI, A., MIN, L. J. & HORIUCHI, M. 2018. Attenuation of stroke damage by angiotensin II type 2 receptor stimulation via peroxisome proliferator-activated receptor-gamma activation. *Hypertens Res,* 41**,** 839-848.

SHARMA, N., BELENCHIA, A. M., TOEDEBUSCH, R., PULAKAT, L. & HANS, C. P. 2020. AT2R agonist NP-6A4 mitigates aortic stiffness and proteolytic activity in mouse model of aneurysm. *J Cell Mol Med,* 24**,** 7393-7404.

SHEINERMAN, K. S., TSIVINSKY, V. G., ABDULLAH, L., CRAWFORD, F. & UMANSKY, S. R. 2013. Plasma microRNA biomarkers for detection of mild cognitive impairment: biomarker validation study. *Aging (Albany NY),* 5**,** 925-38.

SHENG, M., LI, Q., HUANG, W., YU, D., PAN, H., QIAN, K., REN, F., LUO, L. & TANG, L. 2024. Ang-(1–7)/Mas axis ameliorates bleomycin-induced pulmonary fibrosis in mice via restoration of Nox4-Nrf2 redox homeostasis. *European Journal of Pharmacology,* 962**,** 176233.

SHERMAN, C. D., LODHA, S. & SAHOO, S. 2021. EV Cargo Sorting in Therapeutic Development for Cardiovascular Disease. *Cells* [Online], 10.

SHIBUYA, M. 2011. Vascular Endothelial Growth Factor (VEGF) and Its Receptor (VEGFR) Signaling in Angiogenesis: A Crucial Target for Anti- and Pro-Angiogenic Therapies. *Genes Cancer,* 2**,** 1097-105.

SHINOHARA, K., NAKAGAWA, P., GOMEZ, J., MORGAN, D. A., LITTLEJOHN, N. K., FOLCHERT, M. D., WEIDEMANN, B. J., LIU, X., WALSH, S. A., PONTO, L. L., RAHMOUNI, K., GROBE, J. L. & SIGMUND, C. D. 2017. Selective Deletion of Renin-b in the Brain Alters Drinking and Metabolism. *Hypertension,* 70**,** 990-997.

SIEDLINSKI, M., CARNEVALE, L., XU, X., CARNEVALE, D., EVANGELOU, E., CAULFIELD, M. J., MAFFIA, P., WARDLAW, J., SAMANI, N. J., TOMASZEWSKI, M., LEMBO, G., HOLMES, M. V. & GUZIK, T. J. 2023. Genetic analyses identify brain structures related to cognitive impairment associated with elevated blood pressure. *European Heart Journal,* 44, 2114-2125.

SIMÕES E SILVA, A. C., SILVEIRA, K. D., FERREIRA, A. J. & TEIXEIRA, M. M. 2013. ACE2, angiotensin-(1-7) and Mas receptor axis in inflammation and fibrosis. *Br J Pharmacol,* 169**,** 477-92.

SIMS, J. E. & SMITH, D. E. 2010. The IL-1 family: regulators of immunity. *Nature Reviews Immunology,* 10**,** 89-102.

SIMS, N. R. & MUYDERMAN, H. 2010. Mitochondria, oxidative metabolism and cell death in stroke. *Biochimica et Biophysica Acta (BBA) - Molecular Basis of Disease,* 1802**,** 80-91.

SINNING, J. M., LOSCH, J., WALENTA, K., BOHM, M., NICKENIG, G. & WERNER, N. 2011. Circulating CD31+/Annexin V+ microparticles correlate with cardiovascular outcomes. *Eur Heart J,* 32**,** 2034-41.

SIRAGY, H. M. & CAREY, R. M. 1999. Protective Role of the Angiotensin AT2 Receptor in a Renal Wrap Hypertension Model. *Hypertension,* 33**,** 1237-1242.

SIVANANTHAM, A. & JIN, Y. 2022. Impact of Storage Conditions on EV Integrity/Surface Markers and Cargos. *Life (Basel),* 12.

SMITH, C. J., HULME, S., VAIL, A., HEAL, C., PARRY-JONES, A. R., SCARTH, S., HOPKINS, K., HOADLEY, M., ALLAN, S. M., ROTHWELL, N. J., HOPKINS, S. J. & TYRRELL, P. J. 2018. SCIL-STROKE (Subcutaneous Interleukin-1 Receptor Antagonist in Ischemic Stroke). *Stroke,* 49**,** 1210-1216.

SMITH, J. A., DAS, A., RAY, S. K. & BANIK, N. L. 2012. Role of pro-inflammatory cytokines released from microglia in neurodegenerative diseases. *Brain Res Bull,* 87**,** 10-20.

SODAEI, F. & SHAHMAEI, V. 2020. Identification of penumbra in acute ischemic stroke using multimodal MR imaging analysis: A case report study. *Radiol Case Rep,* 15**,** 2041-2046.

SONG, W., WANG, H. & WU, Q. 2015. Atrial natriuretic peptide in cardiovascular biology and disease (NPPA). *Gene,* 569**,** 1-6.

SONG, Y., ZHANG, C., ZHANG, J., JIAO, Z., DONG, N., WANG, G., WANG, Z. & WANG, L. 2019. Localized injection of miRNA-21-enriched extracellular vesicles effectively restores cardiac function after myocardial infarction. *Theranostics,* 9**,** 2346-2360.

SONG, Z., BAI, J., ZHANG, L., SUN, X., ZHANG, M., ZHENG, H. & ZHANG, J. 2014. [Effects of telmisartan on inflammation and fibrosis after acute myocardial infarction in rats]. *Zhonghua Yi Xue Za Zhi,* 94**,** 2628-33.

SOO, C. Y., SONG, Y., ZHENG, Y., CAMPBELL, E. C., RICHES, A. C., GUNN-MOORE, F. & POWIS, S. J. 2012. Nanoparticle tracking analysis monitors microvesicle and exosome secretion from immune cells. *Immunology,* 136**,** 192-7.

SOTOMAYOR-FLORES, C., RIVERA-MEJÍAS, P., VÁSQUEZ-TRINCADO, C., LÓPEZ-CRISOSTO, C., MORALES, P. E., PENNANEN, C., POLAKOVICOVA, I., ALIAGA-TOBAR, V., GARCÍA, L., ROA, J. C., ROTHERMEL, B. A., MARACAJA-COUTINHO, V., HO-XUAN, H., MEISTER, G., CHIONG, M., OCARANZA, M. P., CORVALÁN, A. H., PARRA, V. & LAVANDERO, S. 2020. Angiotensin-(1–9) prevents cardiomyocyte hypertrophy by controlling mitochondrial dynamics via miR-129-3p/PKIA pathway. *Cell Death & Differentiation,* 27**,** 2586-2604.

SOUZA-SILVA, I. M., PELUSO, A. A., MORTENSEN, C., NAZAROVA, A. L., STAGE, T. B., SUMNERS, C., KATRITCH, V. & STECKELINGS, U. M. 2024. Development of an automated, high-throughput assay to detect angiotensin AT2-receptor agonistic compounds by nitric oxide measurements in vitro. *Peptides,* 172**,** 171137.

SOUZA Á, P., SOBRINHO, D. B., ALMEIDA, J. F., ALVES, G. M., MACEDO, L. M., PORTO, J. E., VÊNCIO, E. F., COLUGNATI, D. B., SANTOS, R. A., FERREIRA, A. J., MENDES, E. P. & CASTRO, C. H. 2013. Angiotensin II type 1 receptor blockade restores angiotensin-(1-7)-induced coronary vasodilation in hypertrophic rat hearts. *Clin Sci (Lond),* 125**,** 449-59.

SPRANGER, M., KREMPIEN, S., SCHWAB, S., DONNEBERG, S. & HACKE, W. 1997. Superoxide Dismutase Activity in Serum of Patients With Acute Cerebral Ischemic Injury. *Stroke,* 28**,** 2425-2428.

STANTON, A., JENSEN, C., NUSSBERGER, J. & O'BRIEN, E. 2003. Blood Pressure Lowering in Essential Hypertension With an Oral Renin Inhibitor, Aliskiren. *Hypertension,* 42**,** 1137-1143.

STARKOV, A. A., CHINOPOULOS, C. & FISKUM, G. 2004. Mitochondrial calcium and oxidative stress as mediators of ischemic brain injury. *Cell Calcium,* 36**,** 257-264.

STEPHENSON, D., YIN, T., SMALSTIG, E. B., HSU, M. A., PANETTA, J., LITTLE, S. & CLEMENS, J. 2000. Transcription Factor Nuclear Factor-Kappa B is Activated in Neurons after Focal Cerebral Ischemia. *Journal of Cerebral Blood Flow & Metabolism,* 20**,** 592-603.

STROKE ASSOCIATION. 2023. *Symptoms of Stroke* [Online]. Available: https://www.stroke.org.uk/what-is-stroke/what-are-the-symptoms-of-stroke [Accessed 31.10.2023 2023].

STROKE ASSOCIATION. 2024. *Types of Stroke* [Online]. Available: https://www.stroke.org.uk/what-is-stroke/types-of-stroke?gad_source=1&gclid=CjwKCAiA6KWvBhAREiwAFPZM7mbpHra3jmMeaYH_fjdkiIerzXfZZzbls3tkBKICezzaJ30uHdY89xoCPo4QAvD_BwE [Accessed 07032024 2024].

STROKE THERAPY ACADEMIC INDUSTRY ROUNDTABLE (STAIR) 1999. Recommendations for standards regarding preclinical neuroprotective and restorative drug development. *Stroke,* 30**,** 2752-8.

STUFFERS, S., SEM WEGNER, C., STENMARK, H. & BRECH, A. 2009. Multivesicular endosome biogenesis in the absence of ESCRTs. *Traffic,* 10**,** 925-37.

SUKUMARAN, V., VEERAVEEDU, P. T., GURUSAMY, N., LAKSHMANAN, A. P., YAMAGUCHI, K. I., MA, M., SUZUKI, K., KODAMA, M. & WATANABE, K. 2012. Telmisartan acts through the modulation of ACE-2/ANG 1–7/mas receptor in rats with dilated cardiomyopathy induced by experimental autoimmune myocarditis. *Life Sciences,* 90**,** 289-300.

SUKUMARAN, V., VEERAVEEDU, P. T., GURUSAMY, N., YAMAGUCHI, K., LAKSHMANAN, A. P., MA, M., SUZUKI, K., KODAMA, M. & WATANABE, K. 2011. Cardioprotective effects of telmisartan against heart failure in rats induced by experimental autoimmune myocarditis through the modulation of angiotensin-converting enzyme-2/angiotensin 1-7/mas receptor axis. *Int J Biol Sci,* 7**,** 1077-92.

SUMNERS, C., ALLEYNE, A., RODRÍGUEZ, V., PIOQUINTO, D. J., LUDIN, J. A., KAR, S., WINDER, Z., ORTIZ, Y., LIU, M., KRAUSE, E. G. & DE KLOET, A. D. 2020. Brain angiotensin type-1 and type-2 receptors: cellular locations under normal and hypertensive conditions. *Hypertens Res,* 43**,** 281-295.

SUN, D., LEE, Y. S., MALHOTRA, A., KIM, H. K., MATECIC, M., EVANS, C., JENSEN, R. V., MOSKALUK, C. A. & DUTTA, A. 2011. miR-99 family of MicroRNAs suppresses the expression of prostate-specific antigen and prostate cancer cell proliferation. *Cancer Res,* 71**,** 1313-24.

SUN, Y., LI, Y., WANG, M., YUE, M., BAI, L., BIAN, J., HAO, W., SUN, J., ZHANG, S. & LIU, H. 2020. Increased AT(2)R expression is induced by AT(1)R autoantibody via two axes, Klf-5/IRF-1 and circErbB4/miR-29a-5p, to promote VSMC migration. *Cell Death Dis,* 11**,** 432.

SUN, Y., SAITO, K. & SAITO, Y. 2019. Lipid Profile Characterization and Lipoprotein Comparison of Extracellular Vesicles from Human Plasma and Serum. *Metabolites,* 9.

SUN, Y., ZHANG, J. Q., ZHANG, J. & RAMIRES, F. J. A. 1998. Angiotensin II, Transforming Growth Factor-β1and Repair in the Infarcted Heart. *Journal of Molecular and Cellular Cardiology,* 30**,** 1559-1569.

TAKAKI, H., MINODA, Y., KOGA, K., TAKAESU, G., YOSHIMURA, A. & KOBAYASHI, T. 2006. TGF-β1 suppresses IFN-γ-induced NO production in macrophages by suppressing STAT1 activation and accelerating iNOS protein degradation. *Genes to Cells,* 11**,** 871-882.

TAMARAT, R., SILVESTRE, J.-S., DURIE, M. & LEVY, B. I. 2002. Angiotensin II Angiogenic Effect In Vivo Involves Vascular Endothelial Growth Factor- and Inflammation-Related Pathways. *Laboratory Investigation,* 82**,** 747-756.

TANG, L. L., YE, K., YANG, X. F. & ZHENG, J. S. 2007. Apocynin attenuates cerebral infarction after transient focal ischaemia in rats. *J Int Med Res,* 35**,** 517-22.

TAO, M.-X., XUE, X., LU, J.-L., ZHOU, J.-S., JIANG, T., ZHANG, Y.-D. & GAO, L. 2018. Involvement of angiotensin-(1-7) in the neuroprotection of captopril against focal cerebral ischemia. *Neuroscience Letters,* 687**,** 16-21.

TAO, Z., ZHAO, H., WANG, R., LIU, P., YAN, F., ZHANG, C., JI, X. & LUO, Y. 2015. Neuroprotective effect of microRNA-99a against focal cerebral ischemia-reperfusion injury in mice. *J Neurol Sci,* 355**,** 113-9.

TAYLOR, R. A., CHANG, C.-F., GOODS, B. A., HAMMOND, M. D., MAC GRORY, B., AI, Y., STEINSCHNEIDER, A. F., RENFROE, S. C., ASKENASE, M. H., MCCULLOUGH, L. D., KASNER, S. E., MULLEN, M. T., HAFLER, D. A., LOVE, J. C. & SANSING, L. H. 2017. TGF-β1 modulates microglial phenotype and promotes recovery after intracerebral hemorrhage. *The Journal of Clinical Investigation,* 127**,** 280-292.

TEASDALE, G. & JENNETT, B. 1974. Assessment of coma and impaired consciousness. A practical scale. *Lancet,* 2**,** 81-4.

TER-OVANESYAN, D., GILBOA, T., BUDNIK, B., NIKITINA, A., WHITEMAN, S., LAZAROVITS, R., TRIEU, W., KALISH, D., CHURCH, G. M. & WALT, D. R. 2023. Improved isolation of extracellular vesicles by removal of both free proteins and lipoproteins. *Elife,* 12.

THAMM, T., GUO, J., ROSENBERG, J., LIANG, T., MARKS, M. P., CHRISTENSEN, S., DO, H. M., KEMP, S. M., ADAIR, E., EYNGORN, I., MLYNASH, M., JOVIN, T. G., KEOGH, B. P., CHEN, H. J., LANSBERG, M. G., ALBERS, G. W., ZAHARCHUK, G. & NULL, N. 2019. Contralateral Hemispheric Cerebral Blood Flow Measured With Arterial Spin Labeling Can Predict Outcome in Acute Stroke. *Stroke,* 50**,** 3408-3415.

THE NATIONAL INSTITUTES OF HEALTH. 2024. *NIH Stroke Scale* [Online]. Available: https://www.ninds.nih.gov/health-information/public-education/know-stroke/health-professionals/nih-stroke-scale [Accessed 08032024 2024].

THE UNIPROT CONSORTIUM. 2023. *P08962 · CD63_HUMAN* [Online]. Available: https://www.uniprot.org/uniprotkb/P08962/entry [Accessed 12122023 2023].

THERY, C., AMIGORENA, S., RAPOSO, G. & CLAYTON, A. 2006. Isolation and characterization of exosomes from cell culture supernatants and biological fluids. *Curr Protoc Cell Biol,* Chapter 3**,** Unit 3 22.

THERY, C., WITWER, K. W., AIKAWA, E., ALCARAZ, M. J., ANDERSON, J. D., ANDRIANTSITOHAINA, R., ANTONIOU, A., ARAB, T., ARCHER, F., ATKIN-SMITH, G. K., AYRE, D. C., BACH, J. M., BACHURSKI, D., BAHARVAND, H., BALAJ, L., BALDACCHINO, S., BAUER, N. N., BAXTER, A. A., BEBAWY, M., BECKHAM, C., BEDINA ZAVEC, A., BENMOUSSA, A., BERARDI, A. C., BERGESE, P., BIELSKA, E., BLENKIRON, C., BOBIS-WOZOWICZ, S., BOILARD, E., BOIREAU, W., BONGIOVANNI, A., BORRAS, F. E., BOSCH, S., BOULANGER, C. M., BREAKEFIELD, X., BREGLIO, A. M., BRENNAN, M. A., BRIGSTOCK, D. R., BRISSON, A., BROEKMAN, M. L., BROMBERG, J. F., BRYL-GORECKA, P., BUCH, S., BUCK, A. H., BURGER, D., BUSATTO, S., BUSCHMANN, D., BUSSOLATI, B., BUZAS, E. I., BYRD, J. B., CAMUSSI, G., CARTER, D. R., CARUSO, S., CHAMLEY, L. W., CHANG, Y. T., CHEN, C., CHEN, S., CHENG, L., CHIN, A. R., CLAYTON, A., CLERICI, S. P., COCKS, A., COCUCCI, E., COFFEY, R. J., CORDEIRO-DA-SILVA, A., COUCH, Y., COUMANS, F. A., COYLE, B., CRESCITELLI, R., CRIADO, M. F., D'SOUZA-SCHOREY, C., DAS, S., DATTA

CHAUDHURI, A., DE CANDIA, P., DE SANTANA, E. F., DE WEVER, O., DEL PORTILLO, H. A., DEMARET, T., DEVILLE, S., DEVITT, A., DHONDT, B., DI VIZIO, D., DIETERICH, L. C., DOLO, V., DOMINGUEZ RUBIO, A. P., DOMINICI, M., DOURADO, M. R., DRIEDONKS, T. A., DUARTE, F. V., DUNCAN, H. M., EICHENBERGER, R. M., EKSTROM, K., EL ANDALOUSSI, S., ELIE-CAILLE, C., ERDBRUGGER, U., FALCON-PEREZ, J. M., FATIMA, F., FISH, J. E., FLORES-BELLVER, M., FORSONITS, A., FRELET-BARRAND, A., et al. 2018. Minimal information for studies of extracellular vesicles 2018 (MISEV2018): a position statement of the International Society for Extracellular Vesicles and update of the MISEV2014 guidelines. *J Extracell Vesicles,* 7**,** 1535750.

TIAN, S., ZHOU, X., ZHANG, M., CUI, L., LI, B., LIU, Y., SU, R., SUN, K., HU, Y., YANG, F., XUAN, G., MA, S., ZHENG, X., ZHOU, X., GUO, C., SHANG, Y., WANG, J. & HAN, Y. 2022. Mesenchymal stem cell-derived exosomes protect against liver fibrosis via delivering miR-148a to target KLF6/STAT3 pathway in macrophages. *Stem Cell Res Ther,* 13**,** 330.

TIAN, T., ZHANG, H. X., HE, C. P., FAN, S., ZHU, Y. L., QI, C., HUANG, N. P., XIAO, Z. D., LU, Z. H., TANNOUS, B. A. & GAO, J. 2018. Surface functionalized exosomes as targeted drug delivery vehicles for cerebral ischemia therapy. *Biomaterials,* 150**,** 137-149.

TODA, N., NAKANISHI, S. & TANABE, S. 2013. Aldosterone affects blood flow and vascular tone regulated by endothelium-derived NO: therapeutic implications. *Br J Pharmacol,* 168**,** 519-33.

TORCIA, M., DE CHIARA, G., NENCIONI, L., AMMENDOLA, S., LABARDI, D., LUCIBELLO, M., ROSINI, P., MARLIER, L. N., BONINI, P., DELLO SBARBA, P., PALAMARA, A. T., ZAMBRANO, N., RUSSO, T., GARACI, E. & COZZOLINO, F. 2001. Nerve growth factor inhibits apoptosis in memory B lymphocytes via inactivation of p38 MAPK, prevention of Bcl-2 phosphorylation, and cytochrome c release. *J Biol Chem,* 276**,** 39027-36.

TOUYZ, R. M., ALVES-LOPES, R., RIOS, F. J., CAMARGO, L. L., ANAGNOSTOPOULOU, A., ARNER, A. & MONTEZANO, A. C. 2018. Vascular smooth muscle contraction in hypertension. *Cardiovasc Res,* 114**,** 529-539.

TRAJKOVIC, K., HSU, C., CHIANTIA, S., RAJENDRAN, L., WENZEL, D., WIELAND, F., SCHWILLE, P., BRUGGER, B. & SIMONS, M. 2008. Ceramide triggers budding of exosome vesicles into multivesicular endosomes. *Science,* 319**,** 1244-7.

TRAUB, O., LLOYD, M. C. & WEBB, R. C. 1995. Long-term effects of brief antihypertensive treatment on systolic blood pressure and vascular reactivity in young genetically hypertensive rats. *Cardiovasc Drugs Ther,* 9**,** 421-9.

TÜREYEN, K., VEMUGANTI, R., SAILOR, K. A. & DEMPSEY, R. J. 2004. Infarct volume quantification in mouse focal cerebral ischemia: a comparison of triphenyltetrazolium chloride and cresyl violet staining techniques. *Journal of Neuroscience Methods,* 139**,** 203-207.

TURK, A. S., 3RD, SIDDIQUI, A., FIFI, J. T., DE LEACY, R. A., FIORELLA, D. J., GU, E., LEVY, E. I., SNYDER, K. V., HANEL, R. A., AGHAEBRAHIM, A., WOODWARD, B. K., HIXSON, H. R., CHAUDRY, M. I., SPIOTTA, A. M., RAI, A. T., FREI, D., ALMANDOZ, J. E. D., KELLY, M., ARTHUR, A., BAXTER, B., ENGLISH, J., LINFANTE, I., FARGEN, K. M. & MOCCO, J. 2019. Aspiration thrombectomy versus stent retriever thrombectomy as first-line approach for large vessel occlusion (COMPASS): a multicentre, randomised, open label, blinded outcome, non-inferiority trial. *Lancet,* 393**,** 998-1008.

UHLEN, M., FAGERBERG, L., HALLSTROM, B. M., LINDSKOG, C., OKSVOLD, P., MARDINOGLU, A., SIVERTSSON, A., KAMPF, C., SJOSTEDT, E., ASPLUND, A., OLSSON, I., EDLUND, K., LUNDBERG, E., NAVANI, S., SZIGYARTO, C. A., ODEBERG, J., DJUREINOVIC, D., TAKANEN, J. O., HOBER, S., ALM, T., EDQVIST, P. H., BERLING, H., TEGEL, H., MULDER, J., ROCKBERG, J., NILSSON, P., SCHWENK, J. M., HAMSTEN, M., VON FEILITZEN, K., FORSBERG, M., PERSSON, L., JOHANSSON, F., ZWAHLEN, M., VON HEIJNE, G., NIELSEN, J. & PONTEN, F. 2015. Proteomics. Tissue-based map of the human proteome. *Science,* 347**,** 1260419.

URWYLER, S. A., EBRAHIMI, F., BURKARD, T., SCHUETZ, P., POGLITSCH, M., MUELLER, B., DONATH, M. Y. & CHRIST-CRAIN, M. 2020. IL (Interleukin)-1 Receptor Antagonist Increases Ang (Angiotensin [1-7]) and Decreases Blood Pressure in Obese Individuals. *Hypertension,* 75**,** 1455-1463.

US FOOD AND DRUG ADMINISTRATION. 2024. *FDA approves irinotecan liposome for first-line treatment of metastatic pancreatic adenocarcinoma* [Online]. US Food and Drug Administration, United States Government. Available: https://www.fda.gov/drugs/resources-information-approved-drugs/fda-approves-irinotecan-liposome-first-line-treatment-metastatic-pancreatic-adenocarcinoma#:~:text=FDA%20approves%20irinotecan%20liposome%20for%20first%2Dline%20treatment%20of%20metastatic%20pancreatic%20adenocarcinoma,-Share&text=On%20February%2013%2C%202024%2C%20the,%2C%20Ipsen%20Biopharmaceuticals%2C%20Inc.) [Accessed 25.03.2024 2024].

VAN DEUN, J., MESTDAGH, P., AGOSTINIS, P., AKAY, Ö., ANAND, S., ANCKAERT, J., MARTINEZ, Z. A., BAETENS, T., BEGHEIN, E., BERTIER, L., BERX, G., BOERE, J., BOUKOURIS, S., BREMER, M., BUSCHMANN, D., BYRD, J. B., CASERT, C., CHENG, L., CMOCH, A., DAVELOOSE, D., DE SMEDT, E., DEMIRSOY, S., DEPOORTER, V., DHONDT, B., DRIEDONKS, T. A. P., DUDEK, A., ELSHARAWY, A., FLORIS, I., FOERS, A. D., GÄRTNER, K., GARG, A. D., GEEURICKX, E., GETTEMANS, J., GHAZAVI, F., GIEBEL, B., KORMELINK, T. G., HANCOCK, G., HELSMOORTEL, H., HILL, A. F., HYENNE, V., KALRA, H., KIM, D., KOWAL, J., KRAEMER, S., LEIDINGER, P., LEONELLI, C., LIANG, Y., LIPPENS, L., LIU, S., LO CICERO, A., MARTIN, S., MATHIVANAN, S., MATHIYALAGAN, P., MATUSEK, T., MILANI, G., MONGUIÓ-TORTAJADA, M., MUS, L. M., MUTH, D. C., NÉMETH, A., NOLTE-'T HOEN, E. N. M., O'DRISCOLL, L., PALMULLI, R., PFAFFL, M. W., PRIMDAL-BENGTSON, B., ROMANO, E., ROUSSEAU, Q., SAHOO, S., SAMPAIO, N., SAMUEL, M., SCICLUNA, B., SOEN, B., STEELS, A., SWINNEN, J. V., TAKATALO, M., THAMINY, S., THÉRY, C., TULKENS, J., VAN AUDENHOVE, I., VAN DER GREIN, S., VAN GOETHEM, A., VAN HERWIJNEN, M. J., VAN NIEL, G., VAN ROY, N., VAN VLIET, A. R., VANDAMME, N., VANHAUWAERT, S., VERGAUWEN, G., VERWEIJ, F., WALLAERT, A., WAUBEN, M., WITWER, K. W., ZONNEVELD, M. I., DE WEVER, O., VANDESOMPELE, J., HENDRIX, A. & CONSORTIUM, E.-T. 2017. EV-TRACK: transparent reporting and centralizing knowledge in extracellular vesicle research. *Nature Methods,* 14**,** 228-232.

VAN KRALINGEN, J. C., MCFALL, A., ORD, E. N. J., COYLE, T. F., BISSETT, M., MCCLURE, J. D., MCCABE, C., MACRAE, I. M., DAWSON, J. & WORK, L. M. 2019. Altered Extracellular Vesicle MicroRNA Expression in Ischemic Stroke and Small Vessel Disease. *Transl Stroke Res,* 10**,** 495-508.

VAN SWIETEN, J. C., KOUDSTAAL, P. J., VISSER, M. C., SCHOUTEN, H. J. & VAN GIJN, J. 1988. Interobserver agreement for the assessment of handicap in stroke patients. *Stroke,* 19**,** 604-7.

VEERMAN, R. E., AKPINAR, G. G., OFFENS, A., STEINER, L., LARSSEN, P., LUNDQVIST, A., KARLSSON, M. C. I. & GABRIELSSON, S. 2023. Antigen-Loaded Extracellular Vesicles Induce Responsiveness to Anti-PD-1 and Anti-PD-L1 Treatment in a Checkpoint Refractory Melanoma Model. *Cancer Immunol Res,* 11**,** 217-227.

VERDECCHIA, P., SLEIGHT, P., MANCIA, G., FAGARD, R., TRIMARCO, B., SCHMIEDER, R. E., KIM, J. H., JENNINGS, G., JANSKY, P., CHEN, J. H., LIU, L., GAO, P., PROBSTFIELD, J., TEO, K., YUSUF, S. & INVESTIGATORS, O. T. 2009. Effects of telmisartan, ramipril, and their combination on left ventricular hypertrophy in individuals at high vascular risk in the Ongoing Telmisartan Alone and in Combination With Ramipril Global End Point Trial and the Telmisartan Randomized Assessment Study in ACE Intolerant Subjects With Cardiovascular Disease. *Circulation,* 120**,** 1380-9.

VILLARROYA-BELTRI, C., GUTIÉRREZ-VÁZQUEZ, C., SÁNCHEZ-CABO, F., PÉREZ-HERNÁNDEZ, D., VÁZQUEZ, J., MARTIN-COFRECES, N., MARTINEZ-HERRERA, D. J., PASCUAL-MONTANO, A., MITTELBRUNN, M. & SÁNCHEZ-MADRID, F. 2013. Sumoylated hnRNPA2B1 controls the sorting of miRNAs into exosomes through binding to specific motifs. *Nat Commun,* 4**,** 2980.

VON ENGELHARDT, J., COSEREA, I., PAWLAK, V., FUCHS, E. C., KÖHR, G., SEEBURG, P. H. & MONYER, H. 2007. Excitotoxicity in vitro by NR2A- and NR2B-containing NMDA receptors. *Neuropharmacology,* 53**,** 10-17.

WAKI, H. 2012. Central mechanisms of cardiovascular regulation during exercise: Integrative functions of the nucleus of the solitary tract. *The Journal of Physical Fitness and Sports Medicine,* 1**,** 253-261.

WANET, A., TACHENY, A., ARNOULD, T. & RENARD, P. 2012. miR-212/132 expression and functions: within and beyond the neuronal compartment. *Nucleic Acids Res,* 40**,** 4742-53.

WANG, H.-J., LO, W.-Y. & LIN, L.-J. 2013a. Angiotensin-(1–7) decreases glycated albumin-induced endothelial interleukin-6 expression via modulation of miR-146a. *Biochemical and Biophysical Research Communications,* 430**,** 1157-1163.

WANG, H., LIU, Y., LI, J., WANG, T., HEI, Y., LI, H., WANG, X., WANG, L., ZHAO, R., LIU, W. & LONG, Q. 2021. Tail-vein injection of MSC-derived small extracellular vesicles facilitates the restoration of hippocampal neuronal morphology and function in APP / PS1 mice. *Cell Death Discov,* 7**,** 230.

WANG, J., CHEN, S., ZHANG, W., CHEN, Y. & BIHL, J. C. 2020. Exosomes from miRNA-126-modified endothelial progenitor cells alleviate brain injury and promote functional recovery after stroke. *CNS Neurosci Ther,* 26**,** 1255-1265.

WANG, J., HE, W., GUO, L., ZHANG, Y., LI, H., HAN, S. & SHEN, D. 2017a. The ACE2-Ang (1-7)-Mas receptor axis attenuates cardiac remodeling and fibrosis in post-myocardial infarction. *Mol Med Rep,* 16**,** 1973-1981.

WANG, J., SUN, X., ZHAO, J., YANG, Y., CAI, X., XU, J. & CAO, P. 2017b. Exosomes: A Novel Strategy for Treatment and Prevention of Diseases. *Front Pharmacol,* 8**,** 300.

WANG, W., LI, D.-B., LI, R.-Y., ZHOU, X., YU, D.-J., LAN, X.-Y., LI, J.-P. & LIU, J.-L. 2018. Diagnosis of Hyperacute and Acute Ischaemic Stroke: The Potential Utility of Exosomal MicroRNA-21-5p and MicroRNA-30a-5p. *Cerebrovascular Diseases,* 45**,** 204-212.

WANG, X., KHAIDAKOV, M., DING, Z., MITRA, S., LU, J., LIU, S. & MEHTA, J. L. 2012. Cross-talk between inflammation and angiotensin II: studies based on direct transfection of cardiomyocytes with AT1R and AT2R cDNA. *Exp Biol Med (Maywood),* 237**,** 1394-401.

WANG, X. & LIN, Y. 2008. Tumor necrosis factor and cancer, buddies or foes? *Acta Pharmacol Sin,* 29**,** 1275-88.

WANG, Y., JIN, K., MAO, X. O., XIE, L., BANWAIT, S., MARTI, H. H. & GREENBERG, D. A. 2007. VEGF-overexpressing transgenic mice show enhanced post-ischemic neurogenesis and neuromigration. *J Neurosci Res,* 85**,** 740-7.

WANG, Y., XU, J., ZHAO, X., WANG, D., WANG, C., LIU, L., WANG, A., MENG, X., LI, H. & WANG, Y. 2013b. Association of Hypertension With Stroke Recurrence Depends on Ischemic Stroke Subtype. *Stroke,* 44**,** 1232-1237.

WARACH, S. & LATOUR, L. L. 2004. Evidence of Reperfusion Injury, Exacerbated by Thrombolytic Therapy, in Human Focal Brain Ischemia Using a Novel Imaging Marker of Early Blood–Brain Barrier Disruption. *Stroke,* 35**,** 2659-2661.

WARREN, A. J., BRAVO, J., WILLIAMS, R. L. & RABBITTS, T. H. 2000. Structural basis for the heterodimeric interaction between the acute leukaemia-associated transcription factors AML1 and CBFbeta. *Embo j,* 19**,** 3004-15.

WELSH, J. A., GOBERDHAN, D. C. I., O'DRISCOLL, L., BUZAS, E. I., BLENKIRON, C., BUSSOLATI, B., CAI, H., DI VIZIO, D., DRIEDONKS, T. A. P., ERDBRÜGGER, U., FALCON-PEREZ, J. M., FU, Q. L., HILL, A. F., LENASSI, M., LIM, S. K., MAHONEY, M. G., MOHANTY, S., MÖLLER, A., NIEUWLAND, R., OCHIYA, T., SAHOO, S., TORRECILHAS, A. C., ZHENG, L., ZIJLSTRA, A., ABUELREICH, S., BAGABAS, R., BERGESE, P., BRIDGES, E. M., BRUCALE, M., BURGER, D., CARNEY, R. P., COCUCCI, E., CRESCITELLI, R., HANSER, E., HARRIS, A. L., HAUGHEY, N. J., HENDRIX, A., IVANOV, A. R., JOVANOVIC-TALISMAN, T., KRUH-GARCIA, N. A., KU'ULEI-LYN FAUSTINO, V., KYBURZ, D., LÄSSER, C., LENNON, K. M., LÖTVALL, J., MADDOX, A. L., MARTENS-UZUNOVA, E. S., MIZENKO, R. R., NEWMAN, L. A., RIDOLFI, A., ROHDE, E., ROJALIN, T., ROWLAND, A., SAFTICS, A., SANDAU, U. S., SAUGSTAD, J. A., SHEKARI, F., SWIFT, S., TER-OVANESYAN, D., TOSAR, J. P., USECKAITE, Z., VALLE, F., VARGA, Z., VAN DER POL, E., VAN HERWIJNEN, M. J. C., WAUBEN, M. H. M., WEHMAN, A. M., WILLIAMS, S., ZENDRINI, A., ZIMMERMAN, A. J., THÉRY, C. & WITWER, K. W. 2024. Minimal information for studies of extracellular vesicles (MISEV2023): From basic to advanced approaches. *J Extracell Vesicles,* 13**,** e12404.

WETTERLING, F., CHATZIKONSTANTINOU, E., TRITSCHLER, L., MEAIRS, S., FATAR, M., SCHAD, L. R. & ANSAR, S. 2016. Investigating potentially salvageable penumbra tissue in an in vivo model of transient ischemic stroke using sodium, diffusion, and perfusion magnetic resonance imaging. *BMC Neurosci,* 17**,** 82.

WEVERS, N. R., NAIR, A. L., FOWKE, T. M., PONTIER, M., KASI, D. G., SPIJKERS, X. M., HALLARD, C., RABUSSIER, G., VAN VUGHT, R., VULTO, P., DE VRIES, H. E. & LANZ, H. L. 2021. Modeling ischemic stroke in a triculture neurovascular unit on-a-chip. *Fluids Barriers CNS,* 18**,** 59.

WEXLER, E. J., PETERS, E. E., GONZALES, A., GONZALES, M. L., SLEE, A. M. & KERR, J. S. 2002. An objective procedure for ischemic area evaluation of the stroke intraluminal thread model in the mouse and rat. *Journal of Neuroscience Methods,* 113**,** 51-58.

WHITE, C. L., MCCLURE, L. A., WALLACE, P. M., BRAIMAH, J., LISKAY, A., ROLDAN, A. & BENAVENTE, O. R. 2011. The correlates and course of depression in patients with lacunar stroke: results from the Secondary Prevention of Small Subcortical Strokes (SPS3) study. *Cerebrovasc Dis,* 32**,** 354-60.

WIKLANDER, O. P., NORDIN, J. Z., O'LOUGHLIN, A., GUSTAFSSON, Y., CORSO, G., MAGER, I., VADER, P., LEE, Y., SORK, H., SEOW, Y., HELDRING, N., ALVAREZ-ERVITI, L., SMITH, C. I., LE BLANC, K., MACCHIARINI, P.,

JUNGEBLUTH, P., WOOD, M. J. & ANDALOUSSI, S. E. 2015. Extracellular vesicle in vivo biodistribution is determined by cell source, route of administration and targeting. *J Extracell Vesicles,* 4**,** 26316.

WOLF, G., WENZEL, U., BURNS, K. D., HARRIS, R. C., STAHL, R. A. & THAISS, F. 2002. Angiotensin II activates nuclear transcription factor-kappaB through AT1 and AT2 receptors. *Kidney Int,* 61**,** 1986-95.

WOLL, K. A. & VAN PETEGEM, F. 2021. Calcium-release channels: structure and function of IP3 receptors and ryanodine receptors. *Physiological Reviews,* 102**,** 209-268.

WORLD STROKE ORGANISATION. 2022. *Global Stroke Fact Sheet 2022* [Online]. Available: https://www.world-stroke.org/assets/downloads/WSO_Global_Stroke_Fact_Sheet.pdf [Accessed 31.10.2023 2023].

WRIGHT, J. W. & HARDING, J. W. 2013. The brain renin-angiotensin system: a diversity of functions and implications for CNS diseases. *Pflugers Arch,* 465**,** 133-51.

WU, Q.-L., CUI, L.-Y., MA, W.-Y., WANG, S.-S., ZHANG, Z., FENG, Z.-P., SUN, H.-S., CHU, S.-F., HE, W.-B. & CHEN, N.-H. 2023. A novel small-molecular CCR5 antagonist promotes neural repair after stroke. *Acta Pharmacologica Sinica,* 44**,** 1935-1947.

WYNNE, B. M., CHIAO, C. W. & WEBB, R. C. 2009. Vascular Smooth Muscle Cell Signaling Mechanisms for Contraction to Angiotensin II and Endothelin-1. *J Am Soc Hypertens,* 3**,** 84-95.

XIN, H., LI, Y., CUI, Y., YANG, J. J., ZHANG, Z. G. & CHOPP, M. 2013. Systemic administration of exosomes released from mesenchymal stromal cells promote functional recovery and neurovascular plasticity after stroke in rats. *J Cereb Blood Flow Metab,* 33**,** 1711-5.

XIONG, X.-Y., LIU, L. & YANG, Q.-W. 2016. Functions and mechanisms of microglia/macrophages in neuroinflammation and neurogenesis after stroke. *Progress in Neurobiology,* 142**,** 23-44.

XU, N., LAGROW, T. J., ANUMBA, N., LEE, A., ZHANG, X., YOUSEFI, B., BASSIL, Y., CLAVIJO, G. P., KHALILZAD SHARGHI, V., MALTBIE, E., MEYER-BAESE, L., NEZAFATI, M., PAN, W.-J. & KEILHOLZ, S. 2022. Functional Connectivity of the Brain Across Rodents and Humans. *Frontiers in Neuroscience,* 16.

YAMORI, Y., TOMIMOTO, K., OOSHIMA, A., HAZAMA, F. & OKAMOTO, K. 1974. Proceedings: Developmental course of hypertension in the SHR-substrains susceptible to hypertensive cerebrovascular lesions. *Jpn Heart J,* 15**,** 209-10.

YAN, H., KANKI, H., MATSUMURA, S., KAWANO, T., NISHIYAMA, K., SUGIYAMA, S., TAKEMORI, H., MOCHIZUKI, H. & SASAKI, T. 2021. MiRNA-132/212 regulates tight junction stabilization in blood-brain barrier after stroke. *Cell Death Discov,* 7**,** 380.

YAN, J., LIU, Y., ZHENG, F., LV, D. & JIN, D. 2023. Environmental enrichment enhanced neurogenesis and behavioral recovery after stroke in aged rats. *Aging (Albany NY),* 15**,** 9453-9463.

YÁÑEZ-MÓ, M., SILJANDER, P. R., ANDREU, Z., ZAVEC, A. B., BORRÀS, F. E., BUZAS, E. I., BUZAS, K., CASAL, E., CAPPELLO, F., CARVALHO, J., COLÁS, E., CORDEIRO-DA SILVA, A., FAIS, S., FALCON-PEREZ, J. M., GHOBRIAL, I. M., GIEBEL, B., GIMONA, M., GRANER, M., GURSEL, I., GURSEL, M., HEEGAARD, N. H., HENDRIX, A., KIERULF, P., KOKUBUN, K., KOSANOVIC, M., KRALJ-IGLIC, V., KRÄMER-ALBERS, E. M., LAITINEN, S., LÄSSER, C., LENER, T., LIGETI, E., LINĒ, A., LIPPS, G., LLORENTE, A., LÖTVALL, J., MANČEK-KEBER, M., MARCILLA, A.,

MITTELBRUNN, M., NAZARENKO, I., NOLTE-'T HOEN, E. N., NYMAN, T. A., O'DRISCOLL, L., OLIVAN, M., OLIVEIRA, C., PÁLLINGER, É., DEL PORTILLO, H. A., REVENTÓS, J., RIGAU, M., ROHDE, E., SAMMAR, M., SÁNCHEZ-MADRID, F., SANTARÉM, N., SCHALLMOSER, K., OSTENFELD, M. S., STOORVOGEL, W., STUKELJ, R., VAN DER GREIN, S. G., VASCONCELOS, M. H., WAUBEN, M. H. & DE WEVER, O. 2015. Biological properties of extracellular vesicles and their physiological functions. *J Extracell Vesicles,* 4**,** 27066.

YANG, J., CAO, L. L., WANG, X. P., GUO, W., GUO, R. B., SUN, Y. Q., XUE, T. F., CAI, Z. Y., JI, J., CHENG, H. & SUN, X. L. 2021a. Neuronal extracellular vesicle derived miR-98 prevents salvageable neurons from microglial phagocytosis in acute ischemic stroke. *Cell Death Dis,* 12**,** 23.

YANG, J., WU, S., HOU, L., ZHU, D., YIN, S., YANG, G. & WANG, Y. 2020a. Therapeutic Effects of Simultaneous Delivery of Nerve Growth Factor mRNA and Protein via Exosomes on Cerebral Ischemia. *Molecular Therapy - Nucleic Acids,* 21**,** 512-522.

YANG, L., HAN, B., ZHANG, Z., WANG, S., BAI, Y., ZHANG, Y., TANG, Y., DU, L., XU, L., WU, F., ZUO, L., CHEN, X., LIN, Y., LIU, K., YE, Q., CHEN, B., LI, B., TANG, T., WANG, Y., SHEN, L., WANG, G., JU, M., YUAN, M., JIANG, W., ZHANG, J. H., HU, G., WANG, J. & YAO, H. 2020b. Extracellular Vesicle-Mediated Delivery of Circular RNA SCMH1 Promotes Functional Recovery in Rodent and Nonhuman Primate Ischemic Stroke Models. *Circulation,* 142**,** 556-574.

YANG, X., WANG, Z., HUANG, H., LING, S., ZHANG, R., ZHANG, Y., CHEN, G., LI, C. & WANG, Q. 2021b. A Targeted Activatable NIR-IIb Nanoprobe for Highly Sensitive Detection of Ischemic Stroke in a Photothrombotic Stroke Model. *Adv Healthc Mater,* 10**,** e2001544.

YANG, Z., LI, T., LI, S., WEI, M., QI, H., SHEN, B., CHANG, R. C.-C., LE, W. & PIAO, F. 2019. Altered Expression Levels of MicroRNA-132 and Nurr1 in Peripheral Blood of Parkinson's Disease: Potential Disease Biomarkers. *ACS Chemical Neuroscience,* 10**,** 2243-2249.

YAO, H., FERDAUS, M. Z., ZAHID, H. M., OHARA, H., NAKAHARA, T. & NABIKA, T. 2015. Focal Ischemic Injury with Complex Middle Cerebral Artery in Stroke-Prone Spontaneously Hypertensive Rats with Loss-Of-Function in NADPH Oxidases. *PLOS ONE,* 10**,** e0138551.

YU, H., PAN, Y., DAI, M., WANG, X. & CHEN, H. 2022a. Mesenchymal Stem Cell-Originated Exosomal Lnc A2M-AS1 Alleviates Hypoxia/Reperfusion-Induced Apoptosis and Oxidative Stress in Cardiomyocytes. *Cardiovasc Drugs Ther*.

YU, X., BAI, Y., HAN, B., JU, M., TANG, T., SHEN, L., LI, M., YANG, L., ZHANG, Z., HU, G., CHAO, J., ZHANG, Y. & YAO, H. 2022b. Extracellular vesicle-mediated delivery of circDYM alleviates CUS-induced depressive-like behaviours. *J Extracell Vesicles,* 11**,** e12185.

YUANA, Y., LEVELS, J., GROOTEMAAT, A., STURK, A. & NIEUWLAND, R. 2014. Co-isolation of extracellular vesicles and high-density lipoproteins using density gradient ultracentrifugation. *J Extracell Vesicles,* 3.

YUSUF, S., SLEIGHT, P., POGUE, J., BOSCH, J., DAVIES, R. & DAGENAIS, G. 2000. Effects of an angiotensin-converting-enzyme inhibitor, ramipril, on cardiovascular events in high-risk patients. *N Engl J Med,* 342**,** 145-53.

ZABOROWSKI, M. P., BALAJ, L., BREAKEFIELD, X. O. & LAI, C. P. 2015. Extracellular Vesicles: Composition, Biological Relevance, and Methods of Study. *Bioscience,* 65**,** 783-797.

ZAHEDNEZHAD, F., SAADAT, M., VALIZADEH, H., ZAKERI-MILANI, P. & BARADARAN, B. 2019. Liposome and immune system interplay: Challenges and potentials. *Journal of Controlled Release,* 305**,** 194-209.

ZHANG, A. D., NGUYEN DINH CAT, A., SOUKASEUM, C., ESCOUBET, B., CHERFA, A., MESSAOUDI, S., DELCAYRE, C., SAMUEL, J. L. & JAISSER, F. 2008. Cross-talk between mineralocorticoid and angiotensin II signaling for cardiac remodeling. *Hypertension,* 52**,** 1060-7.

ZHANG, F., TANG, Z., HOU, X., LENNARTSSON, J., LI, Y., KOCH, A. W., SCOTNEY, P., LEE, C., ARJUNAN, P., DONG, L., KUMAR, A., RISSANEN, T. T., WANG, B., NAGAI, N., FONS, P., FARISS, R., ZHANG, Y., WAWROUSEK, E., TANSEY, G., RABER, J., FONG, G.-H., DING, H., GREENBERG, D. A., BECKER, K. G., HERBERT, J.-M., NASH, A., YLA-HERTTUALA, S., CAO, Y., WATTS, R. J. & LI, X. 2009. VEGF-B is dispensable for blood vessel growth but critical for their survival, and VEGF-B targeting inhibits pathological angiogenesis. *Proceedings of the National Academy of Sciences,* 106**,** 6152-6157.

ZHANG, H. & FABER, J. E. 2019. Transient versus Permanent MCA Occlusion in Mice Genetically Modified to Have Good versus Poor Collaterals. *Med One,* 4.

ZHANG, J., SU, R., WANG, Y., WANG, H., LI, S., YANG, X. & LIU, G. 2023. Protective effect of small extracellular vesicles (EVs) derived from ACE2-modified human umbilical cord mesenchymal stem cells against renal ischemia–reperfusion injury. *Nephrology,* n/a.

ZHANG, L., OGUNGBEMI, A., TRIPPIER, S., CLARKE, B., KHAN, U., HALL, C., JI, Q., CLIFTON, A. & CLUCKIE, G. 2021. Hub-and-spoke model for thrombectomy service in UK NHS practice. *Clin Med (Lond),* 21**,** e26-e31.

ZHANG, R., ZHONG, C., ZHANG, Y., XIE, X., ZHU, Z., WANG, A., CHEN, C.-S., PENG, Y., PENG, H., LI, Q., JU, Z., GENG, D., CHEN, J., LIU, L., WANG, Y., XU, T. & HE, J. 2019. Immediate Antihypertensive Treatment for Patients With Acute Ischemic Stroke With or Without History of Hypertension: A Secondary Analysis of the CATIS Randomized Clinical Trial. *JAMA Network Open,* 2**,** e198103-e198103.

ZHANG, S., JIN, T., WANG, L., LIU, W., ZHANG, Y., ZHENG, Y., LIN, Y., YANG, M., HE, X., LIN, H., CHEN, L. & TAO, J. 2020. Electro-Acupuncture Promotes the Differentiation of Endogenous Neural Stem Cells via Exosomal microRNA 146b After Ischemic Stroke. *Front Cell Neurosci,* 14**,** 223.

ZHANG, W. & LIU, H. T. 2002. MAPK signal pathways in the regulation of cell proliferation in mammalian cells. *Cell Research,* 12**,** 9-18.

ZHANG, X., TAKEUCHI, T., TAKEDA, A., MOCHIZUKI, H. & NAGAI, Y. 2022. Comparison of serum and plasma as a source of blood extracellular vesicles: Increased levels of platelet-derived particles in serum extracellular vesicle fractions alter content profiles from plasma extracellular vesicle fractions. *PLoS One,* 17**,** e0270634.

ZHANG, Z. G., ZHANG, L., JIANG, Q., ZHANG, R., DAVIES, K., POWERS, C., BRUGGEN, N. & CHOPP, M. 2000. VEGF enhances angiogenesis and promotes blood-brain barrier leakage in the ischemic brain. *J Clin Invest,* 106**,** 829-38.

ZHAO, F., CHENG, L., SHAO, Q., CHEN, Z., LV, X., LI, J., HE, L., SUN, Y., JI, Q., LU, P., JI, Y. & JI, J. 2020. Characterization of serum small extracellular vesicles and their small RNA contents across humans, rats, and mice. *Scientific Reports,* 10**,** 4197.

ZHAO, L., MULLIGAN, M. K. & NOWAK, T. S. 2017. Substrain- and sex-dependent differences in stroke vulnerability in C57BL/6 mice. *Journal of Cerebral Blood Flow & Metabolism,* 39**,** 426-438.

ZHAO, T., ZHAO, W., CHEN, Y., LIU, L., AHOKAS, R. A. & SUN, Y. 2013. Differential expression of vascular endothelial growth factor isoforms and receptor subtypes in the infarcted heart. *Int J Cardiol,* 167**,** 2638-45.

ZHENG, L., XU, C. C., CHEN, W. D., SHEN, W. L., RUAN, C. C., ZHU, L. M., ZHU, D. L. & GAO, P. J. 2010. MicroRNA-155 regulates angiotensin II type 1 receptor expression and phenotypic differentiation in vascular adventitial fibroblasts. *Biochem Biophys Res Commun,* 400**,** 483-8.

ZHENG, X., ZHANG, L., KUANG, Y., VENKATARAMANI, V., JIN, F., HEIN, K., ZAFEIRIOU, M. P., LENZ, C., MOEBIUS, W., KILIC, E., HERMANN, D. M., WEBER, M. S., URLAUB, H., ZIMMERMANN, W. H., BÄHR, M. & DOEPPNER, T. R. 2021. Extracellular Vesicles Derived from Neural Progenitor Cells--a Preclinical Evaluation for Stroke Treatment in Mice. *Transl Stroke Res,* 12**,** 185-203.

ZHOU, G., FAN, L., LI, Z., LI, J., KOU, X., XIAO, M., GAO, M. & QU, X. 2022. G protein-coupled receptor MAS1 induces an inhibitory effect on myocardial infarction-induced myocardial injury. *International Journal of Biological Macromolecules,* 207**,** 72-80.

ZHOU, J., CHEN, L., CHEN, B., HUANG, S., ZENG, C., WU, H., CHEN, C. & LONG, F. 2018. Increased serum exosomal miR-134 expression in the acute ischemic stroke patients. *BMC Neurology,* 18**,** 198.

ZHOU, X., DENG, X., LIU, M., HE, M., LONG, W., XU, Z., ZHANG, K., LIU, T., SO, K.-F., FU, Q.-L. & ZHOU, L. 2023a. Intranasal delivery of BDNF-loaded small extracellular vesicles for cerebral ischemia therapy. *Journal of Controlled Release,* 357**,** 1-19.

ZHOU, Y., HE, Y., YAN, S., CHEN, L., ZHANG, R., XU, J., HU, H., LIEBESKIND, D. S. & LOU, M. 2023b. Reperfusion Injury Is Associated With Poor Outcome in Patients With Recanalization After Thrombectomy. *Stroke,* 54**,** 96-104.

ZHU, Y., CUI, H., LV, J., LIANG, H., ZHENG, Y., WANG, S., WANG, M., WANG, H. & YE, F. 2019. AT1 and AT2 receptors modulate renal tubular cell necroptosis in angiotensin II-infused renal injury mice. *Sci Rep,* 9**,** 19450.

ZHU, Y., WANG, J. L., HE, Z. Y., JIN, F. & TANG, L. 2015. Association of Altered Serum MicroRNAs with Perihematomal Edema after Acute Intracerebral Hemorrhage. *PLoS One,* 10**,** e0133783.

ZIGOVA, T., PENCEA, V., WIEGAND, S. J. & LUSKIN, M. B. 1998. Intraventricular Administration of BDNF Increases the Number of Newly Generated Neurons in the Adult Olfactory Bulb. *Molecular and Cellular Neuroscience,* 11**,** 234-245.

ZOROV, D. B., FILBURN, C. R., KLOTZ, L. O., ZWEIER, J. L. & SOLLOTT, S. J. 2000. Reactive oxygen species (ROS)-induced ROS release: a new phenomenon accompanying induction of the mitochondrial permeability transition in cardiac myocytes. *J Exp Med,* 192**,** 1001-14.

ZOU, X., LIAO, Y., LIU, Z., XU, X., SUN, W., QIN, H., WANG, H., LIU, J. & JING, T. 2023. Exosomes Derived from AT2R-Overexpressing BMSC Prevent Restenosis After Carotid Artery Injury by Attenuating the Injury-Induced Neointimal Hyperplasia. *J Cardiovasc Transl Res,* 16**,** 112-126.

ZUO, X., LU, J., MANAENKO, A., QI, X., TANG, J., MEI, Q., XIA, Y. & HU, Q. 2019. MicroRNA-132 attenuates cerebral injury by protecting blood-brain-barrier in MCAO mice. *Exp Neurol,* 316**,** 12-19.